Silesian University
of Technology

PREDICTION OF THE MECHANICAL AND ELECTRICAL PROPERTIES OF CEMENTITIOUS COMPOSITES USING ARTIFICIAL NEURAL NETWORKS

MSc. CEng Sofija Kekez

Dissertation is presented at the Faculty of Civil Engineering and Transportation of Silesian University of Technology to obtain the title of Ph.D. – Doctor of Philosophy in Civil Engineering

Gliwice, June 2022

Supervisor: Prof. Jan Kubica, PhD, DSc. CEng.

Assistant supervisor: Dr. Marcin Górski, PhD, CEng.

Content

Abstract

Symbols and abbreviations

Bibliography

List of tables

List of figures

Appendices

   Appendix A – ANSYS simulations

   A1. Materials
   A2. Results
   A3. Validation

   Appendix B – Artificial Neural Networks

   B1. Datasets – Group I
   B2. Datasets – Group II
   B3. Datasets – Evaluation
   B4. Scripts
   B5. Results for prescribed models – Group I
   B6. Results for scripted models – Group I
   B7. Results for prescribed models – Group II
   B8. Results for scripted models – Group II
   B9. Results – Evaluation
   B10. Results – Sensitivity analysis

CHAPTER I Introduction

1.   Research context

Nanotechnology has come a long way since the first conception of controlling matter at the atomic scale. The development of nanotechnology started with the proof that the processes taking place at the nanoscale shall ultimately affect the bulk material's performance. Since then, the field of nanoscience has reported a multitude of groundbreaking discoveries, including the development of novel materials and various devices. The most represented and investigated nanomaterials are nano-SiO_2, nano-TiO_2, and nanocarbons such as C60, carbon black, carbon nanotubes, carbon nanofibers, graphene, etc. because of their superior mechanical properties, as well as their thermal and electrical capabilities. Since concrete has a limited ability for electrical conduction, adding such nanofillers may provide conductive behavior of the composite material. Therefore, the concrete composite material becomes an excellent choice for multi-functional structures, with enhanced mechanical features and the ability of internal strain sensing. Since the optimal mixture of CNT or CNF reinforced concrete is usually developed through a relatively long trial-and-error process, which makes its fabrication a costly venture, research provided in this work focuses on the possibilities of faster production and thus more feasible application of such materials. Implementation and application of the novel concrete mix design method are still strictly in the domain of research, and hopefully this work will bring it closer to the civil engineering practice. It is the idea of the author that exploring the application of numerical simulations, especially using artificial neural networks, for material design and prediction of their behavior could be the key part for the overall development of a new mix design technique, which will minimize the use of time- and cost-consuming experimental testing.

2. Motivation and objectives

Motivation for this work is found in the idea of implementing of self-sensing cementitious materials into residential, industrial, and road structures. Making self-sensing concrete more feasible and cost-effective through the application of numerical simulations and artificial neural networks may be the first step towards standardization and the introduction of self-sensing cementitious materials into everyday civil engineering practice.

The objectives of this dissertation are as follows:

- Forming a comprehensive collection of experiments done on CNT/CNF reinforced concrete, including all possible factors which would affect the final performance of the composite material.
- Developing numerical models and simulating performed experiments to establish a possible alternative to traditional concrete mix design methods.
- Establishing if numerical models are capable of emulating the concrete fabrication process and testing.
- Developing artificial neural networks for predictions of the compressive strength, the flexural strength, and the electrical volume resistivity of the self-sensing cementitious composite materials.
- Establishing the optimal type and architecture of an artificial neural network for this type of problem by varying the parameters of the network.

3.   Methodology of research

This work deals with the topic of reinforcing plain concrete with carbon nanotubes (CNTs) and carbon nanofibers (CNFs) and applying artificial neural networks (ANNs) to predict the properties of the said cementitious composite. The study focuses on two problems in regard to the material. The first part considers the experimental development of CNT/CNF concrete composite materials, exploring different fabrication processes, including the processes of the nanofiller dispersion and further mixing, molding, and curing of the concrete composite. The second part considers the application of numerical simulations of the material design and the testing of the specimens as an alternative to the experimental procedures using ANSYS software. The materials are designed, and experiments reproduced to observe the possibility of using this particular software for this purpose. Lastly, all results from both parts of the multi-physics research are collected, processed, and used to develop artificial neural networks designed to predict the concrete material behavior. Neural networks are developed, built, optimized, and evaluated for each dataset obtained from the experimental work and the numerical simulations. Finally, the results of the network performance are compared, and sensitivity analysis is done to establish the optimal ANN development procedure and the network architecture.

4.   Dissertation outlines

Structure of this dissertation is schematically outlined in Figure 1.1. Chapter I introduces the topic of the study and makes a general introduction to the problem. The theoretical research, including the literature review of the multi-physical approach to the issue of the self-sensing cementitious materials and the use of artificial neural networks within the area of concrete mix design, is presented in Chapter II. Chapter III presents the theoretical background for the research work, and Chapter IV establishes the assumptions and the hypotheses of the practical work. Practical research is the second stage of the dissertation, and it is divided into two parts. The first part consists of multi-physics, including material mechanics and electrical conductivity. Chapter V presents the experimental works concerned with CNT/CNF reinforced concrete. Further on, Chapter VI shows numerical models and simulations of the materials and experiments, whereas Appendix part A includes all results from the numerical simulations. The second part of multi-physics given in Chapter VII consists of the development, application, and evaluation of the ANNs,

with Appendix part B. Chapter VIII presents the conclusions regarding the numerical simulations and the artificial neural networks in terms of their practical application and possible implementation in everyday civil engineering practice. Finally, Chapter IX proposes future work and further development on this topic.
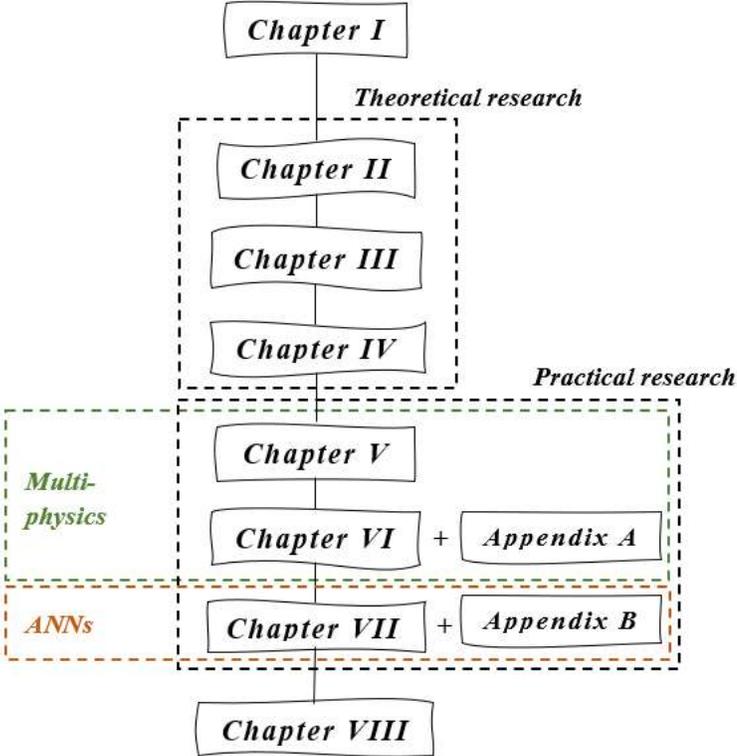
Figure 1.1 Outline of the thesis

CHAPTER II Literature review with critical analysis

1. Concrete mix design

Concrete mix design has been defined in many ways; some of them are as follows:

"Mix design can, therefore, be defined as the process of selecting suitable ingredients of concrete and determining their relative quantities with the purpose of producing an economical concrete which has certain minimum properties, notably workability, strength and durability." [1]

"Concrete mix design is therefore the process of specifying the quantity of concrete ingredients required to produce concrete with a desired fresh and hardened properties." [2]

"Optimization of the concrete mixture design is a process of search for a mixture for which the sum of the costs of the ingredients is the lowest, yet satisfying the required performance of concrete, such as workability strength and durability." [3]

In summary, concrete mix design may be defined as the process of finding the relative quantities of ingredients of concrete to fulfill specific desirable properties in the fresh and hardened states. The properties usually measured in the fresh state are the workability and in the hardened state are the strength and the durability. The property of workability may include several properties of the fresh concrete: (i) mobility (passability), (ii) stability, (iii) compactability, etc. The primary precedence of using concrete mix design is constituted in the economic aspect. In the construction of large voluminous structures such as dams or structures which require high strength of concrete such as high-rise buildings, long bridges, or different megastructures, concrete mix design assures that the required properties of concrete are achieved and, at the same time, keeps the use of costly ingredients at the necessary minimum, making the construction as economically feasible as possible. The general classification of methods used in concrete mix design includes analytical, semi-experimental, experimental, and statistical methods, and their comparative analysis may be found in several review articles, such as the one from Shi et al. [4].

Analytical methods are used to reduce the number of trial mixes to a minimum, rationalizing the initial proportioning procedure into a systematic process based on detailed information about specific weights of mixture components and formulas established from previously conducted experimental works [3]. There are investigations which show applications of mathematical models such as mathematical analysis of the optimal mixture proportions [3,5]; Levenberg-Marquardt method for the nonlinear least-squares analysis [6]; linear function

describing the dependency of compressive strength to hydration kinetics [7,8]; or modified method based on Mohr-Coulomb failure criterion [9]. The application of the particle packing method is introduced by [10] to produce recycled aggregate concrete with comparable mechanical performance as the traditional concrete mixtures and establish the advantage of such mix design approach compared to the traditional one. Li et al. [11] used an improved mix design method based on paste rheological threshold theory through yield stress, and plastic viscosity threshold formulas are modified based on material packing characteristics for self-compacting concrete with ternary blends powder materials. Furthermore, some researchers developed novel methods. Ashish et al. [12] presented the "strength-based mixture design" method, which uses close packing theory to achieve targeted strength, enhanced durability, and minimal paste volume; and [13] used a modified method of the same approach to introduce the recycled aggregate in the concrete mixture, by applying the regression analysis of the relationships between multiple parameters for the defined workability and replacement ratio of the recycled aggregate. Qasrawi [14] developed the "workability-dispersion-cohesion" method, which uses special coefficients to relate workability to mobility and stability of the concrete mix, simultaneously including various types of aggregates water-to-cement ratios, and different degrees of workability. However, not only the mechanical performance of the concrete mixtures is analyzed. The study by Ziaei-Nia et al. [15] puts forward the issue of cost optimization as one of the most important aspects of the construction industry. This study presented a nonlinear dynamic model to investigate the behavior of variables such as cement class, water-to-cement ratio, maximum size of the aggregate, amount of the cement, concrete workability, etc. The dynamic optimization required the separability of the objective function, which was represented as the composition of the individual stage returns to reduce cost over a range of operating conditions actively. The experimental work commonly follows these methods to validate the analytical results and confirm their efficiency.

Experimental methods are based on a trial-and-error process where the testing is provided until the optimal mixture is obtained. The challenge of experimental methods is a high number of effect variables affecting the response variables. Multiple effect variables increase the number of trials. This issue can be seen in the work of Habibi et al. [16], where 42 different design mixtures were tested, with the constraints of 28-day compressive strength and fresh concrete slump flow, considering the importance of sand grading. When only one factor is investigated, the number of trials can be lower, as seen in [17], where 4 formulations were used to determine the impact of the

recycled aggregate on concrete properties. However, the "one-factor-at-a-time" method has the disadvantage of not considering the interaction between the factors, which will affect the final parameters [18]. Experimental methods give the most certainty in results. However, they are also the most time-consuming and expensive procedures.

Statistical methods became an improvement and enlargement of possibilities over entirely experimental, where a set of trial mixes with a prescribed range of proportions for each component is predefined according to some statistical procedure. Afterward, the trial mixes are carried out, specimens are tested, and the results are analyzed using standard statistical methods [3]. Admittedly, statistical methods require a certain amount of experimental work, but the predictability implies somewhat lower degree of certainty. The factorial design approach is often used for determining the optimal mix proportions due to its ability to secure the balance between the variables that affect the workability, deformability, and the strength of concrete [4,19,20]. Analysis of variance (ANOVA) is the most used procedure for fitting of data and examining the weight of factors [3], referring to the materials used for the mixture. Methods such as multivariable linear regression (MLR) are based on previous experience and empirical relationships. Still, the issue of the incapability of modeling the complex nonlinear nature of the relationships between the mixture and the property [21-23] remains because the underlying relationships between all variables need to be known for a proper model. However, novel methods or the combinations of several methods are constantly investigated to establish a more efficient way to obtain the optimal mix design proportions. The work of Anike et al. [24] shows how the application of the equivalent mortar volume mix design method is an improvement over the traditional methods by using it to obtain the mechanical characteristics of steel fiber-reinforced concrete made with recycled aggregate and silica fume addition.

Semi-experimental methods are the combination of experimental dataset or experimentally developed prediction models and various analytical tools [3,16,25], mostly machine learning methods, such as artificial neural network, support vector machine, genetic algorithm, adaptive neuro-fuzzy inference system, random forest, decision tree, and others. The development of more sophisticated non-parametric machine learning methods and the growing availability of experimental datasets are opening opportunities to forecast the properties with higher accuracy and a wider application range [26]. Machine learning methods can establish the nonlinear dependencies between the effect factors through minimizing the error via the regression with a remarkably high

accuracy of results. This kind of methods has been used in concrete mix design to determine and predict various properties of fresh [27] and hardened concrete [28]. Alsini et al. [29] developed the Isolation Forest based on a Sliding window for the Local Outlier Factor (IFS-LOF) algorithm for the evaluation of 1030 concrete mixtures collected from the construction industry. This study is one of the successful examples of using machine learning or data mining tools to process a large quantity of results and establish patterns from the results. Chopra et al. [30-32] have developed ANN models for the compressive strength prediction, focusing on the execution of the model itself. The authors of [30] used seven different algorithms to determine the optimal one for their dataset.

Furthermore, they observed the efficacy of the ANN model compared to genetic programming [31], decision tree, and random forest models [32]. Golafshani et al. [33] compared the results of ANN and ANFIS models and enhanced them further by optimizing the models with Grey Wolf Optimizer to establish the prediction models for plain and high-performance concrete. The works of Akkurt et al. [34], Nikoo et al. [35], and Santosa et al. [36] show a combination of the ANN technique with the genetic algorithm, creating a so-called evolutionary ANN with improved performance. Notable research was done by Yaseen et al. [37], proposing an extreme learning model (ELM) for predicting the compressive strength of foamed concrete and comparing it with multivariate adaptive regression spline, M5 Tree models, and support vector regression. It was concluded that the ELM is a reliable and accurate technique, which may completely exclude the need for the laborious trial batching. Although there are many machine learning techniques and even more types of each technique, as well as the combinations between them, this work focuses on the basic programming of artificial neural network models to provide the basis into further investigation of the application of machine learning in the optimization of mix proportions of CNT/CNF reinforced concrete.

2. Artificial neural networks

Topic of artificial neural networks in concrete mix design was primarily centered towards the prediction of optimal mix proportions rather than predicting the properties of concrete. Back in 1997, Mukherjee et al. [38] presented an ANN for the prediction of the uniaxial behavior of concrete at high temperatures by capturing the stress–strain relationship of the material. Oh et al. [39] first opened this topic by developing a predictive model for proportioning the concrete mixes as a replacement for complex, time-consuming, and uncertain conventional methods. Later, Lee [40] showed an extensive study on the efficacy of ANNs in predicting concrete strength, where five independent models were developed with staggering 73 input variables and 7 outputs. However, as shown in [41], this approach, although somewhat useful, still implies the development of a new model for each change of a constituent material. Vis-à-vis, further research was mainly shifted towards predicting the properties of concrete, thus resolving the functionality problem. Artificial neural network models are based on data, excluding the need for specifying the underlying mechanism of the problem. Since the number of factors influencing the final 28-day compressive strength of concrete is high and the factors themselves are diverse, the simplest and quickest way to obtain the prediction is most surely through an ANN model. Investigations are mostly focused on developing ANNs to predict the compressive strength of high-performance (self-compacting, high strength), green (recycled concrete/rubber aggregate), and plain concrete. There are several investigations that use replacement materials for either the binder or the aggregate to achieve a more environmentally-friendly and sustainable concrete material. Such is the work of Dantas et al. [42], that focused on the impact of construction and demolition waste on the properties of hardened concrete. Elevado et al. [43] presented completely green concrete, replacing Portland cement with fly ash and coarse aggregate with waste ceramic tiles. ANNs were used for compressive strength predictions of this green concrete, and results were promising, showing possible alternative for traditional concrete. Another interesting investigation was given by Yaman et al. [41] focused on highly flowable self-compacting concrete with a high percentage of fly ash and superplasticizer. The authors [41] developed two ANN models with two different datasets, where the first model comprised all six needed outputs and the second one was in the form of a multi-input-single-output network, giving every target value separately as an individual model.

Except for sustainability of the materials, the issue of construction efficiency is also addressed by exploring the possibility of predicting the properties of in situ concrete materials. In situ works comprehend complete or partial lack of controllability of environmental conditions, which influence concrete in both fresh and hardened states. Such variabilities do not occur in the laboratory, which might suggest false positive results of the prediction. It might be concluded that testing of the field concrete is a much more challenging task compared to the laboratory, but the dataset based on the field concrete tests is far more extensive, giving much more insight into the actual condition of the material. Namyong et al. [44] presented a statistical investigation of in situ concrete based on 1442 results from 59 different mixtures. The authors used a relatively large dataset to establish regression equations for predictions of compressive strength. Later, DeRousseau et al. [45] evaluated the efficacy of ANNs and other machine learning methods for the prediction of the compressive strength of field-placed concrete by using two datasets obtained from the field and the laboratory. The first dataset included 1671 data tuples obtained from the Colorado Department of Transportation, and the second included laboratory mixes developed by Yeh in 1998 at the University of California, Irvine (UCI). This work [45] confirmed that the most accurate prediction of compressive strength of field concrete is achieved with ML models trained on field concrete data and that by using hybrid training data, the predictive performance of laboratory concrete models might be significantly improved.

Furthermore, the work of Young et al. [46] included probably the most extensive dataset ever used in this kind of investigations. The ANN models were based on more than ten thousand data tuples obtained from various building sites and the UCI testing to establish the efficacy of using information from the building site. Additionally, the influence of predicting mix proportions on carbon footprint was explored, addressing current alarming environmental situation. The size of the dataset used for predictions of the compressive strength of concrete is presented in Figure 2.2.1.
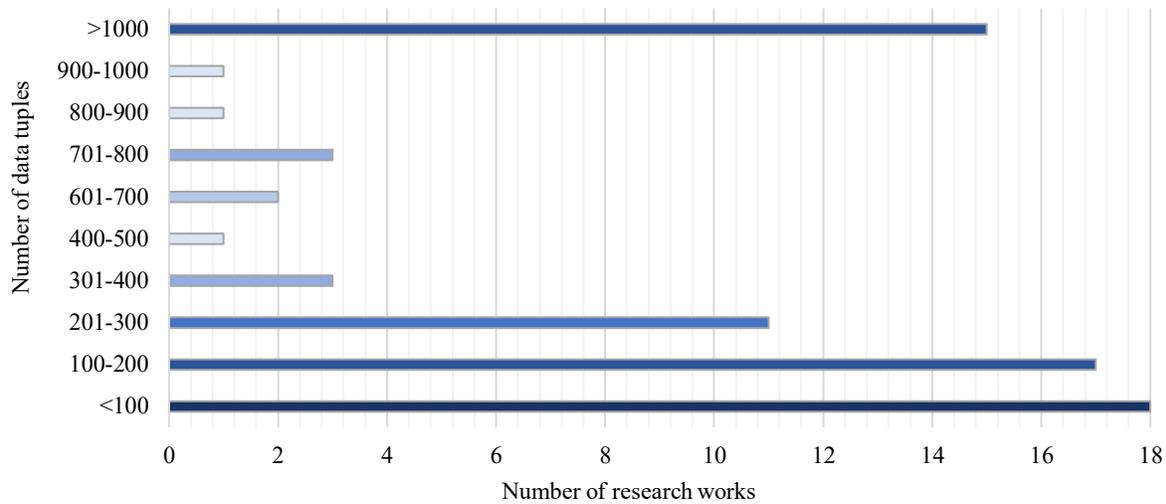
Figure 2.2.1 Representation of the ANN batch sizes used for prediction of compressive strength of concrete

Although most research is focused on predicting the compressive strength, there are notable works dealing with some additional concrete properties. Davraz et al. [47] made models for predicting Poisson's ratio of lightweight aggregate concrete, which gave satisfactory results compared to the experimental testing. Predictions of flexural strength by Onyari et al. [48] for mortar with modified zeolite additive gave excellent results and were proposed to augment the experimental work. Vineela et al. [49] investigated the tensile strength of hybrid short fiber composites with glass fiber, carbon fiber, and epoxy resin using ANN models. Abambres et al. [28] studied fatigue failure by developing a model that can be further used for designing and assessing concrete structures. Karakoc et al. [50] studied the effects of pumice aggregate ratios on the freeze-thaw durability of the high strength concrete and later on modeled ANNs. There have also been investigations focused on the properties of the fresh concrete, such as drying shrinkage [51], the microstructural properties such as chloride permeability [52,53] and diffusivity [54], and air void content [55], as well as the dependency of compressive strength on the microstructure [56].

Not many studies have dealt with the predictions of the electrical property of nano-reinforced concrete composite materials. Shi et al. [57] provided a study on engineered cementitious composite reinforced with polyvinyl alcohol fiber or steel fiber with the predictions of the compressive strength and the electrical resistance using ANN models. However, using keywords artificial neural networks, carbon nanotubes, carbon nanofibers within a research engine such as Scopus or ScienceDirect, the results show only a few studies published during the year

2021. Huang et al. [58] conducted a study using artificial neural networks and support vector machines to map the relationship between the mechanical properties and multiple influential factors for CNT reinforced cement composites. The study [58] used previously published experimental data to demonstrate how machine learning models present a better solution than the response surface methodology, i.e., the traditional statistical methods. Additional sensitivity analysis of the machine learning models shows that the prominent factor influencing the compressive strength of the composite material is the length of the CNTs. Finally, the study presented by Lyngdoh and Das and published in March 2021 [59] shows the multi-physics approach for obtaining the dataset for the predictive ANN models. This paper integrates a validated finite element analysis-based multiscale simulation framework developed in ABAQUS software with machine learning to predict the strain-sensing ability of the self-sensing cementitious composite materials. The material models are enabled by incorporating the nano-engineered interfaces, and the ANNs' predictions are interpreted using a Shapley Additive Explanations algorithm to establish the relative importance of the design parameters on the strain-sensing abilities of the composite materials. The research in [59] presents a similar approach to the study, which was conducted within this thesis, and it allows some expanse for further investigation on the topic.

CHAPTER III   Theoretical background

1. Fundamentals of electronics

Electronics is a field of physics that involves utilizing and controlling the flow of electrons through designed networks of active and passive devices. The electronic circuit is a network of interconnected electronic components that are fundamentally classified as active and passive. Active components such as transistors, diodes, integrated circuits (IC), optoelectronics, and sensors control the flow of electrons through active devices. Passive components made of electrolytes such as resistors, capacitors, inductors etc. complement active components in every respect and are crucial in design of an electronic circuit. Effects such as resistivity, conductivity and capacitance describe passive components. An electronic system may be a constituent of another engineered system or a standalone device.

1.1.   Charge and current

Charge implies a physical property of matter that causes it to experience a force when placed in an electromagnetic field. Positive and negative electric charges are carried by protons and electrons, respectively. Charges of the same type repel each other, and opposite charges attract each other. An object with an absence of charge is referred to as neutral. By convention, the charge of an electron is negative, $^-$e, while that of a proton is positive, $^+$e. An antiparticle is charged equally to its corresponding particle with the opposite sign. The charge can be carried by an ion which is an atom (or group of atoms) that has lost one or more electrons giving it a net positive charge, and an anion is an atom (or group of atoms) that has gained one or more electrons, giving it a negative charge. Coulomb's law defines that the electrostatic force is proportional to the product of their charges and inversely proportional to the square of the distance between them (Eq. 3.1). The electric charge of a macroscopic object is the sum of the electric charges of the particles that constitutes it.

$$\mathbf{F} = \mathbf{k}\frac{\mathbf{q_1 q_2}}{\mathbf{r^2}} \tag{3.1}$$

where F is the electrostatic force, q_1, q_2 are charges of particles, and r is the distance between particles.

Electric current represents the rate of flow of electric charge past a point or a region. An electric current exists when there is a flow of electric charge through a region. Electric current

describes any movement of electric charge carriers, subatomic charged particles electrons, such as protons or ions. Ohm's law (Eq. 3.2) states that the current through a conductor between two points is directly proportional to the voltage across the two points.

$$I = \frac{V}{R} \qquad (3.2)$$

where I is the electrical current, V is voltage, and R is electrical resistance.

1.2. Resistivity and conductivity

Resistivity and conductivity are properties of a material, which are described as passive effects that affect the electrical current flow. Resistivity impedes the current flow and directly opposite, conductivity allows the electrical current flow. While resistivity is a material's intrinsic property, resistance is further a function of geometry, length of the object, and size and shape of the object's cross-section conducting the electrical current. Resistivity occurs when an electron collides with some defect in the crystalline structure of the material through which it is passing, causing the electron to deflect from its path.

Ohm's law (Eq. 3.3) determines resistivity and conductivity.

$$\rho = \frac{E}{J}; \quad \sigma = \frac{J}{E} \qquad (3.3)$$

where:
ρ – electrical resistivity
E – the magnitude of the electric field of the conductor
J – the magnitude of the current density of the conductor
σ – electrical conductivity

Electrical resistance is mostly used to imply the electrical capabilities of different objects. Resistance of an object is a ratio of voltage across it and current through it, while electrical conductance is reciprocal and corresponds to the ease with which the current flows. Pouillet's law (Eq. 3.4) formulates the ideal case of electrical resistance.

$$R = \rho \frac{l}{A} \qquad (3.4)$$

where:
R – electrical resistance
l – length of the object (distance between two electrodes)
A – cross-sectional area of the object

Surface resistivity represents the resistance to the leakage of the current along the surface of the insulating matrix material. It may also be defined as electrical resistance between two parallel electrodes in contact through the surface. The four ends of the electrodes form a square, thus, the resistivity is expressed in ohms per square.

1.3. Piezoresistive effect

The piezoresistive effect represents a change in the electrical resistivity of a semiconductor or conductor when mechanical strain is applied. Opposite to the piezoelectric effect, which causes a change in electrical potential, the piezoresistive effect causes a change only in electrical resistance. In conducting and semiconducting materials, applied strain changes inter-atomic spacing. It thus affects the bandgaps, making it easier (or harder) for electrons to be excited into the conduction band. Since electrons in the conduction band have enough energy to move freely, more (or less) electrons in the conduction band will be shown through resistance change.

The discovery of piezoresistance dates back to 1856, when Lord Kelvin observed the change of resistance in mechanically loaded copper and iron wires. By comparing the difference in the change of resistance measured by a modified Wheatstone bridge, while the elongation of both wires was the same, Kelvin concluded that "the effect observed depends truly on variations in their conductivities." Research on this phenomenon has since continued, but until 1935, the term "piezoresistance" was used to describe the change in resistance/conductivity with stress when Cookson applied it first. Cookson used the already existing term "piezoelectricity", with the prefix "piezo" rooted from the Greek "*piezein*" which means "to press" or "to squeeze". During the 1950s Charles S. Smith reported in his seminal paper on semiconductor piezoresistance, the first measurements of the 'exceptionally large' piezoresistive shear coefficient in silicon and germanium. The discovery of the piezoresistive effect in silicon led to commercial use of piezoresistive sensors and the development of integrated circuits (IC) based on silicon, which were a precursor for MEMS (microelectromechanical system) technology [60]. The most common components that rely on the piezoresistive effects include, but are not restricted to, transducers and sensors with most applications in detection and measurement. The most basic piezoresistive devices are piezoresistors, including integrated resistor networks, potentiometers, and accelerometers.

1.4. Sensors

Sensors are devices that respond to physical stimuli by producing electrical signals. A sensor converts physical parameters into an electrical signal that is further converted to a digital value through a signal conditioning circuitry and the analog-to-digital converter. These components constitute a data acquisition system that processes electrical signals converting them into digital values and enabling further manipulation by a computer. By placing these sensing devices strategically on the structure, where the highest response is expected, and by analyzing the measurands, the occurrence and progression of the changes of internal stresses by the accompanied deformations, the damage can be identified, tracked, and monitored. There are several types of classification of sensing devices. The most general classification of sensors divides them into passive and active. Active sensors require an external power source or an excitation signal, while passive ones do not. According to the type of technology used without considering the type of the measurand, sensors can be fiber optic, piezoelectric, piezoresistive, etc. In terms of size, they may vary from macro, micro to nanoscale. In terms of the type of connection, wired sensors are considered traditional and are less used nowadays, while wireless sensor networks are more common. Wireless sensor networks are spatially and discretely distributed autonomous sensors (nodes) that monitor and record occurrences. They inter-coordinate and cooperatively pass the acquired data through the network and to the central processing computer. The wireless network is built of nodes counting from hundreds to thousands, where each node is connected to one or several sensors. A sensor node might vary in size from macro to nanosensor, allowing the possibility of monitoring issues, ranging from organic such as the human physical conditions to technological such as cracking, corrosion, and other structural or non-structural damage.

1.4.1. Piezoresistive sensors

Piezoresistive sensors are based on the piezoresistive effect, using the change in electrical resistivity of material when it is deformed under applied strain. Piezoresistive sensors are classified as active sensors since they require an external power source and cannot generate electrical signal independently. Many materials show the ability of piezoresistivity, but only those with relatively high sensitivity are suitable for sensing systems. Piezoresistive devices that are the most commonly used may include piezoresistive strain gauges, pressure sensors, accelerometers, and cantilever force/displacement sensors. The most well-known example of a piezoresistive sensor in civil

engineering is the strain gauge that produces a significantly higher gauge factor than that given by the metal wire or the foil gauges, allowing the uncertainty measurement to be reduced to ±0.1%. Piezoresistive materials such as silicon can constitute micro electromechanical systems (MEMS), a combination of traditional silicon integrated circuit electronics with micromechanical sensing and actuating components, or the nano electromechanical systems (NEMS), which integrate a similar functionality at the nanoscale. Other than silicone, carbon-based nanomaterials, such as carbon nanotubes and nanofibers, express piezoresistive behavior, making them perfect for creating a smart self-sensing composite material that would be able to function as a structural material and monitor itself at the same time.

1.4.2. Smart materials

Smart materials are engineered intelligent materials with properties adaptable to external stimuli such as stress, moisture, temperature, light, acidity, radiation, etc., in a controlled fashion. Smart materials are composite materials, usually designed as a compound of the primary insulating material and a macro, micro, or nanofiller material, giving them multifunctionality. Since this work focuses solely on smart concrete with the addition of carbon nanotubes and carbon nanofibers, only these nanofillers will be discussed further. Nano-engineering of concrete encompasses techniques of manipulation of the structure at the nanoscale to develop a new generation of tailored, multifunctional, cementitious composites with superior mechanical performance and durability, potentially having a range of novel properties such as low electrical resistivity, self-sensing capabilities, self-cleaning, self-healing, high ductility, or self-control of cracks.

Smart materials are used as sensors/actuators in medicine, mechanical, civil, and environmental engineering, clothing, and other fields of industry. However, the smart structure may be a passive one as well, thus considered an adaptive structure reacting to external stimulus in a predesigned manner. Within the general field of civil engineering, structural design and structural health monitoring represent the areas that employ these materials. Multifunctionality is introduced to structures exposed to extreme conditions, such as skyscrapers, towers, bridges, massive structures in seismically active areas, retaining walls, industrial reservoirs and cooling towers, and even aesthetically important structures. Smart materials represent an alternative to complex monitoring systems. Whether it means building an entirely new smart structure or introducing a smart material to certain parts of already existing structures to monitor structural health during its exploitation period. The main feature of a smart structure is realized by the system

of distributed sensors/actuators. Most preferably, this is done using a single material with properties that enable it to act as both the sensor and the actuator or by a combination of materials that allow forming of composite structure [61].

2. Concrete mix design

Traditional concrete material is based on the mix of cement, water, fine and coarse aggregate. Cement with water becomes the cement paste, the binder that binds fine and coarse aggregate and forms the concrete mass. The quality of the concrete mass depends on the quality of all the ingredients and their individual ratio. Hence, the quality of the cement paste is dependent mainly on the water-to-cement (w/c) ratio, and the quality of the binding is dependent on the relationship between the cement paste and the type, shape, and size of the aggregate. In the ideal case, cement paste should cover the entire surface of every aggregate grain. However, this is hardly ever achieved due to the air void content, which is governed by the aggregate particle size distribution. Thus, preferably the particle size is as versatile as possible to achieve the occurrence known as particle packing. To this point, the addition of nanomaterials in the concrete would significantly improve the particle packing of the material, so decreasing the air void content and promoting the hydration of cement. The promotion of cement hydration is then twofold: physical, by making more aggregate grains covered in cement paste, and chemical, by allowing further cement hydration due to the high reactivity of nanomaterials. Except for the traditional plain and reinforced concrete, other types of concrete have been introduced, such as high-performance, green, self-compacting, self-healing, self-cleaning, etc. In addition, there is an increase in the use of chemical admixtures and supplementary materials such as fly ash, ground granulated blast-furnace slag, silica fume, metakaolin, etc. [62], which may introduce lower w/c ratios, higher permeability, close packing, or other improvements. Continuing research work is conducted using mix design methods, which have been standardized, as well as the investigations on the impact of the variability of different supplementary and recycled ingredients on the properties of concrete in both fresh and hardened states.

2.1. Standards and methods in concrete mix design

Mix design refers to designed mixtures and does not imply prescribed, standard, or designated concrete mixtures, meaning that the designer specifies the limiting values of some key characteristics, which will affect the properties of the desired type of concrete. Design in the strict sense of the word is not possible: the materials are variable in a number of aspects, and many of their properties cannot be assessed quantitatively, so the designer is making no more than an intelligent guess at the optimum combinations of the ingredients [1] based on empirical evidence and personal experience. Usually, the estimated combinations of mixtures are checked by making trial mixes and adjusting the proportions until the optimal mixture is obtained.

However, concrete mix design is a globally well-established practice. Most countries have standardized their concrete mix design methods and have been using them on a regular basis. There are various methods of concrete mix design now in use:

- DOE method [63,64]
- ACI method [65]
- IS method – Concrete mix proportioning guidelines [66]
- British Road Note No.4 (graphic) method
- Mix design for high-strength concrete
- Mix design for pumpable concrete
- Rapid method
- Arbitrary method
- Maximum density method
- Fineness modulus method
- Surface area method

The first three are the most used in civil engineering practice from the listed methods because they proved to be the most consistent. British standard method was developed for the Department of Environment in 1975 and revised in 1988, American Concrete Institute (ACI) method was established in 1991 and reapproved in 2002, and the Indian standard (IS) method was finally established and applied in 2009. Generally, concrete mix design methods may be classified as analytical, semi-experimental, experimental, and statistical.

Analytical methods are used to reduce the number of trial mixtures to a possible minimum by rationalizing the initial proportioning procedure into a systematic process based on detailed information about specific weights of mixture components and formulae established from the previously conducted experimental works. Entirely analytical methods are quicker and cost-friendly, but the main drawback is the uncertainty of results. Semi-experimental (half-analytical) methods are based on the combination of the experimental database or experimentally developed prediction models and various analytical tools such as artificial neural network, genetic algorithm, and mathematical programming [3]. Fully experimental methods are based on a trial-and-error process where the one starting mix proportion is selected, and then the trial mixes are adjusted, followed by testing, and repeated until the optimal mixture is obtained. These methods give the most certainty in the results but are also the most time-consuming and expensive. Statistical methods, also known as statistical experiment design methods or factorial design methods, are an improvement over the entirely experimental methods, in which a set of trial batches covering a chosen range of proportions for each mixture component is defined according to the established statistical procedures. After establishing all mixture proportions, trial batches are carried out, specimens are fabricated and tested, and the results are analyzed using a standard statistical method. These methods include fitting the empirical models to the data for each performance criterion. Each result, for example, compressive strength, or slump, is expressed as an algebraic function of factors such as w/c ratio, cement content, chemical admixture dosage, and percentage of pozzolana replacement. Statistical methods require a certain amount of experimental work, but they have an advantage because the expected properties can be characterized by a variability a variability can characterize the expected properties [3].

3. Self-sensing concrete

Self-sensing concrete, or intrinsically smart concrete, is produced by adding the functional fillers to concrete to provide it with the ability of sensing strain, stress, cracking, or damage and simultaneously improving its mechanical properties. Conventional concrete serves as a structural material with no sensing ability; hence, it represents an insulating matrix. The presence of functional fillers enables the self-sensing property because the fillers form an electrically conductive network inside the concrete mesoporous environment. Due to the piezoresistive effect, when the conductive network inside the concrete experiences changes under strain, stress, or cracking, the damage can be detected through the measurement of changes in the electrical parameters, for example, resistance. In general, the functional filler phase usually exists in one of three forms: fiber, particle, or a hybrid of fiber and particle [67]. The concrete matrix is composed of fine and coarse mineral aggregates 'glued' together with a binder, which also spreads the filler particles and holds them and the aggregate in place. These fillers range a variety of materials such as carbon or steel fiber, carbon nanotube, carbon nanofiber, carbon black, nano-SiO_2, nano-TiO_2, nano-Fe_2O_3, nickel powder, graphene, or a combination (hybrid) of several. Although some of the latter serve different purposes, by now, more than ten types of functional fillers have been proved effective for providing the sensing ability to the concrete. Table 3.1 shows different types of nanofillers according to their morphological characteristics and conduction capabilities [67].

Table 3.1. Classification of nanoscale functional fillers used in smart concrete

Criteria	Category	Filler
Shape	Fibrous	carbon nanotube, carbon nanofiber
	Particle	carbon black, graphene, nano-TiO_2, nano-Fe_2O_3
Material component	Carbonaceous	carbon nanotube, carbon nanofiber, carbon black, graphene
	Metal oxide	nano-TiO_2, nano-Fe_2O_3
Conduction capability	Conductive	carbon nanotube, carbon nanofiber, carbon black, graphene
	Semi-conductive	nano-TiO_2, nano-Fe_2O_3

The most popular types of nanomaterials used for producing smart concrete are carbon-based ones, such as carbon nanofibers, carbon nanotubes (single- or multi-walled), carbon black graphene. The term nanocarbons in concrete technology usually refers to carbon nanotubes and

carbon nanofibers, which this work focuses on. Nanocarbons are used for the improvement and enhancement of the properties of concrete on one side and as a self-sensing system on the other.

Mix design for self-sensing concrete is based on the procedures established for conventional concrete. However, the presence of nanofillers affects the workability of fresh concrete because of their high specific surface area and application of different dispersion materials. Therefore, it is considered that an appropriate mixing procedure includes experimental design methods for getting an optimal mixing proportion design formula in combination with the trial-mixing method.

3.1. Carbon nanotubes

Sumio Iijima produced a new type of fullerene in 1991, which he called "helical microtubule", now known as the multi-walled carbon nanotube [68]. Later on, in 1993, Iijima and Ichihashi published a paper about synthesizing a "single-shell" carbon nanotubes and their notable properties, proposing further investigations on the features of this material all with regards to the morphology and the structure of the single tube [69].

Carbon nanotubes are allotropes of carbon with a cylindrical structure. As part of the fullerene family, nanotubes have a long hollow structure made of one (single-walled) or more (multi-walled) sheets, which have the thickness of a single carbon atom. Their size is generally spanning a few nanometers in diameter and several micrometers in length. The rolling angles of the carbon sheet are chiral, meaning that the structure and its mirror image are not superimposable. The type of chirality and the radius of a tube influence the properties of an individual nanotube. Notation using the integers *(n,m)* describes the configuration of stacked atoms in the graphene sheet, so the types of nanotube structures with different integers are defined as an armchair, zigzag, or chiral (Figure 3.3.1). This material is occasionally described as a 'one-dimensional' conductor since the high electrical conductivity occurs along the tubular axis. Nanotubes can be electrically semi-conductive or fully conductive depending on the chirality angle (*n,m*) and the uniformity of the production. For a nanotube with the structure described by (*n,m*): if $n = m$, the nanotube is conductive; if $n - m$ is a multiple of 3 and $n \neq m$ and $nm \neq 0$, then the nanotube is moderately semi-conductive.
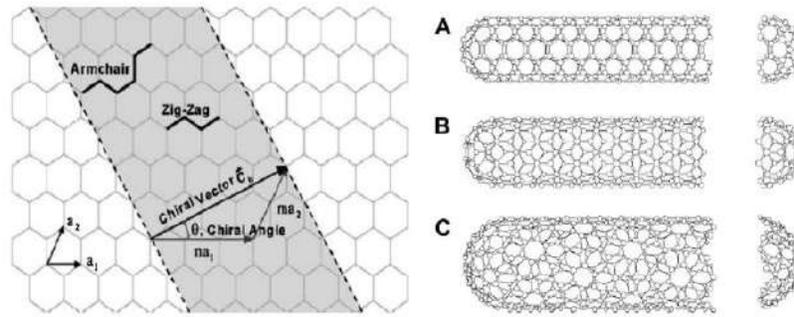
Figure 3.3.2 Schematic of carbon sheet rolling to form a nanotube with different chirality, A) armchair; B) zigzag; C) chiral [70]

Mechanical and other properties of carbon nanotubes are greatly superior in comparison to any traditional civil engineering material (Table 3.2). However, they cannot be used as stand-alone material. Therefore, CNTs are considered to be in use as a suitable material for enhancing the characteristics of the traditional materials, i.e., for creating the engineered composite materials. Aside from the outstanding mechanical or conductive properties, CNTs are considered to be a good filler material because of their features, such as high bonding force with the matrix and the high aspect ratio.

Table 3.2 Comparison of concrete and CNT properties

Material	Carbon nanotubes	Concrete
Tensile strength [MPa]	11000-100 000	2-5
Young's modulus [GPa]	270-1000	30-44
Mass density [g/cm^3]	1.8-2.6	1.9-2.5
Thermal conductivity (longitudinal) [W/m·K]	2000-6000	1.0-1.8
Electrical conductivity (longitudinal) [S/m]	10^2-10^6	10^{-8}

Abovementioned properties offer nanotubes great potential for a wide variety of applications in field emission, conducting plastics, thermal conductors, energy storage, conductive adhesives, thermal interface materials, fibers, reinforcement material, hydrogen containers, supercapacitors, molecular sensors, etc. Primarily CNTs have been applied as fillers in various polymer composite materials, and afterwards the procedures used for manufacturing polymer composite materials served as the guidelines for incorporating CNTs in cementitious materials as well. Within the cement matrix, carbon nanotubes' function is threefold. They serve as a cement nucleus, further promoting the cement hydration and providing higher density and close packing,

33

thus improving the strength of the C-S-H phase and decreasing the autogenous shrinkage; as nano reinforcement enhancing the flexural capability of concrete; and as a filler, improving the durability of the concrete and giving it the new ability of self-sensing.

3.2. Carbon nanofibers

One of the first mentions of carbon nanofibers is a patent from June 1889 on the synthesis of a threadlike carbon by Hughes and Chambers [patent number: US405480A]. However, it was not until the mid-twentieth century that this material could be observed and categorized with the development of electron microscopy. Carbon nanofibers (CNFs), or vapor-grown carbon nanofibers, are cylindrical nanostructures differing from the perfectly formed cylinders of the nanotubes. Moreover, CNF sheets are arranged as stacked cones, cups, or plates. Carbon nanofiber is produced through essentially the same manufacturing process as the vapor-grown carbon fiber. It not only possesses the same low density, high modulus, strength, conductivity, and thermal stability as the carbon fiber, but it exceeds it with its rarity of defects, large aspect ratio, large surface area, and compact structure. According to its structural characteristics, CNF can be categorized as a hollow or solid carbon nanofiber. Its diameter spans the range from 10 to 500 nm, and its length ranges from 0.5 to 200 mm [67]. The great advantage of vapor-grown CNFs lies in the fact that their diameter can be arbitrarily small, limited by the minimum theoretical diameter of a monomolecular single-walled carbon nanotube (0.7 nm) [71].

CNFs are characterized by an extraordinarily high elastic modulus and tensile strength as with all nanofibers. In particular, a fiber as thin as a human hair (50 µm) can withstand a load of 2 kg, whereas a steel wire of the same thickness endures only 200 g. Other relevant properties include high electrical conductivity and corrosion resistance, invariability of mechanical properties over an extensive temperature range (from cryogenic temperatures to more than 1000°C), and excellent compatibility with organic living tissues [71]. Similar to carbon nanotubes, the mechanical properties of CNFs depend on the morphology of the nanofiber, primarily the outer layer orientation and angle. Furthermore, the cylinder's diameter relates to the fiber's tensile strength. Electrical conductivity is directly proportional to the height of the degree of the crystalline orientation, where the normal vapor-grown CNFs have the highest conductivity compared to the additionally treated (carbonized, graphitized) ones [72]. Table 3.3 shows the features of carbon nanofibers in comparison to plain concrete.

When incorporated into composite materials, CNFs can increase the tensile strength, compression strength, Young's modulus, interlaminar shear strength, fracture toughness, and vibration damping of the matrix. The extent of improvement depends upon the matrix type, the degree of dispersion, and the processing history [73]. This material is used for the fabrication of self-sensing concrete, which is then often referred to as fiber reinforced concrete. The composite material is distinguished by the enhanced compressive and tensile strength, elastic modulus, and conductivity. Moreover, the propagation of damage after the germination of fresh cracks is slower, and the overall behavior is more ductile due to the crack bridging provided by the fibers.

Table 3.3 Comparison of concrete and CNF properties

Material	Carbon nanofibers	Concrete
Tensile strength [MPa]	1 000-12 000	2-5
Young's modulus [GPa]	50-775	30-44
Mass density [g/cm^3]	1.8	1.9-2.5
Thermal conductivity (longitudinal) [W/m·K]	1950	1.0-1.8
Electrical conductivity (longitudinal) [S/m]	1000	10^{-8}

Excellent mechanical properties of carbon nanofibers such as high electrical conductivity and high thermal conductivity can be used for a range of matrix materials, including thermoplastics, thermosets, elastomers, ceramics, metals, and concrete. CNFs possess a unique surface state, facilitating functionalization and other surface modification techniques to tailor the nanofiber to the host matrix [73]. Due to their particular properties, CNFs allow the fabrication of the nano-filled thermosetting materials with high electrical conductivity. Therefore, it is feasible to produce composite materials with different electrical resistivity values by controlling the concentration and interaction of the nanofibers inside the matrix itself. This feature is suitable for applications that require variations of the electrical resistivity within different ranges, such as electrostatic dissipation, electrostatic painting, EMI shielding, and lightning strike protection [73,74]. Carbon nanofibers are closely related to ordinary micron-sized carbon fibers, which are widely used in the industry and are produced at an annual rate above ten thousand tons [72] in terms of their properties at the microscale and their influence at the macroscale.

3.3. Percolation threshold

Concrete represents an insulating matrix for the filler material, CNTs and CNFs in this work. At sufficiently low fraction levels of the nanofiller, the conductivity of the composite material remains close to the conductivity level of the insulating matrix. However, when a certain volume fraction is reached, the overall electrical conductivity experiences a drastic increase by many orders of magnitude due to the formation of continuous electron paths, i.e., the conducting networks. This phenomenon is known as percolation, and the critical concentration of the filler as the percolation threshold. The percolation process governs the electrical conductivity of the self-sensing composite material. It is well known that percolation is associated with the ability of electron transfer along with the fiber as well as between adjacent nanotubes/nanofibers at their junctions. Hence, the percolation theory is applied to explain the electrically conducting behavior of composites consisting of the conducting filler and the insulating matrices. There are no electron paths below the percolation transition range, electrons have low energy levels, and the matrix material dominates the electrical properties where no significant conductivity is achieved. When the fillers are physically close enough, Van der Waals force's interatomic action provides the energy needed for the electrons to jump to the valence orbital and thus create a conductive network between themselves. However, since interatomic forces are particularly strong between the nanotubes, the occurrence of agglomeration occasionally may hinder the overall conduction as well as the mechanical properties of the composite material. Research on the self-sensing concrete shows that fibrous fillers with a high aspect ratio, i.e., a high ratio of length to diameter, can contribute more to the sensing ability at a lower concentration than the particle fillers. The effective concentration is not higher than 1.5% for the fibrous filler, whereas it is at least 5% for the particle filler. Furthermore, small radii and large aspect ratios of CNTs and CNFs grant them an exceptionally low percolation threshold, thus, the volume fraction for achieving conductivity is also satisfactorily low [67].

3.4. Processing of self-sensing concrete

Concrete is a heterogeneous composite material by nature, where a mix of cement and water bind the aggregate into an artificial stone material. Portland cement is the most used binder material, and this work considers only PC as the basic binder, considering that the variety of additional materials may lead to a complex multivariable problem. Yet, the concrete containing

Portland cement as the binder material may give different results depending on the mixing proportions and the type of aggregate. Although concrete represents the insulating matrix for the conductive filler material, its structure also affects the conduction of the completely composite system. In addition, the type and the mixing proportions of the materials chosen to build the concrete matrix influence the dispersion of the fillers, their distribution in the matrix, and thus, the mechanical properties of the final composite material, affecting the sensing properties of the composite [67].

First property of concrete matrix, which should be addressed, is the water-to-cement (w/c) ratio. It is a parameter describing the quantity of water compared to the quantity of cement. The influence of w/c ratio to the characteristics of self-sensing concrete is twofold. On one side, it affects the deformation capacity of the composite material, therefore, affecting the fillers' conductive network, and on the other side, it sets the environment for the dispersion of the fillers. Namely, higher w/c ratios indicate higher sensitivity of the sensing property of the composite material by increasing the deformation capacity and ensuring a higher quality dispersion of nanofillers. Further, the type of aggregate and the granulation used for the mixture of self-sensing concrete may influence the mechanical characteristics of the end-product. Since aggregate material is electrically insulating, the grains represent obstacles and interruptions for the conductive network formed by the fillers in the composite material. The best conductive network is, thus, formed in the absence of the coarse aggregate. However, coarse aggregate is necessary in case that self-sensing concrete is used in bulk form. Therefore, the adopted practice is to use the regular crushed rock since it has shown the best results so far. This material is made by crushing larger rocks into grains with relatively similar shape and size, and it is used as the optimal solution because of its higher purity, uniformity, and compressive strength. Fine aggregate is always present in the structure of self-sensing concrete, and in this work, it is only in the form of standardized sand. Usually, some mineral admixture is added to enhance the properties of fresh concrete (workability, passability) and allow close packing, however, this work focuses only on plain concrete without any additional mineral materials.

As previously mentioned, the sensing ability of smart concrete derives from the presence of electrically conductive fillers. In this case, CNTs and CNFs are used as electrically conductive and mechanically superior materials. Firstly, the level of the filler concentration determines whether the conductive network will be formed in the composite material. A percolation threshold

has to be achieved to obtain the sensing property of the material. The final sensing property of the material is not determined only by the concentration level but also by the mixing procedure, meaning the dispersion state of the filler in the concrete matrix and the dispersion of the aggregate material in the cement paste. Since CNTs and CNFs have high aspect ratio, hydrophobicity, and Van der Waals forces, special attention needs to be paid to the dispersion state to avoid the occurrence of agglomeration. Nonuniformly dispersed nanofillers strongly influence the workability and microstructure of the cementitious composites and hinder the ongoing hydration, thus leading to segregation, weak zones, or potential areas for accumulating concentrated stresses. Unlike CNTs, for which Van der Waals forces cause forming of ropes or reassembling after being dispersed, CNFs are less affected and tend to stay dispersed for longer periods of time [74]. Nonetheless, dispersing needs to be carefully carried out. Important factors, which determine if proper dispersion is achieved, are the processing method, equipment, and the energy adopted for the manufacturing. Mixing processes for self-sensing concrete are presented in Figure 3.3.2, where the plot (a) shows the process commonly used for concrete with the addition of CNTs/CNFs [67].
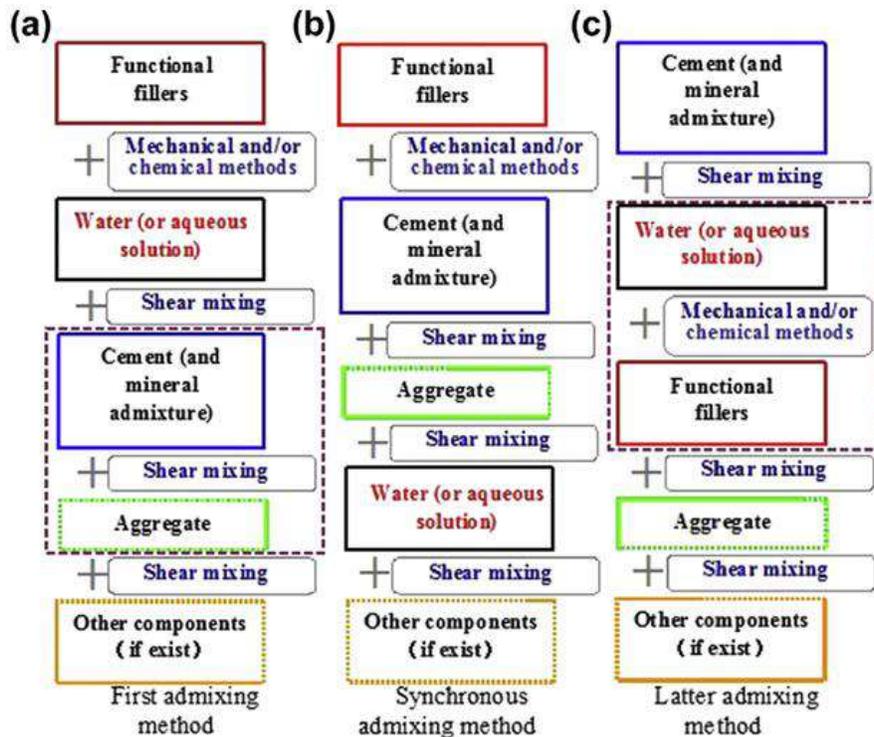
Figure 3.3.3 Mixing procedures for self-sensing concrete [67]

Application of the dispersion materials has three benefits: reproducible and stable properties may be obtained, the full realization of the improvement effects of fillers is achieved,

and the consumption of mechanical mixing energy is decreased [67]. The dispersion material should be compatible with the component materials of the matrix, having no negative effect on cement hydration, workability, and mechanical properties of the final composite material. Dispersion materials can be classified into surfactants and mineral admixtures but sometimes may be conjoined [67]. The dispersion solution contains the surfactant powder and/or mineral material, which are mixed with the distilled water at a specific concentration. Then, CNTs/CNFs are added into the solution and subjected to treatment, which can be of physical (mechanical) or chemical nature. The physical methods of treatment are ultrasonication, ball milling, and mechanical stirring. Ultrasonication provides energy to overcome the Van der Waals interactions. Ball milling is a powder milling method used to break the agglomerates formed by the Van der Waals forces. It can be used to deal with the dispersion with higher filler content, but it can also decrease the aspect ratio of the filler. Mechanical stirring, including magnetic stirring and hand-stirring, is a shear mixing method, usually combined with sonication. Mechanical stirring cannot disperse the fillers well in an aqueous solution, and so it is used as a preliminary treatment for the filler suspension. Physical methods may be effective in separating the fillers from each other, but methods such as shear mixing may significantly damage the fibers. Therefore, ultrasonication is most preferred (Figure 3.3.3) avoiding damaging to the fillers. Chemical treatments are designed to change the surface structure of the filler. They can be helpful for disentanglement of the bundles, thus facilitating a uniform dispersion at the single filler level, above all in an aqueous media. The covalent surface modification method uses the surface functionalization of the fillers to improve their chemical compatibility with the target media, i.e., to improve their wettability and reduce their tendency to agglomerate [67]. Functionalization, which forms a covalent bond, is a chemical method commonly used to modify CNTs by adding polar functionalized groups such as carboxyl (COOH) to the surface of the nanotube. The oxidization of inorganic acid is a typical method used to realize the function process, and it applies acids such as nitric and sulfuric. However, the use of acids may cause structural defects of fillers, and it is not recommended for cementitious composite materials. The last factor influencing the dispersion of the functional fillers is the dispersing energy, which is determined by the dispersing intensity and duration. Higher intensity over longer periods will ensure the uniformity of the dispersion and overall improvement of the composite material. Nevertheless, attention should be paid to the dispersing energy since high shearing forces may be developed, which may lead to severe damage of the fillers.
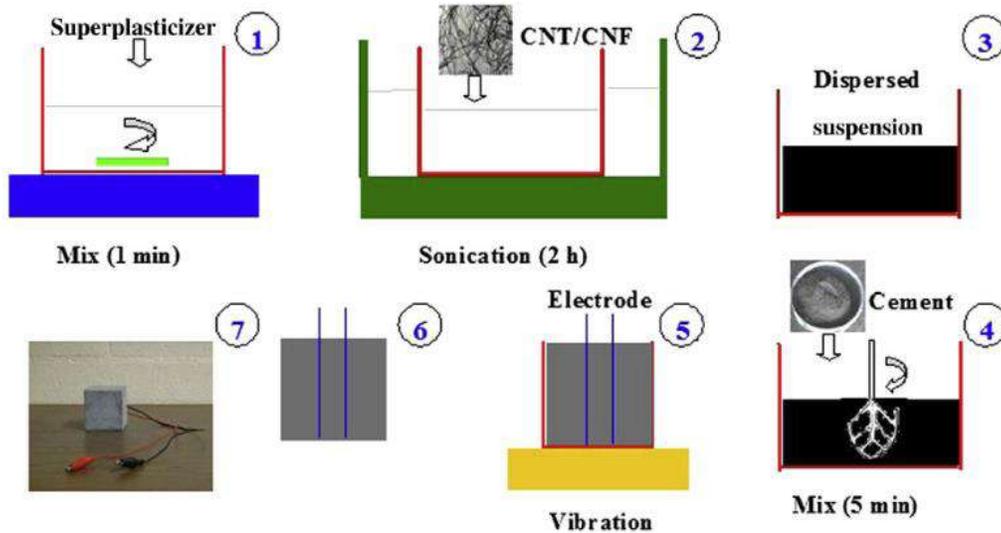
Figure 3.3.4 Fabrication of samples of self-sensing concrete with CNT/CNF [67]

Assuming that appropriate and quality materials are used, and a proper dispersion is achieved, the properties of the self-sensing concrete are also influenced by the molding and curing of the fresh material. The molding technique dictates the compaction, which affects mechanical and sensing performance of the concrete. The techniques that are used for molding are casting and vibration, extrusion, pressing, or hydrothermal hot-pressing technique. Every technique shows more or less satisfactory results, whereas casting and vibration induces the highest sensing sensitivity, but extrusion and pressing show better repeatability and stability. Curing affects the cement hydration and, consequentially the microstructure of the concrete. Different curing techniques influence the bonding level between the filler and the matrix and the water content, leading to eventually different mechanical properties. Curing techniques that are commonly used for self-sensing concrete are standard, hot water, or steam curing [67].

3.5. Properties of self-sensing concrete

Concrete is a nanostructured, multi-phase composite material that changes over time. It is composed of an amorphous phase, nanometer to micrometer size crystals, and bound water. Namely, the properties of concrete exist in multiple length scales, nano to micro to macro, where the properties of each scale are derived from those of the next smaller scale. Any processes that occur at the nanoscale ultimately affect the properties and performance of the bulk cementitious composite material. The amorphous phase, C–S–H, is the 'glue' that holds the concrete together and is itself a material that reacts in the presence of water. Viewed from the bottom-up, concrete at the nanoscale is a composite of molecular assemblages, surfaces, and chemical bonds that

interact through local chemical reactions, intermolecular forces, and interphase diffusion. As a composite material, self-sensing concrete consists of the matrix material, the filler material, and some auxiliary materials used for the dispersion of the fillers. Self-sensing concrete has the matrix phase, functional filler phase, and an interface phase between the fillers and the matrix. CNTs and CNFs reinforce the concrete at the nanoscale, somewhat in the manner as the traditional steel reinforcement bars do at the macroscale. In the mesoporous environment of concrete, nanofillers have multiple functions. Firstly, they can act as fillers to produce a denser, less porous material with higher compressive strength while inhibiting crack growth in the initial stages, thus preventing crack propagation. Secondly, they have the role of the nano-reinforcement, increasing the tensile strength and elastic and shear modulus of the overall composite material. The effect that nanofillers have on the mechanical properties is finally connected to the sensing property of the self-sensing concrete.

Sensing properties are closely related to the structure of the self-sensing concrete, especially the distribution of fillers, which create conducting networks in the concrete matrix and the interfaces between these fillers and the insulating cement matrix. The sensing derives from the intrinsic electrical resistance of the cement-based matrix, as well as the piezoresistive properties of the fillers, further, the contact between the fillers, and the tunneling and field emission conduction that occur in the nanomodified lattice [75]. Furthermore, the self-sensing behavior depends on several parameters of the filler, such as carbonaceous components; morphology, e.g., size, length, surface state, degree of agglomeration; and the concentration level, i.e., the weight fraction [67].

Sensing behavior of the self-sensing concrete can be described by the relationship between the fractional change in electrical resistance and the external force (or stress and strain) as follows:

$$\frac{\Delta\rho}{\rho_0} = f(X) \tag{3.5}$$

Where ρ_0 is the initial electrical resistance, $\Delta\rho$ is the change of resistance, and X may be the external force, stress, or strain.

The last component that influences the sensing behavior is the nature of the loading. It is established that self-sensing concrete exhibits different features when it is subjected to different loads causing stress states such as compression, tension, and flexure. Moreover, different features

are displayed for monotonic, repeated loading, or impact. However, this work considers only the responses of the concrete subjected to monotonic uniaxial compression and pure bending.

As shown in Figure 3.3.4, when under compression, the sensing behavior of the self-sensing concrete usually goes through the state of decrease and further flattening, followed by an increase, which corresponds respectively to the compaction caused by pressure, the occurrence of cracks, and the crack propagation under compression. The compaction causes the fillers to approach each other, thus improving the conductive network inside the composite and enhancing the conductivity. The occurrence of cracks leads to the destruction and reconstruction of the conductive network inside the composite until further crack propagation results in failure and the complete breakdown of the conductive network [67].
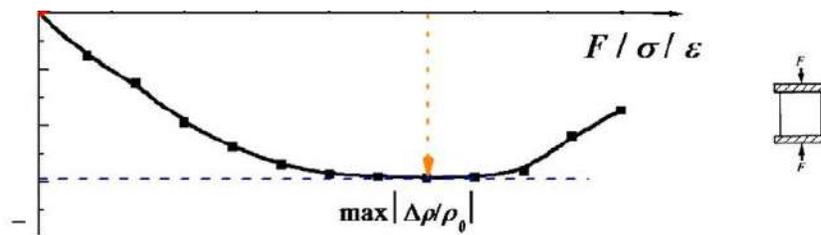
Figure 3.3.4 Sensing behavior of self-sensing concrete under compression [67]

Unlike the state of compression, when a specimen is exposed to the three-point bending test, the upper fiber of the beam is compressed, and the lower fiber undergoes tension in flexure. As a result, the sensing behavior is a composition of sensing properties under both compression and tension. Different sensing behaviors under flexure were observed, meaning that it depends on the material components and the layout of the electrodes. Since the strain in the lower tensile zone is higher, and the distance between the fibers rises, the resistance of this zone is increased and dominating for the whole specimen. Chen and Liu [76] pointed out that the relative change of resistance could be divided into three stages: (1) the elastic stage of the proportional increase of the deflection with the load, where the resistance follows the deflection increase; (2) the nonelastic stage starting with the occurrence of visible cracks, where the load-deflection relationship changes to nonlinear, while the resistance rapidly increases with the deflection; (3) the failure stage, where the resistance remains stable and high since the inner conductive network is broken [67].

3.6.   Mechanisms of electrical conduction in self-sensing concrete

When the percolation threshold is reached, and the conductive network is formed, several types of conduction can be observed within the structure of the self-sensing concrete. Conduction, i.e., the movement of electrons, is enabled by the presence of the fillers. However, conduction mechanisms vary due to the complex heterogeneous structure of concrete, where electrons may face different obstacles. Conduction is happening because of the electrons coming from fillers and the ions already present in the cement matrix. Electronic conduction can be contacting, tunneling, or field emission conduction, and conduction within the matrix is referred to as ionic conduction. As the name suggests, contacting conduction occurs due to a direct contact between the fillers. Electrons flow through the filler paths, forming a conductive network. Tunneling and field emission conduction are both associated with the transmission of electrons between the fillers that are not in direct contact but are close enough. Tunneling conduction occurs when the electrons "jump" through the energy barriers between the fillers (Figure 3.3.5). It actively contributes to the conductivity of the self-sensing concrete in oppose to the field emission conduction, which requires a stronger electric field to induce the conduction. Ionic conduction occurs when free water is present within the voids or pores of the hydrated cement, dissolving ionic species from the solid phases, such as K^{2+}, Na^{2+}, Ca^{2+}, OH^-, and SO_2^{4+}. The result is conduction through the interconnected capillary pores. Therefore, ionic conduction depends on the amount of free water within the voids of hydrated cement, and it is safe to assume that the cement matrix is completely insulating in fully dry conditions. The main issue of the ionic conduction is that it leads to the polarization in the matrix, which may aggravate the results of the resistivity measurement and possibly imply unrealistic resistivity values if not previously addressed.
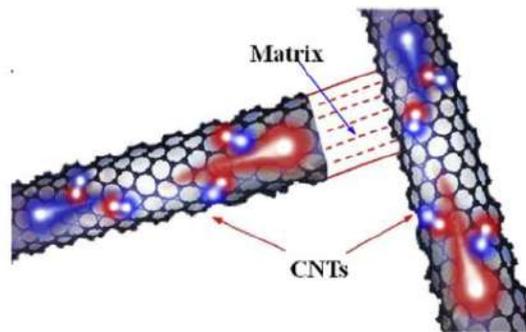
Figure 3.3.5 Schematic of the tunneling conduction between the nanofillers [67]

The sensing property is associated with the piezoresistive effect, so the changes in resistivity are expected under loading. The electrical resistivity of concrete with fibrous nanofillers varies due to several occurrences caused by the strain in the concrete. The first occurrence is the

change in the intrinsic electrical resistance because of the deformation of the individual fillers, which may be considerable in case of fibrous fillers. Next is the change in resistance caused by the deformation of the composite element. The bond between fillers and the matrix is altered under loading, leading to an increase in resistivity as the debonding of the interface takes place. The last two factors are both connected to the change of the distance between the adjacent fillers. The deformation prompts direct contact or complete separation of the fillers, leading to a decrease or increase of resistance, respectively. This deformation also influences the tunneling effect between the fillers, since the distance between them is changed. Under compression, the distance between adjacent fillers decreases, thus enhancing the tunneling and the field-induced tunneling effect conduction. Change of tunneling distance between the fillers is considered the most important factor of the sensing property. All of these mechanisms of conduction under loading are described at the nano to micro scale level. Since the filler-matrix and filler-filler interface surfaces are enormous, the contacting and tunneling conduction mechanisms contribute more than others do to the overall conductivity of the composite material, as well as its sensing behavior. Desirable characteristics of the self-sensing concrete describing a well-balanced sensing ability is low resistivity while simultaneously maintaining high sensing sensitivity with low filler concentration. Exactly this may be achieved around the percolation threshold, thus, it is a critical parameter for the optimization of mix proportions of the self-sensing concrete [67].

3.7. Measuring the sensing property of self-sensing concrete

Methodology of measuring the sensing properties has a direct impact on the response accuracy of the sensing signal. The results of measurements depend on the material of the electrode, type of fixing, and the configuration (layout) of the electrodes. Common materials used are: stainless steel, copper, lead, aluminum, and silver, because of their similar electrical properties, i.e., low electrical resistivity and stable conductivity. These materials can be used in the forms of flakes, mesh, foil, loop, bar, wire, rod, cloth, or paint. Depending on the form of the electrodes, the fixing style may be classified as attached, embedded, and clipped. Most used are the stainless steel or copper; flake, mesh, or rod; attached or clipped. The electrodes are commonly set in a two-probe or four-probe layout (Figure 3.3.6). The three-probe method can be applied as well, however, it is not common since it is complicated to set up, and the responses may not be as reliable. Additionally, the former two schemes are widely used in situ or for the laboratory

measurement of sensing property because there is no negative influence on the mechanical properties of the specimens.

3.7.1. Two-probe method

Two-probe method is the simplest method of measuring electrical resistivity. It involves measuring the voltage drop across and the current through the specimen. In doing so, the two electrodes are both the current and the voltage electrodes. This method is useful when the sample has large resistance [77]. The electrical resistance signal can be directly collected using multimeters or indirectly using a Wheatstone bridge method. In addition, the two-probe method is more convenient to use compared to the four-probe method, therefore, it is still widely used in research and application of self-sensing concrete [67]. Although the two-probe method has a simpler measurement circuit, the four-probe method is sometimes preferred because it can eliminate the contact resistance between the electrodes and the concrete [67].
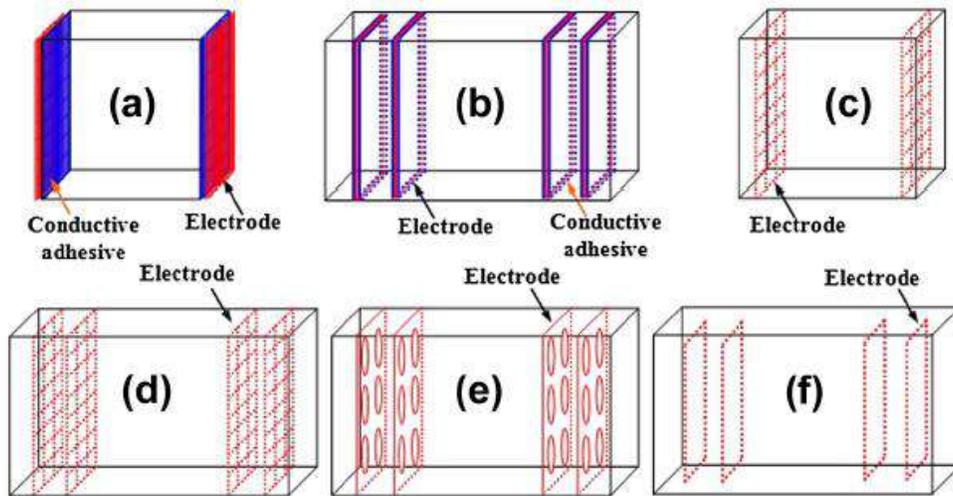
Figure 3.3.6 Fixing styles for two and four-probe methods [67]

3.7.2. Four-probe method

Unlike the two-probe method, the four-probe method uses the inner two electrodes and the outer two electrodes as the voltage electrodes and the current electrodes, respectively. The current passes through the outer contacts, which are closer to the edges of the sample. Then the potential difference is measured across the inner contacts. The potential drop is measured across the two probes and the distance between these probes represents the sample length. This method can eliminate the effects of contact resistance between the sample and the electrical contacts and

therefore is most suitable for low and accurate resistance measurements, however, it is possible that the contact resistance causes error if the probes develop enough heat [77]. The four-probe method showed the best response for the resistivity measurement of small size specimens. It is mostly used for the low resistive samples and it is applicable when the distance between the probes is small compared to the smaller dimension of the sample and provided none of the probes are too close to the edge of the specimen [77]. The four-probe method is recommended for electrical resistance measurements because the response is usually closer to the real value of the resistance of composite materials than the response from the two-probe method. However, it has been proven in numerous researches that the two-probe method has the ability to detect changes in electrical resistance, i.e., relative resistance values under loading.
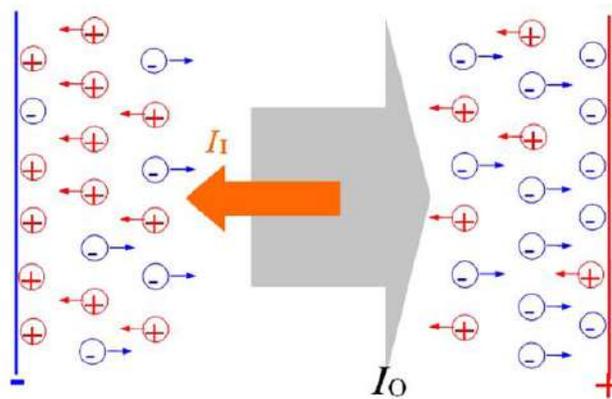
Figure 3.3.7 Polarization in concrete [67]

Regardless of the measuring method, the preferable option is to use a direct current with a fixed voltage applied to the specimen [67]. When a constant electric field is applied, the ions' movements in the cement provoke electrical polarization in the matrix, representing conduction dominated by the ionic conduction mechanism. Since the polarization (Figure 3.3.7) causes an increase of resistance, it is more difficult to obtain the accurate values of changes in the resistance. Possible way of overcoming this problem is to apply the current before applying the load, giving some time for settling the processes activated by polarization until it is completed. The alternative would be to record the change in resistance caused by polarization for an unloaded sample. Since both methods are not feasible on site, especially for larger concrete elements, an alternative method is to employ alternating current (AC) signals with equal magnitudes of positive and negative peaks to the self-sensing concrete [67]. Though the polarization is still present, the effect is decreased by increasing the frequency of the voltage. Finally, the resistance can be measured by using a

differential circuit within a sandwich structure. The measurements of electrical signals are conventionally acquired by a wired system; however, wireless systems are used more and more because of the convenience and the reliability of results. In general, the acquired signals are inevitably polluted by the measurement noise, so a subsequent signal processing procedure should be used to remove the noise effect and to obtain the effective sensing information [67].

4. Numerical simulations

Numerical simulations are used for the mathematical representation of physical objects and their behavior under certain circumstances. Simulations are run by the computer software that is able to implement a mathematical model for a physical system. The analysis is provided through the finite element method (FEM) which is a common numerical method used for solving the partial differential equations within two-dimensional or three-dimensional space. Using FEM, complex problems are solved through the discretization by dividing a larger system into smaller objects called finite elements. Creating finite elements is possible by the meshing of the system. This way, the discretization is achieved, and the numerical domain of the solution with a finite number of points is established. Every finite element of the mesh has a certain number of nodes, depending on its geometry and the complexity of the model. Nodes are prescribed with boundary conditions that further simplify and transform the differential problem into a finite number of algebraic equations. Specific loading of the structure is introduced and modeled as realistically as possible and transformed into discrete loading points of the interconnected mesh. The FEM then approximates the unknown function within the domain by minimizing the error function. After solving the unknown variables, results are presented as a respective reaction, strain, stress, force, etc. of the modeled object under loading.

This work uses ANSYS 2021R2 [78] to analyze the mechanical behavior of CNT/CNF reinforced concrete under compression and bending. Specific features of the ANSYS platform used for each phase of the model development and analysis in this research work are, as follows:

➢ Material Designer feature is used for modeling composite materials involving different length scales by homogenization of the composite material. The homogenization process starts with modeling the representative volume element (RVE), which is meshed and analyzed. The results of the material behavior of the new composite material are represented by the tensor of elasticity. With homogenized material data, the object further needs to be transferred to the Engineering Data feature and further modeled at the macroscopic scale.

➢ Engineering Data feature represents a cell in the Project schematic containing data about the materials used for modeling the object. Data is presented by a singular identifier or a property defined by tabular data, which together define or model the behavior of the material. This

feature is also used for creating a new collection (library) of materials that are homogenized and defined by the Material Designer.

➢ Geometry feature represents a cell in the Project schematic containing geometrical data of the macroscale model. It can be used to create geometry from scratch or prepare existing CAD geometry for analysis. This feature is where the object's macroscale geometry and relevant points for loading are defined.

➢ Static Structural analysis feature represents a linear static analysis solver, which uses previously defined engineering data and geometry to define the mechanical model and establish the FE model and loading parameters. After defining and meshing of the object, and introduction of all loads, the static analysis is performed, and the results of desired reactions are obtained.

Parametrization is a native feature of ANSYS, which allows for the analysis of the model based on the sets of parametric values. All ANSYS features have some variables, which may be parameterized, providing flexibility through the interaction of the parameters between different features of the project This work includes parametrization within the abovementioned features.

5. Artificial neural networks

Machine learning is a field of artificial intelligence used for prediction, i.e., a classification which represents the prediction of the categorical value, or regression which is the prediction of the numerical value [18]. Machine learning methods are used in civil engineering for problems within the area of structural health monitoring, structural system identification, structural analysis and optimization, seismic design, soil mapping, construction site management, road construction, material behavior, concrete mix design, etc. Methods used in concrete mix design are artificial neural networks (ANNs), support vector machine, adaptive neuro-fuzzy inference system, fuzzy logic, random forest, decision tree, genetic programming, and salp swarm algorithm.

Artificial neural networks (ANNs) represent a method where learning of patterns is provided through examples. They may also be a part of the deep learning family of techniques, depending on the amount and the type of data given by the dataset from which the learning proceeds. Their development is inspired by the human brain, a biological neural network functioning based on communication between the neurons through synapses. Although ANNs' complexity is far from an actual human brain, there are key similarities comprised in the neurons and the determination of function (pattern) by the connections (synapses) between them. The theory of connectionism was for the first time proposed in the 1940s with the idea to simulate the processing of the human brain, however, at first, it did not meet a great deal of success. Eventually, it was abandoned for many years until new interest in this subject sparked, and the technology was advanced enough to keep up and develop this technique.

4.1. Definition and types of artificial neural networks

An ANN comprises interconnected neurons, otherwise named nodes, units, or processing elements, for resolving complex non-linear problems that often cannot be described by a direct mathematical formula. The network learns and identifies the causality between the input and the output through iterative training and uses the relationship to carry out the needed prediction. It learns from parallel examples of the input and output pairs of data, called tuples, and then generalizes to extrapolate outputs. Neurons are formulated as follows:

$$Y = \sum (weight * input) + bias \tag{3.6}$$

or specifically:

$$y = x_1 \cdot w_1 + x_2 \cdot w_2 + x_3 \cdot w_3 + \cdots + x_n \cdot w_n + b \cdot 1 \qquad (3.7)$$

$$\hat{y} = a_{out} = af(y) \qquad (3.8)$$

Main advantage of ANNs is the ability to give the correct or nearly correct response to incomplete tasks and noisy data. Additional advantages include an unrestricted number of inputs and outputs, fast implementation, and user-friendliness, implying simple application and more clarity than traditional statistical methods. Disadvantages include the need for a rich dataset, an iterative process of determining the optimal network architecture, and hardware dependence. ANNs may be used in a variety of specific problems, such as recalling data, classifying patterns, performing a general mapping from input to output pattern, grouping similar patterns, or solving constrained optimization problems [79].

There are essentially three types of learning: supervised, unsupervised, and reinforcement learning. In supervised learning, the complete training set is provided, thus, as the input data is applied, the output value of the network is compared to the target value. The weights and biases are adjusted based on the observed error to obtain the output value as close to the target value as possible. It represents an adaptive system capable of change according to the relevant information [80]. In unsupervised learning (self-organization), the weights and bias are modified in response to network inputs only because no target outputs are available. Finally, reinforcement learning is similar to supervised learning, except that instead of being provided with the correct output for each network input, the algorithm is only given a grade. The following work refers only to the supervised learning process since it is used in this research.

4.2. Layers

Artificial neural networks have three levels of layers: input, output, and one or more hidden layers. Each layer is comprised of neurons, which are connected to neurons of the next layer. Neurons within one layer are not interconnected. The number of layers determines if the network has a single layer (Hopfield nets), bilayer (Carpenter/Grossberg adaptive resonance networks), or multiple layers. Non-linear problems are solved by multilayer networks, also known as multiple layer perceptrons. In concrete mix design, the input layer gives information about the quantity of each constituent material, concrete age, and any other significant parameter; and the output layer gives the value of the observed property of concrete. The number of neurons in the input layer may be subsequently changed if it is concluded by the sensitivity analysis that some parameters

ultimately have a negligible effect on the target parameter. Sensitivity analysis shows the cause-and-effect relationship between the inputs and the outputs of the network. In case that some input parameter does not affect the output significantly enough, the network's efficacy may be increased by excluding it, making its complexity and training time lower.

Number of hidden layers usually varies from one to eight. A network with one hidden layer is called "shallow", and with 2-8 hidden layers is "deep" neural network. The function of a hidden layer is to detect and establish the relationships between network inputs and outputs. The size of the hidden layer, i.e., the number of neurons in it, is problem specific and depends on the training patterns. There is no established rule for selecting the number of hidden neurons. It must be sufficiently low to ensure generalization of the network but not too low that the network cannot learn the pattern and generalize to new data. On the other hand, too many neurons can encourage over-fitting, thus modeling the noise in the data or data itself with unnecessarily complex functions. Studies have related the number of neurons in the hidden layer to the number of input and output variables (Table 3.4), however, these are only recommendations and cannot be dogmatically followed. Additionally, some studies suggest that the ratio between the number of neurons in the first and the second hidden layer should be 3:1 to yield the best result [81,82]. In practice, selecting the number of hidden layers and neurons is a time-consuming iterative process based on a trial-and-error procedure, however, it is important to carry it out.

Table 3.4 Empirical recommendations for the number of nodes in a single hidden layer

$2 \cdot N_i$
$N_i + N_o$
$0.75 \cdot N_i$
$2N_i + 1$
N_i
$(N_i + N_o)/2$

N_i – number of input nodes N_o – number of output nodes

4.3.   Dataset

Extensive and reliable dataset ensures the proper training and testing process of the ANN. The form, content and size of the dataset affect the computation of appropriate outputs. One of ANNs' drawbacks is the sensitivity to the sample size, i.e., the size of the training and testing sets. The network learns from information provided by the training set, so the quality and quantity of

data tuples play a critical role in the accuracy and the efficiency of the network. The optimal training dataset should fully represent the modeling domain and have the minimum number of repetitive samples, i.e., identical inputs with different outputs [82]. Larger sample sizes can supply a more accurate prediction of the mean and identify outliers that skew the data. Employing small datasets may lead to overfitting of the data and weak generalization performance on new datasets.

Second factor is the format of the dataset itself because the representation of data affects the training process of the model. Especially in the case where the sigmoid activation function is used, both input and output variables must be preprocessed, usually normalized within the range of [0,1] or scaled to the range of [-1,+1] or [0.1,0.9], depending on the type of the sigmoid function. Data preprocessing improves the learning speed. To determine the actual value of the output, an inverse transformation must be performed.

Third factor is the content of the dataset. If the ANN is developed to predict e.g. compressive strength of concrete, the experimental results must contain relevant information about the material behavior. Such a network should have enough information to reproduce the experimental results and approximate the results of other experiments based on the generalization it has made during training. However, a larger sample does not necessarily lead to a better network. Even though a richer dataset theoretically leads to a better generalization, if the data quality is not at a high level, the sample size itself does not make a big difference in the network performance.

When the corrupted data are excluded from the batch, and preprocessing of data is finished, the dataset is divided into two or three subsets for training, validation, and testing. The validation subset may be excluded, or a different dataset can be used for performing the validation of the network. The training subset contains the highest percentage of the total amount of data, usually from 65-80, or even 90 percent. The rest is then left to be used for testing or is divided between testing and validation sets. Commonly observed practice for training/testing ratio is 70/30, or 70/15/15 for training/validation/testing. Data tuples are randomly shuffled between subsets to avoid the possible effect on the training algorithm and lead to overly positive results (false positive).

Finally, once the training process is finished, sensitivity analysis may be performed to establish the relative contribution of the input variables to the overall performance of the network. It is done by testing the network with each individual input variable missing, thus establishing

which one has the highest and lowest influence on the output. If the ratio is equal to or lower than 1, excluding a variable either has no effect on the network's performance or enhances it.

5.3.1. Dataset normalization

Database normalization regarding an ANN model is twofold. It refers to the format of the table from one side and the values in the table on the other. Regarding the format, database normalization is the process of organizing the data. It represents establishing relationships between columns, rows, and multiple tables between themselves. It serves to protect data and eliminate redundancy of the table and inconsistent dependency within the table. When upgrading the database, unwanted anomalies such as inserting, updating, and deleting may occur if normalization is not implemented.

Other format of normalization is the value normalization. The data values must be within the same domain, meaning that the values cannot be at drastically different scales, as is the case for concrete mix design. In this case, the values of input range from 0-2000 for the weight of constituent materials; from 3-120 for specimen age; or from 1-2 for the demolding age. Therefore, normalization is required to obtain all values within the same range. This can be achieved by using one of the several data processing techniques such as min-max or z-score. In this work, min-max normalization was used, making the minimum value equal to 0, the maximum equal to 1, and all the rest in the interval between 0 and 1 according to the following formula,

$$norm = \frac{value - min}{max - min} \tag{3.9}$$

4.4. Weights and bias

Weight is the parameter, which transforms values from one layer to the next, successively until the final output value is obtained, as shown in Eq. 3.6 and Eq. 3.7. It represents the strength of the connection between two neurons from neighboring layers. If the weight has a greater magnitude, it means that the neuron has a greater influence on the connected neuron in the next layer. Therefore, the weight parameter can also have a negative value meaning that the input-output relationship is inverse. Connections between the neurons are always weighed. During the training, the weights are adjusted through the feed-forward back-propagation process as the learning proceeds. The value of the total error corresponds to the weight adjustment, so the weights are set, and the learning halts at the moment when the minimum error is obtained.

Bias, or offset, represents an additional input to the network. As the learning begins, it is set to 1 and has its own connection to the network. This ensures that even when all inputs are 0, the neuron in the hidden layer will be activated. After the learning process stops, final bias values are obtained and set.

4.5. Algorithm

Learning algorithm, which is used for solving problems of concrete mix design, is the backpropagation (BP) algorithm. The "backpropagation learning rule" dates back to 1985, when it was established as a solution to the problems occurring with single or bilayer networks. It is considered a generalization of the delta rule for multilayer networks, and the idea is to back-propagate the error of the outputs so that the network can adjust the weights until the output is satisfactory.

Learning process is divided in two stages, the first being the feed-forwarding stage, and the second being the back-propagation stage. Forward propagation is a process of feeding input values to the neural network and getting an output, which is the predicted value. The input values are fed to the network's first layer as is, without any operations. The next layer takes values from the previous and applies multiplication, addition, and activation function, and forwards it to the next layer. The same process repeats until an output value, i.e., the prediction is obtained. The error is calculated from comparing the predicted and the target values when the derivative (gradient) of the error for each weight may be acquired. Then, the cycle starts again and repeats until the obtained error is minimal. The number of these cycles is expressed in epochs. An epoch is one forward and one backward pass of all training examples. After training of the network is completed, final connection weights are set and fixed, and the new input patterns can be presented to the network to rapidly produce corresponding output, consistent with the established internal topology. Validation is the intermittent procedure occasionally used to measure the network generalization and halt the training when generalization ceases to improve, meaning that testing no longer has an effect on the training. Parameters that dictate the performance of the network include activation function, number of training iterations (within epochs), minimum error, learning rate (how fast coefficients of regression and weights of the ANN change), momentum (speed of convergence for gradient descent learning algorithm), number of hidden layers, and the number of neurons in the hidden layers. Training algorithms used for the backpropagation network are problem-specific. Some of the most common algorithms used in concrete mix design are shown in

Table 3.5. The favorite is the Levenberg-Marquardt algorithm due to its speed, robustness, and the fact that it is the fastest training algorithm for moderately sized networks with up to a few hundred weights. The ultimate goal of any training procedure is to minimize mean square error (MSE) and mean absolute error (MAE) and maximize the coefficient of determination R^2, or regression coefficient R. The iterations run until no improvement in MSE and MAE value is found. Accuracy of results is usually presented by the value of R or R^2, meaning that in case of a perfect fit between given and predicted output, these values would be equal to 1.

Table 3.5 Most used training algorithms for ANNs in concrete mix design

Algorithm	Description
Levenberg-Marquardt	Fastest for the moderately sized network, has memory reduction feature if needed
Resilient backpropagation	Simple batch mode training algorithm with convergence and minimal storage requirements
BFGS quasi-Newton	Converges in less iterations, but needs appropriate Hessian matrix and has more computation in each iteration
Polak-Ribiere conjugate gradient	Faster convergence, but needs larger storage
Powell-Beale conjugate gradient	Fast convergence, but needs slightly larger storage
Scaled conjugate gradient	Exceptionally good general-purpose algorithm
One-step secant	Requires less storage and computation than BFGS, but more than conjugate gradients.

4.6. Activation function

Activation function represents a mathematical "gate" that data is "passing through" on its way to the next layer of the neural network. The output signal of the neuron relates to the input via the activation function, and the final output value is obtained by relating the output signal to the transfer function. Activation functions are generally divided into three groups: binary step function, linear activation, and non-linear activation function. The binary step function is threshold-based, meaning that if the input is above or below a certain threshold, the neuron is activated and sending the same signal to the next layer, hence, it does not allow categorizing inputs. The linear activation function simply multiplies the inputs by the appropriate weight and creates the output signal. Although this function is not binary based, it does not allow backpropagation in training, thus making the error minimization impossible. Moreover, it is a simple regression model

with limited abilities for solving more complex problems. Non-linear functions are the most used activation functions in modern ANNs. They allow complex mapping between the input and output including images, video, audio, and datasets of high dimensionalities. Non-linear functions allow backpropagation because of the derivative functions connected to the inputs, and allow creating a deep network (layer stacking), thus making learning with high accuracy possible.

Identity		$f(x) = x$	$f'(x) = 1$	$(-\infty, \infty)$
Binary step		$f(x) = \begin{cases} 0 & \text{for } x < 0 \\ 1 & \text{for } x \geq 0 \end{cases}$	$f'(x) = \begin{cases} 0 & \text{for } x \neq 0 \\ ? & \text{for } x = 0 \end{cases}$	$\{0, 1\}$
Logistic (a.k.a. Sigmoid or Soft step)		$f(x) = \sigma(x) = \dfrac{1}{1+e^{-x}}$[1]	$f'(x) = f(x)(1 - f(x))$	$(0, 1)$
TanH		$f(x) = \tanh(x) = \dfrac{(e^x - e^{-x})}{(e^x + e^{-x})}$	$f'(x) = 1 - f(x)^2$	$(-1, 1)$
Rectified linear unit (ReLU)[15]		$f(x) = \begin{cases} 0 & \text{for } x < 0 \\ x & \text{for } x \geq 0 \end{cases}$	$f'(x) = \begin{cases} 0 & \text{for } x < 0 \\ 1 & \text{for } x \geq 0 \end{cases}$	$[0, \infty)$
Leaky rectified linear unit (Leaky ReLU)[17]		$f(x) = \begin{cases} 0.01x & \text{for } x < 0 \\ x & \text{for } x \geq 0 \end{cases}$	$f'(x) = \begin{cases} 0.01 & \text{for } x < 0 \\ 1 & \text{for } x \geq 0 \end{cases}$	$(-\infty, \infty)$
Parameteric rectified linear unit (PReLU)[18]		$f(\alpha, x) = \begin{cases} \alpha x & \text{for } x < 0 \\ x & \text{for } x \geq 0 \end{cases}$	$f'(\alpha, x) = \begin{cases} \alpha & \text{for } x < 0 \\ 1 & \text{for } x \geq 0 \end{cases}$	$(-\infty, \infty)$[2]
Exponential linear unit (ELU)[20]		$f(\alpha, x) = \begin{cases} \alpha(e^x - 1) & \text{for } x \leq 0 \\ x & \text{for } x > 0 \end{cases}$	$f'(\alpha, x) = \begin{cases} f(\alpha, x) + \alpha & \text{for } x \leq 0 \\ 1 & \text{for } x > 0 \end{cases}$	$(-\alpha, \infty)$
SoftPlus[24]		$f(x) = \ln(1 + e^x)$	$f'(x) = \dfrac{1}{1+e^{-x}}$	$(0, \infty)$
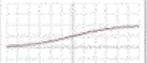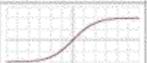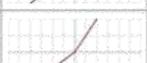
Figure 3.5.1 Activation functions [83]

The most common activation functions, which are presented in Figure 3.5.1, are:

1. Sigmoid (logistic) – smooth gradient, clear predictions, outputs normalized values (between 0 and 1). Drawbacks: vanishing gradient, the output is not zero-centered, computationally expensive. It can be uni-polar or bi-polar sigmoid function.
2. Hyperbolic tangent - same as sigmoid, but the output is zero-centered.
3. Rectified linear unit (ReLU) - computationally efficient but dying ReLU problem occurs.
4. Leaky ReLU - same as ReLU additionally prevents the dying ReLU problem, but the results are not always consistent.
5. Parametric ReLU - same as ReLU, additionally allows learning on the negative slope. However, a manifestation of different behavior for different problems is possible.
6. Exponential linear unit (ELU) - reduces the bias shift effect and achieves faster learning by allowing the negative input, which pushes the mean closer to zero.
7. Softplus – produces outputs in the interval of [0,+∞]. Its derivative is equal to the sigmoid function.

CHAPTER IV   Assumptions and hypotheses

1. Assumptions regarding experimental research

Experimental investigations [84-119] which were observed in this work are, in most cases, have detailed descriptions in regards to materials, specimen preparation, experimental setup, and standardization. However, some works failed to specify certain parts of the procedures or to confirm the quality of the final composite material. For this reason, several assumptions must be made. Firstly, the quality of the nanofiller dispersion is not evaluated and confirmed in [103,106,115] by SEM or TEM analysis. In such cases, it is assumed that proper dispersion of the nanofillers is achieved based on the results of mechanical and electromechanical tests. Since the nanofillers are supposed to enhance the mechanical behavior of concrete and enable the piezoresistive properties, results, which confirm this, were used for further analysis. Investigations, which showed no change or even the opposite effect after the incorporation of the nanofiller, were rejected and exempt from any further analysis.

Further, the structure of the observed composite materials was influenced at the mesoscale by different chemical additives used for the dispersion and mixing processes. Some mixtures included different antifoaming agents (defoamers) and surfactants, and some did not use any additional materials. It is assumed that, regardless of the existence or absence of the additional materials, the final composite material has an appropriate structure and has reached the percolation threshold. It is perceived that if defoamer is not used, there was no occurrence of foaming, and if it is used, it was necessary; and if surfactants were not used, the dispersion was achieved nevertheless. Essentially, it is assumed that any additional material was used only toward obtaining the appropriate structure and has not influenced any property of the final hardened material. Only the superplasticizers were taken into account since their influence on the concrete properties may be significant, and their weight fraction percentage is occurring at significant levels.

Lastly, it is assumed that all experimental investigations followed proper mixing, molding, curing, and testing procedures as specified by any relevant standard. All investigations observed in this work are considered to confirm the latter assumptions by giving satisfactory results after the testing of the specimens. Investigations, which did not comply, were rejected and exempt from further analysis, as it is described in detail within Chapter V.

2. Assumptions regarding numerical simulations

Numerical analysis in this work implies the numerical representation of the experimental fabrication and testing of the CNT/CNF reinforced concrete specimens. Throughout the homogenization stage of the model development, the materials are modeled according to the bottom-up principle over the mezzo-scale (from nano to macro). In order to simplify the procedure and comprehend all materials under a uniform methodology, assumptions are made as follows. The dispersion of nanomaterials is not included in the methodology because it is not supported by the ANSYS Material Designer. The nanomaterials are included as separate idealized materials, and the factor of dispersion quality does not affect the final homogenization process since it is implied. Hydration of cement as a physical process cannot be reproduced by the software, since the Material Designer cannot recognize different aggregate states.

For the same reason, it is not possible to include liquid additive materials such as superplasticizers. Hence, the referential materials are input as already homogenized concrete materials, which will be further reinforced by the nanofiller and so homogenized by the Material Designer. Moreover, Material Designer is incapable of producing the material data regarding the electrical properties of the homogenized material, rendering the electrical analysis impossible. Lastly, Material Designer is capable of providing nonlinear analysis only for the short fiber UD composite RVE. Since none of the needed nonlinear parameters are known from the experimental work, this feature cannot be used, and only linear analysis of the material may be provided.

Because of the latter simplifications included within several levels of modeling of the material, the final models are validated by comparison with their experimental counterparts with the acceptable deviation of up to 15%. The model is considered acceptable if the validation procedure gives relevant and comparable results. Validation of the numerical models is described in detail within Chapter VI.

3. Hypotheses

Hypotheses, which are implied by this research work, are, as follows:

- *The mechanical properties of concrete are enhanced by the presence of CNT or CNF nanofillers.*

- *The electrical properties of concrete are enhanced by the presence of CNT or CNF nanofillers.*

- *CNT/CNF concrete composite material can be modeled by ANSYS Material Designer.*

- *Numerical models of CNT/CNF reinforced concrete can realistically respond to mechanical stimuli.*

- *The mechanical behavior of CNT/CNF reinforced concrete can be predicted by the artificial neural networks.*

- *The electrical behavior of CNT/CNF reinforced concrete can be predicted by the artificial neural networks.*

- *Number of neurons in the hidden layer of the artificial neural network, which equals to $N_h=3 \cdot N_i$ may be used to achieve the satisfactory behavior of the network and valid predictions.*

CHAPTER V   Experimental research

Chapter V observes the experimental research work [84-119] that deals with the dispersion and the fabrication procedures, compression and bending testing, and electrical testing of the CNT/CNF reinforced self-sensing concrete. The following describes materials, nanofiller dispersion, composite fabrication, testing, and the standards, which were used for the experimental work in [84-119], which will further serve for the validation of the numerical models as well as the dataset for the artificial neural networks.

1. Materials

Observed experimental investigations have commonalities in regards to the constituent materials and further the processing procedures. All works have the same basic ingredients for obtaining the insulating concrete matrix. The type of cement is Ordinary Portland cement (OPC), it is a hydraulic cement produced with the minimum of 90% of clinker, containing limited amounts of calcium sulfate (up to 5%) and other minor constituents (up to 5%). Strength classes of the used OPC are 42.5 and 52.5, meaning that the expected 28-day compressive strength of the cement is 42.5 MPa and 52.5 MPa, respectively. OPC represents a basic binding material, and the high purity is chosen so that the possible additional or unexpected factors that may affect the properties of the concrete are brought to a minimum. Distilled water is used for the dispersion of nanofillers, and tap or distilled water was used for mixing of the concrete. The amount of water for every mixture, i.e., the w/c ratio, included the total amount of water used for both nanofiller dispersion and concrete mixing. Experimental works have produced cement pastes [84,94,96,98-100,102-107,113,117-119], mortars with fine aggregate [91-93,97,101,109-112,114,116], or concrete with fine and coarse aggregate [85-90,95,108,115]. In accordance with keeping the threatening factors for the concrete quality at a minimum, the used aggregate material is standardized natural or manufactured siliceous sand for the fine aggregate and gravel or crushed rock for the coarse aggregate. Nanofillers are multi-walled carbon nanotubes, further referred to as CNTs, and carbon nanofibers (CNFs), both with the purity of around 99%. Because of the presence of nanofillers, some additive materials are used to achieve better dispersion and mixing of the materials and avoid phenomena such as segregation or excessive foaming. Those materials are surfactants, superplasticizers, and/or foam reducing (defoamer) agents. These materials serve to enable a

quality dispersion of the nanomaterials and to allow the quality of the concrete mixture. Surfactants used in the observed investigations are noted in Table 5.1. Some dispersions are achieved without the help of any kind of surfactant [91,99,100,103,106,111,114-118].

Table 5.1 Surfactants used in observed investigations

Material	Abbreviation	Reference
polyethylene glycol aromatic imidazole	TNWDIS	84,107,110
sodium dodecyl benzene sulfonate	NaDDBS, SDB, SDS	90,92,96,101,104,113,119
lignosulfonic acid sodium salt	SLS	85-89
sodium lauryl with defoamer	SLDS	92
Triton X-100	TX	92
gum arabic	GA	92
cetyltrimethyl ammonium bromide	CTB	92
polycarboxylate based surfactant	SFC, PCE	93-95,97,98,112,119
Pluronic F-127		101
Adva Cast 575		105
polyvinyl pyrrolidone	PVP	107
sodium dodecyl sulfate	SDS	109
Dolapix PC67		110

2. Specimen fabrication

Specimen fabrication is conducted starting with the dispersion process of the nanomaterials. The dispersion is then mixed with the binder, and finally, the dry aggregate materials are incorporated. The mixtures are molded and cured until testing. The following sections give detailed descriptions of all procedures carried out for specimen preparation for the mechanical and the electrical testing.

2.1. Dispersion of nanomaterials

Dispersion of the nanomaterials is carried out for all cementitious composite mixtures. Several techniques are used depending on the type of the surfactant, and if the surfactant is used at all. To achieve the proper dispersion of the nanofillers, techniques such as hand mixing or mechanical mixing, magnetic stirring, and sonication are used. Fabrication procedures, including surfactants for the dispersions, are summarized in Table 5.2. Dispersions of the nanofillers, which are achieved without the use of chemical surfactants, are summarized in Table 5.3.

Quality of the nanofiller dispersion has been analyzed by observing the final hardened cementitious composite specimens. The techniques used for observing if agglomeration of the nanofiller or the segregation occurred are scanning electron microscopy (SEM), environmental scanning electron microscopy (ESEM), transmission electron microscopy (TEM), ultraviolet-visible spectrum analysis (UV-Vis), and the X-ray diffractometer (XRD).

2.2. Mixing of concrete

Mixing procedure, where the nanofiller dispersion and the concrete constituent materials are mixed, is carried out either by manual mixing or automatic mixer, in this case, it is the mechanical agitator or the rotary mixer. During the mixing of the concrete, superplasticizers and foam reducing agents (defoamers) may be included. Superplasticizers are materials, which effectively influence the amount of water used in the mix and, thus, influence the final strength as well as the electrical conductivity of the material. For this reason, and because the weight is relatively comparable, the amount of superplasticizer is included later on in the datasets as an input parameter. Foam reducing agents, on the other side, influence only the air content of the composite by reducing it. It indirectly influences the final properties of concrete, however, if used only when necessary, the final composite material shows no relative difference in material behavior compared

to other mixtures. Hence, its application in several experiments is not particularly considered or included further in the work and the datasets.

2.3. Molding and curing of specimens

Molding follows the mixing process, where the cementitious mixture is poured into oiled molds of varying dimensions, commonly vibrated for compaction, and left until demolding. The demolding is done after 24 or 48 hours when the specimens are further referred to the curing process. The final but nevertheless, an important part of specimen preparation is the curing process. The curing of concrete is done in a water-saturated environment, where the samples are either submerged in water or kept in a room with controlled humidity and temperature. The duration of the curing process is as long as the planned testing of specimens prescribes. In this work, the specimens are tested after 3, 7, 14, 20, 28, 90, or 120 days, meaning that the curing process lasted until the testing date or at least 28 days for the older specimens.

Table 5.2 Process of fabrication CNT/CNF reinforced concrete with surfactants (1/3)

Materials	Dispersion of nanofillers	Mixing of concrete	Molding and curing	Evaluation	Ref.
OPC 42.5 Sand; Gravel Water Superplasticizer NaDDBS	CNTs and CNFs were dispersed in a solution of deionized water and surfactant. Dispersion was achieved through a series of mixings: 10 minutes of magnetic stirring and 30 min of sonication.	Suspension was added to cement and fine and coarse aggregates to achieve cement paste and concrete. Superplasticizer was added last.	Mixtures were casted in oiled molds. After 48 h, were demolded and cured for 28 days in laboratory conditions	SEM	85,86,88,89,108
OPC 42.5 Sand; Gravel Water de-foamer NaDDBS	The solution of surfactantand CNTs was diluted using double-ionized distilled water and sonicated for 2 hours.	Cement was added to dispersion and mixed in ultrasonic device for 3 min. De-foamer, sand, gravel were added and agitated for 5 min.	Mixtures were poured in oiled molds and vibrated. Demolded after 24h, and kept at RH 100% for 28 days	SEM	90
OPC 42.5 Water de-foamer NaDDBS	Surfactant was mixed with water using a magnetic stirrer for 3 min. Next, CNTs were added and this solution was sonicated for 2 h.	Mortar mixer was used to mix the suspension and cement for 3 min. Then, defoamer was added in the mixture and mixed for 3 min.	Mixes were poured into oiled molds, vibrated, demolded after 24h, and cured at RH 100% for 12 months	SEM	96
OPC 52.5 Sand Water SDB, SLDS, TX,	Each surfactant was individually mixed with distilled water. The solutions were magnetically stirred for 5 min. Then, CNTs were added, and dispersions were sonicated	Cement and f aggregates were mixed. Then dispersion and water was added and mixed thoroughly for 5 min in a rotary mixer with	Mixtures were poured in oiled molds, demolded after 24h, and cured for 28 days in water.	UV-Vis	92
OPC 42.5 Sand Water SFC	CNTs and CNFs were added to aqueous solution with SFC. The suspensions were sonicated at room temperature at cycles of 20 s to prevent overheating until dispersion is achieved.	Dispersion was added to cement and sand, and mixed with robust mixer.	Mixtures were poured in oiled molds, demolded after 24h, and cured for 28 days in lime-saturated water.	SEM, TEM	93-95,97,98,112
OPC 42.5 Sand; Water de-foamer NaDDBS, Pluronic F-127	De-foamer was added to water, and then CNTs and each surfactant. The mix was magnetically stirred for 10 min and then sonicated for 1h in a bath sonicator.	Suspensions, cement, and standardized sand were mixed in a Hobart mixer.	Mixtures were poured in oiled molds, demolded after 24h, and cured for 28 days in water.	SEM	101

Table 5.2 Process of fabrication CNT/CNF reinforced concrete with surfactants (2/3)

Materials	Dispersion of nanofillers	Mixing of concrete	Molding and curing	Evaluation	Ref.
OPC 52.5 Water de-foamer SDBS	CNTs were added to surfactant solution, and magnetically stirred for 10 min. Then, solution was sonicated at room temperature for 4 h.	Cement was first mixed in flat beater Hobart mixer. Dispersion was added to this mixture and mixed for 3 min. Further, deformer was added.	Mixtures were casted in oiled molds and vibrated. After 24 h, were demolded and cured for 28 days at 20°C.	UV-Vis	104
OPC 42.5 Water PVP,TNWDIS	Surfactants were added to beakers, followed by addition of CNTs and water. Suspensions were magnetically stirred for 15 min and then sonicated for 30 min in 2 s intervals to avoid overheating.	Cement was mixed with the solutions for 7 min using a cement paste mixer.	Mixtures were poured in oiled molds and vibrated. Demolded after 24h, and kept at RH 100% for 28 days.	SEM	107
OPC 42.5 Water Adva Cast 575	Water was set at 23°C and CNTs were placed in. Then, surfactant was added and the sonication was carried out for 30 min.	Cement was added to solution in five increments for 10 min. Then, the mixing continued for another 50 min in Hobart mixer.	Mixtures were poured to oiled molds, vibrated, demolded after 24h, and cured at RH 100% for 28 days.	SEM	105
OPC 52.5 Water PCE, SDS	Dispersants, water, and CNTs were poured to the beaker and mixed, and then the solution was mechanically stirred for 5 min and sonicated for 15 minutes.	Cement and mixed solutions were stirred for 2 minutes.	Mixtures were casted in oiled molds and vibrated. After 24 h, were unmolded and cured.	ESEM	119
OPC 42.5 Sand; Gravel Water Superplasticizer SLS	CNTs and dispersant were added to deionized water. Premixing of deionized water, dispersant, and CNTs was manual, followed by 10 min of magnetic stirring. After, suspension was sonicated for 30 min.	After mixing the solution, cement powder, aggregates and superplasticizer were added, and stirred.	Mixtures were poured in oiled molds, demolded after 24h, and cured for 28 days in controlled conditions.	SEM	87
OPC 52.5 Sand; Gravel Water Superplasticizer	CNTs and surfactant were magnetically stirred with 40% of water, and then sonicated in 2 cycles of 15 minutes	Cement, fine, and coarse aggregate were added to the mixer are mixed with 60% of water for 3 min. Then, dispersion and superplasticizer were added and mixed for 1 min.	Mixtures were poured in oiled molds, demolded after 24h, and cured until testing.	/	115

Table 5.2 Process of fabrication CNT/CNF reinforced concrete with surfactants (3/3)

Materials	Dispersion of nanofillers	Mixing of concrete	Molding and curing	Evaluation	Ref.
OPC 52.5 Water PVA	Concentrated H_2SO_4 was cooled at 0°C for 30 min under slow stirring. Then, CNTs were added under stirring for 30 min. After, $KMnO_4$ was added gradually and water temperature was controlled at 20°C. The mixture was stirred for 8 h, filtered and washed by water until neutral. Then, CNTs were dispersed in water under sonication, and mixed with PVA solution.	The suspension was mixed with cement.	The paste was cast into molds and were maintained in condition of high humidity (95% humidity, 20°C) for 28 days to complete the hydration process.	SEM, TEM	102
OPC 42.5 Water TNWDIS	Surfactant was dissolved in water and stirred, CNTs were added and stirred until wetted. Dispersion had 6 cycles of 5 min. Dispersion was placed in ice water because of heating and foaming, and then subjected to centrifugation for 30 min. Sediment was filtered and CNT aggregates were dispersed by repeating entire process until bundles were separated to strands. Final dispersion was stored for 3 months.	Dispersion and water were placed in the JJ-5 mixer and mixed for 60 s. Then, cement was added and stirred for 300 s.	Mixtures were poured in oiled molds and vibrated. Then, demolded after 24h, and cured until testing.	SEM	84
OPC 42.5; Sand Crushed limestone; Water; Superplasticizer de-foamer, SDS	3 types of CNFs were used, 2 non-oxidized and 1 oxidized. Each type is made only with water; with surfactant, and with surfactant and de-foamer. After 3 min of mixing, superplasticizer was added using a paint mixer.	Coarse aggregate, sand, and cement were combined in a centrifugal mixer for 3 min. Then, the CNF mixture was slowly poured into the mixer and stirred for several minutes.	Mixes were poured into oiled molds, vibrated, demolded after 24h, and cured until testing.	SEM	109
OPC 42.5 Water Superplasticizer TNWDIS Dolapix PC67	5 types of CNTs were used – 2 untreated, 1 pristine and 2 acid-treated. Untreated CNTs came in a solution with TNWDIS which was then stirred and sonicated. Pristine and acid-treated CNTs were dispersed with Dolapix PC67 by 4 h of magnetic stirring, followed by 30 min of sonication.	Suspension was added to cement and mixed for 3 min. After 1 min superplasticizer was added. FAggregates were mixed with remaining water. Then, cement paste was added to aggregates and mixed for 2 min.	Mixtures were poured in oiled molds, demolded after 24h, and cured for 28 days in water.	SEM	110

67

Table 5.3 Process of fabrication of CNT/CNF reinforced concrete without dispersion (1/2)

Materials	Dispersion of nanofillers	Mixing of concrete	Molding and curing	Evaluation	Ref.
OPC 42.5 Sand; Gravel Water Superplasticizer	The mix of only CNTs in water was made by mechanical mixing and then 30 minutes of sonication.	After mixing the solution, cement powder, aggregates and superplasticizer were added, and stirred.	Mixtures were poured in oiled molds, demolded after 24h, and cured for 28 days in controlled conditions.	SEM	87
OPC 42.5 Sand Water Superplasticizer Viscofluid SCC	3 types of CNTs: pristine, annealed and functionalized, were dispersed in acetone with 4h of sonication after which the acetone was allowed to evaporate.	Samples were prepared in rotary mixer by adding cement, water, sand, and CNTs. Then, superplasticizer and viscosity modifying agent Viscofluid SCC were added during stirring.	Mixes were poured into oiled molds, vibrated, demolded after 24h, and cured for 28 days.	SEM, XRD	91
OPC 52.5 Water Superplasticizer De-foamer	CNFs and CNTs were added to water, mechanically stirred and sonicated.	Solution, cement and superplasticizer were mixed in rotary mixer for 3 min. Then, a defoamer was added. Mixture was mixed for another 5 min.	Mixes were poured into oiled molds, vibrated, demolded after 24h, and cured until testing.	SEM	99, 100, 111, 116
OPC 42.5 Sand Water	CNTs were mixed with water and stirred with magnetic stirrer for 15–20 min. The solution was sonicated for 9 min at 60 °C.	Solution was hand-mixed with cement and sand until correct consistency.	Mortar was compacted in 3 layers in molds and vibrated, demolded after 24h and immersed in water until testing.	/	103
OPC 42.5 Water Superplasticizer	Probe sonicator was used to disperse the CNTs and CNFs for 5 min.	Mixer was used to mix the water, filler and superplasticizer for 30s in low speed. Cement was put in the mixture slowly mixing for 3 min.	Mixes were poured into oiled molds, vibrated, demolded after 24h, and cured until testing.	/	106

68

Table 5.3 Process of fabrication of CNT/CNF reinforced concrete without dispersion (2/2)

Materials	Dispersion of nanofillers	Mixing of concrete	Molding and curing	Evaluation	Ref.
OPC 42.5 Sand Water De-foamer	CNTs were added to mixed solution of sulfuric and nitric acid (3:1). Mixture was sonicated for 3h. Then mixture was diluted with distilled water in ratio of 1:5. After 24h, top part of diluted solution was removed. Solution was diluted further. After 4 cycles, mixture was filtered and washed with water until no acid was present.	Solution, cement, sand, water and de-foamer were all mixed in the mixer for 5 min.	Mixes were poured into oiled molds, vibrated, demolded after 24h, and cured until testing. All specimens were dried in an oven at $50 \pm 2°C$ for 24 h before testing.	SEM	114
OPC 42.5 Water	CNTs and water were mixed in automatic mixer for 2 minutes.	Cement was added gradually into the dispersion while the mixing continued. Mixing was carried out for another 15 min.	Mixes were poured into oiled molds, vibrated, demolded after 24h, and cured until testing.	SEM	117
	CNTs were soaked in deionized water (pH 6.6) over night, then the solution was stirred for 24h, and then sonicated for 20 minutes.	Dry ingredients (cement, fine, and coarse aggregates) were mixed for 3 min. Solution was added to the dry mixture and mixed for 5 min.	Mixtures were poured in oiled molds and vibrated, demolded after 24h, and cured in lime-saturated water until testing.	SEM	118

3. Testing procedures

3.1. Determination of flexural and compressive strength

Mechanical tests may include a wide spectrum of different procedures, however, the following describes only the destructive testing procedures used for establishing the compressive strength and the flexural strength of the cementitious specimens that were used in this work. The procedures are described in chronological order.

Three-point bending test is one of the standard testing procedures for establishing the flexural strength (tensile under bending) of the concrete specimen. It is performed on a prismatic (small-beam) specimen with the two supporting points and a midpoint where the force is applied (Figure 5.3.1). The force causes bending of the specimen by putting it in the state of flexural strain. Four-point bending test is also a standard testing procedure for establishing the flexural strength of concrete. The main difference between the three-point and the four-point test is that the four-point bending is caused by two force points on the prismatic specimen, causing a more distributed bending moment than with the 3-point bending (Figure 5.3.2). Moreover, shearing stresses do not appear in the area between the two forces, so the three-dimensional strain state is at a minimum. The width, height, and length of the specimens used for bending tests are, respectively, as follows:

- 40×40×160 mm;
- 25×40×80 mm;
- 20×20×80 mm;
- 150×150×150 mm.
- 38×70×80 mm.
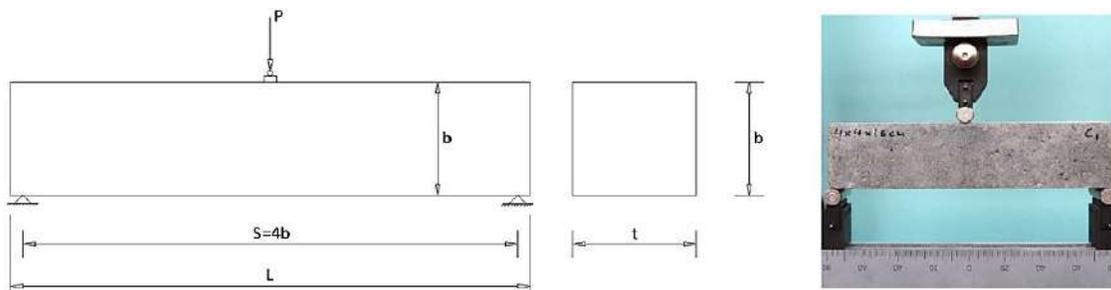
Figure 5.3.5 Experimental setup for three-point bending test [112]
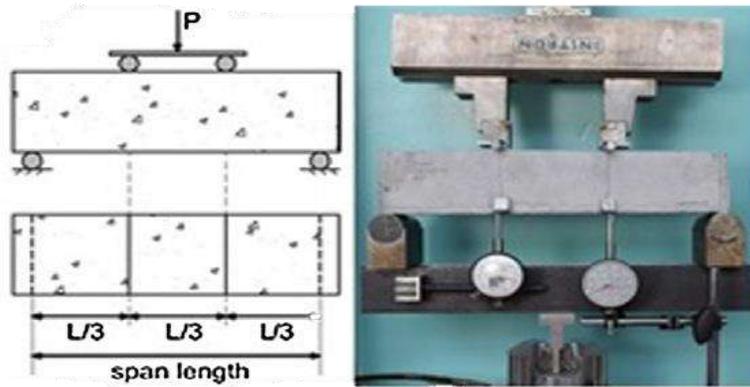
Figure 5.3.6 Experimental setup for four-point bending test [95]

Axial compression test is usually carried out by a compression press machine using the cuboid or cylindrical specimens subjected to the centered compressive force along the longitudinal axis, which is gradually applied until complete failure. The width, height, and length of the specimens are with the tolerance rate of ±1 mm, respectively, as follows:

- 40×40×160 mm;
- 40×40×80 mm;
- 40×40×40 mm;
- 50×50×50 mm;
- 70×70×70 mm;
- 150×150×150 mm;
- 300×150 mm (cylindrical);
- 150×75 mm (cylindrical);
- 140×70 mm (cylindrical).

3.2. Testing of electrical properties

As described in Chapter III, testing of the electrical properties of self-sensing concrete, also including CNT/CNF reinforced concrete, is most often carried out by applying the two- or four-probe method. The occurrence of the polarization effect may interfere with the results, so it should be addressed after the curing process of the concrete specimens but prior to the testing of electrical conductivity, resistivity, or resistance. The observed experiments have used several procedures to eliminate the polarization effect or to subsequently consider it. These procedures include: measuring the variation of current after 3 min [85-87], 20 min [88], or 30 min [89] on a

71

mechanically unloaded specimen; oven-drying the specimens after curing at 60°C for 3 days and at 95°C for another 3 days [98]; or using the AC measurement method [93]. Electrical tests were done by a digital multimeter, and the procedures followed the two-probe method (Figure 5.3.4) [85-90,93,96,104,106,108,113] and the four-probe method (Figure 5.3.5) [98-100,109,119].
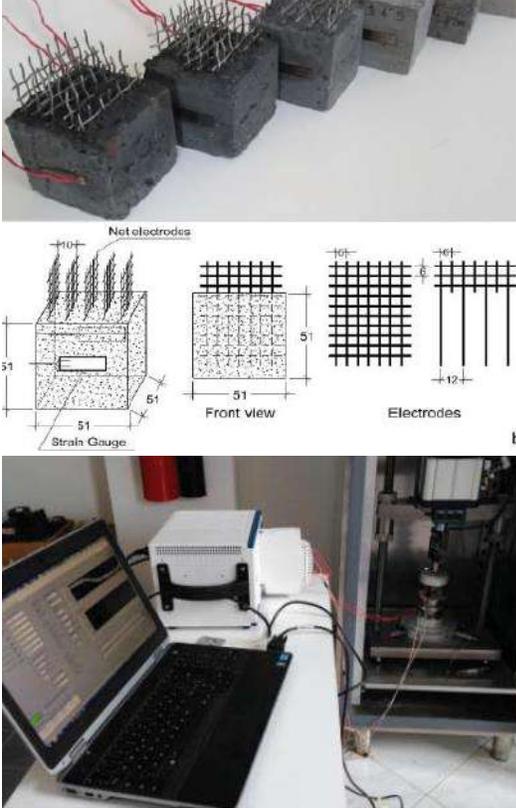
Figure 5.3.3 Specimen preparation and testing using two-probe method [88]
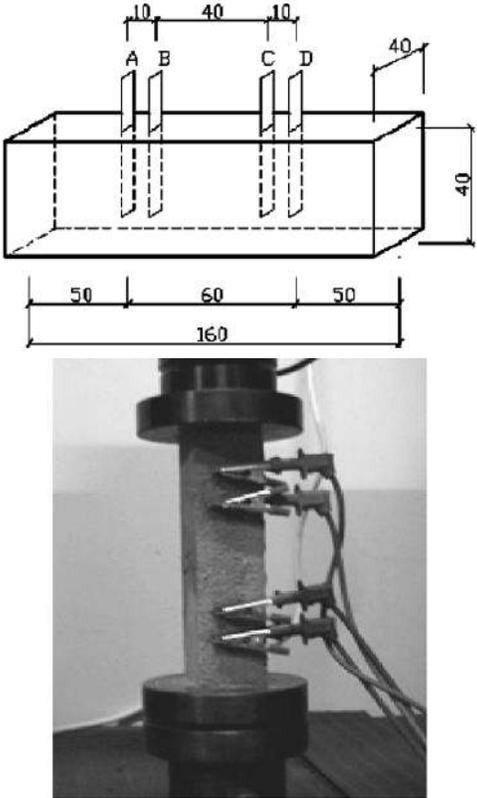
Figure 5.3.4 Specimen preparation and testing using four-probe method [100]

4. Standards

The experiments are based on several standards and standardized procedures for materials, as well as the mixing, molding, curing, and testing procedures. European (EN), American - American Association for Testing and Materials - ASTM, American Concrete Institute - ACI, Spanish (Spanish Association for Standardization - UNE), and Indian (Indian Standard - IS) standards are included. The applied standards are summarized and classified in Table 5.4. It should be noted that standards are given strictly by following the authors' explicit citations. In cases that the procedures only indirectly imply a certain standard, the standard is not referenced.

Table 5.4 Standards used for experimental investigations

Type	Nomenclature	Title	Reference
For materials	EN 197-1[120]	Composition, specifications, and conformity criteria for common cements	90,99,102,105,110
	ASTM C778-17 [121]	Standard Specification for Standard Sand	90
	ACI 544 1R-96 [122]	Report on Fiber Reinforced Concrete	93-95,97,112
	UNE 83258 [123]	Admixtures for concretes, mortars and grouts. Admixtures for masonry mortars. Determination of consistency	99
	IS 8112 (1989) [124]	Ordinary Portland Cement, 43 grade - Specification	103
For mixing	ASTM 305-20 [125]	Standard practice for mechanical mixing of hydraulic cement pastes and mortars of plastic consistency	93-95,97, 112,116,118
	IS 2250:1981 [126]	Code of practice for preparation and use of masonry mortars	103
For molding and curing	ASTM C192 [127]	Standard practice for making and curing concrete test specimens in the laboratory	93-95,97,112, 118
For testing	EN 196-1 [128]	Methods of testing cement. Determination of strength	91,93-95,97, 101,111,112
	ASTM C349 [129]	Standard test method for compressive strength of hydraulic-cement mortars prism-shaped specimens	93,97,107,112
	ASTM C109 [130]	Standard test method for compressive strength of hydraulic cement mortars (using 2-in. or [50 mm] cube specimens)	85-90,92,93, 105,112,116
	ASTM C39 [131]	Standard test method for compressive strength of cylindrical concrete specimens	90,95,109
	ASTM C348 [132]	Standard test method for flexural strength of hydraulic-cement mortars	93-95,97,105, 107,112,116
	ASTM C1760 [133]	Standard test method for bulk electrical conductivity of hardened concrete	85-89
	IS 4031:1988 [134]	Methods of physical tests for hydraulic cement	103
	IS 516:1959 [135]	Method of tests for strength of concrete	115
	EN 1015-11 [136]	Methods of test for mortars for masonry – Determination of flexural and compressive strength of hardened mortar	110

CHAPTER VI   Numerical analysis and simulations

Numerical simulations are employed in this study to establish if it is possible to use ANSYS software package as a substitute for the experimental testing of CNT/CNF reinforced concrete specimens. The analyses and simulations are carried out based on the results of the experimental research. To this end, the materials fabricated in the laboratory, as described in Chapter V [84,93,95,97,100,101,107,110,111,114,119], are numerically simulated and analyzed. The material models are developed using Material Designer and used to build a comprehensive material library, which is later applied in simulations of the mechanical testing of the specimens.

1. Material Designer

Material models are developed through the use of the RVE, a representative volume element in the Material Designer. To simulate the most realistic structure of the composite material, Random UD Composite RVE is used. As it is previously mentioned, the Material Designer is unable to recognize the various aggregate states of materials. Since the concrete microstructure is heterogeneous and it includes solid materials such as cement and aggregate, but also air voids and free and capillary water, all three aggregate states are present in a general concrete composite material. Furthermore, the structure itself at the microlevel consists only of the cement particles and water particles because both fine and coarse aggregate materials have the minimum size of 1-2 mm, and hence exist only on the macro scale. Due to the different scale ranges of the constituent materials and different states in which these materials appear, plain concrete is not modeled at each level, but instead, it is input into the primary material library as the matrix material of the Random UD Composite RVE, whereas the fiber material is represented by the CNT or CNF.

Material Designer RVE is defined by the geometry of the fiber, including the fiber volume fraction, mean misalignment angle, seed, fiber diameter, and the repeat count. After these parameters are provided, the Material Designer generates an appropriate RVE. The fiber volume fraction is provided according to the established material library, and the fiber diameter followed the realistic sizes of the nanofillers (as given within Chapter III). Parametrization is done for the fiber volume fraction, so that each composite group is prescribed with the suitable values. The duration of RVE generation and meshing depends on the seed and the repeat count parameter. It is established that for the smaller fiber weight fractions, from 0.01-0.1%, it is better to use a smaller

mean misalignment angle and repeat count, while the seed should be kept between 15000 and 25000. For the weight fractions higher than 0.1%, the mean misalignment angle can be increased to 5 or even 10 for fractions over 1 wt%. The seed should increase steadily in line with the nanofiller fraction, going up to around 70000 for 2 wt%. Only conformal meshing is used, without a limit for the maximum FE size. It is established that limiting the mesh size leads to difficulties for the model to provide a complete mesh between the matrix and the fiber materials. Conformal meshing coincides with the relatively irregular geometry between the two materials. The analysis is provided for the final material defined as linear orthotropic instead of anisotropic. When the homogenization was attempted for the anisotropic material, the model encountered difficulties and could not converge due to the orthotropic nature of the nanofiller. An example of an RVE from this work is shown in Figure 6.1.1. All results from the Material Designer models are given in Appendix A1. Figure 6.1.2 shows the flow of the ANSYS Workbench project, including the Material Designer model with the parametrization and the compression test and bending test simulation in Static Structural.
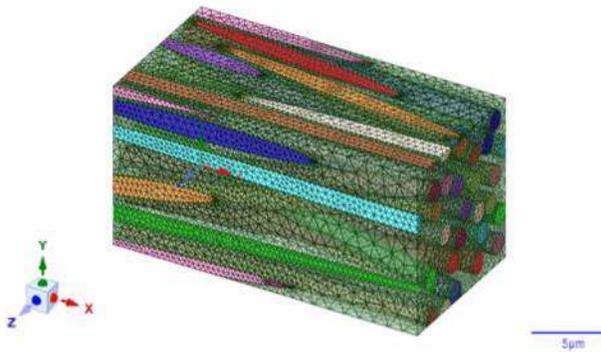
Figure 6.1.1 Random UD Composite RVE
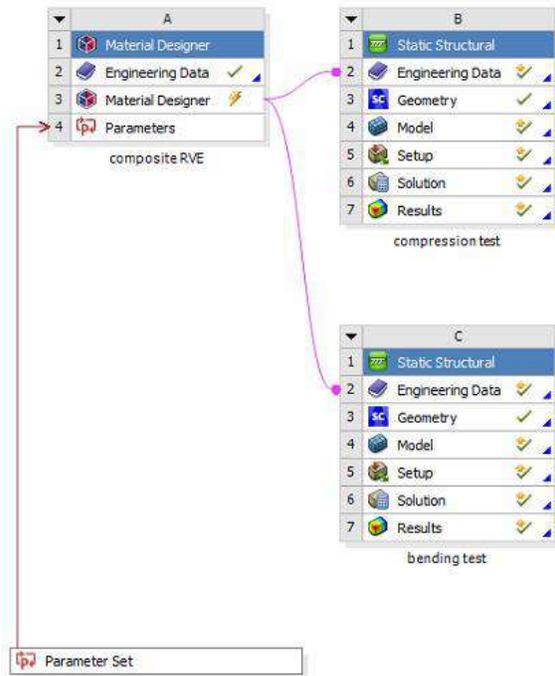
Figure 6.1.2 Schematic of the modeling flow for the ANSYS Workbench project

2. Macroscale models

Material Designer conducts the linear analysis of the material model and the results are then transferred to the Engineering Data, which is a part of the Static Structural model (Figure 6.1.2). Engineering Data contains all relevant parameters of the new composite materials, such as density, Young's modulus, Poisson's ratio, and shear modulus for each global coordinate direction, while the ply type is regular, which indicates isotropy. The Engineering Data material library is provided within Appendix A2. As may be seen in Figure 6.1.2, there are two Static Structural models, one for each mechanical testing. Space Claim is used to build the geometry of the specimen for compression and bending tests, following the realistic testing set-up for the axial compression test and the three-point bending test. Hence, bending test specimens are small beams, and the compression test specimens represent the halved small beams (Figure 6.2.1). In reality, the beam halves cannot be perfectly shaped with uniform geometry, however, it is assumed that the topology of the breaking side does not have a significant impact on the results because the axial force is submitted through the rectangular steel sheets with dimensions of 40×40 mm placed between the machine's heads and the surfaces (upper and bottom edge) of the test sample. The Mechanical part of the Static Structural model defines the meshing of the model, supports loading, and analysis' settings. The meshing of both types of specimens includes hexagonal finite elements (Hex8, Hex20) of 2 mm, type SOLID185, as shown in Figure 6.2.2, which are the default elements for Static Structural models. Linear SOLID185 elements are 8-node three-dimensional finite elements used for the thick shell and solid structures. Figure 6.2.2 shows the meshing element number and quality, where it may be observed that all elements in both compression (Figure 6.2.2a) and tension (Figure 6.2.2b) models have exactly the same size and shape. The number of elements also implies on the geometry of the models. Since the size is 2 mm in both cases, we may conclude that the compression model with 8000 elements represents half of the bending model with 16768 elements.
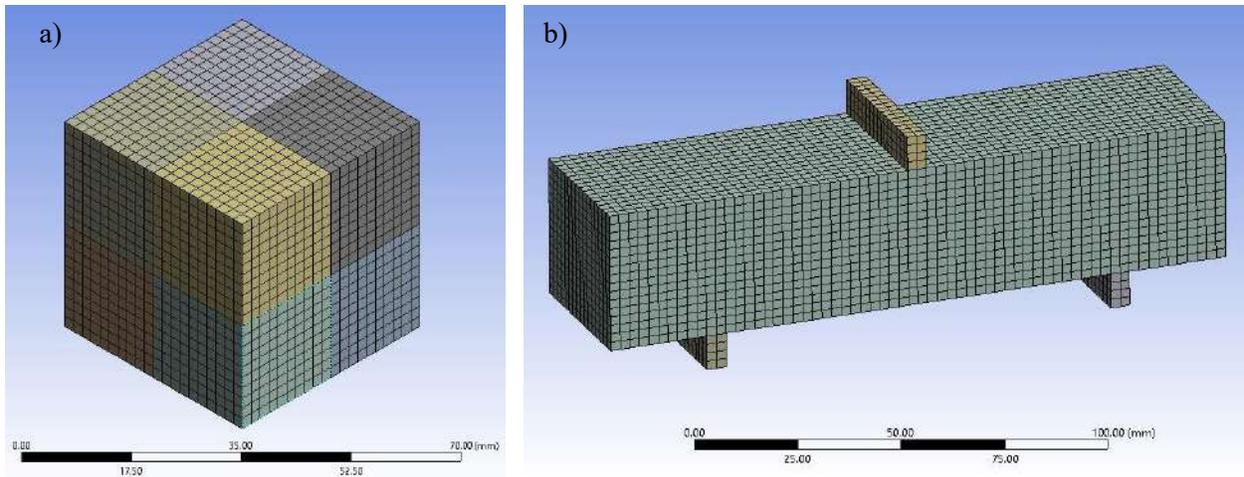
Figure 6.2.1 Meshing of the models for: (a) compression test; (b) bending test
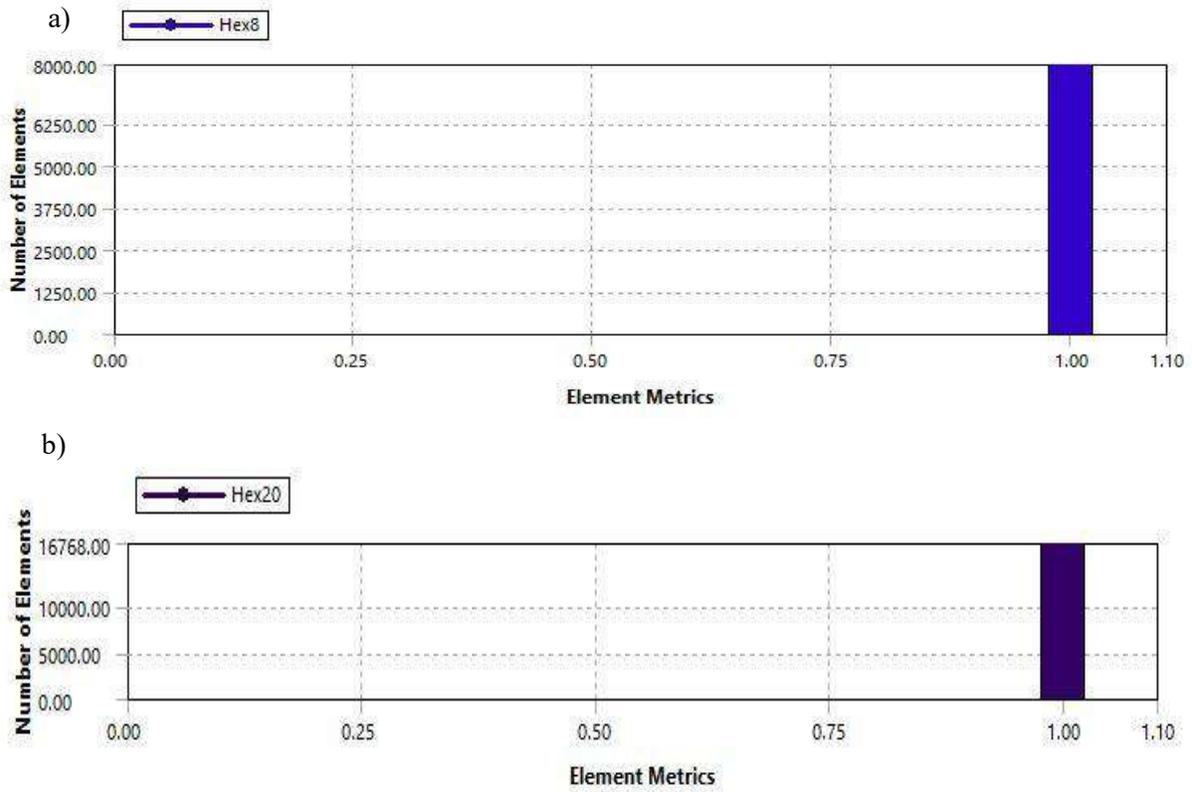
Figure 6.2.2 Quality of the meshing for: (a) compression model; (b) bending model

3. Simulation of loading

Simulation of the loading is indicated by the ultimate strength of the referential plain concrete material from the experimental testing. The compression test model followed the set-up as the laboratory axial compression test. This set-up implies that the sample is oriented so that the vertical loaded axis takes the dimension of 40 mm; that the entire bottom surface is fully supported; and that the entire top plane is loaded. The loading of the model is presented as the displacement of the top surface, which is input as tabular to ensure the steady growth of the stresses. The analysis of the stresses is provided with substeps within one second of the implicit static analysis. The minimum number of steps is 10, and the maximum is 20, to ensure incremental analysis but still keep the speed of convergence.

Bending test model followed the experimental setup of the three-point bending as presented in Chapter III. Unlike the compression test model, where the surfaces of the body are constrained or loaded, the bending test model includes additional bodies in the form of supports and the impactor. The contact surfaces between the support bodies and the beam are defined as "no separation" contacts, where the bodies are fully connected, but the sliding is allowed. Displacement is set to zero in all global directions and is provided for both supports. Even though statically the constraints are in vertical and horizontal longitudinal directions only, this setup helps the software to converge quicker and easier. The impactor body serves to transfer the loading from the press to the beam. Therefore, the contact type is "bonded" and the displacement is provided for the top surface of the impactor.

4. Results

Materials created by the Material Designer are orthotropic linear elastic. Hence, the analysis of the models is linear. The static analysis results are represented with the maximum, minimum, and average values of the maximum principal stress, minimum principal stress, and normal stress. All results are given in detail within the Appendix A2. Figure 6.4.1 represents the resulting maps of the bending and the compression test for the composite material denominated as cem52504NT01, which means it is an OPC 52.5 cement with the ratio of 1/0.4 for cement/water; with the addition of the CNT filler with the weight fraction of 0.1 wt%. It may be observed that the cracking did not occur in any of the composite material specimens. That is also confirmed by the fact that Young's modulus and Poisson's ratio of all homogenized composite materials increased significantly with the addition of the nanofiller.
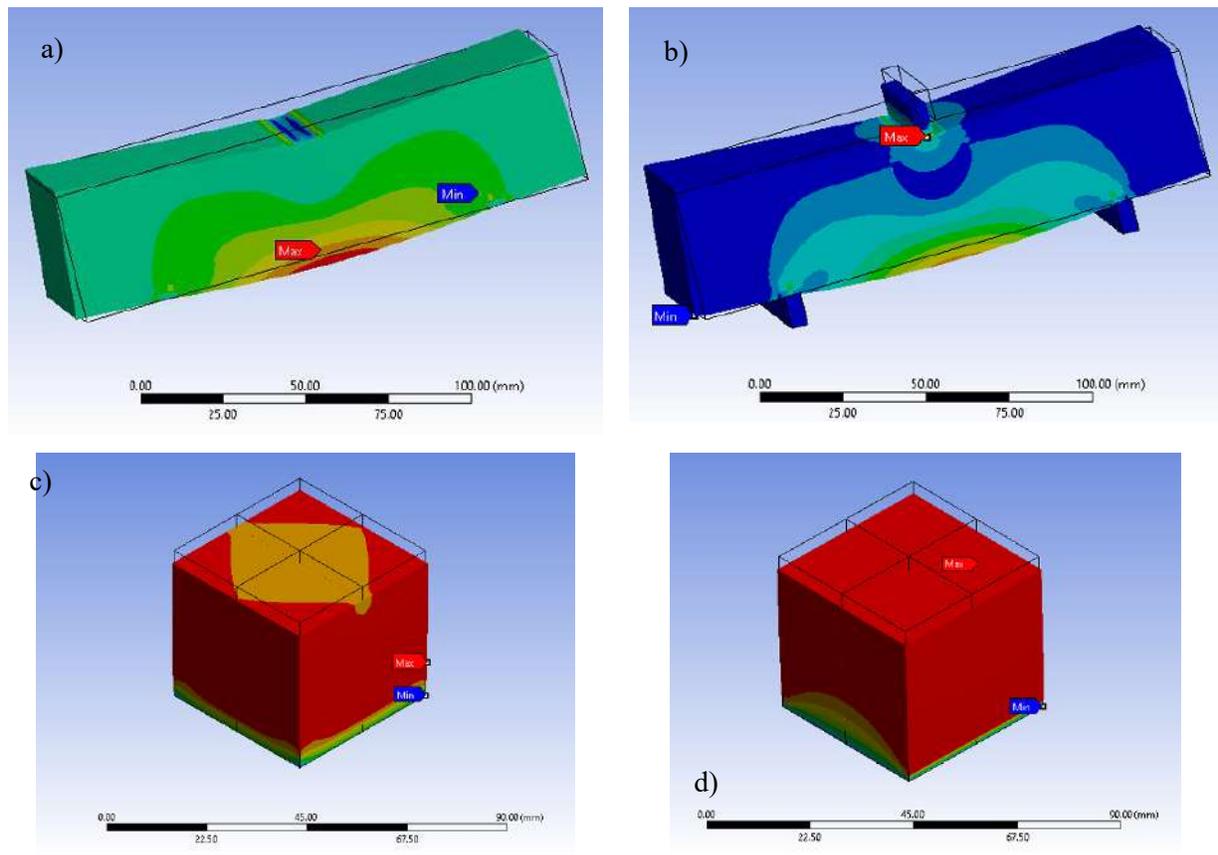
Figure 6.4.1 Results for cem52504NT01: (a) maximum principal bending stress; (b) maximum principal elastic bending strain; (c) minimum principal compressive stress; (d) normal stress under compression.

Table 6.1 gives an overview of the compressive and flexural stresses. It is observed that in some cases, Young's modulus of the composite material is even higher than 200 GPa, and the flexural strength surpasses the value of 20 MPa. It is safe to say that this is an overestimation and that it would not occur in realistic conditions. However, the results show fairly realistic material behavior for the composite materials with the weight fractions of up to 0.1%. Thus, for the lower weight fraction of the nanofiller, the results seem promising and imply further research. As for the weight fractions over 0.1%, it may be concluded that the microstructure should be modeled thoroughly from the bottom up, taking into account individual particles and grains of the constituent materials and modeling the nanofillers more realistically in terms of their interaction with each other and within the concrete matrix.

Table 6.1 Material behavior of the homogenized specimens

Material	Young's modulus [GPa]	Poisson's ratio YZ direction	Compressive strength [MPa]	Tensile strength [MPa]
cem52504	30	0.18	51.13	13.32
cem52504NT005	46.898	0.2014	51.81	12.67
cem52504NT01	69.277	0.21847	52.17	12.06
cem52504NT015	86.57	0.22763	52.19	11.69
cem53504NT02	105.72	0.22958	52.29	11.37
cem52504NT025	127.15	0.25611	52.06	12.99
cem54504NT03	139.8	0.24451	52.29	13.10
cem52504NT035	170.93	0.2412	52.40	14.45
cem52504NT04	191.52	0.24311	52.37	15.35
cem52504NT045	211.4	0.24233	52.44	15.88
cem52504NT05	231.44	0.2327	52.51	16.61
cem425033	30	0.18	76.47	6.12
cem425033NT001	34.755	0.1875	76.86	6.03
cem425033NT002	38.734	0.19256	77.14	5.96
cem425033NT003	43.415	0.1986	77.36	5.88
cem425033NT004	47.15	0.2012	77.52	5.83
cem425033NT005	51.086	0.20554	77.64	5.77
cem425033NT006	56.006	0.20916	77.73	5.70
cem425033NT007	58.794	0.21069	77.73	5.66
cem425033NT008	62.84	0.21281	77.90	5.60
cem425033NT009	69.834	0.22016	77.93	5.56
cem425033NT01	72.756	0.22117	77.97	5.52
cem42505	30	0.18	32.10	10.95
cem42505NT001	34.108	0.18654	32.24	10.80
cem42505NT002	37.642	0.19135	32.35	10.69
cem42505NT003	39.6	0.19437	32.39	10.69
cem42505NT004	46.188	0.20041	32.53	10.44
cem42505NT005	49.448	0.20354	32.56	10.36
cem42505NT006	52.988	0.20597	32.63	10.27
cem42505NT007	57.439	0.21028	32.65	10.17
cem42505NT008	60.504	0.21191	32.71	10.11
cem42505NT009	64.408	0.21624	32.69	10.02

cem42505NT01	63.656	0.21754	32.62	9.98
cem42504	30	0.18	41.03	10.78
cem42504NT001	34.164	0.18673	41.21	10.63
cem42504NT002	37.711	0.19166	41.33	10.52
cem42504NT003	42.076	0.19615	41.47	10.39
cem42504NT004	45.828	0.20066	41.55	10.28
cem42504NT005	50.065	0.20429	41.64	10.18
cem42504NT006	52.12	0.2072	41.64	10.12
cem42504NT007	56.626	0.21149	41.76	9.98
cem42504NT008	63.25	0.21248	41.83	9.89
cem42504NT009	64.01	0.21649	41.79	9.86
cem42504NT01	68.749	0.22117	41.79	9.77
cem42503	30	0.18	59.97	15.46
cem42503NT005	49.418	0.20304	60.84	14.63
cem42503NT01	69.027	0.21823	61.12	14.02
cem42503NT015	81.188	0.2284	61.11	13.66
cem42503NT02	100.39	0.23364	61.26	13.29
cem42503NT025	121.6	0.23448	61.25	13.86
cem42503NT03	132.77	0.24041	61.03	15.76
cem42503NT035	159.43	0.27042	60.76	17.57
cem42503NT04	184.42	0.27442	60.81	18.52
cem42503NT045	178.96	0.28382	60.36	19.64
cem42503NT05	188.25	0.28563	60.04	20.22
mor42504850364	30	0.18	28.59	9.03
mor42504850364NT005	37.12	0.19069	28.79	8.83
mor42504850364NT008	40.907	0.19536	28.87	8.74
mor42504850364NT01	44.364	0.19941	28.94	8.66
mor42504850364NT015	48.591	0.20236	28.94	8.55
mor42504850364NT02	55.918	0.21104	29.05	8.41
mor42504850364NT025	65.009	0.21078	29.17	8.26
mor42504850364NT03	68.574	0.21669	29.15	8.19
mor42504850364NT035	75.726	0.21842	29.14	8.06
mor42504850364NT04	83.29	0.22426	29.17	7.96
mor42504850364NT045	82.758	0.22785	29.04	7.90
more42504850364NT05	88.074	0.23075	29.03	7.81
mor42505033	30	0.18	46.26	12.71
mor42505033NT0025	33.205	0.1852	46.41	12.57
mor42505033NT005	36.496	0.18983	46.57	12.45
mor42505033NT0075	39.332	0.19373	46.65	12.34
mor42505033NT01	42.171	0.19613	46.78	12.25
mor425055033	30	0.18	44.01	11.63
mor425055033NT0025	33.251	0.18528	44.18	11.50
mor425055033NT005	36.426	0.18996	44.28	11.40
mor425055033NT0075	39.931	0.19434	44.40	11.28
mor425055033NT01	41.556	0.19637	44.49	11.20
mor42505033spl	30	0.18	28.68	9.03
mor42505033splNT0025	33.549	0.18578	28.79	8.93
mor42505033splNT005	36.525	0.19002	28.87	8.85
mor42505033splNT0075	40.024	0.19462	28.95	8.76
mor42505033splNT01	42.309	0.19668	28.99	8.70
mor52505033spl	30	0.18	48.70	15.84
mor52505033splNF005	32.133	0.18614	48.78	15.70

mor525033splNF01	34.25	0.19154	48.85	15.56
mor525033splNF015	36.04	0.19613	48.89	15.44
mor525033splNF02	38.16	0.198	48.98	15.30
mor52505033splNF025	40.882	0.20251	49.02	15.13
mor52505033splNF03	41.959	0.20494	48.95	15.03
mor52505033splNF035	45.208	0.20994	49.11	14.89
mor52505033splNF04	46.562	0.20844	49.03	14.69
mor52505033splNF045	47.571	0.20862	49.10	14.61
mor52505033splNF05	48.891	0.21418	49.04	14.56
mor52505033splNF055	48.391	0.21919	48.88	14.51
mor52505033splNF06	55.214	0.22837	49.11	14.31
mor52505033splNF065	58.136	0.23501	49.02	14.14
mor52505033splNF07	58.194	0.21891	49.09	13.93
mor52505033splNF075	56.012	0.2299	48.99	14.06
mor52505033splNF08	63.188	0.23997	48.86	13.72
mor52505033splNF085	65.11	0.23161	48.64	13.68
mor52505033splNF09	47.79	0.22215	48.62	14.06
mor52505033splNF095	68.691	0.24497	49.09	13.59
mor52505033splNF1	69.943	0.28297	48.47	13.70
mor52505033splNF105	67.334	0.24728	48.77	13.31
mor52505033splNF11	72.273	0.25817	48.60	14.39
mor52505033splNF115	74.709	0.28033	48.18	15.54
mor52505033splNF12	74.804	0.2462	48.84	14.21
mor52505033splNF125	77.232	0.27412	48.27	15.82
mor52505033splNF13	82.917	0.25954	48.70	15.38
mor52505033splNF135	84.795	0.23499	49.13	14.94
mor52505033splNF14	90.497	0.22133	49.07	16.41
mor52505033splNF145	90.887	0.23923	48.93	16.35
mor52505033splNF15	93.555	0.25613	48.48	17.60
mor52505033splNF155	90.794	0.28922	47.89	18.46
mor52505033splNF16	99.068	0.30026	47.67	19.85
mor52505033splNF165	97.566	0.28326	48.09	18.66
mor52505033splNF17	99.398	0.33264	47.83	20.43
mor52505033splNF175	106.06	0.29754	47.53	21.03
mor52505033splNF18	102.64	0.29309	47.99	19.35
mor52505033splNF185	121.19	0.20014	49.70	17.09
mor52505033splNF19	114.39	0.19535	49.80	17.15
mor52505033splNF195	116.59	0.18489	49.92	17.35
mor52505033splNF2	118.79	0.19042	49.86	17.56
mor425035033spl	30	0.18	65.02	15.77
mor425035033splNT0025	33.49	0.18559	65.26	15.59
mor425035033splNT005	36.389	0.18974	65.43	15.45
mor425035033splNT0075	39.144	0.19367	65.59	15.33
mor425035033splNT01	43.027	0.19783	65.75	15.17
mor425045033spl	30	0.18	50.86	13.62
mor425045033splNT0025	33.582	0.18585	51.06	13.47
mor425045033splNT005	36.318	0.18963	51.19	13.35
mor425045033splNT0075	39.771	0.19399	51.30	13.22
mor425045033splNT01	42.526	0.1969	51.42	13.12
mor425040263spl	30	0.18	58.62	11.48
mor425040263splNT005	35.972	0.18946	58.98	11.27
mor425040263splNT01	39.568	0.19418	59.12	11.14

mor425040263splNT015	47.211	0.20176	59.39	10.92
mor425040263splNT02	52.965	0.20683	59.56	10.78
mor425040263splNT025	57.318	0.20901	59.61	10.66
mor425040263splNT03	59.63	0.21203	59.71	10.61
mor425040263splNT035	67.894	0.21543	59.84	10.45
mor425040263splNT04	71.044	0.21637	59.81	10.35
mor425040263splNT045	79.463	0.22116	59.85	10.20
mor425040263splNT05	80.873	0.22459	59.80	10.16
mor425045067spl	30	0.18	47.14	10.24
mor425045067splNT005	39.72	0.19425	47.58	9.94
mor425045067splNT01	48.067	0.20207	47.80	9.72
mor425045067splNT015	59.764	0.21199	47.98	9.47
mor425045067splNT02	70.697	0.21908	48.09	9.26
mor425045067splNT025	79.687	0.22307	48.12	9.11
mor425045067splNT03	84.996	0.22647	48.14	9.01
mor425045067splNT035	86.279	0.22504	48.12	8.96
mor425045067splNT04	84.289	0.22864	47.78	8.84
mor425045067splNT045	76.926	0.21766	48.04	8.93
mor425045067splNT05	119.9	0.24438	47.88	9.82
con425051038049	30	0.18	41.30	10.26
con425051038049NT0025	32.336	0.18387	41.42	10.18
con425051038049NT005	34.724	0.18752	41.50	10.10
con425051038049NT0075	37.064	0.19062	41.59	10.03
con425051038049NT01	38.996	0.19295	41.65	9.97
con425051038049NF0025	30.756	0.18232	41.32	10.22
con425051038049NF005	31.558	0.18438	41.36	10.19
con425051038049NF0075	32.168	0.18606	41.37	10.16
con425051038049NF01	32.967	0.18755	41.41	10.13

Similarly, to the results of the bending test, the compression test results scarcely show a realistic situation. Although there is an increase in strength in most cases, this increase is hardly enough to present the realistic raise, which the nanofillers actually provide to the concrete matrix. Figures indicating the change of material behavior with the increase of the nanofiller may be observed within Appendix A2. Figure 6.4.2 shows the change of compressive and flexural strengths with the increase of the nanofiller for the simulated composite mixtures. The figures are divided between similar mixtures of cement, mortar, and concrete. It may be observed that the compressive strength is changed negligibly, with the increase maximum of 1 MPa, while the flexural strength decreases significantly for most of the mixtures, with the maximum decrease of about 4 MPa.

Compressive strength

Legend:
- cem425033NT
- cem42505NT
- cem42504NT

Flexural strength

Legend:
- cem425033NT
- cem42505NT
- cem42504NT

Nanofiller wt%

Compressive strength

Legend:
- mor42505033NT
- mor425055033NT
- mor42505033splNT
- mor425035033splNT
- mor425045033splNT
- con425051038049NT
- con425051038049NF

Nanofiller wt%

Flexural strength

Legend:
- mor42505033NT
- mor425055033NT
- mor42505033splNT
- mor425035033splNT
- mor425045033splNT
- con425051038049NT
- con425051038049NF

Nanofiller wt%

Compressive strength

Legend:
- cem52504NT
- mor42504850364NT
- mor425040263splNT
- mor425045067splNT

Nanofiller wt%

Flexural strength

Legend:
- cem52504NT
- mor42504850364NT
- mor425040263splNT
- mor425045067splNT

Nanofiller wt%

Figure 6.4.2 Change of compressive and flexural strength with the increase of the nanofiller wt%

5. Validation of the numerical models

Validation of the results obtained from numerical simulations is done by comparing them with the results obtained from the experimental works presented in [84,93,95,97,100,101,107,110,111,114,119]. Experimental research included less variations of the nanofiller weight fractions, hence, the validation is implemented for the total of 51 cementitious mixtures, including plain and nano-reinforced concrete. All observed experimental investigations included the specimens with the same geometry (40×40×160 mm) and the type of testing (3-point bending). All validation results are given in detail within Appendix A3. Figure 6.5.1 shows the progression of the compressive strength with the increase of the nanofiller weight fraction, obtained from experimental testing and numerical simulations, and the comparison between them. Figure 6.5.2 shows the outliers in the results of simulations of the compression test, where the increase of the compressive strength after adding the nanofiller surpasses 40% compared to the plain concrete specimen. Figure 6.5.3 shows specimens that expressed a difference in compressive strength higher than 20% between the experimental test and the simulation.
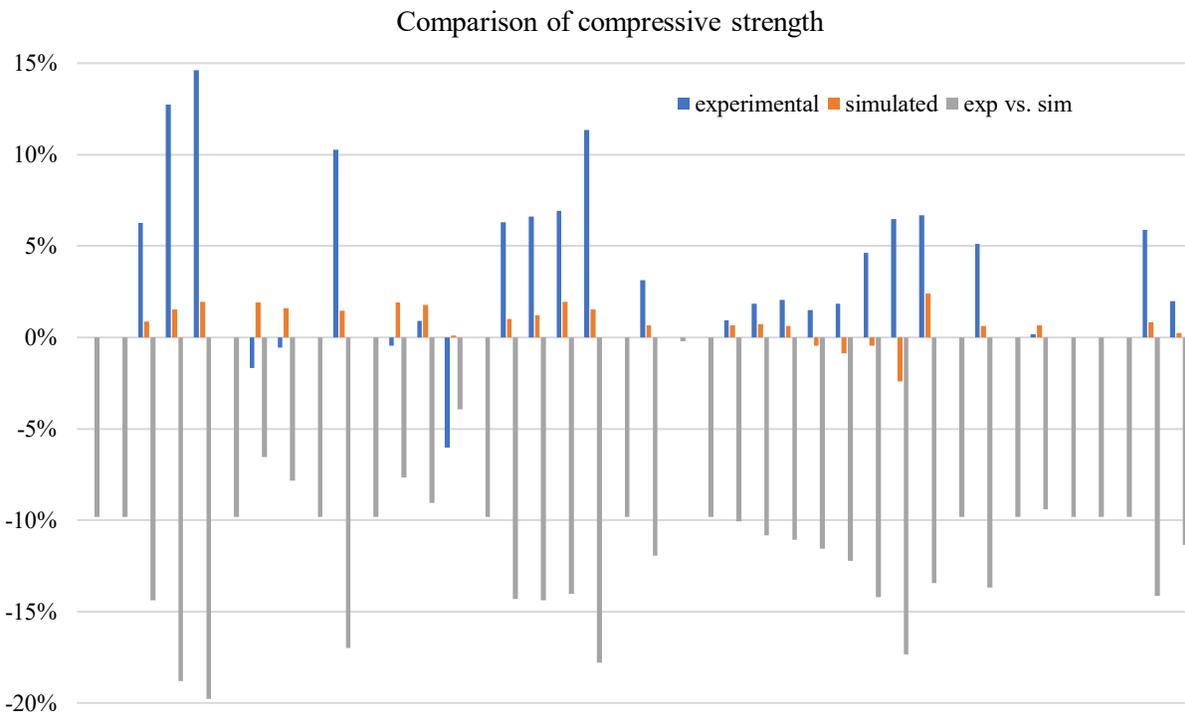
Figure 6.5.1 Histogram of the increase of compressive strength within testing, simulations, and the difference between testing and simulations
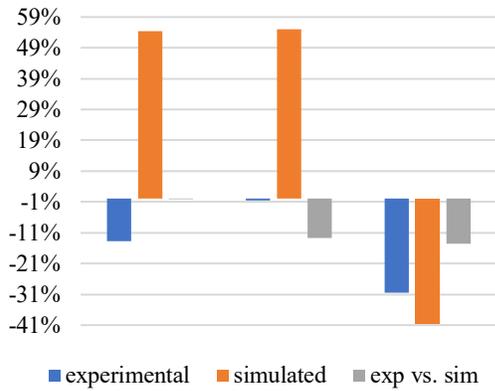
Figure 6.5.2 Specimens with significant change of compressive strength
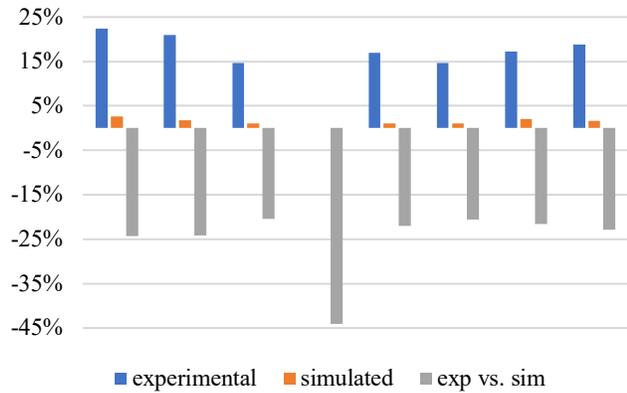
Figure 6.5.3 Specimens with significant change of compressive strength
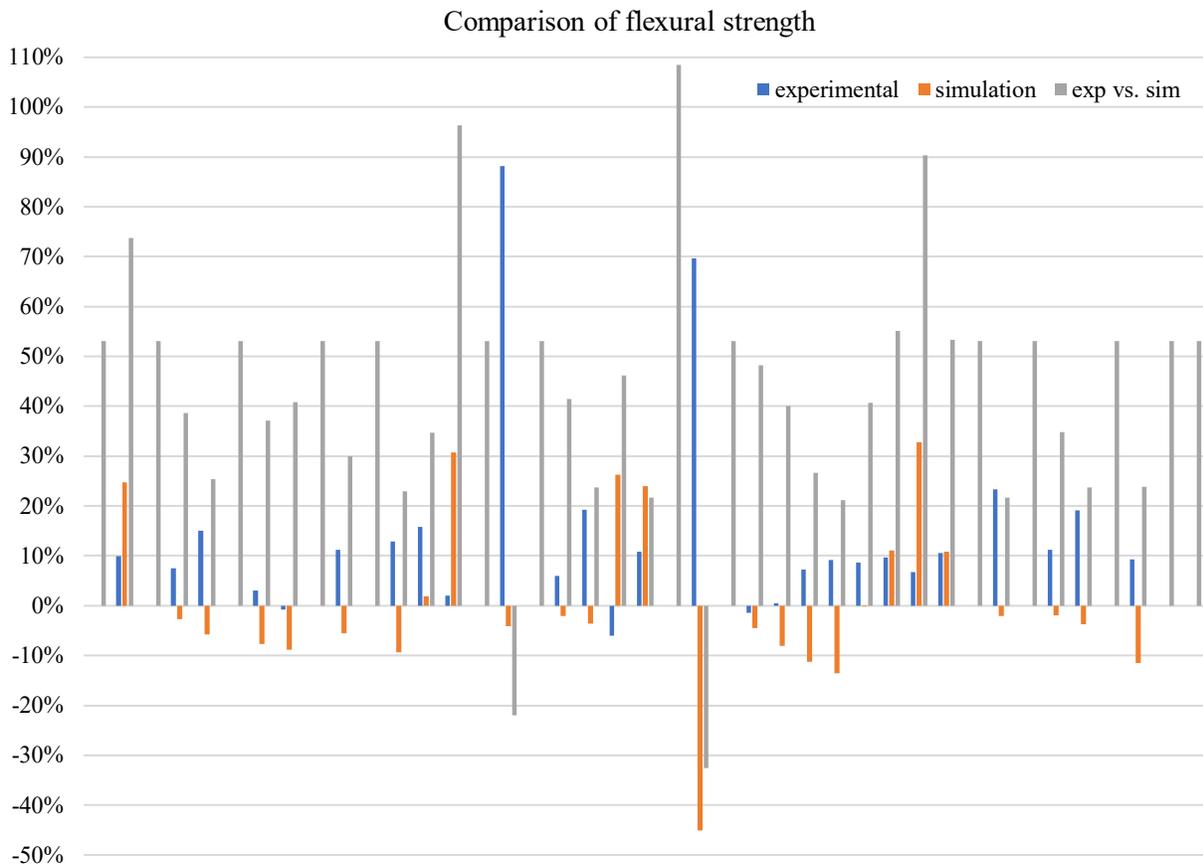
Figure 6.5.4 Histogram of the change of the flexural strength
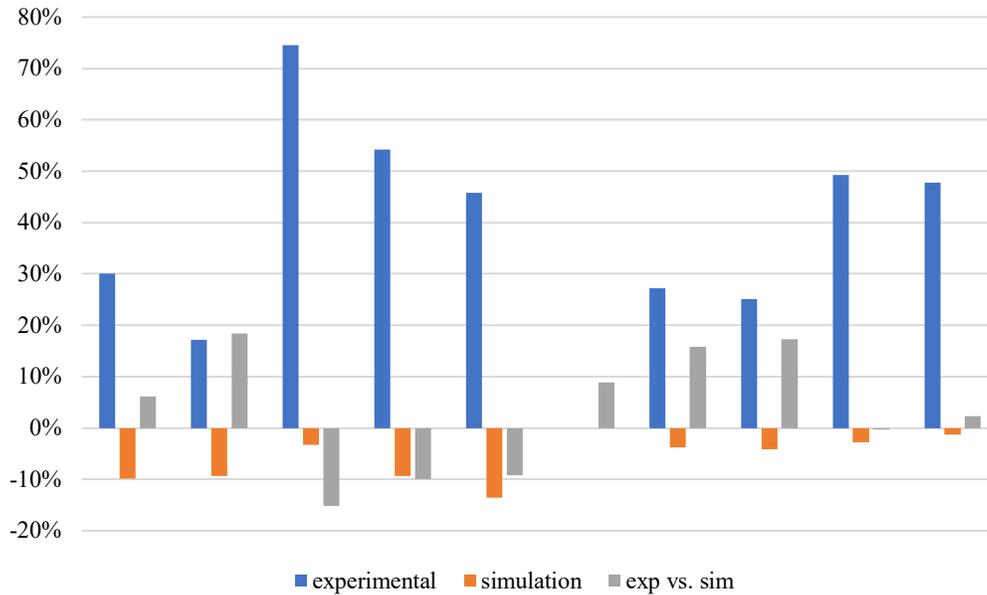
Figure 6.5.5 Experimental samples with significant increase of flexural strength

Figure 6.5.4 shows the progression of the flexural strength with the increase of the nanofiller weight fraction, obtained from the experimental testing, numerical simulations, and the comparison between the two. It may be observed that the difference between the experimental testing and the numerical simulations of the plain concrete mixtures and the nano-reinforced mixtures is much higher than for the compressive strength, going as high as around 110%. This occurrence is extraordinary, however, it cannot be considered possible. So far, there is no evidence that may show such a high increase of strength, regardless of the additional materials or the method of fabrication of the composite material. Hence, the flexural strength results from the simulations are not realistic and, therefore should not be considered acceptable. Figure 6.5.5 shows the increase of flexural strength after adding the nanofiller to the specimens produced experimentally. It may be observed that there are instances of very high increase in flexural strength (up to 75%) in laboratory conditions, however, it is considered as an outlier since the repeatability of these results is not achieved. Even though simulations may produce impressive material results equal to ultra-high performance concretes, we have to be aware of the actual capabilities of concrete as the insulating matrix, which comprehends more than 98% of the composite material. The flexural strength of 20 MPa is impressive but hardly possible to be achieved in a concrete without any macroscale reinforcement.

CHAPTER VII Artificial neural network models

Artificial neural network models are developed using the Neural Fitting (NF) tool within the Matlab R2020b, as well as using the script in the same software. Neural fitting tool is a predefined application used for creating neural networks and providing the initial training, validation, and testing. Datasets, architecture, network parameters, and results and behavior analysis of the developed networks are described within this chapter for the prescribed networks and the scripted models. The goal is to determine if the results obtained from experimental investigations and numerical simulations are applicable and if ANNs are a feasible option for predicting the optimal mix proportions of self-sensing concrete. ANN models are developed using datasets based on experimental investigations and numerical simulations, denominated as Group I and Group II, respectively. The models are built using the NF tool and the script directly. After testing the ANN models from each group, the results and behavior of the ANN models are compared to establish the viability of using the results of ANSYS simulations instead of the experimental testing results.

1. Datasets

Neural network models are based on the research findings, which are of two kinds. The first set of models (Group I) is based on the experimental investigations with results of bending, compression, and electrical testing, as described in Chapter V. The second set of models (Group II) is based on the numerical modeling and results of ANSYS simulations of homogenization, bending and compression tests, and is described in Chapter VI.

1.1. Empirically obtained data – Group I

Empirically obtained data refer to the experimental investigations described in detail in Chapter V. Total of 492 different mixtures have been fabricated in [84-119], out of which 207 were tested for flexural strength, 329 mixtures were tested for compressive strength, and 223 mixtures were tested for electrical conductivity, resistance, or resistivity. The results of compressive and flexural tests are taken as represented in the respective research works. The results of electrical testing are analytically transformed into volume resistivity, using eq. (7.1) in case the electrical conductivity was tested, and eq. (7.2) was used in the case that the electrical resistance was tested.

$$\rho = {}^1\!/_\sigma \qquad\qquad (7.1)$$

$$\rho = R \cdot l \qquad\qquad (7.2)$$

where ρ is electrical resistivity, σ is electrical conductivity, R is electrical resistance, and l is the distance between measuring probes.

After processing, Group I with four initial datasets is formed to give different output signals. Three datasets are formed to give a single output, namely, compressive strength (COMP), flexural strength (FLEX), and electrical resistivity (RESIST). The forth dataset is formed to give two output signals, namely, compressive and flexural strength (C+F), but was also tested with each output separately. Each dataset has a different number of data tuples, as well as different number of parameters, which represent the input neurons, as shown in Table 7.1. List of the input neurons for all datasets is shown in Table 7.2. Complete datasets are given in Appendix B1.

Table 7.4 Summary of datasets in Group I

Dataset	Designation	Data tuples	Input neurons	Output neurons	Minimum value of output	Maximum value of output
1	COMP	329	20	1	4,4 MPa	152 MPa
2	FLEX	207	16	1	2,18 MPa	16,4 MPa
3	RESIST	223	17	1	77,25 Ω·cm	7,7e+6 Ω·cm
4	COMP+FLEX	185	11	2	19,8 MPa/2,18 MPa	97,2 MPa/16,4 MPa

Table 7.5 Input neurons for each dataset in Group I and their minimum/maximum values

COMP		FLEX		RESIST		COMP+FLEX	
Neuron	Min/Max	Neuron	Min/Max	Neuron	Min/Max	Neuron	Min/Max
CEM	317,61/1875	CEM	317,61/1578,95	CEM	448/1875	CEM	317,61/1578,95
WAT	121,6/789,475	WAT	142/789,475	WAT	191/789,475	WAT	142/789,475
FA	0/1994,4	FA	0/1994,4	FA	0/1490,5	FA	0/1994,4
CA	0/1284	CA	0/1284	CA	0/902	CA	0/1284
SPL	0/27,27	SPL	0/27,27	SPL	0/14,0625	SPL	0/27,27
CNT	0/2	CNT	0/0,5	CNT	0/2	CNT	0/0,5
CNF	0/2,5	CNF	0/2	CNF	0/2,5	CNF	0/2
CEM-CLASS	42.5/52.5	CEM-CLASS	42.5/52.5	CEM-CLASS	42.5/52.5	CEM-CLASS	42.5/52.5
FUNCT	0/1 (no/yes)	FUNCT	0/1 (no/yes)	FUNCT	0/1 (no/yes)	FUNCT	0/1 (no/yes)
C_S-A	0/1 (no/yes)	C_S-A	0/1 (no/yes)	C_S-A	0/1 (no/yes)	DEM-AGE	24/48
C_S-B	0/1 (no/yes)	C_S-B	0/1 (no/yes)	C_S-B	0/1 (no/yes)	AGE	3/120

C_S-C	0/1 (no/yes)	C_S-C	0/1 (no/yes)	C_S-C	0/1 (no/yes)
C_S-D	0/1 (no/yes)	C_S-D	0/1 (no/yes)	C_S-D	0/1 (no/yes)
C_S-E	0/1 (no/yes)	C_S-E	0/1 (no/yes)	C_S-E	0/1 (no/yes)
C_S-F	0/1 (no/yes)	DEM-AGE	18/48	PROBE-DIS	1/12
C_S-G	0/1 (no/yes)	AGE	3/120	DEM-AGE	24/48
C_S-H	0/1 (no/yes)			AGE	3/28
C_S-I	0/1 (no/yes)				
DEM-AGE	24/48				
AGE	3/120				
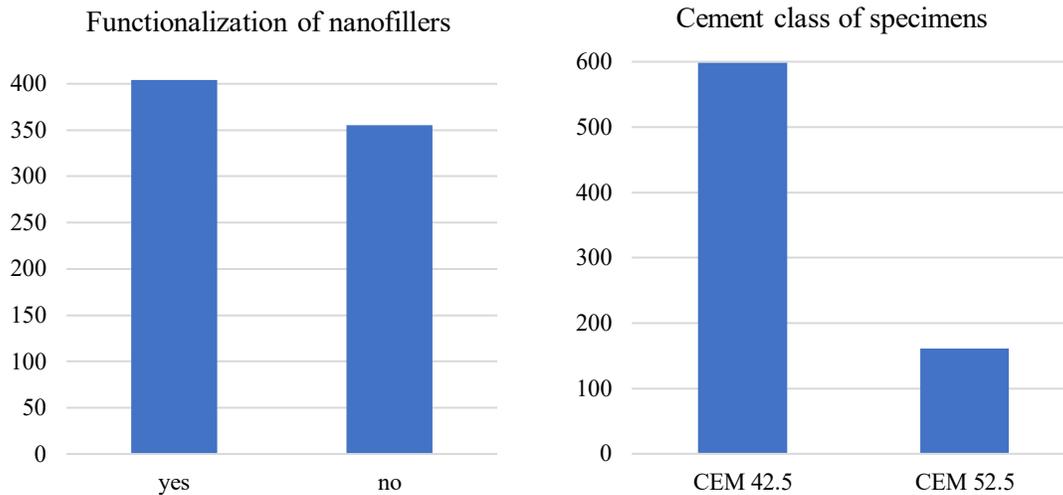
Figure 7.1.1 Histograms of functionalization of nanofillers and cement class
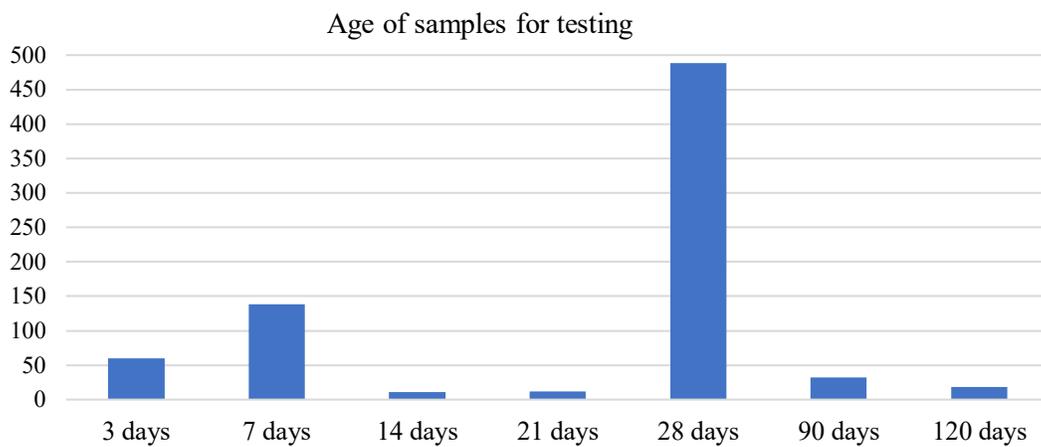
Figure 7.1.2 Histogram of the age of samples at day of testing
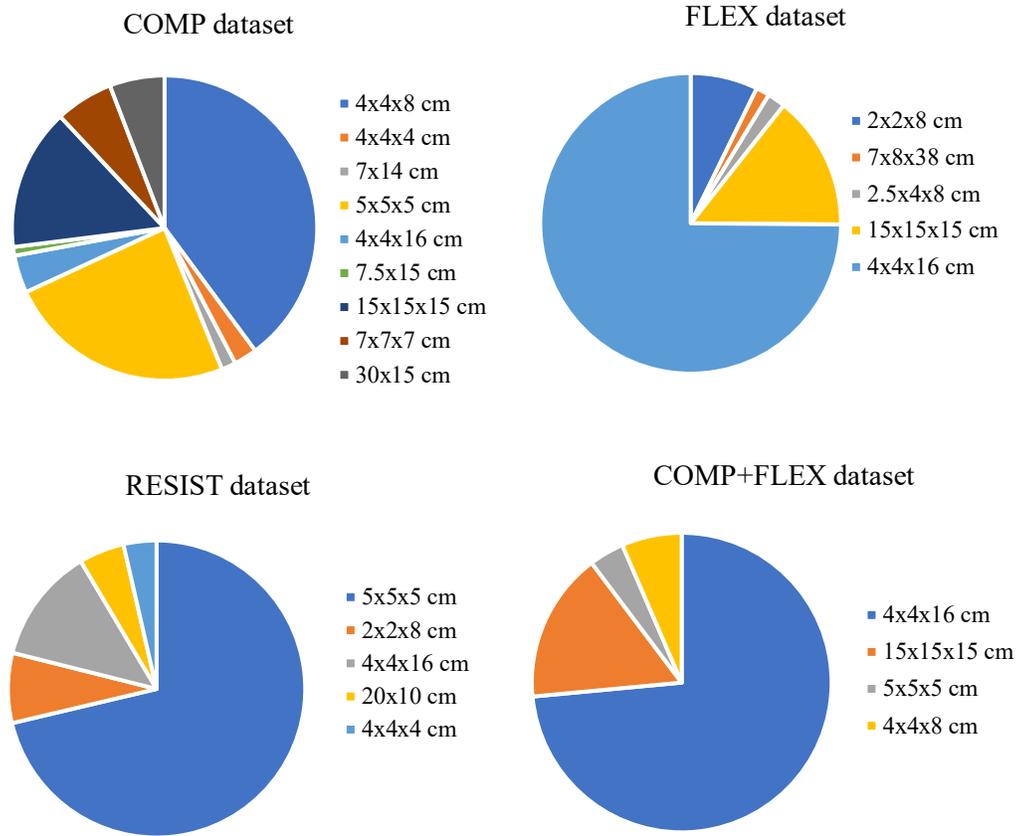
Figure 7.1.3 Cross-section geometry of samples for each dataset

Experimental investigations of CNT/CNF reinforced concrete with certain inconsistencies were ultimately rejected and exempt from the final datasets. Partial or complete results from 13 different investigations were rejected due to several reasons:

- unclear process of specimen fabrication [146,148];
- unstandardized geometry of the specimens [137,145];
- improper dispersion of the nanofillers (high threshold occurring) [138];
- pre-dispersed CNTs, giving only the weight fraction of the admixture [142];
- occurrence of decrease of mechanical properties after adding the nanofillers [139-141,143,144,149];
- hindering of electrical properties after adding the nanofillers [141];
- determining the tensile strength by a split tensile test [147].

1.2. Numerically obtained data – Group II

Results obtained from the numerical simulations, as it is described in detail within Chapter VI, were used for building the dataset in Group II. From the basis of 15 concrete mixture, 149 CNT or CNF reinforced mixtures were developed, making the total of 164 mixtures, which were included in the comprehensive dataset. All samples developed from these mixtures were simulated for compression and bending tests to obtain the compressive strength and the flexural strength, representing the output signals. The comprehensive dataset included 8 input neurons and two output neurons. Moreover, the dataset is also used with the separate output neurons to test the behavior of the ANN models under these conditions. All results are given in detail within Appendix A, and the dataset in its entirety is given in Appendix B2. List of input neurons and their minimum and maximum values before the normalization is shown in Table 7.3.

Table 7.3 Input neurons for the dataset in Group II and their minimum/maximum values

Neuron	CEM	WAT	FA	CA	SPL	CNT	CNF	CCLASS
Min/Max	317,61/1578,95	158,81/789,48	0/1994,4	0/775,2	0/7.9776	0/0,5	0/2	42.5/52.5

Input neurons do not include the geometry of the specimen because all specimens have the same geometry, 40×40×40 mm and 40×40×160 mm for compression and flexural tests, respectively. The age of the specimen is excluded because the specimens, which were used for the material library, are tested for the 28-day compressive and bending strength. Finally, the demolding age is also excluded, as it is redundant. Functionalization is not taken into account since the "ideal" nanofiller material was used for the homogenization in the Material Designer.

2. Architecture of the artificial neural network models

Architecture of artificial neural networks includes the number of layers and the number of neurons in each layer, as well as the algorithm type and the activation function. In this work, all neural network models have matching learning parameters to provide a proper comparison of models within both groups and establish if numerical simulations represent an efficient method for determining the properties of CNT/CNF concrete composite materials. By fixing the learning parameters while varying only the number of the hidden neurons and the subsets size, it should be possible to establish which type of architecture presents the best fit for each group and subgroup of models. Each group of models uses their respective datasets depending on the output variable, according to Table 7.4 and Table 7.5.

2.1. Prescribed (NF tool) models

Total number of layers in all ANN models is three, including the input, one hidden, and the output layer. This type of architecture is called the "shallow" network, and it is commonly used for relatively small datasets in regards to the number of input neurons and data tuples. Number of hidden neurons is connected to the number of neurons in the input layers. This work uses two dependencies given in the literature, as shown in eq. (7.3) and eq. (7.4), and proposes an additional dependence, given in eq. (7.5) to test and observe the behavior of the models. Table 7.4 shows parameters regarding the architecture of neural network models in group I and Table 7.5 shows the network models' parameters in group II.

$$N_h = N_i \tag{7.3}$$

$$N_h = 2 \cdot N_i + 1 \tag{7.4}$$

$$N_h = 3 \cdot N_i \tag{7.5}$$

where N_h is the number of hidden neurons, and N_i is the number of input neurons.

Table 7.4 Architecture of the models in Group I

#	Model	Dataset	Input neurons	Hidden neurons	Output neurons	Training % (#)	Validation % (#)	Testing % (#)
1	COMP_NN70_10_20-20	COMP	20	20	1	70% (230)	10% (33)	20% (66)
2	COMP_NN70_10_20-41	COMP	20	41	1	70% (230)	10% (33)	20% (66)
3	COMP_NN70_10_20-60	COMP	20	60	1	70% (230)	10% (33)	20% (66)
4	COMP_NN80_10_10-20	COMP	20	20	1	80% (263)	10% (33)	10% (33)
5	COMP_NN80_10_10-41	COMP	20	41	1	80% (263)	10% (33)	10% (33)
6	COMP_NN80_10_10-60	COMP	20	60	1	80% (263)	10% (33)	10% (33)
7	COMP_NN80_5_15-20	COMP	20	20	1	80% (264)	5% (16)	15% (49)
8	COMP_NN80_5_15-41	COMP	20	41	1	80% (264)	5% (16)	15% (49)
9	COMP_NN80_5_15-60	COMP	20	60	1	80% (264)	5% (16)	15% (49)

#	Model		Input neurons	Hidden neurons	Output neurons	Training % (#)	Validation % (#)	Testing % (#)
10	COMP_NN85_5_10-20	COMP	20	20	1	85% (280)	5% (16)	10% (33)
11	COMP_NN85_5_10-41	COMP	20	41	1	85% (280)	5% (16)	10% (33)
12	COMP_NN85_5_10-60	COMP	20	60	1	85% (280)	5% (16)	10% (33)
13	FLEX_NN70_10_20-16	FLEX	16	16	1	70% (145)	10% (21)	20% (41)
14	FLEX_NN70_10_20-33	FLEX	16	22	1	70% (145)	10% (21)	20% (41)
15	FLEX_NN70_10_20-48	FLEX	16	48	1	70% (145)	10% (21)	20% (41)
16	FLEX_NN80_10_10-16	FLEX	16	16	1	80% (165)	10% (21)	10% (21)
17	FLEX_NN80_10_10-33	FLEX	16	22	1	80% (165)	10% (21)	10% (21)
18	FLEX_NN80_10_10-48	FLEX	16	48	1	80% (165)	10% (21)	10% (21)
19	FLEX_NN80_5_15-16	FLEX	16	16	1	80% (166)	5% (10)	15% (31)
20	FLEX_NN80_5_15-33	FLEX	16	22	1	80% (166)	5% (10)	15% (31)
21	FLEX_NN80_5_15-48	FLEX	16	48	1	80% (166)	5% (10)	15% (31)
22	FLEX_NN85_5_10-16	FLEX	16	16	1	85% (176)	5% (10)	10% (21)
23	FLEX_NN85_5_10-33	FLEX	16	22	1	85% (176)	5% (10)	10% (21)
24	FLEX_NN85_5_10-48	FLEX	16	48	1	85% (176)	5% (10)	10% (21)
25	RES_NN70_10_20-17	RESIST	17	17	1	70% (156)	10% (22)	20% (45)
26	RES_NN70_10_20-35	RESIST	17	35	1	70% (156)	10% (22)	20% (45)
27	RES_NN70_10_20-51	RESIST	17	51	1	70% (156)	10% (22)	20% (45)
28	RES_NN80_10_10-17	RESIST	17	17	1	80% (179)	10% (22)	10% (22)
29	RES_NN80_10_10-35	RESIST	17	35	1	80% (179)	10% (22)	10% (22)
30	RES_NN80_10_10-51	RESIST	17	51	1	80% (179)	10% (22)	10% (22)
31	RES_NN80_5_15-17	RESIST	17	17	1	80% (179)	5% (11)	15% (33)
32	RES_NN80_5_15-35	RESIST	17	35	1	80% (179)	5% (11)	15% (33)
33	RES_NN80_5_15-51	RESIST	17	51	1	80% (179)	5% (11)	15% (33)
34	RES_NN85_5_10-17	RESIST	17	17	1	85% (190)	5% (11)	10% (22)
35	RES_NN85_5_10-35	RESIST	17	35	1	85% (190)	5% (11)	10% (22)
36	RES_NN85_5_10-51	RESIST	17	51	1	85% (190)	5% (11)	10% (22)
37	C+F_NN70_10_20-11	C+F	11	11	2	70% (129)	10% (19)	20% (37)
38	C+F_NN70_10_20-23	C+F	11	23	2	70% (129)	10% (19)	20% (37)
39	C+F_NN70_10_20-33	C+F	11	33	2	70% (129)	10% (19)	20% (37)
40	C+F_NN80_10_10-11	C+F	11	11	2	80% (147)	10% (19)	10% (19)
41	C+F_NN80_10_10-23	C+F	11	23	2	80% (147)	10% (19)	10% (19)
42	C+F_NN80_10_10-33	C+F	11	33	2	80% (147)	10% (19)	10% (19)
43	C+F_NN80_5_15-11	C+F	11	11	2	80% (147)	5% (9)	15% (28)
44	C+F_NN80_5_15-23	C+F	11	23	2	80% (147)	5% (9)	15% (28)
45	C+F_NN80_5_15-33	C+F	11	33	2	80% (147)	5% (9)	15% (28)
46	C+F_NN85_5_10-11	C+F	11	11	2	85% (157)	5% (9)	10% (19)
47	C+F_NN85_5_10-23	C+F	11	23	2	85% (157)	5% (9)	10% (19)
48	C+F_NN85_5_10-33	C+F	11	33	2	85% (157)	5% (9)	10% (19)

Table 7.5 Architecture of the models in Group II

#	Model	Input neurons	Hidden neurons	Output neurons	Training % (#)	Validation % (#)	Testing % (#)
1	S_C+F_70_10_20-8	8	8	2	70% (115)	10% (16)	20% (33)
2	S_C+F_70_10_20-17	8	17	2	70% (115)	10% (16)	20% (33)
3	S_C+F_70_10_20-24	8	24	2	70% (115)	10% (16)	20% (33)
4	S_C+F_80_10_10-8	8	8	2	80% (130)	10% (17)	10% (17)
5	S_C+F_80_10_10-17	8	17	2	80% (130)	10% (17)	10% (17)
6	S_C+F_80_10_10-24	8	24	2	80% (130)	10% (17)	10% (17)
7	S_C+F_80_5_15-8	8	8	2	80% (130)	5% (8)	15% (26)
8	S_C+F_80_5_15-17	8	17	2	80% (130)	5% (8)	15% (26)
9	S_C+F_80_5_15-24	8	24	2	80% (130)	5% (8)	15% (26)

10	S_C+F_85_5_10-8	8	8	2	85% (139)	5% (8)	10% (17)
11	S_C+F_85_5_10-17	8	17	2	85% (139)	5% (8)	10% (17)
12	S_C+F_85_5_10-24	8	24	2	85% (139)	5% (8)	10% (17)
13	S_C+F(C)_70_10_20-8	8	8	1	70% (115)	10% (16)	20% (33)
14	S_C+F(C)_70_10_20-17	8	17	1	70% (115)	10% (16)	20% (33)
15	S_C+F(C)_70_10_20-24	8	8	1	70% (115)	10% (16)	20% (33)
16	S_C+F(C)_80_10_10-8	8	17	1	80% (130)	10% (17)	10% (17)
17	S_C+F(C)_80_10_10-17	8	24	1	80% (130)	10% (17)	10% (17)
18	S_C+F(C)_80_10_10-24	8	8	1	80% (130)	10% (17)	10% (17)
19	S_C+F(C)_80_5_15-8	8	17	1	80% (130)	5% (8)	15% (26)
20	S_C+F(C)_80_5_15-17	8	24	1	80% (130)	5% (8)	15% (26)
21	S_C+F(C)_80_5_15-24	8	8	1	80% (130)	5% (8)	15% (26)
22	S_C+F(C)_85_5_10-8	8	17	1	85% (139)	5% (8)	10% (17)
23	S_C+F(C)_85_5_10-17	8	24	1	85% (139)	5% (8)	10% (17)
24	S_C+F(C)_85_5_10-24	8	8	1	85% (139)	5% (8)	10% (17)
25	S_C+F(F)_70_10_20-8	8	8	1	70% (115)	10% (16)	20% (33)
26	S_C+F(F)_70_10_20-17	8	17	1	70% (115)	10% (16)	20% (33)
27	S_C+F(F)_70_10_20-24	8	24	1	70% (115)	10% (16)	20% (33)
28	S_C+F(F)_80_10_10-8	8	8	1	80% (130)	10% (17)	10% (17)
29	S_C+F(F)_80_10_10-17	8	17	1	80% (130)	10% (17)	10% (17)
30	S_C+F(F)_80_10_10-24	8	24	1	80% (130)	10% (17)	10% (17)
31	S_C+F(F)_80_5_15-8	8	8	1	80% (130)	5% (8)	15% (26)
32	S_C+F(F)_80_5_15-17	8	17	1	80% (130)	5% (8)	15% (26)
33	S_C+F(F)_80_5_15-24	8	24	1	80% (130)	5% (8)	15% (26)
34	S_C+F(F)_85_5_10-8	8	8	1	85% (139)	5% (8)	10% (17)
35	S_C+F(F)_85_5_10-17	8	17	1	85% (139)	5% (8)	10% (17)
36	S_C+F(F)_85_5_10-24	8	24	1	85% (139)	5% (8)	10% (17)

2.2. Scripted models

Neural network models are developed additionally by direct manual scripting in Matlab R2020b. This way, more options are available in terms of architecture and the process of training and optimization. Complete scripts are given in Appendix B4. All ANN models are initially trained using 80% of the entire dataset, which is applied only for training and validation. The validation is used at this point to halt the training process, and the training/validation subsets are set to the ratio of 85/15 for the initial and optimization stage. After the initial training, the topology is optimized by iterating the number of neurons in the hidden layer from one to $3 \cdot Ni$, respectively. Optimization of the initial model serves to establish the optimal number of neurons in the hidden layer. Improved topology of the network implies better generalization and contributes to the stability of the network. The optimization is indicated via the level and the change of the mean squared error for the varying number of neurons in the hidden layer [150]. Then, two values are chosen to be tested further based on the optimization results. These two models are tested with the rest 20% of the dataset, and based on the results of the testing, a single topology is chosen as the

final working model. The final working ANN model is then trained using the complete dataset and without any validation or testing subsets. It means that the training continues until the minimum training gradient of 10e-7 is reached. If the gradient is not reached as the training reaches a thousand iterations, it is immediately halted.

Number of input and output neurons are the same as given in Table 7.4 and Table 7.5. During the initial stage, the number of hidden neurons equals the number of input neurons. Later, it is adjusted based on the results of the optimization and testing. Another difference from the predefined NF tool models is that some subsets could be omitted in different stages of model development. Therefore, during the initial stage, only training and validation sets are used, only training and validation sets are used during the initial stage. Then, the testing is performed separately, using the rest 20% of the full dataset. Lastly, the final working model uses the entire dataset only for training, meaning that its training is not limited by the cross-validation but rather with the number of iterations, which is set to 1000, or minimal gradient, as it was previously mentioned.

3. Training, validation, and testing

Algorithm used for the training of all ANN models is the back-propagation feed-forward algorithm. It is a gradient descent technique that minimizes error for a particular training pattern by incrementally adjusting the connection weights throughout the training cycles. A cycle consists of two stages, the feed-forward stage, and the back-propagation stage. The former represents computing the input data toward hidden layers from where the total weighed sum passes through the activation function and gives the activation value to the output layer. Then, the latter stage starts, and the obtained error is passed backwards from the output to the input layer with the adjustment of the weights. The cycle repeats until the level of error is acceptable. The learning parameters of all neural network models in this work are as follows:

➢ Uni-polar sigmoid activation function, with linear transfer function;
➢ Levenberg-Marquardt training algorithm;
➢ Shallow architecture (1 hidden layer);
➢ Maximum number of epoch: 1000;
➢ Training momentum: 10e+9;
➢ Learning rate: 10e-6;

➢ Minimum gradient: 10e-7;

➢ Number of cross-validation checks: 6.

Levenberg-Marquardt algorithm is relatively fast for moderately sized datasets with up to a few hundred data tuples. The ultimate goal of any training procedure is to minimize the mean squared error (MSE), root mean squared error (RMSE), and mean absolute error (MAE) and maximize the regression coefficient R. In case of a perfect fit between the output and a target value, this value of R would be equal to 1. Vis-à-vis, the value of error tends toward zero with the increase of network accuracy. Network performance can be observed after the validation check has completed and converged, so the number of iterations within each epoch shows how many cycles the network experienced before converging. The error histogram is a useful tool for observations of the distribution of errors for each stage of development. The optimal error distribution shows Gaussian zero-centered curve.

4. Evaluation and sensitivity analysis

Evaluation of ANNs is provided for the models developed using NF tool, which have shown the best behavior. Datasets are randomly divided into two subsets according to the ratio of 80/20, using 80% of the respective set for repeated training and subsequent testing using the rest 20% of the set. Evaluation datasets are shown in Appendix B3. In this work, evaluation is done only if a model obtained a regression coefficient of 0.8 or higher. Results lower than R=0.8 are considered to be unsatisfactory, and further revisions are made to determine the source of this occurrence.

Sensitivity analysis serves to show the absolute or the relative contribution of each input parameter to the output value, and it is very useful for understanding the relationship of the input parameters [151]. The sensitivity analysis may also influence the topology of the final working model because it may show that some parameters could impair or slow down the learning process. On the other hand, it shows which parameters are crucial, as well as the dependency of the output on each input parameter. There are many methods of performing the sensitivity analysis. This work uses the weights method, otherwise known as the Garson's algorithm [152]. The algorithm is specifically created for supervised neural networks with a single output to describe the relative importance of the input parameters by deconstructing the model weights. The analytical description for a network with a single hidden layer is as follows:

$$D_{ij} = \frac{|W_{ij}|}{\sum_{i=1}^{n_i} |W_{ij}|} \tag{7.6}$$

$$RC_i = \frac{\sum_{j=1}^{n_j} D_{ij}}{\sum_{j=1}^{n_j} \sum_{i=1}^{n_i} D_{ij}} \tag{7.7}$$

Where n_i and n_j are numbers of input and hidden neurons, respectively; W_{ij} is weight corresponding to i-th input and j-th hidden neuron; and RC_i represents the relative importance of i-th input.

5. Response and analysis

5.1. Prescribed models – Group I

Responses of the prescribed ANN models developed using the NF tool are given in Table 7.6 and shown in Figures 7.5.1-7.5.16. Detailed results are given in Appendix B5.

Table 7.6 Response values of the models in Group I

#	Model	Regression coefficient R	Mean squared error MSE	Epoch
1	COMP_NN70_10_20-20	0.95267	0.00195	11
2	**COMP_NN70_10_20-41**	**0.9688**	**0.00107**	**10**
3	COMP_NN70_10_20-60	0.96502	0.00151	11
4	COMP_NN80_10_10-20	0.96367	0.000979	12
5	COMP_NN80_10_10-41	0.98091	0.000766	23
6	**COMP_NN80_10_10-60**	**0.9791**	**0.000415**	**29**
7	**COMP_NN80_5_15-20**	**0.98256**	**0.000391**	**32**
8	COMP_NN80_5_15-41	0.93784	0.00367	8
9	COMP_NN80_5_15-60	0.96813	0.001488	9
10	COMP_NN85_5_10-20	0.97202	0.001193	27
11	**COMP_NN85_5_10-41**	**0.97858**	**0.000681**	**24**
12	COMP_NN85_5_10-60	0.97274	0.001157	11
13	FLEX_NN70_10_20-16	0.91543	0.005345	15
14	FLEX_NN70_10_20-33	0.89097	0.007012	9
15	**FLEX_NN70_10_20-48**	**0.92254**	**0.001995**	**24**
16	FLEX_NN80_10_10-16	0.87775	0.00877	9
17	FLEX_NN80_10_10-33	0.89732	0.00707	9
18	**FLEX_NN80_10_10-48**	**0.90198**	**0.00396**	**23**
19	**FLEX_NN80_5_15-16**	**0.92508**	**0.005**	**20**
20	FLEX_NN80_5_15-33	0.86375	0.008407	8
21	FLEX_NN80_5_15-48	0.87383	0.005773	10
22	**FLEX_NN85_5_10-16**	**0.94388**	**0.00378**	**32**
23	FLEX_NN85_5_10-33	0.93602	0.00461	18
24	FLEX_NN85_5_10-48	0.91121	0.00533	10
25	RES_NN70_10_20-17	0.56728	0.00438	14
26	RES_NN70_10_20-35	0.51622	0.003813	11
27	RES_NN70_10_20-51	0.45509	0.003968	9
28	RES_NN80_10_10-17	0.40192	0.000222	9

29	RES_NN80_10_10-35	0.28895	0.0000537	12
30	RES_NN80_10_10-51	0.68019	0.00183	23
31	RES_NN80_5_15-17	0.41224	0.0000197	10
32	RES_NN80_5_15-35	0.52067	0.003419	11
33	RES_NN80_5_15-51	0.50021	0.00331	8
34	RES_NN85_5_10-17	0.54735	0.00361	10
35	RES_NN85_5_10-35	0.56962	0.003601	11
36	RES_NN85_5_10-51	0.60146	0.0031	11
37	C+F_NN70_10_20-11	0.86913	0.009495	10
38	C+F_NN70_10_20-23	0.90129	0.0076	12
39	**C+F_NN70_10_20-33**	**0.88072**	**0.004027**	**18**
40	**C+F_NN80_10_10-11**	**0.93468**	**0.003361**	**27**
41	C+F_NN80_10_10-23	0.95102	0.003566	21
42	C+F_NN80_10_10-33	0.83489	0.005389	16
43	**C+F_NN80_5_15-11**	**0.94066**	**0.005587**	**19**
44	C+F_NN80_5_15-23	0.93937	0.00511	16
45	C+F_NN80_5_15-33	0.95118	0.004076	12
46	C+F_NN85_5_10-11	0.83851	0.01363	10
47	C+F_NN85_5_10-23	0.88078	0.008397	10
48	**C+F_NN85_5_10-33**	**0.90683**	**0.00636**	**10**
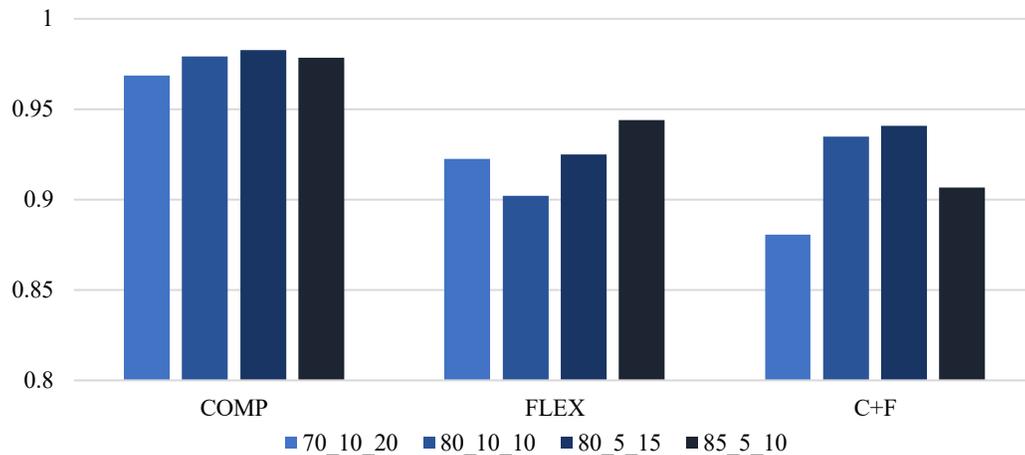
Figure 7.5.1 Regression coefficients for COMP, FLEX, and COMP+FLEX models (Group I)

103
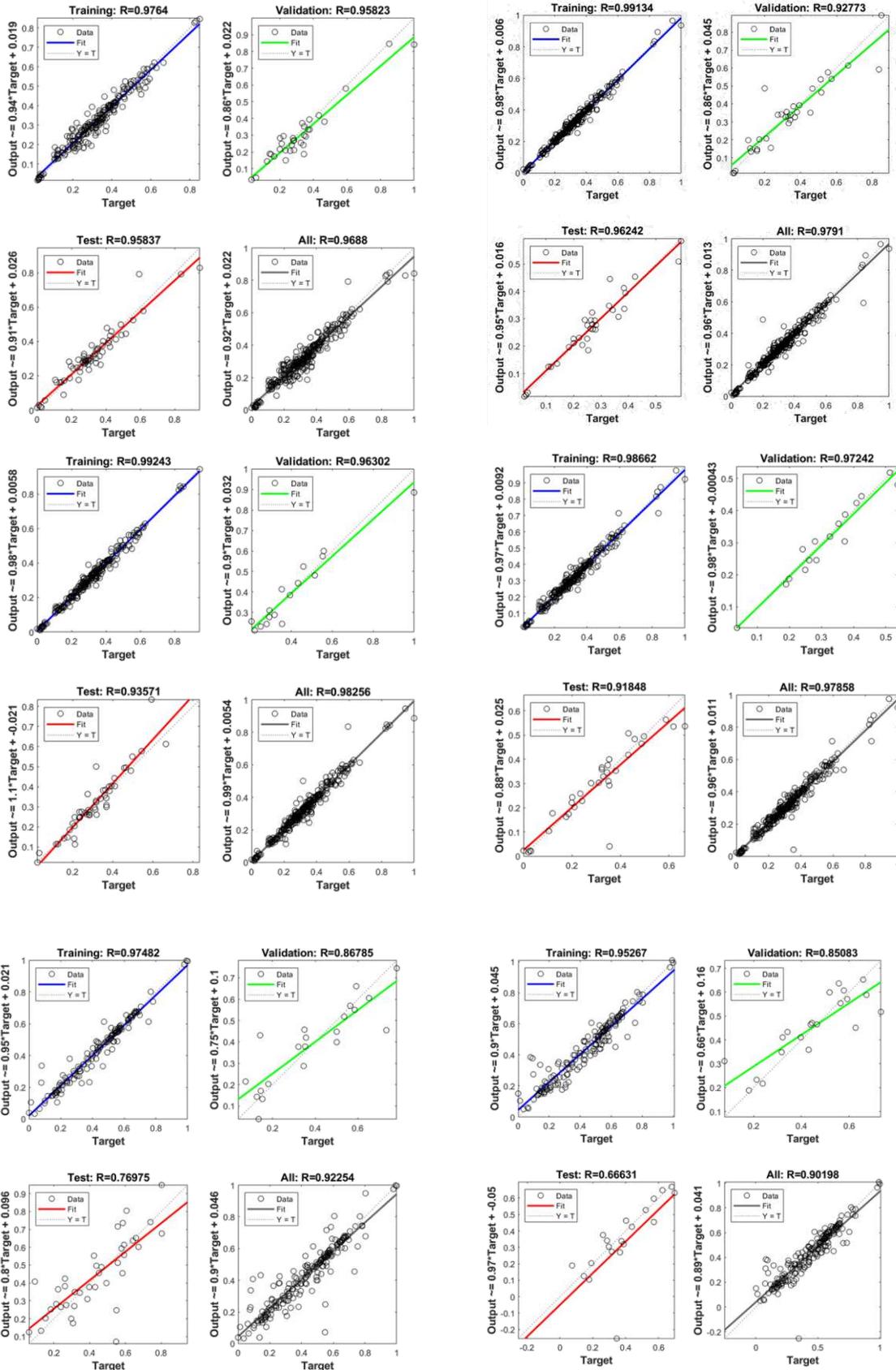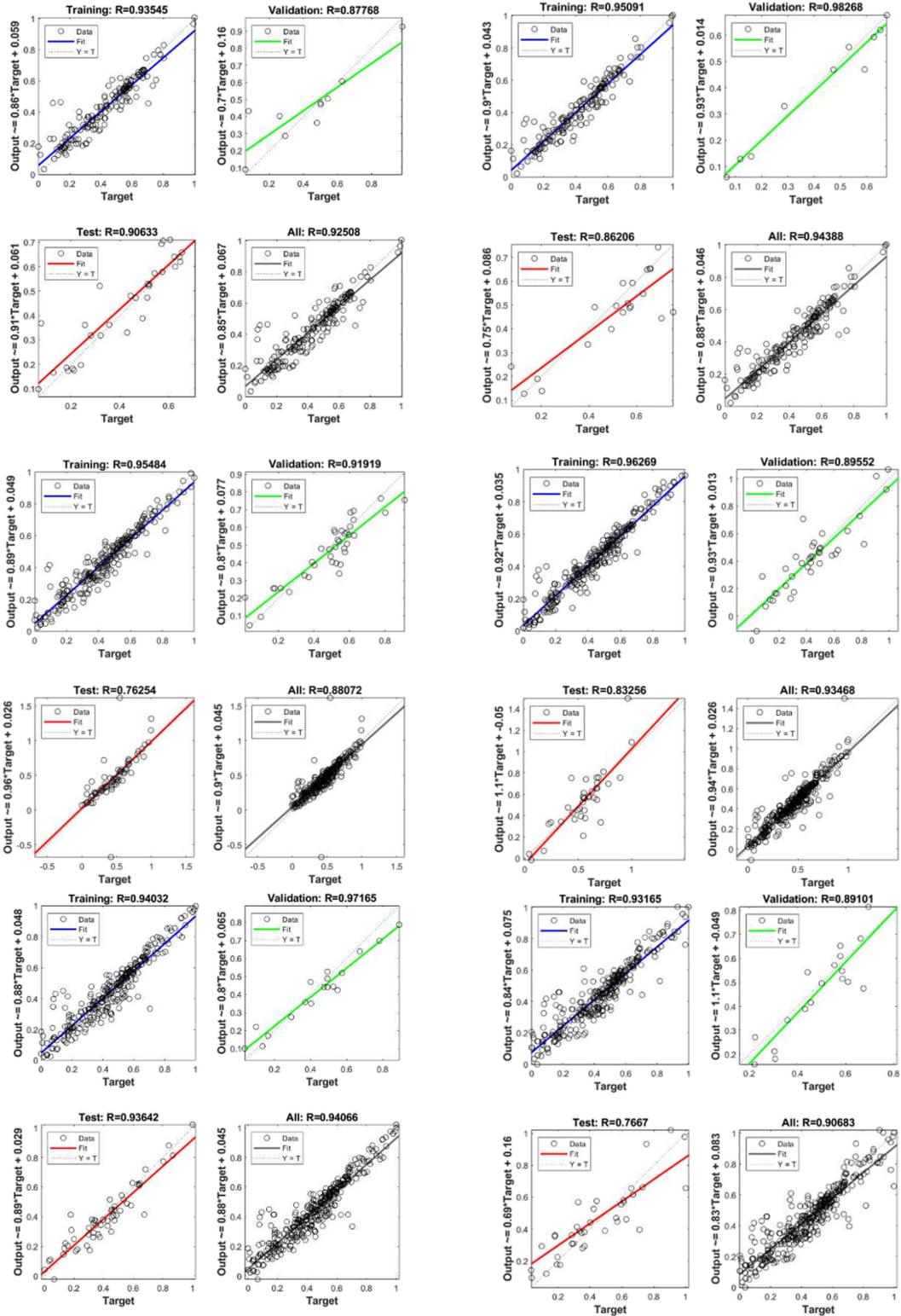
Figure 7.5.2 Regression for model: a) COMP_NN70_10_20-41; b) COMP_NN80_10_10-60; c) COMP_NN80_5_15-20; d) COMP_NN85_5_10-41; e) FLEX_NN70_10_20-48; f) FLEX_NN80_10_10-48; g) FLEX_NN80_5_15-16; h) FLEX_NN85_5_10-16; i) C+F_NN70_10_20-33; j) C+F_NN80_10_10-11; k) C+F_NN80_5_15-11; l) C+F_NN85_5_10-33.

Models in bold within Table 7.6 present the best within each subgroup. As shown in Figure 7.5.1, the total regression coefficients for these models are comparable, so the models will be further evaluated, i.e., checked if the expressed behavior is valid or the obtained results could be falsely positive, and the optimal model within each group will be established. Figures 7.5.2-7.5.13 show regression coefficients for training, validation, testing, and total for models with the best results within each subgroup of every dataset from group I. Graphs showing the R value and error for all models are given in Appendix B5. Models from COMP, FLEX and COMP+FLEX dataset gave satisfactory results with the regression coefficient values higher than 0.8. Error histograms of these models are shown in Figures 7.5.14-7.5.25. The figures show that the most regular distribution is obtained when the number of hidden neurons equals the number of input neurons, as for the models FLEX_NN80_5_15-16 and C+F_NN80_5_15-11. Other occurrence shows that the model COMP_NN70_10_20-41, which has *Nh=2Ni+1*, exhibits the best behavior within its subgroup. Nevertheless, models with *Nh=3Ni* also showed comparable behavior to other models. The models presented in the figures have been evaluated to establish the truthfulness of these results.
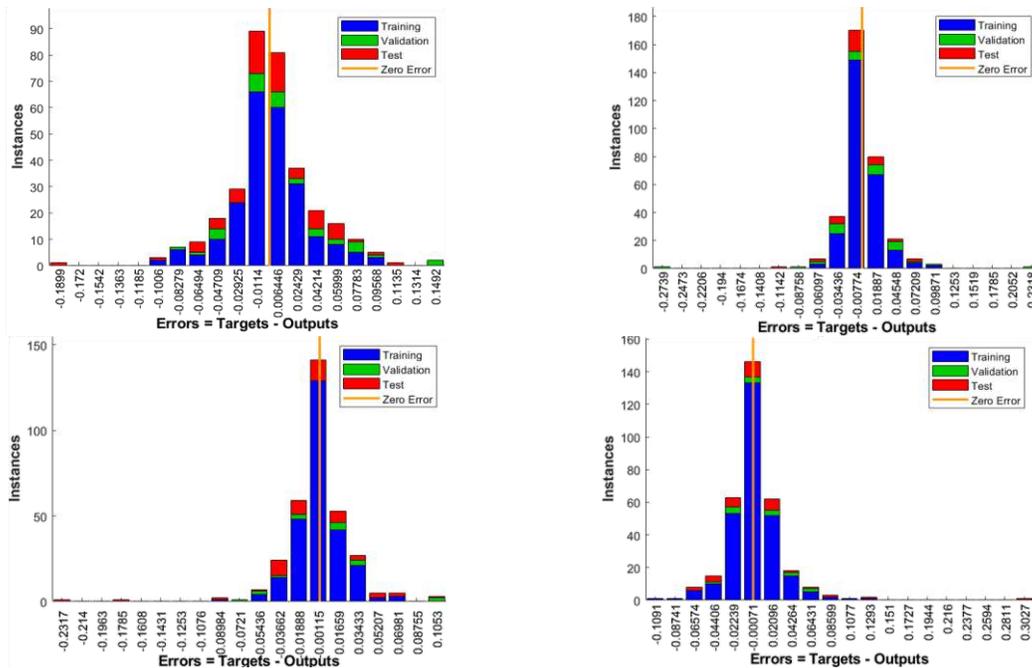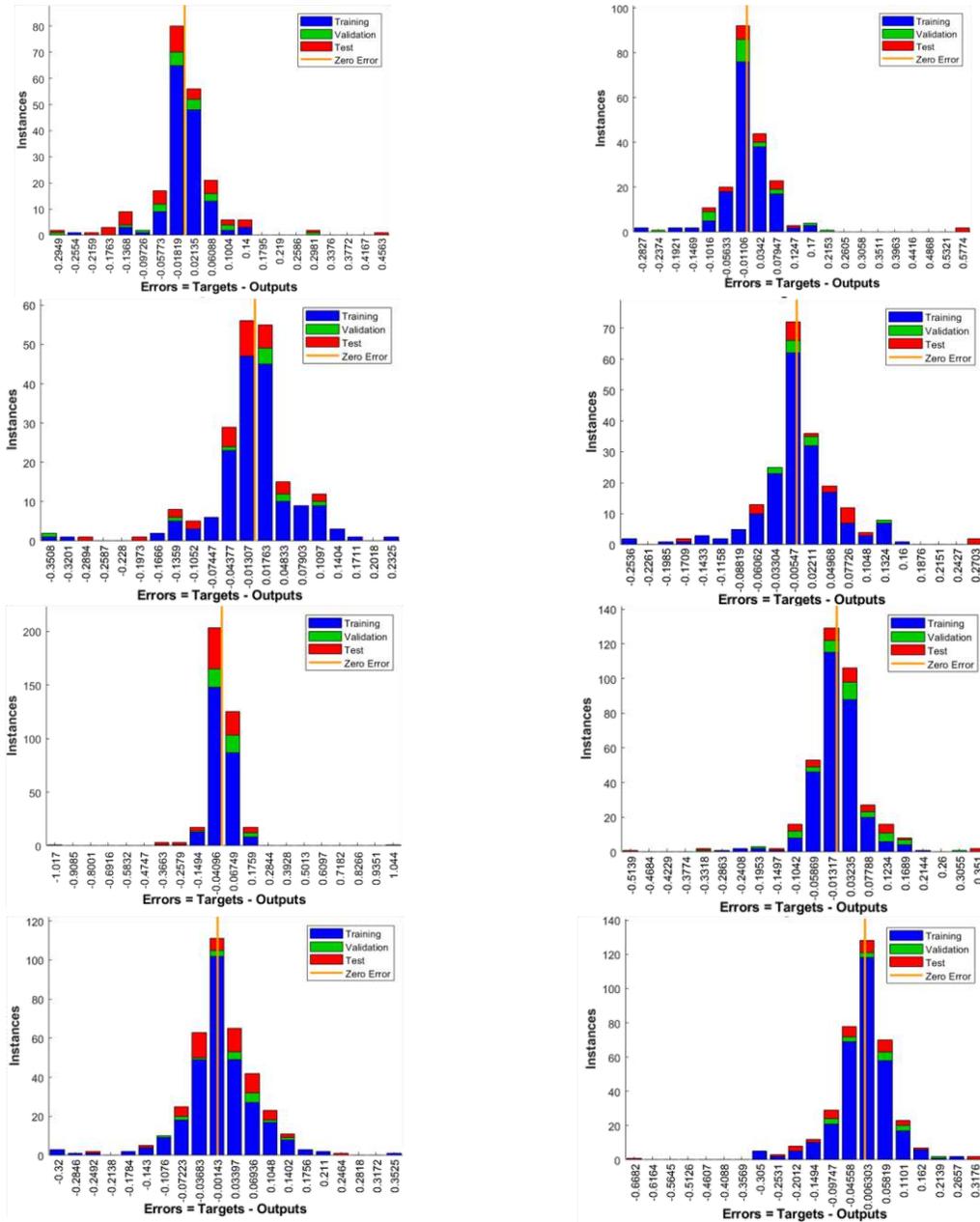
Figure 7.5.3 Error for model: a) COMP_NN70_10_20-41; b) COMP_NN80_10_10-60; c) COMP_NN80_5_15-20; d) COMP_NN85_5_10-41; e) FLEX_NN70_10_20-48; f) FLEX_NN80_10_10-48; g) FLEX_NN80_5_15-16; h) FLEX_NN85_5_10-16; i) C+F_NN70_10_20-33; j) C+F_NN80_10_10-11; k) C+F_NN80_5_15-11; l) C+F_NN85_5_10-33

The models from the RESIST dataset gave the regression coefficient values much lower than the expected 0.8 limit, which is deemed unsatisfactory in this work. Regression coefficients for the best models in this group are shown in Figure 7.5.4 and Figure 7.5.5. Further investigation is made to try to establish the source of this behavior. In that goal, the RESIST dataset was revised. The results of the volume electrical resistivity, which showed that the percolation threshold is not

reached, have been omitted from the dataset with the assumption that the training of the networks was unsuccessful because of the incoherent behavior of samples. In addition, the results, which showed relatively higher resistivity for higher weight fraction of the nanofiller compared to other samples within the same sample group, were rejected as outliers. The revised RESIST dataset is given in Appendix B1. Furthermore, the input neuron, which gave the cross-sectional area of the sample, was added, in order to try to enrich the network with more learning points. After the revision was complete, the new dataset was normalized in the same manner and prepared for training. Other than the increase of the number of input neurons and thus the number of hidden neurons, there was no other changes to the twelve new models. The results for the revised models are shown in Table 7.7.
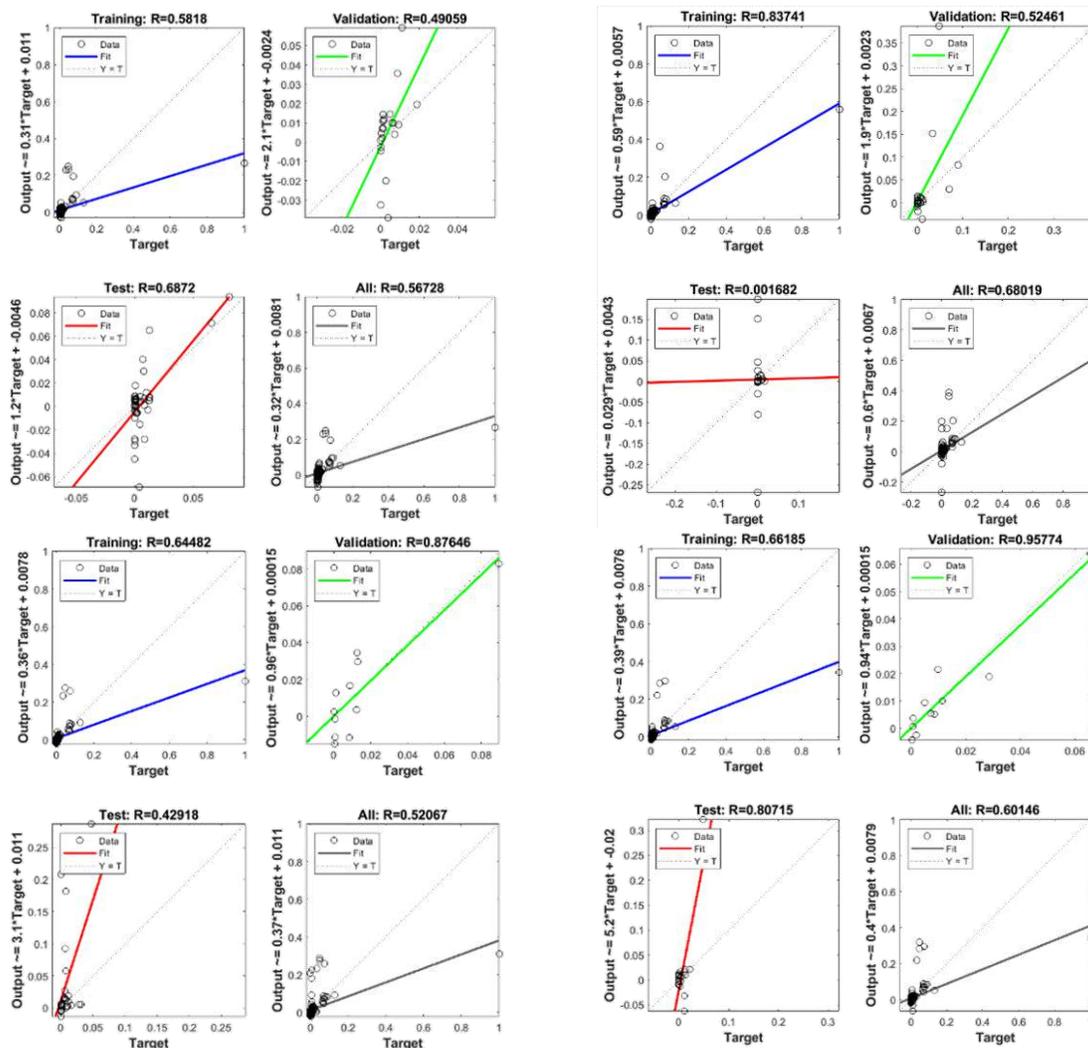
Figure 7.5.4 Regression for model: a) RES_NN70_10_20-17; b) RES_NN80_10_10-51; c) RES_NN80_5_15-35; d) RES_NN85_5_10-51.
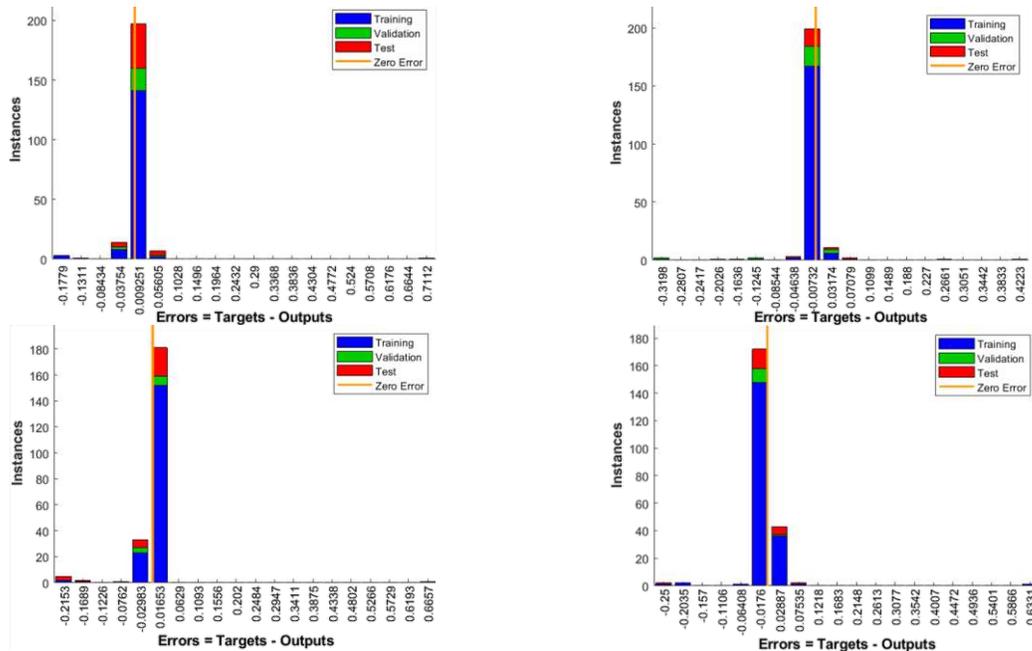
Figure 7.5.5 Error distribution for model: a) RES_NN70_10_20-17; b) RES_NN80_10_10-51; c) RES_NN80_5_15-35; d) RES_NN85_5_10-51

Table 7.7 Results of the revised RESIST models (Group I)

#	Model	Regression coefficient R	Mean squared error MSE	Epoch
1	R-RES_70_10_20-18	0.557	0.00485	15
2	R-RES_70_10_20-37	0.5196	0.00558	9
3	R-RES_70_10_20-54	0.23551	0.0000033	11
4	R-RES_80_10_10-18	0.534	0.005174	10
5	R-RES_80_10_10-37	0.5754	0.00525	10
6	R-RES_80_10_10-54	0.6826	0.003515	15
7	R-RES_80_5_15-18	0.5529	0.00524	9
8	R-RES_80_5_15-37	0.5397	0.00572	9
9	R-RES_80_5_15-54	0.2118	0.00482	10
10	R-RES_85_5_10-18	0.5323	0.00523	11
11	R-RES_85_5_10-37	0.57013	0.00312	11
12	R-RES_85_5_10-54	0.5911	0.00432	10

Results of the revised RESIST models show that the behavior of the models has not improved after the revision of the initial RESIST dataset. A possible explanation for this occurrence could be that the referential samples without nanofillers may be considered outliers in this dataset. The reason is that the samples have several times higher volume resistivity before

adding nanofillers and reaching the percolation threshold. For example, within one sample group [85], the value of the resistivity of the non-reinforced sample is 7700000 Ωcm, while the resistivity after reaching the percolation threshold with 0.048wt% of CNTs is 360000 Ωcm. Hence, the referential non-reinforced sample is considered to be an outlier of the dataset. This occurrence may be seen in Figures 7.5.4 and 7.5.5, where it is obvious that the presence of referential samples is hindering the learning process. This assumption would imply that the dataset needs further revision, however, the further revision would compress the dataset to the point of instability of learning because the total number of tuples would be around 100. Thus, it would be best to make more experimental investigations and collect more data so that a more appropriate dataset could be made, followed by an exclusion of the samples that have not reached the percolation threshold.

5.2. Scripted models – Group I

Response of the ANN models, which were developed using the script editor in Matlab R2020b, are observed at each stage of the development: initial, optimization, testing, and working stage, respectively. Each dataset is used for one model development throughout the former stages. The scripts for all models are given in Appendix B4. The initial stage consists of training the initial network using 80% of the full respective dataset. Table 7.8 shows results for the initial stage of the COMP, FLEX, COMP+FLEX, and RESIST models from Group I.

Table 7.8 Response after the initial training of the scripted ANN models (Group I)

Model	Regression coefficient R	Mean squared error MSE	Mean absolute error MAE
COMP Initial	0.96259	0.0007135	0.00198
FLEX Initial	0.92794	0.0056	0.0479
COMP+FLEX Initial	0.9103	0.085	0.2361
RESIST Initial	0.6173	0.0042	0.0457

As previously mentioned, the initial topology included equal numbers of input and hidden neurons. Results are satisfactory for all models except for the RESIST Initial, as it was already expected. Nevertheless, the topologies are optimized, and the improvement of the prediction is attempted. Figures 7.5.6 and 7.5.7 show R values for training and validation of the initial models, and the error distribution, respectively.
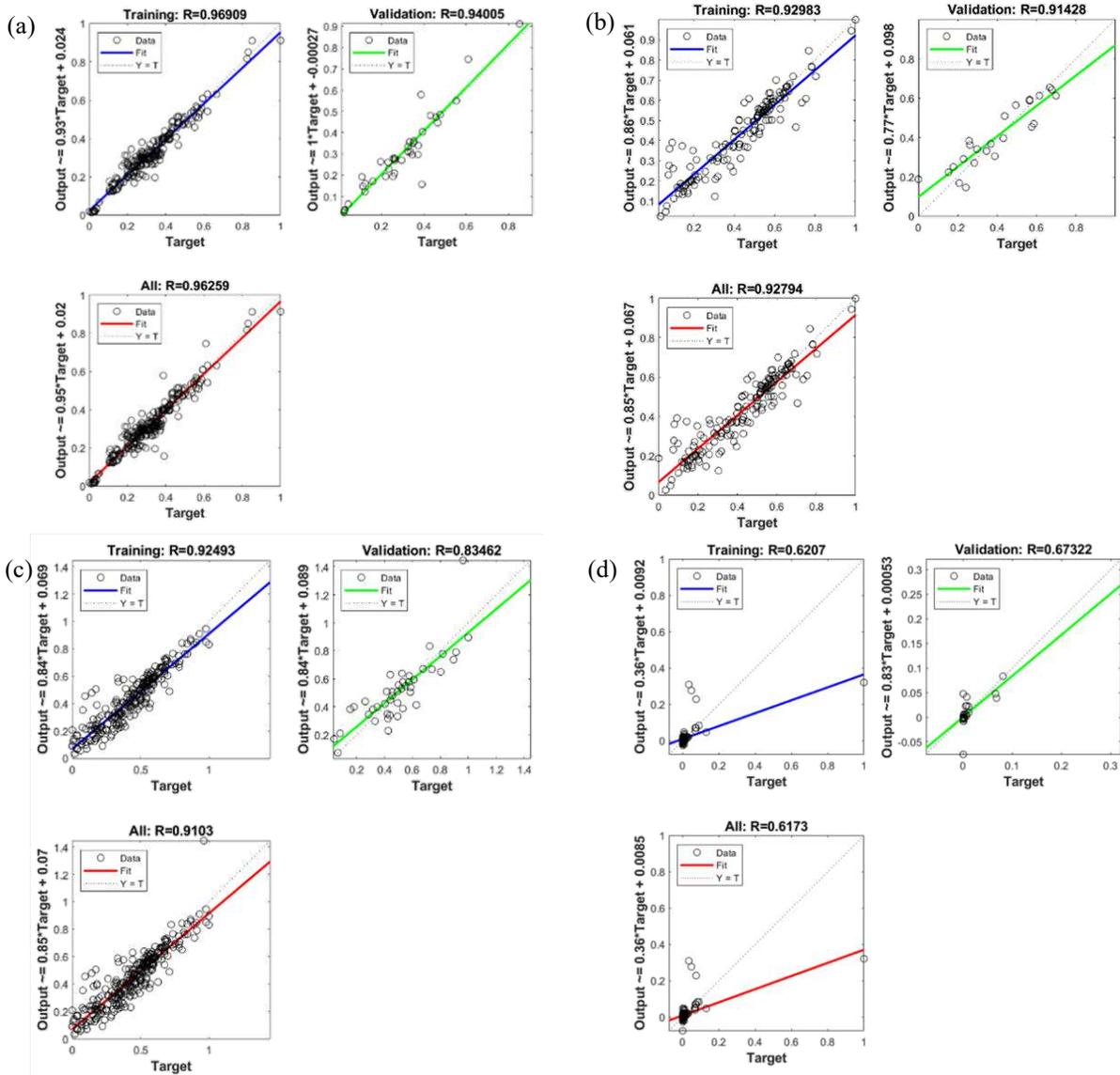
Figure 7.5.6 Regression coefficients for models: (a) COMP Initial; (b) FLEX Initial; (c) COMP+FLEX Initial; (d) RESIST Initial
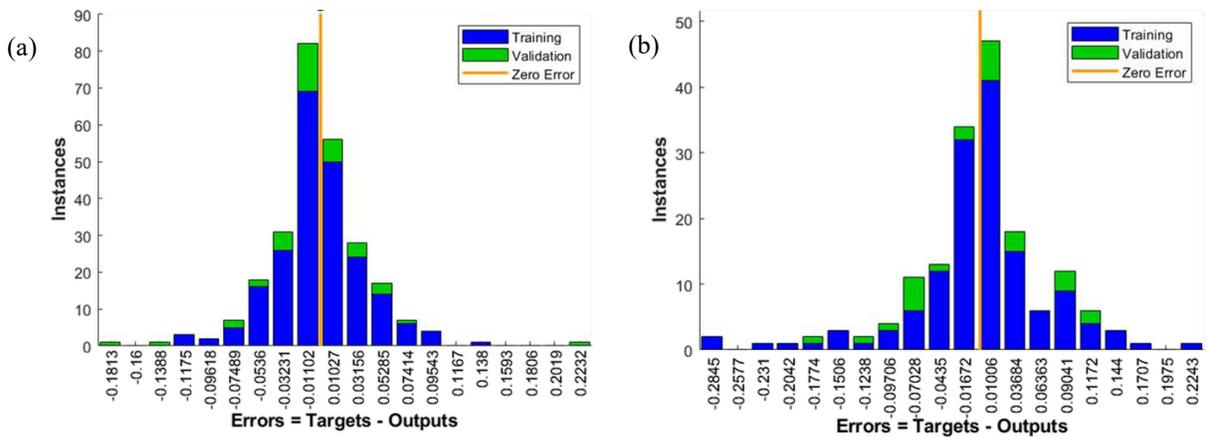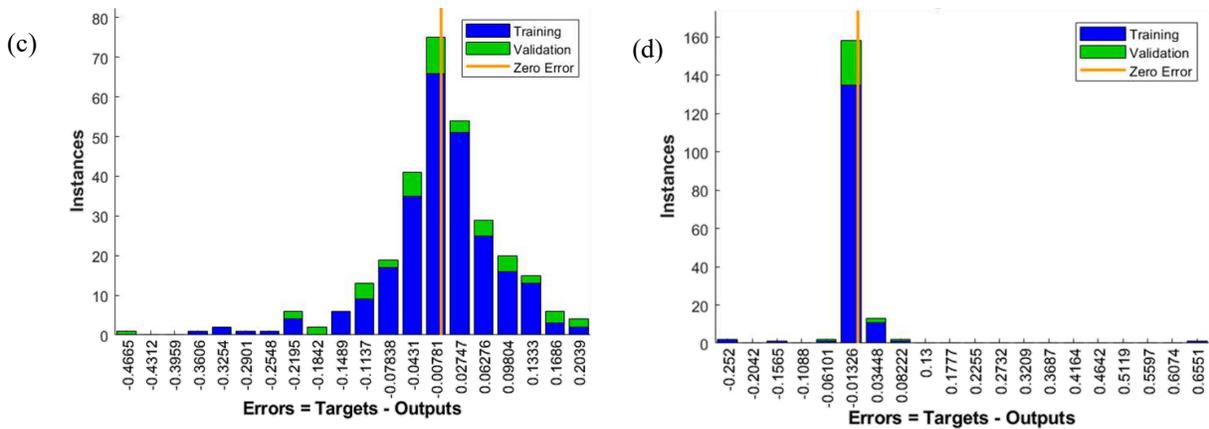
Figure 7.5.7 Error distribution for models: (a) COMP Initial; (b) FLEX Initial; (c) COMP+FLEX Initial; (d) RESIST Initial

After running the initial models, the optimization is performed for each model. The optimization consisted of an iterative change of the number of neurons in the hidden layer, beginning from one and ending at the value of three times the number of input neurons. Figure 7.5.8 shows the change of the RMSE depending on the number of neurons in the hidden layer for training and validation.
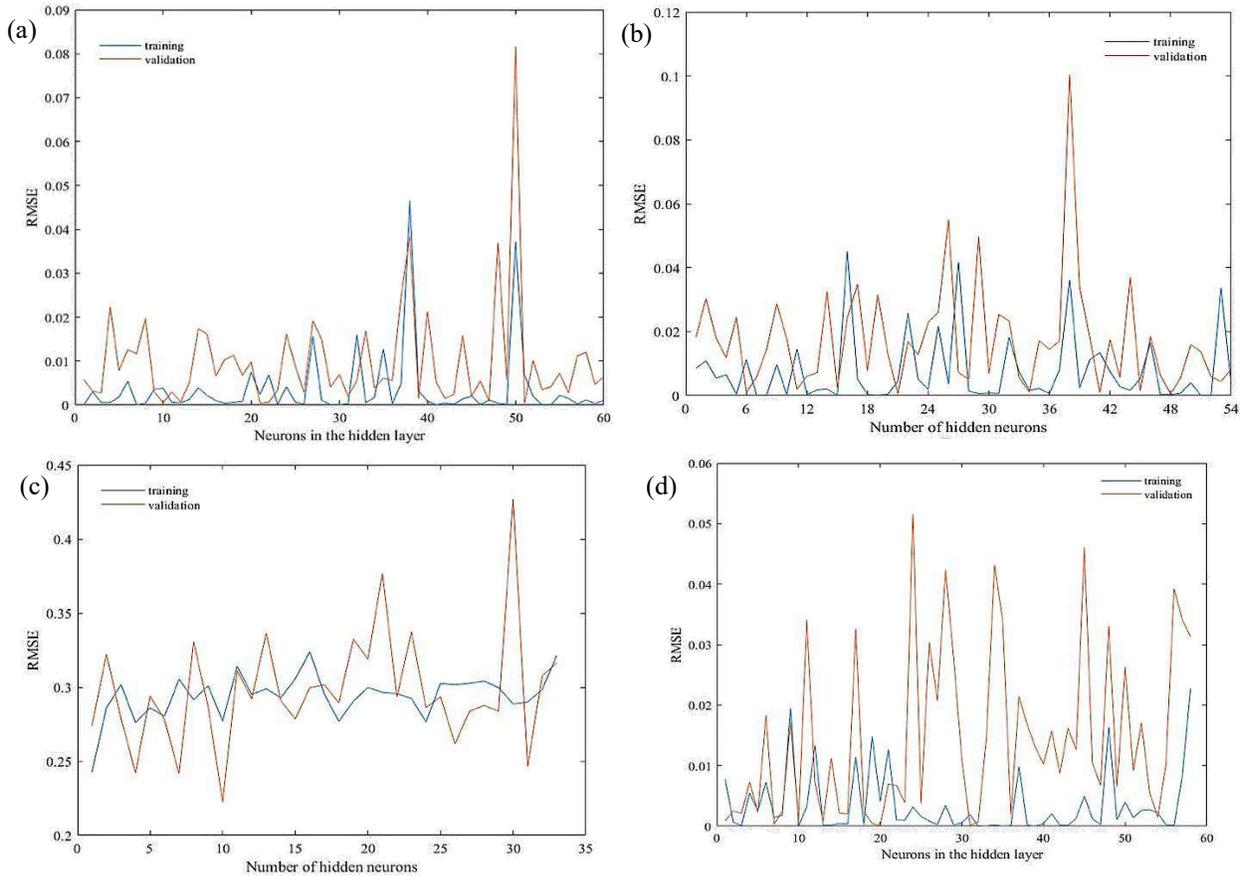
Figure 7.5.8 Optimization for models: (a) COMP; (b) FLEX; (c) COMP+FLEX; (d) RESIST

111

Blue lines in Figure 7.5.8 signify the RMSE after training and the red lines signify the RMSE after validation. As it may be observed for the COMP model, the value of RMSE is very low for the number of hidden neurons lower than the number of input neurons. This may imply the underfitting and therefore exempt from further consideration. The same occurrence may also be observed for the number of hidden neurons lower than 15 for the FLEX model. On the other hand, the overfitting should be pointed for 38 hidden neurons in the COMP model and 58 hidden neurons for the RESIST model. These observations are made only for the training function. Validation function is used only to establish the optimal number, but since validation subset is much smaller than the training subset, the fitting is not examined through this function. The two values, which are giving relatively satisfactory MSE and are within the recommended limits are 25 and 31 for COMP model; 21 and 30 for FLEX model; 18 and 24 for COMP+FLEX model; and 23 and 31 for RESIST model. Following Table 7.9 and Figures 7.5.9-7.5.12, the regression of the optimized models after training may be observed. For COMP and FLEX models, both optimizations show similar results, however, the difference is quite notable for models COMP+FLEX and RESIST. It may be noted that RESIST model continues to give regression values bellow 0.8, although there are some improvements.

Table 7.9 Results of the optimized models

Model	Hidden neurons	Total R value	Hidden neurons	Total R value
COMP Opt.	25	0.97363	31	0.98407
FLEX Opt.	21	0.95773	30	0.95507
COMP+FLEX Opt.	18	0.93429	24	0.97254
RESIST Opt.	23	0.68137	31	0.71474
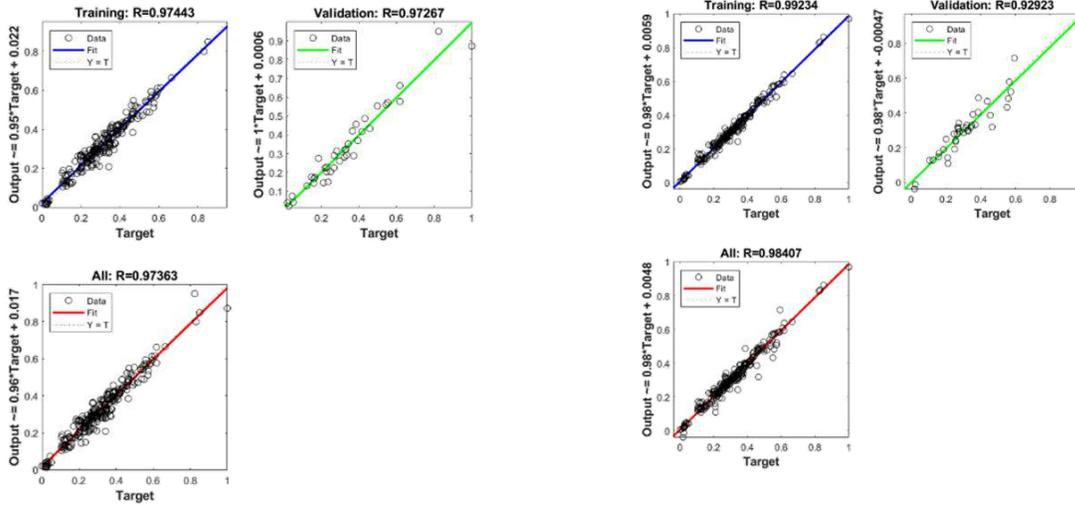
Figure 7.5.9 Regression coefficients for COMP models with: (a) 25, and (b) 31 hidden neurons
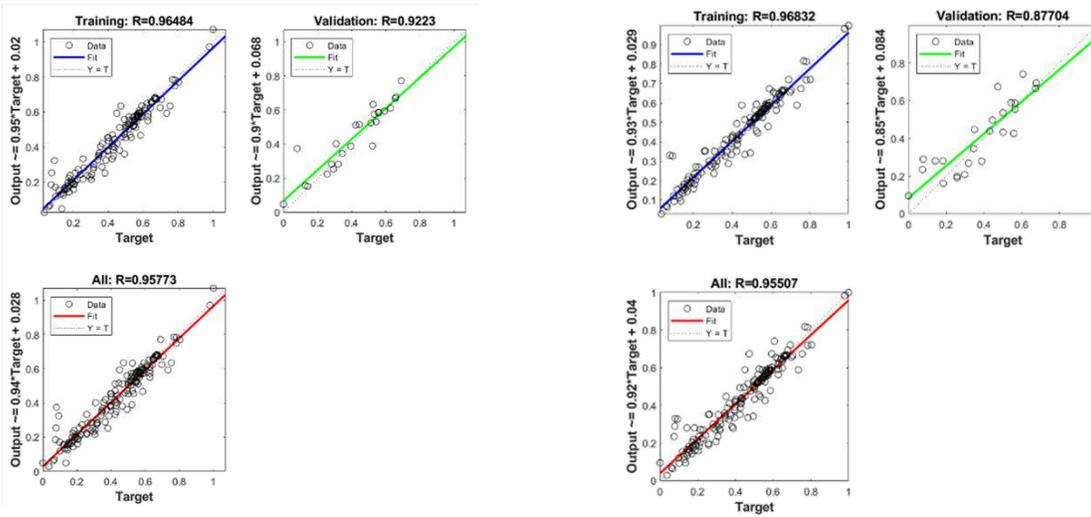
Figure 7.5.10 Regression coefficients for FLEX models with: (a) 21, and (b) 30 hidden neurons
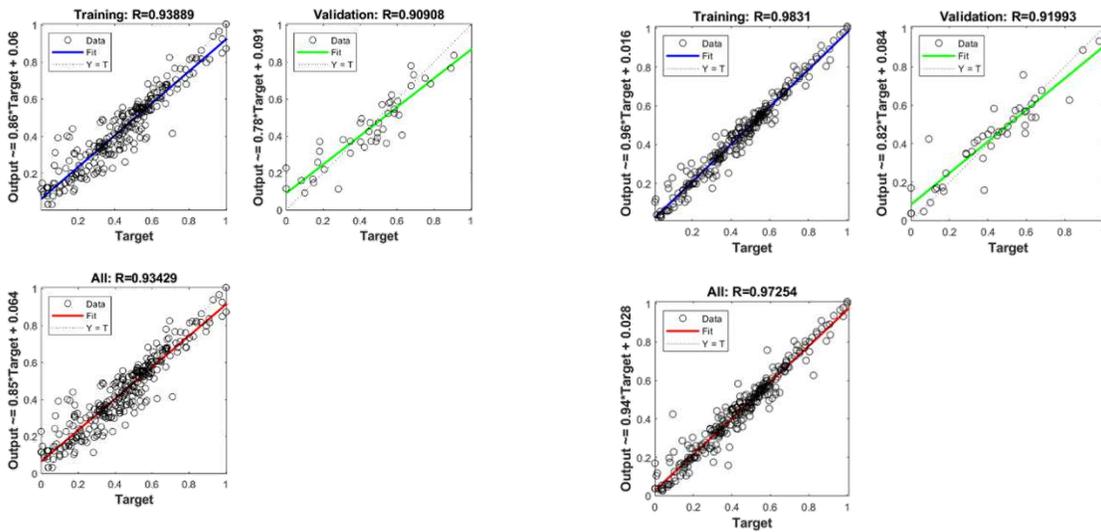
Figure 7.5.11 Regression coefficients for COMP+FLEX models with: (a) 18, and (b) 24 hidden neurons
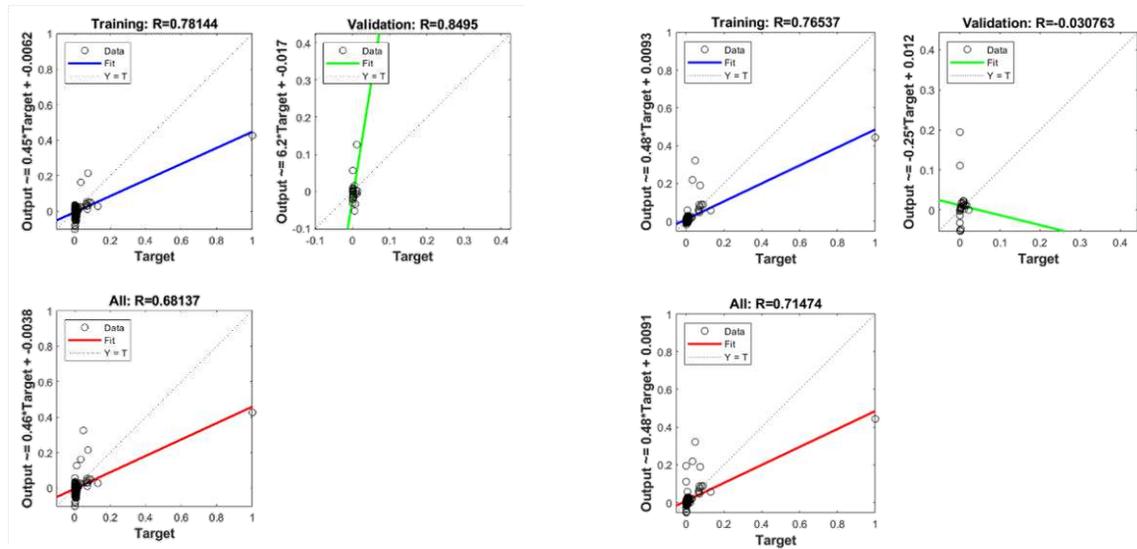
Figure 7.5.12 Regression coefficients for RESIST models with: (a) 23, and (b) 31 hidden neurons

Testing of the optimized models is provided for the topology, which has given better response of the network during the optimization process. Therefore, the testing is provided for the COMP model with 31 neurons in the hidden layer; 21 for the FLEX model; 24 hidden neurons for the COMP+FLEX model; and 31 for the RESIST model. The testing is performed with the simulation function using the 20% of the full dataset. Figure 7.5.13 shows the relationship between the target and the output values for the training and the testing stages.
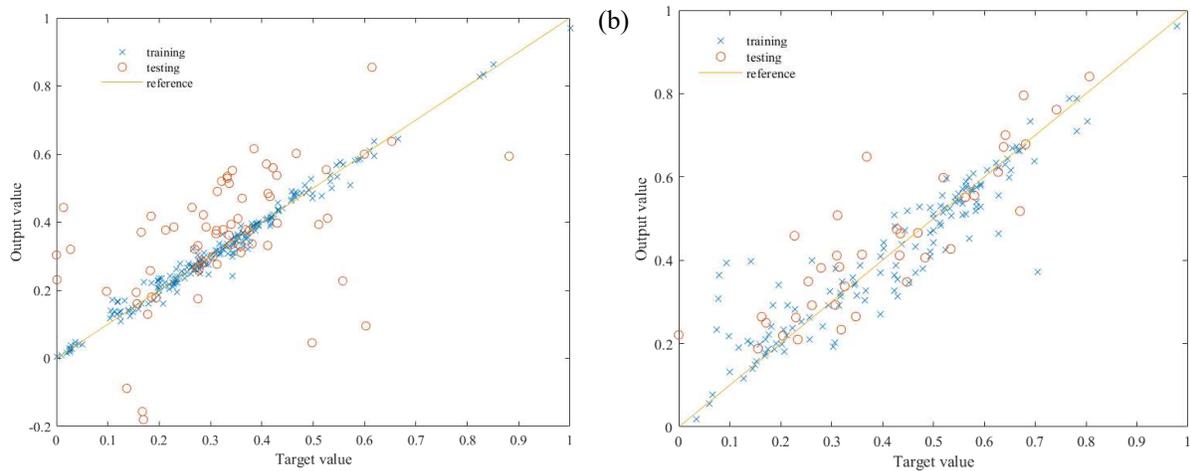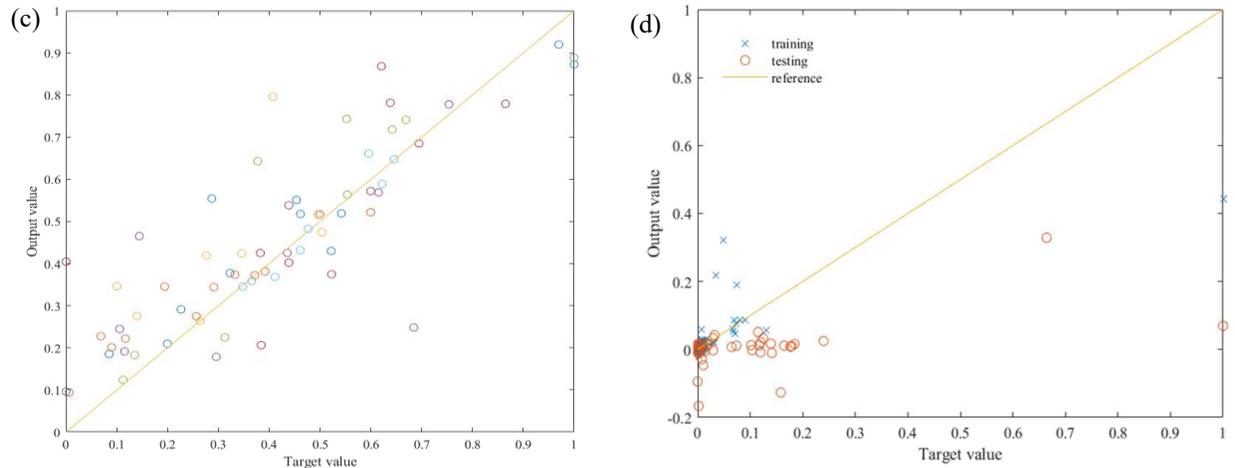
Figure 7.5.13 Target/Output value for: (a) COMP; (b) FLEX; (c) COMP+FLEX; (d) RESIST

After testing, final working models are trained using the full respective dataset. Training is performed without any other subsets, as has been previously described. The results in terms of regression are given in Figure 7.5.14 for all four working models. It may be observed that regression coefficients for all models are extremely high when the learning process is not limited with anything else other than the learning gradient and the number of iterations. From the distribution of the target/output value relationship, it may be observed that model COMP+FLEX shows the most stable behavior and the best convergence.

Furthermore, it is very interesting to observe the response of the RESIST model. Opposite to the expected, the R value is staggering 0.9996, which is also the highest regression value of all models in this group. However, from the distribution function, it is visible that the network forcefully rejected most of the learning tuples and that the R=0.99 is not always a staple of a successful ANN model.
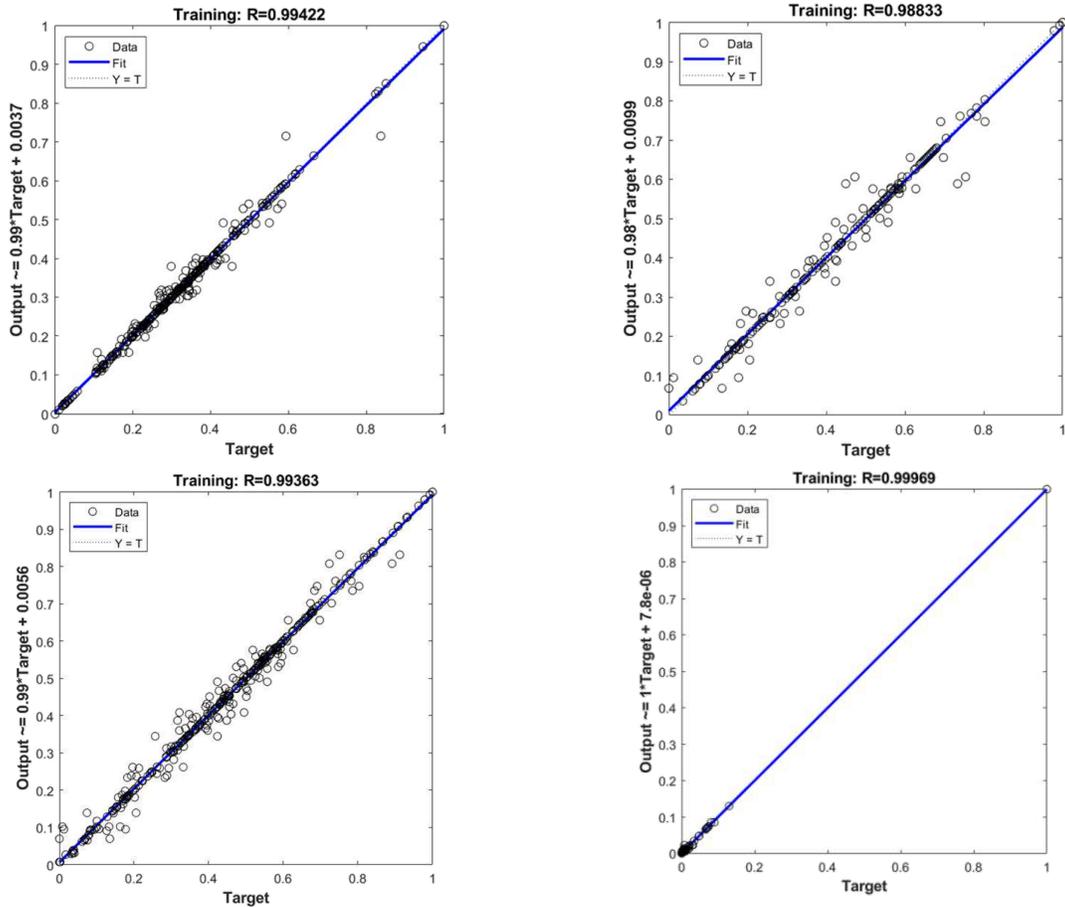
Figure 7.5.14 Training regression for models: (a) COMP; (b) FLEX; (c) COMP+FLEX; (d) RESIST

5.3. Prescribed models – Group II

Results of the ANN models from Group II are given in Table 7.10 and Figures 7.5.15-7.5.17. Models that have expressed the best behavior and were further evaluated by testing are bolded in Table 7.10. Results for all prescribed models using the datasets from Group II are given in Appendix B7, including regression coefficients for training, validation, testing, and error histograms.

Table 7.10 Response values of prescribed models in Group II

#	Model	Regression coefficient R	Mean squared error MSE	Epoch
1	**S_C+F_70_10_20-8**	**0.99333**	**0.00041914**	**70**
2	S_C+F_70_10_20-17	0.99401	0.00009324	81
3	S_C+F_70_10_20-24	0.97471	0.0012624	24
4	**S_C+F_80_10_10-8**	**0.9987**	**0.0001597**	**183**
5	S_C+F_80_10_10-17	0.98778	0.001245	33

6	S_C+F_80_10_10-24	0.97232	0.002636	12
7	S_C+F_80_5_15-8	0.98657	0.0013906	38
8	**S_C+F_80_5_15-17**	**0.99845**	**0.0001255**	**47**
9	S_C+F_80_5_15-24	0.97099	0.00056264	27
10	S_C+F_85_5_10-8	0.98092	0.00190345	38
11	**S_C+F_85_5_10-17**	**0.99851**	**0.0001442**	**78**
12	S_C+F_85_5_10-24	0.99902	0.0000703	113
13	S_C+F(C)_70_10_20-8	0.96522	0.0000045	101
14	**S_C+F(C)_70_10_20-17**	**0.9974**	**0.00003163**	**46**
15	S_C+F(C)_70_10_20-24	0.99494	0.0000101	51
16	S_C+F(C)_80_10_10-8	0.99989	0.00000696	176
17	**S_C+F(C)_80_10_10-17**	**0.99994**	**0.00000473**	**143**
18	S_C+F(C)_80_10_10-24	0.99993	0.0000067	54
19	**S_C+F(C)_80_5_15-8**	**0.98166**	**0.001706**	**21**
20	S_C+F(C)_80_5_15-17	0.97192	0.0000197	32
21	S_C+F(C)_80_5_15-24	0.99863	0.0000495	32
22	**S_C+F(C)_85_5_10-8**	**0.99985**	**0.0000178**	**57**
23	S_C+F(C)_85_5_10-17	0.99298	0.0008709	28
24	S_C+F(C)_85_5_10-24	0.99501	0.0006186	24
25	S_C+F(F)_70_10_20-8	0.9759	0.0020427	12
26	**S_C+F(F)_70_10_20-17**	**0.99651**	**0.0002681**	**39**
27	S_C+F(F)_70_10_20-24	0.98743	0.0002038	61
28	**S_C+F(F)_80_10_10-8**	**0.9904**	**0.0008968**	**45**
29	S_C+F(F)_80_10_10-17	0.98325	0.0011868	17
30	S_C+F(F)_80_10_10-24	0.97864	0.001998	10
31	**S_C+F(F)_80_5_15-8**	**0.99399**	**0.0005593**	**45**
32	S_C+F(F)_80_5_15-17	0.99344	0.000515	34
33	S_C+F(F)_80_5_15-24	0.97076	0.0006981	13
34	**S_C+F(F)_85_5_10-8**	**0.98388**	**0.0015214**	**15**
35	S_C+F(F)_85_5_10-17	0.99793	0.0001675	105
36	S_C+F(F)_85_5_10-24	0.99677	0.0001397	102
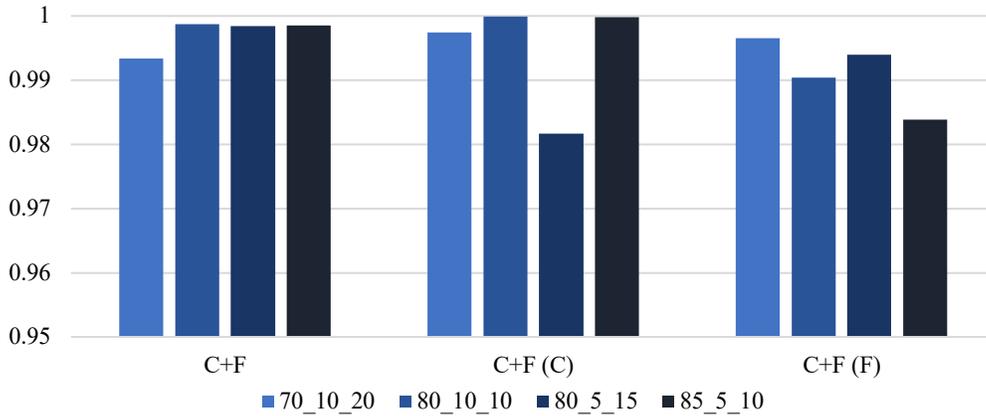
Figure 7.5.15 Histogram of regression coefficients for prescribed C+F, C+F(C), and C+F(F) models (Group II)

Models, which are bolded in Table 7.10, represent the models, which exhibit the best behavior within each subgroup. As it is shown in Figure 7.5.15, the total regression coefficients for these models are very high, going over 0.98. Hence, the models will be analyzed further and then evaluated, i.e., checked for validity, and the optimal model from each group will be established. Figure 7.5.16 shows regression coefficients for training, validation, testing, and total for models with the best results within each subgroup, and Figure 7.5.17 show the error histogram plots for these models to establish the distributions of the mean square errors. Plots showing the regression coefficient and error for all models in Group II are available in Appendix B7.
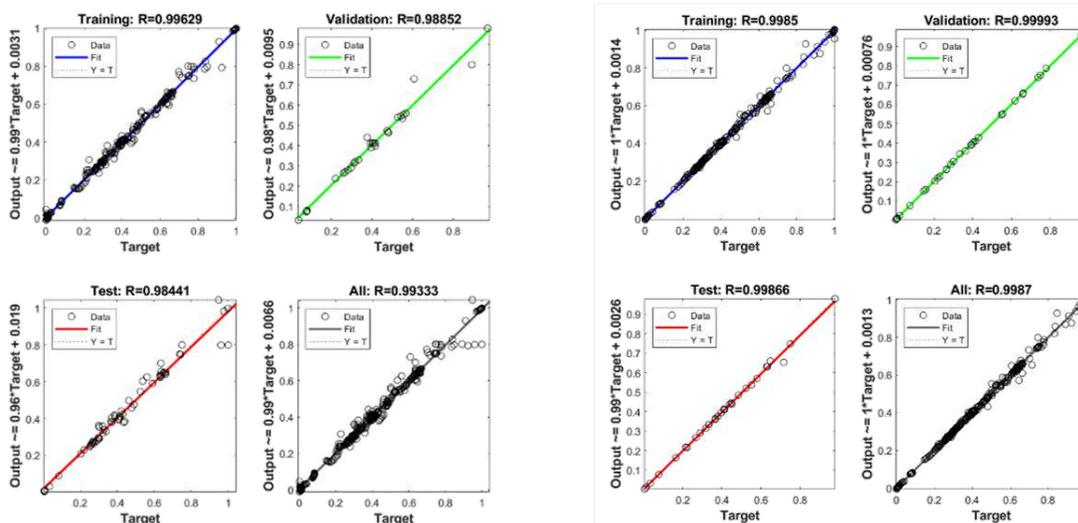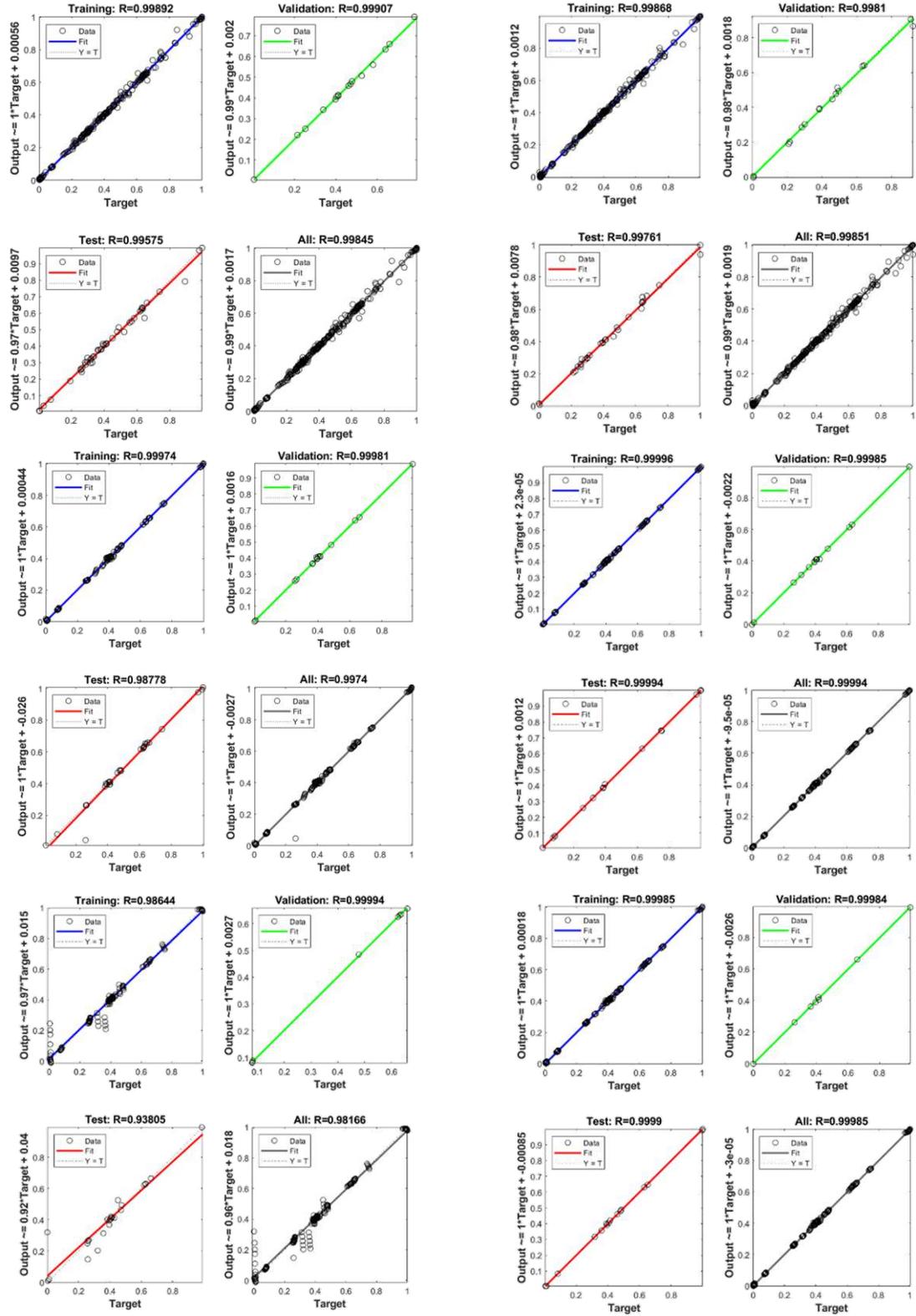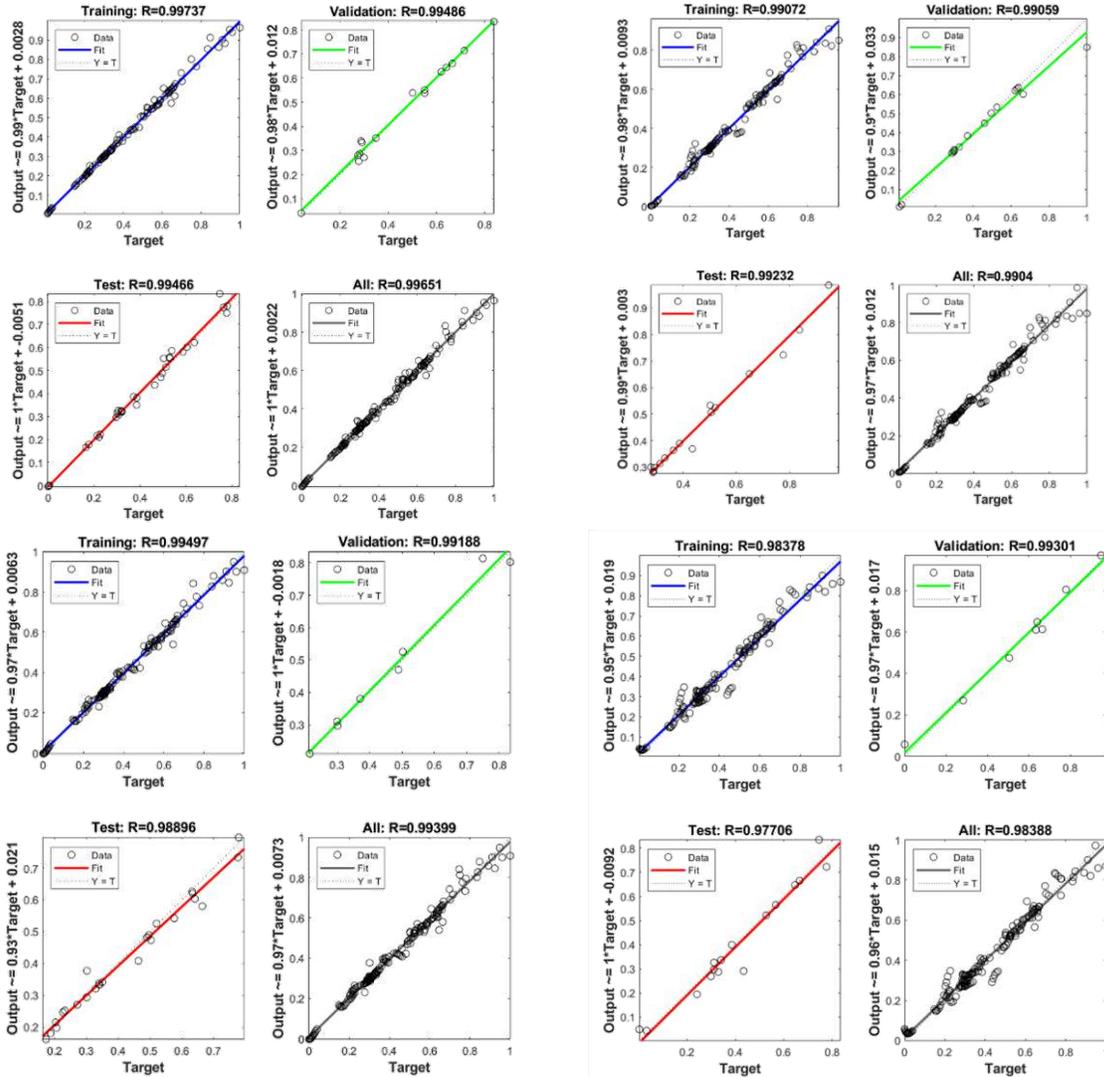
Figure 7.5.16 Regression for model: a) S_C+F_70_10_20-8; b) S_C+F_80_10_10-8; c) S_C+F_80_5_15-17;
d) S_C+F_85_5_10-17; e) S_C+F(C)_70_10_20-17; f) S_C+F(C)_80_10_10-17; g) S_C+F(C)_80_5_15-8;
h) S_C+F(C)_85_5_10-8; i) S_C+F(F)_70_10_20-17; j) S_C+F(F)_80_10_10-8; k) S_C+F(F)_80_5_15-8; l)
S_C+F(F)_85_5_10-8.
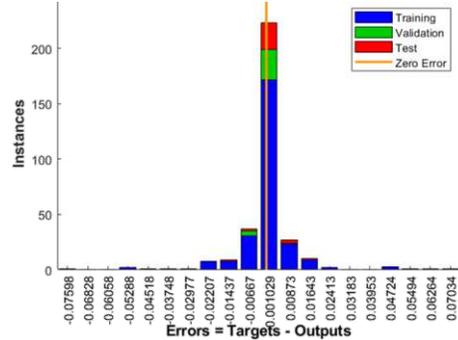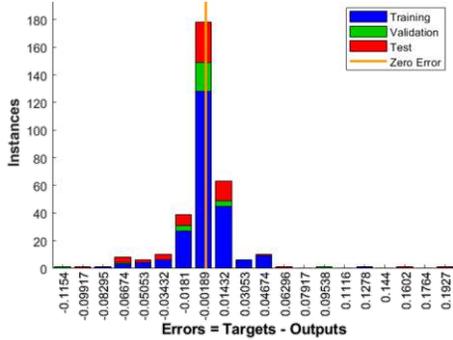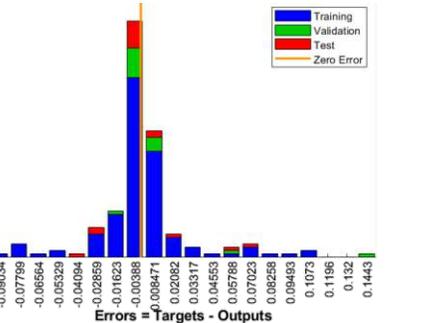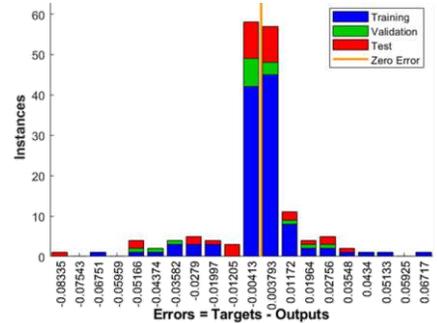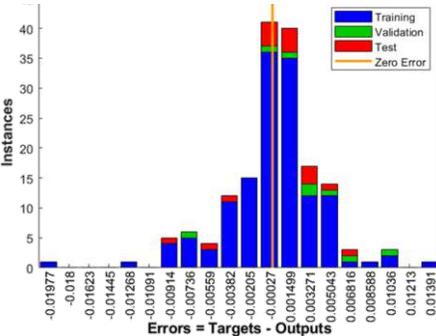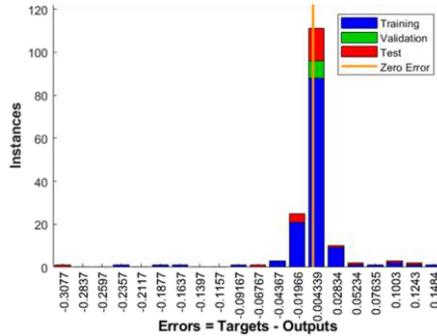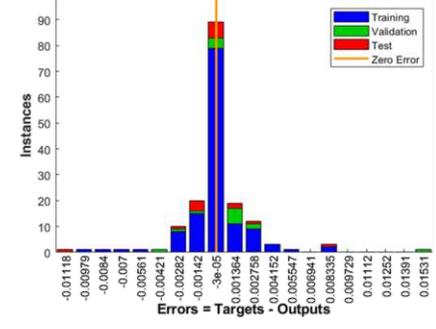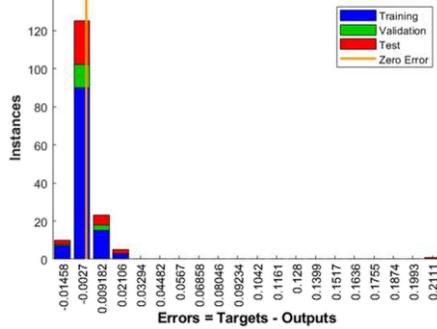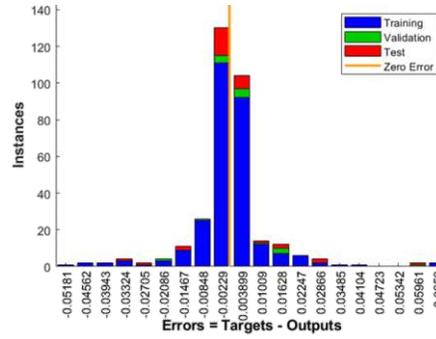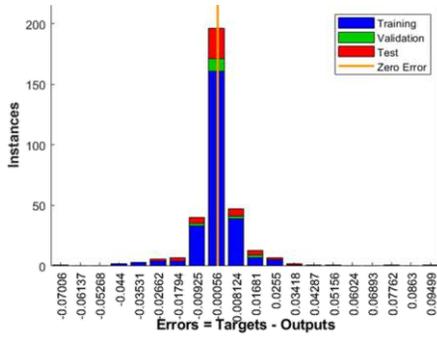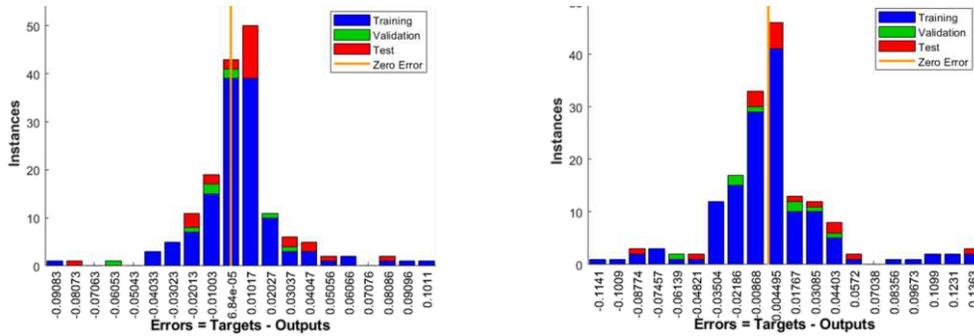
Figure 7.5.17 Error distribution for model: a) S_C+F_70_10_20-8; b) S_C+F_80_10_10-8; c) S_C+F_80_5_15-17; d) S_C+F_85_5_10-17; e) S_C+F(C)_70_10_20-17; f) S_C+F(C)_80_10_10-17; g) S_C+F(C)_80_5_15-8; h) S_C+F(C)_85_5_10-8; i) S_C+F(F)_70_10_20-17; j) S_C+F(F)_80_10_10-8; k) S_C+F(F)_80_5_15-8; l) S_C+F(F)_85_5_10-8

As it may be seen, the highest regression coefficients are obtained when the number of hidden neurons equals the number of input neurons. This situation is very similar to the situation in Group I, so it may be concluded that these ANN models express optimal behavior when the number of hidden neurons is equal to the number of the input neurons. Nevertheless, the models with *Nh=2Ni+1* and *Nh=3Ni* also show comparable behavior to other models, leading to the conclusion that the ANN behavior does not significantly suffer all the while the number of hidden neurons is comparable or within the range of the number of input neurons.

As for the error distribution, it may be seen that even though the models show a Gaussian curve-like behavior, none of them is regularly distributed. It is an unexpected occurrence since the dataset is obtained from the numerical simulations where the models were ideal, and the results showed fairly regular change. It may be prescribed to much higher number of iterations per epoch for these models (Table 7.10). The models presented in the figures have been additionally evaluated to establish the truthfulness of the results. Furthermore, a direct comparison between Group I and Group II is given in the following sub-sections.

5.4. Scripted models – Group II

Models, which have been developed via script editor for the dataset from Group II, refer to the same dataset but with different output signals. As for the prescribed models, the networks are developed for two outputs, compressive and bending strength, as well as single outputs for both parameters. In all three cases, number of input neurons is eight, therefore, the initial number of neurons in the hidden layer is also eight. The procedure follows model's development including initial stage, optimization, testing, and final working model. Table 7.11 shows the response of

initial models, Figure 7.5.18 shows the initial regression, and Figure 7.5.19 shows the error distribution of the initial models.

Table 7.11 Response after the initial training of the scripted ANN models (Group II)

Model	Regression coefficient R	Mean squared error MSE	Mean absolute error MAE
COMP Initial	0.99187	0.001	0.016
FLEX Initial	0.97356	0.0028	0.037
COMP+FLEX Initial	0.97113	0.1461	0.2971

(a)

(b)

(c)
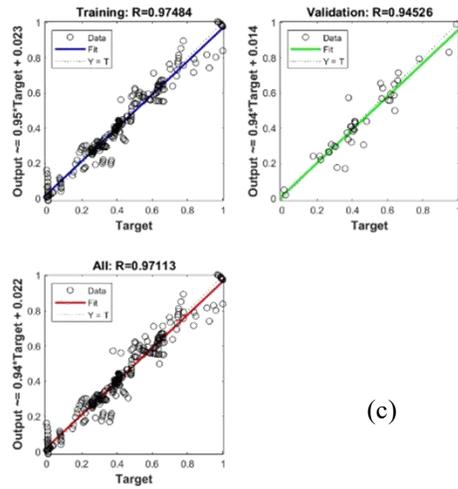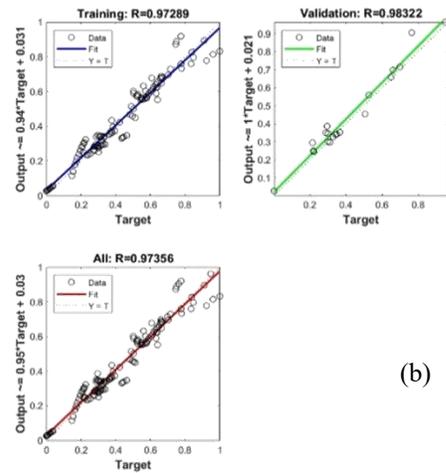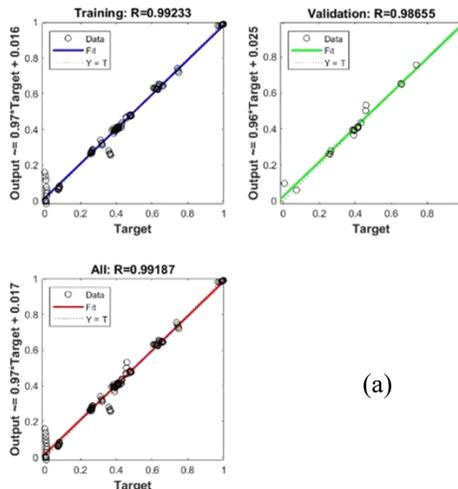
Figure 7.5.18 Regression coefficients for initial model: (a) COMP; (b) FLEX; (c) COMP+FLEX
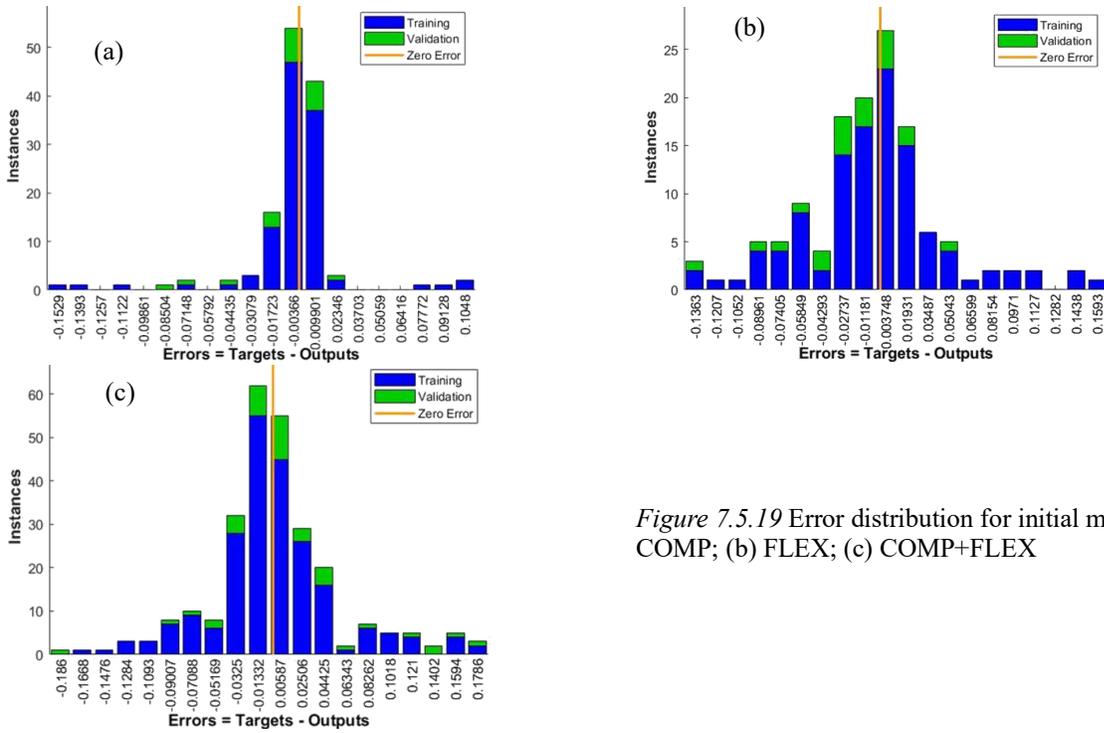
Figure 7.5.19 Error distribution for initial model: (a) COMP; (b) FLEX; (c) COMP+FLEX

Optimization of the initial models is provided by iterating the number of neurons in the hidden layer from one to twenty-four, following the same procedure as previously described. The response is measured using RMSE values, as shown in Figure 7.5.120. Figure 7.5.20 implies that the behavior of the model may change drastically with more or less hidden neurons. For this reason, the number of hidden neurons should be considered carefully, taking into account the general recommendations from the literature and other experimental work. For both COMP and FLEX models, the optimization models take 10 and 13 hidden neurons, while the COMP+FLEX model examines the topology where 13 and 17 neurons are in the hidden layer. Table 7.12 gives the results of training for the optimized models. Figures 7.5.21-7.5.23 show the regression behavior of the optimization models.
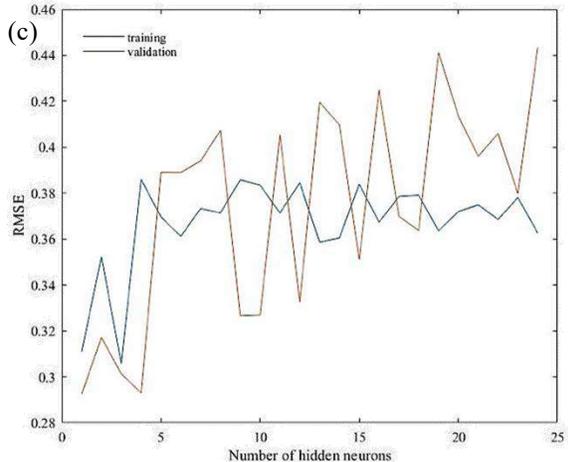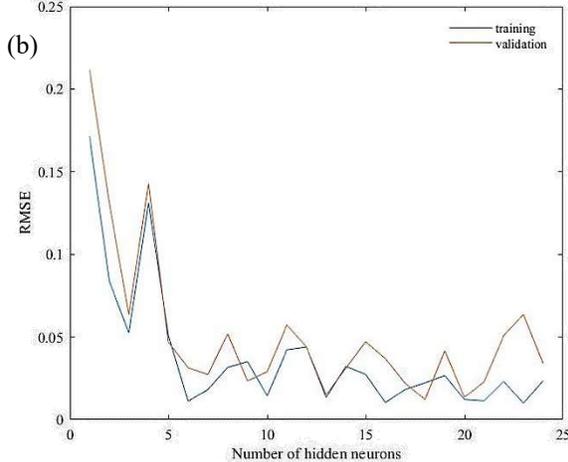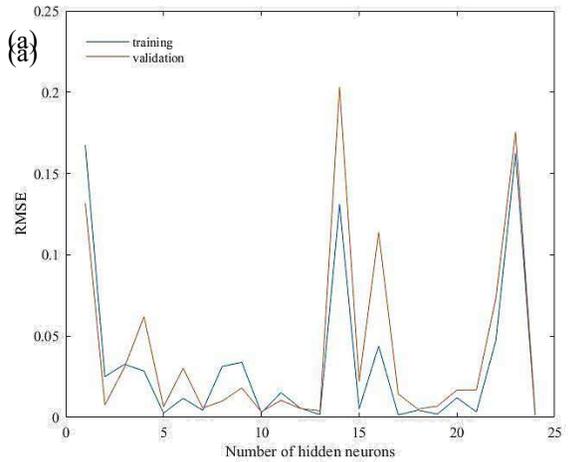
Figure 7.5.20 Optimization for model: (a) COMP; (b) FLEX; (c) COMP+FLEX

Table 7.12 Results of the optimized models

Model	Hidden neurons	Total R value	Hidden neurons	Total R value
COMP Opt.	10	0.98639	13	0.99991
FLEX Opt.	10	0.99642	13	0.98585
COMP+FLEX Opt.	13	0.9915	17	0.99931
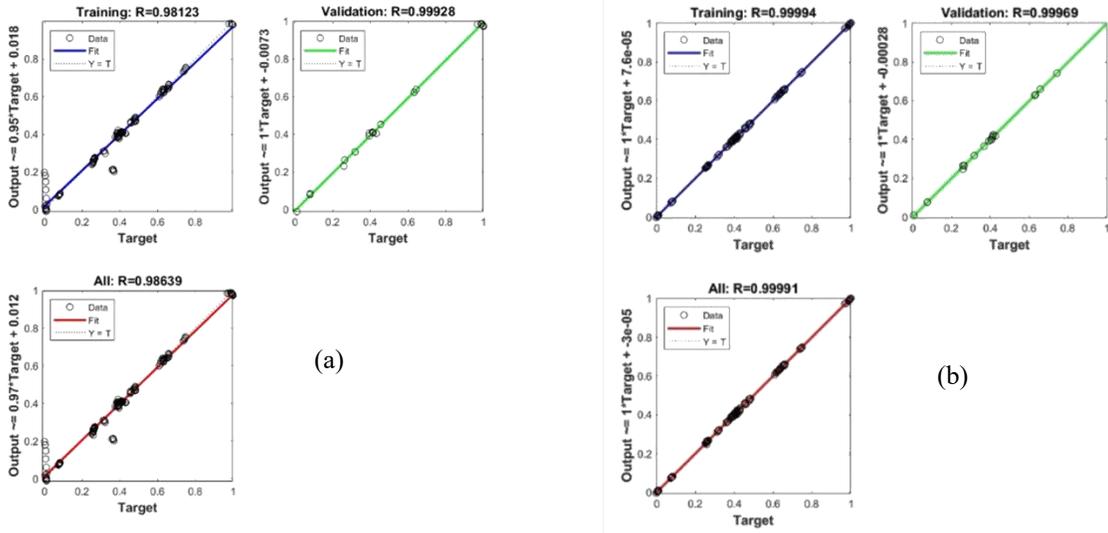
Figure 7.5.21 Regression value for COMP model with: (a) 10; (b) 13 hidden neurons
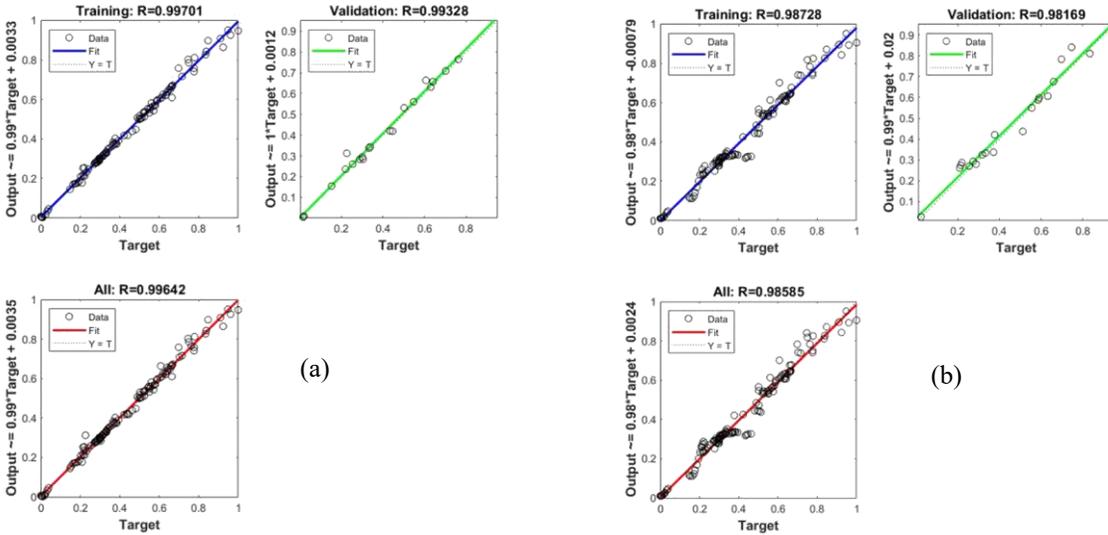
Figure 7.5.22 Regression value for FLEX model with: (a) 10; (b) 13 hidden neurons

126
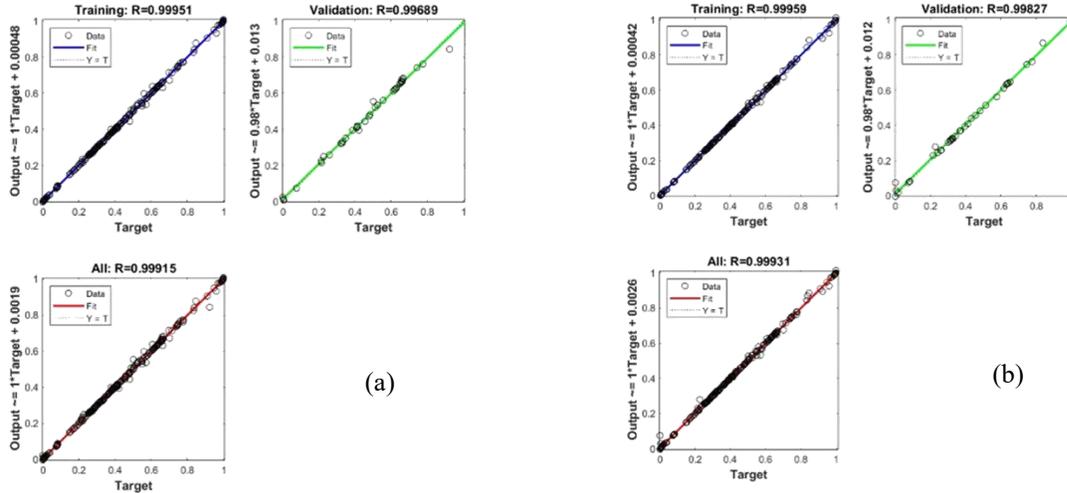
Figure 7.5.23 Regression value for the COMP+FLEX model with: (a) 13; (b) 17 hidden neurons

After the optimization of all three models, the following topologies are adopted. For the COMP model, the number of hidden neurons is 13, for the FLEX model it is 10, and for the COMP+FLEX model there are 17 hidden neurons. These topologies are tested with the 20% of the full dataset, after which the final working models are trained using the full dataset. Testing of the models is represented through the relationship between the target and the output values, as in Figure 7.5.24.
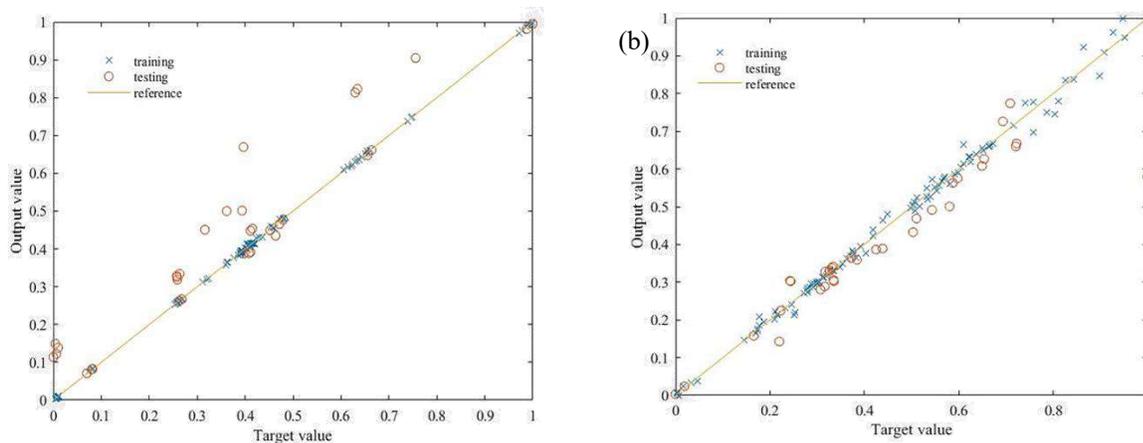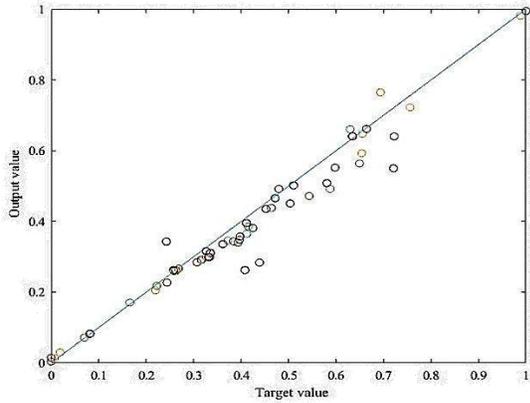
Figure 7.5.24 Testing response for model: (a) COMP; (b) FLEX; (c) COMP+FLEX

After the testing of the adopted models is performed, the final working models may be trained on the full dataset. As it has been described, the training of the working model is performed without the limitations of the learning process. Results of the working models are presented via the regression coefficient in Figure 7.5.25. It may be observed that all three models show exceptionally well and reliable behavior from the initial stage to the working model. Although the results of the ANSYS models matched the experimental results only partially, this data is more or less linear and thus presents the perfect learning material for a neural network. All models show reliability of over 0.99, however, it only implies that the prediction, which the network can provide, matches the simulations and not a realistic situation.

(a)

(b)

128

Training: R=0.99968
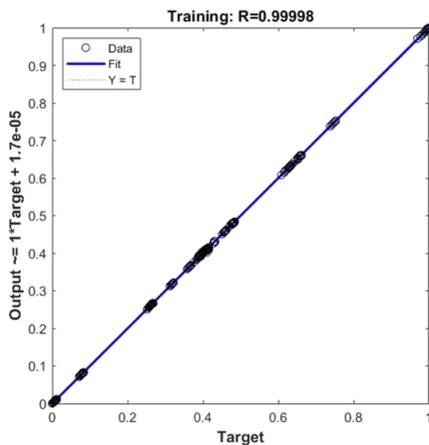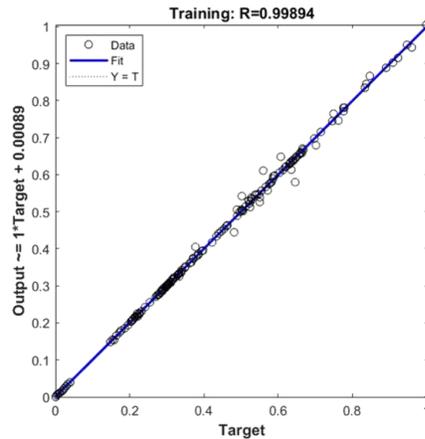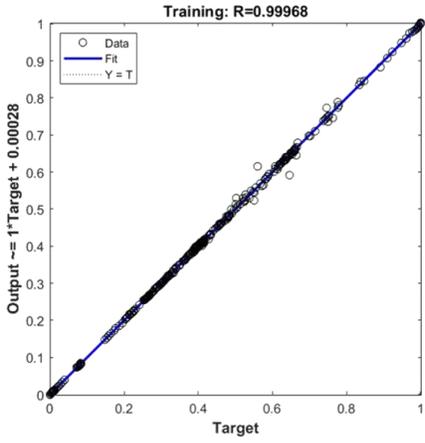
Figure 7.5.25 Regression value of the working model:
(a) COMP; (b) FLEX; (c) COMP+FLEX

(c)

5.5. Evaluation of models

Evaluation for the 12 best ANN models from both Group I and Group II is done to establish the validity of the initial results. As it is previously mentioned, models from the RESIST group have not shown satisfactory behavior, and thus they were not evaluated further. Evaluation models followed precisely the same architecture as their respective initial models and have been trained again with randomly divided 80% of the respective dataset, after which they were tested on the remaining 20% of the respective dataset. The reasoning behind this division of the datasets is that all datasets are too small to be divided by the ratio of 50/50 and still be expected to give meaningful results. Results of the repeated training and testing are shown in Table 7.13 for Group I and Table 7.14 for Group II.

Table 7.13 Results of evaluation of the prescribed models from Group I

#	Model	Training %(#)	R	MSE	Testing %(#)	R	MSE
1	EV-COMP_70_10_20-41	80% (259)	0.9399	0.00234	20% (71)	0.6995	0.02325
2	EV-COMP_80_10_10-60	80% (259)	0.97068	0.00121	20% (71)	0.641	0.02477
3	EV-COMP_80_5_15-20	80% (259)	0.94203	0.00189	20% (71)	0.717	0.0164
4	EV-COMP_85_5_10-41	80% (259)	0.975	0.00104	20% (71)	0.6455	0.0295
5	EV-FLEX_70_10_20-48	80% (167)	0.915	0.004645	20% (40)	0.886	0.01385
6	EV-FLEX_80_10_10-48	80% (167)	0.92495	0.00488	20% (40)	0.873	0.01281
7	EV-FLEX_80_5_15-16	80% (167)	0.90042	0.00741	20% (40)	0.869	0.01255
8	EV-FLEX_85_5_10-16	80% (167)	0.83336	0.01645	20% (40)	0.898	0.0189
9	EV-C+F_70_10_20-33	80% (148)	0.91828	0.000789	20% (37)	0.6658	0.0379
10	EV-C+F_80_10_10-11	80% (148)	0.8954	0.009044	20% (37)	0.8098	0.0218
11	EV-C+F_80_5_15-11	80% (148)	0.93163	0.002162	20% (37)	0.68652	0.06705
12	EV-C+F_85_5_10-33	80% (148)	0.95713	0.003185	20% (37)	0.81361	0.02378

a)

b)
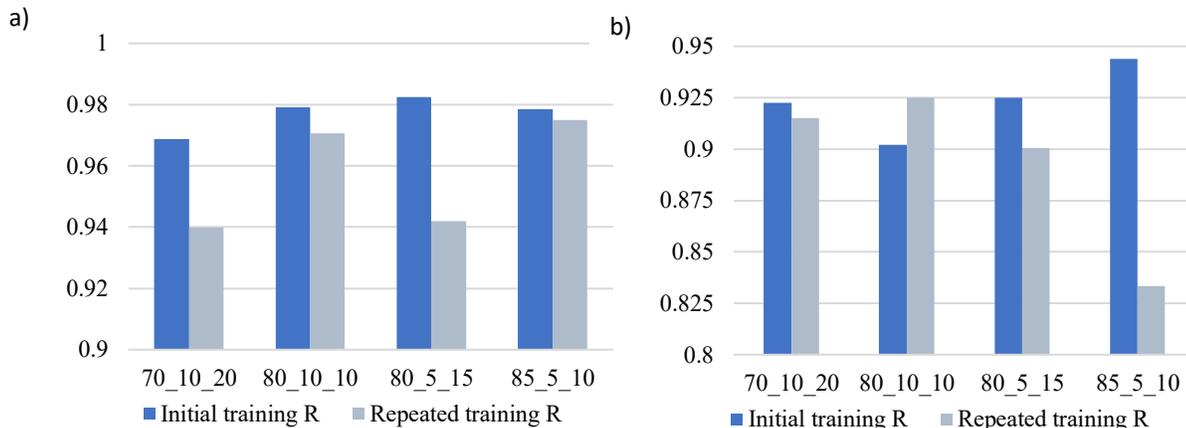
Figure 7.5.26 Initial and repeated training R value for prescribed COMP (a) and FLEX (b) models
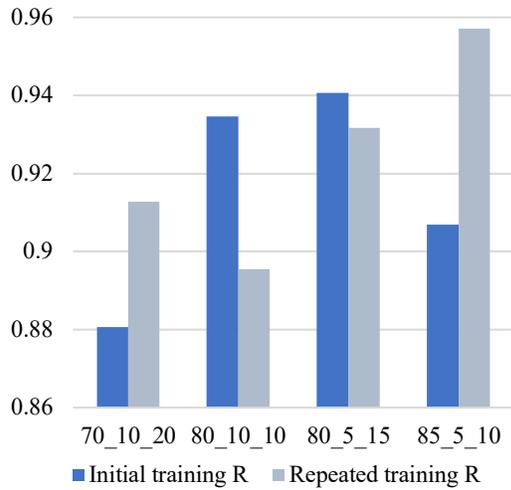
Figure 7.5.27 Comparison of initial and repeated training R value for prescribed COMP+FLEX models

R values of the evaluation models are compared to the initial results in Figures 7.5.26 and 7.5.27. In some cases, regression coefficients of the evaluation models are higher than the initial R values. This may occur due to the favorable distribution of tuples during randomization. That said, the difference between the values does not exceed 0.1, meaning that circumstantially better results can be considered as confirmation of the validity of the models.

The only exception is the model FLEX_85_5_10-16 which shows a difference higher than 0.1, thus implying a false-positive result. However, it may still be considered that the overall behavior of the model is satisfactory, with R value higher than 0.8 in both initial and repeated training. After evaluating the initial models, it may be concluded that all models from Group I showed satisfactory behavior with the given topologies. In addition, all variations of the number of hidden neurons may be used for this type of neural network to achieve successful training of the network.

Table 7.14 Results of evaluation of the prescribed models from Group II

#	Model	Training %(#)	R	MSE	Testing %(#)	R	MSE
1	EV-S_C+F_70_10_20-8	80% (130)	0.94562	0.001621	20% (34)	0.8957	0.01294
2	EV-S_C+F_80_10_10-8	80% (130)	0.99714	0.000124	20% (34)	0.8222	0.01889
3	EV-S_C+F_80_5_15-17	80% (130)	0.99382	0.000549	20% (34)	0.9806	0.00273
4	EV-S_C+F_85_5_10-17	80% (130)	0.99484	0.00047	20% (34)	0.9765	0.00422
5	EV-S_C+F(C)_70_10_20-17	80% (130)	0.99775	0.00038	20% (34)	0.9871	0.0017
6	EV-SC+F(C)_80_10_10-17	80% (130)	0.98194	0.00123	20% (34)	0.9789	0.0028
7	EV-S_C+F(C)_80_5_15-8	80% (130)	0.93353	0.00593	20% (34)	0.93531	0.00892
8	EV-S_C+F(C)_85_5_10-8	80% (130)	0.95678	0.00447	20% (34)	0.9544	0.00578
9	EV-S_C+F(F)_70_10_20-17	80% (130)	0.99738	0.000055	20% (34)	0.958	0.00697
10	EV-S_C+F(F)_80_10_10-8	80% (130)	0.9822	0.00196	20% (34)	0.9796	0.00329
11	EV-S_C+F(F)_80_5_15-8	80% (130)	0.97939	0.0017	20% (34)	0.9669	0.00483
12	EV-S_C+F(F)_85_5_10-8	80% (130)	0.99039	0.0007	20% (34)	0.9346	0.00741
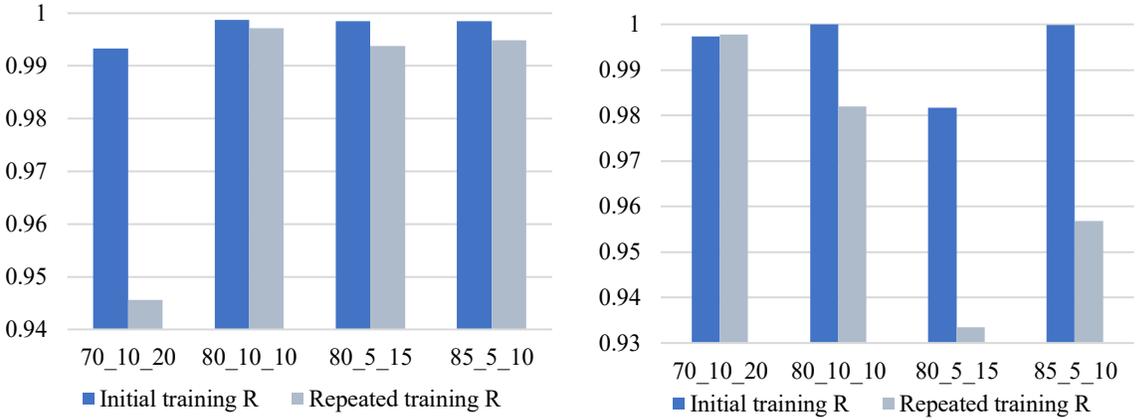
Figure 7.5.28 Comparison of initial and repeated training R values for C+F and C+F(C) models
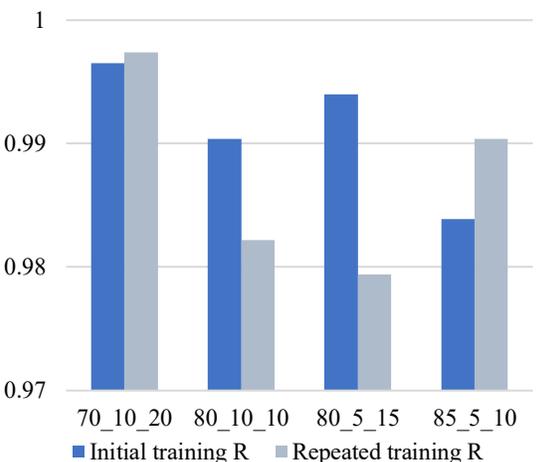
Figure 7.5.29 Comparison of initial and repeated training R values for C+F(F) models

Regression coefficients of the evaluation models and the initial models are compared in Figure 7.5.28 and 7.5.29. It may be observed that the differences between the R values are extremely small, in some cases negligible. It may also be noted that the trainings were repeated several times and gave exactly the same results, i.e., the same R values. This occurrence leads to the conclusion that the models are stable for the given database.

Additionally, the difference between the datasets is expectedly minute because the same dataset was tested with both target values and with the independent target values (C+F(C); C+F(F)). Nevertheless, some occurrences may be observed. Dataset C+F shows the worst results for the 70/10/20 subset ratio, while the independent target value datasets, show the highest values with the same subset ratio. Obviously, the target value significantly affects the behavior of the ANN with the exactly same architecture. However, satisfactory, most logical results are observed for the subset ratio of 85/5/10 for all three datasets. Hence, it may be concluded that the stability and accuracy are preserved, and that the optimal architecture is indeed the one described by the subset ratio of 85/5/10 and the number of hidden neurons equal to $Nh=Ni$ or $Nh=2Ni+1$.

Moreover, the initial investigation shows that the mechanical properties of CNT/CNF reinforced concrete can be successfully predicted using the described ANN models. The evaluation shows that models COMP_70_10_20-41, FLEX_80_5_15-16, and C+F_80_5_15-11 from

Group I; and S_C+F_85_5_10-17, S_C+F(C)_85_5_10-8, and S_C+F(F)_85_5_10-8 from Group II, exhibited optimal results in terms of high R values and the most uniform error distribution, and therefore, the overall most favorable behavior. All evaluation results are given in Appendix B9.

5.6 Sensitivity analysis

Sensitivity analysis is provided for the scripted ANN models using the weights method, as described in Section 4 of this chapter. The analysis is done after establishing the working models for the respective datasets. The weights are used to show the influence of each input parameter on the output variable. The weights between the input and hidden layer (w1), bias between input and hidden layer (b1), weights between hidden and output layer (w2), and bias at the output layer (b2) of the respective final working models for datasets from Group I and Group II are presented in detail within Appendix B10. The nomenclature is followed as in Table 2 and Table 3. Figure 7.5.30 shows the relative influence of the input parameters on the output for the respective models from Group I.

(a)

(b)
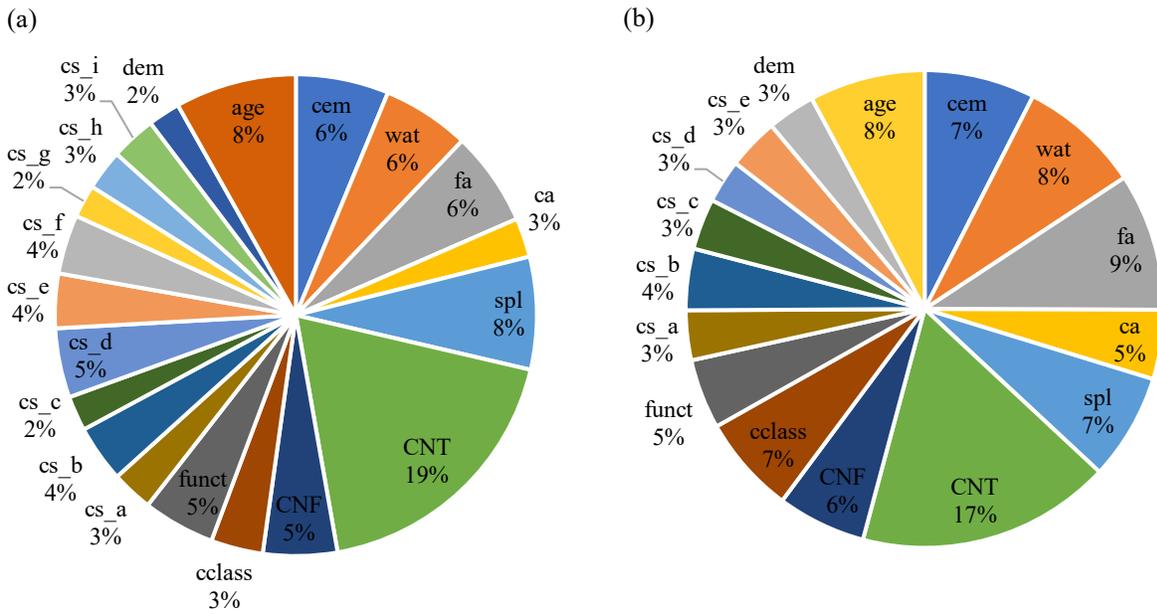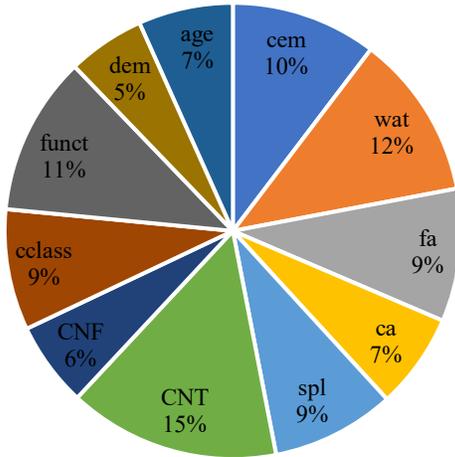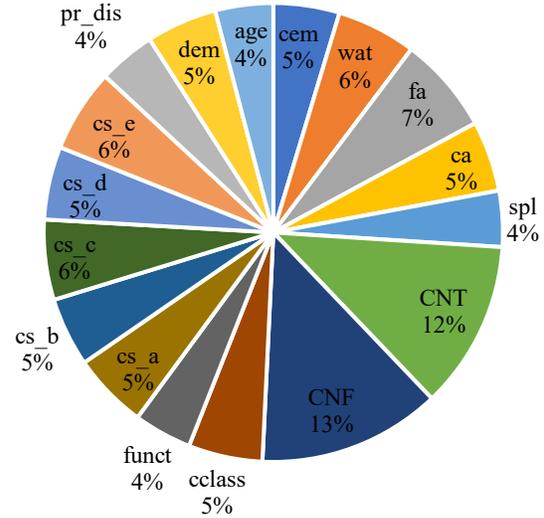
Figure 7.5.30 Contribution of the input parameters to the output value, for models: (a) COMP; (b) FLEX; (c) COMP+FLEX; (d) RESIST

Input parameter, which is predominating for all models, is the amount of the nanofiller. This is expected, and confirms the validity of the datasets. In general, there are no input parameters which could be omitted from the learning process. The implication may be that more input parameters would give more specificity and quality to the learning since Figure 7.5.30 refers to Group I ,i.e., the experimental investigation of CNT/CNF reinforced concrete composite material. Further expansion might include the dispersion technique and materials. Figure 7.5.31 shows the sensitivity analysis results for Group II datasets.
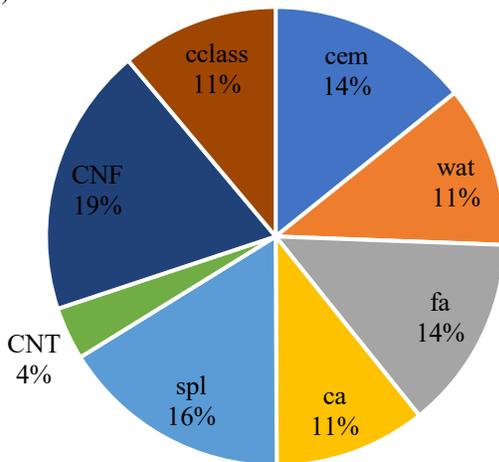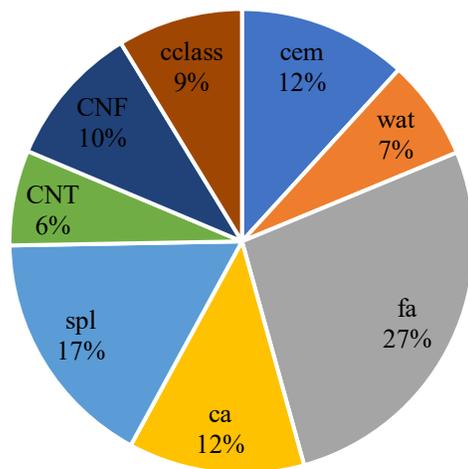
(c)
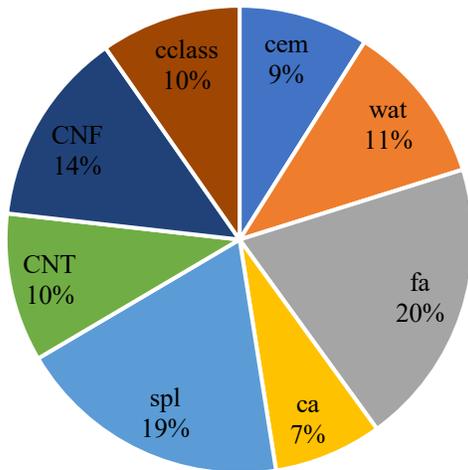
Figure 7.5.31 Contribution of the input parameters to the output value, for models: (a) COMP; (b) FLEX; (c) COMP+FLEX

For the models from Group II, the situation is quite different. The influence of nanofillers is much lesser, which serves to show how the simulated material did not acknowledge realistically the influence of the nanomaterial on the overall enhancement of concrete properties. The sensitivity analysis shows that aggregate and superplasticizer affect the learning process the most compared to other input parameters, while in Group I, these factors had significant but not overruling contribution.

5.7 Comparison of results

Comparison of the behavior of the models from Group I and Group II is provided by comparing the models using the COMP+FLEX dataset. In order to properly compare the ANN models, an adjustment to the COMP+FLEX dataset was provided to additionally give the independent target values (C+F(C) for compressive strength and C+F(F) for flexural strength). To this end, another two sets of 12 ANN models were tested with the single target value from the experimental research dataset. The complete datasets are given in Appendix B1 and B2, and the results of the ANN models in Appendix B5 and B7 for Group I and Group II, respectively. The architecture between these sets differs in the number of the input neurons and thus the number of neurons in the hidden layer. However, this difference may still be considered minimal since the Group I dataset counts 11 and the Group II dataset has 8 input neurons. Moreover, the subset ratios coincide, and the size of the sets is very similar. With 175 data tuples in Group I dataset and 164 data tuples in the Group II dataset, the difference may be considered negligible.

The comparison of results is made separately for the prescribed models developed using Neural Fitting tool and the scripted models using the script editor in Matlab R2020b. Since the procedure differs between the prescribed and the scripted models, the comparison between them will be discussed on a global level reviewing the overall process of development and learning.

Prescribed models

Table 7.15 Results for prescribed models from Group I

#	Model	R - training	R - validation	R - testing	R - total	MSE	Epoch
1	C+F_70_10_20-11	0.90648	0.69973	0.78576	0.86913	0.01605	10
2	C+F_70_10_20-23	0.92494	0.72127	0.90038	0.90129	0.02143	12
3	C+F_70_10_20-33	0.95484	0.91919	0.76254	0.88072	0.00657	18
4	C+F_80_10_10-11	0.96269	0.89552	0.83256	0.93468	0.0126	27
5	C+F_80_10_10-23	0.96423	0.89838	0.8659	0.95102	0.008822	21
6	C+F_80_10_10-33	0.94185	0.61875	0.48269	0.83489	0.04276	16
7	C+F_80_5_15-11	0.94032	0.97165	0.93642	0.94066	0.00431	19
8	C+F_80_5_15-23	0.94552	0.93936	0.90559	0.93937	0.007035	16
9	C+F_80_5_15-33	0.95811	0.97166	0.89735	0.95118	0.003036	12
10	C+F_85_5_10-11	0.85493	0.7315	0.79043	0.83851	0.02148	10
11	C+F_85_5_10-23	0.91374	0.80006	0.51481	0.88078	0.02081	10
12	C+F_85_5_10-33	0.93165	0.89101	0.7667	0.90683	0.006886	10
13	C+F(C)_70_10_20-11	0.94306	0.88933	0.79261	0.90407	0.00638	16
14	C+F(C)_70_10_20-23	0.99035	0.93642	0.91792	0.97062	0.0011	36
15	C+F(C)_70_10_20-33	0.99088	0.92069	0.53997	0.83021	0.00105	21
16	C+F(C)_80_10_10-11	0.8804	0.96462	0.92023	0.89466	0.01221	12
17	C+F(C)_80_10_10-23	0.98931	0.97563	0.85569	0.97368	0.001218	41
18	C+F(C)_80_10_10-33	0.99117	0.94651	0.8712	0.97231	0.00097	40
19	C+F(C)_80_5_15-11	0.91441	0.86477	0.76372	0.8765	0.00913	14
20	C+F(C)_80_5_15-23	0.98657	0.8777	0.79109	0.94961	0.00154	25
21	C+F(C)_80_5_15-33	0.92851	0.85586	0.91949	0.91782	0.00754	9
22	C+F(C)_85_5_10-11	0.94219	0.95031	0.6253	0.88351	0.0061	20
23	C+F(C)_85_5_10-23	0.98928	0.98212	0.80141	0.94613	0.00117	28
24	C+F(C)_85_5_10-33	0.98615	0.97294	0.73419	0.97554	0.00166	19
25	C+F(F)_70_10_20-11	0.95316	0.88552	0.77722	0.9085	0.00371	21
26	C+F(F)_70_10_20-23	0.94468	0.75063	0.87348	0.91439	0.00459	14
27	C+F(F)_70_10_20-33	0.93485	0.82416	0.74891	0.89831	0.00624	10

28	C+F(F)_80_10_10-11	0.91492	0.9691	0.8446	0.90721	0.0071	17
29	C+F(F)_80_10_10-23	0.93363	0.78578	0.92823	0.92145	0.00528	11
30	C+F(F)_80_10_10-33	0.95331	0.92088	0.72288	0.92353	0.00356	13
31	C+F(F)_80_5_15-11	0.89549	0.59091	0.88892	0.87907	0.00736	10
32	C+F(F)_80_5_15-23	0.94491	0.98692	0.90541	0.93861	0.00455	27
33	C+F(F)_80_5_15-33	0.92103	0.60936	0.84939	0.87552	0.0068	8
34	C+F(F)_85_5_10-11	0.93448	0.95476	0.95327	0.93617	0.00524	21
35	C+F(F)_85_5_10-23	0.87832	0.56263	0.91745	0.87404	0.00938	8
36	C+F(F)_85_5_10-33	0.91805	0.94984	0.91167	0.91785	0.0065	9

Table 7.16 Results for prescribed models from Group II

#	Model	R - training	R - validation	R - testing	R - total	MSE	Epoch
1	S_C+F_70_10_20-8	0.99629	0.98852	0.98441	0.99333	0.000419	70
2	S_C+F_70_10_20-17	0.99918	0.99693	0.9643	0.99401	0.000093	81
3	S_C+F_70_10_20-24	0.98782	0.98054	0.93792	0.97471	0.00126	24
4	S_C+F_80_10_10-8	0.9985	0.99993	0.99866	0.9987	0.00016	183
5	S_C+F_80_10_10-17	0.98866	0.99668	0.9673	0.98778	0.0012	33
6	S_C+F_80_10_10-24	0.97764	0.9449	0.94194	0.97232	0.00264	12
7	S_C+F_80_5_15-8	0.98663	0.97822	0.98998	0.98657	0.00139	38
8	S_C+F_80_5_15-17	0.99892	0.99907	0.99575	0.99845	0.00013	47
9	S_C+F_80_5_15-24	0.99497	0.98721	0.85313	0.97099	0.000563	27
10	S_C+F_85_5_10-8	0.98122	0.95136	0.9919	0.98092	0.001904	38
11	S_C+F_85_5_10-17	0.99868	0.9981	0.99761	0.99851	0.00014	78
12	S_C+F_85_5_10-24	0.99933	0.99988	0.99622	0.99902	0.00007	113
13	S_C+F(C)_70_10_20-8	0.99996	0.99984	0.88325	0.96522	0.000005	101
14	S_C+F(C)_70_10_20-17	0.99974	0.99981	0.98778	0.9974	0.000032	46
15	S_C+F(C)_70_10_20-24	0.99991	0.99976	0.97514	0.99494	0.00001	51
16	S_C+F(C)_80_10_10-8	0.99995	0.99982	0.99908	0.99989	0.000007	176
17	S_C+F(C)_80_10_10-17	0.99996	0.99985	0.9994	0.99994	0.000005	143
18	S_C+F(C)_80_10_10-24	0.9999	0.99992	0.99992	0.99993	0.000007	54
19	S_C+F(C)_80_5_15-8	0.98644	0.99994	0.93805	0.98166	0.0017	21
20	S_C+F(C)_80_5_15-17	0.99984	0.99978	0.85702	0.97192	0.00002	32
21	S_C+F(C)_80_5_15-24	0.99957	0.99986	0.99375	0.99863	0.00005	32
22	S_C+F(C)_85_5_10-8	0.99985	0.99984	0.9999	0.99985	0.00002	57
23	S_C+F(C)_85_5_10-17	0.99334	0.99921	0.98391	0.99298	0.00087	28
24	S_C+F(C)_85_5_10-24	0.99522	0.99884	0.99226	0.99501	0.00062	24

25	S_C+F(F)_70_10_20-8	0.97565	0.98298	0.9758	0.9759	0.00204	12
26	S_C+F(F)_70_10_20-17	0.99737	0.99486	0.99466	0.99651	0.00027	39
27	S_C+F(F)_70_10_20-24	0.9978	0.98805	0.96117	0.98743	0.00021	61
28	S_C+F(F)_80_10_10-8	0.99072	0.99059	0.99232	0.9904	0.0009	45
29	S_C+F(F)_80_10_10-17	0.98722	0.9862	0.93984	0.98325	0.00119	17
30	S_C+F(F)_80_10_10-24	0.98046	0.98952	0.962	0.97864	0.002	10
31	S_C+F(F)_80_5_15-8	0.99497	0.99188	0.98896	0.99399	0.00056	45
32	S_C+F(F)_80_5_15-17	0.99504	0.97509	0.98947	0.99344	0.00052	34
33	S_C+F(F)_80_5_15-24	0.99262	0.9974	0.88519	0.97076	0.0007	13
34	S_C+F(F)_85_5_10-8	0.98378	0.99301	0.97706	0.98388	0.0015	15
35	S_C+F(F)_85_5_10-17	0.99827	0.99146	0.99801	0.99793	0.00017	105
36	S_C+F(F)_85_5_10-24	0.99855	0.99954	0.98348	0.99677	0.00014	102

The R values for training, validation, and testing stages and total R values, as well as the total mean squared error and number of iterations within a single epoch which were needed for convergence, are given in Table 7.15 for models using the dataset formed from experimental measurements (Group I), and in Table 7.16 for models using the dataset from numerical simulations (Group II). Figures 7.5.32-7.5.34 show the comparison of total regression coefficients for the dataset with compressive strength and flexural strength as the target value (Figure 7.5.32); for the dataset with only compressive strength as the output (Figure 7.5.33); and for the dataset with only flexural strength as the output (Figure 7.5.34).
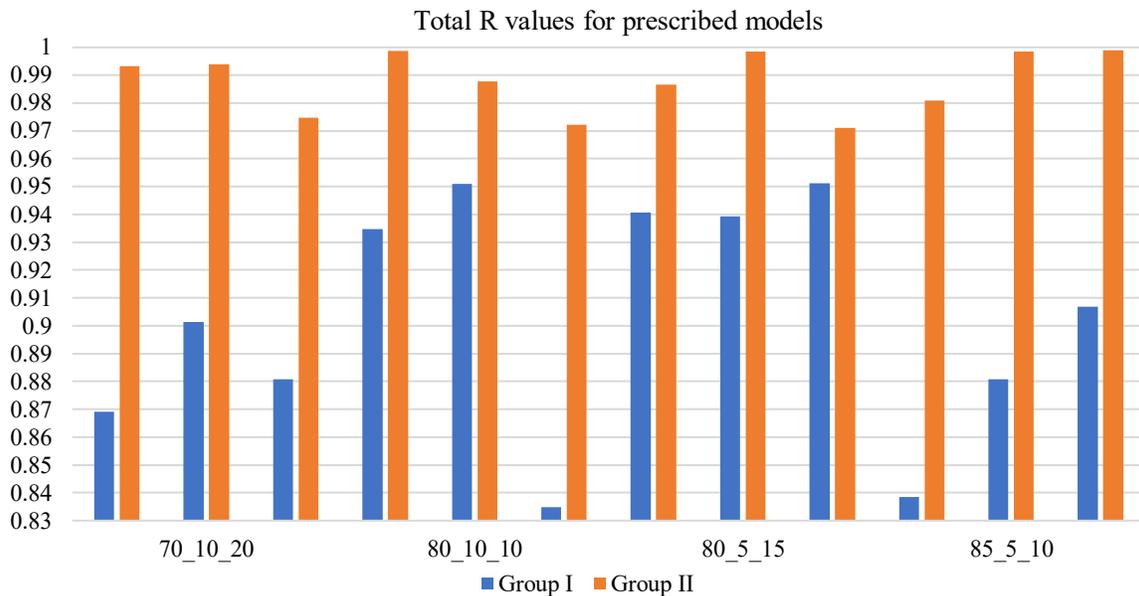
Figure 7.5.32 Total R values for prescribed ANN models for COMP+FLEX dataset

Total R values for C+F(C) dataset
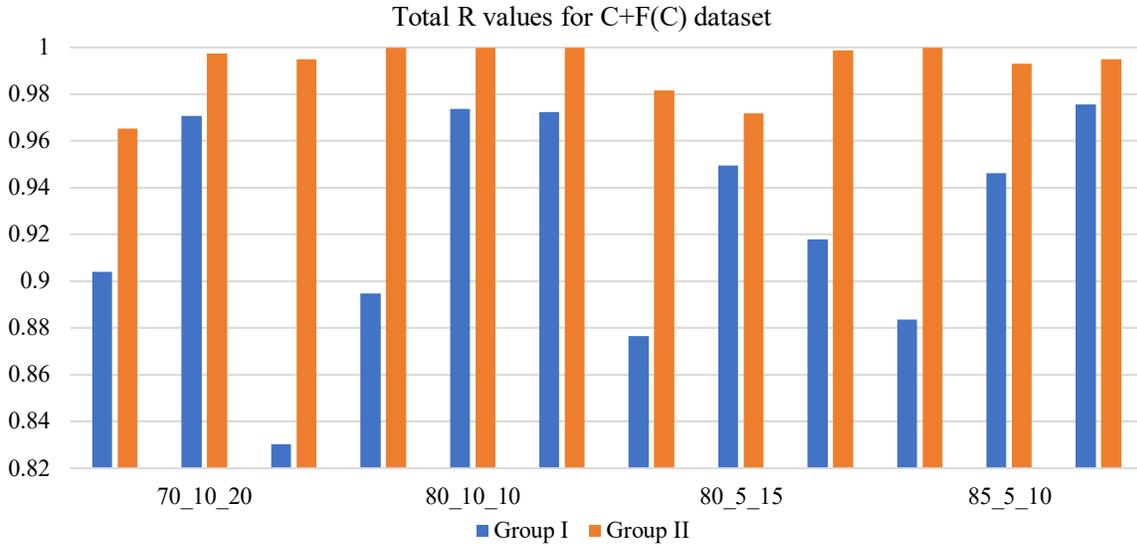
Figure 7.5.33 Total R values for prescribed models using the dataset with compressive strength as output

Total R values for C+F(F) dataset
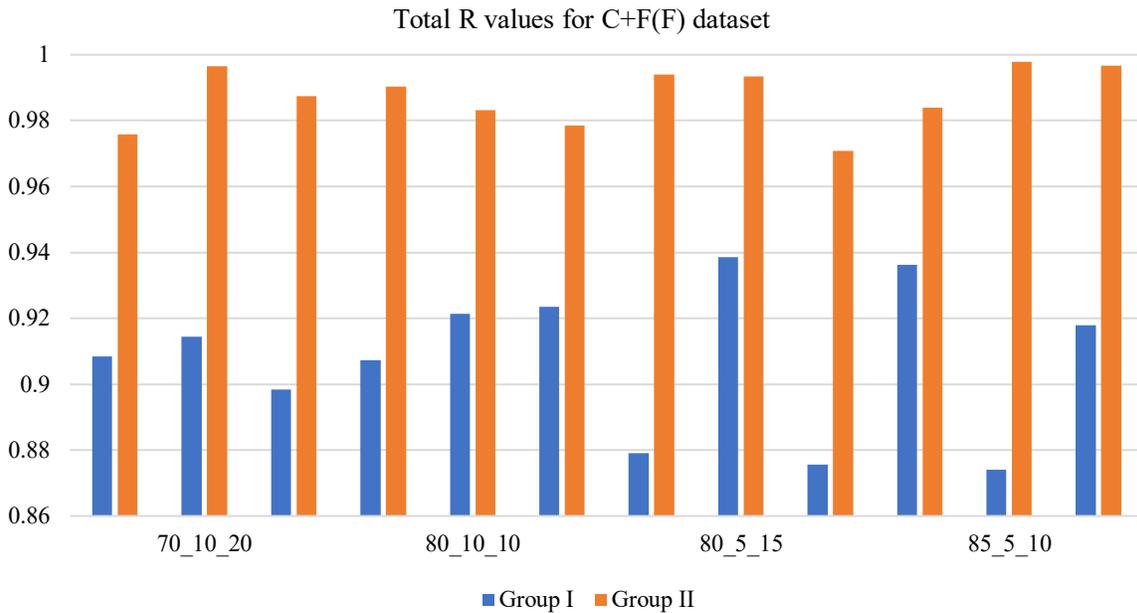
Figure 7.5.34 Total R values for prescribed models using the dataset with flexural strength as output

The histogram given in Figure 7.5.32 shows that the best match between the models with coupled outputs is established for the architecture presented by the subset ratio of 80/5/15 for training/validation/testing for all three varieties of the number of hidden neurons. Within this subgroup, the best match is shown for the models with the number of hidden neurons that equals *Nh=3Ni*. Similarly, for the models with a single output for the compressive strength, the best match is shown for the subset ratio of 80/10/10 and for the number of hidden neurons that equals *Nh=2Ni+1* and *Nh=3Ni*. The interesting occurrence is visible when the final dataset with the single

output of the flexural strength is observed. The optimal architecture is represented by the subset ratio of 70/10/20 for training/validation/testing, showing consistency when the number of hidden neurons varies. However, it should be noted that the deviations of the total R value between models are the smallest comparing to other subset ratios. Although the results of flexural strength obtained from the numerical simulations are unrealistically high, as shown in Chapter VI, the total R values are very comparable, with the deviations of only around 0.05.

Scripted models

Table 7.17 Results for scripted models based on datasets from Group I

#	Model	R - training	R - validation	R - total	MSE	RMSE
1	COMP Initial	0.9609	0.94005	0.96259	0.0007135	0.0023
2	COMP Optimized n=25	0.97443	0.97267	0.97363	0.0012	0.0073
3	COMP Optimized n=31	0.99234	0.92923	0.98407	0.00039729	0.000019355
4	COMP Working	0.99422	/	0.99422	0.0004653	0.0001329
5	FLEX Initial	0.92983	0.91428	0.92794	0.0056	0.00043963
6	FLEX Optimized n=21	0.96484	0.9223	0.95773	0.0028	0.0029
7	FLEX Optimized n=30	0.96832	0.87704	0.95507	0.0025	0.000071645
8	FLEX Working	0.98833	/	0.98833	0.00093724	0.00065467
9	COMP+FLEX Initial	0.92493	0.83462	0.9103	0.018	0.134
10	COMP+FLEX Optimized n=18	0.93889	0.90908	0.93429	0.0986	0.2495
11	COMP+FLEX Optimized n=24	0.9831	0.91993	0.97254	0.0813	0.2851
12	COMP+FLEX Working	0.99363	/	0.99363	0.0892	0.3033

Table 7.18 Results for scripted models based on datasets from Group II

#	Model	R - training	R - validation	R - total	MSE	RMSE
1	COMP Initial	0.99233	0.98655	0.99187	0.001	0.0319
2	COMP Optimized n=10	0.98123	0.99928	0.98639	0.0019	0.00065577
3	COMP Optimized n=13	0.9994	0.99969	0.99991	0.000007986	0.0028
4	COMP Working	0.99998	/	0.99998	0.00000231	0.0028
5	FLEX Initial	0.97289	0.98322	0.97356	0.0028	0.0533
6	FLEX Optimized n=10	0.99701	0.99238	0.99642	0.0003194	0.00006157
7	FLEX Optimized n=13	0.98728	0.98169	0.98585	0.0014	0.0378
8	FLEX Working	0.99894	/	0.99894	0.0001047	0.0378
9	COMP+FLEX Initial	0.97484	0.94526	0.97113	0.1461	0.3823
10	COMP+FLEX Optimized n=13	0.99951	0.99689	0.99915	0.1438	0.2505

11	COMP+FLEX Optimized n=17	0.99959	0.99827	0.99931	0.135	0.3674
12	COMP+FLEX Working	0.99968	/	0.99968	0.138	0.3674

Comparison between the scripted ANN models is provided by observing the response of COMP, FLEX, and COMP+FLEX models, as shown in Tables 7.17 and 7.18. The RESIST models are excluded since the datasets formed from the numerical simulations do not contain information on electrical resistivity. As it was previously described, the number of hidden neurons was determined through the optimization process, so the architecture of models from the two groups differ according to the behavior of an individual network. Nevertheless, the numbers of neurons in the hidden layer do not vary significantly since the upper limit equals $Nh=3Ni$ in all cases of optimization. Figures 7.5.35-7.5.37 show the comparison of the total R values for initial, optimized, and working models from each set.
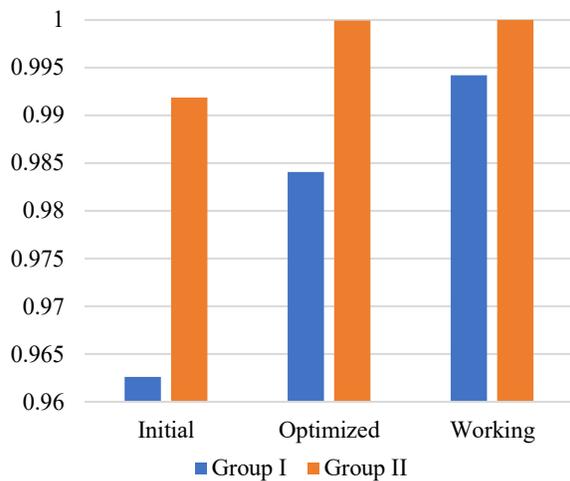
Figure 7.5.35 Comparison of COMP models
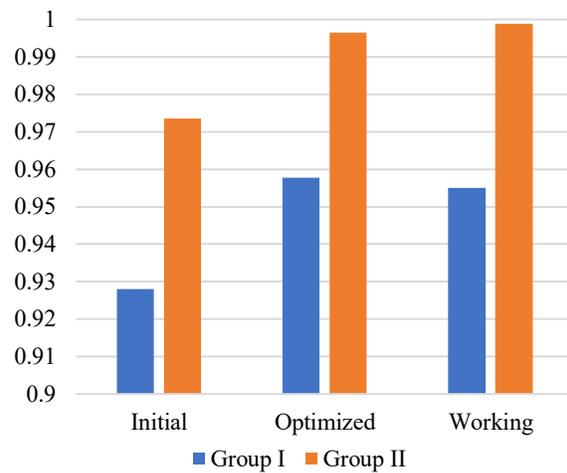
Figure 7.5.36 Comparison of FLEX models
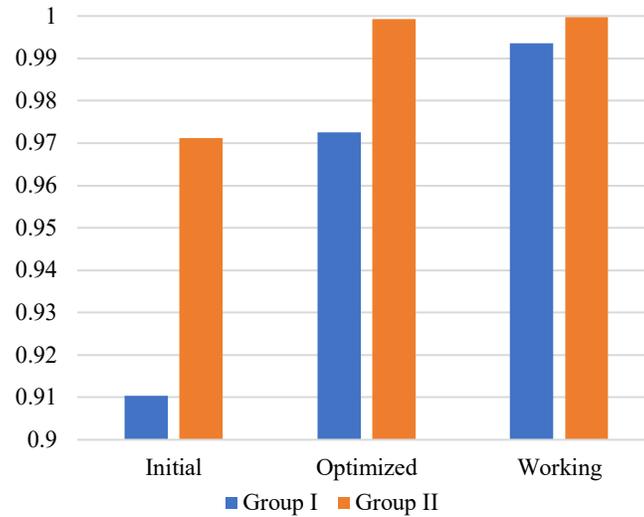
Figure 7.5.37 Comparison of COMP+FLEX models

Regression coefficients are very high, over 0.9, for all models even in the initial stage where the number of hidden neurons equals the number of input neurons. As expected, in all cases, datasets from Group II give a much better response because of their linear progression. Nevertheless, it is useful to observe and validate the experimental testing by comparing the realistic and the 'idealized' mixtures.

Moreover, the consideration of the prescribed and the scripted models leads to the conclusion that even though it demands more time and expertise, the scripted models express much better behavior. The point of improvement lies in the significant control that the designer has over the learning process when the network is manually scripted. This way, the basic premise of the user-friendliness is somewhat hindered, however, the script itself for this kind of a simple shallow architecture of the network and basic learning parameters does not demand any deeper knowledge of programming. Additionally, less models are needed to obtain a very high probability of prediction, which implies that the duration of exploring different architectures in NF tool is longer than conducting the optimization of the initial network.

CHAPTER VIII Summary and conclusions

1.   Numerical simulations

Numerical simulations in this research are provided using ANSYS platform and its various features. Mainly, the application of the Material Designer feature was inspected to establish if it is possible to model the CNT/CNF reinforced cementitious composite materials realistically. The first issue which arouse was the fact that Material Designer is not able to generate the electrical properties of the composite material, making it impossible to inspect the sensing property. Secondly, the homogenization and, later on the static analysis for the mixtures with weight fractions of the nanofiller above 0.1% gave unrealistic results in terms of the flexural capabilities of the composite materials. The mixtures with higher weight fractions showed exceptionally high values of Young's modulus and flexural strength, which in actuality, the concrete matrix material could not support. Furthermore, the results of the compression test showed an insignificant increase, or even decrease, of the compressive strength of the composite materials for higher weight fractions, which does not coincide with the experimental results. However, the composite materials with lower weight fractions of up to 0.1% did show satisfactory behavior, considering the expected deviation of up to 15% between the experimental and numerical results.

It may be concluded that ANSYS Material Designer is a useful tool for the investigation of material properties and strength of CNT/CNF reinforced cementitious composite materials with lower weight fractions of the nanofiller material. Although some issues have been encountered, it may be used successfully the for initial stages of the semi-experimental concrete mix design methods, in terms of setting the initial mixture constituents and weight fractions of the nanofiller. It shows satisfactory results for the mixtures with weight fractions of up to 0.1% if the following recommendations are carried out:

-   Type of RVE: Random UD Composite
-   Seeding: 10 000-25 000
-   Mean misalignment angle: 2
-   Repeat count: 1
-   Meshing type: Conformal

2. Artificial neural networks

Artificial neural networks were developed using the Neural Fitting tool and script editor in Matlab R2020b for the creation of the models and providing the initial training, validation, testing, evaluation, and sensitivity analysis. Neural Fitting tool provides pre-set shallow topology networks with the sigmoid activation function and linear transfer function. Subsets are set by the user, allowing limited manipulation of the dataset and the architecture. The information, which is collected from several experimental investigations and the numerical simulations done in this work, is further used to form several datasets for the ANN models. The datasets are classified depending on their origin, i.e., whether the data tuples are obtained experimentally or numerically. Every dataset is used for 12 prescribed ANN models organized in four subgroups by three. Every subgroup differs in the subset ratio, and the three models within each subgroup have a different number of hidden neurons. Every dataset is also used for developing scripted ANN models, where each dataset was provided for an initial model with optimization, two optimized models, and a final working model.

Results are presented via mean squared error (MSE), root mean squared error (RMSE), mean absolute error (MAE), and the regression coefficient (R value). Regression coefficients are higher than 0.8 for all models that have a mechanical property as an output signal. As for the RESIST dataset, models based on it have not shown satisfactory behavior or prediction probability. As for the results of models from Group II, all R values are higher than 0.95, which is somewhat expected when the dataset is obtained through idealized materials and numerical simulations. The numerical analysis in ANSYS is linear, therefore, the data presented to the ANN is very favorable for the learning process. The mean squared error values for all models are exceedingly low, and the error distribution is more or less regular, especially for the models using the experimental data.

After initial training, validation, and testing, the prescribed ANN models showed satisfactory results in predicting the compressive strength and the flexural strength of CNT/CNF reinforced concrete. Considering only the prescribed ANN models, it may be concluded that the optimal architecture includes subset ratios where the training subset consists of 70 to 80% of the dataset, and the number of hidden neurons equals the number of input neurons or is equal to $Nh=2Ni+1$. The tested variation of the number of hidden neurons which equals $Nh=3Ni$ has shown satisfactory results. The difference between the variations of Nh within a single subgroup is not significant. It can be assumed that $Nh=3Ni$ would be most optimal in cases where the number of

input neurons is lower than 8 to allow enough iterations for convergence and proper generalization. The validity of all results is confirmed after the final evaluation of the best behaving prescribed models from each group. This work has been published by the author under the title "Application of artificial neural networks for prediction of mechanical properties of CNT/CNF reinforced concrete" [153] in the international journal *Materials*.

Artificial neural network models based on the RESIST dataset, where the input gives information on the mixtures, geometry, and age of specimens, and the test set-up, did not give satisfactory results. All models from this group gave R values lower than 0.6, going even as low as 0.28. Moreover, the distribution of the regression and errors is very irregular. Since the initial results were unsatisfactory, the initial RESIST dataset was revised, and a reduced dataset was formed. The volume electrical resistivity for which it was suspected that have not reached the percolation threshold, as well as the cases where the resistivity is higher for the higher nanofiller wt.%, were excluded from the revised dataset. Furthermore, a new input neuron is added to provide information on the cross-sectional area of the sample. After the revision, the new dataset was employed, keeping the topology of the models intact. The training, validation, and testing is repeated, and the results have not shown much improvement. The regression coefficients are again lower than 0.6, and the network shows instability and scattering of the results. Since the results repeatedly showed to be unsatisfactory, the conclusion is that the quality of the dataset is too low.

Scripted models showed better prediction probability than the prescribed models. All models have R values higher than 0.9, and even the RESIST models showed better results even though their behavior is still not satisfactory. The scattering appears again very similar to the prescribed models, which implies that the problem is, in fact primarily in the dataset. An interesting occurrence is observed for the RESIST working model. This model uses a full dataset only for training, and the learning process is barely limited, and the consequence is that the probability of the prediction is slightly higher. The RESIST working model, however, has shown significant raise in the R value after training. If only the R value would be observed, it could be concluded that this network is highly functioning. However, seeing the scattering (Figure 7.5.14) is enough to imply that this R value is not realistic and that this network is not reliably able to generalize. As for the prescribed models based on the mechanical properties of the CNT/CNF concrete composites, very good behavior and results are provided. Developing the networks manually gives more freedom to the designer to use different algorithms or just the learning parameters. It is much more

informative in terms of the topology of the network since the number of hidden neurons may iteratively change and provide the wanted information, showing which topology is the most favorable. Moreover, results may be represented through many statistical values instead of only the R value and MSE as it is for the prescribed networks.

3.   Final conclusions

These investigations included the multi-physics approach in addressing the issue of concrete mix design and the application of numerical simulations and of artificial neural networks for predicting mechanical and electrical properties of CNT/CNF reinforced cementitious composite materials. Summarizing all the works and analyzes carried out in this dissertation, the following may be concluded:

-    *Mechanical properties are improved by the presence of the CNT or CNF nanofiller.* It has been shown that if proper dispersion is achieved, and the mixing and molding of the concrete is made according to the standard, the mechanical properties of the composite material are improved.

-    *Electrical properties of concrete may be enhanced by the presence of the CNT or CNF nanofiller.* Crossing the percolation threshold of the nanofillers allows electrical conductivity through the concrete composite material. In addition, proper dispersion of the nanofiller and avoidance of the agglomeration is a prerequisite.

-    *Numerical models of CNT/CNF reinforced concrete cannot realistically respond to mechanical stimuli.* ANSYS models of the CNT/CNF concrete composite material showed promising results only for up to 0.1 wt.% of the nanofiller.

-    *The mechanical behavior of CNT/CNF reinforced concrete may be predicted using artificial neural networks.* Neural networks for the prediction of compressive and flexural strength of the concrete composite material show a very high probability of prediction.

-    *The electrical behavior of the CNT/CNF reinforced concrete cannot be predicted using artificial neural networks.* The lack of comprehensive information on the electrical behavior of these materials leads to insufficient learning materials for the neural network. It is shown how only false-positive results may be achieved.

-    *The number of neurons in the hidden layer of the artificial neural network, which equals to $N_h = 3 \cdot N_i$, may be used to achieve the satisfactory behavior of the network and valid predictions.*

The assumed value of the number of hidden neurons shows satisfactory behavior and does not exhibit overfitting of the networks in this work.

CHAPTER IX Directions for further research

Several different problems have been detected during research, which should be included and investigated in the future work regarding this topic. First of all, the experimental research for the electrically sensitive type of concrete is not comprehensively standardized. To this date, the fabrication is based on a trial-and-error process using the combination of several different standards. Hence, the results between different authors are hardly comparable and useful in practice. The fabrication procedures, which were attempted to numerically reproduce, were too different to comprehend under a parametric analysis. In that sense, the first step to obtain results that are more worthwhile would be making comprehensive experimental research and establishing a reliable and comprehensive experimental procedure based on the most commonly available equipment and materials, including some simpler methods of nanofiller dispersion. Since the problem arises with the determination of the electrical properties, the focus should turn on the methodology of dispersion and mixing, probe material and distance, and the testing method. It has been proven on several occasions that the improvement of the mechanical properties is the consequence of the proper dispersion of the nanofiller, so the focus should transfer to the electrical abilities to develop a multifunctional smart material that could be easily used in practice.

After establishing the experimental portion of the procedure and providing concrete and detailed fabrication methodology, the next step should be examining the possibilities in terms of other softwares that are able to encompass meso-structure of concrete and the complexity of multi-physics, including both the constituent materials and the interfaces between them, such as ABAQUS for building the mesostructured and providing the mechanical tests, or FLUENT and CFX for the microstructure and the chemical simulations of porosity, diffusivity, and permeability, as well as durability simulations such as the freeze-thaw cycle testing. Application of numerical simulations could represent a substitute for the expensive and timely experimental procedure of fabrication and testing. Furthermore, some research work has been done, such as simulations of contact resistance of carbon nanotubes in polymers [154] or simulations of CNT reinforced mortar [59], which may be used for implementation of the electrical behavior of the carbon nanomaterials. Lastly, the artificial neural networks should be reprogrammed to give the optimal mixture

proportions for the wanted properties of the composite material. This research shows that the initial stage is completed, and it is proven that machine learning is effective in this matter. Further work should include the development of more powerful programming so that the predictions could also be extrapolate and not only interpolated within a dataset. If a stable ready-to-use model for prediction of the mix proportions of CNT/CNF reinforced cementitious composite material will be successfully produced, the use of smart material could finally be transferred from the laboratory research. It could be implemented in a wider application in civil engineering practice, and a system of custom ordering of the smart and sustainable materials could be developed and opened for wider population.

Abstract

Concrete mix design is becoming essential in concrete construction due to the rising prices of construction materials, and recent implementation of alternative materials in civil engineering practice. Concrete mix design serves to optimize the concrete mixture and explore possibilities of adding materials such as recycled plastic, recycled aggregate, different types of nanomaterials, etc. Nanomaterials are especially attractive as a filler material in concrete because they may provide additional function to the concrete, including self-cleaning, self-healing, self-sensing, and others. Most popular nanomaterials used in concrete matrix are carbon black, C60, nano-TiO_2, nano-Fe_2O_3, carbon nanotubes, carbon nanofibers, and graphene. This research work concerns with the development, fabrication process, and alternative methods of concrete mix design for carbon nanotube (CNT) or carbon nanofiber (CNF) concrete composite material. This composite material is a structural material with enhanced mechanical properties and it expresses self-sensing capabilities as an additional function. The ability of self-sensing may be very significant for the development of the sensing systems, and structural monitoring field in general. If sensing is possible within the material itself, the monitoring of the structure can be constant and self-sufficient if provided with a powerful processing unit and data storage. Currently, self-sensing concrete is not used in civil engineering practice, partly due to the lack of appropriate sensing equipment and partly due to the high costs of a relatively experimental material. This dissertation presents novel methods of predicting the behavior of CNT/CNF reinforced concrete, including numerical simulations of the composite material in ANSYS and the application of artificial neural networks for predictions of compressive strength, flexural strength, and volume electrical resistivity of the material. Experimental work that deals with the fabrication and testing of these materials is found in literature and collected for validation and predictions. The numerical models are developed in ANSYS to simulate the properties of the composite material, as well as to simulate the experimental testing including axial compression test and three-point bending test. Furthermore, artificial neural network are developed in Matlab, using neural fitting tool and the script editor. The networks are trained using both experimental results and numerical results to establish the applicability of these methods in the civil engineering practice.

Symbols and abbreviations

Symbols

F – electrostatic force

q – charge of particles

r – distance between particles

I – electric current

V – voltage

R – electrical resistance; coefficient of regression

ρ – electrical resistivity

E – magnitude of the electric field of conductor

J – magnitude of the current density of conductor

σ – electrical conductivity

l – length of the sample, distance between two electrodes

A – cross-sectional area of object

n, m – vectors describing the chirality angle

f(X) – function of any external stimuli such as stress, strain, force, etc.

$\Delta\rho$ – change in electrical resistivity

ρ_0 – electrical resistivity at t=0s

K^{2+} - potassium

Na^{2+} - sodium

Ca^{2+} - calcium

OH^- - hydroxide

SO_2^{4+} - sulfur dioxide

x – input signal

y – output signal

w – weight of connection

b - bias

N_i – number of input nodes

N_o – number of output nodes

norm - normalization

min – minimum value

max – maximum value

R^2 – multiple coefficient of determination

b – width of the sample

d – height of the sample

°C – Celsius degrees

min – minutes

Min – minimum

Max – maximum

Abbreviations

w/c – water to cement

wt% - weight fraction percentage

ACI – American Concrete Institute

IS – Indian Standard

CNT – carbon nanotube

CNF – carbon nanofiber

C-S-H – calcium-silicate-hydrate

EMI – electromagnetic interference

FEM – finite element method

RVE – representative volume element

CAD – computer aided design

SEM – scanning electron microscopy

TEM – transmission electron microscopy

OPC – Ordinary Portland cement

TNWDIS – polyethylene glycol aromatic imidazole

NaDDBS, SDB, SDS – sodium dodecyl benzene sulfonate

SLS – lignosulfonic acid sodium salt

SLDS – sodium lauryl with defoamer

TX – Triton X-100

GA – Gum arabic

CTB – cetyltrimethyl ammonium bromide

SFC, PCE – polycarboxylate based surfactant

PVP – polyvinyl pyrrolidone

SDS – sodium dodecyl sulfate

ESEM – environmental scanning electron microscopy

XRD – X-ray diffractometer

UV-Vis – ultra-violet visible spectrum analysis

AC – alternating current

ASTM - American Association for Testing and Materials

UNE - Spanish Association for Standardization

ANN – artificial neural network

BP – backpropagation

LM – Levenberg-Marquardt

MSE – minimum squared error

MAE – minimum absolute error

ReLU – rectified linear unit

ELU – exponential linear unit

NF – neural fitting

COMP – dataset with compressive strength as output value

FLEX – dataset with flexural strength as output value

RESIST – dataset with electrical volume resistivity as output value

C+F – dataset with compressive and flexural strength as output value

CEM – cement

WAT – water

FA – fine aggregate

CA – coarse aggregate

SPL – superplasticizer

CEM_CLASS – cement class

FUNCT – functionalization

C-S_A – cross-section A

C-S_B – cross-section B

C-S_C – cross-section C

C-S_D – cross-section D

C-S_E – cross-section E

C-S_F – cross-section F

C-S_G – cross-section G

C-S_H – cross-section H

C-S_I – cross-section I

DEM-AGE –age of sample at the moment of demolding

AGE – age of sample at the day of testing

Bibliography

[1]   Neville, A.M., J.J. Brooks, J.J. Concrete Technology, 2nd edition, 2010, Pearson Education Limited, Harlow, England. ISBN 978-0-273-73219-8

[2]   https://structville.com/2017/08/full-process-on-how-to-carry-out-concrete-mix-design.html

[3]   Ahmad, S., Alghamdi, S.A. A Statistical Approach to Optimizing Concrete Mixture Design, The Scientific World Journal, 2014 (2014) 561539-7. http://dx.doi.org/10.1155/2014/561539

[4]   Shi, C., Wu, Z., Lv, K., Wu, L. A review on mixture design methods for self-compacting concrete, Construct. Build. Mater. 84 (2015) 387–398. http://dx.doi.org/10.1016/j.conbuildmat.2015.03.079.

[5]   Shakhmenko, G., Birsh, J. Concrete mix design and optimization, 2nd International PhD Symposium in Civil Engineering, Budapest, 1998.

[6]   Sayed-Ahmed, M. Statistical Modelling and Prediction of Compressive Strength of Concrete, Concr. Res. Lett. 3/2 (2012) 452-458. DOI: 10.6084/M9.FIGSHARE.105905

[7]   Zelić, J., Rušić, D., Krstulović, R. A mathematical model for prediction of compressive strength in cement–silica fume blends, Cem. Concr. Res. 34 (2004) 2319–2328. doi:10.1016/j.cemconres.2004.04.015.

[8]   Wang, X.-Y., Park, K.-B. Analysis of compressive strength development of concrete containing high volume fly ash, Construct. Build. Mater. 98 (2015) 810–819. http://dx.doi.org/10.1016/j.conbuildmat.2015.08.099.

[9]   Yu, F., Sun, D., Sun, G., Ling, S., Hu, M., Ma, J. A modified mix design method for pervious concrete based on Mohr-Coulomb failure criterion, Constr. Build. Mater. 269 (2021) 121801. https://doi.org/10.1016/j.conbuildmat.2020.121801

[10]   Pradhan, S., Kumar, S., Barai, S.V. Recycled aggregate concrete: Particle Packing Method (PPM) of mix design approach, Constr. Build. Mater. 152 (2017) 269–284. http://dx.doi.org/10.1016/j.conbuildmat.2017.06.171

[11]   Li, P., Ran, J., Nie, D., Zhang, W. Improvement of mix design method based on paste rheological threshold theory for self-compacting concrete using different mineral additions in ternary blends of powders, Constr. Build. Mater. 276 (2021) 122194. https://doi.org/10.1016/j.conbuildmat.2020.122194

[12]   Ashish, D.K., Verma, S.K. Determination of optimum mixture design method for self-compacting concrete: Validation of method with experimental results, Construct. Build. Mater. 217 (2019) 664–678. https://doi.org/10.1016/j.conbuildmat.2019.05.034.

[13]   Meng, D., Wu, X., Quan, H., Zhu, C. A strength-based mix design method for recycled aggregate concrete and consequent durability performance, Constr. Build. Mater. 281 (2021) 122616. https://doi.org/10.1016/j.conbuildmat.2021.122616

[14]   Qasrawi, H. Design of Normal Concrete Mixtures Using Workability-Dispersion-Cohesion Method, Adv. Civ. Eng. 2016 (2016) e1035946. http://dx.doi.org/10.1155/2016/1035946.

[15]   Ziaei-Nia, A., Tadayonfar, G.-R., Eskandari-Naddaf, H. Dynamic Cost Optimization Method of Concrete Mix Design, ICMPC 2017, Materials Today: Proceedings 5 (2018) 4669–4677. ISBN 2214-7853

[16]   Habibi, A., Ghomashi, J. Development of an optimum mix design method for self-compacting concrete based on experimental results, Construct. Build. Mater. 168 (2018) 113–123. https://doi.org/10.1016/j.conbuildmat.2018.02.113.

[17]   Wardeh, G., Ghorbel, E., Gomart, H. Mix Design and Properties of Recycled Aggregate Concretes: Applicability of Eurocode 2, Int. J. Concr. Struct. Mater. 9/1 (2015) 1–20. DOI 10.1007/s40069-014-0087-y.

[18]   Cihan, M.T. Prediction of Concrete Compressive Strength and Slump by Machine Learning Methods, Adv. Civ. Eng. 2019 (2019) e3069046. https://doi.org/10.1155/2019/3069046.

[19]   Correia, S.L., Partala, T., Loch, F.C., Segadães, A.M. Factorial design used to model the compressive strength of mortars containing recycled rubber, Compos. Struct. 92 (2010) 2047–2051. doi:10.1016/j.compstruct.2009.11.007.

[20]   Svinning, K., Høskuldsson, A., Justnes, H. Prediction of compressive strength up to 28 days from microstructure of Portland cement, Cem. Concr. Compos. 30 (2008) 138–151. doi:10.1016/j.cemconcomp.2007.05.016.

[21]   Słonski, M. A comparison of model selection methods for compressive strength prediction of high-performance concrete using neural networks, Comput. Struct. 88 (2010) 1248–1253. doi:10.1016/j.compstruc.2010.07.003.

[22]   Feng, D.-C., Liu, Z.-T., Wang, X.-D., Chen, Y., Chang, J.-Q., Wei, D.-F., Jiang, Z.-M. Machine learning-based compressive strength prediction for concrete: An adaptive boosting approach, Construct. Build. Mater. 230 (2020) e117000. https://doi.org/10.1016/j.conbuildmat.2019.117000.

[23]   Bui, D.-K., Nguyen, T., Chou, J.-S., Nguyen-Xuan, H., Ngo, T.D. A modified firefly algorithm-artificial neural network expert system for predicting compressive and tensile strength of high-performance concrete, Construct. Build. Mater. 180 (2018) 320–333. https://doi.org/10.1016/j.conbuildmat.2018.05.201.

[24]   Anike, E.E., Saidani, M., Olubanwo, A.O., Tyrer, M., Ganjian, E., Effect of mix design methods on the mechanical properties of steel fibrereinforced concrete prepared with recycled aggregates from precast waste, Structures 27 (2020) 664–672. https://doi.org/10.1016/j.istruc.2020.05.038

[25]   Nasr, D., Behforouz, B., Borujeni, P.R., Borujeni, S.A., Zehtab, B. Effect of nano-silica on mechanical properties and durability of self-compacting mortar containing natural zeolite: Experimental investigations and artificial neural network modeling, Construct. Build. Mater. 229 (2019) e116888. https://doi.org/10.1016/j.conbuildmat.2019.116888.

[26]   Erdal, H.I. Two-level and hybrid ensembles of decision trees for high performance concrete compressive strength prediction, Engineering Appl. Artif. Intell. 26 (2013) 1689–1697. https://dx.doi.org/10.1016/j.engappai.2013.03.014.

[27]   Chandwani, V., Agrawal, V., Nagar, R. Modeling slump of ready mix concrete using genetic algorithms assisted training of Artificial Neural Networks, Expert Syst. Appl. 42 (2015) 885–893. http://dx.doi.org/10.1016/j.eswa.2014.08.048.

[28]   Abambres, M., Lantsoght, E.O.L. ANN-Based Fatigue Strength of Concrete under Compression, Mater. 12 (2019) e3787. doi:10.3390/ma12223787.

[29]   Alsini, R., Almakrab, A., Ibrahim, A., Ma, X. Improving the outlier detection method in concrete mix design by combining the isolation forest and local outlier factor, Construction and Building Materials 270 (2021) 121396. https://doi.org/10.1016/j.conbuildmat.2020.121396

[30]   Chopra, P., Sharma, R.K., Kumar, M. Artificial Neural Networks for the Prediction of Compressive Strength of Concrete, Int. J. Appl. Sci. Eng. 13/3 (2015) 187-204.

[31]   Chopra, P., Sharma, R.K., Kumar, M. Prediction of Compressive Strength of Concrete Using Artificial Neural Network and Genetic Programming, Adv. Mater. Sci. Eng. 2016 (2016) e7648467. http://dx.doi.org/10.1155/2016/7648467.

[32]   Chopra, P., Sharma, R.K., Kumar, M., Chopra, T. Comparison of Machine Learning Techniques for the Prediction of Compressive Strength of Concrete, Adv. Civ. Eng. 2018 (2018) e5481705. https://doi.org/10.1155/2018/5481705.

[33]   Kandiri, A., Golafshani, E.M., Behnood, A. Estimation of the compressive strength of concretes containing ground granulated blast furnace slag using hybridized multi-objective ANN and salp swarm algorithm, Construct. Build. Mater. 248 (2020) e118676. https://doi.org/10.1016/j.conbuildmat.2020.118676.

[34]   Akkurt, S., Ozdemir, S., Tayfur, G., Akyol, B. The use of GA–ANNs in the modelling of compressive strength of cement mortar, Cem. Concr. Res. 33 (2003) 973–979. doi:10.1016/S0008-8846(03)00006-1.

[35]   Nikoo, M., Moghadam, F.T., Sadowski, A. Prediction of Concrete Compressive Strength by Evolutionary Artificial Neural Networks, Adv. Mater. Sci. Eng. 2015 (2015) e849126. http://dx.doi.org/10.1155/2015/849126.

[36]   Santosa, S., Santosa, Y.P. Evolutionary Artificial Neural Networks for Concrete Mix Design Modelling, Int. J. Comput. Appl. 7/5 (2017) 62-70. DOI: https://dx.doi.org/10.26808/rs.ca.i7v5.06

[37]   Yaseen, Z.M., Deo, R.C., Hilal, A., Abd, A.M., Cornejo Bueno, L., Salcedo-Sanz, S., Nehdi, M.L. Predicting compressive strength of lightweight foamed concrete using extreme learning machine model, Adv. Eng. Software 115 (2018) 112–125. http://dx.doi.org/10.1016/j.advengsoft.2017.09.004.

[38]   Mukherjee, A., Biswas, S.N. Artificial neural networks in prediction of mechanical behavior of concrete at high temperature, Nuclear Eng. Des. 178 (1997) 1–11.

[39]   Oh, J.-W., Lee, I.-W., Kim, J.-T., Lee, G.-W. Application of Neural networks for proportioning of concrete mixes, ACI Mater. J. 96/1 (1999) 61-67.

[40]   Lee, S.-C. Prediction of concrete strength using artificial neural networks, Eng. Struct. 25 (2003) 849–857. doi:10.1016/S0141-0296(03)00004-X.

[41]   Yaman, M.A., Elaty, M.A., Taman, Predicting the ingredients of self compacting concrete using artificial neural network, Alexandria Eng. J. 56 (2017) 523–532. http://dx.doi.org/10.1016/j.aej.2017.04.007.

[42]   Dantas, T.A., Leite, M.B., Nagahama, K.d.J. Prediction of compressive strength of concrete containing construction and demolition waste using artificial neural networks, Construct. Build. Mater. 38 (2013) 717–722. http://dx.doi.org/10.1016/j.conbuildmat.2012.09.026.

[43]   Elevado, K.J.T., Galupino, J.G., Gallardo, R.S. Artificial Neural Network (ANN) Modelling of Concrete Mixed with Waste Ceramic Tiles and Fly Ash, Int. J. GEOMATE 15/51 (2018) 154-159. https://doi.org/10.21660/2018.51.58567.

[44]   Namyong, J., Sangchun, Y., Hongbum, C. Prediction of Compressive Strength of In-Situ Concrete Based on Mixture Proportions, J. Asian Arch. Build. Eng. 3/1 (2004) 9-16. DOI: 10.3130/jaabe.3.9.

[45]   DeRousseau, M.A., Laftchiev, E., Kasprzyk, J.R., Rajagopalan, B., Srubar III, W.V. A comparison of machine learning methods for predicting the compressive strength of field-placed concrete, Construct. Build. Mater. 228 (2019) e116661. https://doi.org/10.1016/j.conbuildmat.2019.08.042.

[46]   Young, B.A., Hall, A., Pilon, L., Gupta, P., Sant, G. Can the compressive strength of concrete be estimated from knowledge of the mixture proportions?: New insights from statistical analysis and machine learning methods, Cem. Concr. Res. 115 (2019) 379–388. https://doi.org/10.1016/j.cemconres.2018.09.006.

[47]   Davraz, M., Kilinçarslan, S., Ceylan, H. Predicting the Poisson Ratio of Lightweight Concretes using Artificial Neural Network, Acta Phys. Pol. A 128/2-B (2015) 184-186. doi: 10.12693/APhysPolA.128.B-184.

[48]   Onyari, E.K., Ikotun, B.D Prediction of compressive and flexural strengths of a modified zeolite additive mortar using artificial neural network, Construct. Build. Mater. 187 (2018) 1232–1241. https://doi.org/10.1016/j.conbuildmat.2018.08.079.

[49]   Vineela, M.G., Dave, A., Chaganti, P.K. Artificial neural network based prediction of tensile strength of hybrid composites, Materials Today: Proceedings 5/9 (2018) 19908-19915. https://doi.org/10.1016/j.matpr.2018.06.356.

[50]   Karakoç, M.B., Demirboga, R., Türkmen, I., Can, I. Modeling with ANN and effect of pumice aggregate and air entrainment on the freeze–thaw durabilities of HSC, Construct. Build. Mater. 25 (2011) 4241–4249. doi:10.1016/j.conbuildmat.2011.04.068.

[51]   Bal, L., Buyle-Bodin, F. Artificial neural network for predicting drying shrinkage of concrete, Construct. Build. Mater. 38 (2013) 248–254. http://dx.doi.org/10.1016/j.conbuildmat.2012.08.043.

[52]   Marks, M., Glinicki, M.A., Gibas, K. Prediction of the Chloride Resistance of Concrete Modified with High Calcium Fly Ash Using Machine Learning, Mater. 8 (2015) 8714–8727. doi:10.3390/ma8125483.

[53]   Boga, A.R., Öztürk, M., Topçu, I.B. Using ANN and ANFIS to predict the mechanical and chloride permeability properties of concrete containing GGBFS and CNI, Composites: Part B 45 (2013) 688–696. http://dx.doi.org/10.1016/j.compositesb.2012.05.054.

[54]   Hodhod, O.A., Ahmed, H.I. Developing an artificial neural network model to evaluate chloride diffusivity in high performance concrete, HBRC J. 9 (2013) 15–21. http://dx.doi.org/10.1016/j.hbrcj.2013.04.001.

[55]   Zavrtanik, N., Prosen, J., Tušar, M., Turk, G. The use of artificial neural networks for modeling air void content in aggregate mixture, Autom. Construct. 63 (2016) 155–161. http://dx.doi.org/10.1016/j.autcon.2015.12.009.

[56]   Onal, O., Ozturk, A.U. Artificial neural network application on microstructure–compressive strength relationship of cement mortar, Adv. Eng. Software 41 (2010) 165–169. doi:10.1016/j.advengsoft.2009.09.004.

[57]   Shi, L., Lin, S.T.K., Lua, Y., Yeb, L., Zhang, Y.X. Artificial neural network based mechanical and electrical property prediction of engineered cementitious composites, Construct. Build. Mater. 174 (2018) 667–674. https://doi.org/10.1016/j.conbuildmat.2018.04.127.

[58]   Huang, J.S., Liew, J.X., Liew, K.M. Data-driven machine learning approach for exploring and assessing mechanical properties of carbon nanotube-reinforced cement composites, Composite Structures 267 (2021) 113917. https://doi.org/10.1016/j.compstruct.2021.113917

[59]   Lyngdoh, G.A., Das, S. Integrating multiscale numerical simulations with machine learning to predict the strain sensing efficiency of nano-engineered smart cementitious composites, Mater. Design 209 (2021) 109995. https://doi.org/10.1016/j.matdes.2021.109995

[60]   Barlian, A.A., Park, W.-T., Mallon Jr, J.R., Rastegars, A.J., Pruitt, B.L. Review: Semiconductor Piezoresistance for Microsystems, Proc IEEE Institute of Electrical and Electronics Engineers, 2009; 97(3): 513–552.

[61]   Górski, M., Knoppik-Wróbel, A., Kozłowski, M. Active monitoring with use of smart structures based on high-strength fibre composites as a method of structural elements optimization, Proceedings of the 11th International Conference on New Trends in Statics and Dynamics of Buildings, Bratislava, Slovakia, October 2013.

[62]   Chandrakar, J.K., Mishra, S.P. Comparison of IS, BS and ACI Methods of Concrete Mix Design and Proposing Function Equations Based Design, IJCSEIERD, 2(1) 2012 20-56.

[63]   BS 206-1:2000, Concrete. Specification, performance, production and conformity.

[64]   BS 8500-2:2015+A2:2019, Concrete. Complementary British Standard to BS EN 206. Specification for constituent materials and concrete.

[65]   ACI PRC-211.1-91: Standard Practice for Selecting Proportions for Normal, Heavyweight, and Mass Concrete (Reapproved 2009).

[66]   IS 10262 (2009): Guidelines for concrete mix design proportioning.

[67]   Han, B., Xu X., Ou, J. Self-Sensing Concrete in Smart Structures, 2014, Butterworth-Heineman.

[68]   Iijima, S. Synthesis of Carbon Nanotubes. Nature, 354 (1991) 56-58. http://dx.doi.org/10.1038/354056a0

[69]   Iijima, S., Ichihashi, T. Single-shell carbon nanotubes of 1-nm diameter. Nature 363 (1993) 603–605. https://doi.org/10.1038/363603a0

[70]   Ma, P.-C., Siddiqui, N.A., Marom, G., Kim, J.-K. Dispersion and functionalization of carbon nanotubes for polymer-based nanocomposites: A review, Composites: Part A 41 (2010) 1345–67.

[71]   Mordkovich, V.Z. Carbon Nanofibers: A New Ultrahigh-Strength Material for Chemical Technology, Theoretical Foundations of Chemical Engineering, 37(5) (2003) 429–438.

[72]   Endo, M., Kim, Y.A., Hayashi, T., Nishimura, K., Matusita, T., Miyashita, K., Dresselhaus, M.S. Vapor-grown carbon fibers (VGCFs): Basic properties and their battery applications, Carbon, 39(9) (2001) 1287-1297.

[73]   https://www.sigmaaldrich.com/technical-documents/articles/materials-science/nanomaterials/carbon-nanofibers.html

[74]   Guadagno, L., Raimondo, M., Vittoria, V., Vertuccio, L., Lafdi, K., De Vivo, B., Lamberti, P., Spinelli, G., Tucci, V. The role of carbon nanofiber defects on the electrical and mechanical properties of CNF-based resins, Nanotech. 24(30) (2013) IOP Publishing Ltd.

[75]   Han, B., Yu, X., Ou, J. Multifunctional and smart nanotube reinforced cement-based materials. In Nanotechnology in Civil Infrastructure. A Paradigm shift. Gipalakrishnan K., Birgisson B., Taylor P., Attoh-Okine N. Editors – Springer 2011; p. 1-48.

[76]   Chen, B., Liu, J. Damage in carbon fiber-reinforced concrete, monitored by both electrical resistance measurement and acoustic emission analysis, Constr. Build. Mater. 22(11) (2008) 2196-2201.

[77]   Singh, Y. Electrical Resistivity Measurements: a Review, International Conference on Ceramics, Bikaner, India, Int. J, Modern Physics: Conference Series, 22 (2013) 745–756.

[78]   ANSYS® Academic Research Mechanical, 2021 R2. Release 21.0. ANSYS, Inc. Canonsburg, USA.

[79]   Sonawane, D.A., Jadhav, R.M. Prediction of Compression Strength of Concrete by Using Artificial Neural Network, IJREAM Special Issue – ICRTET-2018, 6th International Conference on Recent Trends in Engineering & Technology, 2018.

[80]   Duan, Z.H., Kou, S.C., Poon, C.S. Prediction of compressive strength of recycled aggregate concrete using artificial neural networks, Constr. Build. Mater. 40 (2013) 1200–6. http://dx.doi.org/10.1016/j.conbuildmat.2012.04.063.

[81]   Alshihri, M.M., Azmy, A.M., El-Bisy, M.S. Neural networks for predicting compressive strength of structural light weight concrete, Constr. Build. Mater. 23 (2009) 2214–19. doi:10.1016/j.conbuildmat.2008.12.003.

[82]   Özturan, M., Kutlu, B., Özturan, T. Comparison of Concrete Strength Prediction Techniques with Artificial Neural Network Approach, Build. Res. J. 56(1) (2008) 23-36.

[83]   https://himanshuxd.medium.com/activation-functions-sigmoid-relu-leaky-relu-and-softmax-basics-for-neural-networks-and-deep-8d9c70eed91e

[84]   Kahidan, A., Shirmohammadian, M. Properties of Carbon Nanotube (CNT) Reinforced Cement, Int. J. Eng. Res.5(6) (2016) 497-503. doi:10.17950/ijer/v5s6/616

[85]   D'Alessandro, A., Rallini, M., Ubertini, F., Materazzi, A.L., Kenny, J.M., Laflamme, S. A comparative study between carbon nanotubes and carbon nanofibers as nanoinclusions in self-sensing concrete, Proceedings of the 15th IEEE International Conference on Nanotechnology, 2015, Rome, Italy, 698-701.

[86]   D'Alessandro, A., Ubertini, F., Materazzi, A.L., Laflamme, S., Cancelli, A., Micheli, L. Carbon cement-based sensors for dynamic monitoring of structures, 2016 IEEE 16th International Conference on Environment and Electrical Engineering (EEEIC), Florence, 2016, 1-4, doi:10.1109/EEEIC.2016.7555628

[87]   D'Alessandro, A., Rallini, M., Ubertini, F., Materazzi, A.L., Kenny, J.M. Investigations on scalable fabrication procedures for self-sensing carbon nanotube cement-matrix composites for SHM applications, Cem. Concr. Compos. 65 (2016) 200-213. http://dx.doi.org/10.1016/j.cemconcomp.2015.11.001

[88]   D'Alessandro, A., Ubertini, F., Materazzi, A.L. Self-Sensing Concrete Nanocomposites for Smart Structures, World Academy of Science, Engineering and Technology, Int. J. Civ. Environ. Eng. 10(5) (2016) 599-604.

[89]   D'Alessandro, A., Meoni, A., Ubertini, F., Materazzi, A.L. Strain measurement in a reinforced concrete beam using embedded smart concrete sensors, Proceedings of Italian Concrete Days 42 (2018) 289-300. DOI:10.1007/978-3-030-23748-6_22

[90]   Parvaneh, V., Khiabani, S.H. Mechanical and piezoresistive properties of self-sensing smart concretes reinforced by carbon nanotubes, Mech. Adv. Mater. Struct. 26(11) (2019) 993-1000. DOI:10.1080/15376494.2018.1432789

[91]   Musso, S., Tulliani, J.-M., Ferro, G., Tagliaferro, A. Influence of carbon nanotubes structure on the mechanical behavior of cement composites, Compos. Sci. Tech. 69 (2009) 1985–1990. doi:10.1016/j.compscitech.2009.05.002

[92]   Sindu, B.S., Sasmal, S. Properties of carbon nanotube reinforced cement composite synthesized using different types of surfactants, Constr. Build. Mater. 155 (2017) 389–399. http://dx.doi.org/10.1016/j.conbuildmat.2017.08.059

[93]   Konsta-Gdoutos, M.S., Batis, G., Danoglidis, P.A., Zacharopoulou, A.K., Zacharopoulou, E.K., Falara, M.G., Shah, S.P. Effect of CNT and CNF loading and count on the corrosion resistance, conductivity and mechanical properties of nanomodified OPC mortars, Constr. Build. Mater. 147 (2017) 48–57. http://dx.doi.org/10.1016/j.conbuildmat.2017.04.112

[94]   Konsta-Gdoutos, M.S., Metaxa, Z.S., Shah, S.P. Highly dispersed carbon nanotube reinforced cement based materials, Cem. Concr. Res. 40 (2010) 1052–1059. doi:10.1016/j.cemconres.2010.02.015

[95]   Konsta-Gdoutos, M.S., Danoglidis, P.A., Shah, S.P. High modulus concrete: Effects of low carbon nanotube and nanofiber additions, Theor. Appl. Fracture Mech. 103 (2019) 102295. https://doi.org/10.1016/j.tafmec.2019.102295

[96]   Han, B., Yu, X., Zhang, K., Kwon, E., Ou, J. Sensing properties of CNT-filled cement-based stress sensors, J. Civ. Struct. Health Monitoring 1 (2011) 17–24. DOI 10.1007/s13349-010-0001-5

[97]   Konsta-Gdoutos, M.S., Danoglidis, P.A., Falara, M.G., Nitodas, S.F. Fresh and mechanical properties, and strain sensing of nanomodified cement mortars: The effects of MWCNT aspect ratio, density and functionalization, Cem. Concr. Compos. 82 (2017) 137-151. http://dx.doi.org/10.1016/j.cemconcomp.2017.05.004

[98]   Konsta-Gdoutos, M.S., Aza, C.A. Self sensing carbon nanotube (CNT) and nanofiber (CNF) cementitious composites for real time damage assessment in smart structures, Cem. Concr. Compos. 53 (2014) 162–169. http://dx.doi.org/10.1016/j.cemconcomp.2014.07.003

[99]   Galao, O., Baeza, F.J., Zornoza, E., Garcés, P. Strain and damage sensing properties on multifunctional cement composites with CNF admixture, Cem. Concr. Compos. 46 (2014) 90–98. http://dx.doi.org/10.1016/j.cemconcomp.2013.11.009

[100]   Li, G.Y., Wang, P.M., Zhao, X. Pressure-sensitive properties and microstructure of carbon nanotube reinforced cement composites, Cem. Concr. Compos. 29 (2017) 377–382. doi:10.1016/j.cemconcomp.2006.12.011

[101]   Parveen, S., Rana, S., Fangueiro, R., Paiva, M.C. Microstructure and mechanical properties of carbon nanotube reinforced cementitious composites developed using a novel dispersion technique, Cem. Concr. Res. 73 (2015) 215–227. http://dx.doi.org/10.1016/j.cemconres.2015.03.006

[102]   Sun, G., Liang, R., Lu, Z., Zhang, J., Li, Z. Mechanism of cement/carbon nanotube composites with enhanced mechanical properties achieved by interfacial strengthening, Constr. Build. Mater. 115 (2016) 87–92. http://dx.doi.org/10.1016/j.conbuildmat.2016.04.034

[103]   Jeevanagoudar, Y.V., Hari Krishna, R., Gowda, R., Preetham, R., Prabhakara, R. Improved mechanical properties and piezoresistive sensitivity evaluation of MWCNTs reinforced cement mortars, Constr. Build. Mater. 144 (2017) 188–194. http://dx.doi.org/10.1016/j.conbuildmat.2017.03.139

[104]   Sasmal, S., Ravivarman, N., Sindu, B.S., Vignesh, K. Electrical conductivity and piezo-resistive characteristics of CNT and CNF incorporated cementitious nanocomposites under static and dynamic loading, Compos.: Part A 100 (2017) 227–243. http://dx.doi.org/10.1016/j.compositesa.2017.05.018

[105]   Mohsen, M.O., Taha, R., Abu Taqa, A., Shaat, A. Optimum carbon nanotubes' content for improving flexural and compressive strength of cement paste, Constr. Build. Mater. 150 (2017) 395–403. http://dx.doi.org/10.1016/j.conbuildmat.2017.06.020

[106]   Jiang, S., Zhou, D., Zhang, L., Ouyang, J., Yu, X., Cui, X., Han, B. Comparison of compressive strength and electrical resistivity of cementitious composites with different nano- and micro-fillers, Arch. Civ. Mech. Eng. 18 (2018) 60-68. http://dx.doi.org/10.1016/j.acme.2017.05.010

[107]   Liew, K.M., Kai, M.F., Zhang, L.W. Mechanical and damping properties of CNT-reinforced cementitious composites, Compos. Struct. 160 (2017) 81–88. http://dx.doi.org/10.1016/j.compstruct.2016.10.043

[108]   Meoni, A., D'Alessandro, A., Downey, A., García-Macías, E., Rallini, M., Materazzi, A.L., Torre, L., Laflamme, S., Castro-Triguero, R., Ubertini, F. An Experimental Study on Static and Dynamic Strain Sensitivity of Embeddable Smart Concrete Sensors Doped with Carbon Nanotubes for SHM of Large Structures, Sensors, 18 (2018) 831-850. doi:10.3390/s18030831

[109]   Gao, D., Sturm, M., Mo, Y.L. Electrical resistance of carbon-nanofiber concrete, Smart Mater. Struct. 18 (2019) 095039. doi:10.1088/0964-1726/18/9/095039

[110]   Hawreen, A., Bogas, J.A., Dias, A.P.S. On the mechanical and shrinkage behavior of cement mortars reinforced with carbon nanotubes, Constr. Build. Mater. 168 (2018) 459–470. https://doi.org/10.1016/j.conbuildmat.2018.02.146

[111]   Galao, O., Zornoza, E., Baeza, F.J., Bernabeu, A., Garcés, P. Effect of carbon nanofiber addition in the mechanical properties and durability of cementitious materials, Materiales de Construcción, 2012, 62(307) 343-357. doi: 10.3989/mc.2012.01211

[112]   Danoglidis, P.A., Konsta-Gdoutos, M.S., Gdoutos, E.E., Shah, S.P. Strength, energy absorption capability and self-sensing properties of multifunctional carbon nanotube reinforced mortars, Constr. Build. Mater. 120 (2016) 265–274. http://dx.doi.org/10.1016/j.conbuildmat.2016.05.049

[113]   Han, B., Zhang, K., Yu, X., Kwon, E., Ou, J. Electrical characteristics and pressure-sensitive response measurements of carboxyl MWNT/cement composites, Cem. Concr. Compos. 34 (2012) 794–800. doi:10.1016/j.cemconcomp.2012.02.012

[114]   Li, G.Y., Wang, P.M., Zhao, X. Mechanical behavior and microstructure of cement composites incorporating surface-treated multi-walled carbon nanotubes, Carbon 43 (2005) 1239-1245. doi:10.1016/j.carbon.2004.12.017

[115]   Rashmi, R., Padmapriya, P. Mechanical and durability characteristics of multiwalled carbon nano tube in concrete, ICMSMT 2020, OIP Conf. Series: Materials Science and Engineering 872 (2020) 012110. doi:10.1088/1757-899X/872/1/012110

[116]   Irshidat, M.R., Al-Nuaimi Soheb Salim, N., Rabie, M. Carbon Nanotubes Dosage Optimization for Strength Enhancement of Cementitious Composites, Procedia Manufacturing, 44 (2020) 366–370. doi: 10.1016/j.promfg.2020.02.282

[117]   Azeem, M., Saleem, M.A. Role of electrostatic potential energy in carbon nanotube augmented cement paste matrix, Constr. Build. Mater. 239 (2020) 117875. https://doi.org/10.1016/j.conbuildmat.2019.117875

[118]   Assi, L.N., Al-Hamadani, Y.A.J., Deaver, E., Soltangharaei, V., Ziehl, P., Yoon, Y. Effect of Sonicated Deionized Water on The Early Age Behavior of Portland Cement-Based Concrete and Paste, Constr. Build. Mater. 247 (2020) 118571. https://doi.org/10.1016/j.conbuildmat.2020.118571

[119]   Zhang, J., Kea, Y., Zhang, J., Han, Q., Dong, B. Cement paste with well-dispersed multi-walled carbon nanotubes: Mechanism and performance, Constr. Build. Mater. 262 (2020) 120746. https://doi.org/10.1016/j.conbuildmat.2020.120746

[120]   EN 197-1:2011, Cement – Part 1: Composition, specification, and conformity criteria for common cement.

[121]   ASTM C778-17, Standard Specification for Standard Sand

[122]   ACI 544.1R-96, Report on Fiber Reinforced Concrete.

[123]   UNE 83258:2005, Admixtures for concretes, mortars and grouts. Admixtures for masonry mortars. Determination of consistency.

[124]   I.S.: 8112 (1989): 43 Grade Ordinary Portland Cement Specifications (First Revision).

[125]   ASTM 305-20, Standard Practice for Mechanical Mixing of Hydraulic Cement Pastes and Mortars of Plastic Consistency.

[126]   I.S.: 2250 (1981): Preparation and Use of Masonry Mortars.

[127]   ASTM C192/C192M-19, Standard Practice for Making and Curing Concrete Test Specimens in the Laboratory.

[128]   EN 196-1:2016, Methods of testing cement - Part 1: Determination of strength.

[129]   ASTM 349-18, Standard Test Method for Compressive Strength of Hydraulic-Cement Mortars (Using Portions of Prisms Broken in Flexure).

[130]   ASTM C109/C109M-20b, Standard Test Method for Compressive Strength of Hydraulic Cement Mortars (Using 2-in. or [50 mm] Cube Specimens).

[131]   ASTM C39/C39M-21, Standard Test Method for Compressive Strength of Cylindrical Concrete Specimens.

[132]   ASTM C348-21, Standard Test Method for Flexural Strength of Hydraulic-Cement Mortars.

[133]   ASTM C1760-12, Standard Test Method for Bulk Electrical Conductivity of Hardened Concrete (Withdrawn 2021).

[134]   I.S.: 4031 (1988): Methods of physical tests for hydraulic cement.

[135]   I.S.: 516 (1959): Methods of Test for Strength of Concrete.

[136]   EN 1015-11:2020, Methods of test for mortar for masonry - Part 11: Determination of flexural and compressive strength of hardened mortar.

[137]   Gdoutos, E.E., Konsta-Gdoutos, M.S., Danoglidis, P.A., Portland cement mortar nanocomposites at low carbon nanotube and carbon nanofiber content: A fracture mechanics experimental study, Cem. Concr. Compos. 70 (2016) 110-118. http://dx.doi.org/10.1016/j.cemconcomp.2016.03.010

[138]   Dalla, P.T., Dassios, K.G., Tragazikis, I.K., Exarchos, D.A., Matikas, T.E. Carbon nanotubes and nanofibers as strain and damage sensors for smart cement, Mater. Today Com. 8 (2016) 196–204. http://dx.doi.org/10.1016/j.mtcomm.2016.07.004

[139]   Collins, F., Lambert, J., Duan, W.H. The influences of admixtures on the dispersion, workability, and strength of carbon nanotube–OPC paste mixtures, Cem. Concr. Compos. 34 (2012) 201–207. doi:10.1016/j.cemconcomp.2011.09.013

[140]   Hongyu, S., Binmeng, C., Bob, L., Shengwen, T., L. Zongjin, L. Influence of dispersants on the properties of CNTs reinforced cement-based materials, Construction and Building Materials 131 (2017) 186–194. http://dx.doi.org/10.1016/j.conbuildmat.2016.11.053

[141]   Liu, M. The influence of modified carbon nanotubes on the performance of bridge concrete, Functional Materials, 26, No. 3 (2019), p. 567-572. https://doi.org/10.15407/fm26.03.567

[142]   MacLeod, A.J.N., Fehervari, A., Gates, W.P., Garcez, E.O., Aldridge, L.P., Collins, F. Enhancing fresh properties and strength of concrete with a pre-dispersed carbon nanotube liquid admixture, Constr. Build. Mater. 247 (2020) 118524. https://doi.org/10.1016/j.conbuildmat.2020.118524

[143]   Sobolkina, A., Mechtcherine, V., Khavrus, V., Maier, D., Mende, M., Ritschel, M., Leonhardt, A. Dispersion of carbon nanotubes and its influence on the mechanical properties of the cement matrix, Cem. Concr. Compos. 34 (2012) 1104–1113. http://dx.doi.org/10.1016/j.cemconcomp.2012.07.008

[144]   Mohsen, M.., Al Ansari, M.S., Taha, R., Al Nuaimi, N., Abu Taqa, A. Carbon Nanotube Effect on the Ductility, Flexural Strength, and Permeability of Concrete, Journal of Nanomaterials, 2019 (2019) 6490984. https://doi.org/10.1155/2019/6490984

[145]   Yazdanbakhsh, A., Grasley, Z., Tyson, B., Abu Al-Rub, R. Challenges and Benefits of Utilizing Carbon Nanofilaments in Cementitious Materials, J. Nanomater. 2012 (2012) 371927. doi:10.1155/2012/371927

[146]   Ghosal, M., Chakraborty, A.K. Short Term V/S Long Term Optimization of Nano-Additions of Ordinary Portland Cement, European J. Adv. Eng. Tech. 3(7) (2016) 71-77.

[147]   Sindu, B.S., Sasmal, S. Properties of carbon nanotube reinforced cement composite synthesized using different types of surfactants, Constr. Build. Mater. 155 (2017) 389–399. http://dx.doi.org/10.1016/j.conbuildmat.2017.08.059

[148]   Camacho, M.d.C., Galao, O., Baeza, F.J., Zornoza, E., Garces, P. Mechanical Properties and Durability of CNT Cement Composites, Mater. 7 (2014) 1640-1651; doi:10.3390/ma7031640

[149]   Musso, S., Tulliani, J.-M., Ferro, G., Tagliaferro, A. Influence of carbon nanotubes structure on the mechanical behavior of cement composites, Compos. Sci. Tech. 69 (2009) 1985–1990. doi:10.1016/j.compscitech.2009.05.002.

[150]   Kekez, S., Krzywon, R. Prediction of Bonding Strength of Externally Bonded SRP Composites Using Artificial Neural Networks, Materials (2022) 15, 1314. https://doi.org/10.3390/ma15041314.

[151]   Kröse, B., van der Smagt, P. An introduction to neural networks, University of Amsterdam, Netherlands, 1996.

[152]   Garson, G.D. Interpreting neural network connection weights. AI Expert 1991, 6(4),46–51.

[153]   Kekez, S., Kubica, J. Application of artificial neural networks for prediction of mechanical properties of cnt/cnf reinforced concrete, Mater. (2021) 14 (19), 5637. DOI: 10.3390/ma14195637

[154]   Li, C., Chou, T.-W. Modeling of damage sensing in fiber composites using carbon nanotube network, Composites Science and Technology (2008), 68, 3373–3379. doi:10.1016/j.compscitech.2008.09.025

List of Tables

List of Figures

APPENDICES

Appendix A – ANSYS Numerical Simulations

A1. Materials

Table A1.1 Materials library for Material Designer models

Material	Density [kg/m^3]	Coefficient of thermal expansion [C^{-1}]	Young's modulus [GPa]	Poisson's ratio	Tensile ultimate strength [MPa]	Compressive ultimate strength [MPa]	Isotropic thermal conductivity [Wm^{-1}C^{-1}]	Specific heat constant pressure [Jkg^{-1}C^{-1}]	Isotropic electrical resistivity [Ωcm]
OPC 42.5	2300	1.40E-05	30	0.18	5	42.5	0.72	780	8.0E+06
OPC 52.5	2300	1.40E-05	30	0.18	5	52.5	0.72	780	8.0E+06
CNT	1800	0.005483	635/6/6	0.2/0.4/0.2	55500	0.0002	4400	/	0.0001
CNF	1800	0.005483	230/2.3/2.3	0.2/0.4/0.2	6500	0.0002	448	/	0.001
cem42503	2300	1.40E-05	30	0.18	10.1	66.5	0.72	780	7.7E+06
cem425033	2300	1.40E-05	30	0.18	4	84.8	0.72	780	7.7E+06
cem42504	2300	1.40E-05	30	0.18	7.04	45.5	0.72	780	6.6E+06
cem42505	2300	1.40E-05	30	0.18	7.15	35.6	0.72	780	6.6E+06
cem52504	2300	1.40E-05	30	0.18	6	56.7	0.72	780	6.6E+06
mor425035033spl	2300	1.40E-05	30	0.18	10.3	72.1	0.72	780	1.00E+05
mor425040263spl	2300	1.40E-05	30	0.18	7.5	65	0.72	780	1.00E+05
mor425045033spl	2300	1.40E-05	30	0.18	8.9	56.4	0.72	780	1.00E+05
mor425045067spl	2300	1.40E-05	30	0.18	6.69	52.27	0.72	780	1.00E+05
mor42504850364	2300	1.40E-05	30	0.18	5.9	31.7	0.72	780	1.00E+05
mor42505033	2300	1.40E-05	30	0.18	8.3	51.3	0.72	780	1.00E+04
mor42505033spl	2300	1.40E-05	30	0.18	5.9	31.8	0.72	780	1.00E+04
mor425055033	2300	1.40E-05	30	0.18	7.6	48.8	0.72	780	1.00E+04
mor52505033spl	2300	1.40E-05	30	0.18	10.35	54	0.72	780	1.00E+04
con425051038049	2300	1.40E-05	30	0.18	6.7	45.8	0.72	780	1.00E+06

A2. Results

Table A2.1 Resulting material properties and strength of simulated samples

Material	Density [kg/m^3]	Young's modulus [GPa]	Poisson's ratio YZ direction	Shear modulus XY direction [GPa]	Compressive ultimate strength [MPa]	Tensile ultimate strength [MPa]
cem52504	2300	30	0.18	/	51.13	13.32
cem52504NT005	2283.4	46.898	0.2014	12.659	51.81	12.67
cem52504NT01	2266.4	69.277	0.21847	12.5	52.17	12.06
cem52504NT015	2249.8	86.57	0.22763	12.408	52.19	11.69
cem53504NT02	2233.2	105.72	0.22958	12.326	52.29	11.37
cem52504NT025	2216.3	127.15	0.25611	12.051	52.06	12.99
cem54504NT03	2199.5	139.8	0.24451	12.157	52.29	13.10
cem52504NT035	2183.5	170.93	0.2412	11.739	52.40	14.45
cem52504NT04	2166.5	191.52	0.24311	11.602	52.37	15.35
cem52504NT045	2150	211.4	0.24233	11.483	52.44	15.88
cem52504NT05	2133.5	231.44	0.2327	11.339	52.51	16.61
cem425033	2300	30	0.18	/	76.47	6.12
cem425033NT001	2296	34.755	0.1875	12.687	76.86	6.03
cem425033NT002	2292.5	38.734	0.19256	12.652	77.14	5.96
cem425033NT003	2288.5	43.415	0.1986	12.619	77.36	5.88
cem425033NT004	2285	47.15	0.2012	12.607	77.52	5.83
cem425033NT005	2280.9	51.086	0.20554	12.596	77.64	5.77
cem425033NT006	2277.4	56.006	0.20916	12.601	77.73	5.70
cem425033NT007	2273.1	58.794	0.21069	12.695	77.73	5.66
cem425033NT008	2269.8	62.84	0.21281	12.575	77.90	5.60
cem425033NT009	2266	69.834	0.22016	12.47	77.93	5.56
cem425033NT01	2262.3	72.756	0.22117	12.45	77.97	5.52
cem42505	2300	30	0.18	/	32.10	10.95
cem42505NT001	2296.5	34.108	0.18654	12.705	32.24	10.80
cem42505NT002	2293.5	37.642	0.19135	12.665	32.35	10.69
cem42505NT003	2289.9	39.6	0.19437	12.637	32.39	10.69
cem42505NT004	2286.5	46.188	0.20041	12.609	32.53	10.44
cem42505NT005	2283.5	49.448	0.20354	12.631	32.56	10.36
cem42505NT006	2279.9	52.988	0.20597	12.585	32.63	10.27
cem42505NT007	2276	57.439	0.21028	12.598	32.65	10.17
cem42505NT008	2273.4	60.504	0.21191	12.489	32.71	10.11
cem42505NT009	2269.9	64.408	0.21624	12.57	32.69	10.02
cem42505NT01	2266.2	63.656	0.21754	12.761	32.62	9.98
cem42504	2300	30	0.18	/	41.03	10.78
cem42504NT001	2296.5	34.164	0.18673	12.697	41.21	10.63
cem42504NT002	2293	37.711	0.19166	12.695	41.33	10.52
cem42504NT003	2289.5	42.076	0.19615	12.649	41.47	10.39
cem42504NT004	2285.5	45.828	0.20066	12.655	41.55	10.28
cem42504NT005	2281.9	50.065	0.20429	12.635	41.64	10.18
cem42504NT006	2278.4	52.12	0.2072	12.623	41.64	10.12
cem42504NT007	2275	56.626	0.21149	12.527	41.76	9.98

cem42504NT008	2271.4	63.25	0.21248	12.506	41.83	9.89
cem42504NT009	2267.9	64.01	0.21649	12.551	41.79	9.86
cem42504NT01	2264.4	68.749	0.22117	12.502	41.79	9.77
cem42503	2300	30	0.18	/	59.97	15.46
cem42503NT005	2283.5	49.418	0.20304	12.609	60.84	14.63
cem42503NT01	2266.4	69.027	0.21823	12.538	61.12	14.02
cem42503NT015	2249.7	81.188	0.2284	12.609	61.11	13.66
cem42503NT02	2233.2	100.39	0.23364	12.399	61.26	13.29
cem42503NT025	2215.6	121.6	0.23448	12.368	61.25	13.86
cem42503NT03	2199.2	132.77	0.24041	12.431	61.03	15.76
cem42503NT035	2182.8	159.43	0.27042	11.936	60.76	17.57
cem42503NT04	2166.2	184.42	0.27442	11.741	60.81	18.52
cem42503NT045	2149	178.96	0.28382	11.675	60.36	19.64
cem42503NT05	2131.8	188.25	0.28563	12.851	60.04	20.22
mor42504850364	2300	30	0.18	/	28.59	9.03
mor42504850364NT005	2294	37.12	0.19069	12.672	28.79	8.83
mor42504850364NT008	2290.5	40.907	0.19536	12.649	28.87	8.74
mor42504850364NT01	2288	44.364	0.19941	12.613	28.94	8.66
mor42504850364NT015	2282.3	48.591	0.20236	12.808	28.94	8.55
mor42504850364NT02	2276.4	55.918	0.21104	12.597	29.05	8.41
mor42504850364NT025	2270.4	65.009	0.21078	12.524	29.17	8.26
mor42504850364NT03	2264.4	68.574	0.21669	12.493	29.15	8.19
mor42504850364NT035	2258.1	75.726	0.21842	12.645	29.14	8.06
mor42504850364NT04	2252.7	83.29	0.22426	12.521	29.17	7.96
mor42504850364NT045	2246	82.758	0.22785	13.156	29.04	7.90
more42504850364NT05	2239.5	88.074	0.23075	13.354	29.03	7.81
mor42505033	2300	30	0.18	/	46.26	12.71
mor42505033NT0025	2297	33.205	0.1852	12.721	46.41	12.57
mor42505033NT005	2294.5	36.496	0.18983	12.671	46.57	12.45
mor42505033NT0075	2291.5	39.332	0.19373	12.708	46.65	12.34
mor42505033NT01	2288.9	42.171	0.19613	12.643	46.78	12.25
mor425055033	2300	30	0.18	/	44.01	11.63
mor425055033NT0025	2297	33.251	0.18528	12.739	44.18	11.50
mor425055033NT005	2294.5	36.426	0.18996	12.696	44.28	11.40
mor425055033NT0075	2291.5	39.931	0.19434	12.704	44.40	11.28
mor425055033NT01	2288.9	41.556	0.19637	12.636	44.49	11.20
mor42505033spl	2300	30	0.18	/	28.68	9.03
mor42505033splNT0025	2297	33.549	0.18578	12.687	28.79	8.93
mor42505033splNT005	2294.5	36.525	0.19002	12.668	28.87	8.85
mor42505033splNT0075	2291.5	40.024	0.19462	12.641	28.95	8.76
mor42505033splNT01	2289	42.309	0.19668	12.627	28.99	8.70
mor52505033spl	2300	30	0.18	/	48.70	15.84
mor52505033splNF005	2294.5	32.133	0.18614	12.67	48.78	15.70
mor525033splNF01	2289	34.25	0.19154	12.625	48.85	15.56
mor525033splNF015	2283.4	36.04	0.19613	12.592	48.89	15.44

mor525033splNF02	2277.9	38.16	0.198	12.523	48.98	15.30
mor52505033splNF025	2271.9	40.882	0.20251	12.501	49.02	15.13
mor525033splNF03	2266.2	41.959	0.20494	12.477	48.95	15.03
mor525033splNF035	2260.9	45.208	0.20994	12.396	49.11	14.89
mor525033splNF04	2255	46.562	0.20844	12.44	49.03	14.69
mor525033splNF045	2249.5	47.571	0.20862	12.286	49.10	14.61
mor52505033splNF05	2243.8	48.891	0.21418	12.301	49.04	14.56
mor525033splNF055	2237.5	48.391	0.21919	12.712	48.88	14.51
mor525033splNF06	2233.2	55.214	0.22837	12.19	49.11	14.31
mor525033splNF065	2227.8	58.136	0.23501	12.139	49.02	14.14
mor525033splNF07	2221.3	58.194	0.21891	12.272	49.09	13.93
mor52505033splNF075	2214.2	56.012	0.2299	12.028	48.99	14.06
mor525033splNF08	2210.3	63.188	0.23997	12.159	48.86	13.72
mor525033splNF085	2204.6	65.11	0.23161	12.107	48.64	13.68
mor525033splNF09	2191.6	47.79	0.22215	12.728	48.62	14.06
mor525033splNF095	2193.8	68.691	0.24497	11.994	49.09	13.59
mor52505033splNF1	2188.3	69.943	0.28297	12.006	48.47	13.70
mor525033splNF105	2181.8	67.334	0.24728	12.243	48.77	13.31
mor525033splNF11	2177.1	72.273	0.25817	11.764	48.60	14.39
mor525033splNF115	2171.2	74.709	0.28033	11.739	48.18	15.54
mor525033splNF12	2164.8	74.804	0.2462	12.031	48.84	14.21
mor52505033splNF125	2159.4	77.232	0.27412	11.559	48.27	15.82
mor525033splNF13	2154.6	82.917	0.25954	11.681	48.70	15.38
mor525033splNF135	2149.1	84.795	0.23499	11.569	49.13	14.94
mor525033splNF14	2144.3	90.497	0.22133	11.431	49.07	16.41
mor525033splNF145	2138.4	90.887	0.23923	11.471	48.93	16.35
mor52505033splNF15	2132.7	93.555	0.25613	11.472	48.48	17.60
mor525033splNF155	2126.9	90.794	0.28922	11.305	47.89	18.46
mor525033splNF16	2121.7	99.068	0.30026	11.284	47.67	19.85
mor525033splNF165	2115.5	97.566	0.28326	11.285	48.09	18.66
mor525033splNF17	2110	99.398	0.33264	11.402	47.83	20.43
mor52505033splNF175	2105.1	106.06	0.29754	11.196	47.53	21.03
mor525033splNF18	2098.9	102.64	0.29309	11.306	47.99	19.35
mor525033splNF185	2094.4	121.19	0.20014	11.044	49.70	17.09
mor525033splNF19	2089.1	114.39	0.19535	11.005	49.80	17.15
mor525033splNF195	2083.5	116.59	0.18489	10.956	49.92	17.35
mor52505033splNF2	2078	118.79	0.19042	10.922	49.86	17.56
mor425035033spl	2300	30	0.18	/	65.02	15.77
mor425035033splNT0025	2297	33.49	0.18559	12.71	65.26	15.59
mor425035033splNT005	2294.5	36.389	0.18974	12.697	65.43	15.45
mor425035033splNT0075	2291.4	39.144	0.19367	12.645	65.59	15.33
mor425035033splNT01	2289	43.027	0.19783	12.644	65.75	15.17
mor425045033spl	2300	30	0.18	/	50.86	13.62
mor425045033splNT0025	2297	33.582	0.18585	12.693	51.06	13.47
mor425045033splNT005	2294.5	36.318	0.18963	12.682	51.19	13.35

mor425045033splNT0075	2291.5	39.771	0.19399	12.662	51.30	13.22
mor425045033splNT01	2289	42.526	0.1969	12.632	51.42	13.12
mor425040263spl	2300	30	0.18	/	58.62	11.48
mor425040263splNT005	2295	35.972	0.18946	12.672	58.98	11.27
mor425040263splNT01	2226.2	39.568	0.19418	12.69	59.12	11.14
mor425040263splNT015	2285.5	47.211	0.20176	12.627	59.39	10.92
mor425040263splNT02	2280.5	52.965	0.20683	12.563	59.56	10.78
mor425040263splNT025	2275.9	57.318	0.20901	12.659	59.61	10.66
mor425040263splNT03	2271.3	59.63	0.21203	12.48	59.71	10.61
mor425040263splNT035	2266.4	67.894	0.21543	12.429	59.84	10.45
mor425040263splNT04	2261.2	71.044	0.21637	12.535	59.81	10.35
mor425040263splNT045	2256.9	79.463	0.22116	12.436	59.85	10.20
mor425040263splNT05	2251.6	80.873	0.22459	12.536	59.80	10.16
mor425045067spl	2300	30	0.18	/	47.14	10.24
mor425045067splNT005	2291.5	39.72	0.19425	12.647	47.58	9.94
mor425045067splNT01	2282.9	48.067	0.20207	12.635	47.80	9.72
mor425045067splNT015	2274.5	59.764	0.21199	12.553	47.98	9.47
mor425045067splNT02	2266	70.697	0.21908	12.433	48.09	9.26
mor425045067splNT025	2257.4	79.687	0.22307	12.496	48.12	9.11
mor425045067splNT03	2248.6	84.996	0.22647	12.41	48.14	9.01
mor425045067splNT035	2239.9	86.279	0.22504	12.416	48.12	8.96
mor425045067splNT04	2230.1	84.289	0.22864	13.386	47.78	8.84
mor425045067splNT045	2219	76.926	0.21766	12.78	48.04	8.93
mor425045067splNT05	2214.7	119.9	0.24438	12.526	47.88	9.82
con425051038049	2300	30	0.18	/	41.30	10.26
con425051038049NT0025	2298	32.336	0.18387	12.715	41.42	10.18
con425051038049NT005	2295.9	34.724	0.18752	12.705	41.50	10.10
con425051038049NT0075	2294	37.064	0.19062	12.679	41.59	10.03
con425051038049NT01	2292	38.996	0.19295	12.671	41.65	9.97
con425051038049NF0025	2298	30.756	0.18232	12.704	41.32	10.22
con425051038049NF005	2295.9	31.558	0.18438	12.684	41.36	10.19
con425051038049NF0075	2293.9	32.168	0.18606	12.687	41.37	10.16
con425051038049NF01	2292	32.967	0.18755	12.646	41.41	10.13
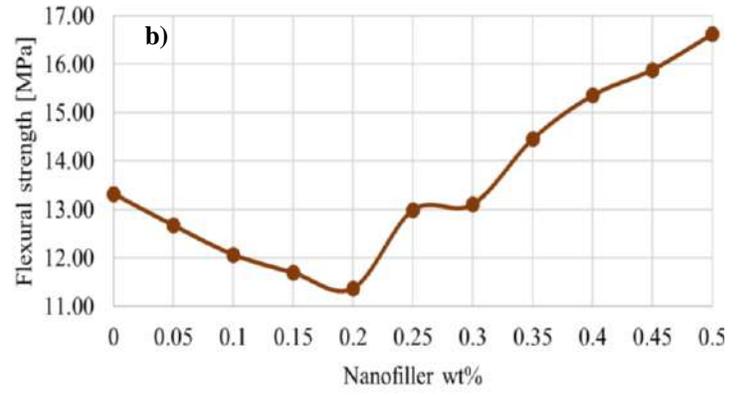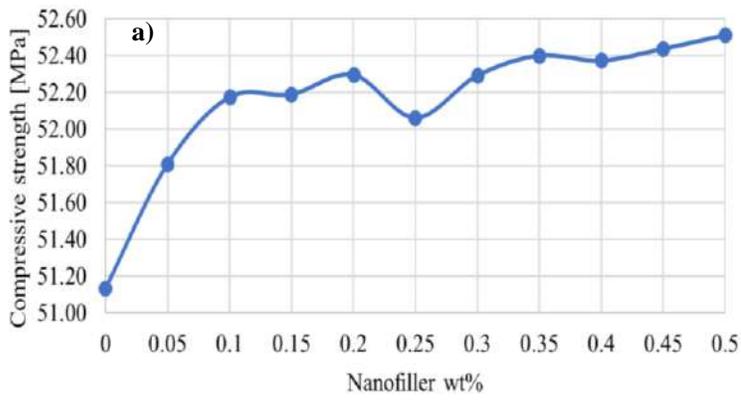
Figure A2.1 Change of compressive strength (a) and flexural strength (b) of material cem52504 with increase of nanofiller wt%
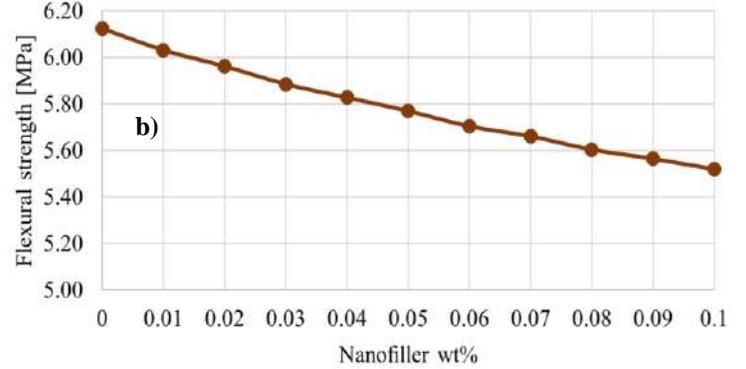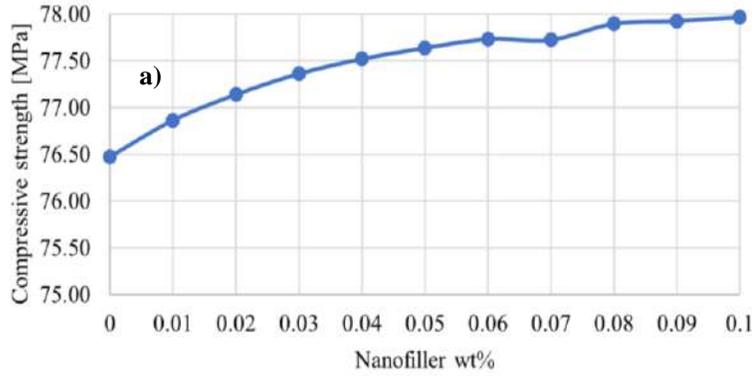
Figure A2.2 Change of compressive strength (a) and flexural strength (b) of material cem425033 with increase of nanofiller wt%
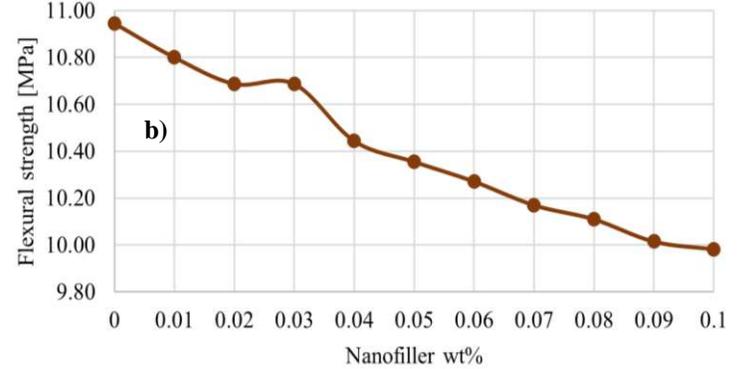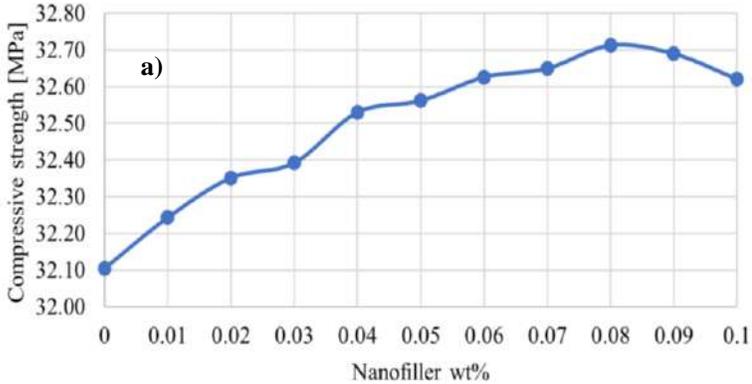
Figure A2.3 Change of compressive strength (a) and flexural strength (b) of material cem42505 with increase of nanofiller wt%
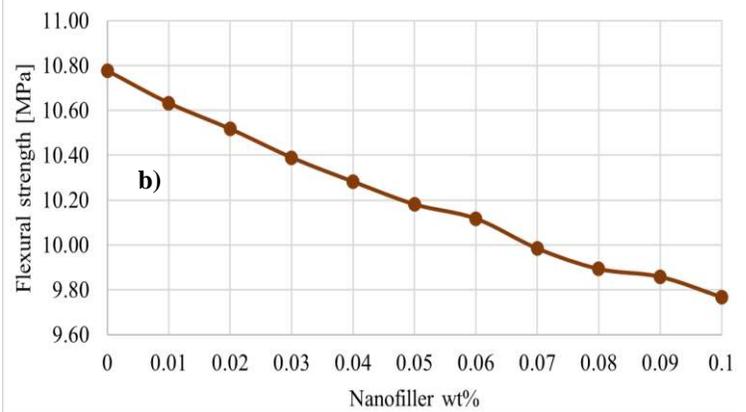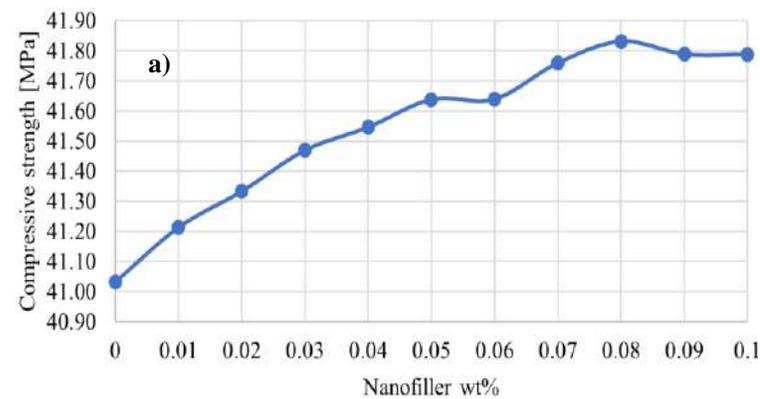
Figure A2.4 Change of compressive strength (a) and flexural strength (b) of material cem42504 with increase of nanofiller wt%
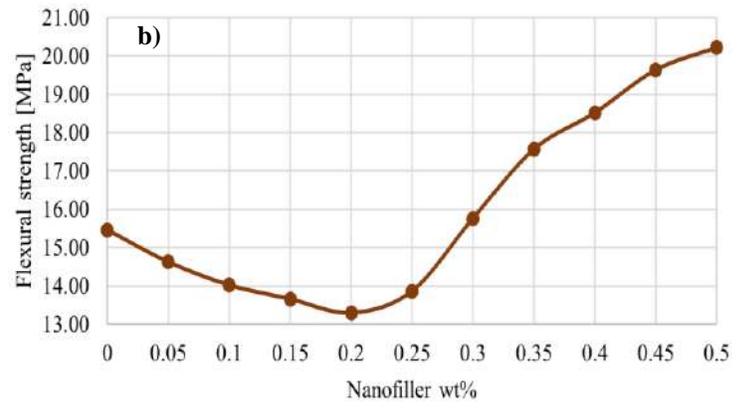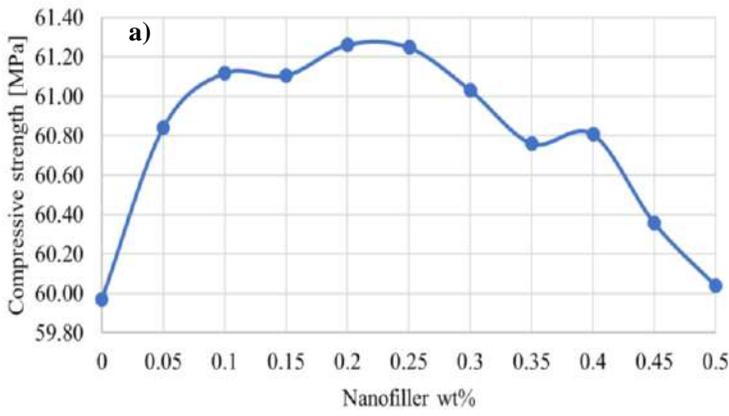
Figure A2.5 Change of compressive strength (a) and flexural strength (b) of material cem42503 with increase of nanofiller wt%
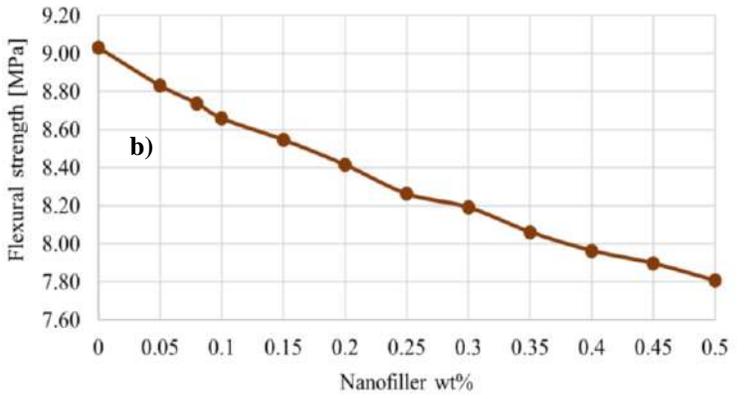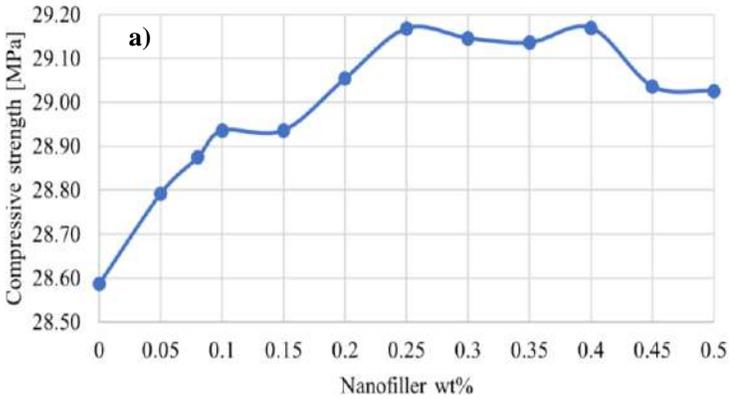
Figure A2.6 Change of compressive strength (a) and flexural strength (b) of material mor42504850364 with increase of nanofiller wt%
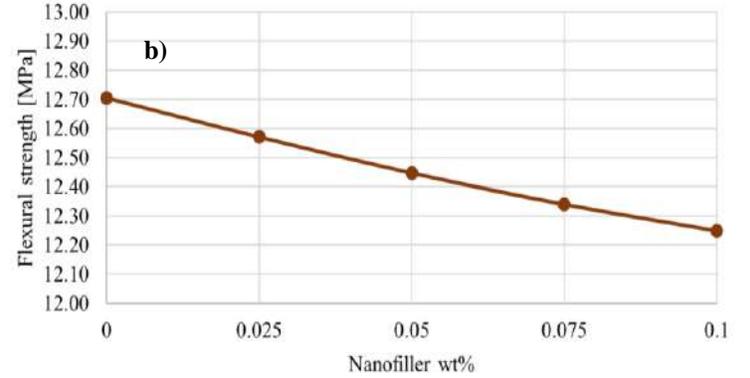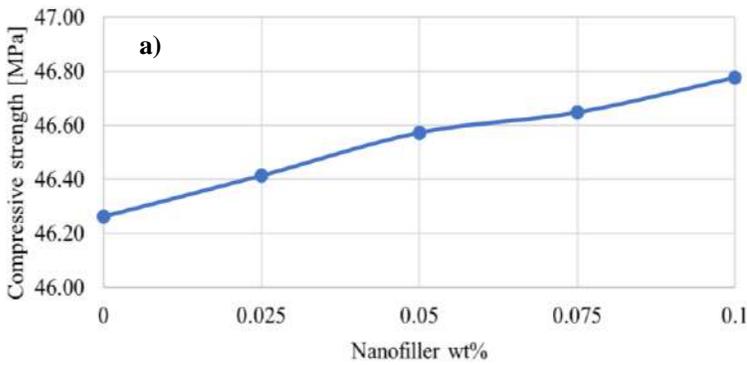
Figure A2.7 Change of compressive strength (a) and flexural strength (b) of material mor42505033 with increase of nanofiller wt%
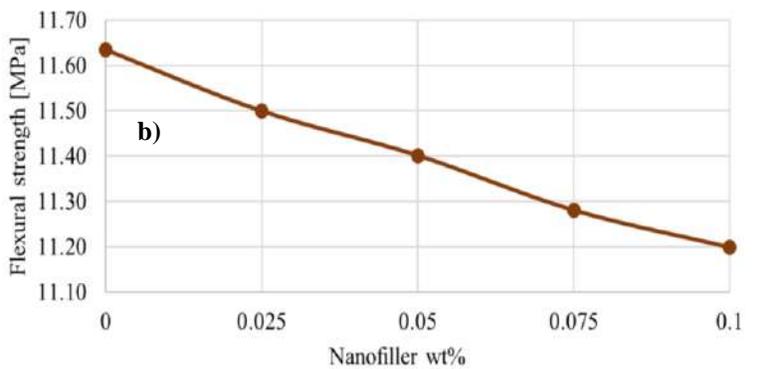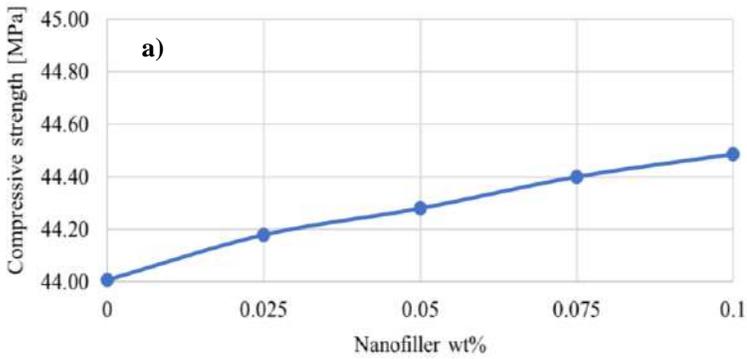
Figure A2.8 Change of compressive strength (a) and flexural strength (b) of material mor425055033 with increase of nanofiller wt%
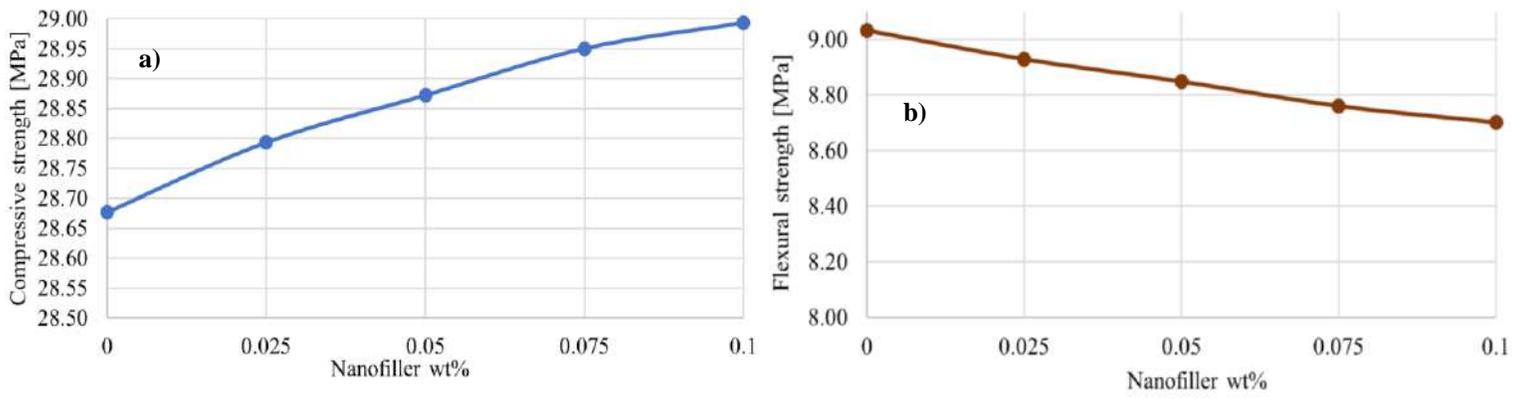
Figure A2.9 Change of compressive strength (a) and flexural strength (b) of material mor42505033spl with increase of nanofiller wt%
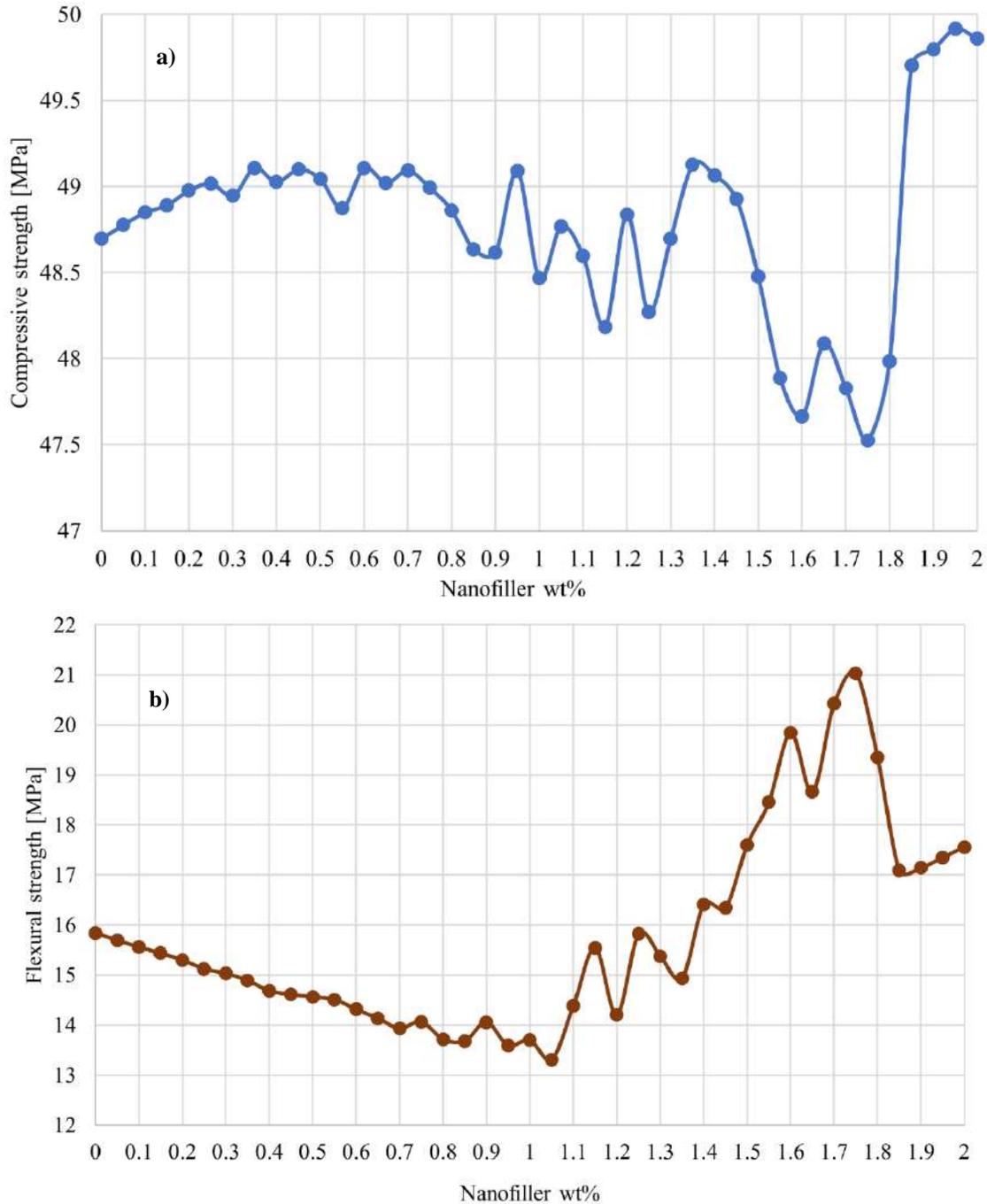
Figure A2.10 Change of compressive strength (a) and flexural strength (b) of material mor52505033spl with increase of nanofiller wt%
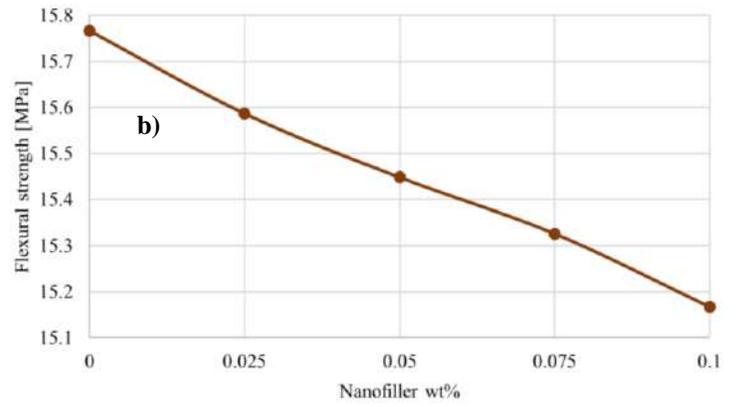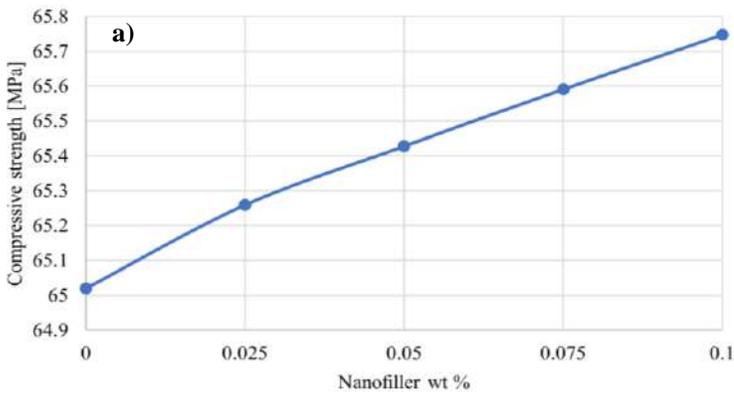
Figure A2.11 Change of compressive strength (a) and flexural strength (b) of material mor425035033spl with increase of nanofiller wt%
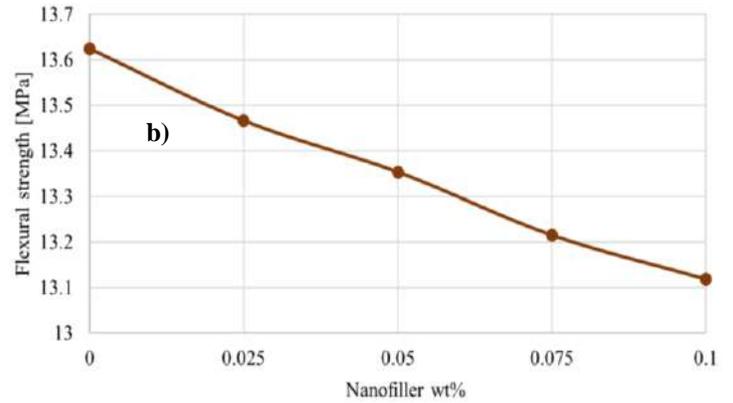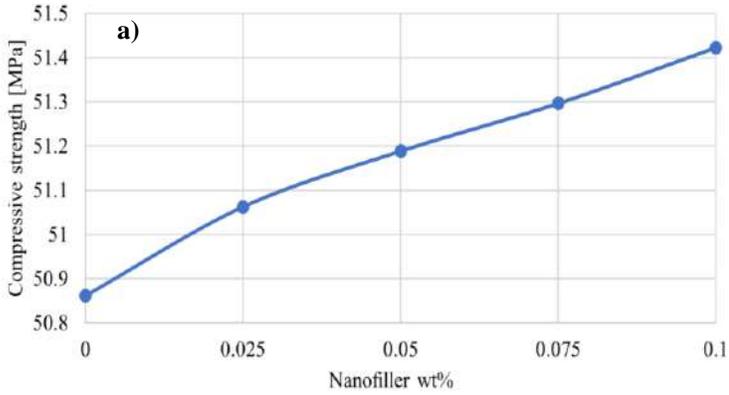
Figure A2.12 Change of compressive strength (a) and flexural strength (b) of material mor425045033spl with increase of nanofiller wt%
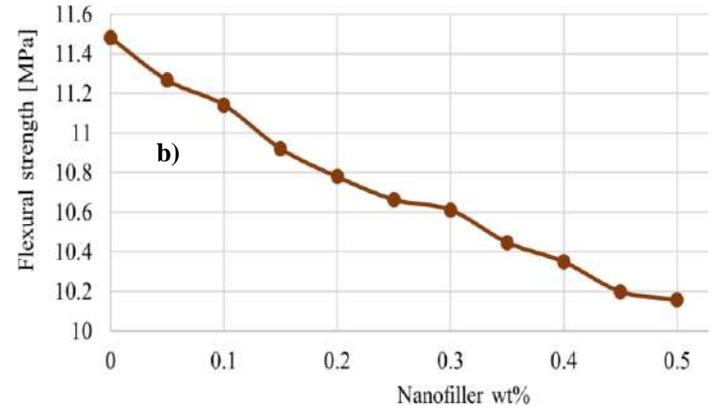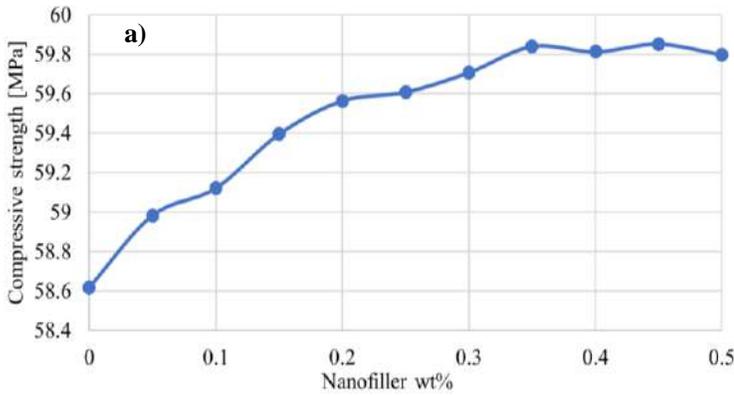
Figure A2.13 Change of compressive strength (a) and flexural strength (b) of material mor425040263spl with increase of nanofiller wt%
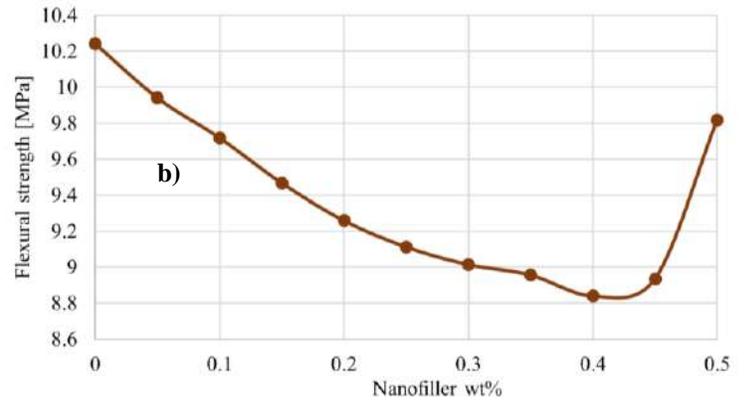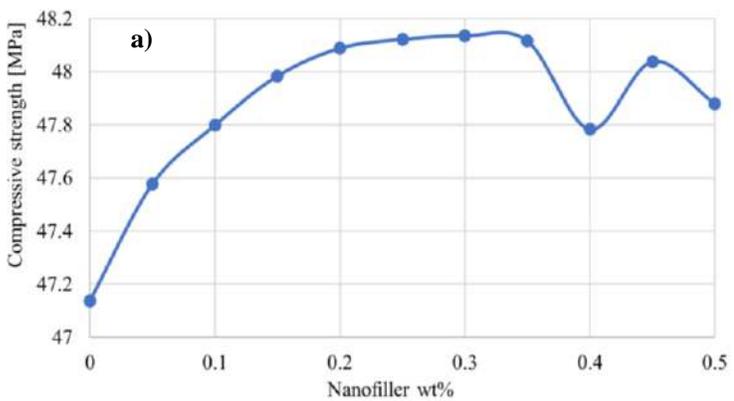
Figure A2.14 Change of compressive strength (a) and flexural strength (b) of material mor425045067spl with increase of nanofiller wt%
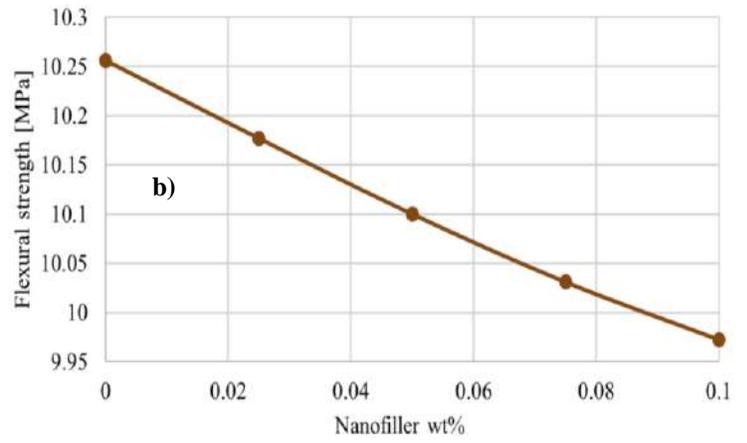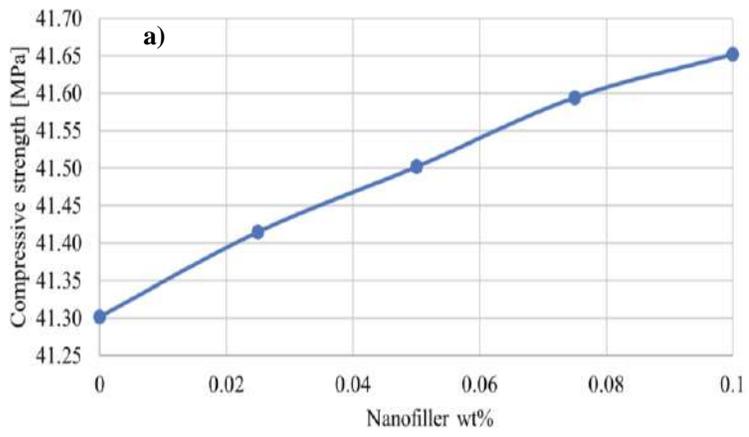
Figure A2.15 Change of compressive strength (a) and flexural strength (b) of material con425051038049 with increase of CNT wt%
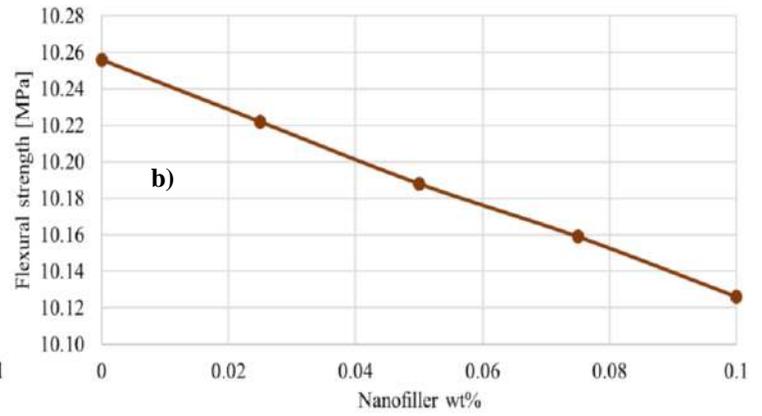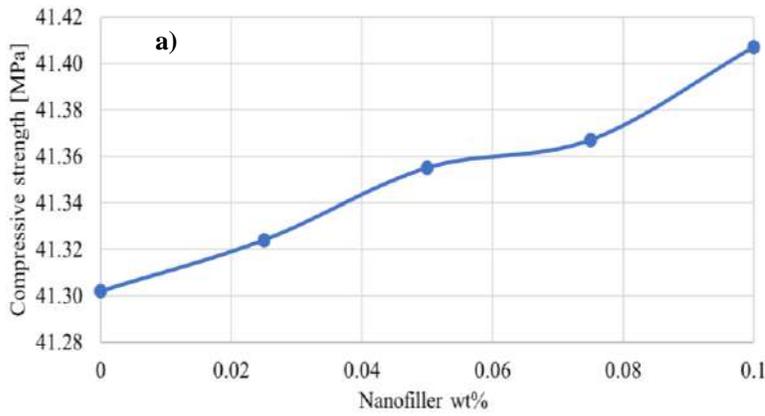
Figure A2.16 Change of compressive strength (a) and flexural strength (b) of material con425051038049 with increase of CNF wt%

A3. Validation

Table A3.1 Validation of results of numerical simulations by comparison to experimental testing results

| | Experimental testing (exp) | | | | Simulated testing (sim) | | | | Difference between exp & sim | |
| | Compression | | Bending | | Compression | | Bending | | Compression | Bending |
Validated sample	[MPa]	Increase %	[MPa]	Increase %	[MPa]	Increase %	[MPa]	Increase %	%	%
cem52504	56.7	0	8.7	0	51.132	0	13.318	0	-9.82%	53.08%
cem52504NT05	69.41	22.42%	9.56	9.89%	52.509	2.69%	16.614	24.75%	-24.35%	73.79%
cem425033	84.8	0	4	0	76.473	0	6.123	0	-9.82%	53.08%
cem425033NT002	90.1	6.25%	4.3	7.50%	77.139	0.87%	5.9609	-2.65%	-14.39%	38.63%
cem425033NT005	95.6	12.74%	4.6	15.00%	77.637	1.52%	5.7689	-5.78%	-18.79%	25.41%
cem425033NT01	97.2	14.62%	5.2	30.00%	77.969	1.96%	5.5192	-9.86%	-19.78%	6.14%
cem42505	35.6	0	7.15	0	32.104	0	10.945	0	-9.82%	53.08%
cem42505NT008	35	-1.69%	7.37	3.08%	32.713	1.90%	10.11	-7.63%	-6.53%	37.18%
cem42505NT01	35.4	-0.56%	7.09	-0.84%	32.621	1.61%	9.9818	-8.80%	-7.85%	40.79%
cem42504	45.5	0	7.04	0	41.032	0	10.776	0	-9.82%	53.07%
cem42504NT005	50.17	10.26%	7.83	11.22%	41.638	1.48%	10.181	-5.52%	-17.01%	30.03%
cem42504NT01	55.05	20.99%	8.25	17.19%	41.788	1.84%	9.7671	-9.36%	-24.09%	18.39%
cem42503	66.5	0	10.1	0	59.97	0	15.461	0	-9.82%	53.08%
cem42503NT01	66.2	-0.45%	11.4	12.87%	61.118	1.91%	14.022	-9.31%	-7.68%	23.00%
cem42503NT03	67.1	0.90%	11.7	15.84%	61.031	1.77%	15.756	1.91%	-9.04%	34.67%
cem42503NT05	62.5	-6.02%	10.3	1.98%	60.038	0.11%	20.224	30.81%	-3.94%	96.35%
mor42504850364	31.7	0	5.9	0	28.587	0	9.0314	0	-9.82%	53.07%
mor42504850364NT008	33.7	6.31%	10.3	74.58%	28.874	1.00%	8.7375	-3.25%	-14.32%	-15.17%
mor42504850364NT01	33.8	6.62%	11.1	88.14%	28.935	1.22%	8.6584	-4.13%	-14.39%	-22.00%
mor42504850364NT03	33.9	6.94%	9.1	54.24%	29.146	1.96%	8.1917	-9.30%	-14.02%	-9.98%
more42504850364NT05	35.3	11.36%	8.6	45.76%	29.025	1.53%	7.8063	-13.56%	-17.78%	-9.23%
mor42505033	51.3	0	8.3	0	46.262	0	12.705	0	-9.82%	53.07%
mor42505033NT005	52.9	3.12%	8.8	6.02%	46.573	0.67%	12.447	-2.03%	-11.96%	41.44%
mor42505033NT01	58.8	14.62%	9.9	19.28%	46.776	1.11%	12.249	-3.59%	-20.45%	23.73%
mor425055033	51.3	0	8.3	0	28.677	0	9.0314	0	-44.10%	8.81%
mor425055033NT005	44.3	-13.65%	7.8	-6.02%	44.28	54.41%	11.401	26.24%	-0.05%	46.17%
mor425055033NT01	51	-0.58%	9.2	10.84%	44.486	55.13%	11.198	23.99%	-12.77%	21.72%
mor42505033spl	48.8	0	7.6	0	48.697	0	15.843	0	-0.21%	108.46%
mor42505033splNT01	33.9	-30.53%	12.9	69.74%	28.993	-40.46%	8.7014	-45.08%	-14.47%	-32.55%
mor52505033spl	54	0	10.35	0	48.697	0	15.843	0	-9.82%	53.07%
mor52505033splNF025	54.5	0.93%	10.2	-1.45%	49.018	0.66%	15.126	-4.53%	-10.06%	48.29%
mor52505033splNF05	55	1.85%	10.4	0.48%	49.044	0.71%	14.563	-8.08%	-10.83%	40.03%
mor52505033splNF075	55.1	2.04%	11.1	7.25%	48.994	0.61%	14.063	-11.24%	-11.08%	26.69%
mor52505033splNF1	54.8	1.48%	11.3	9.18%	48.469	-0.47%	13.699	-13.53%	-11.55%	21.23%
mor52505033splNF125	55	1.85%	11.25	8.70%	48.273	-0.87%	15.823	-0.13%	-12.23%	40.65%
mor52505033splNF15	56.5	4.63%	11.35	9.66%	48.479	-0.45%	17.603	11.11%	-14.20%	55.09%
mor52505033splNF175	57.5	6.48%	11.05	6.76%	47.526	-2.40%	21.032	32.75%	-17.35%	90.33%
mor52505033splNF2	57.6	6.67%	11.45	10.63%	49.862	2.39%	17.559	10.83%	-13.43%	53.35%
mor425035033spl	72.1	0	10.3	0	65.02	0	15.767	0	-9.82%	53.08%

mor425035033splNT005	75.8	5.13%	12.7	23.30%	65.428	0.63%	15.448	-2.02%	-13.68%	21.64%
mor425035033splNT01	84.3	16.92%	13.1	27.18%	65.748	1.12%	15.167	-3.81%	-22.01%	15.78%
mor425045033spl	56.4	0	8.9	0	50.861	0	13.624	0	-9.82%	53.08%
mor425045033splNT005	56.5	0.18%	9.9	11.24%	51.188	0.64%	13.353	-1.99%	-9.40%	34.88%
mor425045033splNT01	64.7	14.72%	10.6	19.10%	51.422	1.10%	13.118	-3.71%	-20.52%	23.75%
mor425040263spl	65	0	7.5	0	58.617	0	11.481	0	-9.82%	53.08%
mor425040263splNT05	76.25	17.31%	8.2	9.33%	59.798	2.01%	10.157	-11.53%	-21.58%	23.87%
mor425045067spl	52.27	0	6.69	0	47.137	0	10.241	0	-9.82%	53.08%
mor425045067splNT05	62.13	18.86%	8.37	25.11%	47.88	1.58%	9.818	-4.13%	-22.94%	17.30%
con425051038049	45.8	0	6.7	0	41.302	0	10.256	0	-9.82%	53.07%
con425051038049NT01	48.5	5.90%	10	49.25%	41.652	0.85%	9.9725	-2.76%	-14.12%	-0.27%
con425051038049NF01	46.7	1.97%	9.9	47.76%	41.407	0.25%	10.126	-1.27%	-11.33%	2.28%

Appendix B – Artificial Neural Networks

B1. Datasets - Group I

Table B1.1 Dataset 1 - COMP

#	Cement [kg/m³]	Water [kg/m³]	Fine aggregate [kg/m³]	Coarse aggregate [kg/m³]	Superplasticizer [kg/m³]	Nanofiller [wt%]		Cement class	Functionalization	Cross-section [cm]	Demolding age [h]	Age [h]	Compressive strength [MPa]
						CNT	CNF	0/1	0/1	0/1			
	min/max	min/max	min/max	min/max	min/max	min/max	min/max	0/1	0/1	0/1	min/max	min/max	min/max
1	542	262.87	1490.5	0	0	0	0	42.5	no	4x4x8	24	3	19.8
2	542	262.87	1490.5	0	0	0	0	42.5	no	4x4x8	24	7	25.6
3	542	262.87	1490.5	0	0	0	0	42.5	no	4x4x8	24	28	31.7
4	542	262.87	1490.5	0	0	0.1	0	42.5	no	4x4x8	24	3	22.6
5	542	262.87	1490.5	0	0	0.1	0	42.5	no	4x4x8	24	7	26.5
6	542	262.87	1490.5	0	0	0.1	0	42.5	no	4x4x8	24	28	33.8
7	542	262.87	1490.5	0	0	0.5	0	42.5	no	4x4x8	24	3	22.7
8	542	262.87	1490.5	0	0	0.5	0	42.5	no	4x4x8	24	7	27.6
9	542	262.87	1490.5	0	0	0.5	0	42.5	no	4x4x8	24	28	35.3
10	542	262.87	1490.5	0	0	0	0.1	42.5	no	4x4x8	24	3	22.5
11	542	262.87	1490.5	0	0	0	0.1	42.5	no	4x4x8	24	7	25.2
12	542	262.87	1490.5	0	0	0	0.1	42.5	no	4x4x8	24	28	33.7
13	380	193.8	999.4	775.2	0	0	0	42.5	no	7x14	24	28	45.8
14	380	193.8	999.4	775.2	0	0.1	0	42.5	no	7x14	24	28	48.5
15	380	193.8	999.4	775.2	0	0	0.1	42.5	no	7x14	24	28	46.7
16	380	121.6	547.2	839.8	0	0	0	42.5	no	7x14	24	28	64.5
17	380	121.6	547.2	839.8	0	0.1	0	42.5	no	7x14	24	28	66
18	512.10	256.05	1536.3	0	2.048	0	0	42.5	no	4x4x8	24	28	31.8
19	512.10	256.05	1536.3	0	2.048	0.1	0	42.5	no	4x4x8	24	28	33.5
20	512.10	256.05	1536.3	0	2.048	0.1	0	42.5	no	4x4x8	24	28	33.1
21	512.10	256.05	1536.3	0	2.048	0.1	0	42.5	yes	4x4x8	24	28	33.9
22	1071.43	642.85	0	0	0	0.1	0	42.5	yes	5x5x5	24	28	40
23	1363.64	681.82	0	0	0	0	0	52.5	no	4x4x16	24	28	56.7
24	1338.21	669.10	0	0	0	0.5	0	52.5	no	4x4x16	24	28	69.41
25	1338.21	669.10	0	0	0	0.5	0	52.5	yes	4x4x16	24	28	72.13
26	1363.64	681.82	0	0	0	0	0	42.5	no	5x5x5	24	28	74.8
27	1363.64	681.82	0	0	1.636	0.03	0	42.5	no	5x5x5	24	28	83.1
28	1363.64	681.82	0	0	4.364	0.08	0	42.5	no	5x5x5	24	28	80
29	1363.64	681.82	0	0	8.182	0.15	0	42.5	no	5x5x5	24	28	86.9
30	1363.64	681.82	0	0	13.636	0.25	0	42.5	no	5x5x5	24	28	91.8
31	1363.64	681.82	0	0	19.091	0.35	0	42.5	no	5x5x5	24	28	90
32	1363.64	681.82	0	0	27.273	0.5	0	42.5	no	5x5x5	24	28	94.3
33	359.20	179.6	1077.6	0	0	0	0	52.5	no	4x4x8	24	7	43.5
34	359.20	179.6	1077.6	0	0	0	0	52.5	no	4x4x8	24	28	54
35	359.20	179.6	1077.6	0	0	0	0	52.5	no	4x4x8	24	120	58
36	353.72	176.86	1061.1	0	1.03	0	0.25	52.5	no	4x4x8	24	7	43
37	353.72	176.86	1061.1	0	1.03	0	0.25	52.5	no	4x4x8	24	28	54.5
38	353.72	176.86	1061.1	0	1.03	0	0.25	52.5	no	4x4x8	24	120	60.6
39	348.32	174.16	1044.9	0	2.02	0	0.5	52.5	no	4x4x8	24	7	43.5
40	348.32	174.16	1044.9	0	2.02	0	0.5	52.5	no	4x4x8	24	28	55
41	348.32	174.16	1044.9	0	2.02	0	0.5	52.5	no	4x4x8	24	120	61
42	343	171.50	1029.0	0	2.95	0	0.75	52.5	no	4x4x8	24	7	44
43	343	171.50	1029.0	0	2.95	0	0.75	52.5	no	4x4x8	24	28	55.1
44	343	171.50	1029.0	0	2.95	0	0.75	52.5	no	4x4x8	24	120	62.5
45	337.77	168.88	1013.3	0	3.85	0	1	52.5	no	4x4x8	24	7	46.5
46	337.77	168.88	1013.3	0	3.85	0	1	52.5	no	4x4x8	24	28	54.8
47	337.77	168.88	1013.3	0	3.85	0	1	52.5	no	4x4x8	24	120	61.8
48	332.61	166.31	997.83	0	4.86	0	1.25	52.5	no	4x4x8	24	7	47.5
49	332.61	166.31	997.83	0	4.86	0	1.25	52.5	no	4x4x8	24	28	55
50	332.61	166.31	997.83	0	4.86	0	1.25	52.5	no	4x4x8	24	120	62.5
51	327.53	163.77	982.60	0	5.86	0	1.5	52.5	no	4x4x8	24	7	46
52	327.53	163.77	982.60	0	5.86	0	1.5	52.5	no	4x4x8	24	28	56.5
53	327.53	163.77	982.60	0	5.86	0	1.5	52.5	no	4x4x8	24	120	65
54	322.53	161.27	967.60	0	6.29	0	1.75	52.5	no	4x4x8	24	7	45.5
55	322.53	161.27	967.60	0	6.29	0	1.75	52.5	no	4x4x8	24	28	57.5

56	322.53	161.27	967.60	0	6.29	0	1.75	52.5	no	4x4x8	24	120	65.8
57	317.61	158.81	952.84	0	6.73	0	2	52.5	no	4x4x8	24	7	50
58	317.61	158.81	952.84	0	6.73	0	2	52.5	no	4x4x8	24	28	57.6
59	317.61	158.81	952.84	0	6.73	0	2	52.5	no	4x4x8	24	120	67
60	1200	600	0	0	0	0	0	52.5	no	4x4x16	24	7	38.65
61	1200	600	0	0	0	0	0	52.5	no	4x4x16	24	28	46.7
62	1200	600	0	0	1.8	0	0.5	52.5	no	4x4x16	24	7	39.12
63	1200	600	0	0	1.8	0	0.5	52.5	no	4x4x16	24	28	47.2
64	1200	600	0	0	3.6	0	1	52.5	no	4x4x16	24	7	38.78
65	1200	600	0	0	3.6	0	1	52.5	no	4x4x16	24	28	45.67
66	1200	600	0	0	6.6	0	2	52.5	no	4x4x16	24	7	37.8
67	1200	600	0	0	6.6	0	2	52.5	no	4x4x16	24	28	44.56
68	542	262.87	1490.5	0	0	0	0	42.5	no	4x4x8	24	3	19.95
69	542	262.87	1490.5	0	0	0	0	42.5	no	4x4x8	24	7	25
70	542	262.87	1490.5	0	0	0	0	42.5	no	4x4x8	24	28	31.7
71	542	262.87	1490.5	0	0	0.08	0	42.5	no	4x4x8	24	3	22.3
72	542	262.87	1490.5	0	0	0.08	0	42.5	no	4x4x8	24	7	26.1
73	542	262.87	1490.5	0	0	0.08	0	42.5	no	4x4x8	24	28	33.7
74	542	262.87	1490.5	0	0	0.1	0	42.5	no	4x4x8	24	3	22.9
75	542	262.87	1490.5	0	0	0.1	0	42.5	no	4x4x8	24	7	26.2
76	542	262.87	1490.5	0	0	0.1	0	42.5	no	4x4x8	24	28	33.8
77	542	262.87	1490.5	0	0	0.3	0	42.5	no	4x4x8	24	3	21.1
78	542	262.87	1490.5	0	0	0.3	0	42.5	no	4x4x8	24	7	28
79	542	262.87	1490.5	0	0	0.3	0	42.5	no	4x4x8	24	28	33.9
80	542	262.87	1490.5	0	0	0.5	0	42.5	no	4x4x8	24	3	22.8
81	542	262.87	1490.5	0	0	0.5	0	42.5	no	4x4x8	24	7	27.6
82	542	262.87	1490.5	0	0	0.5	0	42.5	no	4x4x8	24	28	35.3
83	664.80	232.68	1994.4	0	7.9776	0	0	42.5	no	4x4x8	24	7	68.1
84	664.80	232.68	1994.4	0	7.9776	0	0	42.5	no	4x4x8	24	28	72.1
85	664.80	232.68	1994.4	0	7.9776	0	0	42.5	no	4x4x8	24	90	73.6
86	644.66	225.63	1933.9	0	7.7359	0.1	0	42.5	no	4x4x8	24	7	76.8
87	644.66	225.63	1933.9	0	7.7359	0.1	0	42.5	no	4x4x8	24	28	84.3
88	644.66	225.63	1933.9	0	7.7359	0.1	0	42.5	no	4x4x8	24	90	86.8
89	654.65	229.12	1963.9	0	7.8558	0.05	0	42.5	no	4x4x8	24	7	72.7
90	654.65	229.12	1963.9	0	7.8558	0.05	0	42.5	no	4x4x8	24	28	75.8
91	654.65	229.12	1963.9	0	7.8558	0.05	0	42.5	no	4x4x8	24	90	77.9
92	654.65	229.12	1963.9	0	7.8558	0.05	0	42.5	no	4x4x8	24	7	80.6
93	654.65	229.12	1963.9	0	7.8558	0.05	0	42.5	no	4x4x8	24	28	88.8
94	654.65	229.12	1963.9	0	7.8558	0.05	0	42.5	no	4x4x8	24	90	90.4
95	525.56	236.50	709.50	0	0.78834	0	0	42.5	no	4x4x8	24	7	45.3
96	525.56	236.50	709.50	0	0.78834	0	0	42.5	no	4x4x8	24	28	56.4
97	525.56	236.50	709.50	0	0.78834	0	0	42.5	no	4x4x8	24	90	57.9
98	509.64	229.33	688.01	0	0.7645	0.1	0	42.5	no	4x4x8	24	7	53.2
99	509.64	229.33	688.01	0	0.7645	0.1	0	42.5	no	4x4x8	24	28	64.7
100	509.64	229.33	688.01	0	0.7645	0.1	0	42.5	no	4x4x8	24	90	65.8
101	517.54	232.89	698.67	0	0.7763	0.05	0	42.5	no	4x4x8	24	7	46.7
102	517.54	232.89	698.67	0	0.7763	0.05	0	42.5	no	4x4x8	24	28	56.5
103	517.54	232.89	698.67	0	0.7763	0.05	0	42.5	no	4x4x8	24	90	57.5
104	517.54	232.89	698.67	0	0.7763	0.05	0	42.5	no	4x4x8	24	7	55.4
105	517.54	232.89	698.67	0	0.7763	0.05	0	42.5	no	4x4x8	24	28	65.2
106	517.54	232.89	698.67	0	0.7763	0.05	0	42.5	no	4x4x8	24	90	65.7
107	512.10	256.05	1536.3	0	0	0	0	42.5	no	4x4x8	24	7	38.1
108	512.10	256.05	1536.3	0	0	0	0	42.5	no	4x4x8	24	28	51.3
109	512.10	256.05	1536.3	0	0	0	0	42.5	no	4x4x8	24	90	52.4
110	496.59	248.29	1489.7	0	0	0.1	0	42.5	no	4x4x8	24	7	46.3
111	496.59	248.29	1489.7	0	0	0.1	0	42.5	no	4x4x8	24	28	58.8
112	496.59	248.29	1489.7	0	0	0.1	0	42.5	no	4x4x8	24	90	61.5
113	504.28	252.14	1512.8	0	0	0.05	0	42.5	no	4x4x8	24	7	43
114	504.28	252.14	1512.8	0	0	0.05	0	42.5	no	4x4x8	24	28	52.9
115	504.28	252.14	1512.8	0	0	0.05	0	42.5	no	4x4x8	24	90	56.5
116	504.28	252.14	1512.8	0	0	0.05	0	42.5	no	4x4x8	24	7	45.6
117	504.28	252.14	1512.8	0	0	0.05	0	42.5	no	4x4x8	24	28	58.8
118	504.28	252.14	1512.8	0	0	0.05	0	42.5	no	4x4x8	24	90	59.5
119	499.30	274.62	1497.9	0	0	0	0	42.5	no	4x4x8	24	7	36.9
120	499.30	274.62	1497.9	0	0	0	0	42.5	no	4x4x8	24	28	48.8
121	499.30	274.62	1497.9	0	0	0	0	42.5	no	4x4x8	24	90	50.6
122	484.17	266.3	1452.5	0	0	0.1	0	42.5	no	4x4x8	24	7	38.9

123	484.17	266.3	1452.5	0	0	0.1	0	42.5	no	4x4x8	24	28	51
124	484.17	266.3	1452.5	0	0	0.1	0	42.5	no	4x4x8	24	90	52
125	491.68	270.42	1475	0	0	0.05	0	42.5	no	4x4x8	24	7	34.7
126	491.68	270.42	1475	0	0	0.05	0	42.5	no	4x4x8	24	28	44.3
127	491.68	270.42	1475	0	0	0.05	0	42.5	no	4x4x8	24	90	44.7
128	491.68	270.42	1475	0	0	0.05	0	42.5	no	4x4x8	24	7	42.1
129	491.68	270.42	1475	0	0	0.05	0	42.5	no	4x4x8	24	28	54.5
130	491.68	270.42	1475	0	0	0.05	0	42.5	no	4x4x8	24	90	58.1
131	572	188	572	1015	0	0	0	42.5	no	30x15	24	28	51.23
132	571	188	572	1015	0.22	0	0.16	42.5	no	30x15	24	28	73.08
133	570	188	572	1015	0.31	0	0.31	42.5	no	30x15	24	28	64.604
134	569	188	572	1015	0.71	0	0.78	42.5	no	30x15	24	28	53.5
135	566	188	572	1015	1.38	0	1.55	42.5	no	30x15	24	28	50.26
136	480	191	1005	901	0.49	0	0	42.5	no	30x15	24	28	45.505
137	480	191	942	901	0.49	0	0.25	42.5	no	30x15	24	28	43.44
138	448	191	877	838	0.62	0	0.5	42.5	no	30x15	24	28	51.64
139	448	191	877	838	0.62	0	1	42.5	yes	30x15	24	28	41.16
140	448	191	877	838	0.71	0	1.5	42.5	yes	30x15	24	28	39.78
141	478	191	1008	902	0.49	0	1	42.5	no	30x15	24	28	47.71
142	478	191	1008	902	0.85	0	1.5	42.5	no	30x15	24	28	52.33
143	478	191	1008	902	1.02	0	2	42.5	no	30x15	24	28	56.6
144	478	191	1008	902	1.56	0	2.5	42.5	no	30x15	24	28	51.57
145	478	191	1008	902	0.31	0	0.7	42.5	no	30x15	24	28	44.75
146	478	191	1008	902	0.49	0	1	42.5	no	30x15	24	28	55.23
147	478	191	1008	902	0.85	0	1.5	42.5	no	30x15	24	28	51.15
148	478	191	1008	902	1.02	0	2	42.5	no	30x15	24	28	43.78
149	478	191	1008	902	1.56	0	2.5	42.5	no	30x15	24	28	44.33
150	1500	495	0	0	0	0	0	42.5	no	5x5x5	24	7	40.4
151	1500	495	0	0	0	0.025	0	42.5	no	5x5x5	24	7	44.2
152	1500	495	0	0	0	0.05	0	42.5	no	5x5x5	24	7	47.8
153	1500	495	0	0	0	0.1	0	42.5	no	5x5x5	24	7	49.2
154	1500	495	0	0	0	0	0	42.5	no	5x5x5	24	28	84.8
155	1500	495	0	0	0	0.025	0	42.5	no	5x5x5	24	28	90.1
156	1500	495	0	0	0	0.05	0	42.5	no	5x5x5	24	28	95.6
157	1500	495	0	0	0	0.1	0	42.5	no	5x5x5	24	28	97.2
158	1277	574	0	0	0	0	0	42.5	yes	5x5x5	24	28	37.6
159	1274.55	573.55	0	0	0	0.1	0	42.5	yes	5x5x5	24	28	44.3
160	1264.77	569.14	0	0	0	0.5	0	42.5	yes	5x5x5	24	28	51.2
161	1252.77	563.74	0	0	0	1	0	42.5	yes	5x5x5	24	28	58.4
162	1241.01	558.45	0	0	0	1.5	0	42.5	yes	5x5x5	24	28	59.8
163	1071.43	642.86	0	0	0	0	0	42.5	yes	5x5x5	24	28	41.3
164	1069.40	641.64	0	0	0	0.1	0	42.5	yes	5x5x5	24	28	48.2
165	1061.87	637.12	0	0	0	0.5	0	42.5	yes	5x5x5	24	28	56.8
166	1031.95	619.17	0	0	0	1	0	42.5	yes	5x5x5	24	28	66.3
167	1002.86	601.72	0	0	0	1.5	0	42.5	yes	5x5x5	24	28	68.2
168	974.60	584.76	0	0	0	2	0	42.5	yes	5x5x5	24	28	61.5
169	897.91	538.75	628.54	0	0	0	0	42.5	yes	5x5x5	24	28	40.6
170	887.63	532.58	621.34	0	0	0.1	0	42.5	yes	5x5x5	24	28	51.3
171	877.47	526.48	614.23	0	0	0.5	0	42.5	yes	5x5x5	24	28	60.7
172	867.43	520.45	607.2	0	0	1	0	42.5	yes	5x5x5	24	28	76.3
173	857.50	514.5	600.25	0	0	1.5	0	42.5	yes	5x5x5	24	28	87.7
174	847.68	508.61	593.38	0	0	2	0	42.5	yes	5x5x5	24	28	95.6
175	1040.37	468.17	728.26	0	0	0	0	42.5	yes	5x5x5	24	28	38.6
176	1028.46	462.81	719.92	0	0	0.1	0	42.5	yes	5x5x5	24	28	46.3
177	1016.69	457.51	711.68	0	0	0.5	0	42.5	yes	5x5x5	24	28	56.1
178	1005.05	452.27	703.53	0	0	1	0	42.5	yes	5x5x5	24	28	68.1
179	993.54	447.09	695.48	0	0	1.5	0	42.5	yes	5x5x5	24	28	78
180	899.93	539.96	629.95	0	0	0	0	42.5	yes	5x5x5	24	28	42.27
181	889.63	533.78	622.74	0	0	0.1	0	42.5	yes	5x5x5	24	28	53.7
182	879.44	527.66	615.61	0	0	0.5	0	42.5	yes	5x5x5	24	28	60.7
183	869.38	521.62	608.56	0	0	1	0	42.5	yes	5x5x5	24	28	80.33
184	859.42	515.65	601.59	0	0	1.5	0	42.5	yes	5x5x5	24	28	91
185	849.59	509.75	594.71	0	0	2	0	42.5	yes	5x5x5	24	28	102.57
186	1200	600	0	0	0	0	0	42.5	no	4x4x8	24	28	35.6
187	1200	600	0	0	0	0.1	0	42.5	no	4x4x8	24	28	20.4
188	1200	600	0	0	0	0.1	0	42.5	no	4x4x8	24	28	30.1
189	1200	600	0	0	0	0.1	0	42.5	no	4x4x8	24	28	32.4

190	1200	600	0	0	0	0.08	0	42.5	no	4x4x8	24	28	35
191	1200	600	0	0	0	0.1	0	42.5	yes	4x4x8	48	28	32
192	1200	600	0	0	0	0.1	0	42.5	yes	4x4x8	48	28	35.4
193	1500	600	0	0	0	0	0	42.5	no	4x4x8	24	28	45.5
194	1500	600	0	0	0	0.05	0	42.5	no	4x4x8	24	28	45.92
195	1500	600	0	0	0	0.05	0	42.5	no	4x4x8	24	28	50.17
196	1500	600	0	0	0	0.1	0	42.5	no	4x4x8	24	28	50.09
197	1500	600	0	0	0	0.1	0	42.5	no	4x4x8	24	28	55.05
198	320.17	252.93	1921	0	0	0	0	42.5	no	7x7x7	24	3	5.9
199	320.17	252.93	1921	0	0	0	0	42.5	no	7x7x7	24	7	8.9
200	320.17	252.93	1921	0	0	0	0	42.5	no	7x7x7	24	14	9.9
201	320.17	252.93	1921	0	0	0	0	42.5	no	7x7x7	24	28	11
202	320.17	252.93	1921	0	0	0.2	0	42.5	no	7x7x7	24	3	7.4
203	320.17	252.93	1921	0	0	0.2	0	42.5	no	7x7x7	24	7	8.3
204	320.17	252.93	1921	0	0	0.2	0	42.5	no	7x7x7	24	14	9.15
205	320.17	252.93	1921	0	0	0.2	0	42.5	no	7x7x7	24	28	11.9
206	320.17	252.93	1921	0	0	0.4	0	42.5	no	7x7x7	24	3	8.2
207	320.17	252.93	1921	0	0	0.4	0	42.5	no	7x7x7	24	7	8.2
208	320.17	252.93	1921	0	0	0.4	0	42.5	no	7x7x7	24	14	8.45
209	320.17	252.93	1921	0	0	0.4	0	42.5	no	7x7x7	24	28	12.85
210	320.17	252.93	1921	0	0	0.6	0	42.5	no	7x7x7	24	3	4.4
211	320.17	252.93	1921	0	0	0.6	0	42.5	no	7x7x7	24	7	7.98
212	320.17	252.93	1921	0	0	0.6	0	42.5	no	7x7x7	24	14	9.9
213	320.17	252.93	1921	0	0	0.6	0	42.5	no	7x7x7	24	28	10.9
214	320.17	252.93	1921	0	0	0.8	0	42.5	no	7x7x7	24	3	7.15
215	320.17	252.93	1921	0	0	0.8	0	42.5	no	7x7x7	24	7	7.9
216	320.17	252.93	1921	0	0	0.8	0	42.5	no	7x7x7	24	14	8.2
217	320.17	252.93	1921	0	0	0.8	0	42.5	no	7x7x7	24	28	9.3
218	496	272.8	1488	0	0	0	0	42.5	no	5x5x5	24	28	48
219	496	272.8	1488	0	0	0.05	0	42.5	no	5x5x5	24	28	55
220	496	272.8	1488	0	0	0.1	0	42.5	no	5x5x5	24	28	52
221	496	272.8	1488	0	0	0.15	0	42.5	no	5x5x5	24	28	53
222	620	250	0	0	0	0	0	42.5	no	5x5x5	24	3	21.72
223	620	250	0	0	0	0	0	42.5	no	5x5x5	24	3	23
224	620	250	0	0	0	0	0	42.5	no	5x5x5	24	3	20.36
225	620	250	0	0	0	0	0	42.5	no	5x5x5	24	7	30.76
226	620	250	0	0	0	0	0	42.5	no	5x5x5	24	7	30.32
227	620	250	0	0	0	0	0	42.5	no	5x5x5	24	7	28.8
228	620	250	0	0	0	0	0	42.5	no	5x5x5	24	14	38.16
229	620	250	0	0	0	0	0	42.5	no	5x5x5	24	14	35.44
230	620	250	0	0	0	0	0	42.5	no	5x5x5	24	14	39.36
231	620	250	0	0	0	0	0	42.5	no	5x5x5	24	28	61.2
232	620	250	0	0	0	0	0	42.5	no	5x5x5	24	28	48.44
233	620	250	0	0	0	0	0	42.5	no	5x5x5	24	28	71.56
234	620	250	0	0	0	0.2	0	42.5	no	5x5x5	24	7	43.8
235	620	250	0	0	0	0.2	0	42.5	no	5x5x5	24	28	73.1
236	620	250	0	0	0	0.4	0	42.5	no	5x5x5	24	7	43.9
237	620	250	0	0	0	0.4	0	42.5	no	5x5x5	24	28	64.3
238	620	250	0	0	0	0.2	0	42.5	yes	5x5x5	24	7	45.4
239	620	250	0	0	0	0.2	0	42.5	yes	5x5x5	24	28	68.2
240	620	250	0	0	0	0.4	0	42.5	yes	5x5x5	24	7	46
241	620	250	0	0	0	0.4	0	42.5	yes	5x5x5	24	28	69
242	620	250	0	0	0	0.2	0	42.5	yes	5x5x5	24	7	43.3
243	620	250	0	0	0	0.2	0	42.5	yes	5x5x5	24	28	85.7
244	620	250	0	0	0	0.4	0	42.5	yes	5x5x5	24	7	45.7
245	620	250	0	0	0	0.4	0	42.5	yes	5x5x5	24	28	57.9
246	474	237	793	793	0	0	0	42.5	no	7.5x15	24	28	34
247	474	237	793	793	0	0	0	42.5	no	7.5x15	24	28	39.9
248	474	237	793	793	0	0.01	0	42.5	no	7.5x15	24	28	41.2
249	400	160	660	1168	2.4	0	0	52.5	no	15x15x15	24	3	20
250	400	160	660	1168	2.4	0	0	52.5	no	15x15x15	24	7	39
251	400	160	660	1168	2.4	0	0	52.5	no	15x15x15	24	28	49
252	400	160	660	1168	2.4	0.05	0	52.5	yes	15x15x15	24	3	22
253	400	160	660	1168	2.4	0.05	0	52.5	yes	15x15x15	24	7	40
254	400	160	660	1168	2.4	0.05	0	52.5	yes	15x15x15	24	28	45
255	400	160	660	1168	2.4	0.07	0	52.5	yes	15x15x15	24	3	22
256	400	160	660	1168	2.4	0.07	0	52.5	yes	15x15x15	24	7	42

257	400	160	660	1168	2.4	0.07	0	52.5	yes	15x15x15	24	28	54
258	400	160	660	1168	2.4	0.08	0	52.5	yes	15x15x15	24	3	28
259	400	160	660	1168	2.4	0.08	0	52.5	yes	15x15x15	24	7	55
260	400	160	660	1168	2.4	0.08	0	52.5	yes	15x15x15	24	28	67
261	400	160	660	1168	2.4	0.1	0	52.5	yes	15x15x15	24	3	24
262	400	160	660	1168	2.4	0.1	0	52.5	yes	15x15x15	24	7	48
263	400	160	660	1168	2.4	0.1	0	52.5	yes	15x15x15	24	28	54
264	422	147	621	1284	5.06	0	0	52.5	no	15x15x15	24	3	34.1
265	422	147	621	1284	5.06	0	0	52.5	no	15x15x15	24	7	38.6
266	422	147	621	1284	5.06	0	0	52.5	no	15x15x15	24	28	61.2
267	422	147	621	1284	5.06	0.05	0	52.5	yes	15x15x15	24	3	31.4
268	422	147	621	1284	5.06	0.05	0	52.5	yes	15x15x15	24	7	55
269	422	147	621	1284	5.06	0.05	0	52.5	yes	15x15x15	24	28	78
270	422	147	621	1284	5.06	0.07	0	52.5	yes	15x15x15	24	3	29.6
271	422	147	621	1284	5.06	0.07	0	52.5	yes	15x15x15	24	7	50.8
272	422	147	621	1284	5.06	0.07	0	52.5	yes	15x15x15	24	28	72.6
273	422	147	621	1284	5.06	0.08	0	52.5	yes	15x15x15	24	3	38.6
274	422	147	621	1284	5.06	0.08	0	52.5	yes	15x15x15	24	7	51.4
275	422	147	621	1284	5.06	0.08	0	52.5	yes	15x15x15	24	28	73.2
276	422	147	621	1284	5.06	0.1	0	52.5	yes	15x15x15	24	3	33.4
277	422	147	621	1284	5.06	0.1	0	52.5	yes	15x15x15	24	7	59.3
278	422	147	621	1284	5.06	0.1	0	52.5	yes	15x15x15	24	28	83.6
279	422	147	621	1284	5.06	0.15	0	52.5	yes	15x15x15	24	7	52.5
280	422	147	621	1284	5.06	0.15	0	52.5	yes	15x15x15	24	28	77.6
281	504	142	683	1108	4.7	0	0	52.5	no	15x15x15	24	3	38
282	504	142	683	1108	4.7	0	0	52.5	no	15x15x15	24	7	42
283	504	142	683	1108	4.7	0	0	52.5	no	15x15x15	24	28	72
284	504	142	683	1108	4.7	0.05	0	52.5	yes	15x15x15	24	3	34
285	504	142	683	1108	4.7	0.05	0	52.5	yes	15x15x15	24	7	58
286	504	142	683	1108	4.7	0.05	0	52.5	yes	15x15x15	24	28	89
287	504	142	683	1108	4.7	0.07	0	52.5	yes	15x15x15	24	3	34
288	504	142	683	1108	4.7	0.07	0	52.5	yes	15x15x15	24	7	55
289	504	142	683	1108	4.7	0.07	0	52.5	yes	15x15x15	24	28	85
290	504	142	683	1108	4.7	0.08	0	52.5	yes	15x15x15	24	3	39
291	504	142	683	1108	4.7	0.08	0	52.5	yes	15x15x15	24	7	54
292	504	142	683	1108	4.7	0.08	0	52.5	yes	15x15x15	24	28	83
293	504	142	683	1108	4.7	0.1	0	52.5	yes	15x15x15	24	3	37
294	504	142	683	1108	4.7	0.1	0	52.5	yes	15x15x15	24	7	60
295	504	142	683	1108	4.7	0.1	0	52.5	yes	15x15x15	24	28	92
296	504	142	683	1108	4.7	0.15	0	52.5	yes	15x15x15	24	7	56
297	504	142	683	1108	4.7	0.15	0	52.5	yes	15x15x15	24	28	86
298	1875	375	0	0	14.0625	0	0	42.5	no	4x4x4	24	28	130
299	1875	375	0	0	14.0625	0.1	0	42.5	no	4x4x4	24	28	152
300	1875	375	0	0	14.0625	0.5	0	42.5	no	4x4x4	24	28	144
301	1875	375	0	0	14.0625	1	0	42.5	no	4x4x4	24	28	126
302	1875	375	0	0	14.0625	0	0	42.5	no	4x4x4	24	28	130
303	1875	375	0	0	14.0625	0	0.1	42.5	no	4x4x4	24	28	127
304	1875	375	0	0	14.0625	0	0.5	42.5	no	4x4x4	24	28	128
305	1875	375	0	0	14.0625	0	0.5	42.5	no	4x4x4	24	28	92
306	1277	574	0	0	0	0	0	42.5	no	5x5x5	48	28	27.1
307	1161.12	522.50	0	0	0	0.5	0	42.5	no	5x5x5	48	28	41.8
308	1578.95	789.47	0	0	0.00	0	0	42.5	yes	4x4x8	24	3	54.9
309	1578.95	789.47	0	0	0.00	0.1	0	42.5	yes	4x4x8	24	21	61
310	1578.95	789.47	0	0	0.00	0	0	42.5	yes	4x4x8	24	28	66.5
311	1578.95	789.47	0	0	0.00	0.1	0	42.5	yes	4x4x8	24	3	60.5
312	1578.95	789.47	0	0	0.00	0	0	42.5	yes	4x4x8	24	21	62.3
313	1578.95	789.47	0	0	0.00	0.1	0	42.5	yes	4x4x8	24	28	66.2
314	1578.95	789.47	0	0	0.00	0.3	0	42.5	yes	4x4x8	24	3	58.7
315	1578.95	789.47	0	0	0.00	0	0	42.5	yes	4x4x8	24	21	66
316	1578.95	789.47	0	0	0.00	0.3	0	42.5	yes	4x4x8	24	28	67.1
317	1578.95	789.47	0	0	0.00	0.5	0	42.5	yes	4x4x8	24	3	52
318	1578.95	789.47	0	0	0.00	0	0	42.5	yes	4x4x8	24	21	60.5
319	1578.95	789.47	0	0	0.00	0.5	0	42.5	yes	4x4x8	24	28	62.5
320	675.86	270.34	1351.7	0	0	0.02	0	42.5	yes	5x5x5	24	28	59.49
321	675.86	270.34	1351.7	0	0	0.04	0	42.5	yes	5x5x5	24	28	55.659
322	675.86	270.34	1351.7	0	0	0.08	0	42.5	yes	5x5x5	24	28	55.343
323	675.86	270.34	1351.7	0	0	0.1	0	42.5	yes	5x5x5	24	28	55.659

#	Cement [kg/m³]	Water [kg/m³]	Fine aggregate [kg/m³]	Coarse aggregate [kg/m³]	Super plasticizer [kg/m³]	CNT	CNF	Cement class	Functionalization	Cross-section [cm]	Demolding age [h]	Age [h]	Strength
324	675.86	270.34	1351.7	0	0	0.3	0	42.5	yes	5x5x5	24	28	36.783
325	450	180	1720	0	4.95	0	0	42.5	no	4x4x8	24	28	65
326	450	180	1720	0	4.95	0.5	0	42.5	no	4x4x8	24	28	71.875
327	450	180	1720	0	4.95	0.5	0	42.5	no	4x4x8	24	28	76.25
328	1103.2	496.44	1654.8	0	1.43416	0	0	42.5	no	4x4x16	24	28	52.27
329	1103.2	496.44	1654.8	0	1.43416	0.5	0	42.5	yes	4x4x16	24	28	62.13

Table B1.2 Dataset 2 – FLEX

	Cement [kg/m³]	Water [kg/m³]	Fine aggregate [kg/m³]	Coarse aggregate [kg/m³]	Super plasticizer [kg/m³]	Nanofiler wt%		Cement class	Functio nalization	Cross-section [cm]	Demolding age [h]	Age [h]	Flexural strength [MPa]
						CNT	CNF						
#	min/max	min/max	min/max	min/max	min/max	min/max	min/max	0/1	0/1	0/1	min/max	min/max	min/max
1	1200	600	0	0	0	0	0	42.5	no	2x2x8	18	3	3.86
2	1200	600	0	0	0	0	0	42.5	no	2x2x8	18	7	4.89
3	1200	600	0	0	0	0	0	42.5	no	2x2x8	18	28	5.43
4	1200	600	0	0	0	0.048	0	42.5	no	2x2x8	18	3	4.35
5	1200	600	0	0	0	0.048	0	42.5	no	2x2x8	18	7	5.56
6	1200	600	0	0	0	0.048	0	42.5	no	2x2x8	18	28	6.181
7	1200	600	0	0	0	0.048	0	42.5	no	2x2x8	18	3	4.74
8	1200	600	0	0	0	0.048	0	42.5	no	2x2x8	18	7	5.83
9	1200	600	0	0	0	0.048	0	42.5	no	2x2x8	18	28	6.75
10	1200	600	0	0	0	0.008	0	42.5	no	2x2x8	18	3	5.055
11	1200	600	0	0	0	0.008	0	42.5	no	2x2x8	18	7	5.83
12	1200	600	0	0	0	0.008	0	42.5	no	2x2x8	18	28	6.64
13	1200	600	0	0	0	0.008	0	42.5	no	2x2x8	18	3	4.45
14	1200	600	0	0	0	0.008	0	42.5	no	2x2x8	18	7	5.61
15	1200	600	0	0	0	0.008	0	42.5	no	2x2x8	18	28	6.66
16	542	262.87	1490	0	0	0	0	42.5	no	4x4x16	24	3	2.18
17	542	262.87	1490	0	0	0	0	42.5	no	4x4x16	24	7	3.23
18	542	262.87	1490	0	0	0	0	42.5	no	4x4x16	24	28	5.9
19	542	262.87	1490	0	0	0.1	0	42.5	no	4x4x16	24	3	4.97
20	542	262.87	1490	0	0	0.1	0	42.5	no	4x4x16	24	7	5.83
21	542	262.87	1490	0	0	0.1	0	42.5	no	4x4x16	24	28	11.1
22	542	262.87	1490	0	0	0.5	0	42.5	no	4x4x16	24	3	2.35
23	542	262.87	1490	0	0	0.5	0	42.5	no	4x4x16	24	7	4.77
24	542	262.87	1490	0	0	0.5	0	42.5	no	4x4x16	24	28	8.6
25	542	262.87	1490	0	0	0	0.1	42.5	no	4x4x16	24	3	3.57
26	542	262.87	1490	0	0	0	0.1	42.5	no	4x4x16	24	7	7.69
27	542	262.87	1490	0	0	0	0.1	42.5	no	4x4x16	24	28	12.2
28	380	193.8	999.4	775.2	0	0	0	42.5	no	7x8x38	24	28	6.7
29	380	193.8	999.4	775.2	0	0.1	0	42.5	no	7x8x38	24	28	10
30	380	193.8	999.4	775.2	0	0	0.1	42.5	no	7x8x38	24	28	9.9
31	512.10	256.05	1536	0	2.048	0	0	42.5	no	4x4x16	24	28	5.9
32	512.10	256.05	1536	0	2.048	0.1	0	42.5	no	4x4x16	24	28	10.5
33	512.10	256.05	1536	0	2.048	0.1	0	42.5	no	4x4x16	24	28	10.2
34	512.10	256.05	1536	0	2.048	0.1	0	42.5	yes	4x4x16	24	28	12.9
35	512.10	256.05	1536	0	2.048	0.1	0	42.5	yes	4x4x16	24	28	10.6
36	512.10	256.05	1536	0	2.048	0.1	0	42.5	yes	4x4x16	24	28	8.9
37	1338.2	669.11	0	0	0	0.5	0	52.5	no	4x4x16	24	28	9.56
38	1338.2	669.11	0	0	0	0.5	0	52.5	yes	4x4x16	24	28	9.97
39	1363.6	681.82	0	0	0	0	0	42.5	no	4x4x16	24	28	10.2
40	1363.6	681.82	0	0	1.64	0.03	0	42.5	no	4x4x16	24	28	11.1
41	1363.6	681.82	0	0	4.36	0.08	0	42.5	no	4x4x16	24	28	10.8
42	1363.6	681.82	0	0	8.18	0.15	0	42.5	no	4x4x16	24	28	13.6
43	1363.6	681.82	0	0	13.64	0.25	0	42.5	no	4x4x16	24	28	16.1
44	1363.6	681.82	0	0	19.09	0.35	0	42.5	no	4x4x16	24	28	16.3
45	1363.6	681.82	0	0	27.27	0.5	0	42.5	no	4x4x16	24	28	16.4
46	359.20	179.6	1077	0	0	0	0	52.5	no	4x4x16	24	7	9.5
47	359.20	179.6	1077	0	0.00	0	0	52.5	no	4x4x16	24	28	10.35
48	359.20	179.6	1077	0	0.00	0	0	52.5	no	4x4x16	24	120	11.75
49	353.72	176.86	1061	0	1.03	0	0.25	52.5	no	4x4x16	24	7	9.8
50	353.72	176.86	1061	0	1.03	0	0.25	52.5	no	4x4x16	24	28	10.2
51	353.72	176.86	1061	0	1.03	0	0.25	52.5	no	4x4x16	24	120	11.3
52	348.32	174.16	1045	0	2.02	0	0.5	52.5	no	4x4x16	24	7	9.75
53	348.32	174.16	1045	0	2.02	0	0.5	52.5	no	4x4x16	24	28	10.4
54	348.32	174.16	1045	0	2.02	0	0.5	52.5	no	4x4x16	24	120	11.85

55	343.00	171.50	1029	0	2.95	0	0.75	52.5	no	4x4x16	24	7	10.1
56	343.00	171.50	1029	0	2.95	0	0.75	52.5	no	4x4x16	24	28	11.1
57	343.00	171.50	1029	0	2.95	0	0.75	52.5	no	4x4x16	24	120	11.8
58	337.77	168.88	1013	0	3.85	0	1	52.5	no	4x4x16	24	7	10
59	337.77	168.88	1013	0	3.85	0	1	52.5	no	4x4x16	24	28	11.3
60	337.77	168.88	1013	0	3.85	0	1	52.5	no	4x4x16	24	120	11.7
61	332.61	166.31	997.8	0	4.86	0	1.25	52.5	no	4x4x16	24	7	10.05
62	332.61	166.31	997.8	0	4.86	0	1.25	52.5	no	4x4x16	24	28	11.25
63	332.61	166.31	997.8	0	4.86	0	1.25	52.5	no	4x4x16	24	120	11.65
64	327.53	163.77	982.6	0	5.86	0	1.5	52.5	no	4x4x16	24	7	9.9
65	327.53	163.77	982.6	0	5.86	0	1.5	52.5	no	4x4x16	24	28	11.35
66	327.53	163.77	982.6	0	5.86	0	1.5	52.5	no	4x4x16	24	120	11.5
67	322.53	161.27	967.6	0	6.29	0	1.75	52.5	no	4x4x16	24	7	9.6
68	322.53	161.27	967.6	0	6.29	0	1.75	52.5	no	4x4x16	24	28	11.05
69	322.53	161.27	967.6	0	6.29	0	1.75	52.5	no	4x4x16	24	120	11.55
70	317.61	158.81	952.8	0	6.73	0	2	52.5	no	4x4x16	24	7	9.5
71	317.61	158.81	952.8	0	6.73	0	2	52.5	no	4x4x16	24	28	11.45
72	317.61	158.81	952.8	0	6.73	0	2	52.5	no	4x4x16	24	120	11.6
73	542	262.87	1490	0	0	0	0	42.5	no	4x4x16	24	3	4.1
74	542	262.87	1490	0	0	0	0	42.5	no	4x4x16	24	7	5.1
75	542	262.87	1490	0	0	0	0	42.5	no	4x4x16	24	28	5.9
76	542	262.87	1490	0	0	0.08	0	42.5	no	4x4x16	24	3	6.4
77	542	262.87	1490	0	0	0.08	0	42.5	no	4x4x16	24	7	7.5
78	542	262.87	1490	0	0	0.08	0	42.5	no	4x4x16	24	28	10.3
79	542	262.87	1490	0	0	0.1	0	42.5	no	4x4x16	24	3	6.9
80	542	262.87	1490	0	0	0.1	0	42.5	no	4x4x16	24	7	8.2
81	542	262.87	1490	0	0	0.1	0	42.5	no	4x4x16	24	28	11.1
82	542	262.87	1490	0	0	0.3	0	42.5	no	4x4x16	24	3	4.8
83	542	262.87	1490	0	0	0.3	0	42.5	no	4x4x16	24	7	6.7
84	542	262.87	1490	0	0	0.3	0	42.5	no	4x4x16	24	28	9.1
85	542	262.87	1490	0	0	0.5	0	42.5	no	4x4x16	24	3	4.7
86	542	262.87	1490	0	0	0.5	0	42.5	no	4x4x16	24	7	6.2
87	542	262.87	1490	0	0	0.5	0	42.5	no	4x4x16	24	28	8.6
88	664.80	232.68	1994	0	7.98	0	0	42.5	no	4x4x16	24	7	9.6
89	664.80	232.68	1994	0	7.98	0	0	42.5	no	4x4x16	24	28	10.3
90	664.80	232.68	1994	0	7.98	0	0	42.5	no	4x4x16	24	90	10.4
91	644.66	225.63	1934	0	7.74	0.1	0	42.5	no	4x4x16	24	7	11.8
92	644.66	225.63	1934	0	7.74	0.1	0	42.5	no	4x4x16	24	28	13.1
93	644.66	225.63	1934	0	7.74	0.1	0	42.5	no	4x4x16	24	90	13.3
94	654.65	229.13	1964	0	7.86	0.05	0	42.5	no	4x4x16	24	7	10.9
95	654.65	229.13	1964	0	7.86	0.05	0	42.5	no	4x4x16	24	28	12.7
96	654.65	229.13	1964	0	7.86	0.05	0	42.5	no	4x4x16	24	90	12
97	654.65	229.13	1964	0	7.86	0.05	0	42.5	no	4x4x16	24	7	12.1
98	654.65	229.13	1964	0	7.86	0.05	0	42.5	no	4x4x16	24	28	13.3
99	654.65	229.13	1964	0	7.86	0.05	0	42.5	no	4x4x16	24	90	13.6
100	525.56	236.50	709.5	0	0.79	0	0	42.5	no	4x4x16	24	7	7.1
101	525.56	236.50	709.5	0	0.79	0	0	42.5	no	4x4x16	24	28	8.9
102	525.56	236.50	709.5	0	0.79	0	0	42.5	no	4x4x16	24	90	9.6
103	509.64	229.34	688	0	0.76	0.1	0	42.5	no	4x4x16	24	7	9.3
104	509.64	229.34	688	0	0.76	0.1	0	42.5	no	4x4x16	24	28	10.6
105	509.64	229.34	688	0	0.76	0.1	0	42.5	no	4x4x16	24	90	11.1
106	517.54	232.89	699	0	0.78	0.05	0	42.5	no	4x4x16	24	7	7.9
107	517.54	232.89	699	0	0.78	0.05	0	42.5	no	4x4x16	24	28	9.9
108	517.54	232.89	699	0	0.78	0.05	0	42.5	no	4x4x16	24	90	10.2
109	517.54	232.89	699	0	0.78	0.05	0	42.5	no	4x4x16	24	7	9.3
110	517.54	232.89	699	0	0.78	0.05	0	42.5	no	4x4x16	24	28	10.5
111	517.54	232.89	699	0	0.78	0.05	0	42.5	no	4x4x16	24	90	10.6
112	512.10	256.05	1536	0	0	0	0	42.5	no	4x4x16	24	7	6.8
113	512.10	256.05	1536	0	0	0	0	42.5	no	4x4x16	24	28	8.3
114	512.10	256.05	1536	0	0	0	0	42.5	no	4x4x16	24	90	9.2
115	496.59	248.29	1490	0	0	0.1	0	42.5	no	4x4x16	24	7	9
116	496.59	248.29	1490	0	0	0.1	0	42.5	no	4x4x16	24	28	9.9
117	496.59	248.29	1490	0	0	0.1	0	42.5	no	4x4x16	24	90	10.2
118	504.28	252.14	1513	0	0	0.05	0	42.5	no	4x4x16	24	7	7.4
119	504.28	252.14	1513	0	0	0.05	0	42.5	no	4x4x16	24	28	8.8
120	504.28	252.14	1513	0	0	0.05	0	42.5	no	4x4x16	24	90	9.2
121	504.28	252.14	1513	0	0	0.05	0	42.5	no	4x4x16	24	7	8.2

122	504.28	252.14	1513	0	0	0.05	0	42.5	no	4x4x16	24	28	9.8
123	504.28	252.14	1513	0	0	0.05	0	42.5	no	4x4x16	24	90	10.1
124	499.30	274.62	1498	0	0	0	0	42.5	no	4x4x16	24	7	6.5
125	499.30	274.62	1498	0	0	0	0	42.5	no	4x4x16	24	28	7.6
126	499.30	274.62	1498	0	0	0	0	42.5	no	4x4x16	24	90	8.4
127	484.17	266.30	1452	0	0	0.1	0	42.5	no	4x4x16	24	7	8.3
128	484.17	266.30	1452	0	0	0.1	0	42.5	no	4x4x16	24	28	9.2
129	484.17	266.30	1452	0	0	0.1	0	42.5	no	4x4x16	24	90	9.3
130	491.68	270.42	1475	0	0	0.05	0	42.5	no	4x4x16	24	7	7.2
131	491.68	270.42	1475	0	0	0.05	0	42.5	no	4x4x16	24	28	7.8
132	491.68	270.42	1475	0	0	0.05	0	42.5	no	4x4x16	24	90	8.5
133	491.68	270.42	1475	0	0	0.05	0	42.5	no	4x4x16	24	7	7.8
134	491.68	270.42	1475	0	0	0.05	0	42.5	no	4x4x16	24	28	8.8
135	491.68	270.42	1475	0	0	0.05	0	42.5	no	4x4x16	24	90	9.3
136	1500	495	0	0	0	0	0	42.5	no	4x4x16	24	28	4
137	1500	495	0	0	0	0.025	0	42.5	no	4x4x16	24	28	4.3
138	1500	495	0	0	0	0.05	0	42.5	no	4x4x16	24	28	4.6
139	1500	495	0	0	0	0.1	0	42.5	no	4x4x16	24	28	5.2
140	1500	495	0	0	0	0.2	0	42.5	no	4x4x16	24	28	5.6
141	1200	600	0	0	0	0	0	42.5	no	4x4x16	24	28	7.15
142	1200	600	0	0	0	0.1	0	42.5	no	4x4x16	24	28	5.21
143	1200	600	0	0	0	0.1	0	42.5	no	4x4x16	24	28	6.35
144	1200	600	0	0	0	0.1	0	42.5	no	4x4x16	24	28	6
145	1200	600	0	0	0	0.08	0	42.5	no	4x4x16	24	28	7.37
146	1200	600	0	0	0	0.1	0	42.5	yes	4x4x16	48	28	7.09
147	1200	600	0	0	0	0.1	0	42.5	yes	4x4x16	48	28	7.09
148	1500	600	0	0	0	0	0	42.5	no	4x4x16	24	28	7.04
149	1500	600	0	0	0	0.05	0	42.5	no	4x4x16	24	28	6.75
150	1500	600	0	0	0	0.05	0	42.5	no	4x4x16	24	28	7.83
151	1500	600	0	0	0	0.1	0	42.5	no	4x4x16	24	28	7.25
152	1500	600	0	0	0	0.1	0	42.5	no	4x4x16	24	28	8.25
153	1579	789.5	0	0	0	0	0	52.5	yes	2.5x4x8	24	28	5.52
154	1579	789.5	0	0	0	0.05	0	52.5	yes	2.5x4x8	24	28	10.47
155	1579	789.5	0	0	0	0.05	0	52.5	yes	2.5x4x8	24	28	12.61
156	1579	789.5	0	0	0	0.05	0	52.5	yes	2.5x4x8	24	28	8.57
157	496	272.8	1488	0	0	0	0	42.5	no	4x4x16	24	28	3.28
158	496	272.8	1488	0	0	0.05	0	42.5	no	4x4x16	24	28	3.31
159	496	272.8	1488	0	0	0.1	0	42.5	no	4x4x16	24	28	3.5
160	496	272.8	1488	0	0	0.15	0	42.5	no	4x4x16	24	28	4.2
161	400	160	660	1168	2.4	0	0	52.5	no	15x15x15	24	7	2.68
162	400	160	660	1168	2.4	0	0	52.5	no	15x15x15	24	28	4.85
163	400	160	660	1168	2.4	0.05	0	52.5	yes	15x15x15	24	7	3.61
164	400	160	660	1168	2.4	0.05	0	52.5	yes	15x15x15	24	28	6.25
165	400	160	660	1168	2.4	0.07	0	52.5	yes	15x15x15	24	7	3.98
166	400	160	660	1168	2.4	0.07	0	52.5	yes	15x15x15	24	28	7.37
167	400	160	660	1168	2.4	0.08	0	52.5	yes	15x15x15	24	7	4.57
168	400	160	660	1168	2.4	0.08	0	52.5	yes	15x15x15	24	28	9.2
169	400	160	660	1168	2.4	0.1	0	52.5	yes	15x15x15	24	7	4.2
170	400	160	660	1168	2.4	0.1	0	52.5	yes	15x15x15	24	28	8.42
171	422	147	621	1284	5.06	0	0	52.5	no	15x15x15	24	7	3.04
172	422	147	621	1284	5.06	0	0	52.5	no	15x15x15	24	28	5.2
173	422	147	621	1284	5.06	0.05	0	52.5	yes	15x15x15	24	7	4.24
174	422	147	621	1284	5.06	0.05	0	52.5	yes	15x15x15	24	28	6.57
175	422	147	621	1284	5.06	0.07	0	52.5	yes	15x15x15	24	7	4.52
176	422	147	621	1284	5.06	0.07	0	52.5	yes	15x15x15	24	28	7.82
177	422	147	621	1284	5.06	0.08	0	52.5	yes	15x15x15	24	7	5.12
178	422	147	621	1284	5.06	0.08	0	52.5	yes	15x15x15	24	28	9.64
179	422	147	621	1284	5.06	0.1	0	52.5	yes	15x15x15	24	7	4.61
180	422	147	621	1284	5.06	0.1	0	52.5	yes	15x15x15	24	28	8.32
181	504	142	683	1108	4.7	0	0	52.5	no	15x15x15	24	7	3.12
182	504	142	683	1108	4.7	0	0	52.5	no	15x15x15	24	28	5.35
183	504	142	683	1108	4.7	0.05	0	52.5	yes	15x15x15	24	7	4.35
184	504	142	683	1108	4.7	0.05	0	52.5	yes	15x15x15	24	28	6.68
185	504	142	683	1108	4.7	0.07	0	52.5	yes	15x15x15	24	7	4.68
186	504	142	683	1108	4.7	0.07	0	52.5	yes	15x15x15	24	28	7.91
187	504	142	683	1108	4.7	0.08	0	52.5	yes	15x15x15	24	7	6.54
188	504	142	683	1108	4.7	0.08	0	52.5	yes	15x15x15	24	28	9.74

189	504	142	683	1108	4.7	0.1	0	52.5	yes	15x15x15	24	7	4.62
190	504	142	683	1108	4.7	0.1	0	52.5	yes	15x15x15	24	28	8.21
191	1579	789.5	0	0	0	0	0	42.5	yes	4x4x16	24	3	9.47
192	1579	789.5	0	0	0	0.1	0	42.5	yes	4x4x16	24	21	9.65
193	1579	789.5	0	0	0	0	0	42.5	yes	4x4x16	24	28	10.1
194	1579	789.5	0	0	0	0.1	0	42.5	yes	4x4x16	24	3	10.35
195	1579	789.5	0	0	0	0	0	42.5	yes	4x4x16	24	21	10.45
196	1579	789.5	0	0	0	0.1	0	42.5	yes	4x4x16	24	28	11.4
197	1579	789.5	0	0	0	0	0	42.5	yes	4x4x16	24	3	10.5
198	1579	789.5	0	0	0	0	0	42.5	yes	4x4x16	24	21	11.1
199	1579	789.5	0	0	0	0.3	0	42.5	yes	4x4x16	24	28	11.7
200	1579	789.5	0	0	0	0.5	0	42.5	yes	4x4x16	24	3	8.4
201	1579	789.5	0	0	0	0	0	42.5	yes	4x4x16	24	21	9.55
202	1579	789.5	0	0	0	0.5	0	42.5	yes	4x4x16	24	28	10.3
203	450	180	1720	0	4.95	0	0	42.5	no	4x4x16	24	28	7.5
204	450	180	1720	0	4.95	0.5	0	42.5	no	4x4x16	24	28	10.1
205	450	180	1720	0	4.95	0.5	0	42.5	no	4x4x16	24	28	8.2
206	1103.2	496.44	1655	0	1.43416	0	0	42.5	no	4x4x16	24	28	6.69
207	1103.2	496.44	1655	0	1.43416	0.5	0	42.5	yes	4x4x16	24	28	8.37

Table B1.3 Dataset 3 - RESIST

#	Cement [kg/m^3]	Water [kg/m^3]	Fine aggregate [kg/m^3]	Coarse aggregate [kg/m^3]	Super plasticizer [kg/m^3]	Nanofiller wt% CNT	CNF	Cement class	Functionalization	Cross-section [cm]	Probe distance [cm]	Demolding age [h]	Age [h]	Volume resistivity [Ω·cm]
	min/max	min/max	min/max	min/max	min/max	min/max		0/1	0/1	0/1	min/max	min/max	0/1	min/max
1	1277	574	0	0	0	0	0	42.5	yes	5x5x5	4	48	28	76862.18
2	1270.5	571.88	0	0	0	0.25	0	42.5	yes	5x5x5	4	48	28	67699.31
3	1264.8	569.15	0	0	0	0.5	0	42.5	yes	5x5x5	4	48	28	56248.82
4	1258.7	566.43	0	0	0	0.75	0	42.5	yes	5x5x5	4	48	28	56248.82
5	1252.8	563.75	0	0	0	1	0	42.5	yes	5x5x5	4	48	28	6058.77
6	1241	558.45	0	0	0	1.5	0	42.5	yes	5x5x5	4	48	28	6769.93
7	654	294.3	1308	0	0	0	0	42.5	yes	5x5x5	4	48	28	100000
8	652.31	293.54	1304.62	0	0	0.25	0	42.5	yes	5x5x5	4	48	28	98522.17
9	650.63	292.78	1301.26	0	0	0.5	0	42.5	yes	5x5x5	4	48	28	67699.31
10	648.96	292.03	1297.92	0	0	0.75	0	42.5	yes	5x5x5	4	48	28	51170.79
11	647.30	291.29	1294.6	0	0	1	0	42.5	yes	5x5x5	4	48	28	71990.61
12	644.02	289.81	1288.04	0	0	1.5	0	42.5	yes	5x5x5	4	48	28	62419.63
13	524	235.8	951	638	2.62	0	0	42.5	yes	5x5x5	4	48	28	689655.17
14	523	235.35	946.61	638.05	7.84	0.25	0	42.5	yes	5x5x5	4	48	28	562382.25
15	522	234.89	944.79	636.82	7.83	0.5	0	42.5	yes	5x5x5	4	48	28	541978.98
16	521	234.44	942.97	635.60	7.81	0.75	0	42.5	yes	5x5x5	4	48	28	67699.31
17	520	233.99	941.16	634.38	7.80	1	0	42.5	yes	5x5x5	4	48	28	7686.22
18	518	233.1	937.58	631.96	7.77	1.5	0	42.5	yes	5x5x5	4	48	28	6058.77
19	1277	574	0	0	0	0	0	42.5	yes	5x5x5	4	48	28	76862.18
20	1270.8	571.88	0	0	0	0	0.25	42.5	yes	5x5x5	4	48	28	76599
21	1264.8	569.15	0	0	0	0	0.5	42.5	yes	5x5x5	4	48	28	69779.29
22	1258.7	566.43	0	0	0	0	0.75	42.5	yes	5x5x5	4	48	28	68259.39
23	1252.8	563.75	0	0	0	0	1	42.5	yes	5x5x5	4	48	28	67699.31
24	1241	558.45	0	0	0	0	1.5	42.5	yes	5x5x5	4	48	28	64956.15
25	1229.4	553.25	0	0	0	0	2	42.5	yes	5x5x5	4	48	28	64956.15
26	654	294.3	1308	0	0	0	0	42.5	yes	5x5x5	4	48	28	97077.67
27	652.31	293.54	1304.62	0	0	0	0.25	42.5	yes	5x5x5	4	48	28	89253.84
28	650.63	292.78	1301.26	0	0	0	0.5	42.5	yes	5x5x5	4	48	28	86918.73
29	648.96	292.03	1297.92	0	0	0	0.75	42.5	yes	5x5x5	4	48	28	94321.83
30	647.30	291.29	1294.6	0	0	0	1	42.5	yes	5x5x5	4	48	28	95693.78
31	644.02	289.81	1288.04	0	0	0	1.5	42.5	yes	5x5x5	4	48	28	85795.67
32	640.73	288.33	1281.46	0	0	0	2	42.5	yes	5x5x5	4	48	28	84732.84
33	524	235.8	951	638	2.62	0	0	42.5	yes	5x5x5	4	48	28	624196.35
34	523	235.35	946.61	638.05	7.84	0	0.25	42.5	yes	5x5x5	4	48	28	536912.75
35	522	234.89	944.79	636.82	7.83	0	0.5	42.5	yes	5x5x5	4	48	28	541978.98
36	521	234.44	942.97	635.60	7.81	0	0.75	42.5	yes	5x5x5	4	48	28	505786.19
37	520	233.99	941.16	634.38	7.80	0	1	42.5	yes	5x5x5	4	48	28	521259.57
38	518	233.10	937.58	631.96	7.77	0	1.5	42.5	yes	5x5x5	4	48	28	97077.67
39	516	232.21	934.01	629.56	7.74	0	2	42.5	yes	5x5x5	4	48	28	85795.67
40	1277	574	0	0	0	0	0	42.5	no	5x5x5	4	48	28	5405.41
41	1270.6	571.8	0	0	0	0.25	0	42.5	no	5x5x5	4	48	28	5555.56

42	1264.6	569.1	0	0	0	0.5	0	42.5	no	5x5x5	4	48	28	526.32
43	1258.6	566.38	0	0	0	0.75	0	42.5	no	5x5x5	4	48	28	512.82
44	1252.7	563.71	0	0	0	1	0	42.5	no	5x5x5	4	48	28	769.23
45	1241	558.45	0	0	0	1.5	0	42.5	no	5x5x5	4	48	28	666.67
46	654	294	1308	0	0	0	0	42.5	no	5x5x5	4	48	28	5025.13
47	652.34	293.55	1304.67	0	0	0.25	0	42.5	no	5x5x5	4	48	28	5128.21
48	650.68	292.81	1301.36	0	0	0.5	0	42.5	no	5x5x5	4	48	28	512.82
49	649	292.05	1298	0	0	0.75	0	42.5	no	5x5x5	4	48	28	518.13
50	647.33	291.3	1294.67	0	0	1	0	42.5	no	5x5x5	4	48	28	5555.56
51	644.02	289.81	1288	0	0	1.5	0	42.5	no	5x5x5	4	48	28	7692.31
52	524	234	951	638	2.62	0	0	42.5	no	5x5x5	4	48	28	54054.05
53	523	235.33	946.55	638	7.84	0.25	0	42.5	no	5x5x5	4	48	28	100000
54	522	234.87	944.7	636.75	7.83	0.5	0	42.5	no	5x5x5	4	48	28	5128.21
55	521	234.42	942.9	635.55	7.81	0.75	0	42.5	no	5x5x5	4	48	28	5555.56
56	520	233.98	941.13	634.35	7.80	1	0	42.5	no	5x5x5	4	48	28	526.32
57	518	233.09	937.56	631.95	7.77	1.5	0	42.5	no	5x5x5	4	48	28	571.43
58	1578.9	789.48	0	0	0	0		42.5	yes	2x2x8	6	24	28	7700000
59	1578.9	789.48	0	0	0	0.048	0	42.5	yes	2x2x8	6	24	28	360000
60	1578.9	789.48	0	0	0	0.1	0	42.5	yes	2x2x8	6	24	28	260000
61	1578.9	789.48	0	0	0	0	0.048	42.5	yes	2x2x8	6	24	28	370000
62	1578.9	789.48	0	0	0	0	0.1	42.5	yes	2x2x8	6	24	28	570000
63	542	262.87	1490.5	0	0	0	0	42.5	no	2x2x8	6	24	3	75600
64	542	262.87	1490.5	0	0	0	0	42.5	no	2x2x8	6	24	7	75600
65	542	262.87	1490.5	0	0	0	0	42.5	no	2x2x8	6	24	28	75600
66	542	262.87	1490.5	0	0	0.1	0	42.5	no	2x2x8	6	24	3	55200
67	542	262.87	1490.5	0	0	0.1	0	42.5	no	2x2x8	6	24	7	55200
68	542	262.87	1490.5	0	0	0.1	0	42.5	no	2x2x8	6	24	28	55200
69	542	262.87	1490.5	0	0	0.5	0	42.5	no	2x2x8	6	24	3	63600
70	542	262.87	1490.5	0	0	0.5	0	42.5	no	2x2x8	6	24	7	63600
71	542	262.87	1490.5	0	0	0.5	0	42.5	no	2x2x8	6	24	28	63600
72	542	262.87	1490.5	0	0	0	0.1	42.5	no	2x2x8	6	24	3	64800
73	542	262.87	1490.5	0	0	0	0.1	42.5	no	2x2x8	6	24	7	64800
74	542	262.87	1490.5	0	0	0	0.1	42.5	no	2x2x8	6	24	28	64800
75	1071.4	642.86	0	0	0	0.1	0	42.5	yes	5x5x5	1	24	28	9810
76	1338.2	669.11	0	0	0	0.5	0	52.5	no	4x4x16	6	24	28	145.83
77	1338.2	669.11	0	0	0	0.5	0	52.5	yes	4x4x16	6	24	28	129.17
78	1200	600	0	0	2	0	0.5	52.5	no	4x4x16	12	24	7	1340
79	1200	600	0	0	1.8	0	0.5	52.5	no	4x4x16	12	24	28	1340
80	1200	600	0	0	3.6	0	1	52.5	no	4x4x16	12	24	7	1292.70
81	1200	600	0	0	3.6	0	1	52.5	no	4x4x16	12	24	28	1292.70
82	1200	600	0	0	6.6	0	2	52.5	no	4x4x16	12	24	7	1118.20
83	1200	600	0	0	6.6	0	2	52.5	no	4x4x16	12	24	28	1118.2
84	448	191	877	838	0.62	0	1	42.5	yes	20x10	9	24	28	84100
85	448	191	877	838	0.71	0	1.5	42.5	yes	20x10	9	24	28	59300
86	478	191	1008	902	0.49	0	1	42.5	no	20x10	9	24	28	20100
87	478	191	1008	902	0.85	0	1.5	42.5	no	20x10	9	24	28	10000
88	478	191	1008	902	1.02	0	2	42.5	no	20x10	9	24	28	6000
89	4780	191	1008	902	1.56	0	2.5	42.5	no	20x10	9	24	28	5400
90	478	191	1008	902	0.31	0	0.7	42.5	no	20x10	9	24	28	17500
91	478	191	1008	902	0.49	0	1	42.5	no	20x10	9	24	28	20000
92	478	191	1008	902	0.85	0	1.5	42.5	no	20x10	9	24	28	9600
93	478	191	1008	902	1.02	0	2	42.5	no	20x10	9	24	28	10000
94	478	191	1008	902	1.56	0	2.5	42.5	no	20x10	9	24	28	5400
95	1277	574	0	0	0	0	0	42.5	yes	5x5x5	1	24	28	604.7
96	1274.5	573.55	0	0	0	0.1	0	42.5	yes	5x5x5	1	24	28	550.3
97	1264.8	569.15	0	0	0	0.5	0	42.5	yes	5x5x5	1	24	28	249.8
98	1252.8	563.75	0	0	0	1	0	42.5	yes	5x5x5	1	24	28	141.3
99	1241	558.45	0	0	0	1.5	0	42.5	yes	5x5x5	1	24	28	119.5
100	1071.4	642.86	0	0	0	0	0	42.5	yes	5x5x5	1	24	28	574.9
101	1069.4	641.64	0	0	0	0.1	0	42.5	yes	5x5x5	1	24	28	523.1
102	1061.8	637.12	0	0	0	0.5	0	42.5	yes	5x5x5	1	24	28	225.6
103	1031.9	619.17	0	0	0	1	0	42.5	yes	5x5x5	1	24	28	127.2
104	1002.8	601.72	0	0	0	1.5	0	42.5	yes	5x5x5	1	24	28	108.2
105	974.60	584.76	0	0	0	2	0	42.5	yes	5x5x5	1	24	28	77.25
106	897.91	538.74	628.54	0	0	0	0	42.5	yes	5x5x5	1	24	28	1941.9
107	887.63	532.58	621.34	0	0	0.1	0	42.5	yes	5x5x5	1	24	28	1842.5
108	877.47	526.48	614.23	0	0	0.5	0	42.5	yes	5x5x5	1	24	28	1057

109	867.43	520.45	607.2	0	0	1	0	42.5	yes	5x5x5	1	24	28	552.3
110	857.5	514.5	600.25	0	0	1.5	0	42.5	yes	5x5x5	1	24	28	314.8
111	847.68	508.61	593.38	0	0	2	0	42.5	yes	5x5x5	1	24	28	206.6
112	1040.3	468.17	728.26	0	0	0	0	42.5	yes	5x5x5	1	24	28	1502.3
113	1028.5	462.81	719.92	0	0	0.1	0	42.5	yes	5x5x5	1	24	28	1396.6
114	1016.7	457.51	711.68	0	0	0.5	0	42.5	yes	5x5x5	1	24	28	827.2
115	1005	452.27	703.53	0	0	1	0	42.5	yes	5x5x5	1	24	28	421.2
116	993.54	447.1	695.48	0	0	1.5	0	42.5	yes	5x5x5	1	24	28	273.4
117	899.93	539.95	629.95	0	0	0	0	42.5	yes	5x5x5	1	24	28	1463.9
118	889.63	533.77	622.74	0	0	0.1	0	42.5	yes	5x5x5	1	24	28	1363.6
119	879.44	527.67	615.61	0	0	0.5	0	42.5	yes	5x5x5	1	24	28	800
120	869.38	521.62	608.56	0	0	1	0	42.5	yes	5x5x5	1	24	28	415.5
121	859.42	515.65	601.6	0	0	1.5	0	42.5	yes	5x5x5	1	24	28	265.1
122	849.59	509.75	594.7	0	0	2	0	42.5	yes	5x5x5	1	24	28	132.7
123	1875	375	0	0	14.06	0	0	42.5	no	4x4x4	2	24	28	7200
124	1875	375	0	0	14.06	0.1	0	42.5	no	4x4x4	2	24	28	6900
125	1875	375	0	0	14.06	0.5	0	42.5	no	4x4x4	2	24	28	3200
126	1875	375	0	0	14.06	1	0	42.5	no	4x4x4	2	24	28	1000
127	1875	375	0	0	14.06	0	0	42.5	no	4x4x4	2	24	28	7200
128	1875	375	0	0	14.06	0	0.1	42.5	no	4x4x4	2	24	28	4000
129	1875	375	0	0	14.06	0	0.5	42.5	no	4x4x4	2	24	28	600
130	1875	375	0	0	14.06	0	0.5	42.5	no	4x4x4	2	24	28	350
131	1277	574	0	0	0	0	0	42.5	no	5x5x5	4	48	28	80645.16
132	1270.6	571.79	0	0	0	0.25	0	42.5	no	5x5x5	4	48	28	5128.21
133	1161.1	522.5	0	0	0	0.5	0	42.5	no	5x5x5	4	48	28	5882.35
134	1258.6	566.38	0	0	0	0.75	0	42.5	no	5x5x5	4	48	28	10000.00
135	1252.7	563.71	0	0	0	1	0	42.5	no	5x5x5	4	48	28	625.00
136	1241	558.45	0	0	0	1.5	0	42.5	no	5x5x5	4	48	28	526.32
137	524	235.8	943.2	639.28	2.62	0	0	42.5	no	5x5x5	4	48	28	1000000
138	523	235.33	941.32	638	1.07	0.25	0	42.5	no	5x5x5	4	48	28	54054.05
139	522	234.87	939.47	636.75	1.07	0.5	0	42.5	no	5x5x5	4	48	28	55555.56
140	521	234.42	937.7	635.55	1.07	0.75	0	42.5	no	5x5x5	4	48	28	5263.16
141	520	233.98	935.93	634.35	1.07	1	0	42.5	no	5x5x5	4	48	28	526.32
142	518	233.1	932.38	631.95	1.06	1.5	0	42.5	no	5x5x5	4	48	28	666.67
143	1578.9	789.48	0	0	0	0	0	42.5	yes	4x4x16	4	24	3	6000
144	1578.9	789.48	0	0	0	0	0	42.5	yes	4x4x16	4	24	7	11100
145	1578.9	789.48	0	0	0	0	0	42.5	yes	4x4x16	4	24	14	13300
146	1578.9	789.48	0	0	0	0.1	0	42.5	yes	4x4x16	4	24	21	13600
147	1578.9	789.48	0	0	0	0	0	42.5	yes	4x4x16	4	24	28	16000
148	1578.9	789.48	0	0	0	0.1	0	42.5	yes	4x4x16	4	24	3	5000
149	1578.9	789.48	0	0	0	0	0	42.5	yes	4x4x16	4	24	7	9000
150	1578.9	789.48	0	0	0	0.1	0	42.5	yes	4x4x16	4	24	14	10500
151	1578.9	789.48	0	0	0	0	0	42.5	yes	4x4x16	4	24	21	11900
152	1578.9	789.48	0	0	0	0.1	0	42.5	yes	4x4x16	4	24	28	13000
153	1578.9	789.48	0	0	0	0.3	0	42.5	yes	4x4x16	4	24	3	4500
154	1578.9	789.48	0	0	0	0	0	42.5	yes	4x4x16	4	24	7	8500
155	1578.9	789.48	0	0	0	0.1	0	42.5	yes	4x4x16	4	24	14	10300
156	1578.9	789.48	0	0	0	0	0	42.5	yes	4x4x16	4	24	21	10400
157	1578.9	789.48	0	0	0	0.3	0	42.5	yes	4x4x16	4	24	28	12700
158	1578.9	789.48	0	0	0	0.5	0	42.5	yes	4x4x16	4	24	3	3200
159	1578.9	789.48	0	0	0	0	0	42.5	yes	4x4x16	4	24	7	6000
160	1578.9	789.48	0	0	0	0.1	0	42.5	yes	4x4x16	4	24	14	7500
161	1578.9	789.48	0	0	0	0	0	42.5	yes	4x4x16	4	24	21	7300
162	1578.9	789.48	0	0	0	0.5	0	42.5	yes	4x4x16	4	24	28	9500
163	1363.6	545.44	0	0	3.41	0.1	0	42.5	no	5x5x5	1.5	24	28	11500
164	1363.6	545.44	0	0	3.41	0.5	0	42.5	no	5x5x5	1.5	24	28	11100
165	1363.6	681.82	0	0	0	0.05	0	52.5	no	5x5x5	1	24	28	50000.
166	1363.6	681.82	0	0	0	0.1	0	52.5	no	5x5x5	1	24	28	39215.69
167	1363.6	681.82	0	0	0	0.5	0	52.5	no	5x5x5	1	24	28	21505.38
168	1277	574	0	0	0	0	0	42.5	no	5x5x5	4	24	28	39000
169	1270.6	571.8	0	0	0	0.25	0	42.5	no	5x5x5	4	24	28	20000
170	1161.1	522.5	0	0	0	0.5	0	42.5	no	5x5x5	4	24	28	16000
171	1258.6	566.38	0	0	0	0.75	0	42.5	no	5x5x5	4	24	28	15500
172	1252.7	563.71	0	0	0	1	0	42.5	no	5x5x5	4	24	28	1600
173	1241	558.45	0	0	0	1.5	0	42.5	no	5x5x5	4	24	28	2700
174	654	294	1308	0	0	0	0	42.5	no	5x5x5	4	24	28	50000
175	652.34	293.55	1304.67	0	6.52	0.25	0	42.5	no	5x5x5	4	24	28	30000

#														
176	650.68	292.80	1301.36	0	6.51	0.5	0	42.5	no	5x5x5	4	24	28	20000
177	649.00	292.05	1298	0	6.49	0.75	0	42.5	no	5x5x5	4	24	28	7000
178	647.33	291.3	1294.66	0	6.47	1	0	42.5	no	5x5x5	4	24	28	18000
179	644.02	289.81	1288.04	0	6.44	1.5	0	42.5	no	5x5x5	4	24	28	10000
180	524	234	951	638	2.62	0	0	42.5	no	5x5x5	4	24	28	60000
181	523	235.33	941.32	627.55	7.87	0.25	0	42.5	no	5x5x5	4	24	28	50000
182	522	234.87	939.47	626.31	7.855	0.5	0	42.5	no	5x5x5	4	24	28	38000
183	521	234.42	937.7	625.13	7.84	0.75	0	42.5	no	5x5x5	4	24	28	19000
184	520	233.98	935.93	623.95	7.825	1	0	42.5	no	5x5x5	4	24	28	4000
185	518	233.1	932.38	621.59	7.795	1.5	0	42.5	no	5x5x5	4	24	28	2000
186	1277	574	0	0	0	0	0	42.5	no	5x5x5	4	24	28	50000
187	1270.6	571.79	0	0	0	0	0.25	42.5	no	5x5x5	4	24	28	47000
188	1161.1	522.50	0	0	0	0	0.5	42.5	no	5x5x5	4	24	28	38000
189	1258.6	566.38	0	0	0	0	0.75	42.5	no	5x5x5	4	24	28	37000
190	1252.7	563.71	0	0	0	0	1	42.5	no	5x5x5	4	24	28	35000
191	1241	558.45	0	0	0	0	1.5	42.5	no	5x5x5	4	24	28	30000
192	1229.3	558.45	0	0	0	0	2	42.5	no	5x5x5	4	24	28	31000
193	654	294	1308	0	0	0	0	42.5	no	5x5x5	4	24	28	97000
194	652.34	293.55	1304.67	0	6.52	0	0.25	42.5	no	5x5x5	4	24	28	87000
195	650.68	292.81	1301.36	0	6.51	0	0.5	42.5	no	5x5x5	4	24	28	82000
196	649	292.05	1298	0	6.49	0	0.75	42.5	no	5x5x5	4	24	28	92000
197	647.33	291.3	1294.66	0	6.47	0	1	42.5	no	5x5x5	4	24	28	96000
198	644.02	289.81	1288.03	0	6.44	0	1.5	42.5	no	5x5x5	4	24	28	62000
199	640.80	289.81	1288.03	0	6.44	0	2	42.5	no	5x5x5	4	24	28	60000
200	524	234	951	638	2.62	0	0	42.5	no	5x5x5	4	24	28	240000
201	523	235.33	941.32	627.55	7.87	0	0.25	42.5	no	5x5x5	4	24	28	145000
202	522	234.87	939.47	626.31	7.855	0	0.5	42.5	no	5x5x5	4	24	28	170000
203	521	234.42	937.7	625.13	7.84	0	0.75	42.5	no	5x5x5	4	24	28	100000
204	520	233.98	935.93	623.95	7.825	0	1	42.5	no	5x5x5	4	24	28	130000
205	518	233.09	932.38	621.59	7.795	0	1.5	42.5	no	5x5x5	4	24	28	99000
206	516	233.09	932.38	621.59	7.795	0	2	42.5	no	5x5x5	4	24	28	65000
207	1277	574	0	0	0	0	0	42.5	no	5x5x5	4	24	28	50000
208	1270.6	571.79	0	0	0	0.25	0	42.5	no	5x5x5	4	24	28	35000
209	1161.1	522.50	0	0	0	0.5	0	42.5	no	5x5x5	4	24	28	18000
210	1258.6	566.38	0	0	0	0.75	0	42.5	no	5x5x5	4	24	28	21000
211	1252.7	563.71	0	0	0	1	0	42.5	no	5x5x5	4	24	28	1800
212	1241	558.45	0	0	0	1.5	0	42.5	no	5x5x5	4	24	28	3200
213	654	294	1308	0	0	0	0	42.5	no	5x5x5	4	24	28	90000
214	652.34	293.55	1304.67	0	6.52	0.25	0	42.5	no	5x5x5	4	24	28	80000
215	650.68	292.81	1301.36	0	6.51	0.5	0	42.5	no	5x5x5	4	24	28	40000
216	649	292.05	1298	0	6.49	0.75	0	42.5	no	5x5x5	4	24	28	11000
217	524	234	951	638	2.62	0	0	42.5	no	5x5x5	4	24	28	220000
218	523	235.33	941.32	627.55	7.87	0.25	0	42.5	no	5x5x5	4	24	28	160000
219	522	234.87	939.47	626.31	7.855	0.5	0	42.5	no	5x5x5	4	24	28	130000
220	521	234.42	937.7	625.13	7.84	0.75	0	42.5	no	5x5x5	4	24	28	45000
221	520	233.98	935.93	623.95	7.825	1	0	42.5	no	5x5x5	4	24	28	5500
222	518	233.09	932.38	621.59	7.795	1.5	0	42.5	no	5x5x5	4	24	28	2000
223	1277	575	0	0	6.3	1	0	42.5	no	5x5x5	4	24	28	614.3

Table B1.4 Dataset 4 – COMP+FLEX

	Cement [kg/m³]	Water [kg/m³]	Fine aggregate [kg/m³]	Coarse aggregate [kg/m³]	Super plasticizer [kg/m³]	Nanofiller wt%		Cement class	Function alization	Demolding age [h]	Age [h]	Compressive strength [MPa]	Flexural strength [MPa]
						CNT	CNF						
#	min/max	min/max	min/max	min/max	min/max	min/max		0/1	0/1	min/max	min/max	min/max	min/max
1	542	262.87	1490.5	0	0	0	0	42.5	no	24	3	19.8	2.18
2	542	262.87	1490.5	0	0	0	0	42.5	no	24	7	25.6	3.23
3	542	262.87	1490.5	0	0	0	0	42.5	no	24	28	31.7	5.9
4	542	262.87	1490.5	0	0	0.1	0	42.5	no	24	3	22.6	4.97
5	542	262.87	1490.5	0	0	0.1	0	42.5	no	24	7	26.5	5.83
6	542	262.87	1490.5	0	0	0.1	0	42.5	no	24	28	33.8	11.1
7	542	262.87	1490.5	0	0	0.5	0	42.5	no	24	3	22.7	2.35
8	542	262.87	1490.5	0	0	0.5	0	42.5	no	24	7	27.6	4.77
9	542	262.87	1490.5	0	0	0.5	0	42.5	no	24	28	35.3	8.6
10	542	262.87	1490.5	0	0	0	0.1	42.5	no	24	3	22.5	3.57
11	542	262.87	1490.5	0	0	0	0.1	42.5	no	24	7	25.2	7.69
12	542	262.87	1490.5	0	0	0	0.1	42.5	no	24	28	33.7	12.2

13	380	193.8	999.4	775.2	0	0	0	42.5	no	24	28	45.8	6.7
14	380	193.8	999.4	775.2	0	0.1	0	42.5	no	24	28	48.5	10
15	380	193.8	999.4	775.2	0	0	0.1	42.5	no	24	28	46.7	9.9
16	512.10	256.05	1536.3	0	2.05	0	0	42.5	no	24	28	31.8	5.9
17	512.10	256.05	1536.3	0	2.05	0.1	0	42.5	no	24	28	33.5	10.5
18	512.10	256.05	1536.3	0	2.05	0.1	0	42.5	no	24	28	33.1	10.2
19	512.10	256.05	1536.3	0	2.05	0.1	0	42.5	yes	24	28	33.9	12.9
20	1338.2	669.11	0	0	0	0.5	0	52.5	no	24	28	69.41	9.56
21	1338.2	669.11	0	0	0	0.5	0	52.5	yes	24	28	72.13	9.97
22	1363.6	681.82	0	0	0	0	0	42.5	no	24	28	74.8	10.2
23	1363.6	681.82	0	0	1.64	0.03	0	42.5	no	24	28	83.1	11.1
24	1363.6	681.82	0	0	4.36	0.08	0	42.5	no	24	28	80	10.8
25	1363.6	681.82	0	0	8.18	0.15	0	42.5	no	24	28	86.9	13.6
26	1363.6	681.82	0	0	13.64	0.25	0	42.5	no	24	28	91.8	16.1
27	1363.6	681.82	0	0	19.09	0.35	0	42.5	no	24	28	90	16.3
28	1363.6	681.82	0	0	27.27	0.5	0	42.5	no	24	28	94.3	16.4
29	359.20	179.6	1077.6	0	0	0	0	52.5	no	24	7	43.5	9.5
30	359.20	179.6	1077.6	0	0.00	0	0	52.5	no	24	28	54	10.35
31	359.20	179.6	1077.6	0	0.00	0	0	52.5	no	24	120	58	11.75
32	353.72	176.86	1061.15	0	1.03	0	0.25	52.5	no	24	7	43	9.8
33	353.72	176.86	1061.15	0	1.03	0	0.25	52.5	no	24	28	54.5	10.2
34	353.72	176.86	1061.15	0	1.03	0	0.25	52.5	no	24	120	60.6	11.3
35	348.32	174.16	1044.96	0	2.02	0	0.5	52.5	no	24	7	43.5	9.75
36	348.32	174.16	1044.96	0	2.02	0	0.5	52.5	no	24	28	55	10.4
37	348.32	174.16	1044.96	0	2.02	0	0.5	52.5	no	24	120	61	11.85
38	343	171.50	1029.01	0	2.95	0	0.75	52.5	no	24	7	44	10.1
39	343	171.50	1029.01	0	2.95	0	0.75	52.5	no	24	28	55.1	11.1
40	343	171.50	1029.01	0	2.95	0	0.75	52.5	no	24	120	62.5	11.8
41	337.77	168.88	1013.30	0	3.85	0	1	52.5	no	24	7	46.5	10
42	337.77	168.88	1013.30	0	3.85	0	1	52.5	no	24	28	54.8	11.3
43	337.77	168.88	1013.30	0	3.85	0	1	52.5	no	24	120	61.8	11.7
44	332.61	166.31	997.83	0	4.86	0	1.25	52.5	no	24	7	47.5	10.05
45	332.61	166.31	997.83	0	4.86	0	1.25	52.5	no	24	28	55	11.25
46	332.61	166.31	997.83	0	4.86	0	1.25	52.5	no	24	120	62.5	11.65
47	327.53	163.77	982.60	0	5.86	0	1.5	52.5	no	24	7	46	9.9
48	327.53	163.77	982.60	0	5.86	0	1.5	52.5	no	24	28	56.5	11.35
49	327.53	163.77	982.60	0	5.86	0	1.5	52.5	no	24	120	65	11.5
50	322.53	161.27	967.60	0	6.29	0	1.75	52.5	no	24	7	45.5	9.6
51	322.53	161.27	967.60	0	6.29	0	1.75	52.5	no	24	28	57.5	11.05
52	322.53	161.27	967.60	0	6.29	0	1.75	52.5	no	24	120	65.8	11.55
53	317.61	158.81	952.84	0	6.73	0	2	52.5	no	24	7	50	9.5
54	317.61	158.81	952.84	0	6.73	0	2	52.5	no	24	28	57.6	11.45
55	317.61	158.81	952.84	0	6.73	0	2	52.5	no	24	120	67	11.6
56	542	262.87	1490.5	0	0	0	0	42.5	no	24	3	19.95	4.1
57	542	262.87	1490.5	0	0	0	0	42.5	no	24	7	25	5.1
58	542	262.87	1490.5	0	0	0	0	42.5	no	24	28	31.7	5.9
59	542	262.87	1490.5	0	0	0.08	0	42.5	no	24	3	22.3	6.4
60	542	262.87	1490.5	0	0	0.08	0	42.5	no	24	7	26.1	7.5
61	542	262.87	1490.5	0	0	0.08	0	42.5	no	24	28	33.7	10.3
62	542	262.87	1490.5	0	0	0.1	0	42.5	no	24	3	22.9	6.9
63	542	262.87	1490.5	0	0	0.1	0	42.5	no	24	7	26.2	8.2
64	542	262.87	1490.5	0	0	0.1	0	42.5	no	24	28	33.8	11.1
65	542	262.87	1490.5	0	0	0.3	0	42.5	no	24	3	21.1	4.8
66	542	262.87	1490.5	0	0	0.3	0	42.5	no	24	7	28	6.7
67	542	262.87	1490.5	0	0	0.3	0	42.5	no	24	28	33.9	9.1
68	542	262.87	1490.5	0	0	0.5	0	42.5	no	24	3	22.8	4.7
69	542	262.87	1490.5	0	0	0.5	0	42.5	no	24	7	27.6	6.2
70	542	262.87	1490.5	0	0	0.5	0	42.5	no	24	28	35.3	8.6
71	664.80	232.68	1994.4	0	7.98	0	0	42.5	no	24	7	68.1	9.6
72	664.80	232.68	1994.4	0	7.98	0	0	42.5	no	24	28	72.1	10.3
73	664.80	232.68	1994.4	0	7.98	0	0	42.5	no	24	90	73.6	10.4
74	644.66	225.63	1933.98	0	7.735	0.1	0	42.5	no	24	7	76.8	11.8
75	644.66	225.63	1933.98	0	7.735	0.1	0	42.5	no	24	28	84.3	13.1
76	644.66	225.63	1933.98	0	7.735	0.1	0	42.5	no	24	90	86.8	13.3
77	654.65	229.13	1963.96	0	7.855	0.05	0	42.5	no	24	7	72.7	10.9
78	654.65	229.13	1963.96	0	7.855	0.05	0	42.5	no	24	28	75.8	12.7
79	654.65	229.13	1963.96	0	7.855	0.05	0	42.5	no	24	90	77.9	12

80	654.65	229.13	1963.96	0	7.855	0.05	0	42.5	no	24	7	80.6	12.1
81	654.65	229.13	1963.96	0	7.855	0.05	0	42.5	no	24	28	88.8	13.3
82	654.65	229.13	1963.96	0	7.855	0.05	0	42.5	no	24	90	90.4	13.6
83	525.56	236.5	709.5	0	0.788	0	0	42.5	no	24	7	45.3	7.1
84	525.56	236.5	709.5	0	0.788	0	0	42.5	no	24	28	56.4	8.9
85	525.56	236.5	709.5	0	0.788	0	0	42.5	no	24	90	57.9	9.6
86	509.64	229.34	688.01	0	0.764	0.1	0	42.5	no	24	7	53.2	9.3
87	509.64	229.34	688.01	0	0.764	0.1	0	42.5	no	24	28	64.7	10.6
88	509.64	229.34	688.012	0	0.764	0.1	0	42.5	no	24	90	65.8	11.1
89	517.54	232.89	698.68	0	0.776	0.05	0	42.5	no	24	7	46.7	7.9
90	517.54	232.89	698.68	0	0.776	0.05	0	42.5	no	24	28	56.5	9.9
91	517.54	232.89	698.68	0	0.776	0.05	0	42.5	no	24	90	57.5	10.2
92	517.54	232.89	698.68	0	0.776	0.05	0	42.5	no	24	7	55.4	9.3
93	517.54	232.89	698.68	0	0.776	0.05	0	42.5	no	24	28	65.2	10.5
94	517.54	232.89	698.68	0	0.776	0.05	0	42.5	no	24	90	65.7	10.6
95	512.10	256.05	1536.3	0	0	0	0	42.5	no	24	7	38.1	6.8
96	512.10	256.05	1536.3	0	0	0	0	42.5	no	24	28	51.3	8.3
97	512.10	256.05	1536.3	0	0	0	0	42.5	no	24	90	52.4	9.2
98	496.59	248.29	1489.76	0	0	0.1	0	42.5	no	24	7	46.3	9
99	496.59	248.29	1489.76	0	0	0.1	0	42.5	no	24	28	58.8	9.9
100	496.59	248.29	1489.76	0	0	0.1	0	42.5	no	24	90	61.5	10.2
101	504.28	252.14	1512.85	0	0	0.05	0	42.5	no	24	7	43	7.4
102	504.28	252.14	1512.85	0	0	0.05	0	42.5	no	24	28	52.9	8.8
103	504.28	252.14	1512.85	0	0	0.05	0	42.5	no	24	90	56.5	9.2
104	504.28	252.14	1512.85	0	0	0.05	0	42.5	no	24	7	45.6	8.2
105	504.28	252.14	1512.85	0	0	0.05	0	42.5	no	24	28	58.8	9.8
106	504.28	252.14	1512.85	0	0	0.05	0	42.5	no	24	90	59.5	10.1
107	499.30	274.61	1497.9	0	0	0	0	42.5	no	24	7	36.9	6.5
108	499.30	274.61	1497.9	0	0	0	0	42.5	no	24	28	48.8	7.6
109	499.30	274.61	1497.9	0	0	0	0	42.5	no	24	90	50.6	8.4
110	484.17	266.3	1452.52	0	0	0.1	0	42.5	no	24	7	38.9	8.3
111	484.17	266.3	1452.52	0	0	0.1	0	42.5	no	24	28	51	9.2
112	484.17	266.3	1452.52	0	0	0.1	0	42.5	no	24	90	52	9.3
113	491.68	270.42	1475.04	0	0	0.05	0	42.5	no	24	7	34.7	7.2
114	491.68	270.42	1475.04	0	0	0.05	0	42.5	no	24	28	44.3	7.8
115	491.68	270.42	1475.04	0	0	0.05	0	42.5	no	24	90	44.7	8.5
116	491.68	270.42	1475.04	0	0	0.05	0	42.5	no	24	7	42.1	7.8
117	491.68	270.42	1475.04	0	0	0.05	0	42.5	no	24	28	54.5	8.8
118	491.68	270.42	1475.04	0	0	0.05	0	42.5	no	24	90	58.1	9.3
119	1500	495	0	0	0	0	0	42.5	no	24	28	84.8	4
120	1500	495	0	0	0	0.025	0	42.5	no	24	28	90.1	4.3
121	1500	495	0	0	0	0.05	0	42.5	no	24	28	95.6	4.6
122	1500	495	0	0	0	0.1	0	42.5	no	24	28	97.2	5.2
123	1200	600	0	0	0	0	0	42.5	no	24	28	35.6	7.15
124	1200	600	0	0	0	0.1	0	42.5	no	24	28	20.4	5.21
125	1200	600	0	0	0	0.1	0	42.5	no	24	28	30.1	6.35
126	1200	600	0	0	0	0.1	0	42.5	no	24	28	32.4	6
127	1200	600	0	0	0	0.08	0	42.5	no	24	28	35	7.37
128	1200	600	0	0	0	0.1	0	42.5	yes	48	28	32	7.09
129	1200	600	0	0	0	0.1	0	42.5	yes	48	28	35.4	7.09
130	1500	600	0	0	0	0	0	42.5	no	24	28	45.5	7.04
131	1500	600	0	0	0	0.05	0	42.5	no	24	28	45.92	6.75
132	1500	600	0	0	0	0.05	0	42.5	no	24	28	50.17	7.83
133	1500	600	0	0	0	0.1	0	42.5	no	24	28	50.09	7.25
134	1500	600	0	0	0	0.1	0	42.5	no	24	28	55.05	8.25
135	496	272.8	1488	0	0	0	0	42.5	no	24	28	48	3.28
136	496	272.8	1488	0	0	0.05	0	42.5	no	24	28	55	3.31
137	496	272.8	1488	0	0	0.1	0	42.5	no	24	28	52	3.5
138	496	272.8	1488	0	0	0.15	0	42.5	no	24	28	53	4.2
139	400	160	660	1168	2.4	0	0	52.5	no	24	7	39	2.68
140	400	160	660	1168	2.4	0	0	52.5	no	24	28	49	4.85
141	400	160	660	1168	2.4	0.05	0	52.5	yes	24	7	40	3.61
142	400	160	660	1168	2.4	0.05	0	52.5	yes	24	28	45	6.25
143	400	160	660	1168	2.4	0.07	0	52.5	yes	24	7	42	3.98
144	400	160	660	1168	2.4	0.07	0	52.5	yes	24	28	54	7.37
145	400	160	660	1168	2.4	0.08	0	52.5	yes	24	7	55	4.57
146	400	160	660	1168	2.4	0.08	0	52.5	yes	24	28	67	9.2

147	400	160	660	1168	2.4	0.1	0	52.5	yes	24	7	48	4.2
148	400	160	660	1168	2.4	0.1	0	52.5	yes	24	28	54	8.42
149	422	147	621	1284	5.06	0	0	52.5	no	24	7	38.6	3.04
150	422	147	621	1284	5.06	0	0	52.5	no	24	28	61.2	5.2
151	422	147	621	1284	5.06	0.05	0	52.5	yes	24	7	55	4.24
152	422	147	621	1284	5.06	0.05	0	52.5	yes	24	28	78	6.57
153	422	147	621	1284	5.06	0.07	0	52.5	yes	24	7	50.8	4.52
154	422	147	621	1284	5.06	0.07	0	52.5	yes	24	28	72.6	7.82
155	422	147	621	1284	5.06	0.08	0	52.5	yes	24	7	51.4	5.12
156	422	147	621	1284	5.06	0.08	0	52.5	yes	24	28	73.2	9.64
157	422	147	621	1284	5.06	0.1	0	52.5	yes	24	7	59.3	4.61
158	422	147	621	1284	5.06	0.1	0	52.5	yes	24	28	83.6	8.32
159	504	142	683	1108	4.7	0	0	52.5	no	24	7	42	3.12
160	504	142	683	1108	4.7	0	0	52.5	no	24	28	72	5.35
161	504	142	683	1108	4.7	0.05	0	52.5	yes	24	7	58	4.35
162	504	142	683	1108	4.7	0.05	0	52.5	yes	24	28	89	6.68
163	504	142	683	1108	4.7	0.07	0	52.5	yes	24	7	55	4.68
164	504	142	683	1108	4.7	0.07	0	52.5	yes	24	28	85	7.91
165	504	142	683	1108	4.7	0.08	0	52.5	yes	24	7	54	6.54
166	504	142	683	1108	4.7	0.08	0	52.5	yes	24	28	83	9.74
167	504	142	683	1108	4.7	0.1	0	52.5	yes	24	7	60	4.62
168	504	142	683	1108	4.7	0.1	0	52.5	yes	24	28	92	8.21
169	1578.9	789.48	0	0	0	0	0	42.5	yes	24	3	54.9	9.47
170	1578.9	789.48	0	0	0	0.1	0	42.5	yes	24	21	61	9.65
171	1578.9	789.48	0	0	0	0	0	42.5	yes	24	28	66.5	10.1
172	1578.9	789.48	0	0	0	0.1	0	42.5	yes	24	3	60.5	10.35
173	1578.9	789.48	0	0	0	0	0	42.5	yes	24	21	62.3	10.45
174	1578.9	789.48	0	0	0	0.1	0	42.5	yes	24	28	66.2	11.4
175	1578.9	789.48	0	0	0	0.3	0	42.5	yes	24	3	58.7	10.5
176	1578.9	789.48	0	0	0	0	0	42.5	yes	24	21	66	11.1
177	1578.9	789.48	0	0	0	0.3	0	42.5	yes	24	28	67.1	11.7
178	1578.9	789.48	0	0	0	0.5	0	42.5	yes	24	3	52	8.4
179	1578.9	789.48	0	0	0	0	0	42.5	yes	24	21	60.5	9.55
180	1578.9	789.48	0	0	0	0.5	0	42.5	yes	24	28	62.5	10.3
181	450	180	1720	0	4.95	0	0	42.5	no	24	28	65	7.5
182	450	180	1720	0	4.95	0.5	0	42.5	no	24	28	71.875	10.1
183	450	180	1720	0	4.95	0.5	0	42.5	no	24	28	76.25	8.2
184	1103.2	496.44	1654.8	0	1.434	0	0	42.5	no	24	28	52.27	6.69
185	1103.2	496.44	1654.8	0	1.434	0.5	0	42.5	yes	24	28	62.13	8.37

Table B1.5 Dataset 3 – RESIST after revision

	Cement [kg/m³]	Water [kg/m³]	Fine aggregate [kg/m³]	Coarse aggregate [kg/m³]	Super plasticizer [kg/m³]	Nanofiller wt%		Cement class	Function alization	Cross-section [cm]	Area of cross-section [cm²]	Probe distance [cm]	Demolding age [h]	Age [h]	Volume resistivity [Ω·cm]
						CNT	CNF								
#	min/max	min/max	min/max	min/max	min/max	min/max		0/1	0/1	0/1	min/max	min/max	min/max	0/1	min/max
1	1277	574	0	0	0	0	0	42.5	yes	5x5x5	25	4	48	28	76862.18
2	1270.85	571.88	0	0	0	0.25	0	42.5	yes	5x5x5	25	4	48	28	67699.31
3	1264.77	569.15	0	0	0	0.5	0	42.5	yes	5x5x5	25	4	48	28	56248.82
4	1258.74	566.43	0	0	0	0.75	0	42.5	yes	5x5x5	25	4	48	28	56248.82
5	1252.77	563.75	0	0	0	1	0	42.5	yes	5x5x5	25	4	48	28	6058.77
6	1241	558.45	0	0	0	1.5	0	42.5	yes	5x5x5	25	4	48	28	6769.93
7	654	294.3	1308	0	0	0	0	42.5	yes	5x5x5	25	4	48	28	100000
8	652.31	293.54	1304.62	0	0	0.25	0	42.5	yes	5x5x5	25	4	48	28	98522.17
9	650.63	292.78	1301.26	0	0	0.5	0	42.5	yes	5x5x5	25	4	48	28	67699.31
10	649	292	1297.92	0	0	0.75	0	42.5	yes	5x5x5	25	4	48	28	51170.79
11	647	291.29	1294.6	0	0	1	0	42.5	yes	5x5x5	25	4	48	28	71990.61
12	644	289.81	1288.04	0	0	1.5	0	42.5	yes	5x5x5	25	4	48	28	62419.63
13	524	235.8	951	638	2.62	0	0	42.5	yes	5x5x5	25	4	48	28	689655.17
14	521	234.44	942.97	635.60	7.81	0.75	0	42.5	yes	5x5x5	25	4	48	28	67699.31
15	520	234	941.16	634.38	7.80	1	0	42.5	yes	5x5x5	25	4	48	28	7686.22
16	518	233.1	937.58	632	7.77	1.5	0	42.5	yes	5x5x5	25	4	48	28	6058.77
17	518	233.10	937.58	632	7.77	0	1.5	42.5	yes	5x5x5	25	4	48	28	97077.67
18	516	232.21	934.01	629.56	7.74	0	2	42.5	yes	5x5x5	25	4	48	28	85795.67
19	1277	574	0	0	0	0	0	42.5	no	5x5x5	25	4	48	28	5405.41
20	511	229.96	0	0	0	0.5	0	42.5	no	5x5x5	25	4	48	28	526.32
21	508.60	228.87	0	0	0	0.75	0	42.5	no	5x5x5	25	4	48	28	512.82
22	506.21	227.79	0	0	0	1	0	42.5	no	5x5x5	25	4	48	28	769.23
23	501.49	225.67	0	0	0	1.5	0	42.5	no	5x5x5	25	4	48	28	666.67

28

24	654	294	1308	0	0	0	0	42.5	no	5x5x5	25	4	48	28	5025.13
25	498.94	224.52	997.88	0	0	0.5	0	42.5	no	5x5x5	25	4	48	28	512.82
26	497.65	223.94	995.31	0	0	0.75	0	42.5	no	5x5x5	25	4	48	28	518.13
27	524	234	951	638	2.62	0	0	42.5	no	5x5x5	25	4	48	28	54054.05
28	495.69	223.06	897.19	604.74	7.44	0.5	0	42.5	no	5x5x5	25	4	48	28	5128.21
29	494.75	222.64	895.50	603.60	7.42	0.75	0	42.5	no	5x5x5	25	4	48	28	5555.56
30	493.82	222.22	893.81	602.46	7.41	1	0	42.5	no	5x5x5	25	4	48	28	526.32
31	491.95	221.38	890.43	600.18	7.38	1.5	0	42.5	no	5x5x5	25	4	48	28	571.43
32	1579	789.48	0	0	0	0		42.5	yes	2x2x8	4	6	24	28	7700000
33	1579	789.48	0	0	0	0.048	0	42.5	yes	2x2x8	4	6	24	28	360000
34	1579	789.48	0	0	0	0.1	0	42.5	yes	2x2x8	4	6	24	28	260000
35	1579	789.48	0	0	0	0	0.048	42.5	yes	2x2x8	4	6	24	28	370000
36	1579	789.48	0	0	0	0	0.1	42.5	yes	2x2x8	4	6	24	28	570000
37	542	262.87	1490.5	0	0	0	0	42.5	no	2x2x8	4	6	24	28	75600
38	542	262.87	1490.5	0	0	0.1	0	42.5	no	2x2x8	4	6	24	28	55200
39	542	262.87	1490.5	0	0	0.5	0	42.5	no	2x2x8	4	6	24	28	63600
40	542	262.87	1490.5	0	0	0	0.1	42.5	no	2x2x8	4	6	24	28	64800
41	1071.43	642.86	0	0	0	0.1	0	42.5	yes	5x5x5	25	1	24	28	9810
42	448	191	877	838	0.62	0	1	42.5	yes	20x10	314	9	24	28	84100
43	448	191	877	838	0.71	0	1.5	42.5	yes	20x10	314	9	24	28	59300
44	478	191	1008	902	0.49	0	1	42.5	no	20x10	314	9	24	28	20100
45	478	191	1008	902	0.85	0	1.5	42.5	no	20x10	314	9	24	28	10000
46	478	191	1008	902	1.02	0	2	42.5	no	20x10	314	9	24	28	6000
47	478	191	1008	902	1.56	0	2.5	42.5	no	20x10	314	9	24	28	5400
48	478	191	1008	902	0.31	0	0.7	42.5	no	20x10	314	9	24	28	17500
49	478	191	1008	902	0.85	0	1.5	42.5	no	20x10	314	9	24	28	9600
50	478	191	1008	902	1.56	0	2.5	42.5	no	20x10	314	9	24	28	5400
51	1277	574	0	0	0	0	0	42.5	yes	5x5x5	25	1	24	28	604.7
52	1264.77	569.15	0	0	0	0.5	0	42.5	yes	5x5x5	25	1	24	28	249.8
53	1252.77	563.75	0	0	0	1	0	42.5	yes	5x5x5	25	1	24	28	141.3
54	1241.01	558.45	0	0	0	1.5	0	42.5	yes	5x5x5	25	1	24	28	119.5
55	1071.43	642.86	0	0	0	0	0	42.5	yes	5x5x5	25	1	24	28	574.9
56	1061.87	637.12	0	0	0	0.5	0	42.5	yes	5x5x5	25	1	24	28	225.6
57	1031.95	619.17	0	0	0	1	0	42.5	yes	5x5x5	25	1	24	28	127.2
58	1002.86	601.72	0	0	0	1.5	0	42.5	yes	5x5x5	25	1	24	28	108.2
59	974.60	584.76	0	0	0	2	0	42.5	yes	5x5x5	25	1	24	28	77.25
60	897.91	538.75	628.54	0	0	0	0	42.5	yes	5x5x5	25	1	24	28	1941.9
61	877.47	526.48	614.23	0	0	0.5	0	42.5	yes	5x5x5	25	1	24	28	1057
62	867.43	520.46	607.20	0	0	1	0	42.5	yes	5x5x5	25	1	24	28	552.3
63	857.50	514.50	600.25	0	0	1.5	0	42.5	yes	5x5x5	25	1	24	28	314.8
64	847.68	508.61	593.38	0	0	2	0	42.5	yes	5x5x5	25	1	24	28	206.6
65	1040.37	468.17	728.26	0	0	0	0	42.5	yes	5x5x5	25	1	24	28	1502.3
66	1016.69	457.51	711.68	0	0	0.5	0	42.5	yes	5x5x5	25	1	24	28	827.2
67	1005.05	452.27	703.53	0	0	1	0	42.5	yes	5x5x5	25	1	24	28	421.2
68	993.54	447.09	695.48	0	0	1.5	0	42.5	yes	5x5x5	25	1	24	28	273.4
69	899.93	539.96	630	0	0	0	0	42.5	yes	5x5x5	25	1	24	28	1463.9
70	879.44	527.67	615.61	0	0	0.5	0	42.5	yes	5x5x5	25	1	24	28	800
71	869.38	521.63	608.56	0	0	1	0	42.5	yes	5x5x5	25	1	24	28	415.5
72	859.42	515.65	601.60	0	0	1.5	0	42.5	yes	5x5x5	25	1	24	28	265.1
73	849.59	509.75	594.71	0	0	2	0	42.5	yes	5x5x5	25	1	24	28	132.7
74	1875	375	0	0	14.06	0	0	42.5	no	4x4x4	16	2	24	28	7200
75	1875	375	0	0	14.06	0.5	0	42.5	no	4x4x4	16	2	24	28	3200
76	1875	375	0	0	14.06	1	0	42.5	no	4x4x4	16	2	24	28	1000
77	1875	375	0	0	14.06	0	0	42.5	no	4x4x4	16	2	24	28	7200
78	1875	375	0	0	14.06	0	0.1	42.5	no	4x4x4	16	2	24	28	4000
79	1875	375	0	0	14.06	0	0.5	42.5	no	4x4x4	16	2	24	28	600
80	1875	375	0	0	14.06	0	0.5	42.5	no	4x4x4	16	2	24	28	350
81	1277	574	0	0	0	0	0	42.5	no	5x5x5	25	4	48	28	80645.16
82	1270.65	571.79	0	0	0	0.25	0	42.5	no	5x5x5	25	4	48	28	5128.21
83	1161.12	522.50	0	0	0	0.5	0	42.5	no	5x5x5	25	4	48	28	5882.35
84	1252.70	563.71	0	0	0	1	0	42.5	no	5x5x5	25	4	48	28	625.00
85	1241	558.45	0	0	0	1.5	0	42.5	no	5x5x5	25	4	48	28	526.32
86	524	235.8	943.2	639.28	2.62	0	0	42.5	no	5x5x5	25	4	48	28	1000000
87	523	235.33	941.32	638	1.07	0.25	0	42.5	no	5x5x5	25	4	48	28	54054.05
88	521	234.42	937.70	635.55	1.07	0.75	0	42.5	no	5x5x5	25	4	48	28	5263.16
89	520	233.98	935.93	634.35	1.07	1	0	42.5	no	5x5x5	25	4	48	28	526.32
90	518	233.10	932.38	632	1.06	1.5	0	42.5	no	5x5x5	25	4	48	28	666.67
91	1579	789.48	0	0	0	0	0	42.5	yes	4x4x16	16	4	24	7	11800
92	1579	789.48	0	0	0	0	0	42.5	yes	4x4x16	16	4	24	14	13100
93	1579	789.48	0	0	0	0	0	42.5	yes	4x4x16	16	4	24	21	13300
94	1579	789.48	0	0	0	0	0	42.5	yes	4x4x16	16	4	24	28	15500
95	1579	789.48	0	0	0	0.1	0	42.5	yes	4x4x16	16	4	24	7	9000
96	1579	789.48	0	0	0	0.1	0	42.5	yes	4x4x16	16	4	24	14	11550
97	1579	789.48	0	0	0	0.1	0	42.5	yes	4x4x16	16	4	24	21	11900
98	1579	789.48	0	0	0	0.1	0	42.5	yes	4x4x16	16	4	24	28	12200

99	1579	789.48	0	0	0	0.3	0	42.5	yes	4x4x16	16	4	24	7	7800
100	1579	789.48	0	0	0	0.3	0	42.5	yes	4x4x16	16	4	24	14	11500
101	1579	789.48	0	0	0	0.3	0	42.5	yes	4x4x16	16	4	24	21	11300
102	1579	789.48	0	0	0	0.3	0	42.5	yes	4x4x16	16	4	24	28	12100
103	1579	789.48	0	0	0	0.5	0	42.5	yes	4x4x16	16	4	24	7	6000
104	1579	789.48	0	0	0	0.5	0	42.5	yes	4x4x16	16	4	24	14	7500
105	1579	789.48	0	0	0	0.5	0	42.5	yes	4x4x16	16	4	24	21	7300
106	1579	789.48	0	0	0	0.5	0	42.5	yes	4x4x16	16	4	24	28	9150
107	1363.60	545.44	0	0	3.41	0.1	0	42.5	no	5x5x5	25	1.5	24	28	11500
108	1363.60	545.44	0	0	3.41	0.5	0	42.5	no	5x5x5	25	1.5	24	28	11100
109	1363.64	681.82	0	0	0	0.1	0	52.5	no	5x5x5	25	1	24	28	39215.69
110	1363.64	681.82	0	0	0	0.5	0	52.5	no	5x5x5	25	1	24	28	21505.38
111	1277	574	0	0	0	0	0	42.5	no	5x5x5	25	4	24	28	39000
112	1270.65	571.79	0	0	0	0.25	0	42.5	no	5x5x5	25	4	24	28	20000
113	1161.12	522.50	0	0	0	0.5	0	42.5	no	5x5x5	25	4	24	28	16000
114	1258.62	566.38	0	0	0	0.75	0	42.5	no	5x5x5	25	4	24	28	15500
115	1252.70	563.71	0	0	0	1	0	42.5	no	5x5x5	25	4	24	28	1600
116	1241	558.45	0	0	0	1.5	0	42.5	no	5x5x5	25	4	24	28	2700
117	654	294	1308	0	0	0	0	42.5	no	5x5x5	25	4	24	28	50000
118	652.34	293.55	1304.67	0	6.52	0.25	0	42.5	no	5x5x5	25	4	24	28	30000
119	650.68	292.81	1301.36	0	6.51	0.5	0	42.5	no	5x5x5	25	4	24	28	20000
120	649	292.05	1298	0	6.49	0.75	0	42.5	no	5x5x5	25	4	24	28	7000
121	647.33	291.30	1294.66	0	6.47	1	0	42.5	no	5x5x5	25	4	24	28	18000
122	644	289.81	1288	0	6.44	1.5	0	42.5	no	5x5x5	25	4	24	28	10000
123	524	234	951	638	2.62	0	0	42.5	no	5x5x5	25	4	24	28	60000
124	523	235.33	941.32	627.54	7.87	0.25	0	42.5	no	5x5x5	25	4	24	28	50000
125	522	234.87	939.47	626.31	7.86	0.5	0	42.5	no	5x5x5	25	4	24	28	38000
126	521	234.42	937.70	625.13	7.84	0.75	0	42.5	no	5x5x5	25	4	24	28	19000
127	520	233.98	935.93	624	7.83	1	0	42.5	no	5x5x5	25	4	24	28	4000
128	518	233.10	932.38	621.59	7.80	1.5	0	42.5	no	5x5x5	25	4	24	28	2000
129	1277	574	0	0	0	0	0	42.5	no	5x5x5	25	4	24	28	50000
130	1270.65	571.79	0	0	0	0	0.25	42.5	no	5x5x5	25	4	24	28	47000
131	1161.12	522.50	0	0	0	0	0.5	42.5	no	5x5x5	25	4	24	28	38000
132	1258.62	566.38	0	0	0	0	0.75	42.5	no	5x5x5	25	4	24	28	37000
133	1252.70	563.71	0	0	0	0	1	42.5	no	5x5x5	25	4	24	28	35000
134	1241	558.45	0	0	0	0	1.5	42.5	no	5x5x5	25	4	24	28	30000
135	1229.30	558.45	0	0	0	0	2	42.5	no	5x5x5	25	4	24	28	31000
136	654	294	1308	0	0	0	0	42.5	no	5x5x5	25	4	24	28	97000
137	652.34	293.55	1304.67	0	6.52	0	0.25	42.5	no	5x5x5	25	4	24	28	87000
138	650.68	292.81	1301.36	0	6.51	0	0.5	42.5	no	5x5x5	25	4	24	28	82000
139	649	292.05	1298	0	6.49	0	0.75	42.5	no	5x5x5	25	4	24	28	92000
140	647.33	291.30	1294.66	0	6.47	0	1	42.5	no	5x5x5	25	4	24	28	96000
141	644	289.81	1288	0	6.44	0	1.5	42.5	no	5x5x5	25	4	24	28	62000
142	640.80	289.81	1288	0	6.44	0	2	42.5	no	5x5x5	25	4	24	28	60000
143	524	234	951	638	2.62	0	0	42.5	no	5x5x5	25	4	24	28	240000
144	523	235.33	941.32	627.54	7.87	0	0.25	42.5	no	5x5x5	25	4	24	28	145000
145	521	234.42	937.70	625.13	7.84	0	0.75	42.5	no	5x5x5	25	4	24	28	100000
146	518	233.10	932.38	621.59	7.80	0	1.5	42.5	no	5x5x5	25	4	24	28	99000
147	516	233.10	932.38	621.59	7.80	0	2	42.5	no	5x5x5	25	4	24	28	65000
148	1277	574	0	0	0	0	0	42.5	no	5x5x5	25	4	24	28	50000
149	1270.65	571.79	0	0	0	0.25	0	42.5	no	5x5x5	25	4	24	28	35000
150	1161.12	522.50	0	0	0	0.5	0	42.5	no	5x5x5	25	4	24	28	18000
151	1252.70	563.71	0	0	0	1	0	42.5	no	5x5x5	25	4	24	28	1800
152	654	294	1308	0	0	0	0	42.5	no	5x5x5	25	4	24	28	90000
153	652.34	293.55	1304.67	0	6.52	0.25	0	42.5	no	5x5x5	25	4	24	28	80000
154	650.68	292.81	1301.36	0	6.51	0.5	0	42.5	no	5x5x5	25	4	24	28	40000
155	649	292	1298	0	6.49	0.75	0	42.5	no	5x5x5	25	4	24	28	11000
156	524	234	951	638	2.62	0	0	42.5	no	5x5x5	25	4	24	28	220000
157	523	235.33	941.32	627.54	7.87	0.25	0	42.5	no	5x5x5	25	4	24	28	160000
158	522	234.87	939.47	626.31	7.86	0.5	0	42.5	no	5x5x5	25	4	24	28	130000
159	521	234.42	937.70	625.13	7.84	0.75	0	42.5	no	5x5x5	25	4	24	28	45000
160	520	234	935.93	624	7.83	1	0	42.5	no	5x5x5	25	4	24	28	5500
161	518	233.10	932.38	621.59	7.80	1.5	0	42.5	no	5x5x5	25	4	24	28	2000
162	1277	575	0	0	6.3	1	0	42.5	no	5x5x5	25	4	24	28	614.3

Appendix B – Artificial Neural Networks

B2. Datasets - Group II

Table B2.1 Dataset 1 – C+F

#	Cement [kg/m³] min/max	Water [kg/m³] min/max	Fine aggregate [kg/m³] min/max	Coarse aggregate [kg/m³] min/max	Superplasticizer [kg/m³] min/max	Nanofiller [wt%] CNT min/max	CNF min/max	Cement class 0/1	Compressive strength [MPa] min/max	Flexural strength [MPa] min/max
1	1363.64	681.82	0	0	0	0	0	52.5	51.13	13.32
2	1361.09	680.55	0	0	0	0.05	0	52.5	51.81	12.67
3	1358.55	679.28	0	0	0	0.1	0	52.5	52.17	12.06
4	1356.01	678.01	0	0	0	0.15	0	52.5	52.19	11.69
5	1353.47	676.74	0	0	0	0.2	0	52.5	52.29	11.37
6	1350.92	675.46	0	0	0	0.25	0	52.5	52.06	12.99
7	1348.38	674.19	0	0	0	0.3	0	52.5	52.29	13.10
8	1345.84	672.92	0	0	0	0.35	0	52.5	52.40	14.45
9	1343.30	671.65	0	0	0	0.4	0	52.5	52.37	15.35
10	1340.75	670.38	0	0	0	0.45	0	52.5	52.44	15.88
11	1338.21	669.11	0	0	0	0.5	0	52.5	52.51	16.61
12	1500	495	0	0	0	0	0	42.5	76.47	6.12
13	1500	495	0	0	0	0.01	0	42.5	76.86	6.03
14	1500	495	0	0	0	0.02	0	42.5	77.14	5.96
15	1500	495	0	0	0	0.03	0	42.5	77.36	5.88
16	1500	495	0	0	0	0.04	0	42.5	77.52	5.83
17	1500	495	0	0	0	0.05	0	42.5	77.64	5.77
18	1500	495	0	0	0	0.06	0	42.5	77.73	5.70
19	1500	495	0	0	0	0.07	0	42.5	77.73	5.66
20	1500	495	0	0	0	0.08	0	42.5	77.90	5.60
21	1500	495	0	0	0	0.09	0	42.5	77.93	5.56
22	1500	495	0	0	0	0.1	0	42.5	77.97	5.52
23	1200	600	0	0	0	0	0	42.5	32.10	10.95
24	1200	600	0	0	0	0.01	0	42.5	32.24	10.80
25	1200	600	0	0	0	0.02	0	42.5	32.35	10.69
26	1200	600	0	0	0	0.03	0	42.5	32.39	10.69
27	1200	600	0	0	0	0.04	0	42.5	32.53	10.44
28	1200	600	0	0	0	0.05	0	42.5	32.56	10.36
29	1200	600	0	0	0	0.06	0	42.5	32.63	10.27
30	1200	600	0	0	0	0.07	0	42.5	32.65	10.17
31	1200	600	0	0	0	0.08	0	42.5	32.71	10.11
32	1200	600	0	0	0	0.09	0	42.5	32.69	10.02
33	1200	600	0	0	0	0.1	0	42.5	32.62	9.98
34	1500	600	0	0	0	0	0	42.5	41.03	10.78
35	1500	600	0	0	0	0.01	0	42.5	41.21	10.63
36	1500	600	0	0	0	0.02	0	42.5	41.33	10.52
37	1500	600	0	0	0	0.03	0	42.5	41.47	10.39
38	1500	600	0	0	0	0.04	0	42.5	41.55	10.28
39	1500	600	0	0	0	0.05	0	42.5	41.64	10.18
40	1500	600	0	0	0	0.06	0	42.5	41.64	10.12
41	1500	600	0	0	0	0.07	0	42.5	41.76	9.98
42	1500	600	0	0	0	0.08	0	42.5	41.83	9.89
43	1500	600	0	0	0	0.09	0	42.5	41.79	9.86
44	1500	600	0	0	0	0.1	0	42.5	41.79	9.77
45	1578.95	789.475	0	0	0	0	0	42.5	59.97	15.46
46	1578.95	789.475	0	0	0	0.05	0	42.5	60.84	14.63
47	1578.95	789.475	0	0	0	0.1	0	42.5	61.12	14.02
48	1578.95	789.475	0	0	0	0.15	0	42.5	61.11	13.66
49	1578.95	789.475	0	0	0	0.2	0	42.5	61.26	13.29
50	1578.95	789.475	0	0	0	0.25	0	42.5	61.25	13.86
51	1578.95	789.475	0	0	0	0.3	0	42.5	61.03	15.76
52	1578.95	789.475	0	0	0	0.35	0	42.5	60.76	17.57
53	1578.95	789.475	0	0	0	0.4	0	42.5	60.81	18.52
54	1578.95	789.475	0	0	0	0.45	0	42.5	60.36	19.64
55	1578.95	789.475	0	0	0	0.5	0	42.5	60.04	20.22
56	542	262.87	1490.5	0	0	0	0	42.5	28.59	9.03
57	542	262.87	1490.5	0	0	0.05	0	42.5	28.79	8.83
58	542	262.87	1490.5	0	0	0.08	0	42.5	28.87	8.74
59	542	262.87	1490.5	0	0	0.1	0	42.5	28.94	8.66
60	542	262.87	1490.5	0	0	0.15	0	42.5	28.94	8.55
61	542	262.87	1490.5	0	0	0.2	0	42.5	29.05	8.41
62	542	262.87	1490.5	0	0	0.25	0	42.5	29.17	8.26
63	542	262.87	1490.5	0	0	0.3	0	42.5	29.15	8.19
64	542	262.87	1490.5	0	0	0.35	0	42.5	29.14	8.06

65	542	262.87	1490.5	0	0	0.4	0	42.5	29.17	7.96
66	542	262.87	1490.5	0	0	0.45	0	42.5	29.04	7.90
67	542	262.87	1490.5	0	0	0.5	0	42.5	29.03	7.81
68	512.1	256.05	1536.30	0	0	0	0	42.5	46.26	12.71
69	508.19	254.10	1524.58	0	0	0.025	0	42.5	46.41	12.57
70	504.28	252.14	1512.85	0	0	0.05	0	42.5	46.57	12.45
71	500.44	250.22	1501.31	0	0	0.075	0	42.5	46.65	12.34
72	496.59	248.29	1489.76	0	0	0.1	0	42.5	46.78	12.25
73	499.30	274.62	1497.90	0	0	0	0	42.5	44.01	11.63
74	495.49	272.52	1486.47	0	0	0.025	0	42.5	44.18	11.50
75	491.68	270.42	1475.04	0	0	0.05	0	42.5	44.28	11.40
76	487.93	268.36	1463.78	0	0	0.075	0	42.5	44.40	11.28
77	484.17	266.30	1452.52	0	0	0.1	0	42.5	44.49	11.20
78	512.1	256.05	1536.3	0	2.05	0	0	42.5	28.68	9.03
79	512.1	256.05	1536.3	0	2.05	0.025	0	42.5	28.79	8.93
80	512.1	256.05	1536.3	0	2.05	0.05	0	42.5	28.87	8.85
81	512.1	256.05	1536.3	0	2.05	0.075	0	42.5	28.95	8.76
82	512.1	256.05	1536.3	0	2.05	0.1	0	42.5	28.99	8.70
83	359.2	179.6	1077.6	0	0	0	0	52.5	48.70	15.84
84	358.1	179.05	1074.31	0	0.21	0	0.05	52.5	48.78	15.70
85	357.01	178.50	1071.02	0	0.41	0	0.1	52.5	48.85	15.56
86	355.91	177.96	1067.73	0	0.62	0	0.15	52.5	48.89	15.44
87	354.81	177.41	1064.44	0	0.82	0	0.2	52.5	48.98	15.30
88	353.72	176.86	1061.15	0	1.03	0	0.25	52.5	49.02	15.13
89	352.70	176.35	1058.11	0	1.22	0	0.3	52.5	48.95	15.03
90	351.61	175.80	1054.82	0	1.42	0	0.35	52.5	49.11	14.89
91	350.51	175.26	1051.53	0	1.62	0	0.4	52.5	49.03	14.69
92	349.41	174.71	1048.24	0	1.82	0	0.45	52.5	49.10	14.61
93	348.32	174.16	1044.96	0	2.02	0	0.5	52.5	49.04	14.56
94	347.39	173.69	1042.16	0	2.15	0	0.55	52.5	48.88	14.51
95	346.29	173.15	1038.87	0	2.35	0	0.6	52.5	49.11	14.31
96	345.19	172.60	1035.58	0	2.55	0	0.65	52.5	49.02	14.14
97	344.10	172.05	1032.30	0	2.75	0	0.7	52.5	49.09	13.93
98	343	171.50	1029.01	0	2.95	0	0.75	52.5	48.99	14.06
99	342.15	171.08	1026.46	0	3.05	0	0.8	52.5	48.86	13.72
100	341.06	170.53	1023.17	0	3.25	0	0.85	52.5	48.64	13.68
101	339.96	169.98	1019.88	0	3.45	0	0.9	52.5	48.62	14.06
102	338.86	169.43	1016.59	0	3.65	0	0.95	52.5	49.09	13.59
103	337.77	168.88	1013.30	0	3.85	0	1	52.5	48.47	13.70
104	337	168.50	1010.99	0	4.06	0	1.05	52.5	48.77	13.31
105	335.90	167.95	1007.70	0	4.26	0	1.1	52.5	48.60	14.39
106	334.80	167.40	1004.41	0	4.46	0	1.15	52.5	48.18	15.54
107	333.71	166.85	1001.12	0	4.66	0	1.2	52.5	48.84	14.21
108	332.61	166.31	997.83	0	4.86	0	1.25	52.5	48.27	15.82
109	331.92	165.96	995.76	0	5.07	0	1.3	52.5	48.70	15.38
110	330.82	165.41	992.47	0	5.27	0	1.35	52.5	49.13	14.94
111	329.73	164.86	989.18	0	5.47	0	1.4	52.5	49.07	16.41
112	328.63	164.32	985.89	0	5.66	0	1.45	52.5	48.93	16.35
113	327.53	163.77	982.60	0	5.86	0	1.5	52.5	48.48	17.60
114	326.92	163.46	980.76	0	5.49	0	1.55	52.5	47.89	18.46
115	325.82	162.91	977.47	0	5.69	0	1.6	52.5	47.67	19.85
116	324.73	162.36	974.18	0	5.89	0	1.65	52.5	48.09	18.66
117	323.63	161.82	970.89	0	6.09	0	1.7	52.5	47.83	20.43
118	322.53	161.27	967.60	0	6.29	0	1.75	52.5	47.53	21.03
119	322	161.00	965.99	0	5.94	0	1.8	52.5	47.99	19.35
120	320.90	160.45	962.70	0	6.14	0	1.85	52.5	49.70	17.09
121	319.81	159.90	959.42	0	6.34	0	1.9	52.5	49.80	17.15
122	318.71	159.35	956.13	0	6.53	0	1.95	52.5	49.92	17.35
123	317.61	158.81	952.84	0	6.73	0	2	52.5	49.86	17.56
124	664.80	232.68	1994.4	0	7.98	0	0	42.5	65.02	15.77
125	659.73	230.90	1979.18	0	7.92	0.025	0	42.5	65.26	15.59
126	654.65	229.13	1963.96	0	7.86	0.05	0	42.5	65.43	15.45
127	649.66	227.38	1948.97	0	7.80	0.075	0	42.5	65.59	15.33
128	644.66	225.63	1933.98	0	7.74	0.1	0	42.5	65.75	15.17
129	525.56	236.50	709.51	0	0.79	0	0	42.5	50.86	13.62
130	521.48	234.66	704.02	0	0.79	0.025	0	42.5	51.06	13.47
131	517.54	232.89	698.68	0	0.78	0.05	0	42.5	51.19	13.35
132	513.60	231.12	693.34	0	0.77	0.075	0	42.5	51.30	13.22
133	509.64	229.34	688.01	0	0.76	0.1	0	42.5	51.42	13.12
134	450	180	1720	0	4.95	0	0	42.5	58.62	11.48
135	450	180	1720	0	4.95	0.05	0	42.5	58.98	11.27
136	450	180	1720	0	4.95	0.1	0	42.5	59.12	11.14
137	450	180	1720	0	4.95	0.15	0	42.5	59.39	10.92
138	450	180	1720	0	4.95	0.2	0	42.5	59.56	10.78
139	450	180	1720	0	4.95	0.25	0	42.5	59.61	10.66

140	450	180	1720	0	4.95	0.3	0	42.5	59.71	10.61
141	450	180	1720	0	4.95	0.35	0	42.5	59.84	10.45
142	450	180	1720	0	4.95	0.4	0	42.5	59.81	10.35
143	450	180	1720	0	4.95	0.45	0	42.5	59.85	10.20
144	450	180	1720	0	4.95	0.5	0	42.5	59.80	10.16
145	1103.2	496.44	1654.8	0	1.43	0	0	42.5	47.14	10.24
146	1103.2	496.44	1654.8	0	1.43	0.05	0	42.5	47.58	9.94
147	1103.2	496.44	1654.8	0	1.43	0.1	0	42.5	47.80	9.72
148	1103.2	496.44	1654.8	0	1.43	0.15	0	42.5	47.98	9.47
149	1103.2	496.44	1654.8	0	1.43	0.2	0	42.5	48.09	9.26
150	1103.2	496.44	1654.8	0	1.43	0.25	0	42.5	48.12	9.11
151	1103.2	496.44	1654.8	0	1.43	0.3	0	42.5	48.14	9.01
152	1103.2	496.44	1654.8	0	1.43	0.35	0	42.5	48.12	8.96
153	1103.2	496.44	1654.8	0	1.43	0.4	0	42.5	47.78	8.84
154	1103.2	496.44	1654.8	0	1.43	0.45	0	42.5	48.04	8.93
155	1103.2	496.44	1654.8	0	1.43	0.5	0	42.5	47.88	9.82
156	380	193.8	999.4	775.2	0	0	0	42.5	41.30	10.26
157	380	193.8	999.4	775.2	0	0.025	0	42.5	41.42	10.18
158	380	193.8	999.4	775.2	0	0.5	0	42.5	41.50	10.10
159	380	193.8	999.4	775.2	0	0.075	0	42.5	41.59	10.03
160	380	193.8	999.4	775.2	0	0.1	0	42.5	41.65	9.97
161	380	193.8	999.4	775.2	0	0	0.025	42.5	41.32	10.22
162	380	193.8	999.4	775.2	0	0	0.5	42.5	41.36	10.19
163	380	193.8	999.4	775.2	0	0	0.075	42.5	41.37	10.16
164	380	193.8	999.4	775.2	0	0	0.1	42.5	41.41	10.13

Appendix B – Artificial Neural Networks

B3. Datasets – Evaluation

Table B3.1 COMP dataset for repeated training (80% of the initial set)

#	Cement [kg/m³]	Water [kg/m³]	Fine aggregate [kg/m³]	Coarse aggregate [kg/m³]	Superplasticizer [kg/m³]	Nanofiller [wt%] CNT	Nanofiller [wt%] CNF	Cement class	Functionalization	Cross-section [cm]	Demolding age [h]	Age [h]	Compressive strength [MPa]
	min/max	min/max	min/max	min/max	min/max	min/max	min/max	0/1	0/1	0/1	min/max	min/max	min/max
1	542	262.9	1490.5	0	0	0	0	42.5	no	4x4x8	24	3	19.8
2	542	262.9	1490.5	0	0	0	0	42.5	no	4x4x8	24	7	25.6
3	542	262.9	1490.5	0	0	0.1	0	42.5	no	4x4x8	24	3	22.6
4	542	262.9	1490.5	0	0	0.1	0	42.5	no	4x4x8	24	7	26.5
5	542	262.9	1490.5	0	0	0.1	0	42.5	no	4x4x8	24	28	33.8
6	542	262.9	1490.5	0	0	0.5	0	42.5	no	4x4x8	24	3	22.7
7	542	262.9	1490.5	0	0	0.5	0	42.5	no	4x4x8	24	7	27.6
8	542	262.9	1490.5	0	0	0	0.1	42.5	no	4x4x8	24	3	22.5
9	542	262.9	1490.5	0	0	0	0.1	42.5	no	4x4x8	24	7	25.2
10	542	262.9	1490.5	0	0	0	0.1	42.5	no	4x4x8	24	28	33.7
11	380	193.8	999.4	775.2	0	0	0	42.5	no	7x14	24	28	45.8
12	380	193.8	999.4	775.2	0	0.1	0	42.5	no	7x14	24	28	48.5
13	380	193.8	999.4	775.2	0	0	0.1	42.5	no	7x14	24	28	46.7
14	3800	121.6	547.2	839.8	0	0	0	42.5	no	7x14	24	28	64.5
15	512.1	256.1	1536.3	0	2.0484	0	0	42.5	no	4x4x16	24	28	31.8
16	512.1	256.1	1536.3	0	2.0484	0.1	0	42.5	no	4x4x16	24	28	33.5
17	512.1	256.1	1536.3	0	2.0484	0.1	0	42.5	yes	4x4x16	24	28	33.9
18	1071	642.9	0	0	0	0.1	0	42.5	yes	5x5x5	24	28	40
19	1364	681.8	0	0	0	0	0	52.5	no	4x4x16	24	28	56.7
20	1338	669.1	0	0	0	0.5	0	52.5	no	4x4x16	24	28	69.41
21	1364	681.82	0.00	0.00	0	0	0	42.5	no	5x5x5	24	28	74.8
22	1364	681.82	0.00	0.00	1.6364	0.03	0	42.5	no	5x5x5	24	28	83.1
23	1364	681.82	0.00	0.00	8.1818	0.15	0	42.5	no	5x5x5	24	28	86.9
24	1364	681.82	0.00	0.00	13.636	0.25	0	42.5	no	5x5x5	24	28	91.8
25	1364	681.82	0.00	0.00	27.273	0.5	0	42.5	no	5x5x5	24	28	94.3
26	359.2	179.6	1077.6	0	0	0	0	52.5	no	4x4x16	24	7	43.5
27	359.2	179.6	1077.6	0	0.00	0	0	52.5	no	4x4x16	24	28	54
28	359.2	179.6	1077.6	0	0.00	0	0	52.5	no	4x4x16	24	120	58
29	353.7	176.86	1061.2	0	1.03	0	0.25	52.5	no	4x4x16	24	7	43
30	353.7	176.86	1061.2	0	1.03	0	0.25	52.5	no	4x4x16	24	120	60.6
31	348.3	174.16	1045	0	2.02	0	0.5	52.5	no	4x4x16	24	7	43.5
32	348.3	174.16	1045	0	2.02	0	0.5	52.5	no	4x4x16	24	28	55
33	343	171.50	1029	0	2.95	0	0.75	52.5	no	4x4x16	24	7	44
34	343	171.50	1029	0	2.95	0	0.75	52.5	no	4x4x16	24	28	55.1
35	343	171.50	1029	0	2.95	0	0.75	52.5	no	4x4x16	24	120	62.5
36	337.8	168.88	1013.3	0	3.85	0	1	52.5	no	4x4x16	24	28	54.8
37	337.8	168.88	1013.3	0	3.85	0	1	52.5	no	4x4x16	24	120	61.8
38	332.6	166.31	997.83	0	4.86	0	1.25	52.5	no	4x4x16	24	7	47.5
39	332.6	166.31	997.83	0	4.86	0	1.25	52.5	no	4x4x16	24	120	62.5
40	327.5	163.77	982.6	0	5.86	0	1.5	52.5	no	4x4x16	24	7	46
41	327.5	163.77	982.6	0	5.86	0	1.5	52.5	no	4x4x16	24	28	56.5
42	327.5	163.77	982.6	0	5.86	0	1.5	52.5	no	4x4x16	24	120	65
43	322.5	161.27	967.6	0	6.29	0	1.75	52.5	no	4x4x16	24	7	45.5
44	322.5	161.27	967.6	0	6.29	0	1.75	52.5	no	4x4x16	24	120	65.8
45	317.6	158.81	952.84	0	6.73	0	2	52.5	no	4x4x16	24	7	50
46	317.6	158.81	952.84	0	6.73	0	2	52.5	no	4x4x16	24	120	67
47	1200	600	0	0	0	0	0	52.5	no	4x4x16	24	7	38.65
48	1200	600	0	0	0	0	0	52.5	no	4x4x16	24	28	46.7
49	1200	600	0	0	1.8	0	0.5	52.5	no	4x4x16	24	7	39.12
50	1200	600	0	0	3.6	0	1	52.5	no	4x4x16	24	7	38.78
51	1200	600	0	0	3.6	0	1	52.5	no	4x4x16	24	28	45.67
52	1200	600	0	0	6.6	0	2	52.5	no	4x4x16	24	28	44.56
53	542	262.9	1490.5	0	0	0	0	42.5	no	4x4x16	24	3	19.95
54	542	262.9	1490.5	0	0	0	0	42.5	no	4x4x16	24	7	25
55	542	262.9	1490.5	0	0	0	0	42.5	no	4x4x16	24	28	31.7
56	542	262.9	1490.5	0	0	0.08	0	42.5	no	4x4x16	24	7	26.1

57	542	262.9	1490.5	0	0	0.08	0	42.5	no	4x4x16	24	28	33.7
58	542	262.9	1490.5	0	0	0.1	0	42.5	no	4x4x16	24	3	22.9
59	542	262.9	1490.5	0	0	0.1	0	42.5	no	4x4x16	24	7	26.2
60	542	262.9	1490.5	0	0	0.3	0	42.5	no	4x4x16	24	3	21.1
61	542	262.9	1490.5	0	0	0.3	0	42.5	no	4x4x16	24	7	28
62	542	262.9	1490.5	0	0	0.3	0	42.5	no	4x4x16	24	28	33.9
63	542	262.9	1490.5	0	0	0.5	0	42.5	no	4x4x16	24	3	22.8
64	542	262.9	1490.5	0	0	0.5	0	42.5	no	4x4x16	24	28	35.3
65	664.8	232.7	1994.4	0	7.9776	0	0	42.5	no	4x4x16	24	7	68.1
66	664.8	232.7	1994.4	0	7.9776	0	0	42.5	no	4x4x16	24	28	72.1
67	664.8	232.7	1994.4	0	7.9776	0	0	42.5	no	4x4x16	24	90	73.6
68	644.7	225.6	1934	0	7.7359	0.1	0	42.5	no	4x4x16	24	7	76.8
69	644.7	225.6	1934	0	7.7359	0.1	0	42.5	no	4x4x16	24	90	86.8
70	654.7	229.1	1964	0	7.8558	0.05	0	42.5	no	4x4x16	24	7	72.7
71	654.7	229.1	1964	0	7.8558	0.05	0	42.5	no	4x4x16	24	28	75.8
72	654.7	229.1	1964	0	7.8558	0.05	0	42.5	no	4x4x16	24	90	77.9
73	654.7	229.1	1964	0	7.8558	0.05	0	42.5	no	4x4x16	24	7	80.6
74	654.7	229.1	1964	0	7.8558	0.05	0	42.5	no	4x4x16	24	28	88.8
75	525.6	236.5	709.5	0	0.7883	0	0	42.5	no	4x4x16	24	7	45.3
76	525.6	236.5	709.5	0	0.7883	0	0	42.5	no	4x4x16	24	28	56.4
77	525.6	236.5	709.5	0	0.7883	0	0	42.5	no	4x4x16	24	90	57.9
78	509.6	229.3	688	0	0.7645	0.1	0	42.5	no	4x4x16	24	7	53.2
79	509.6	229.3	688	0	0.7645	0.1	0	42.5	no	4x4x16	24	90	65.8
80	517.5	232.9	698.68	0	0.7763	0.05	0	42.5	no	4x4x16	24	7	46.7
81	517.5	232.9	698.68	0	0.7763	0.05	0	42.5	no	4x4x16	24	28	56.5
82	517.5	232.9	698.68	0	0.7763	0.05	0	42.5	no	4x4x16	24	90	57.5
83	517.5	232.9	698.68	0	0.7763	0.05	0	42.5	no	4x4x16	24	7	55.4
84	517.5	232.9	698.68	0	0.7763	0.05	0	42.5	no	4x4x16	24	90	65.7
85	512.1	256.1	1536.3	0	0	0	0	42.5	no	4x4x16	24	7	38.1
86	512.1	256.1	1536.3	0	0	0	0	42.5	no	4x4x16	24	28	51.3
87	512.1	256.1	1536.3	0	0	0	0	42.5	no	4x4x16	24	90	52.4
88	496.6	248.3	1489.8	0	0	0.1	0	42.5	no	4x4x16	24	28	58.8
89	496.6	248.3	1489.8	0	0	0.1	0	42.5	no	4x4x16	24	90	61.5
90	504.3	252.1	1512.9	0	0	0.05	0	42.5	no	4x4x16	24	7	43
91	504.3	252.1	1512.9	0	0	0.05	0	42.5	no	4x4x16	24	90	56.5
92	504.3	252.1	1512.9	0	0	0.05	0	42.5	no	4x4x16	24	7	45.6
93	504.3	252.1	1512.9	0	0	0.05	0	42.5	no	4x4x16	24	90	59.5
94	499.3	274.6	1497.9	0	0	0	0	42.5	no	4x4x16	24	7	36.9
95	499.3	274.6	1497.9	0	0	0	0	42.5	no	4x4x16	24	28	48.8
96	499.3	274.6	1497.9	0	0	0	0	42.5	no	4x4x16	24	90	50.6
97	484.2	266.3	1452.5	0	0	0.1	0	42.5	no	4x4x16	24	7	38.9
98	484.2	266.3	1452.5	0	0	0.1	0	42.5	no	4x4x16	24	90	52
99	491.7	270.4	1475	0	0	0.05	0	42.5	no	4x4x16	24	7	34.7
100	491.7	270.4	1475	0	0	0.05	0	42.5	no	4x4x16	24	28	44.3
101	491.7	270.4	1475	0	0	0.05	0	42.5	no	4x4x16	24	90	44.7
102	491.7	270.4	1475	0	0	0.05	0	42.5	no	4x4x16	24	7	42.1
103	491.7	270.4	1475	0	0	0.05	0	42.5	no	4x4x16	24	90	58.1
104	572	188	572	1015	0	0	0	42.5	no	30x15	24	28	51.23
105	571	188	572	1015	0.22	0	0.16	42.5	no	30x15	24	28	73.08
106	569	188	572	1015	0.71	0	0.78	42.5	no	30x15	24	28	53.5
107	566	188	572	1015	1.38	0	1.55	42.5	no	30x15	24	28	50.26
108	480	191	942	901	0.49	0	0.25	42.5	no	30x15	24	28	43.44
109	448	191	877	838	0.62	0	0.5	42.5	no	30x15	24	28	51.64
110	448	191	877	838	0.62	0	1	42.5	yes	30x15	24	28	41.16
111	448	191	877	838	0.71	0	1.5	42.5	yes	30x15	24	28	39.78
112	478	191	1008	902	0.85	0	1.5	42.5	no	30x15	24	28	52.33
113	478	191	1008	902	1.02	0	2	42.5	no	30x15	24	28	56.6
114	478	191	1008	902	1.56	0	2.5	42.5	no	30x15	24	28	51.57
115	478	191	1008	902	0.49	0	1	42.5	no	30x15	24	28	55.23
116	478	191	1008	902	1.02	0	2	42.5	no	30x15	24	28	43.78
117	478	191	1008	902	1.56	0	2.5	42.5	no	30x15	24	28	44.33
118	1500	495	0	0	0	0	0	42.5	no	4x4x16	24	7	40.4
119	1500	495	0	0	0	0.025	0	42.5	no	4x4x16	24	7	44.2
120	1500	495	0	0	0	0.1	0	42.5	no	4x4x16	24	7	49.2
121	1500	495	0	0	0	0	0	42.5	no	4x4x16	24	28	84.8
122	1500	495	0	0	0	0.025	0	42.5	no	4x4x16	24	28	90.1
123	1500	495	0	0	0	0.05	0	42.5	no	4x4x16	24	28	95.6

124	1277	574	0	0	0	0	0	42.5	yes	5x5x5	24	28	37.6
125	1275	573.5	0	0	0	0.1	0	42.5	yes	5x5x5	24	28	44.3
126	1265	569.1	0	0	0	0.5	0	42.5	yes	5x5x5	24	28	51.2
127	1253	563.7	0	0	0	1	0	42.5	yes	5x5x5	24	28	58.4
128	1071	642.9	0	0	0	0	0	42.5	yes	5x5x5	24	28	41.3
129	1069	641.6	0	0	0	0.1	0	42.5	yes	5x5x5	24	28	48.2
130	1032	619.2	0	0	0	1	0	42.5	yes	5x5x5	24	28	66.3
131	1003	601.7	0	0	0	1.5	0	42.5	yes	5x5x5	24	28	68.2
132	974.6	584.8	0	0	0	2	0	42.5	yes	5x5x5	24	28	61.5
133	897.9	538.7	628.54	0	0	0	0	42.5	yes	5x5x5	24	28	40.6
134	877.5	526.5	614.23	0	0	0.5	0	42.5	yes	5x5x5	24	28	60.7
135	867.4	520.5	607.2	0	0	1	0	42.5	yes	5x5x5	24	28	76.3
136	857.5	514.5	600.25	0	0	1.5	0	42.5	yes	5x5x5	24	28	87.7
137	847.7	508.6	593.38	0	0	2	0	42.5	yes	5x5x5	24	28	95.6
138	1040	468.2	728.26	0	0	0	0	42.5	yes	5x5x5	24	28	38.6
139	1017	457.5	711.68	0	0	0.5	0	42.5	yes	5x5x5	24	28	56.1
140	1005	452.3	703.53	0	0	1	0	42.5	yes	5x5x5	24	28	68.1
141	899.9	540	629.95	0	0	0	0	42.5	yes	5x5x5	24	28	42.27
142	889.6	533.8	622.74	0	0	0.1	0	42.5	yes	5x5x5	24	28	53.7
143	879.4	527.7	615.61	0	0	0.5	0	42.5	yes	5x5x5	24	28	60.7
144	859.4	515.7	601.6	0	0	1.5	0	42.5	yes	5x5x5	24	28	91
145	849.6	509.8	594.71	0	0	2	0	42.5	yes	5x5x5	24	28	102.57
146	1200	600	0	0	0	0	0	42.5	no	4x4x16	24	28	35.6
147	1200	600	0	0	0	0.1	0	42.5	no	4x4x16	24	28	20.4
148	1200	600	0	0	0	0.1	0	42.5	no	4x4x16	24	28	32.4
149	1200	600	0	0	0	0.08	0	42.5	no	4x4x16	24	28	35
150	1200	600	0	0	0	0.1	0	42.5	yes	4x4x16	48	28	35.4
151	1500	600	0	0	0	0	0	42.5	no	4x4x16	24	28	45.5
152	1500	600	0	0	0	0.05	0	42.5	no	4x4x16	24	28	45.92
153	1500	600	0	0	0	0.1	0	42.5	no	4x4x16	24	28	50.09
154	1500	600	0	0	0	0.1	0	42.5	no	4x4x16	24	28	55.05
155	320.2	252.93	1921	0	0	0	0	42.5	no	7x7x7	24	3	5.9
156	320.2	252.93	1921	0	0	0	0	42.5	no	7x7x7	24	7	8.9
157	320.2	252.93	1921	0	0	0	0	42.5	no	7x7x7	24	14	9.9
158	320.2	252.93	1921	0	0	0.2	0	42.5	no	7x7x7	24	3	7.4
159	320.2	252.93	1921	0	0	0.2	0	42.5	no	7x7x7	24	7	8.3
160	320.2	252.93	1921	0	0	0.2	0	42.5	no	7x7x7	24	28	11.9
161	320.2	252.93	1921	0	0	0.4	0	42.5	no	7x7x7	24	3	8.2
162	320.2	252.93	1921	0	0	0.4	0	42.5	no	7x7x7	24	7	8.2
163	320.2	252.93	1921	0	0	0.4	0	42.5	no	7x7x7	24	14	8.45
164	320.2	252.93	1921	0	0	0.6	0	42.5	no	7x7x7	24	3	4.4
165	320.2	252.93	1921	0	0	0.6	0	42.5	no	7x7x7	24	7	7.98
166	320.2	252.93	1921	0	0	0.6	0	42.5	no	7x7x7	24	14	9.9
167	320.2	252.93	1921	0	0	0.6	0	42.5	no	7x7x7	24	28	10.9
168	320.2	252.93	1921	0	0	0.8	0	42.5	no	7x7x7	24	3	7.15
169	320.2	252.93	1921	0	0	0.8	0	42.5	no	7x7x7	24	7	7.9
170	320.2	252.93	1921	0	0	0.8	0	42.5	no	7x7x7	24	14	8.2
171	496	272.8	1488	0	0	0	0	42.5	no	4x4x16	24	28	48
172	496	272.8	1488	0	0	0.05	0	42.5	no	4x4x16	24	28	55
173	496	272.8	1488	0	0	0.1	0	42.5	no	4x4x16	24	28	52
174	496	272.8	1488	0	0	0.15	0	42.5	no	4x4x16	24	28	53
175	620	250	0	0	0	0	0	42.5	no	5x5x5	24	3	21.72
176	620	250	0	0	0	0	0	42.5	no	5x5x5	24	3	23
177	620	250	0	0	0	0	0	42.5	no	5x5x5	24	3	20.36
178	620	250	0	0	0	0	0	42.5	no	5x5x5	24	7	30.76
179	620	250	0	0	0	0	0	42.5	no	5x5x5	24	7	28.8
180	620	250	0	0	0	0	0	42.5	no	5x5x5	24	14	38.16
181	620	250	0	0	0	0	0	42.5	no	5x5x5	24	14	35.44
182	620	250	0	0	0	0	0	42.5	no	5x5x5	24	14	39.36
183	620	250	0	0	0	0	0	42.5	no	5x5x5	24	28	61.2
184	620	250	0	0	0	0	0	42.5	no	5x5x5	24	28	71.56
185	620	250	0	0	0	0.2	0	42.5	no	5x5x5	24	7	43.8
186	620	250	0	0	0	0.2	0	42.5	no	5x5x5	24	28	73.1
187	620	250	0	0	0	0.4	0	42.5	no	5x5x5	24	7	43.9
188	620	250	0	0	0	0.2	0	42.5	yes	5x5x5	24	7	45.4
189	620	250	0	0	0	0.2	0	42.5	yes	5x5x5	24	28	68.2
190	620	250	0	0	0	0.4	0	42.5	yes	5x5x5	24	28	69

191	620	250	0	0	0	0.2	0	42.5	yes	5x5x5	24	7	43.3
192	620	250	0	0	0	0.2	0	42.5	yes	5x5x5	24	28	85.7
193	620	250	0	0	0	0.4	0	42.5	yes	5x5x5	24	7	45.7
194	474	237	793	793	0	0	0	42.5	no	7.5x15	24	28	34
195	474	237	793	793	0	0.01	0	42.5	no	7.5x15	24	28	41.2
196	400	160	660	1168	2.4	0	0	52.5	no	15x15x15	24	3	20
197	400	160	660	1168	2.4	0	0	52.5	no	15x15x15	24	7	39
198	400	160	660	1168	2.4	0	0	52.5	no	15x15x15	24	28	49
199	400	160	660	1168	2.4	0.05	0	52.5	yes	15x15x15	24	3	22
200	400	160	660	1168	2.4	0.05	0	52.5	yes	15x15x15	24	28	45
201	400	160	660	1168	2.4	0.07	0	52.5	yes	15x15x15	24	3	22
202	400	160	660	1168	2.4	0.07	0	52.5	yes	15x15x15	24	7	42
203	400	160	660	1168	2.4	0.08	0	52.5	yes	15x15x15	24	3	28
204	400	160	660	1168	2.4	0.08	0	52.5	yes	15x15x15	24	7	55
205	400	160	660	1168	2.4	0.1	0	52.5	yes	15x15x15	24	3	24
206	400	160	660	1168	2.4	0.1	0	52.5	yes	15x15x15	24	7	48
207	400	160	660	1168	2.4	0.1	0	52.5	yes	15x15x15	24	28	54
208	422	147	621	1284	5.06	0	0	52.5	no	15x15x15	24	7	38.6
209	422	147	621	1284	5.06	0	0	52.5	no	15x15x15	24	28	61.2
210	422	147	621	1284	5.06	0.05	0	52.5	yes	15x15x15	24	7	55
211	422	147	621	1284	5.06	0.05	0	52.5	yes	15x15x15	24	28	78
212	422	147	621	1284	5.06	0.07	0	52.5	yes	15x15x15	24	3	29.6
213	422	147	621	1284	5.06	0.07	0	52.5	yes	15x15x15	24	7	50.8
214	422	147	621	1284	5.06	0.07	0	52.5	yes	15x15x15	24	28	72.6
215	422	147	621	1284	5.06	0.08	0	52.5	yes	15x15x15	24	3	38.6
216	422	147	621	1284	5.06	0.08	0	52.5	yes	15x15x15	24	28	73.2
217	422	147	621	1284	5.06	0.1	0	52.5	yes	15x15x15	24	3	33.4
218	422	147	621	1284	5.06	0.1	0	52.5	yes	15x15x15	24	7	59.3
219	422	147	621	1284	5.06	0.1	0	52.5	yes	15x15x15	24	28	83.6
220	422	147	621	1284	5.06	0.15	0	52.5	yes	15x15x15	24	28	77.6
221	504	142	683	1108	4.7	0	0	52.5	no	15x15x15	24	3	38
222	504	142	683	1108	4.7	0	0	52.5	no	15x15x15	24	7	42
223	504	142	683	1108	4.7	0	0	52.5	no	15x15x15	24	28	72
224	504	142	683	1108	4.7	0.05	0	52.5	yes	15x15x15	24	3	34
225	504	142	683	1108	4.7	0.05	0	52.5	yes	15x15x15	24	7	58
226	504	142	683	1108	4.7	0.05	0	52.5	yes	15x15x15	24	28	89
227	504	142	683	1108	4.7	0.07	0	52.5	yes	15x15x15	24	7	55
228	504	142	683	1108	4.7	0.07	0	52.5	yes	15x15x15	24	28	85
229	504	142	683	1108	4.7	0.08	0	52.5	yes	15x15x15	24	3	39
230	504	142	683	1108	4.7	0.08	0	52.5	yes	15x15x15	24	28	83
231	504	142	683	1108	4.7	0.1	0	52.5	yes	15x15x15	24	3	37
232	504	142	683	1108	4.7	0.1	0	52.5	yes	15x15x15	24	7	60
233	504	142	683	1108	4.7	0.15	0	52.5	yes	15x15x15	24	7	56
234	504	142	683	1108	4.7	0.15	0	52.5	yes	15x15x15	24	28	86
235	1875	375	0	0	14.063	0	0	42.5	no	4x4x4	24	28	130
236	1875	375	0	0	14.063	0.1	0	42.5	no	4x4x4	24	28	152
237	1875	375	0	0	14.063	1	0	42.5	no	4x4x4	24	28	126
238	1875	375	0	0	14.063	0	0	42.5	no	4x4x4	24	28	130
239	1875	375	0	0	14.063	0	0.1	42.5	no	4x4x4	24	28	127
240	1875	375	0	0	14.063	0	0.5	42.5	no	4x4x4	24	28	92
241	1277	574	0	0	0	0	0	42.5	no	5x5x5	48	28	27.1
242	1161	522.5	0	0	0	0.5	0	42.5	no	5x5x5	48	28	41.8
243	1579	789.5	0	0	0.00	0.1	0	42.5	yes	4x4x16	24	21	61
244	1579	789.5	0	0	0.00	0	0	42.5	yes	4x4x16	24	28	66.5
245	1579	789.5	0	0	0.00	0	0	42.5	yes	4x4x16	24	21	62.3
246	1579	789.5	0	0	0.00	0.1	0	42.5	yes	4x4x16	24	28	66.2
247	1579	789.5	0	0	0.00	0.3	0	42.5	yes	4x4x16	24	3	58.7
248	1579	789.5	0	0	0.00	0	0	42.5	yes	4x4x16	24	21	66
249	1579	789.5	0	0	0.00	0.5	0	42.5	yes	4x4x16	24	3	52
250	1579	789.5	0	0	0.00	0	0	42.5	yes	4x4x16	24	21	60.5
251	1579	789.5	0	0	0.00	0.5	0	42.5	yes	4x4x16	24	28	62.5
252	675.9	270.3	1351.7	0	0	0.02	0	42.5	yes	5x5x5	24	28	59.49
253	675.9	270.3	1351.7	0	0	0.04	0	42.5	yes	5x5x5	24	28	55.659
254	675.9	270.3	1351.7	0	0	0.1	0	42.5	yes	5x5x5	24	28	55.659
255	675.9	270.3	1351.7	0	0	0.3	0	42.5	yes	5x5x5	24	28	36.783
256	450	180	1720	0	4.95	0	0	42.5	no	4x4x16	24	28	65
257	450	180	1720	0	4.95	0.5	0	42.5	no	4x4x16	24	28	71.875

#	1103	496.4	1654.8	0	1.4342	0	0	42.5	no	4x4x16	24	28	52.27
258	1103	496.4	1654.8	0	1.4342	0	0	42.5	no	4x4x16	24	28	52.27
259	1103	496.4	1654.8	0	1.4342	0.5	0	42.5	yes	4x4x16	24	28	62.13

Table B3.2 COMP dataset for testing (20% of the initial set)

#	Cement [kg/m³]	Water [kg/m³]	Fine aggregate [kg/m³]	Coarse aggregate [kg/m³]	Superplasticizer [kg/m³]	Nanofiller [wt%] CNT	Nanofiller [wt%] CNF	Cement class	Functionalization	Cross-section [cm]	Demolding age [h]	Age [h]	Compressive strength [MPa]
	min/max	min/max	min/max	min/max	min/max	min/max	min/max	0/1	0/1	0/1	min/max	min/max	min/max
1	542	262.9	1490.5	0	0	0	0	42.5	no	4x4x8	24	28	31.7
2	542	262.9	1490.5	0	0	0.5	0	42.5	no	4x4x8	24	28	35.3
3	512.1	256.1	1536.3	0	2.05	0.1	0	42.5	no	4x4x16	24	28	33.1
4	1338.21	669.1	0	0	0	0.5	0	52.5	yes	4x4x16	24	28	72.13
5	1363.6	681.82	0	0	4.36	0.08	0	42.5	no	5x5x5	24	28	80
6	1363.6	681.82	0	0	19.09	0.35	0	42.5	no	5x5x5	24	28	90
7	353.7	176.86	1061.2	0	1.03	0	0.25	52.5	no	4x4x16	24	28	54.5
8	348.3	174.16	1045	0	2.02	0	0.5	52.5	no	4x4x16	24	120	61
9	1342.83	671.41	4028.5	0	15.31	0	1	52.5	no	4x4x16	24	7	46.5
10	337.8	168.88	1013.3	0	3.85	0	1	52.5	no	4x4x16	24	7	46.5
11	332.61	166.31	997.83	0	4.86	0	1.25	52.5	no	4x4x16	24	28	55
12	322.5	161.27	967.60	0	6.29	0	1.75	52.5	no	4x4x16	24	28	57.5
13	317.6	158.81	952.84	0	6.73	0	2	52.5	no	4x4x16	24	28	57.6
14	1200	600	0	0	1.8	0	0.5	52.5	no	4x4x16	24	28	47.2
15	1200	600	0	0	6.6	0	2	52.5	no	4x4x16	24	7	37.8
16	542	262.9	1490.5	0	0	0.08	0	42.5	no	4x4x16	24	3	22.3
17	542	262.9	1490.5	0	0	0.1	0	42.5	no	4x4x16	24	28	33.8
18	542	262.9	1490.5	0	0	0.5	0	42.5	no	4x4x16	24	7	27.6
19	644.7	225.6	1934	0	7.74	0.1	0	42.5	no	4x4x16	24	28	84.3
20	654.6	229.1	1964	0	7.86	0.05	0	42.5	no	4x4x16	24	90	90.4
21	509.6	229.3	688	0	0.76	0.1	0	42.5	no	4x4x16	24	28	64.7
22	517.5	232.9	698.68	0	0.78	0.05	0	42.5	no	4x4x16	24	28	65.2
23	496.6	248.3	1489.8	0	0	0.1	0	42.5	no	4x4x16	24	7	46.3
24	504.3	252.1	1512.9	0	0	0.05	0	42.5	no	4x4x16	24	28	52.9
25	504.3	252.1	1512.9	0	0	0.05	0	42.5	no	4x4x8	24	28	58.8
26	484.2	266.3	1452.5	0	0	0.1	0	42.5	no	4x4x16	24	28	51
27	491.7	270.4	1475	0	0	0.05	0	42.5	no	4x4x16	24	28	54.5
28	570	188	572	1015	0.31	0	0.31	42.5	no	30x15	24	28	64.604
29	480	191	1005	901	0.49	0	0	42.5	no	30x15	24	28	45.505
30	478	191	1008	902	0.49	0	1	42.5	no	30x15	24	28	47.71
31	478	191	1008	902	0.31	0	0.7	42.5	no	30x15	24	28	44.75
32	478	191	1008	902	0.85	0	1.5	42.5	no	30x15	24	28	51.15
33	1500	495	0	0	0	0.05	0	42.5	no	4x4x16	24	7	47.8
34	1500	495	0	0	0	0.1	0	42.5	no	4x4x16	24	28	97.2
35	1241	558.5	0	0	0	1.5	0	42.5	yes	5x5x5	24	28	59.8
36	1061.87	637.1	0	0	0	0.5	0	42.5	yes	5x5x5	24	28	56.8
37	887.6	532.6	621.34	0	0	0.1	0	42.5	yes	5x5x5	24	28	51.3
38	1028.5	462.8	719.92	0	0	0.1	0	42.5	ization	5x5x5	24	28	46.3
39	993.5	447.1	695.48	0	0	1.5	0	42.5	yes	5x5x5	24	28	78
40	869.4	521.6	608.56	0	0	1	0	42.5	yes	5x5x5	24	28	80.33
41	1200	600	0	0	0	0.1	0	42.5	no	4x4x16	24	28	30.1
42	1200	600	0	0	0	0.1	0	42.5	yes	4x4x16	48	28	32
43	1500	600	0	0	0	0.05	0	42.5	no	4x4x16	24	28	50.17
44	320.2	252.93	1921	0	0	0	0	42.5	no	7x7x7	24	28	11
45	320.2	252.93	1921	0	0	0.2	0	42.5	no	7x7x7	24	14	9.15
46	320.2	252.93	1921	0	0	0.4	0	42.5	no	7x7x7	24	28	12.85
47	320.2	252.93	1921	0	0	0.8	0	42.5	no	7x7x7	24	28	9.3
48	620	250	0	0	0	0	0	42.5	no	5x5x5	24	7	30.32
49	620	250	0	0	0	0	0	42.5	no	5x5x5	24	28	48.44
50	620	250	0	0	0	0.4	0	42.5	no	5x5x5	24	28	64.3
51	620	250	0	0	0	0.4	0	42.5	yes	5x5x5	24	7	46
52	620	250	0	0	0	0.4	0	42.5	yes	5x5x5	24	28	57.9
53	400	160	660	1168	2.4	0.05	0	52.5	yes	15x15x15	24	7	40
54	400	160	660	1168	2.4	0.07	0	52.5	yes	15x15x15	24	28	54
55	400	160	660	1168	2.4	0.08	0	52.5	yes	15x15x15	24	28	67
56	422	147	621	1284	5.06	0	0	52.5	no	15x15x15	24	3	34.1
57	422	147	621	1284	5.06	0.05	0	52.5	yes	15x15x15	24	3	31.4
58	422	147	621	1284	5.06	0.08	0	52.5	yes	15x15x15	24	7	51.4

#	Cement	Water	Fine agg.	Coarse agg.	Super plast.	CNT	CNF	Cement class	Funct.	Cross-section	Demolding age	Age	Flexural strength
59	422	147	621	1284	5.06	0.15	0	52.5	yes	15x15x15	24	7	52.5
60	504	142	683	1108	4.7	0.07	0	52.5	yes	15x15x15	24	3	34
61	504	142	683	1108	4.7	0.08	0	52.5	yes	15x15x15	24	7	54
62	504	142	683	1108	4.7	0.1	0	52.5	yes	15x15x15	24	28	92
63	1875	375	0	0	14.06	0.5	0	42.5	no	4x4x4	24	28	144
64	1875	375	0	0	14.06	0	0.5	42.5	no	4x4x4	24	28	128
65	1579	789.5	0	0	0.00	0	0	42.5	yes	4x4x16	24	3	54.9
66	1579	789.5	0	0	0.00	0.1	0	42.5	yes	4x4x16	24	3	60.5
67	1579	789.5	0	0	0.00	0.3	0	42.5	yes	4x4x16	24	28	67.1
68	675.9	270.3	1351.7	0	0	0.08	0	42.5	yes	5x5x5	24	28	55.34
69	450	180	1720	0	4.95	0.5	0	42.5	no	4x4x16	24	28	76.25
70	380	121.6	547.2	839.8	0	0.1	0	42.5	no	7x14	24	28	66
71	474	237	793	793	0	0	0	42.5	no	7.5x15	24	28	39.9

Table B3.3 FLEX dataset for repeated training (80% of the initial set)

#	Cement [kg/m^3]	Water [kg/m^3]	Fine aggregate [kg/m^3]	Coarse aggregate [kg/m^3]	Super plasticizer [kg/m^3]	Nanofiler wt% CNT	Nanofiler wt% CNF	Cement class	Functio nalization	Cross-section [cm]	Demolding age [h]	Age [h]	Flexural strength [MPa]
	min/max	min/max	min/max	min/max	min/max	min/max	min/max	0/1	0/1	0/1	min/max	min/max	min/max
1	1200	600	0	0	0	0	0	42.5	no	2x2x8	18	3	3.86
2	1200	600	0	0	0	0	0	42.5	no	2x2x8	18	7	4.89
3	1200	600	0	0	0	0	0	42.5	no	2x2x8	18	28	5.43
4	1200	600	0	0	0	0.048	0	42.5	no	2x2x8	18	3	4.35
5	1200	600	0	0	0	0.048	0	42.5	no	2x2x8	18	28	6.181
6	1200	600	0	0	0	0.048	0	42.5	no	2x2x8	18	7	5.83
7	1200	600	0	0	0	0.048	0	42.5	no	2x2x8	18	28	6.75
8	1200	600	0	0	0	0.008	0	42.5	no	2x2x8	18	3	5.055
9	1200	600	0	0	0	0.008	0	42.5	no	2x2x8	18	7	5.83
10	1200	600	0	0	0	0.008	0	42.5	no	2x2x8	18	3	4.45
11	1200	600	0	0	0	0.008	0	42.5	no	2x2x8	18	28	6.66
12	542	262.87	1490.5	0	0	0	0	42.5	no	4x4x16	24	3	2.18
13	542	262.87	1490.5	0	0	0	0	42.5	no	4x4x16	24	7	3.23
14	542	262.87	1490.5	0	0	0.1	0	42.5	no	4x4x16	24	3	4.97
15	542	262.87	1490.5	0	0	0.1	0	42.5	no	4x4x16	24	7	5.83
16	542	262.87	1490.5	0	0	0.1	0	42.5	no	4x4x16	24	28	11.1
17	542	262.87	1490.5	0	0	0.5	0	42.5	no	4x4x16	24	7	4.77
18	542	262.87	1490.5	0	0	0.5	0	42.5	no	4x4x16	24	28	8.6
19	542	262.87	1490.5	0	0	0	0.1	42.5	no	4x4x16	24	3	3.57
20	542	262.87	1490.5	0	0	0	0.1	42.5	no	4x4x16	24	7	7.69
21	542	262.87	1490.5	0	0	0	0.1	42.5	no	4x4x16	24	28	12.2
22	380	193.8	999.4	775.2	0	0.1	0	42.5	no	7x8x38	24	28	10
23	380	193.8	999.4	775.2	0		0.1	42.5	no	7x8x38	24	28	9.9
24	512.1	256.05	1536.3	0	2.0484	0	0	42.5	no	4x4x16	24	28	5.9
25	512.1	256.05	1536.3	0	2.0484	0.1	0	42.5	no	4x4x16	24	28	10.5
26	512.1	256.05	1536.3	0	2.0484	0.1	0	42.5	yes	4x4x16	24	28	12.9
27	512.1	256.05	1536.3	0	2.0484	0.1	0	42.5	yes	4x4x16	24	28	10.6
28	512.1	256.05	1536.3	0	2.0484	0.1	0	42.5	yes	4x4x16	24	28	8.9
29	1338.2	669.107	0	0	0	0.5	0	52.5	no	4x4x16	24	28	9.56
30	1338.2	669.107	0	0	0	0.5	0	52.5	yes	4x4x16	24	28	9.97
31	1363.6	681.82	0	0	0	0	0	42.5	no	4x4x16	24	28	10.2
32	1363.6	681.82	0	0	1.64	0.03	0	42.5	no	4x4x16	24	28	11.1
33	1363.6	681.82	0	0	4.36	0.08	0	42.5	no	4x4x16	24	28	10.8
34	1363.6	681.82	0	0	13.64	0.25	0	42.5	no	4x4x16	24	28	16.1
35	1363.6	681.82	0	0	27.27	0.5	0	42.5	no	4x4x16	24	28	16.4
36	359.2	179.6	1077.6	0	0	0	0	52.5	no	4x4x16	24	7	9.5
37	359.2	179.6	1077.6	0	0.00	0	0	52.5	no	4x4x16	24	28	10.35
38	359.2	179.6	1077.6	0	0.00	0	0	52.5	no	4x4x16	24	120	11.75
39	353.7	176.86	1061.2	0	1.03	0	0.25	52.5	no	4x4x16	24	7	9.8
40	353.7	176.86	1061.2	0	1.03	0	0.25	52.5	no	4x4x16	24	28	10.2
41	348.3	174.16	1045	0	2.02	0	0.5	52.5	no	4x4x16	24	7	9.75
42	348.3	174.16	1045	0	2.02	0	0.5	52.5	no	4x4x16	24	28	10.4
43	343	171.50	1029	0	2.95	0	0.75	52.5	no	4x4x16	24	7	10.1
44	343	171.50	1029	0	2.95	0	0.75	52.5	no	4x4x16	24	28	11.1
45	343	171.50	1029	0	2.95	0	0.75	52.5	no	4x4x16	24	120	11.8
46	337.8	168.88	1013.3	0	3.85	0	1	52.5	no	4x4x16	24	7	10
47	337.8	168.88	1013.3	0	3.85	0	1	52.5	no	4x4x16	24	28	11.3

48	337.8	168.88	1013.3	0	3.85	0	1	52.5	no	4x4x16	24	120	11.7
49	332.6	166.31	997.83	0	4.86	0	1.25	52.5	no	4x4x16	24	7	10.05
50	332.6	166.31	997.83	0	4.86	0	1.25	52.5	no	4x4x16	24	120	11.65
51	327.5	163.77	982.60	0	5.86	0	1.5	52.5	no	4x4x16	24	7	9.9
52	327.5	163.77	982.60	0	5.86	0	1.5	52.5	no	4x4x16	24	28	11.35
53	327.5	163.77	982.60	0	5.86	0	1.5	52.5	no	4x4x16	24	120	11.5
54	322.5	161.27	967.60	0	6.29	0	1.75	52.5	no	4x4x16	24	28	11.05
55	322.5	161.27	967.60	0	6.29	0	1.75	52.5	no	4x4x16	24	120	11.55
56	317.6	158.81	952.84	0	6.73	0	2	52.5	no	4x4x16	24	7	9.5
57	317.6	158.81	952.84	0	6.73	0	2	52.5	no	4x4x16	24	28	11.45
58	317.6	158.81	952.84	0	6.73	0	2	52.5	no	4x4x16	24	120	11.6
59	542	262.87	1490.5	0	0	0	0	42.5	no	4x4x16	24	3	4.1
60	542	262.87	1490.5	0	0	0	0	42.5	no	4x4x16	24	7	5.1
61	542	262.87	1490.5	0	0	0.08	0	42.5	no	4x4x16	24	3	6.4
62	542	262.87	1490.5	0	0	0.08	0	42.5	no	4x4x16	24	7	7.5
63	542	262.87	1490.5	0	0	0.08	0	42.5	no	4x4x16	24	28	10.3
64	542	262.87	1490.5	0	0	0.1	0	42.5	no	4x4x16	24	7	8.2
65	542	262.87	1490.5	0	0	0.1	0	42.5	no	4x4x16	24	28	11.1
66	542	262.87	1490.5	0	0	0.3	0	42.5	no	4x4x16	24	3	4.8
67	542	262.87	1490.5	0	0	0.3	0	42.5	no	4x4x16	24	7	6.7
68	542	262.87	1490.5	0	0	0.5	0	42.5	no	4x4x16	24	3	4.7
69	542	262.87	1490.5	0	0	0.5	0	42.5	no	4x4x16	24	7	6.2
70	664.8	232.68	1994.4	0	7.98	0	0	42.5	no	4x4x16	24	7	9.6
71	664.8	232.68	1994.4	0	7.98	0	0	42.5	no	4x4x16	24	28	10.3
72	664.8	232.68	1994.4	0	7.98	0	0	42.5	no	4x4x16	24	90	10.4
73	644.7	225.63	1934	0	7.74	0.1	0	42.5	no	4x4x16	24	28	13.1
74	644.7	225.63	1934	0	7.74	0.1	0	42.5	no	4x4x16	24	90	13.3
75	654.7	229.13	1964	0	7.86	0.05	0	42.5	no	4x4x16	24	7	10.9
76	654.7	229.13	1964	0	7.86	0.05	0	42.5	no	4x4x16	24	90	12
77	654.7	229.13	1964	0	7.86	0.05	0	42.5	no	4x4x16	24	7	12.1
78	654.7	229.13	1964	0	7.86	0.05	0	42.5	no	4x4x16	24	28	13.3
79	654.7	229.13	1964	0	7.86	0.05	0	42.5	no	4x4x16	24	90	13.6
80	525.6	236.5	709.5	0	0.79	0	0	42.5	no	4x4x16	24	7	7.1
81	525.6	236.5	709.5	0	0.79	0	0	42.5	no	4x4x16	24	90	9.6
82	509.6	229.34	688	0	0.76	0.1	0	42.5	no	4x4x16	24	7	9.3
83	509.6	229.34	688	0	0.76	0.1	0	42.5	no	4x4x16	24	28	10.6
84	517.5	232.89	698.7	0	0.78	0.05	0	42.5	no	4x4x16	24	7	7.9
85	517.5	232.89	698.7	0	0.78	0.05	0	42.5	no	4x4x16	24	28	9.9
86	517.5	232.89	698.7	0	0.78	0.05	0	42.5	no	4x4x16	24	90	10.2
87	517.5	232.89	698.7	0	0.78	0.05	0	42.5	no	4x4x16	24	7	9.3
88	517.5	232.89	698.7	0	0.78	0.05	0	42.5	no	4x4x16	24	28	10.5
89	517.5	232.89	698.7	0	0.78	0.05	0	42.5	no	4x4x16	24	90	10.6
90	512.1	256.05	1536.3	0	0	0	0	42.5	no	4x4x16	24	28	8.3
91	512.1	256.05	1536.3	0	0	0	0	42.5	no	4x4x16	24	90	9.2
92	496.6	248.29	1489.8	0	0	0.1	0	42.5	no	4x4x16	24	7	9
93	496.6	248.29	1489.8	0	0	0.1	0	42.5	no	4x4x16	24	28	9.9
94	496.6	248.29	1489.8	0	0	0.1	0	42.5	no	4x4x16	24	90	10.2
95	504.3	252.14	1512.9	0	0	0.05	0	42.5	no	4x4x16	24	7	7.4
96	504.3	252.14	1512.9	0	0	0.05	0	42.5	no	4x4x16	24	28	8.8
97	504.3	252.14	1512.9	0	0	0.05	0	42.5	no	4x4x16	24	90	9.2
98	504.3	252.14	1512.9	0	0	0.05	0	42.5	no	4x4x16	24	7	8.2
99	504.3	252.14	1512.9	0	0	0.05	0	42.5	no	4x4x16	24	90	10.1
100	499.3	274.62	1497.9	0	0	0	0	42.5	no	4x4x16	24	7	6.5
101	499.3	274.62	1497.9	0	0	0	0	42.5	no	4x4x16	24	28	7.6
102	484.2	266.3	1452.5	0	0	0.1	0	42.5	no	4x4x16	24	7	8.3
103	484.2	266.3	1452.5	0	0	0.1	0	42.5	no	4x4x16	24	28	9.2
104	484.2	266.3	1452.5	0	0	0.1	0	42.5	no	4x4x16	24	90	9.3
105	491.7	270.42	1475	0	0	0.05	0	42.5	no	4x4x16	24	28	7.8
106	491.7	270.42	1475	0	0	0.05	0	42.5	no	4x4x16	24	90	8.5
107	491.7	270.42	1475	0	0	0.05	0	42.5	no	4x4x16	24	7	7.8
108	491.7	270.42	1475	0	0	0.05	0	42.5	no	4x4x16	24	28	8.8
109	491.7	270.42	1475	0	0	0.05	0	42.5	no	4x4x16	24	90	9.3
110	1500	495	0	0	0	0	0	42.5	no	4x4x16	24	28	4
111	1500	495	0	0	0	0.025	0	42.5	no	4x4x16	24	28	4.3
112	1500	495	0	0	0	0.05	0	42.5	no	4x4x16	24	28	4.6
113	1500	495	0	0	0	0.2	0	42.5	no	4x4x16	24	28	5.6
114	1200	600	0	0	0	0	0	42.5	no	4x4x16	24	28	7.15

#	Cement	Water	Fine agg	Coarse agg	Super plast	CNT	CNF	Cement class	Funct	Cross-section	Demolding	Age	Flex
115	1200	600	0	0	0	0.1	0	42.5	no	4x4x16	24	28	5.21
116	1200	600	0	0	0	0.1	0	42.5	no	4x4x16	24	28	6.35
117	1200	600	0	0	0	0.08	0	42.5	no	4x4x16	24	28	7.37
118	1200	600	0	0	0	0.1	0	42.5	yes	4x4x16	48	28	7.09
119	1200	600	0	0	0	0.1	0	42.5	yes	4x4x16	48	28	7.09
120	1500	600	0	0	0	0	0	42.5	no	4x4x16	24	28	7.04
121	1500	600	0	0	0	0.05	0	42.5	no	4x4x16	24	28	7.83
122	1500	600	0	0	0	0.1	0	42.5	no	4x4x16	24	28	7.25
123	1500	600	0	0	0	0.1	0	42.5	no	4x4x16	24	28	8.25
124	1579	789.48	0	0	0	0.05	0	52.5	yes	2.5x4x8	576	28	10.47
125	1579	789.48	0	0	0	0.05	0	52.5	yes	2.5x4x8	576	28	12.61
126	1579	789.48	0	0	0	0.05	0	52.5	yes	2.5x4x8	576	28	8.57
127	496	272.8	1488	0	0	0	0	42.5	no	4x4x16	24	28	3.28
128	496	272.8	1488	0	0	0.05	0	42.5	no	4x4x16	24	28	3.31
129	496	272.8	1488	0	0	0.1	0	42.5	no	4x4x16	24	28	3.5
130	496	272.8	1488	0	0	0.15	0	42.5	no	4x4x16	24	28	4.2
131	400	160	660	1168	2.4	0	0	52.5	no	15x15x15	24	7	2.68
132	400	160	660	1168	2.4	0	0	52.5	no	15x15x15	24	28	4.85
133	400	160	660	1168	2.4	0.05	0	52.5	yes	15x15x15	24	7	3.61
134	400	160	660	1168	2.4	0.07	0	52.5	yes	15x15x15	24	7	3.98
135	400	160	660	1168	2.4	0.08	0	52.5	yes	15x15x15	24	7	4.57
136	400	160	660	1168	2.4	0.08	0	52.5	yes	15x15x15	24	28	9.2
137	400	160	660	1168	2.4	0.1	0	52.5	yes	15x15x15	24	7	4.2
138	422	147	621	1284	5.06	0	0	52.5	no	15x15x15	24	7	3.04
139	422	147	621	1284	5.06	0	0	52.5	no	15x15x15	24	28	5.2
140	422	147	621	1284	5.06	0.05	0	52.5	yes	15x15x15	24	7	4.24
141	422	147	621	1284	5.06	0.05	0	52.5	yes	15x15x15	24	28	6.57
142	422	147	621	1284	5.06	0.07	0	52.5	yes	15x15x15	24	28	7.82
143	422	147	621	1284	5.06	0.08	0	52.5	yes	15x15x15	24	7	5.12
144	422	147	621	1284	5.06	0.08	0	52.5	yes	15x15x15	24	28	9.64
145	422	147	621	1284	5.06	0.1	0	52.5	yes	15x15x15	24	7	4.61
146	504	142	683	1108	4.7	0	0	52.5	no	15x15x15	24	7	3.12
147	504	142	683	1108	4.7	0	0	52.5	no	15x15x15	24	28	5.35
148	504	142	683	1108	4.7	0.05	0	52.5	yes	15x15x15	24	7	4.35
149	504	142	683	1108	4.7	0.07	0	52.5	yes	15x15x15	24	7	4.68
150	504	142	683	1108	4.7	0.07	0	52.5	yes	15x15x15	24	28	7.91
151	504	142	683	1108	4.7	0.08	0	52.5	yes	15x15x15	24	7	6.54
152	504	142	683	1108	4.7	0.08	0	52.5	yes	15x15x15	24	28	9.74
153	504	142	683	1108	4.7	0.1	0	52.5	yes	15x15x15	24	28	8.21
154	1579	789.48	0	0	0.00	0	0	42.5	yes	4x4x16	24	3	9.47
155	1579	789.48	0	0	0.00	0.1	0	42.5	yes	4x4x16	24	21	9.65
156	1579	789.48	0	0	0.00	0	0	42.5	yes	4x4x16	24	28	10.1
157	1579	789.48	0	0	0.00	0.1	0	42.5	yes	4x4x16	24	3	10.35
158	1579	789.48	0	0	0.00	0.1	0	42.5	yes	4x4x16	24	28	11.4
159	1579	789.48	0	0	0.00	0.3	0	42.5	yes	4x4x16	24	3	10.5
160	1579	789.48	0	0	0.00	0	0	42.5	yes	4x4x16	24	21	11.1
161	1579	789.48	0	0	0.00	0.5	0	42.5	yes	4x4x16	24	3	8.4
162	1579	789.48	0	0	0.00	0	0	42.5	yes	4x4x16	24	21	9.55
163	1579	789.48	0	0	0.00	0.5	0	42.5	yes	4x4x16	24	28	10.3
164	450	180	1720	0	4.95	0.5	0	42.5	no	4x4x16	24	28	10.1
165	450	180	1720	0	4.95	0.5	0	42.5	no	4x4x16	24	28	8.2
166	1103.2	496.44	1654.8	0	1.4342	0	0	42.5	no	4x4x16	24	28	6.69
167	1103.2	496.44	1654.8	0	1.4342	0.5	0	42.5	yes	4x4x16	24	28	8.37

Table B3.4 FLEX dataset for testing (20% of the initial set)

#	Cement [kg/m³]	Water [kg/m³]	Fine aggregate [kg/m³]	Coarse aggregate [kg/m³]	Super plasticizer [kg/m³]	Nanofiler wt% CNT	Nanofiler wt% CNF	Cement class	Functionalization	Cross-section [cm]	Demolding age [h]	Age [h]	Flexural strength [MPa]
	min/max	min/max	min/max	min/max	min/max	min/max	min/max	0/1	0/1	0/1	min/max	min/max	min/max
1	1200	600	0	0	0	0.048	0	42.5	no	2x2x8	18	7	5.56
2	1200	600	0	0	0	0.048	0	42.5	no	2x2x8	18	3	4.74
3	1200	600	0	0	0	0.008	0	42.5	no	2x2x8	18	28	6.64
4	1200	600	0	0	0	0.008	0	42.5	no	2x2x8	18	7	5.61
5	542	262.87	1490.5	0	0	0	0	42.5	no	4x4x16	24	28	5.9
6	542	262.87	1490.5	0	0	0.5	0	42.5	no	4x4x16	24	3	2.35
7	380	193.8	999.4	775.2	0	0	0	42.5	no	7x8x38	24	28	6.7
8	512.10	256	1536.3	0	2.05	0.1	0	42.5	no	4x4x16	24	28	10.2

#												
9	1363.6	681.82	0	0	8.18	0.15	0	42.5	no	4x4x16	24	28	13.6
10	1363.6	681.82	0	0	19.09	0.35	0	42.5	no	4x4x16	24	28	16.3
11	353.72	176.86	1061.2	0	1.03	0	0.25	52.5	no	4x4x16	24	120	11.3
12	348.32	174.16	1045	0	2.02	0	0.5	52.5	no	4x4x16	24	120	11.85
13	332.61	166.31	997.83	0	4.86	0	1.25	52.5	no	4x4x16	24	28	11.25
14	322.53	161.27	967.60	0	6.29	0	1.75	52.5	no	4x4x16	24	7	9.6
15	542	262.87	1490.5	0	0	0	0	42.5	no	4x4x16	24	28	5.9
16	542	262.87	1490.5	0	0	0.1	0	42.5	no	4x4x16	24	3	6.9
17	542	262.87	1490.5	0	0	0.3	0	42.5	no	4x4x16	24	28	9.1
18	542	262.87	1490.5	0	0	0.5	0	42.5	no	4x4x16	24	28	8.6
19	644.66	225.63	1934	0	7.74	0.1	0	42.5	no	4x4x16	24	7	11.8
20	654.65	229.13	1964	0	7.86	0.05	0	42.5	no	4x4x16	24	28	12.7
21	525.56	236.50	709.51	0	0.79	0	0	42.5	no	4x4x16	24	28	8.9
22	509.64	229.34	688	0	0.76	0.1	0	42.5	no	4x4x16	24	90	11.1
23	512.10	256	1536.3	0	0	0	0	42.5	no	4x4x16	24	7	6.8
24	504.28	252.14	1512.9	0	0	0.05	0	42.5	no	4x4x16	24	28	9.8
25	499.30	274.62	1497.9	0	0	0	0	42.5	no	4x4x16	24	90	8.4
26	491.68	270.42	1475	0	0	0.05	0	42.5	no	4x4x16	24	7	7.2
27	1500	495	0	0	0	0.1	0	42.5	no	4x4x16	24	28	5.2
28	1200	600	0	0	0	0.1	0	42.5	no	4x4x16	24	28	6
29	1500	600	0	0	0	0.05	0	42.5	no	4x4x16	24	28	6.75
30	1579	789.48	0	0	0	0	0	52.5	yes	2.5x4x8	576	28	5.52
31	400	160	660	1168	2.4	0.05	0	52.5	yes	15x15x15	24	28	6.25
32	400	160	660	1168	2.4	0.07	0	52.5	yes	15x15x15	24	28	7.37
33	400	160	660	1168	2.4	0.1	0	52.5	yes	15x15x15	24	28	8.42
34	422	147	621	1284	5.06	0.07	0	52.5	yes	15x15x15	24	7	4.52
35	422	147	621	1284	5.06	0.1	0	52.5	yes	15x15x15	24	28	8.32
36	504	142	683	1108	4.7	0.05	0	52.5	yes	15x15x15	24	28	6.68
37	504	142	683	1108	4.7	0.1	0	52.5	yes	15x15x15	24	7	4.62
38	1579	789.48	0	0	0	0	0	42.5	yes	4x4x16	24	21	10.45
39	1579	789.48	0	0	0	0.3	0	42.5	yes	4x4x16	24	28	11.7
40	450	180	1720	0	4.95	0		42.5	no	4x4x16	24	28	7.5

Table B3.5 COMP+FLEX dataset for repeated training (80% of the initial set)

#	Cement [kg/m³]	Water [kg/m³]	Fine aggregate [kg/m³]	Coarse aggregate [kg/m³]	Super plasticizer [kg/m³]	Nanofiller wt% CNT	Nanofiller wt% CNF	Cement class	Function alization	Demolding age [h]	Age [h]	Compressive strength [MPa]	Flexural strength [MPa]
	min/max	min/max	min/max	min/max	min/max	min/max	min/max	0/1	0/1	min/max	min/max	min/max	min/max
1	542	262.87	1490.5	0	0	0	0	42.5	no	24	3	19.8	2.18
2	542	262.87	1490.5	0	0	0	0	42.5	no	24	7	25.6	3.23
3	542	262.87	1490.5	0	0	0.1	0	42.5	no	24	3	22.6	4.97
4	542	262.87	1490.5	0	0	0.1	0	42.5	no	24	28	33.8	11.1
5	542	262.87	1490.5	0	0	0.5	0	42.5	no	24	3	22.7	2.35
6	542	262.87	1490.5	0	0	0.5	0	42.5	no	24	7	27.6	4.77
7	542	262.87	1490.5	0	0	0	0.1	42.5	no	24	3	22.5	3.57
8	542	262.87	1490.5	0	0	0	0.1	42.5	no	24	7	25.2	7.69
9	380	193.8	999.4	775.2	0	0	0	42.5	no	24	28	45.8	6.7
10	380	193.8	999.4	775.2	0	0.1	0	42.5	no	24	28	48.5	10
11	380	193.8	999.4	775.2	0		0.1	42.5	no	24	28	46.7	9.9
12	512.1	256.05	1536.3	0	2.048	0	0	42.5	no	24	28	31.8	5.9
13	512.1	256.05	1536.3	0	2.048	0.1	0	42.5	no	24	28	33.1	10.2
14	512.1	256.05	1536.3	0	2.048	0.1	0	42.5	yes	24	28	33.9	12.9
15	1338.2	669.11	0	0	0	0.5	0	52.5	yes	24	28	72.13	9.97
16	1363.6	681.82	0	0	0	0	0	42.5	no	24	28	74.8	10.2
17	1363.6	681.82	0	0	4.36	0.08	0	42.5	no	24	28	80	10.8
18	1363.6	681.82	0	0	8.18	0.15	0	42.5	no	24	28	86.9	13.6
19	1363.6	681.82	0	0	13.64	0.25	0	42.5	no	24	28	91.8	16.1
20	1363.6	681.82	0	0	27.27	0.5	0	42.5	no	24	28	94.3	16.4
21	359.2	179.6	1077.6	0	0	0	0	52.5	no	24	7	43.5	9.5
22	359.2	179.6	1077.6	0	0.00	0	0	52.5	no	24	28	54	10.35
23	359.2	179.6	1077.6	0	0.00	0	0	52.5	no	24	120	58	11.75
24	353.7	176.86	1061.15	0	1.03	0	0.25	52.5	no	24	28	54.5	10.2
25	353.7	176.86	1061.15	0	1.03	0	0.25	52.5	no	24	120	60.6	11.3
26	348.3	174.16	1044.96	0	2.02	0	0.5	52.5	no	24	28	55	10.4
27	348.3	174.16	1044.96	0	2.02	0	0.5	52.5	no	24	120	61	11.85
28	343	171.50	1029.01	0	2.95	0	0.75	52.5	no	24	7	44	10.1
29	343	171.50	1029.01	0	2.95	0	0.75	52.5	no	24	28	55.1	11.1

30	343	171.50	1029.01	0	2.95	0	0.75	52.5	no	24	120	62.5	11.8
31	337.8	168.88	1013.30	0	3.85	0	1	52.5	no	24	7	46.5	10
32	337.8	168.88	1013.30	0	3.85	0	1	52.5	no	24	120	61.8	11.7
33	332.6	166.31	997.83	0	4.86	0	1.25	52.5	no	24	7	47.5	10.05
34	332.6	166.31	997.83	0	4.86	0	1.25	52.5	no	24	28	55	11.25
35	327.5	163.77	982.60	0	5.86	0	1.5	52.5	no	24	7	46	9.9
36	327.5	163.77	982.60	0	5.86	0	1.5	52.5	no	24	28	56.5	11.35
37	327.5	163.77	982.60	0	5.86	0	1.5	52.5	no	24	120	65	11.5
38	322.5	161.27	967.60	0	6.29	0	1.75	52.5	no	24	7	45.5	9.6
39	322.5	161.27	967.60	0	6.29	0	1.75	52.5	no	24	120	65.8	11.55
40	317.6	158.81	952.84	0	6.73	0	2	52.5	no	24	7	50	9.5
41	317.6	158.81	952.84	0	6.73	0	2	52.5	no	24	28	57.6	11.45
42	542	262.87	1490.5	0	0	0	0	42.5	no	24	3	19.95	4.1
43	542	262.87	1490.5	0	0	0	0	42.5	no	24	7	25	5.1
44	542	262.87	1490.5	0	0	0	0	42.5	no	24	28	31.7	5.9
45	542	262.87	1490.5	0	0	0.08	0	42.5	no	24	3	22.3	6.4
46	542	262.87	1490.5	0	0	0.08	0	42.5	no	24	28	33.7	10.3
47	542	262.87	1490.5	0	0	0.1	0	42.5	no	24	3	22.9	6.9
48	542	262.87	1490.5	0	0	0.1	0	42.5	no	24	7	26.2	8.2
49	542	262.87	1490.5	0	0	0.3	0	42.5	no	24	3	21.1	4.8
50	542	262.87	1490.5	0	0	0.3	0	42.5	no	24	7	28	6.7
51	542	262.87	1490.5	0	0	0.3	0	42.5	no	24	28	33.9	9.1
52	542	262.87	1490.5	0	0	0.5	0	42.5	no	24	3	22.8	4.7
53	542	262.87	1490.5	0	0	0.5	0	42.5	no	24	7	27.6	6.2
54	664.8	232.68	1994.4	0	7.978	0	0	42.5	no	24	7	68.1	9.6
55	664.8	232.68	1994.4	0	7.978	0	0	42.5	no	24	28	72.1	10.3
56	664.8	232.68	1994.4	0	7.978	0	0	42.5	no	24	90	73.6	10.4
57	644.7	225.63	1933.98	0	7.736	0.1	0	42.5	no	24	7	76.8	11.8
58	644.7	225.63	1933.98	0	7.736	0.1	0	42.5	no	24	90	86.8	13.3
59	654.7	229.13	1963.96	0	7.856	0.05	0	42.5	no	24	7	72.7	10.9
60	654.7	229.13	1963.96	0	7.856	0.05	0	42.5	no	24	28	75.8	12.7
61	654.7	229.13	1963.96	0	7.856	0.05	0	42.5	no	24	7	80.6	12.1
62	654.7	229.13	1963.96	0	7.856	0.05	0	42.5	no	24	28	88.8	13.3
63	654.7	229.13	1963.96	0	7.856	0.05	0	42.5	no	24	90	90.4	13.6
64	525.6	236.50	709.51	0	0.788	0	0	42.5	no	24	7	45.3	7.1
65	525.6	236.50	709.51	0	0.788	0	0	42.5	no	24	28	56.4	8.9
66	525.6	236.50	709.51	0	0.788	0	0	42.5	no	24	90	57.9	9.6
67	509.6	229.34	688.01	0	0.764	0.1	0	42.5	no	24	28	64.7	10.6
68	509.6	229.34	688.01	0	0.764	0.1	0	42.5	no	24	90	65.8	11.1
69	517.5	232.89	698.68	0	0.776	0.05	0	42.5	no	24	7	46.7	7.9
70	517.5	232.89	698.68	0	0.776	0.05	0	42.5	no	24	28	56.5	9.9
71	517.5	232.89	698.68	0	0.776	0.05	0	42.5	no	24	90	57.5	10.2
72	517.5	232.89	698.68	0	0.776	0.05	0	42.5	no	24	7	55.4	9.3
73	517.5	232.89	698.68	0	0.776	0.05	0	42.5	no	24	28	65.2	10.5
74	517.5	232.89	698.68	0	0.776	0.05	0	42.5	no	24	90	65.7	10.6
75	512.1	256.05	1536.3	0	0	0	0	42.5	no	24	7	38.1	6.8
76	512.1	256.05	1536.3	0	0	0	0	42.5	no	24	90	52.4	9.2
77	496.6	248.29	1489.76	0	0	0.1	0	42.5	no	24	7	46.3	9
78	496.6	248.29	1489.76	0	0	0.1	0	42.5	no	24	28	58.8	9.9
79	496.6	248.29	1489.76	0	0	0.1	0	42.5	no	24	90	61.5	10.2
80	504.3	252.14	1512.85	0	0	0.05	0	42.5	no	24	7	43	7.4
81	504.3	252.14	1512.85	0	0	0.05	0	42.5	no	24	28	52.9	8.8
82	504.3	252.14	1512.85	0	0	0.05	0	42.5	no	24	7	45.6	8.2
83	504.3	252.14	1512.85	0	0	0.05	0	42.5	no	24	28	58.8	9.8
84	504.3	252.14	1512.85	0	0	0.05	0	42.5	no	24	90	59.5	10.1
85	499.3	274.62	1497.9	0	0	0	0	42.5	no	24	7	36.9	6.5
86	499.3	274.62	1497.9	0	0	0	0	42.5	no	24	28	48.8	7.6
87	484.2	266.30	1452.52	0	0	0.1	0	42.5	no	24	7	38.9	8.3
88	484.2	266.30	1452.52	0	0	0.1	0	42.5	no	24	28	51	9.2
89	484.2	266.30	1452.52	0	0	0.1	0	42.5	no	24	90	52	9.3
90	491.7	270.42	1475.04	0	0	0.05	0	42.5	no	24	7	34.7	7.2
91	491.7	270.42	1475.04	0	0	0.05	0	42.5	no	24	90	44.7	8.5
92	491.7	270.42	1475.04	0	0	0.05	0	42.5	no	24	7	42.1	7.8
93	491.7	270.42	1475.04	0	0	0.05	0	42.5	no	24	28	54.5	8.8
94	491.7	270.42	1475.04	0	0	0.05	0	42.5	no	24	90	58.1	9.3
95	1500	495	0	0	0	0	0	42.5	no	24	28	84.8	4
96	1500	495	0	0	0	0.025	0	42.5	no	24	28	90.1	4.3

#	Cement [kg/m³]	Water [kg/m³]	Fine aggregate [kg/m³]	Coarse aggregate [kg/m³]	Super plasticizer [kg/m³]	Nanofiller wt% CNT	Nanofiller wt% CNF	Cement class	Functionalization	Demolding age [h]	Age [h]	Compressive strength [MPa]	Flexural strength [MPa]
97	1500	495	0	0	0	0.05	0	42.5	no	24	28	95.6	4.6
98	1500	495	0	0	0	0.1	0	42.5	no	24	28	97.2	5.2
99	1200	600	0	0	0	0.1	0	42.5	no	24	28	20.4	5.21
100	1200	600	0	0	0	0.1	0	42.5	no	24	28	30.1	6.35
101	1200	600	0	0	0	0.1	0	42.5	no	24	28	32.4	6
102	1200	600	0	0	0	0.1	0	42.5	yes	48	28	32	7.09
103	1200	600	0	0	0	0.1	0	42.5	yes	48	28	35.4	7.09
104	1500	600	0	0	0	0	0	42.5	no	24	28	45.5	7.04
105	1500	600	0	0	0	0.05	0	42.5	no	24	28	45.92	6.75
106	1500	600	0	0	0	0.1	0	42.5	no	24	28	50.09	7.25
107	1500	600	0	0	0	0.1	0	42.5	no	24	28	55.05	8.25
108	496	272.8	1488	0	0	0	0	42.5	no	24	28	48	3.28
109	496	272.8	1488	0	0	0.1	0	42.5	no	24	28	52	3.5
110	496	272.8	1488	0	0	0.15	0	42.5	no	24	28	53	4.2
111	400	160	660	1168	2.4	0	0	52.5	no	24	7	39	2.68
112	400	160	660	1168	2.4	0	0	52.5	no	24	28	49	4.85
113	400	160	660	1168	2.4	0.05	0	52.5	yes	24	7	40	3.61
114	400	160	660	1168	2.4	0.07	0	52.5	yes	24	7	42	3.98
115	400	160	660	1168	2.4	0.07	0	52.5	yes	24	28	54	7.37
116	400	160	660	1168	2.4	0.08	0	52.5	yes	24	7	55	4.57
117	400	160	660	1168	2.4	0.08	0	52.5	yes	24	28	67	9.2
118	400	160	660	1168	2.4	0.1	0	52.5	yes	24	28	54	8.42
119	422	147	621	1284	5.06	0	0	52.5	no	24	7	38.6	3.04
120	422	147	621	1284	5.06	0	0	52.5	no	24	28	61.2	5.2
121	422	147	621	1284	5.06	0.05	0	52.5	yes	24	7	55	4.24
122	422	147	621	1284	5.06	0.05	0	52.5	yes	24	28	78	6.57
123	422	147	621	1284	5.06	0.07	0	52.5	yes	24	7	50.8	4.52
124	422	147	621	1284	5.06	0.07	0	52.5	yes	24	28	72.6	7.82
125	422	147	621	1284	5.06	0.08	0	52.5	yes	24	7	51.4	5.12
126	422	147	621	1284	5.06	0.08	0	52.5	yes	24	28	73.2	9.64
127	422	147	621	1284	5.06	0.1	0	52.5	yes	24	28	83.6	8.32
128	504	142	683	1108	4.7	0	0	52.5	no	24	7	42	3.12
129	504	142	683	1108	4.7	0	0	52.5	no	24	28	72	5.35
130	504	142	683	1108	4.7	0.05	0	52.5	yes	24	7	58	4.35
131	504	142	683	1108	4.7	0.05	0	52.5	yes	24	28	89	6.68
132	504	142	683	1108	4.7	0.07	0	52.5	yes	24	28	85	7.91
133	504	142	683	1108	4.7	0.08	0	52.5	yes	24	7	54	6.54
134	504	142	683	1108	4.7	0.08	0	52.5	yes	24	28	83	9.74
135	504	142	683	1108	4.7	0.1	0	52.5	yes	24	7	60	4.62
136	1579	789.48	0	0	0.00	0	0	42.5	yes	24	3	54.9	9.47
137	1579	789.48	0	0	0.00	0.1	0	42.5	yes	24	21	61	9.65
138	1579	789.48	0	0	0.00	0	0	42.5	yes	24	28	66.5	10.1
139	1579	789.48	0	0	0.00	0	0	42.5	yes	24	21	62.3	10.45
140	1579	789.48	0	0	0.00	0.1	0	42.5	yes	24	28	66.2	11.4
141	1579	789.48	0	0	0.00	0.3	0	42.5	yes	24	3	58.7	10.5
142	1579	789.48	0	0	0.00	0	0	42.5	yes	24	21	66	11.1
143	1579	789.48	0	0	0.00	0.5	0	42.5	yes	24	3	52	8.4
144	1579	789.48	0	0	0.00	0	0	42.5	yes	24	21	60.5	9.55
145	1579	789.48	0	0	0.00	0.5	0	42.5	yes	24	28	62.5	10.3
146	450	180	1720	0	4.95	0	0	42.5	no	24	28	65	7.5
147	450	180	1720	0	4.95	0.5	0	42.5	no	24	28	76.25	8.2
148	1103.2	496.44	1654.8	0	1.43416	0	0	42.5	no	24	28	52.27	6.69
149	1103.2	496.44	1654.8	0	1.43416	0.5	0	42.5	yes	24	28	62.13	8.37

Table B3.6 COMP+FLEX dataset for training (20% of the initial set)

	Cement [kg/m³]	Water [kg/m³]	Fine aggregate [kg/m³]	Coarse aggregate [kg/m³]	Super plasticizer [kg/m³]	Nanofiller wt%		Cement class	Function alization	Demolding age [h]	Age [h]	Compressive strength [MPa]	Flexural strength [MPa]
						CNT	CNF						
#	min/max	min/max	min/max	min/max	min/max	min/max	min/max	0/1	0/1	min/max	min/max	min/max	min/max
1	542	262.87	1490.5	0	0	0	0	42.5	no	24	28	31.7	5.9
2	542	262.87	1490.5	0	0	0.1	0	42.5	no	24	7	26.5	5.83
3	542	262.87	1490.5	0	0	0.5	0	42.5	no	24	28	35.3	8.6
4	542	262.87	1490.5	0	0	0	0.1	42.5	no	24	28	33.7	12.2
5	512.10	256.05	1536.3	0	2.05	0.1	0	42.5	no	24	28	33.5	10.5
6	1338.21	669.11	0	0	0	0.5	0	52.5	no	24	28	69.41	9.56
7	1363.64	681.82	0	0	1.64	0.03	0	42.5	no	24	28	83.1	11.1
8	1363.64	681.82	0	0	19.09	0.35	0	42.5	no	24	28	90	16.3

45

9	353.72	176.86	1061.15	0	1.03	0	0.25	52.5	no	24	7	43	9.8
10	348.32	174.16	1044.96	0	2.02	0	0.5	52.5	no	24	7	43.5	9.75
11	337.77	168.88	1013.30	0	3.85	0	1	52.5	no	24	28	54.8	11.3
12	332.61	166.31	997.83	0	4.86	0	1.25	52.5	no	24	120	62.5	11.65
13	322.53	161.27	967.60	0	6.29	0	1.75	52.5	no	24	28	57.5	11.05
14	317.61	158.81	952.84	0	6.73	0	2	52.5	no	24	120	67	11.6
15	542	262.87	1490.5	0	0	0.08	0	42.5	no	24	7	26.1	7.5
16	542	262.87	1490.5	0	0	0.1	0	42.5	no	24	28	33.8	11.1
17	542	262.87	1490.5	0	0	0.5	0	42.5	no	24	28	35.3	8.6
18	644.66	225.63	1934	0	7.74	0.1	0	42.5	no	24	28	84.3	13.1
19	654.65	229.13	1964	0	7.86	0.05	0	42.5	no	24	90	77.9	12
20	509.64	229.34	688	0	0.76	0.1	0	42.5	no	24	7	53.2	9.3
21	512.10	256.05	1536.3	0	0	0	0	42.5	no	24	28	51.3	8.3
22	504.28	252.14	1512.85	0	0	0.05	0	42.5	no	24	90	56.5	9.2
23	499.30	274.62	1497.90	0	0	0	0	42.5	no	24	90	50.6	8.4
24	491.68	270.42	1475	0	0	0.05	0	42.5	no	24	28	44.3	7.8
25	1200	600	0	0	0	0	0	42.5	no	24	28	35.6	7.15
26	1200	600	0	0	0	0.08	0	42.5	no	24	28	35	7.37
27	1500	600	0	0	0	0.05	0	42.5	no	24	28	50.17	7.83
28	496	272.8	1488	0	0	0.05	0	42.5	no	24	28	55	3.31
29	400	160	660	1168	2.4	0.05	0	52.5	yes	24	28	45	6.25
30	400	160	660	1168	2.4	0.1	0	52.5	yes	24	7	48	4.2
31	422	147	621	1284	5.06	0.1	0	52.5	yes	24	7	59.3	4.61
32	504	142	683	1108	4.7	0.07	0	52.5	yes	24	7	55	4.68
33	504	142	683	1108	4.7	0.1	0	52.5	yes	24	28	92	8.21
34	1579	789.48	0	0	0.00	0.3	0	42.5	yes	24	28	67.1	11.7
35	450	180	1720	0	4.95	0.5	0	42.5	no	24	28	71.88	10.1
36	1579	789.48	0	0	0.00	0.1	0	42.5	yes	24	3	60.5	10.35
37	1200	600	0	0	0	0.1	0	42.5	yes	48	28	32	7.09

Table B3.7 Group II C+F dataset for repeated training (80% of the initial set)

	Cement [kg/m3]	Water [kg/m3]	Fine aggregate [kg/m3]	Coarse aggregate [kg/m3]	Superplasticizer [kg/m3]	Nanofiller [wt%]		Cement class	Compressive strength [MPa]	Flexural strength [MPa]
						CNT	CNF			
#	min/max	min/max	min/max	min/max	min/max	min/max	min/max	0/1	min/max	min/max
1	1363.64	681.82	0	0	0	0	0	52.5	51.13	13.32
2	1358.55	679.28	0	0	0	0.1	0	52.5	52.17	12.06
3	1353.47	676.74	0	0	0	0.2	0	52.5	52.29	11.37
4	1350.92	675.46	0	0	0	0.25	0	52.5	52.06	12.99
5	1348.38	674.19	0	0	0	0.3	0	52.5	52.29	13.10
6	1345.84	672.92	0	0	0	0.35	0	52.5	52.40	14.45
7	1343.30	671.65	0	0	0	0.4	0	52.5	52.37	15.35
8	1340.75	670.38	0	0	0	0.45	0	52.5	52.44	15.88
9	1338.21	669.11	0	0	0	0.5	0	52.5	52.51	16.61
10	1500	495	0	0	0	0	0	42.5	76.47	6.12
11	1500	495	0	0	0	0.01	0	42.5	76.86	6.03
12	1500	495	0	0	0	0.03	0	42.5	77.36	5.88
13	1500	495	0	0	0	0.04	0	42.5	77.52	5.83
14	1500	495	0	0	0	0.05	0	42.5	77.64	5.77
15	1500	495	0	0	0	0.07	0	42.5	77.73	5.66
16	1500	495	0	0	0	0.08	0	42.5	77.90	5.60
17	1500	495	0	0	0	0.09	0	42.5	77.93	5.56
18	1500	495	0	0	0	0.1	0	42.5	77.97	5.52
19	1200	600	0	0	0	0.01	0	42.5	32.24	10.80
20	1200	600	0	0	0	0.02	0	42.5	32.35	10.69
21	1200	600	0	0	0	0.03	0	42.5	32.39	10.69
22	1200	600	0	0	0	0.04	0	42.5	32.53	10.44
23	1200	600	0	0	0	0.05	0	42.5	32.56	10.36
24	1200	600	0	0	0	0.07	0	42.5	32.65	10.17
25	1200	600	0	0	0	0.08	0	42.5	32.71	10.11
26	1200	600	0	0	0	0.1	0	42.5	32.62	9.98
27	1500	600	0	0	0	0	0	42.5	41.03	10.78
28	1500	600	0	0	0	0.01	0	42.5	41.21	10.63
29	1500	600	0	0	0	0.02	0	42.5	41.33	10.52
30	1500	600	0	0	0	0.03	0	42.5	41.47	10.39
31	1500	600	0	0	0	0.05	0	42.5	41.64	10.18
32	1500	600	0	0	0	0.06	0	42.5	41.64	10.12
33	1500	600	0	0	0	0.07	0	42.5	41.76	9.98
34	1500	600	0	0	0	0.09	0	42.5	41.79	9.86
35	1500	600	0	0	0	0.1	0	42.5	41.79	9.77
36	1578.95	789.475	0	0	0	0	0	42.5	59.97	15.46

37	1578.95	789.475	0	0	0	0.1	0	42.5	61.12	14.02
38	1578.95	789.475	0	0	0	0.15	0	42.5	61.11	13.66
39	1578.95	789.475	0	0	0	0.2	0	42.5	61.26	13.29
40	1578.95	789.475	0	0	0	0.3	0	42.5	61.03	15.76
41	1578.95	789.475	0	0	0	0.35	0	42.5	60.76	17.57
42	1578.95	789.475	0	0	0	0.4	0	42.5	60.81	18.52
43	1578.95	789.475	0	0	0	0.45	0	42.5	60.36	19.64
44	1578.95	789.475	0	0	0	0.5	0	42.5	60.04	20.22
45	542	262.87	1490.5	0	0	0	0	42.5	28.59	9.03
46	542	262.87	1490.5	0	0	0.05	0	42.5	28.79	8.83
47	542	262.87	1490.5	0	0	0.1	0	42.5	28.94	8.66
48	542	262.87	1490.5	0	0	0.15	0	42.5	28.94	8.55
49	542	262.87	1490.5	0	0	0.2	0	42.5	29.05	8.41
50	542	262.87	1490.5	0	0	0.25	0	42.5	29.17	8.26
51	542	262.87	1490.5	0	0	0.3	0	42.5	29.15	8.19
52	542	262.87	1490.5	0	0	0.35	0	42.5	29.14	8.06
53	542	262.87	1490.5	0	0	0.45	0	42.5	29.04	7.90
54	542	262.87	1490.5	0	0	0.5	0	42.5	29.03	7.81
55	512.10	256.05	1536.30	0	0	0	0	42.5	46.26	12.71
56	504.28	252.14	1512.85	0	0	0.05	0	42.5	46.57	12.45
57	500.44	250.22	1501.31	0	0	0.075	0	42.5	46.65	12.34
58	496.59	248.29	1489.76	0	0	0.1	0	42.5	46.78	12.25
59	499.30	274.62	1497.90	0	0	0	0	42.5	44.01	11.63
60	491.68	270.42	1475.04	0	0	0.05	0	42.5	44.28	11.40
61	487.93	268.36	1463.78	0	0	0.075	0	42.5	44.40	11.28
62	484.17	266.30	1452.52	0	0	0.1	0	42.5	44.49	11.20
63	512.1	256.05	1536.3	0	2.05	0.025	0	42.5	28.79	8.93
64	512.1	256.05	1536.3	0	2.05	0.05	0	42.5	28.87	8.85
65	512.1	256.05	1536.3	0	2.05	0.075	0	42.5	28.95	8.76
66	359.20	179.6	1077.6	0	0	0	0	52.5	48.70	15.84
67	353.72	176.87	1061.15	0	0.21	0	0.05	52.5	48.78	15.70
68	353.72	176.86	1061.15	0	0.62	0	0.15	52.5	48.89	15.44
69	353.72	176.86	1061.15	0	0.82	0	0.2	52.5	48.98	15.30
70	353.72	176.86	1061.15	0	1.03	0	0.25	52.5	49.02	15.13
71	348.32	174.17	1044.96	0	1.22	0	0.3	52.5	48.95	15.03
72	348.32	174.16	1044.96	0	1.42	0	0.35	52.5	49.11	14.89
73	348.32	174.16	1044.96	0	1.62	0	0.4	52.5	49.03	14.69
74	348.32	174.16	1044.96	0	1.82	0	0.45	52.5	49.10	14.61
75	343.01	171.51	1029.01	0	2.15	0	0.55	52.5	48.88	14.51
76	343	171.51	1029.01	0	2.35	0	0.6	52.5	49.11	14.31
77	343	171.50	1029.01	0	2.55	0	0.65	52.5	49.02	14.14
78	343	171.50	1029.01	0	2.75	0	0.7	52.5	49.09	13.93
79	343	171.50	1029.01	0	2.95	0	0.75	52.5	48.99	14.06
80	337.77	168.89	1013.3	0	3.25	0	0.85	52.5	48.64	13.68
81	337.77	168.89	1013.3	0	3.45	0	0.9	52.5	48.62	14.06
82	337.77	168.88	1013.3	0	3.65	0	0.95	52.5	49.09	13.59
83	337.77	168.88	1013.3	0	3.85	0	1	52.5	48.47	13.70
84	332.61	166.31	997.83	0	4.06	0	1.05	52.5	48.77	13.31
85	332.61	166.31	997.83	0	4.26	0	1.1	52.5	48.60	14.39
86	332.61	166.31	997.83	0	4.66	0	1.2	52.5	48.84	14.21
87	332.61	166.31	997.83	0	4.86	0	1.25	52.5	48.27	15.82
88	327.54	163.77	982.6	0	5.27	0	1.35	52.5	49.13	14.94
89	327.54	163.77	982.6	0	5.47	0	1.4	52.5	49.07	16.41
90	327.54	163.77	982.6	0	5.66	0	1.45	52.5	48.93	16.35
91	327.53	163.77	982.6	0	5.86	0	1.5	52.5	48.48	17.60
92	322.54	161.27	967.6	0	5.49	0	1.55	52.5	47.89	18.46
93	322.54	161.27	967.6	0	5.69	0	1.6	52.5	47.67	19.85
94	322.54	161.27	967.6	0	5.89	0	1.65	52.5	48.09	18.66
95	322.54	161.27	967.6	0	6.09	0	1.7	52.5	47.83	20.43
96	322.53	161.27	967.6	0	6.29	0	1.75	52.5	47.53	21.03
97	317.61	158.81	952.84	0	6.14	0	1.85	52.5	49.70	17.09
98	317.61	158.81	952.84	0	6.34	0	1.9	52.5	49.80	17.15
99	317.61	158.81	952.84	0	6.53	0	1.95	52.5	49.92	17.35
100	317.61	158.81	952.84	0	6.73	0	2	52.5	49.86	17.56
101	664.80	232.68	1994.4	0	7.98	0	0	42.5	65.02	15.77
102	659.73	230.90	1979.18	0	7.92	0.025	0	42.5	65.26	15.59
103	654.65	229.13	1963.96	0	7.86	0.05	0	42.5	65.43	15.45
104	649.66	227.38	1948.97	0	7.80	0.075	0	42.5	65.59	15.33
105	521.48	234.66	704.02	0	0.79	0.025	0	42.5	51.06	13.47
106	517.54	232.89	698.68	0	0.78	0.05	0	42.5	51.19	13.35
107	513.60	231.12	693.34	0	0.77	0.075	0	42.5	51.30	13.22
108	450	180	1720	0	4.95	0	0	42.5	58.62	11.48
109	450	180	1720	0	4.95	0.05	0	42.5	58.98	11.27
110	450	180	1720	0	4.95	0.1	0	42.5	59.12	11.14
111	450	180	1720	0	4.95	0.15	0	42.5	59.39	10.92

112	450	180	1720	0	4.95	0.25	0	42.5	59.61	10.66
113	450	180	1720	0	4.95	0.3	0	42.5	59.71	10.61
114	450	180	1720	0	4.95	0.35	0	42.5	59.84	10.45
115	450	180	1720	0	4.95	0.4	0	42.5	59.81	10.35
116	450	180	1720	0	4.95	0.45	0	42.5	59.85	10.20
117	1103.2	496.44	1654.8	0	1.43	0	0	42.5	47.14	10.24
118	1103.2	496.44	1654.8	0	1.43	0.05	0	42.5	47.58	9.94
119	1103.2	496.44	1654.8	0	1.43	0.1	0	42.5	47.80	9.72
120	1103.2	496.44	1654.8	0	1.43	0.15	0	42.5	47.98	9.47
121	1103.2	496.44	1654.8	0	1.43	0.2	0	42.5	48.09	9.26
122	1103.2	496.44	1654.8	0	1.43	0.25	0	42.5	48.12	9.11
123	1103.2	496.44	1654.8	0	1.43	0.35	0	42.5	48.12	8.96
124	1103.2	496.44	1654.8	0	1.43	0.4	0	42.5	47.78	8.84
125	1103.2	496.44	1654.8	0	1.43	0.45	0	42.5	48.04	8.93
126	1103.2	496.44	1654.8	0	1.43	0.5	0	42.5	47.88	9.82
127	380	193.8	999.4	775.2	0	0.025	0	42.5	41.42	10.18
128	380	193.8	999.4	775.2	0	0.5	0	42.5	41.50	10.10
129	380	193.8	999.4	775.2	0	0.1	0	42.5	41.65	9.97
130	380	193.8	999.4	775.2	0	0	0.5	42.5	41.36	10.19
131	380	193.8	999.4	775.2	0	0	0.1	42.5	41.41	10.13

Table B3.8 Group II C+F dataset for testing (20% of the initial set)

	Cement [kg/m3]	Water [kg/m3]	Fine aggregate [kg/m3]	Coarse aggregate [kg/m3]	Superplasticizer [kg/m3]	Nanofiller [wt%]		Cement class	Compressive strength [MPa]	Flexural strength [MPa]
						CNT	CNF			
#	min/max	min/max	min/max	min/max	min/max	min/max	min/max	0/1	min/max	min/max
1	1361.09	680.55	0	0	0	0.05	0	52.5	51.81	12.67
2	1356.01	678.01	0	0	0	0.15	0	52.5	52.19	11.69
3	1500	495	0	0	0	0.02	0	42.5	77.14	5.96
4	1500	495	0	0	0	0.06	0	42.5	77.73	5.70
5	1200	600	0	0	0	0	0	42.5	32.10	10.95
6	1200	600	0	0	0	0.06	0	42.5	32.63	10.27
7	1200	600	0	0	0	0.09	0	42.5	32.69	10.02
8	1500	600	0	0	0	0.04	0	42.5	41.55	10.28
9	1500	600	0	0	0	0.08	0	42.5	41.83	9.89
10	1578.95	789.475	0	0	0	0.05	0	42.5	60.84	14.63
11	1578.95	789.475	0	0	0	0.25	0	42.5	61.25	13.86
12	542	262.87	1490.5	0	0	0.08	0	42.5	28.87	8.74
13	542	262.87	1490.5	0	0	0.4	0	42.5	29.17	7.96
14	508.19	254.10	1524.58	0	0	0.025	0	42.5	46.41	12.57
15	495.49	272.52	1486.47	0	0	0.025	0	42.5	44.18	11.50
16	512.1	256.05	1536.3	0	2.05	0	0	42.5	28.68	9.03
17	512.1	256.05	1536.3	0	2.05	0.1	0	42.5	28.99	8.70
18	353.72	176.86	1061.15	0	0.41	0	0.1	52.5	48.85	15.56
19	348.32	174.16	1044.96	0	2.02	0	0.5	52.5	49.04	14.56
20	337.77	168.89	1013.3	0	3.05	0	0.8	52.5	48.86	13.72
21	332.61	166.31	997.83	0	4.46	0	1.15	52.5	48.18	15.54
22	327.54	163.77	982.6	0	5.07	0	1.3	52.5	48.70	15.38
23	317.62	158.81	952.84	0	5.94	0	1.8	52.5	47.99	19.35
24	644.66	225.63	1933.98	0	7.74	0.1	0	42.5	65.75	15.17
25	525.56	236.50	709.51	0	0.79	0	0	42.5	50.86	13.62
26	509.64	229.34	688.01	0	0.76	0.1	0	42.5	51.42	13.12
27	450	180	1720	0	4.95	0.2	0	42.5	59.56	10.78
28	450	180	1720	0	4.95	0.5	0	42.5	59.80	10.16
29	1103.2	496.44	1654.8	0	1.43	0.3	0	42.5	48.14	9.01
30	380	193.8	999.4	775.2	0	0	0	42.5	41.30	10.26
31	380	193.8	999.4	775.2	0	0.075	0	42.5	41.59	10.03
32	380	193.8	999.4	775.2	0	0	0.025	42.5	41.32	10.22
33	380	193.8	999.4	775.2	0	0	0.075	42.5	41.37	10.16

B4. Scripts

Script for model COMP from Group I

```
data = readmatrix('Comp_trainingset');

x = data(:,1:20);

y = data(:,21);

xt = x';

yt = y';

hiddenlayerSize = 20;

net0 = feedforwardnet(hiddenlayerSize);

net0.divideParam.trainRatio = 85/100;

net0.divideParam.testRatio = 0/100;

net0.divideParam.valRatio = 15/100;

[net0,tr0] = train(net0,xt,yt);

%% Results of the initial model

ytrain0 = net0(xt(:,tr0.trainInd));

ytraintarget0 = yt(tr0.trainInd);

rmse_train = sqrt(mean(ytrain0-ytraintarget0).^2);

yval0 = net0(xt(:,tr0.valInd));

yvaltarget0 = yt(tr0.valInd);

rmse_val = sqrt(mean(yval0-yvaltarget0).^2);

plot(ytraintarget0,ytrain0,'o');hold on;

plot(yvaltarget0,yval0,'x');hold on;

plot(0:1,0:1);hold off;

mse_tr = mean((ytrain0-ytraintarget0).^2);

mse_val = mean((yval0-yvaltarget0).^2);

%% Optimization of the network architecture

for i=1:60

   hiddenLayerSize = i;

   net = feedforwardnet(hiddenLayerSize);

   net.divideParam.trainRatio = 85/100;

   net.divideParam.testRatio = 0/100;

   net.divideParam.valRatio = 15/100;

   [net,tr] = train(net,xt,yt);

   ytrain = net(xt(:,tr.trainInd));

   ytraintarget = yt(tr.trainInd);
```

```matlab
    rmse_train(i) = sqrt(mean(ytrain-ytraintarget).^2);

    yval = net(xt(:,tr.valInd));

    yvaltarget = yt(tr.valInd);

    rmse_val(i) = sqrt(mean(yval-yvaltarget).^2);

    mse_tr(i) = mean((ytrain-ytraintarget).^2);

    mse_val(i) = mean((yval-yvaltarget).^2);

end
%% Optimization plot

trainrmse = plot(1:60,rmse_train); hold on;

valrmse = plot(1:60,rmse_val); hold off;
%% Training the optimized network

hiddenlayerSize1 = 31;

net1 = feedforwardnet(hiddenlayerSize1);

net1.divideParam.trainRatio = 85/100;

net1.divideParam.testRatio = 0/100;

net1.divideParam.valRatio = 15/100;

[net1,tr1] = train(net1,xt,yt);
%% Results of the optimized model

ytrain1 = net1(xt(:,tr1.trainInd));

ytraintarget1 = yt(tr1.trainInd);

rmse_train1 = sqrt(mean(ytrain1-ytraintarget1).^2);

yval1 = net1(xt(:,tr1.valInd));

yvaltarget1 = yt(tr1.valInd);

rmse_val1 = sqrt(mean(yval1-yvaltarget1).^2);

mse_tr1 = mean((ytrain1-ytraintarget1).^2);

mse_val1 = mean((yval1-yvaltarget1).^2);
%% Visualization for optimized model

plot(ytraintarget1,ytrain1,'o'); hold on;

plot(yvaltarget1,yval1,'x'); hold on;

plot(0:1,0:1); hold off;
 %% Training the optimized network#2

hiddenlayerSize2 = 25;

net2 = feedforwardnet(hiddenlayerSize2);

net2.divideParam.trainRatio = 85/100;

net2.divideParam.testRatio = 0/100;

net2.divideParam.valRatio = 15/100;
```

```matlab
[net2,tr2] = train(net2,xt,yt);
%% Results of the optimized model
ytrain2 = net2(xt(:,tr2.trainInd));
ytraintarget2 = yt(tr2.trainInd);
rmse_tr2 = sqrt(mean(ytrain2-ytraintarget2).^2);
yval2 = net2(xt(:,tr2.valInd));
yvaltarget2 = yt(tr2.valInd);
rmse_val2 = sqrt(mean(yval2-yvaltarget2).^2);
mse_tr2 = mean((ytrain2-ytraintarget2).^2);
mse_val2 = mean((yval2-yvaltarget2).^2);
%% Visualization for optimized model
plot(ytraintarget2,ytrain2,'o'); hold on;
plot(yvaltarget2,yval2,'x'); hold on;
plot(0:1,0:1); hold off;
%% Testing the trained network
data1 = readmatrix('Comp_testingset');
x1 = data1(:,1:20);
y1 = data1(:,21);
xt1 = x1';
yt1 = y1';
ytest = sim(net1,xt1);
%% Results of testing vs training
plot(ytraintarget1,ytrain1,'x');hold on;
plot(yt1,ytest,'o');hold on;
plot(0:1,0:1);hold off;
%% Visualization for testing
plot(yt1,ytest,'o'); hold on;
plot(0:1,0:1); hold off;
%% Training on final model
data = readmatrix('Comp_fullset');
x2 = data(:,1:20);
y2 = data(:,21);
xt2 = x2';
yt2 = y2';
net3 = feedforwardnet(hiddenlayerSize1);
net3.divideParam.trainRatio = 100/100;
```

```matlab
net3.divideParam.testRatio = 0/100;

net3.divideParam.valRatio = 0/100;

[net3,tr3] = train(net3,xt2,yt2);

%% Results of the final model

ytrain3 = net3(xt2(:,tr3.trainInd));

ytraintarget3 = yt2(tr3.trainInd);

rmse_train3 = sqrt(mean(ytrain2-ytraintarget2).^2);

mse_tr3 = mean((ytrain3-ytraintarget3).^2);

%% Visualization for final model

plot(ytraintarget3,ytrain3,'o'); hold on;

plot(ytesttarget3,ytest3,'*'); hold on;

plot(yvaltarget3,yval3,'x'); hold on;

plot(0:1,0:1); hold off;

%% Sensitivity analysis weight method

w1 = net3.IW{1} %the input-to-hidden layer weights

w2 = net3.LW{2} %the hidden-to-output layer weights

b1 = net3.b{1} %the input-to-hidden layer bias

b2 = net3.b{2}  %the hidden-to-output layer bias
```

Script for model FLEX from Group I

```matlab
data = readmatrix('Flex_trainingset');

x = data(:,1:16);

y = data(:,17);

xt = x';

yt = y';

hiddenlayerSize = 16;

net0 = feedforwardnet(hiddenlayerSize);

net0.divideParam.trainRatio = 85/100;

net0.divideParam.testRatio = 0/100;

net0.divideParam.valRatio = 15/100;

[net0,tr0] = train(net0,xt,yt);

%% Results of the initial model

ytrain0 = net0(xt(:,tr0.trainInd));

ytraintarget0 = yt(tr0.trainInd);

rmse_train0 = sqrt(mean(ytrain0-ytraintarget0).^2);

yval0 = net0(xt(:,tr0.valInd));
```

```matlab
yvaltarget0 = yt(tr0.valInd);

rmse_val0 = sqrt(mean(yval0-yvaltarget0).^2);

plot(ytraintarget0,ytrain0,'o');hold on;

plot(yvaltarget0,yval0,'x');hold on;

plot(0:1,0:1);hold off;

mse_tr0 = mean((ytrain0-ytraintarget0).^2);

mse_val0 = mean((yval0-yvaltarget0).^2);

%% Optimization of the network architecture

for i=1:54

    hiddenLayerSize = i;

    net = feedforwardnet(hiddenLayerSize);

    net.divideParam.trainRatio = 85/100;

    net.divideParam.testRatio = 0/100;

    net.divideParam.valRatio = 15/100;

    [net,tr] = train(net,xt,yt);

    ytrain = net(xt(:,tr.trainInd));

    ytraintarget = yt(tr.trainInd);

    rmse_train(i) = sqrt(mean(ytrain-ytraintarget).^2);

    yval = net(xt(:,tr.valInd));

    yvaltarget = yt(tr.valInd);

    rmse_val(i) = sqrt(mean(yval-yvaltarget).^2);

    mse_tr(i) = mean((ytrain-ytraintarget).^2);

    mse_val(i) = mean((yval-yvaltarget).^2);

end

%% Optimization plot

trainrmse = plot(1:54,rmse_train); hold on;

valrmse = plot(1:54,rmse_val); hold off;

%% Training the optimized network

hiddenlayerSize1 = 21;

net1 = feedforwardnet(hiddenlayerSize1);

net1.divideParam.trainRatio = 85/100;

net1.divideParam.testRatio = 0/100;

net1.divideParam.valRatio = 15/100;

[net1,tr1] = train(net1,xt,yt);

%% Results of the optimized model

ytrain1 = net1(xt(:,tr1.trainInd));
```

```matlab
ytraintarget1 = yt(tr1.trainInd);

rmse_train1 = sqrt(mean(ytrain1-ytraintarget1).^2);

yval1 = net1(xt(:,tr1.valInd));

yvaltarget1 = yt(tr1.valInd);

rmse_val1 = sqrt(mean(yval1-yvaltarget1).^2);

mse_tr1 = mean((ytrain1-ytraintarget1).^2);

mse_val1 = mean((yval1-yvaltarget1).^2);

%% Visualization for optimized model

plot(ytraintarget1,ytrain1,'o'); hold on;

plot(yvaltarget1,yval1,'x'); hold on;

plot(0:1,0:1); hold off;

%% %% Training the optimized network#2

hiddenlayerSize2 = 30;

net2 = feedforwardnet(hiddenlayerSize2);

net2.divideParam.trainRatio = 85/100;

net2.divideParam.testRatio = 0/100;

net2.divideParam.valRatio = 15/100;

[net2,tr2] = train(net2,xt,yt);

%% Results of the optimized model

ytrain2 = net2(xt(:,tr2.trainInd));

ytraintarget2 = yt(tr2.trainInd);

rmse_tr2 = sqrt(mean(ytrain2-ytraintarget2).^2);

yval2 = net2(xt(:,tr2.valInd));

yvaltarget2 = yt(tr2.valInd);

rmse_val2 = sqrt(mean(yval2-yvaltarget2).^2);

mse_tr2 = mean((ytrain2-ytraintarget2).^2);

mse_val2 = mean((yval2-yvaltarget2).^2);

%% Visualization for optimized model

plot(ytraintarget2,ytrain2,'o'); hold on;

plot(yvaltarget2,yval2,'x'); hold on;

plot(0:1,0:1); hold off;

%% Testing the trained network

data1 = readmatrix('Flex_testingset');

x1 = data1(:,1:16);

y1 = data1(:,17);

xt1 = x1';
```

```matlab
yt1 = y1';

ytest = sim(net2,xt1);
%% Results of testing vs training
plot(ytraintarget2,ytrain2,'x');hold on;

plot(yt1,ytest,'o');hold on;

plot(0:1,0:1);hold off;
%% Visualization for testing
plot(yt1,ytest,'o'); hold on;

plot(0:1,0:1); hold off;
%% Training on final model
data = readmatrix('Flex_fullset');

x2 = data(:,1:16);

y2 = data(:,17);

xt2 = x2';

yt2 = y2';

net3 = feedforwardnet(hiddenlayerSize2);

net3.divideParam.trainRatio = 100/100;

net3.divideParam.testRatio = 0/100;

net3.divideParam.valRatio = 0/100;

[net3,tr3] = train(net3,xt2,yt2);
%% Results of the final model
ytrain3 = net3(xt2(:,tr3.trainInd));

ytraintarget3 = yt2(tr3.trainInd);

rmse_train3 = sqrt(mean(ytrain2-ytraintarget2).^2);

mse_tr3 = mean((ytrain3-ytraintarget3).^2);
%% Visualization for final model
plot(ytraintarget3,ytrain3,'o'); hold on;

plot(ytesttarget3,ytest3,'*'); hold on;

plot(yvaltarget3,yval3,'x'); hold on;

plot(0:1,0:1); hold off;
%% Sensitivity analysis weight method
w1 = net3.IW{1} %the input-to-hidden layer weights

w2 = net3.LW{2} %the hidden-to-output layer weights

b1 = net3.b{1} %the input-to-hidden layer bias

b2 = net3.b{2}  %the hidden-to-output layer bias
```

Script for model COMP+FLEX from Group I

```
data = readmatrix('C+F_trainingset');

x = data(:,1:11);

y = data(:,12:13);

y01 = data(:,12);

y02 = data(:,13);

xt = x';

yt = y';

yt01 = y01';

yt02 = y02';

hiddenlayerSize = 11;

net0 = feedforwardnet(hiddenlayerSize);

net0.divideParam.trainRatio = 85/100;

net0.divideParam.testRatio = 0/100;

net0.divideParam.valRatio = 15/100;

[net0,tr0] = train(net0,xt,yt);

%% Results of the initial model

ytrain0 = net0(xt(:,tr0.trainInd));

ytraintarget0 = yt(tr0.trainInd);

perf_tr0 = mse(ytrain0-ytraintarget0);

yval0 = net0(xt(:,tr0.valInd));

yvaltarget0 = yt(tr0.valInd);

perf_val0 = mse(yval0-yvaltarget0);

mae_tr0 = mae(ytrain0-ytraintarget0);

mae_val0 = mae(yval0-yvaltarget0);

%% Optimization of the network architecture

for i=1:33

    hiddenLayerSize = i;

    net = feedforwardnet(hiddenLayerSize);

    net.divideParam.trainRatio = 85/100;

    net.divideParam.testRatio = 0/100;

    net.divideParam.valRatio = 15/100;

    [net,tr] = train(net,xt,yt);

    ytrain = net(xt(:,tr.trainInd));

    ytraintarget = yt(tr.trainInd);

    rmse_train(i) = sqrt(mse(ytrain-ytraintarget));
```

```matlab
    yval = net(xt(:,tr.valInd));

    yvaltarget = yt(tr.valInd);

    rmse_val(i) = sqrt(mse(yval-yvaltarget));

end
%% Optimization plot

trainmse01 = plot(1:33,rmse_train); hold on;

trainmse02 = plot(1:33,rmse_val); hold off;

%% Training the optimized network

hiddenlayerSize1 = 18;

net1 = feedforwardnet(hiddenlayerSize1);

net1.divideParam.trainRatio = 85/100;

net1.divideParam.testRatio = 0/100;

net1.divideParam.valRatio = 15/100;

[net1,tr1] = train(net1,xt,yt);

%% Results of the optimized model

ytrain1 = net1(xt(:,tr1.trainInd));

ytraintarget1 = yt(tr1.trainInd);

rmse_train1 = sqrt(mean(ytrain1-ytraintarget1).^2);

yval1 = net1(xt(:,tr1.valInd));

yvaltarget1 = yt(tr1.valInd);

rmse_val1 = sqrt(mean(yval1-yvaltarget1).^2);

mse_tr1 = mean((ytrain1-ytraintarget1).^2);

mse_val1 = mean((yval1-yvaltarget1).^2);

% %% Training the optimized network#2

hiddenlayerSize2 = 24;

net2 = feedforwardnet(hiddenlayerSize2);

net2.divideParam.trainRatio = 85/100;

net2.divideParam.testRatio = 0/100;

net2.divideParam.valRatio = 15/100;

[net2,tr2] = train(net2,xt,yt);

%% Results of the optimized model

ytrain2 = net2(xt(:,tr2.trainInd));

ytraintarget2 = yt(tr2.trainInd);

rmse_tr2 = sqrt(mse(ytrain2-ytraintarget2));

yval2 = net2(xt(:,tr2.valInd));

yvaltarget2 = yt(tr2.valInd);
```

```
rmse_val2 = sqrt(mse(yval2-yvaltarget2));

mse_tr2 = mse(ytrain2-ytraintarget2);

mse_val2 = mse(yval2-yvaltarget2);

%% Testing the trained network

data1 = readmatrix('C+F_testingset');

x1 = data1(:,1:11);

y1 = data1(:,12:13);

xt1 = x1';

yt1 = y1';

ytest = sim(net2,xt1);

%% Results of testing vs training

plot(ytraintarget2,ytrain2,'x');hold on;

plot(yt1,ytest,'o');hold on;

plot(0:1,0:1);hold off;

%% Visualization for testing

plot(yt1,ytest,'o'); hold on;

plot(0:1,0:1); hold off;

%% Training on final model

data = readmatrix('C+F_fullset');

x2 = data(:,1:11);

y2 = data(:,12:13);

xt2 = x2';

yt2 = y2';

net3 = feedforwardnet(hiddenlayerSize2);

net3.divideParam.trainRatio = 100/100;

net3.divideParam.testRatio = 0/100;

net3.divideParam.valRatio = 0/100;

[net3,tr3] = train(net3,xt2,yt2);

%% Results of the final model

ytrain3 = net3(xt2(:,tr3.trainInd));

ytraintarget3 = yt2(tr3.trainInd);

rmse_train3 = sqrt(mse(ytrain2-ytraintarget2));

mse_tr3 = mse(ytrain3-ytraintarget3);

%% Visualization for final model

plot(ytraintarget3,ytrain3,'o'); hold on;

plot(ytesttarget3,ytest3,'*'); hold on;
```

```matlab
plot(yvaltarget3,yval3,'x'); hold on;

plot(0:1,0:1); hold off;
%% Sensitivity analysis weight method
w1 = net3.IW{1} %the input-to-hidden layer weights
w2 = net3.LW{2} %the hidden-to-output layer weights
b1 = net3.b{1} %the input-to-hidden layer bias
b2 = net3.b{2}  %the hidden-to-output layer bias
```

Script for model RESIST from Group I

```matlab
data = readmatrix('Resist_trainingset');
x = data(:,1:17);
y = data(:,18);
xt = x';
yt = y';
hiddenlayerSize = 17;
net0 = feedforwardnet(hiddenlayerSize);
net0.divideParam.trainRatio = 85/100;
net0.divideParam.testRatio = 0/100;
net0.divideParam.valRatio = 15/100;
[net0,tr0] = train(net0,xt,yt);
%% Results of the initial model
ytrain0 = net0(xt(:,tr0.trainInd));
ytraintarget0 = yt(tr0.trainInd);
rmse_train0 = sqrt(mean(ytrain0-ytraintarget0).^2);
yval0 = net0(xt(:,tr0.valInd));
yvaltarget0 = yt(tr0.valInd);
rmse_val0 = sqrt(mean(yval0-yvaltarget0).^2);
plot(ytraintarget0,ytrain0,'o');hold on;
plot(yvaltarget0,yval0,'x');hold on;
plot(0:1,0:1);hold off;
mse_tr0 = mean((ytrain0-ytraintarget0).^2);
mse_val0 = mean((yval0-yvaltarget0).^2);
rmse_tr0 = sqrt(mean(ytrain0-ytraintarget0).^2);
rmse_val0 = sqrt(mean(yval0-yvaltarget0).^2);
%% Optimization of the network architecture
for i=1:58
```

```matlab
    hiddenLayerSize = i;

    net = feedforwardnet(hiddenLayerSize);

    net.divideParam.trainRatio = 85/100;

    net.divideParam.testRatio = 0/100;

    net.divideParam.valRatio = 15/100;

    [net,tr] = train(net,xt,yt);

    ytrain = net(xt(:,tr.trainInd));

    ytraintarget = yt(tr.trainInd);

    rmse_train(i) = sqrt(mean(ytrain-ytraintarget).^2);

    yval = net(xt(:,tr.valInd));

    yvaltarget = yt(tr.valInd);

    rmse_val(i) = sqrt(mean(yval-yvaltarget).^2);

    mse_tr(i) = mean((ytrain-ytraintarget).^2);

    mse_val(i) = mean((yval-yvaltarget).^2);

end

%% Optimization plot

trainrmse = plot(1:58,rmse_train); hold on;

valrmse = plot(1:58,rmse_val); hold off;

%% Training the optimized network

hiddenlayerSize1 = 23;

net1 = feedforwardnet(hiddenlayerSize1);

net1.divideParam.trainRatio = 85/100;

net1.divideParam.testRatio = 0/100;

net1.divideParam.valRatio = 15/100;

[net1,tr1] = train(net1,xt,yt);

%% Results of the optimized model

ytrain1 = net1(xt(:,tr1.trainInd));

ytraintarget1 = yt(tr1.trainInd);

rmse_train1 = sqrt(mean(ytrain1-ytraintarget1).^2);

yval1 = net1(xt(:,tr1.valInd));

yvaltarget1 = yt(tr1.valInd);

rmse_val1 = sqrt(mean(yval1-yvaltarget1).^2);

mse_tr1 = mean((ytrain1-ytraintarget1).^2);

mse_val1 = mean((yval1-yvaltarget1).^2);

%% Visualization for optimized model

plot(ytraintarget1,ytrain1,'o'); hold on;
```

```matlab
plot(yvaltarget1,yval1,'x'); hold on;

plot(0:1,0:1); hold off;

%% %% Training the optimized network#2

hiddenlayerSize2 = 31;

net2 = feedforwardnet(hiddenlayerSize2);

net2.divideParam.trainRatio = 85/100;

net2.divideParam.testRatio = 0/100;

net2.divideParam.valRatio = 15/100;

[net2,tr2] = train(net2,xt,yt);

%% Results of the optimized model

ytrain2 = net2(xt(:,tr2.trainInd));

ytraintarget2 = yt(tr2.trainInd);

rmse_tr2 = sqrt(mean(ytrain2-ytraintarget2).^2);

yval2 = net2(xt(:,tr2.valInd));

yvaltarget2 = yt(tr2.valInd);

rmse_val2 = sqrt(mean(yval2-yvaltarget2).^2);

mse_tr2 = mean((ytrain2-ytraintarget2).^2);

mse_val2 = mean((yval2-yvaltarget2).^2);

%% Visualization for optimized model

plot(ytraintarget2,ytrain2,'o'); hold on;

plot(yvaltarget2,yval2,'x'); hold on;

plot(0:1,0:1); hold off;

%% Testing the trained network

data1 = readmatrix('Resist_testingset');

x1 = data1(:,1:17);

y1 = data1(:,18);

xt1 = x1';

yt1 = y1';

ytest = sim(net2,xt1);

%% Results of testing vs training

plot(ytraintarget2,ytrain2,'x');hold on;

plot(yt1,ytest,'o');hold on;

plot(0:1,0:1);hold off;

%% Visualization for testing

plot(yt1,ytest,'o'); hold on;

plot(0:1,0:1); hold off;
```

```
%% Training on final model

data = readmatrix('Resist_fullset');

x2 = data(:,1:17);

y2 = data(:,18);

xt2 = x2';

yt2 = y2';

net3 = feedforwardnet(hiddenlayerSize2);

net3.divideParam.trainRatio = 100/100;

net3.divideParam.testRatio = 0/100;

net3.divideParam.valRatio = 0/100;

[net3,tr3] = train(net3,xt2,yt2);

%% Results of the final model

ytrain3 = net3(xt2(:,tr3.trainInd));

ytraintarget3 = yt2(tr3.trainInd);

rmse_train3 = sqrt(mean(ytrain2-ytraintarget2).^2);

mse_tr3 = mean((ytrain3-ytraintarget3).^2);

%% Visualization for final model

plot(ytraintarget3,ytrain3,'o'); hold on;

plot(ytesttarget3,ytest3,'*'); hold on;

plot(yvaltarget3,yval3,'x'); hold on;

plot(0:1,0:1); hold off;

%% Sensitivity analysis weight method

w1 = net3.IW{1} %the input-to-hidden layer weights

w2 = net3.LW{2} %the hidden-to-output layer weights

b1 = net3.b{1} %the input-to-hidden layer bias

b2 = net3.b{2}  %the hidden-to-output layer bias
```

Script for model C+F from Group II

```
data = readmatrix('C&F_trainingset');

x = data(:,1:8);

y = data(:,9:10);

y01 = data(:,9);

y02 = data(:,10);

xt = x';

yt = y';

yt01 = y01';
```

```matlab
yt02 = y02';

hiddenlayerSize = 8;

net0 = feedforwardnet(hiddenlayerSize);

net0.divideParam.trainRatio = 85/100;

net0.divideParam.testRatio = 0/100;

net0.divideParam.valRatio = 15/100;

[net0,tr0] = train(net0,xt,yt);

%% Results of the initial model

ytrain0 = net0(xt(:,tr0.trainInd));

ytraintarget0 = yt(tr0.trainInd);

perf_tr0 = mse(ytrain0-ytraintarget0);

yval0 = net0(xt(:,tr0.valInd));

yvaltarget0 = yt(tr0.valInd);

perf_val0 = mse(yval0-yvaltarget0);

mae_tr0 = mae(ytrain0-ytraintarget0);

mae_val0 = mae(yval0-yvaltarget0);

rmse_tr0 = sqrt(perf_tr0);

rmse_val0 = sqrt(perf_val0);

%% Optimization of the network architecture

for i=1:24

    hiddenLayerSize = i;

    net = feedforwardnet(hiddenLayerSize);

    net.divideParam.trainRatio = 85/100;

    net.divideParam.testRatio = 0/100;

    net.divideParam.valRatio = 15/100;

    [net,tr] = train(net,xt,yt);

    ytrain = net(xt(:,tr.trainInd));

    ytraintarget = yt(tr.trainInd);

    rmse_train(i) = sqrt(mse(ytrain-ytraintarget));

    yval = net(xt(:,tr.valInd));

    yvaltarget = yt(tr.valInd);

    rmse_val(i) = sqrt(mse(yval-yvaltarget));

end

%% Optimization plot

trainmse01 = plot(1:24,rmse_train); hold on;

trainmse02 = plot(1:24,rmse_val); hold off;
```

```matlab
%% Training the optimized network
hiddenlayerSize1 = 13;
net1 = feedforwardnet(hiddenlayerSize1);
net1.divideParam.trainRatio = 85/100;
net1.divideParam.testRatio = 0/100;
net1.divideParam.valRatio = 15/100;
[net1,tr1] = train(net1,xt,yt);
%% Results of the optimized model
ytrain1 = net1(xt(:,tr1.trainInd));
ytraintarget1 = yt(tr1.trainInd);
rmse_train1 = sqrt(mean(ytrain1-ytraintarget1).^2);
yval1 = net1(xt(:,tr1.valInd));
yvaltarget1 = yt(tr1.valInd);
rmse_val1 = sqrt(mean(yval1-yvaltarget1).^2);
mse_tr1 = mean((ytrain1-ytraintarget1).^2);
mse_val1 = mean((yval1-yvaltarget1).^2);
%% Training the optimized network#2
hiddenlayerSize2 = 17;
net2 = feedforwardnet(hiddenlayerSize2);
net2.divideParam.trainRatio = 85/100;
net2.divideParam.testRatio = 0/100;
net2.divideParam.valRatio = 15/100;
[net2,tr2] = train(net2,xt,yt);
%% Results of the optimized model
ytrain2 = net2(xt(:,tr2.trainInd));
ytraintarget2 = yt(tr2.trainInd);
rmse_tr2 = sqrt(mse(ytrain2-ytraintarget2));
yval2 = net2(xt(:,tr2.valInd));
yvaltarget2 = yt(tr2.valInd);
rmse_val2 = sqrt(mse(yval2-yvaltarget2));
mse_tr2 = mse(ytrain2-ytraintarget2);
mse_val2 = mse(yval2-yvaltarget2);
%% Testing the trained network
data1 = readmatrix('C&F_testingset');
x1 = data1(:,1:8);
y1 = data1(:,9:10);
```

```
xt1 = x1';

yt1 = y1';

ytest = sim(net2,xt1);

%% Visualization for testing

plot(yt1,ytest,'o'); hold on;

plot(0:1,0:1); hold off;

%% Training on final model

data = readmatrix('C&F_fullset');

x2 = data(:,1:8);

y2 = data(:,9:10);

xt2 = x2';

yt2 = y2';

net3 = feedforwardnet(hiddenlayerSize2);

net3.divideParam.trainRatio = 100/100;

net3.divideParam.testRatio = 0/100;

net3.divideParam.valRatio = 0/100;

[net3,tr3] = train(net3,xt2,yt2);

%% Results of the final model

ytrain3 = net3(xt2(:,tr3.trainInd));

ytraintarget3 = yt2(tr3.trainInd);

rmse_train3 = sqrt(mse(ytrain2-ytraintarget2));

mse_tr3 = mse(ytrain3-ytraintarget3);

%% Sensitivity analysis weight method

w1 = net3.IW{1} %the input-to-hidden layer weights

w2 = net3.LW{2} %the hidden-to-output layer weights

b1 = net3.b{1} %the input-to-hidden layer bias

b2 = net3.b{2}  %the hidden-to-output layer bias
```

Script for model C+F(C) from Group II

```
data = readmatrix('C&F_trainingset');

x = data(:,1:8);

y = data(:,9);

xt = x';

yt = y';

hiddenlayerSize = 8;

net0 = feedforwardnet(hiddenlayerSize);
```

```matlab
net0.divideParam.trainRatio = 85/100;

net0.divideParam.testRatio = 0/100;

net0.divideParam.valRatio = 15/100;

[net0,tr0] = train(net0,xt,yt);
%% Results of the initial model
ytrain0 = net0(xt(:,tr0.trainInd));

ytraintarget0 = yt(tr0.trainInd);

perf_tr0 = mse(ytrain0-ytraintarget0);

yval0 = net0(xt(:,tr0.valInd));

yvaltarget0 = yt(tr0.valInd);

perf_val0 = mse(yval0-yvaltarget0);

mae_tr0 = mae(ytrain0-ytraintarget0);

mae_val0 = mae(yval0-yvaltarget0);

rmse_tr0 = sqrt(perf_tr0);

rmse_val0 = sqrt(perf_val0);
%% Optimization of the network architecture
for i=1:24

    hiddenLayerSize = i;

    net = feedforwardnet(hiddenLayerSize);

    net.divideParam.trainRatio = 85/100;

    net.divideParam.testRatio = 0/100;

    net.divideParam.valRatio = 15/100;

    [net,tr] = train(net,xt,yt);

    ytrain = net(xt(:,tr.trainInd));

    ytraintarget = yt(tr.trainInd);

    rmse_train(i) = sqrt(mse(ytrain-ytraintarget));

    yval = net(xt(:,tr.valInd));

    yvaltarget = yt(tr.valInd);

    rmse_val(i) = sqrt(mse(yval-yvaltarget));
end
%% Optimization plot
trainmse01 = plot(1:24,rmse_train); hold on;

trainmse02 = plot(1:24,rmse_val); hold off;
%% Training the optimized network
hiddenlayerSize1 = 10;

net1 = feedforwardnet(hiddenlayerSize1);
```

```matlab
net1.divideParam.trainRatio = 85/100;

net1.divideParam.testRatio = 0/100;

net1.divideParam.valRatio = 15/100;

[net1,tr1] = train(net1,xt,yt);

%% Results of the optimized model

ytrain1 = net1(xt(:,tr1.trainInd));

ytraintarget1 = yt(tr1.trainInd);

rmse_train1 = sqrt(mean(ytrain1-ytraintarget1).^2);

yval1 = net1(xt(:,tr1.valInd));

yvaltarget1 = yt(tr1.valInd);

rmse_val1 = sqrt(mean(yval1-yvaltarget1).^2);

mse_tr1 = mean((ytrain1-ytraintarget1).^2);

mse_val1 = mean((yval1-yvaltarget1).^2);

%% Training the optimized network#2

hiddenlayerSize2 = 13;

net2 = feedforwardnet(hiddenlayerSize2);

net2.divideParam.trainRatio = 85/100;

net2.divideParam.testRatio = 0/100;

net2.divideParam.valRatio = 15/100;

[net2,tr2] = train(net2,xt,yt);

%% Results of the optimized model

ytrain2 = net2(xt(:,tr2.trainInd));

ytraintarget2 = yt(tr2.trainInd);

rmse_tr2 = sqrt(mse(ytrain2-ytraintarget2));

yval2 = net2(xt(:,tr2.valInd));

yvaltarget2 = yt(tr2.valInd);

rmse_val2 = sqrt(mse(yval2-yvaltarget2));

mse_tr2 = mse(ytrain2-ytraintarget2);

mse_val2 = mse(yval2-yvaltarget2);

%% Testing the trained network

data1 = readmatrix('C&F_testingset');

x1 = data1(:,1:8);

y1 = data1(:,9);

xt1 = x1';

yt1 = y1';

ytest = sim(net2,xt1);
```

```
%% Results of testing vs training
plot(ytrain2,ytraintarget2,'x');hold on;
plot(yt1,ytest,'o');hold on;
plot(0:1,0:1);hold off;
%% Visualization for testing
plot(yt1,ytest,'o'); hold on;
plot(0:1,0:1); hold off;
%% Training on final model
data = readmatrix('C&F_fullset');
x2 = data(:,1:8);
y2 = data(:,9);
xt2 = x2';
yt2 = y2';
net3 = feedforwardnet(hiddenlayerSize2);
net3.divideParam.trainRatio = 100/100;
net3.divideParam.testRatio = 0/100;
net3.divideParam.valRatio = 0/100;
[net3,tr3] = train(net3,xt2,yt2);
%% Results of the final model
ytrain3 = net3(xt2(:,tr3.trainInd));
ytraintarget3 = yt2(tr3.trainInd);
rmse_train3 = sqrt(mse(ytrain2-ytraintarget2));
mse_tr3 = mse(ytrain3-ytraintarget3);
%% Visualization for final model
plot(ytraintarget3,ytrain3,'o'); hold on;
plot(0:1,0:1); hold off;
%% Sensitivity analysis weight method
w1 = net3.IW{1} %the input-to-hidden layer weights
w2 = net3.LW{2} %the hidden-to-output layer weights
b1 = net3.b{1} %the input-to-hidden layer bias
b2 = net3.b{2}  %the hidden-to-output layer bias
```

Script for model C+F(F) from Group II

```
data = readmatrix('C&F_trainingset');
x = data(:,1:8);
y = data(:,10);
```

```
xt = x';

yt = y';

hiddenlayerSize = 8;

net0 = feedforwardnet(hiddenlayerSize);

net0.divideParam.trainRatio = 85/100;

net0.divideParam.testRatio = 0/100;

net0.divideParam.valRatio = 15/100;

[net0,tr0] = train(net0,xt,yt);

%% Results of the initial model

ytrain0 = net0(xt(:,tr0.trainInd));

ytraintarget0 = yt(tr0.trainInd);

perf_tr0 = mse(ytrain0-ytraintarget0);

yval0 = net0(xt(:,tr0.valInd));

yvaltarget0 = yt(tr0.valInd);

perf_val0 = mse(yval0-yvaltarget0);

mae_tr0 = mae(ytrain0-ytraintarget0);

mae_val0 = mae(yval0-yvaltarget0);

rmse_tr0 = sqrt(perf_tr0);

rmse_val0 = sqrt(perf_val0);

%% Optimization of the network architecture

for i=1:24

    hiddenLayerSize = i;

    net = feedforwardnet(hiddenLayerSize);

    net.divideParam.trainRatio = 85/100;

    net.divideParam.testRatio = 0/100;

    net.divideParam.valRatio = 15/100;

    [net,tr] = train(net,xt,yt);

    ytrain = net(xt(:,tr.trainInd));

    ytraintarget = yt(tr.trainInd);

    rmse_train(i) = sqrt(mse(ytrain-ytraintarget));

    yval = net(xt(:,tr.valInd));

    yvaltarget = yt(tr.valInd);

    rmse_val(i) = sqrt(mse(yval-yvaltarget));

end

%% Optimization plot

trainmse01 = plot(1:24,rmse_train); hold on;
```

```matlab
trainmse02 = plot(1:24,rmse_val); hold off;
%% Training the optimized network
hiddenlayerSize1 = 10;
net1 = feedforwardnet(hiddenlayerSize1);
net1.divideParam.trainRatio = 85/100;
net1.divideParam.testRatio = 0/100;
net1.divideParam.valRatio = 15/100;
[net1,tr1] = train(net1,xt,yt);
%% Results of the optimized model
ytrain1 = net1(xt(:,tr1.trainInd));
ytraintarget1 = yt(tr1.trainInd);
rmse_train1 = sqrt(mean(ytrain1-ytraintarget1).^2);
yval1 = net1(xt(:,tr1.valInd));
yvaltarget1 = yt(tr1.valInd);
rmse_val1 = sqrt(mean(yval1-yvaltarget1).^2);
mse_tr1 = mean((ytrain1-ytraintarget1).^2);
mse_val1 = mean((yval1-yvaltarget1).^2);
%% Training the optimized network#2
hiddenlayerSize2 = 13;
net2 = feedforwardnet(hiddenlayerSize2);
net2.divideParam.trainRatio = 85/100;
net2.divideParam.testRatio = 0/100;
net2.divideParam.valRatio = 15/100;
[net2,tr2] = train(net2,xt,yt);
%% Results of the optimized model
ytrain2 = net2(xt(:,tr2.trainInd));
ytraintarget2 = yt(tr2.trainInd);
rmse_tr2 = sqrt(mse(ytrain2-ytraintarget2));
yval2 = net2(xt(:,tr2.valInd));
yvaltarget2 = yt(tr2.valInd);
rmse_val2 = sqrt(mse(yval2-yvaltarget2));
mse_tr2 = mse(ytrain2-ytraintarget2);
mse_val2 = mse(yval2-yvaltarget2);
%% Testing the trained network
data1 = readmatrix('C&F_testingset');
x1 = data1(:,1:8);
```

```matlab
y1 = data1(:,10);

xt1 = x1';

yt1 = y1';

ytest = sim(net1,xt1);
%% Results of testing vs training
plot(ytrain1,ytraintarget1,'x');hold on;

plot(yt1,ytest,'o');hold on;

plot(0:1,0:1);hold off;
%% Visualization for testing
plot(yt1,ytest,'o'); hold on;

plot(0:1,0:1); hold off;
%% Training on final model
data = readmatrix('C&F_fullset');

x2 = data(:,1:8);

y2 = data(:,10);

xt2 = x2';

yt2 = y2';

net3 = feedforwardnet(hiddenlayerSize1);

net3.divideParam.trainRatio = 100/100;

net3.divideParam.testRatio = 0/100;

net3.divideParam.valRatio = 0/100;

[net3,tr3] = train(net3,xt2,yt2);
%% Results of the final model
ytrain3 = net3(xt2(:,tr3.trainInd));

ytraintarget3 = yt2(tr3.trainInd);

rmse_train3 = sqrt(mse(ytrain2-ytraintarget2));

mse_tr3 = mse(ytrain3-ytraintarget3);
%% Sensitivity analysis weight method
w1 = net3.IW{1} %the input-to-hidden layer weights

w2 = net3.LW{2} %the hidden-to-output layer weights

b1 = net3.b{1} %the input-to-hidden layer bias

b2 = net3.b{2}  %the hidden-to-output layer bias
```

B5. Results for prescribed models – Group I
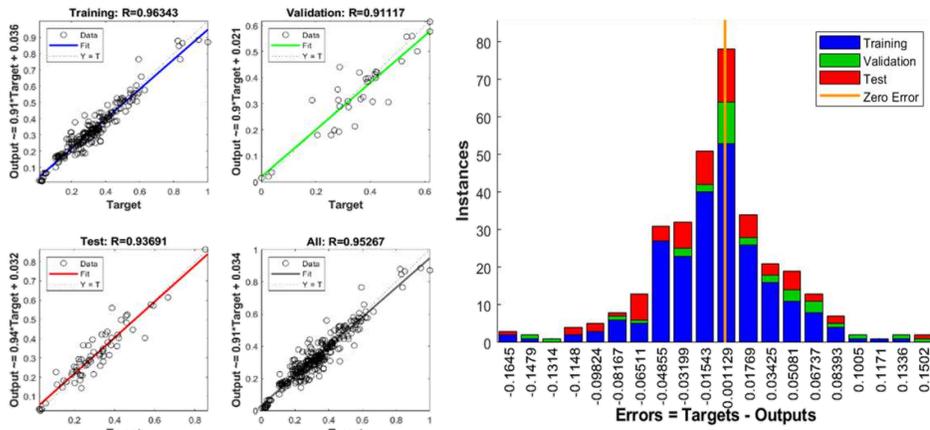
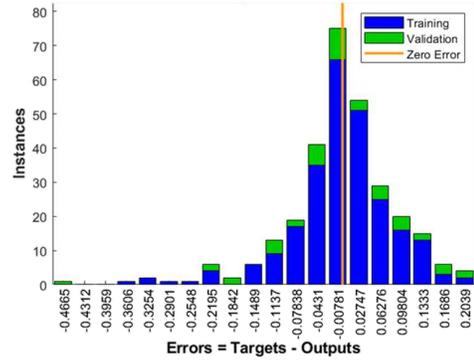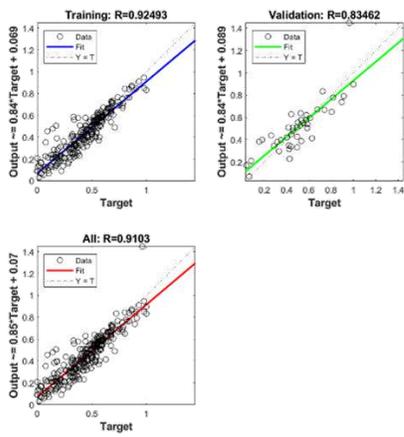*Figure B5.1* Regression coefficient and error histogram for model COMP_70_10_20-20
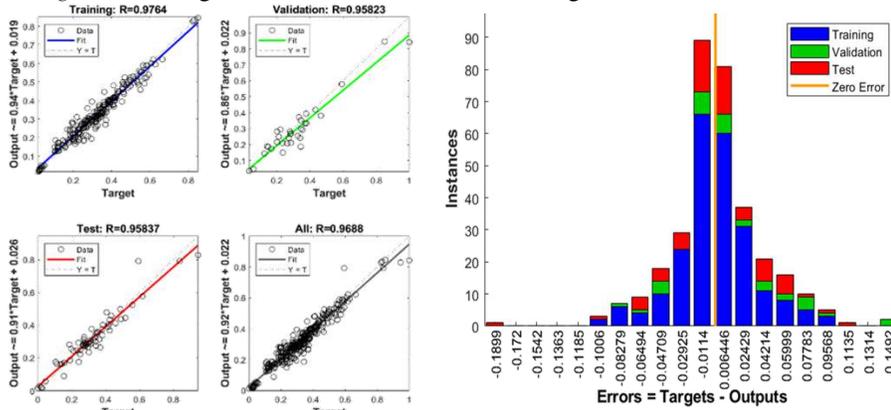
Figure B5.2. Regression coefficient and error histogram for model COMP_70_10_20-41
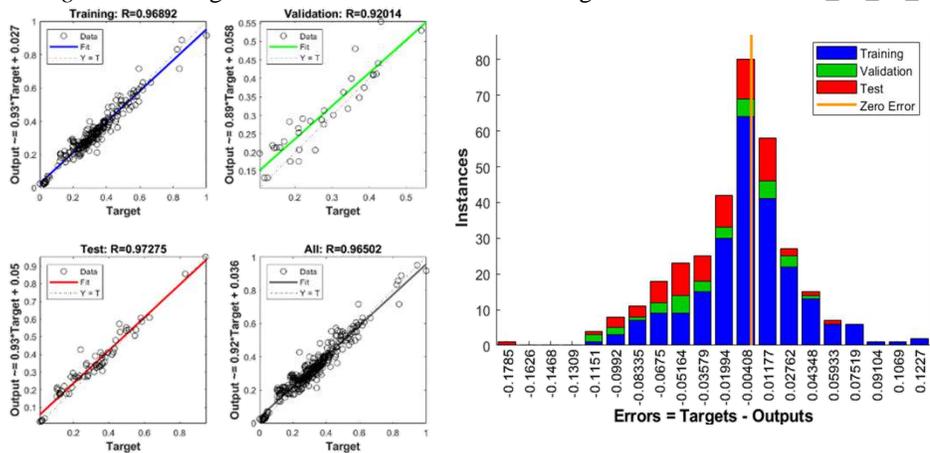
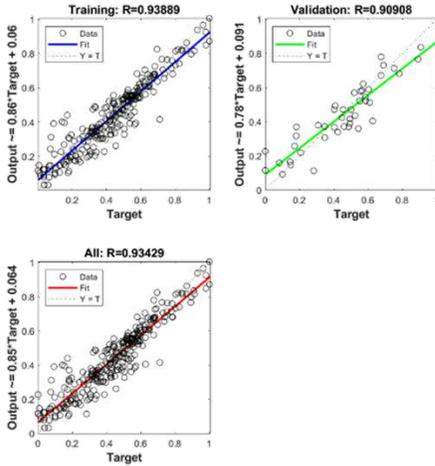*Figure B5.3.* Regression coefficient and error histogram for model COMP_70_10_20-60
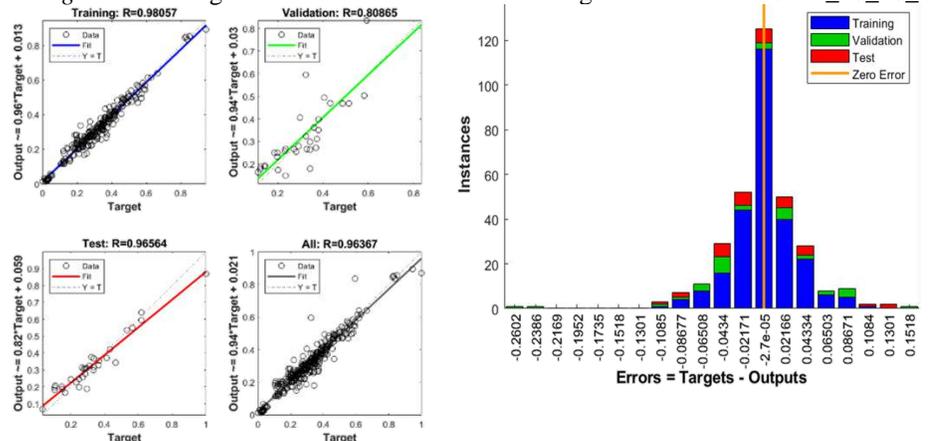
Figure B5.4 Regression coefficient and error histogram for model COMP_80_10_10-20
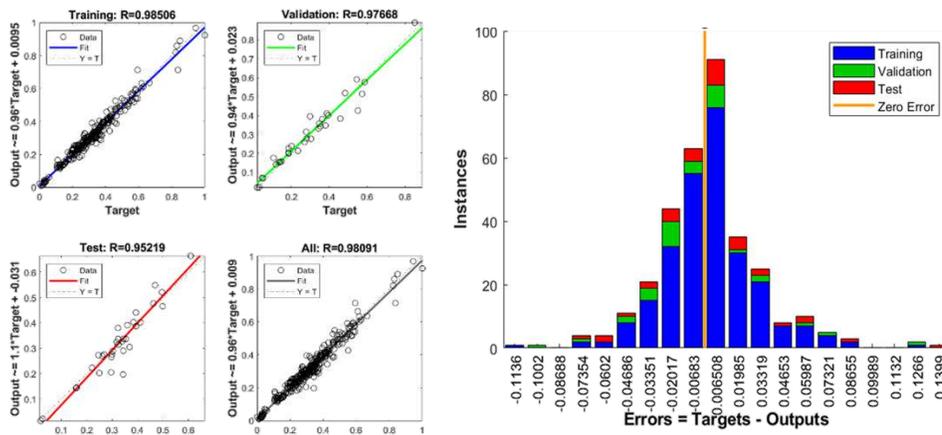
Figure B5.5 Regression coefficient and error histogram for model COMP_80_10_10-41
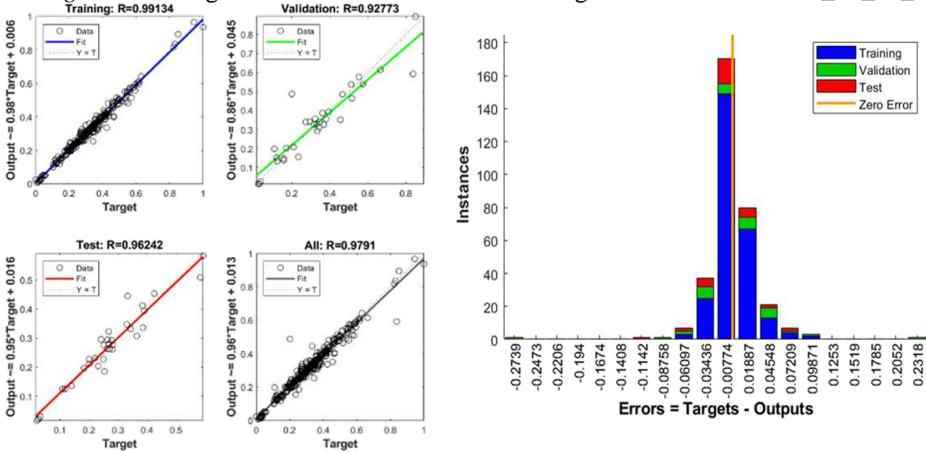
Figure B5.6 Regression coefficient and error histogram for model COMP_80_10_10-60
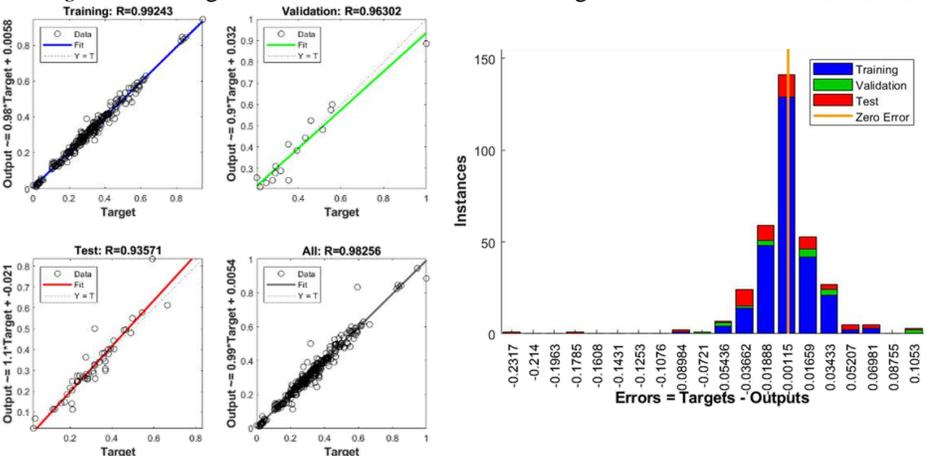
Figure B5.7 Regression coefficient and error histogram for model COMP_80_5_15-20
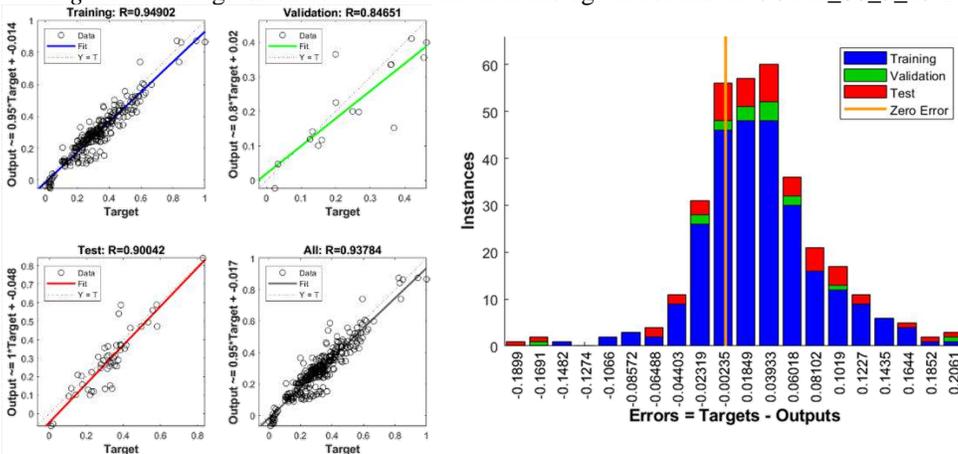
Figure B5.8 Regression coefficient and error histogram for model COMP_80_5_15-41

74
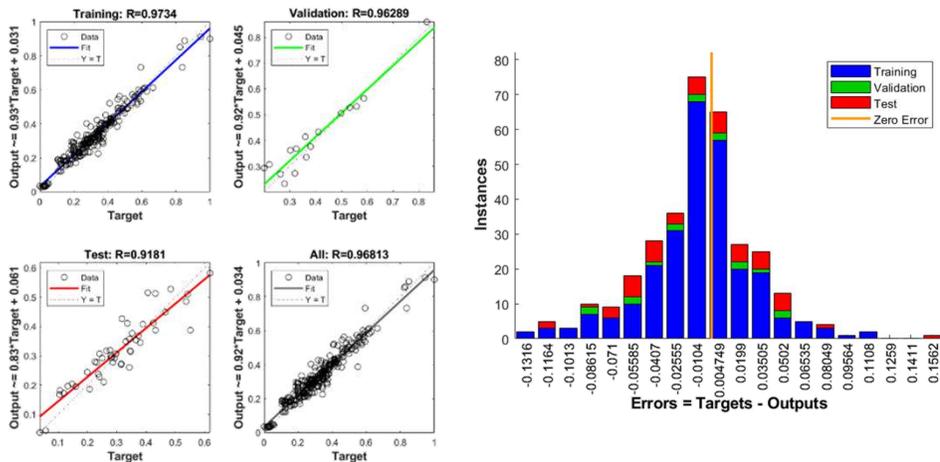
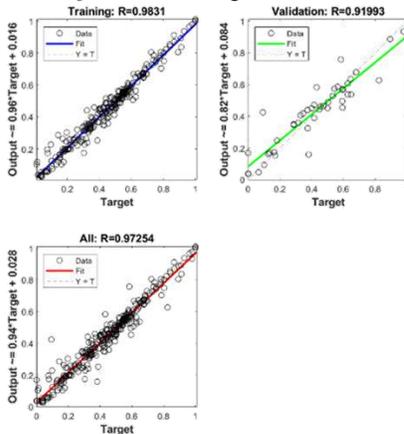*Figure B5.9* Regression coefficient and error histogram for model COMP_80_5_15-60
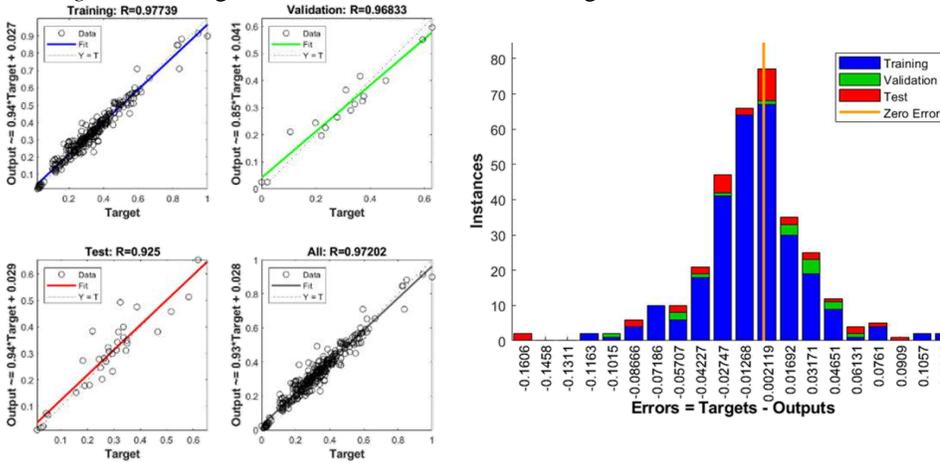
Figure B5.10 Regression coefficient and error histogram for model COMP_85_5_10-20
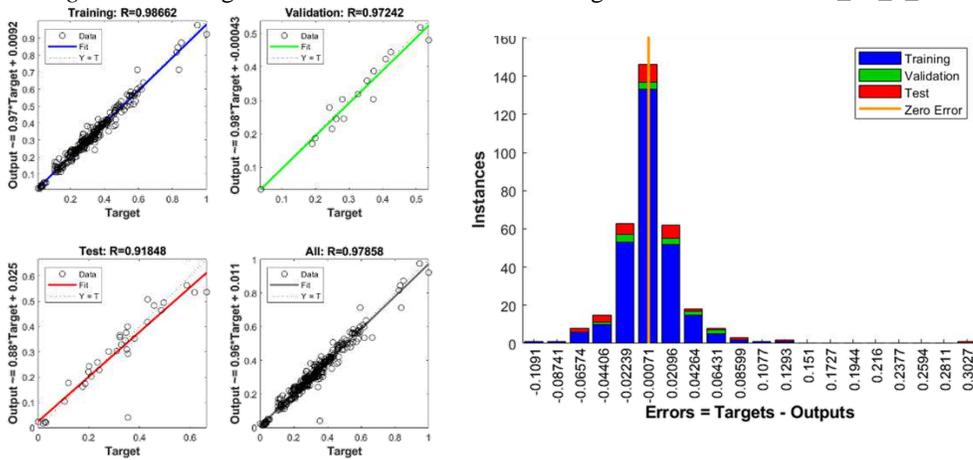
Figure B5.11 Regression coefficient and error histogram for model COMP_85_5_10-41
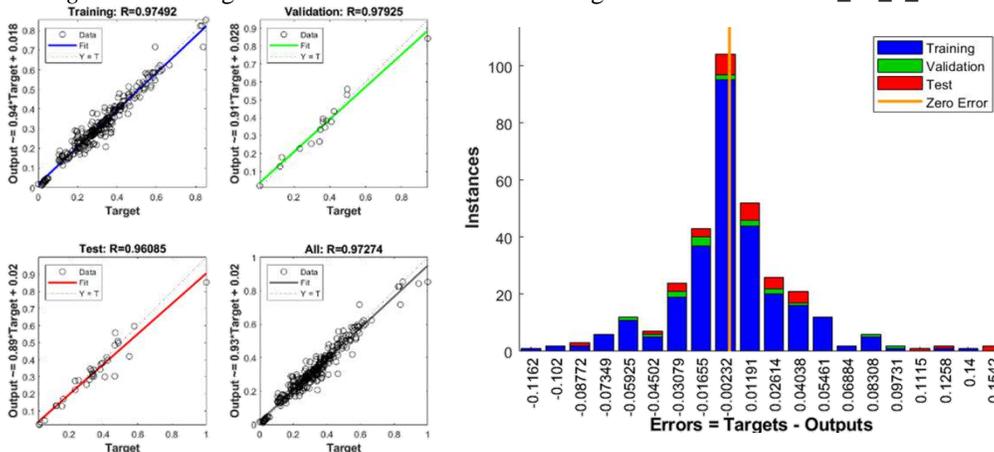
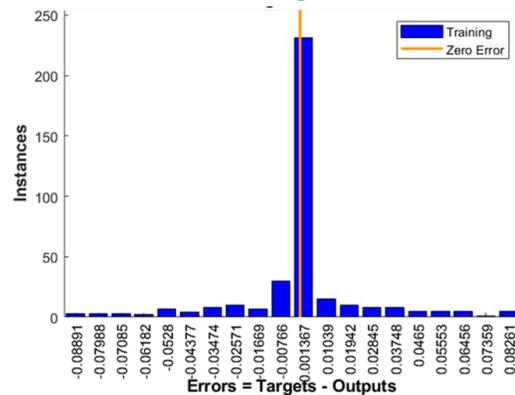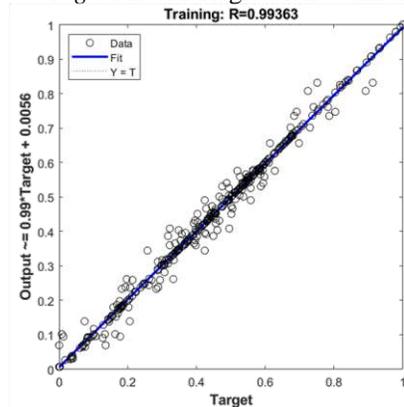*Figure B5.12* Regression coefficient and error histogram for model COMP_85_5_10-60
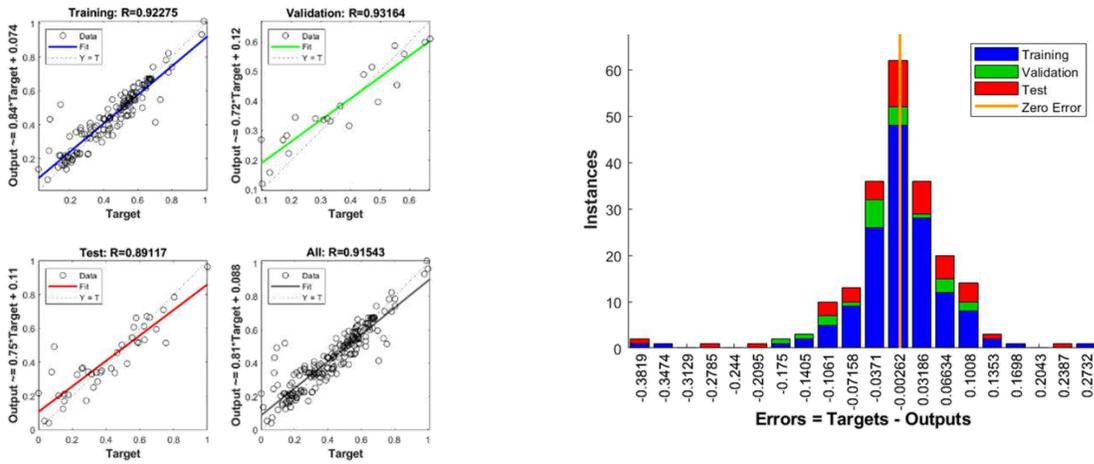
Figure B5.13 Regression coefficient and error histogram for model FLEX_70_10_20-16
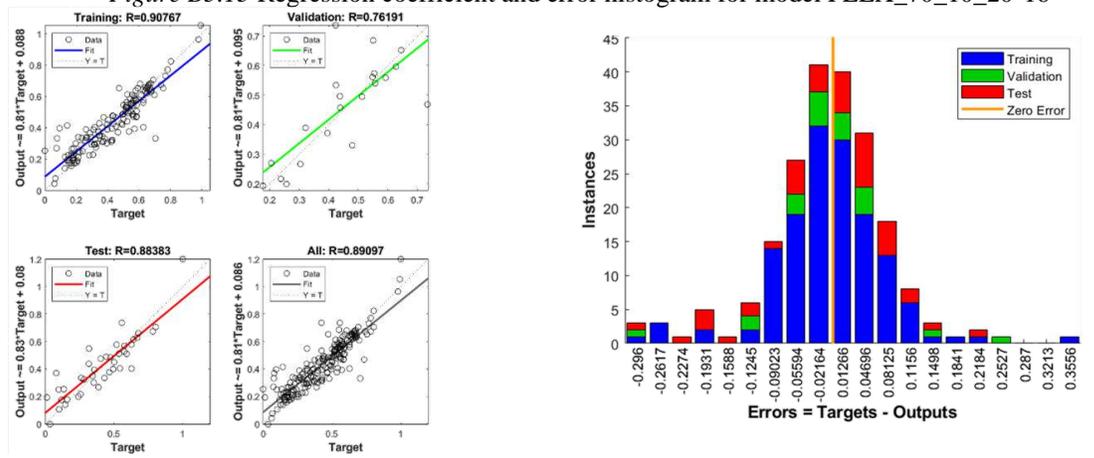
Figure B5.14 Regression coefficient and error histogram for model FLEX_70_10_20-33
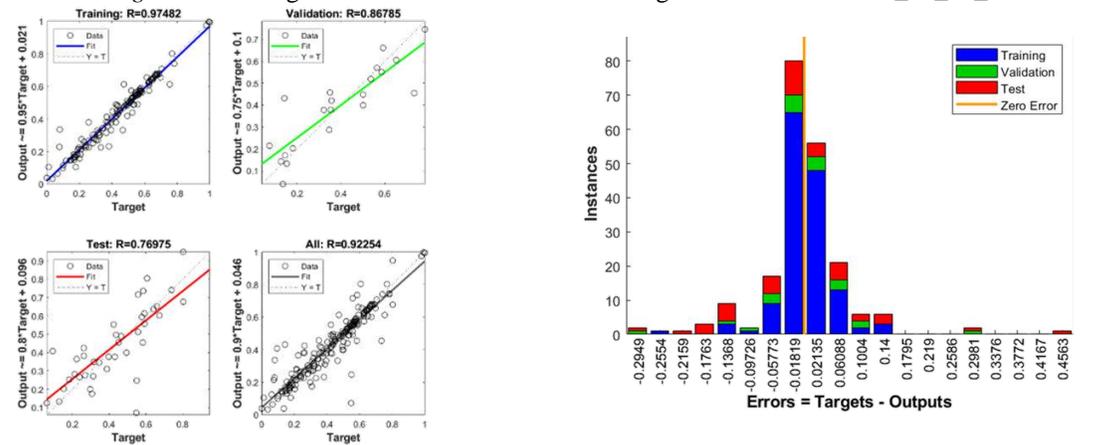
Figure B5.15 Regression coefficient and error histogram for model FLEX_70_10_20-48
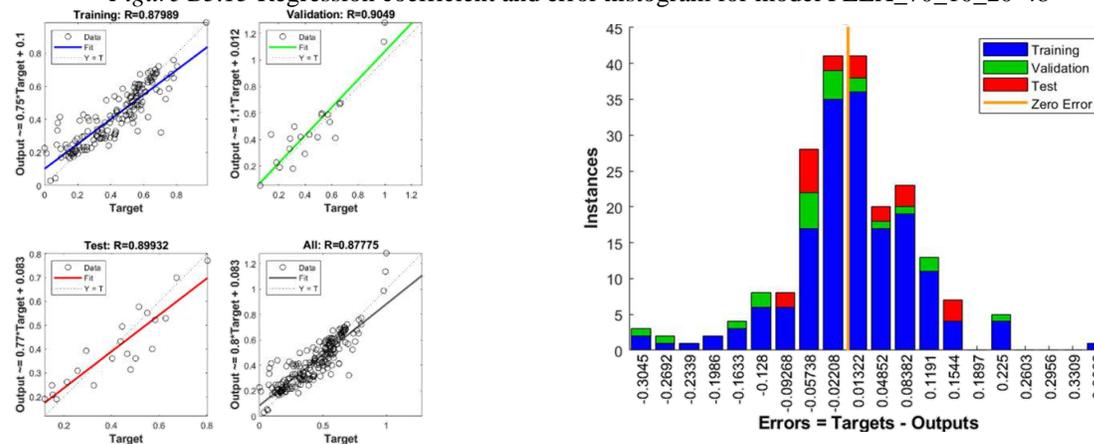
Figure B5.16 Regression coefficient and error histogram for model FLEX_80_10_10-16
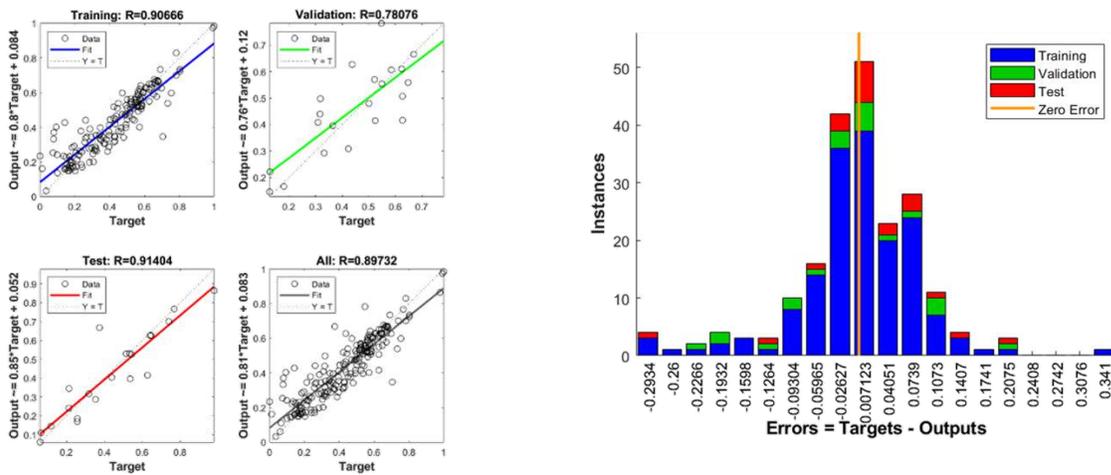
Figure B5.17 Regression coefficient and error histogram for model FLEX_80_10_10-33
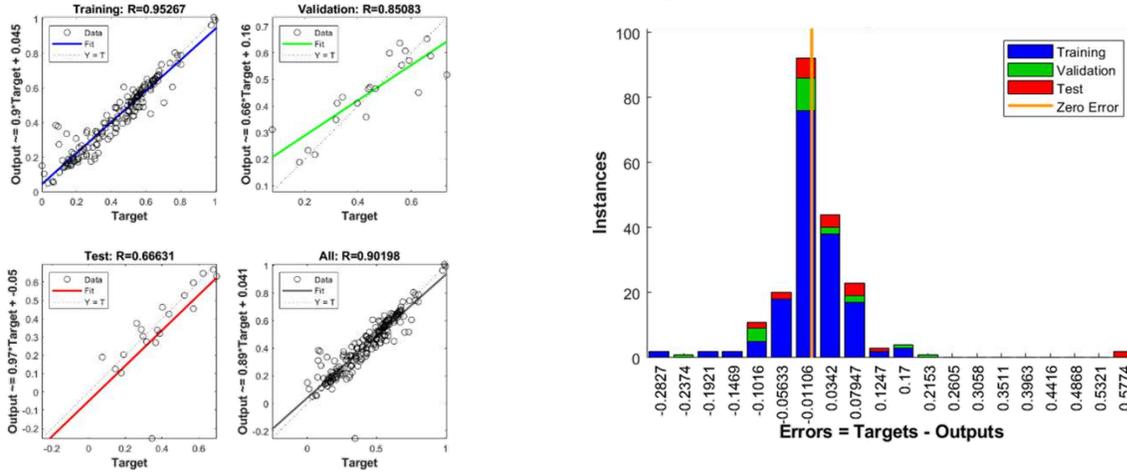
Figure B5.18 Regression coefficient and error histogram for model FLEX_80_10_10-48
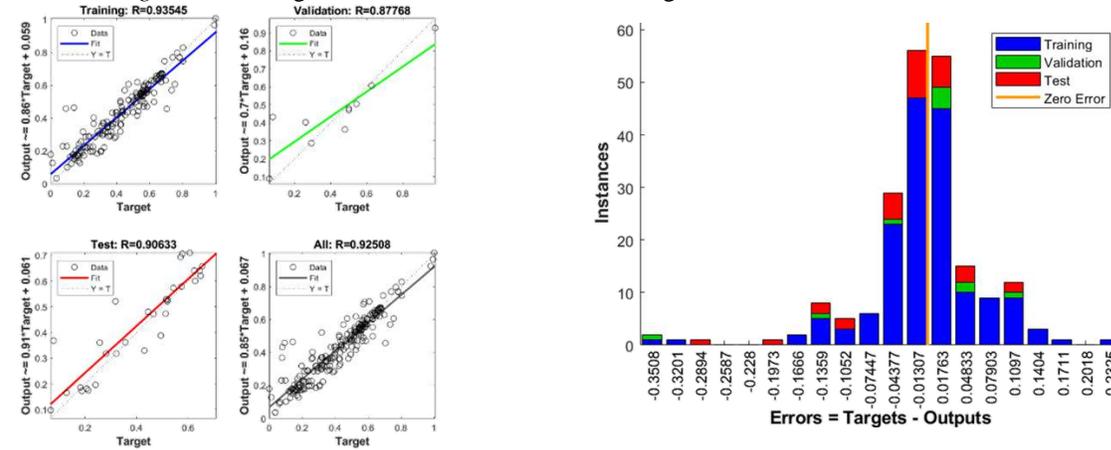
Figure B5.19 Regression coefficient and error histogram for model FLEX_80_5_15-16
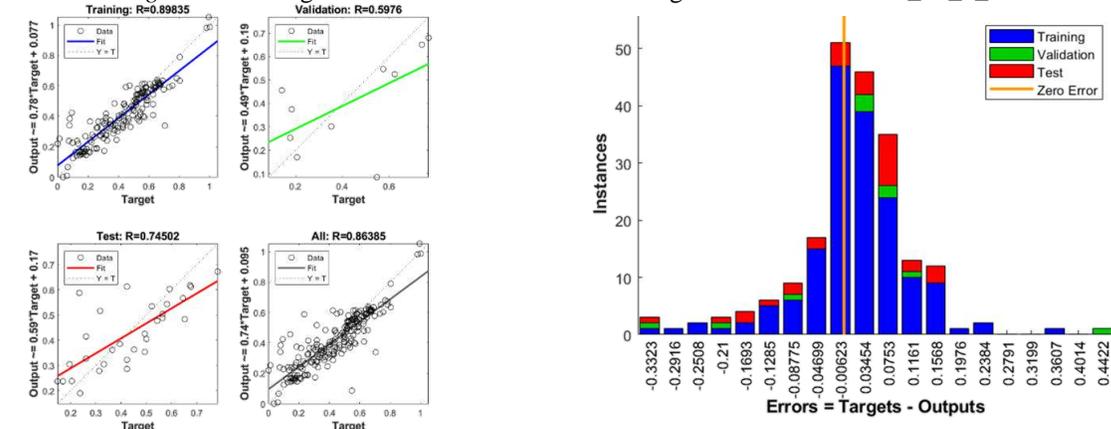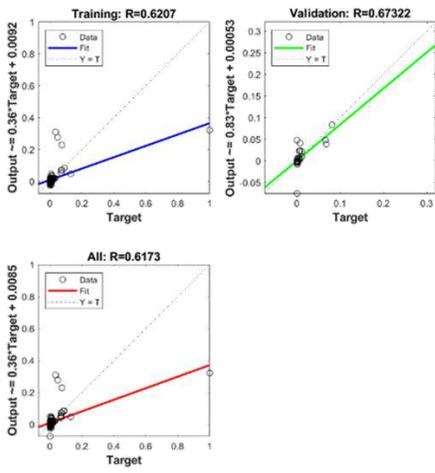

Figure B5.20 Regression coefficient and error histogram for model FLEX_80_5_15-33
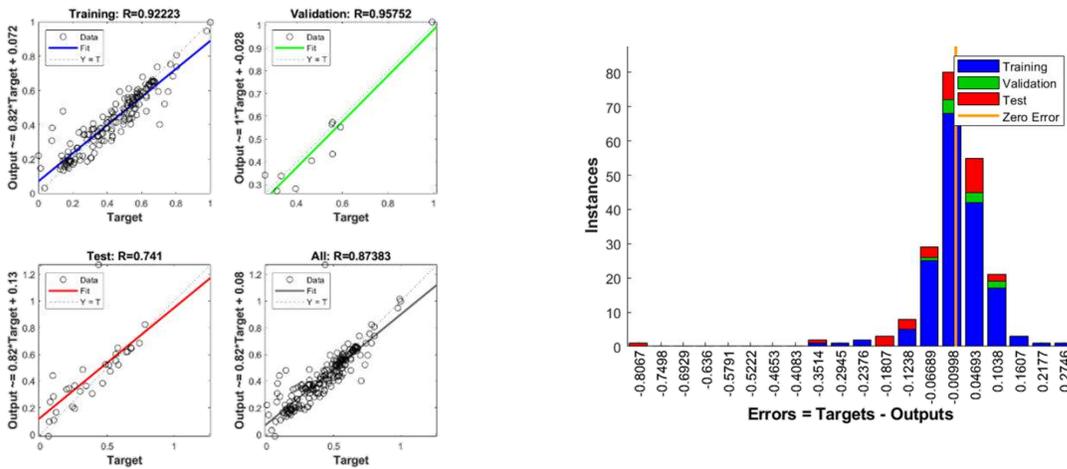
Figure B5.21 Regression coefficient and error histogram for model FLEX_80_5_15-48
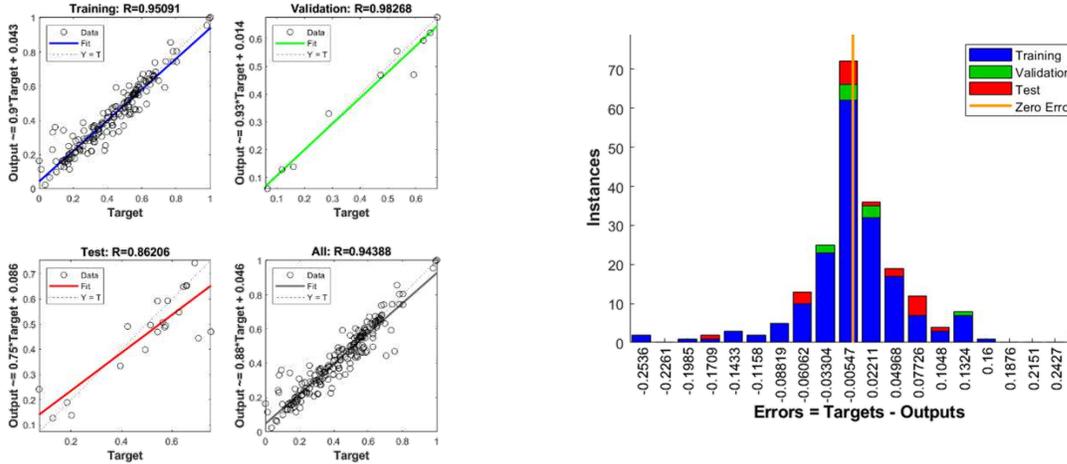
Figure B5.22 Regression coefficient and error histogram for model FLEX_85_5_10-16
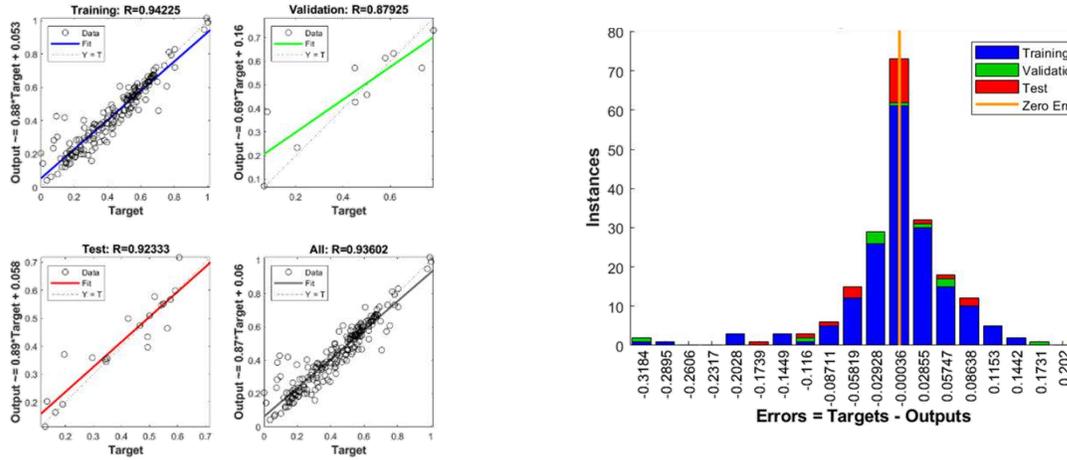
Figure B5.23 Regression coefficient and error histogram for model FLEX_85_5_10-33
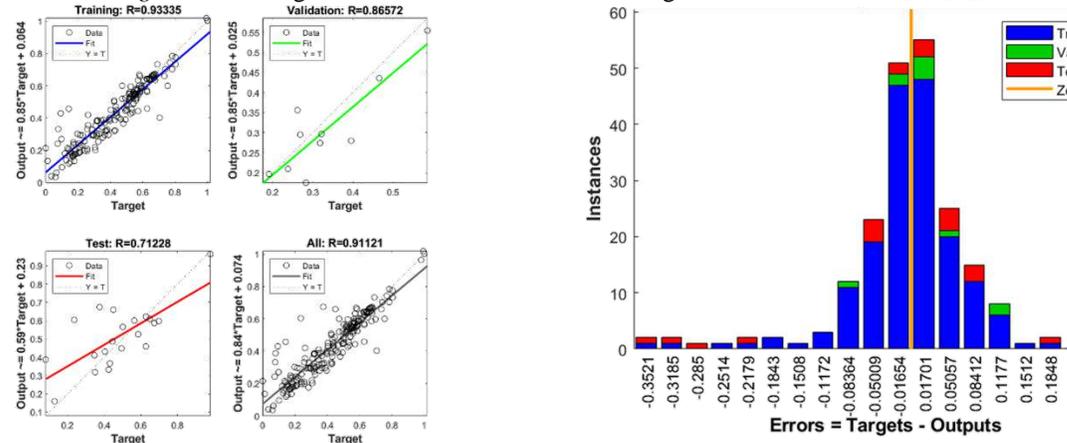
Figure B5.24 Regression coefficient and error histogram for model FLEX_85_5_10-48
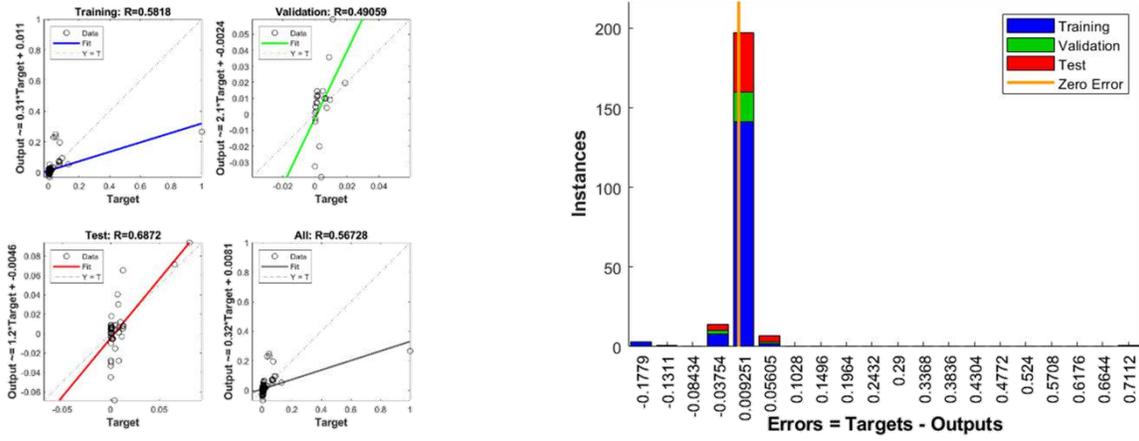
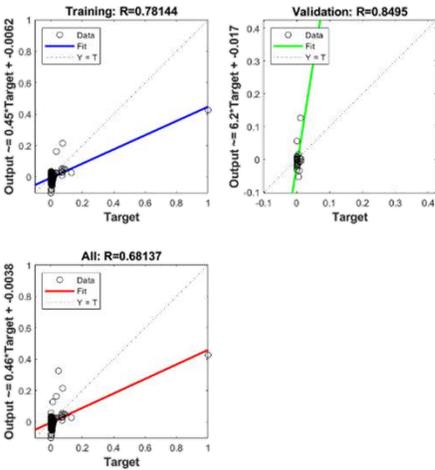*Figure B5.25* Regression coefficient and error histogram for model RES_70_10_20-17
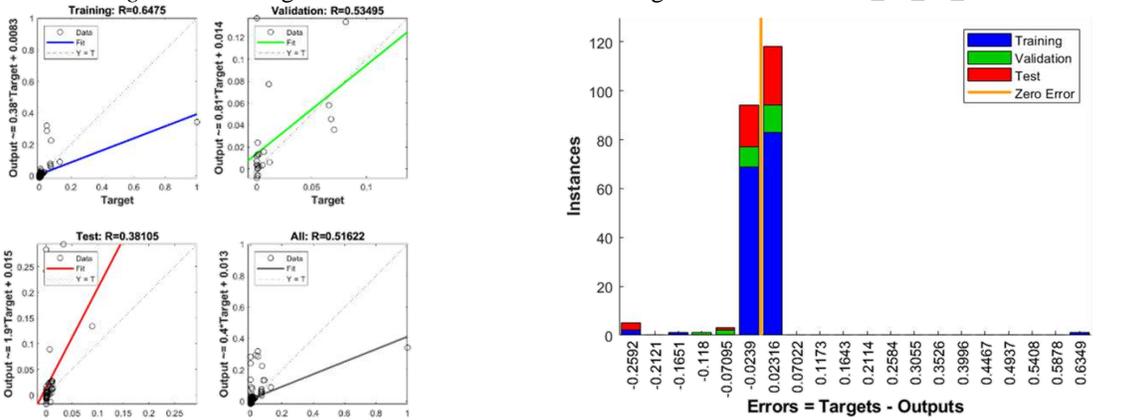
Figure B5.26 Regression coefficient and error histogram for model RES_70_10_20-35
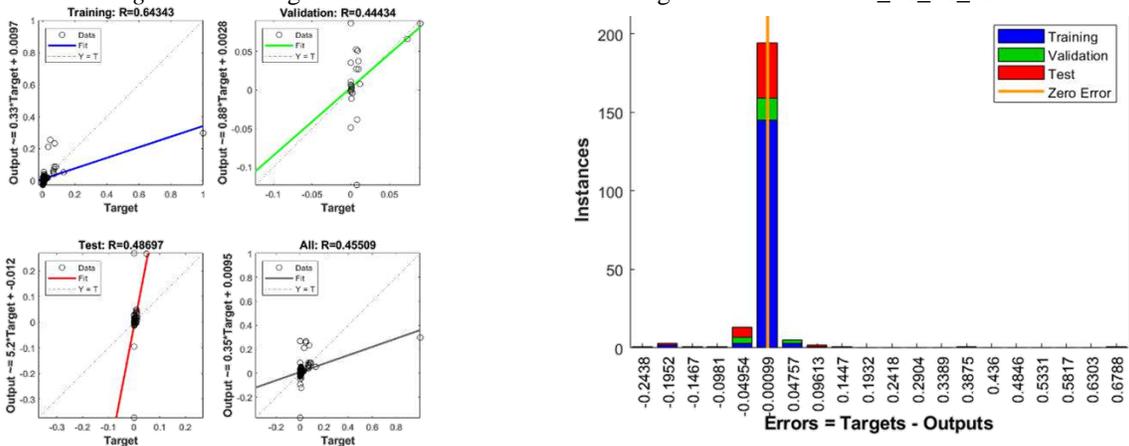
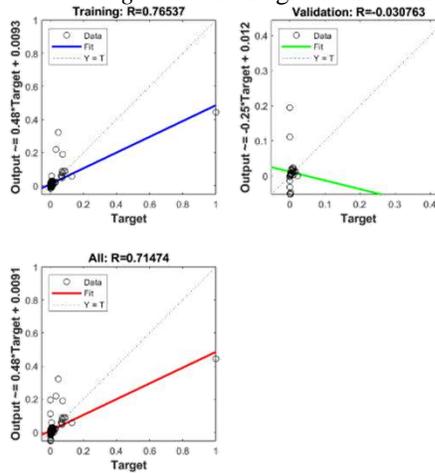*Figure B5.27* Regression coefficient and error histogram for model RES_70_10_20-51
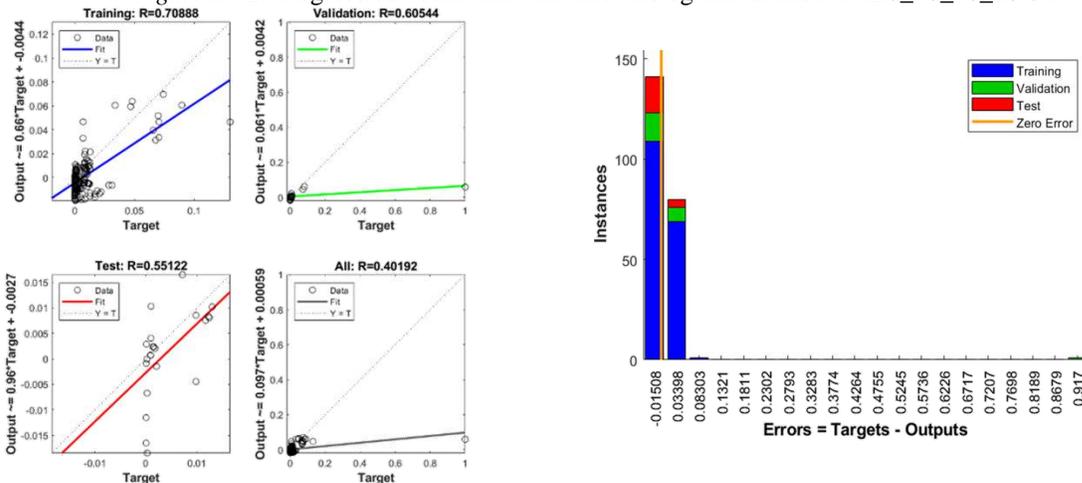
Figure B5.28 Regression coefficient and error histogram for model RES_80_10_10-17
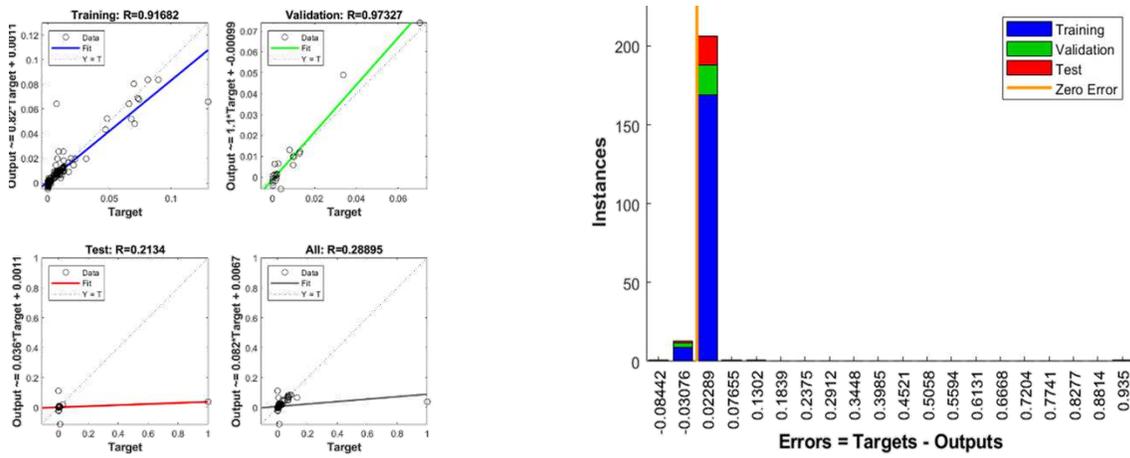
Figure B5.29 Regression coefficient and error histogram for model RES_80_10_10-35
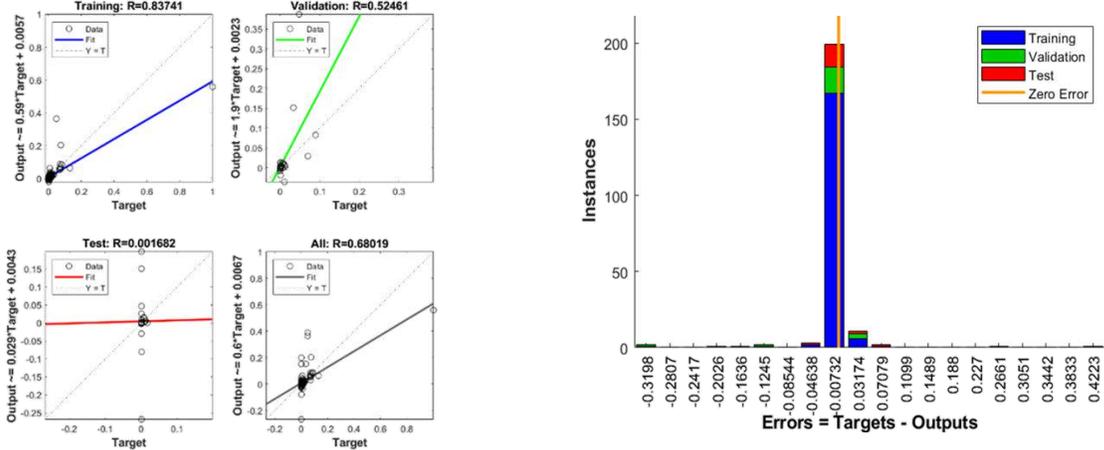
Figure B5.30 Regression coefficient and error histogram for model RES_80_10_10-51
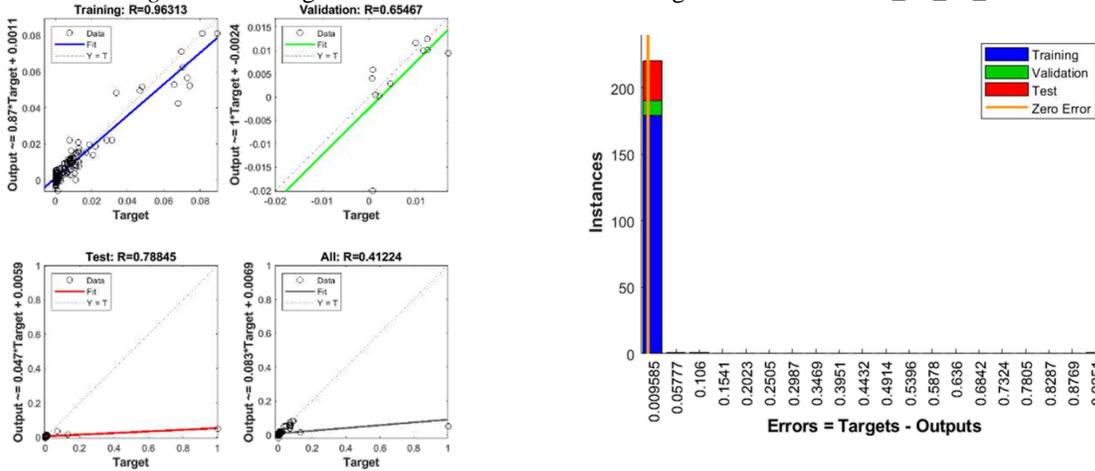
Figure B5.31 Regression coefficient and error histogram for model RES_80_5_15-17
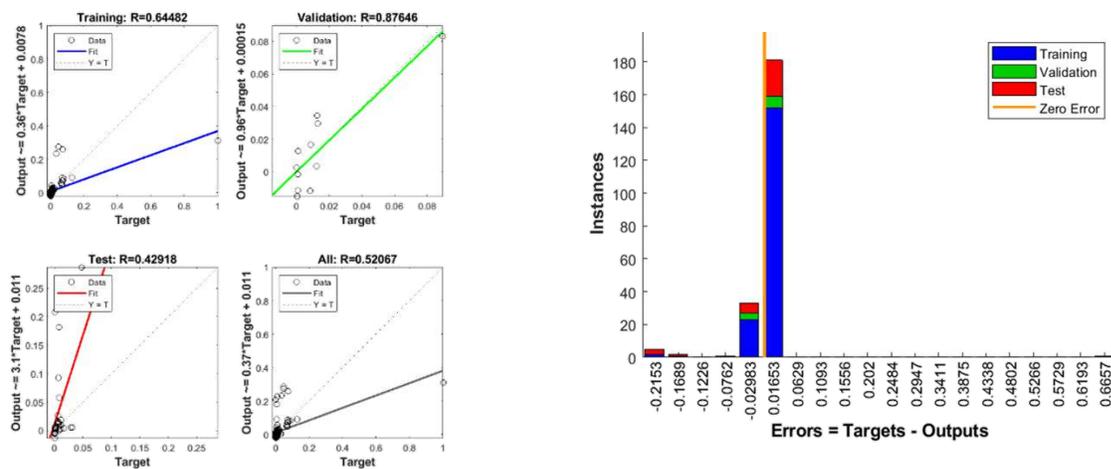
Figure B5.32 Regression coefficient and error histogram for model RES_80_5_15-35
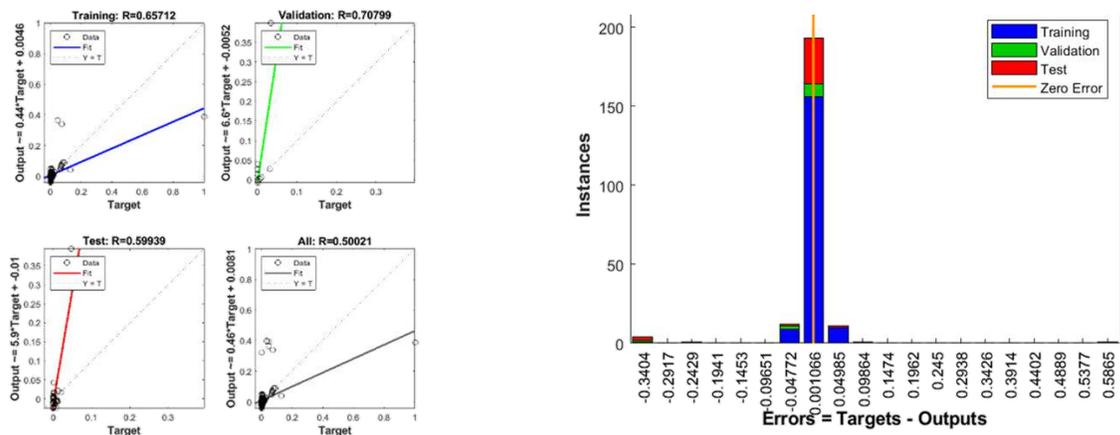
Figure B5.33 Regression coefficient and error histogram for model RES_80_5_15-51
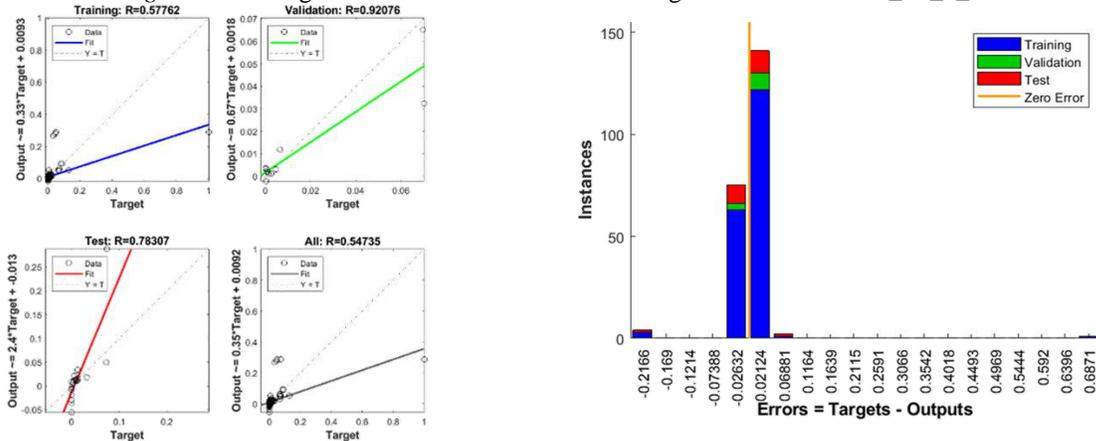
Figure B5.34 Regression coefficient and error histogram for model RES_85_5_10-17
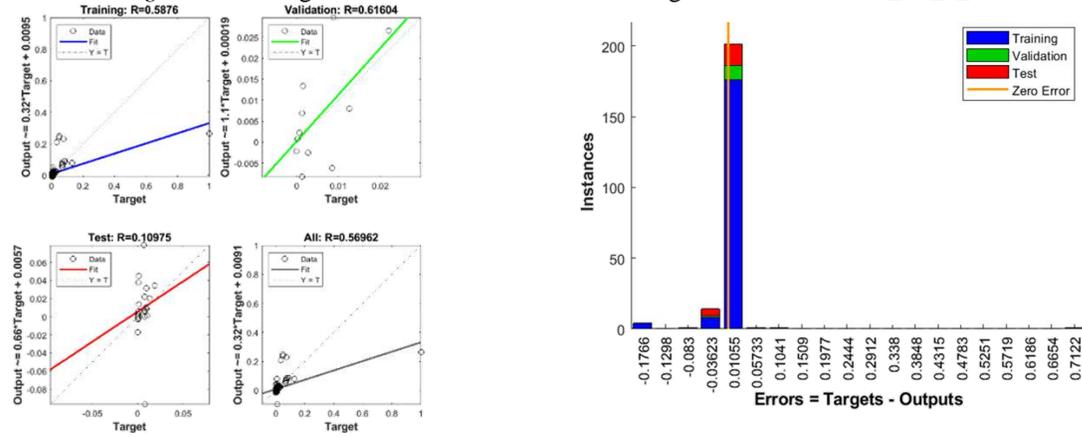
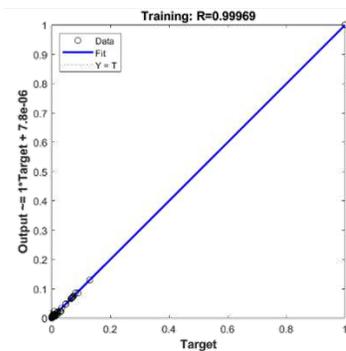*Figure B5.35* Regression coefficient and error histogram for model RES_85_5_10-35
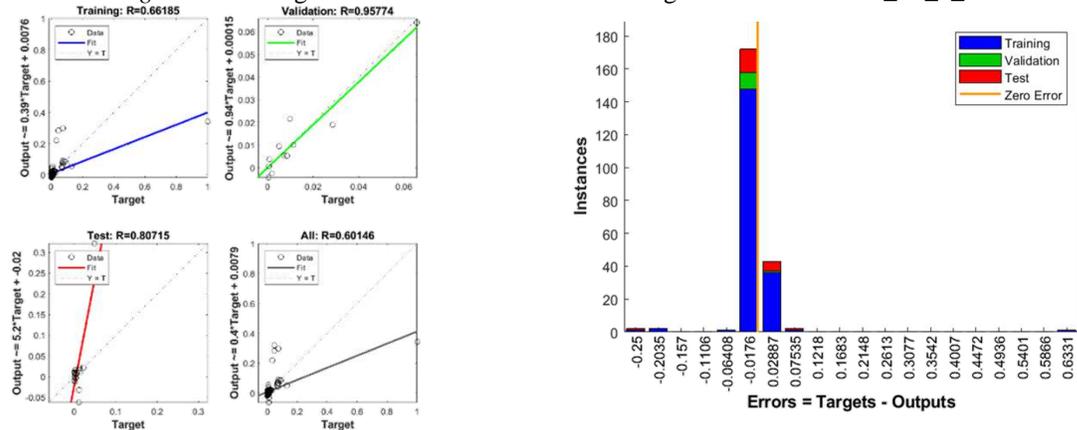
Figure B5.36 Regression coefficient and error histogram for model RES_85_5_10-51
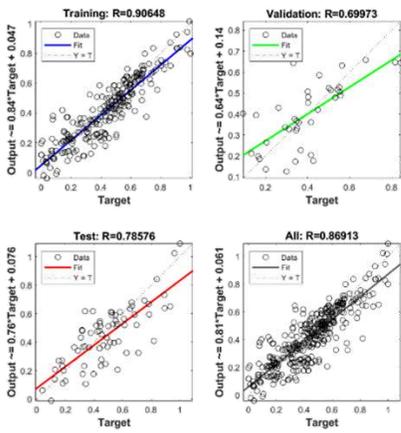
Figure B5.37 Regression coefficient and error histogram for model C+F_70_10_20-11
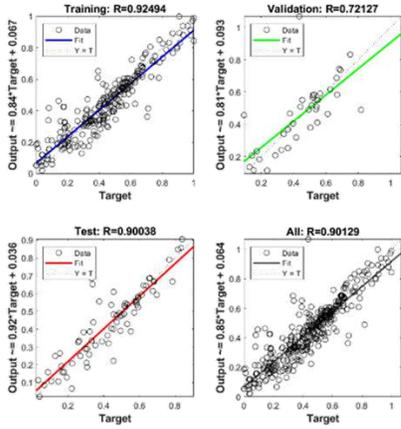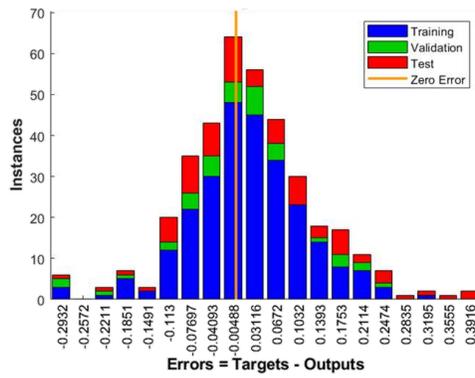
Figure B5.38 Regression coefficient and error histogram for model C+F_70_10_20-23
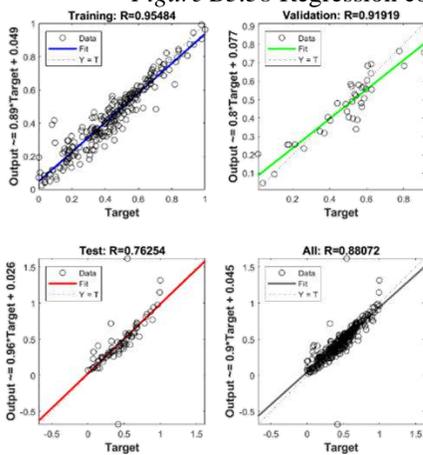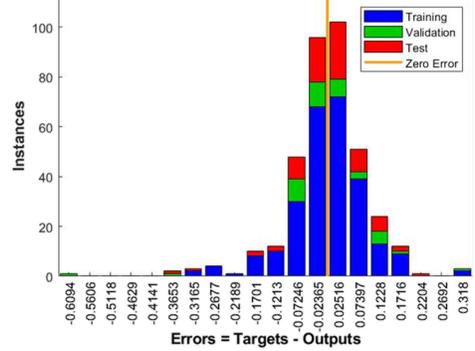
Figure B5.39 Regression coefficient and error histogram for model C+F_70_10_20-33
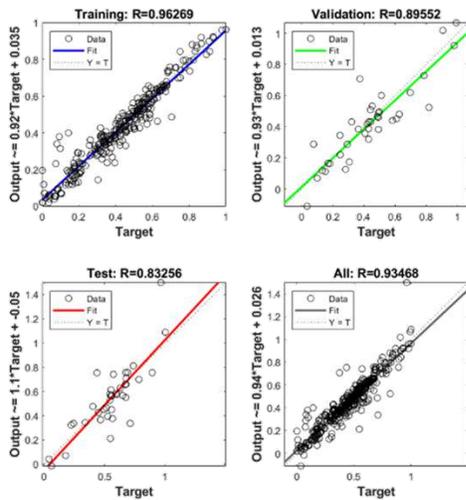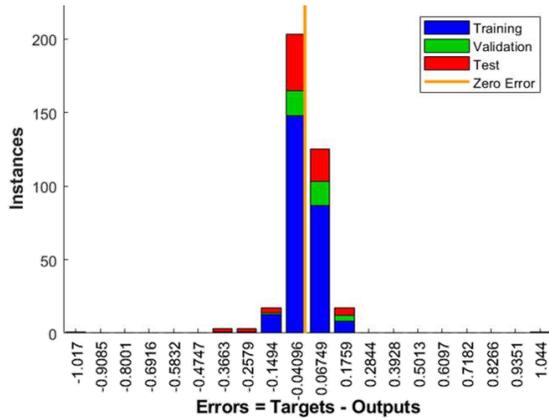
Figure B5.40 Regression coefficient and error histogram for model C+F_80_10_10-11
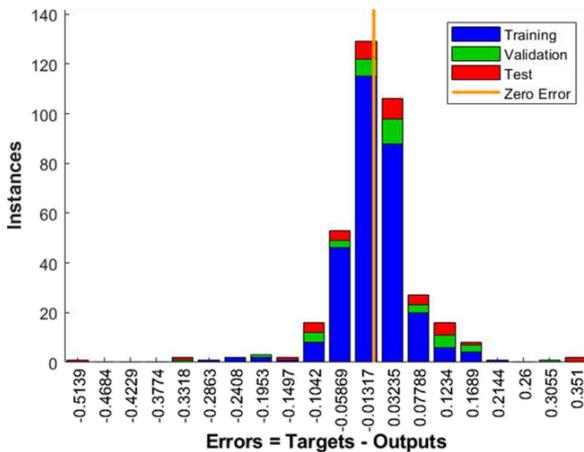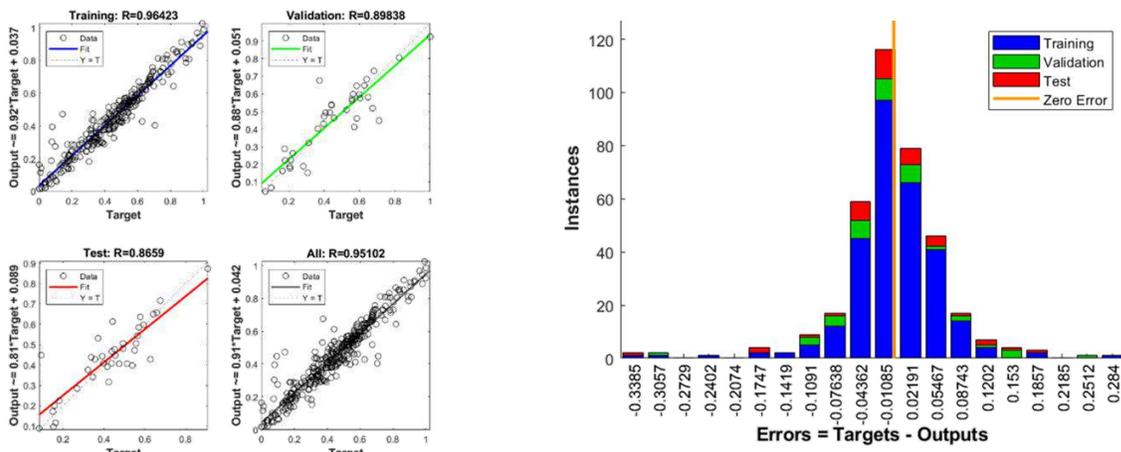
Figure B5.41 Regression coefficient and error histogram for model C+F_80_10_10-23
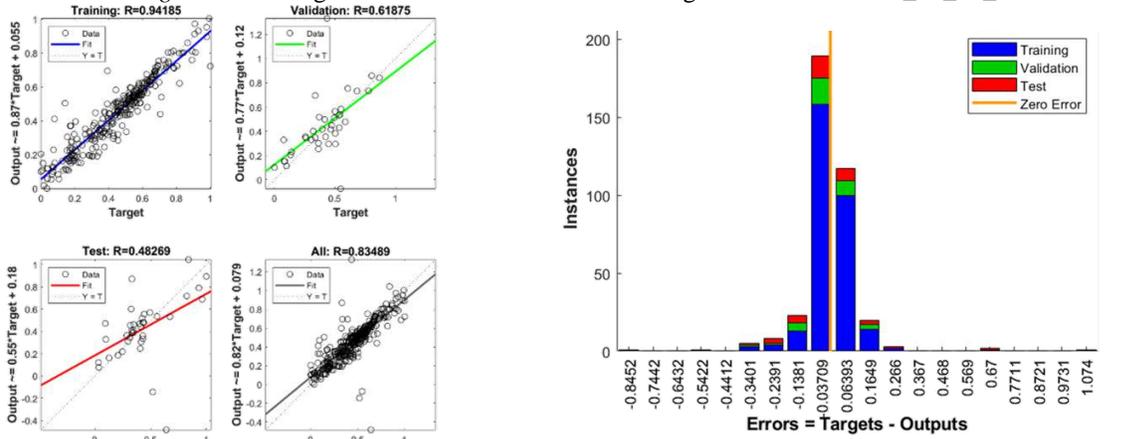
Figure B5.42 Regression coefficient and error histogram for model C+F_80_10_10-33
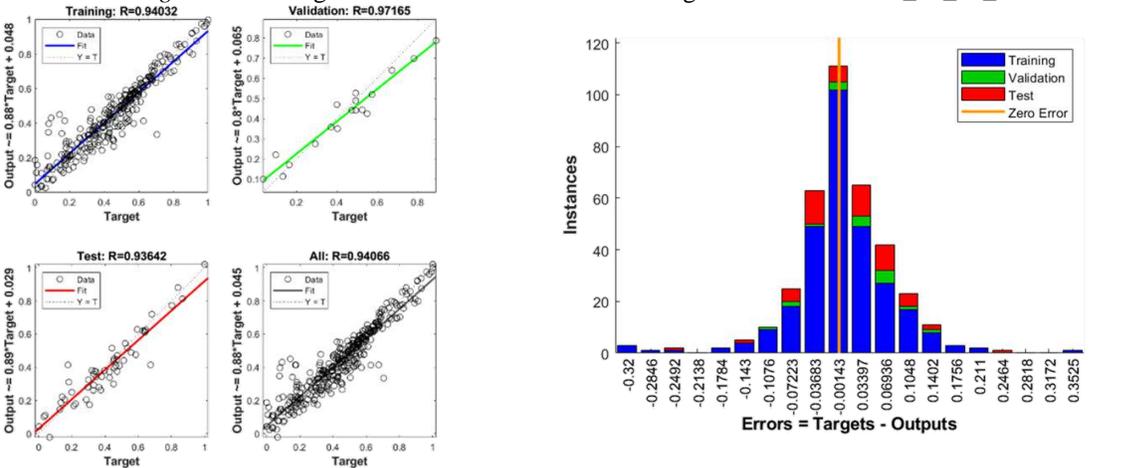
Figure B5.43 Regression coefficient and error histogram for model C+F_80_5_15-11
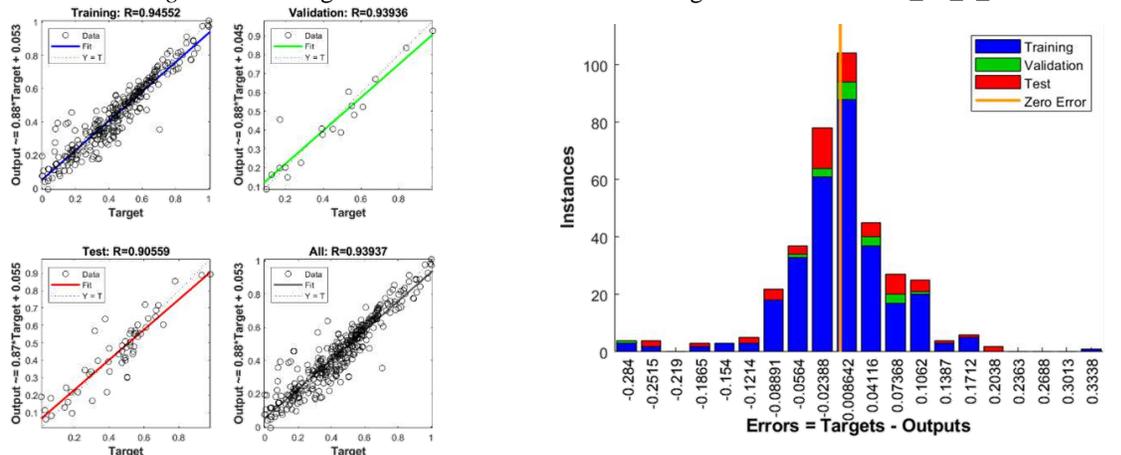
Figure B5.44 Regression coefficient and error histogram for model C+F_80_5_15-23

83
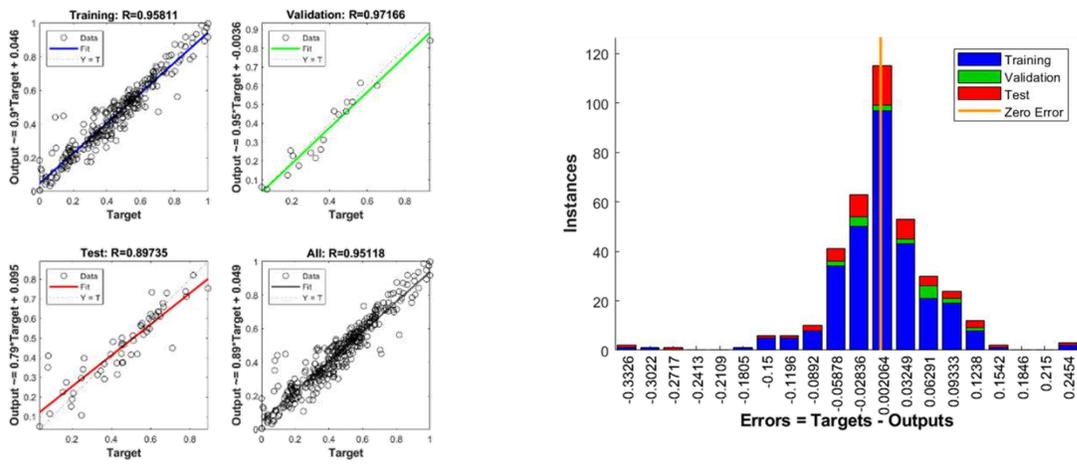
Figure B5.45 Regression coefficient and error histogram for model C+F_80_5_15-33
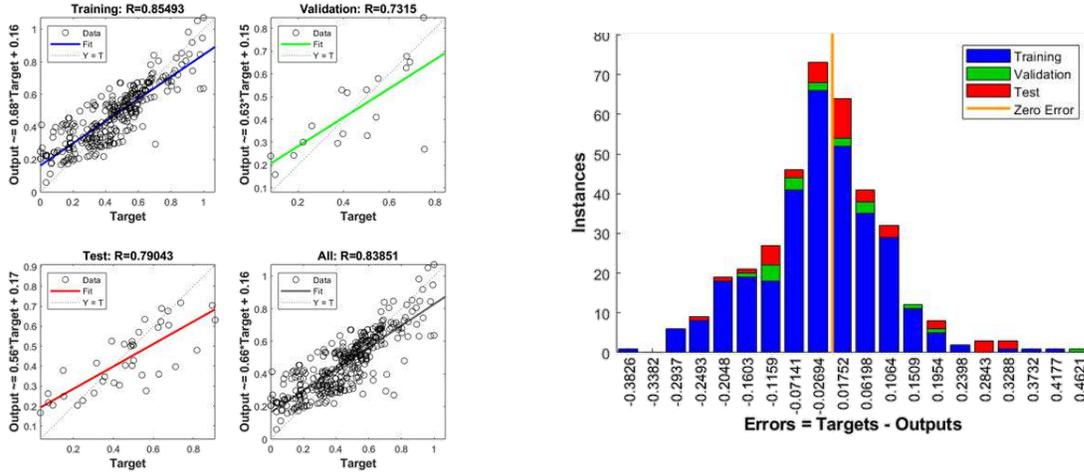
Figure B5.46 Regression coefficient and error histogram for model C+F_85_5_10-11
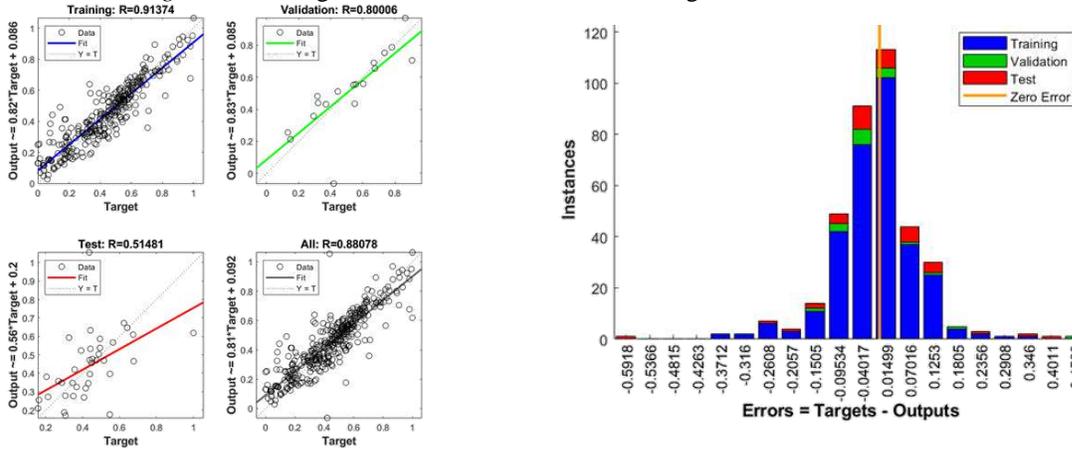
Figure B5.47 Regression coefficient and error histogram for model C+F_85_5_10-23
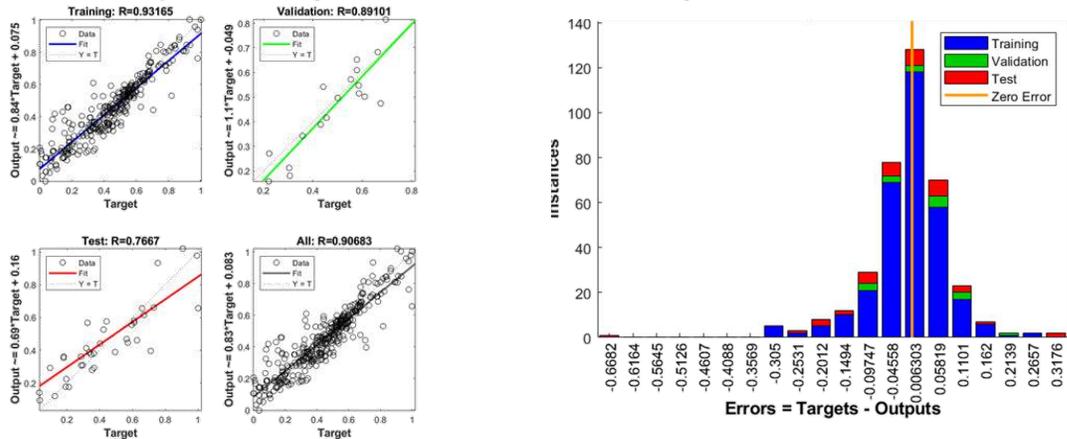
Figure B5.48 Regression coefficient and error histogram for model C+F_85_5_10-33
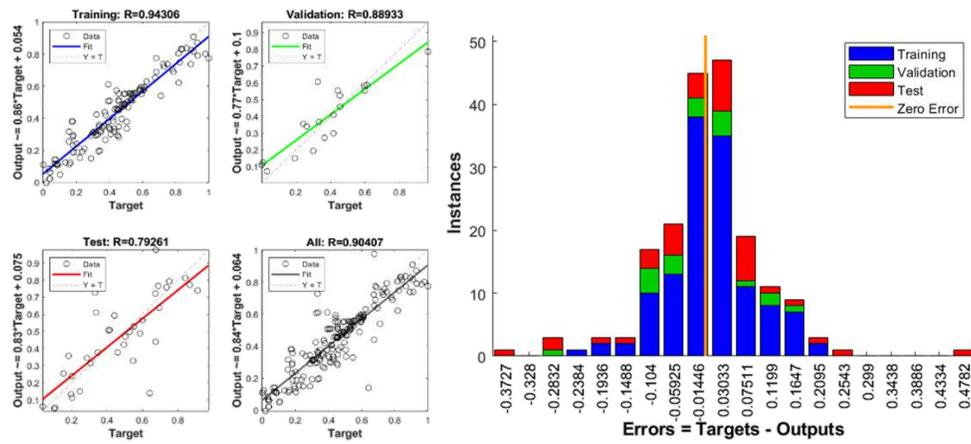
Figure B5.49 Regression coefficient and error histogram for model C+F(C)_70_10_20-11
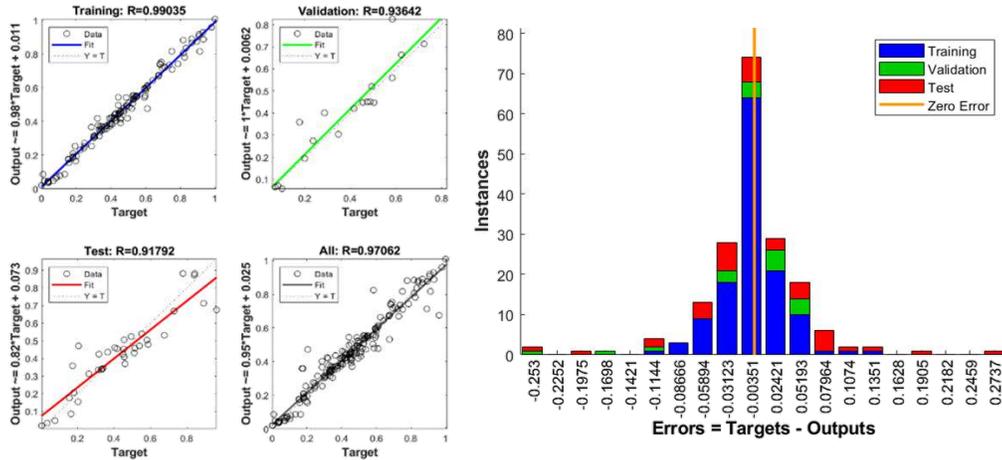
Figure B5.50 Regression coefficient and error histogram for model C+F(C)_70_10_20-23
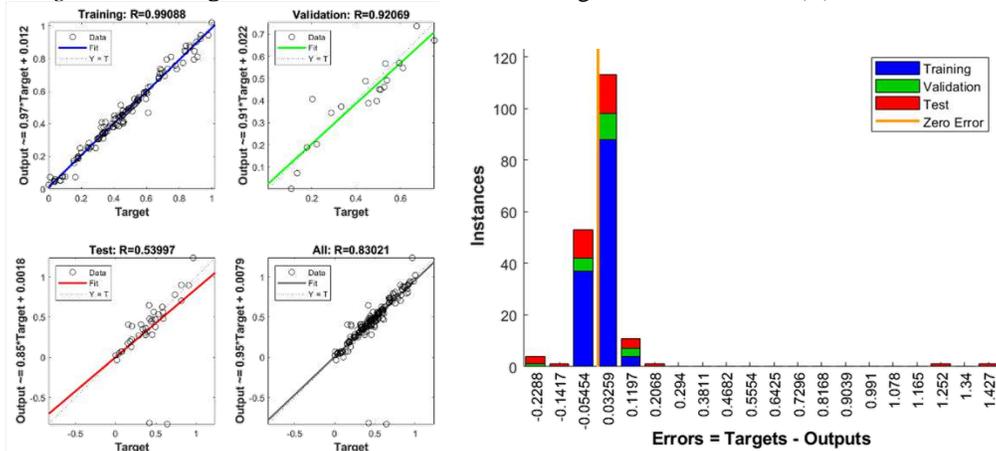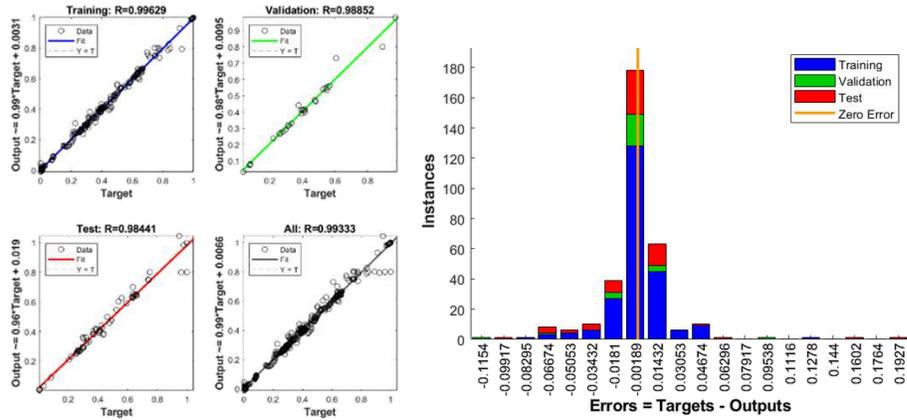

Figure B5.51 Regression coefficient and error histogram for model C+F(C)_70_10_20-33
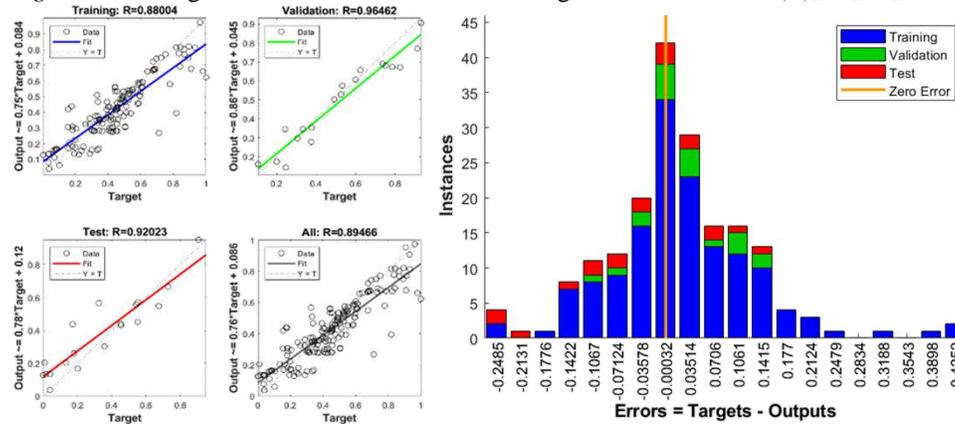
Figure B5.52 Regression coefficient and error histogram for model C+F(C)_80_10_10-11
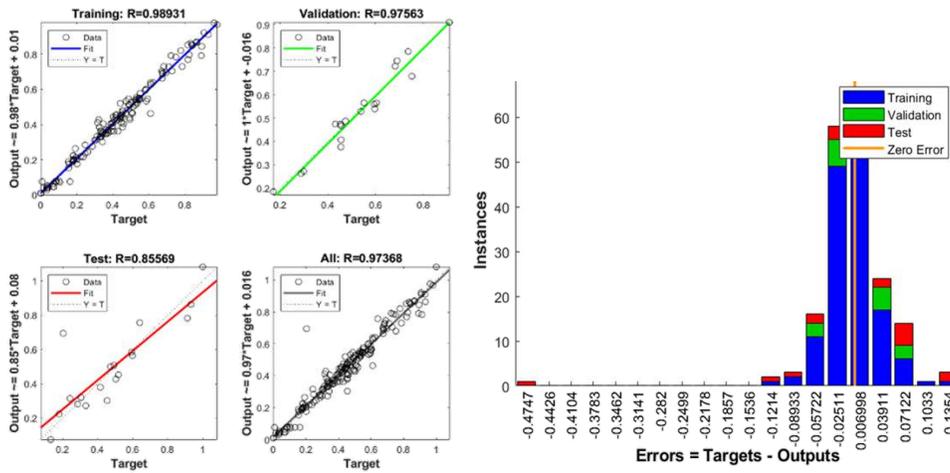
Figure B5.53 Regression coefficient and error histogram for model C+F(C)_80_10_10-23
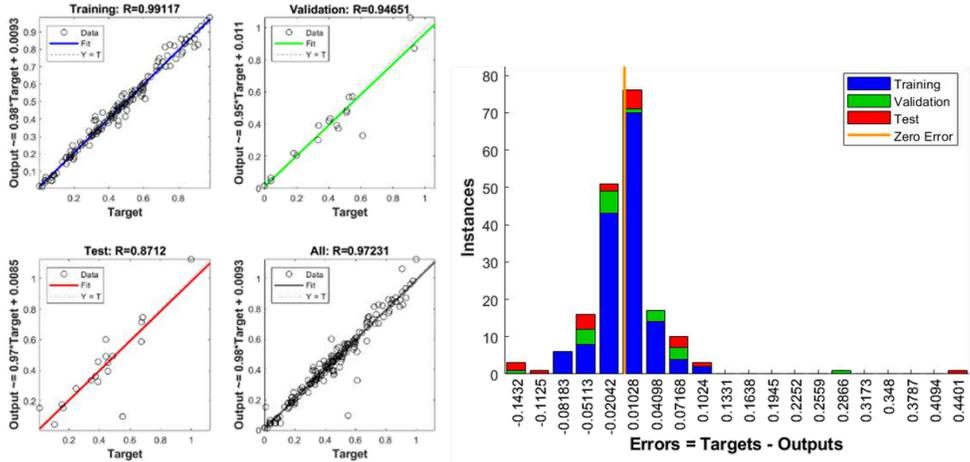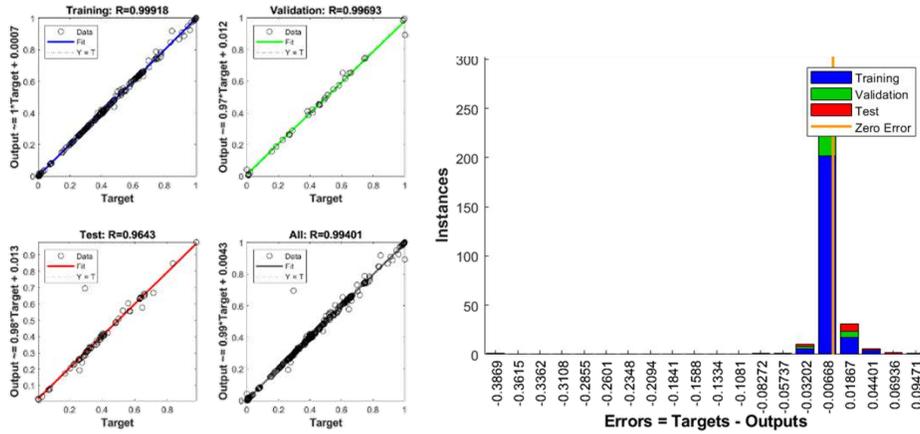

Figure B5.54 Regression coefficient and error histogram for model C+F(C)_80_10_10-33
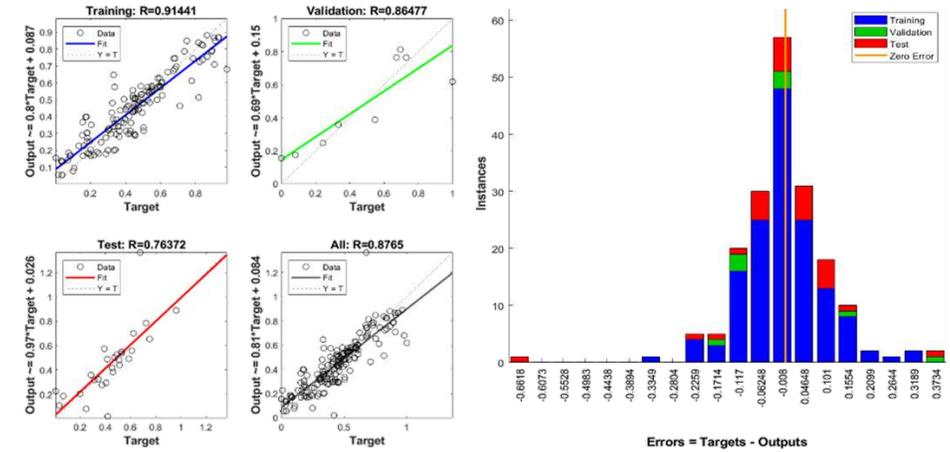
Figure B5.55 Regression coefficient and error histogram for model C+F(C)_80_5_15-11
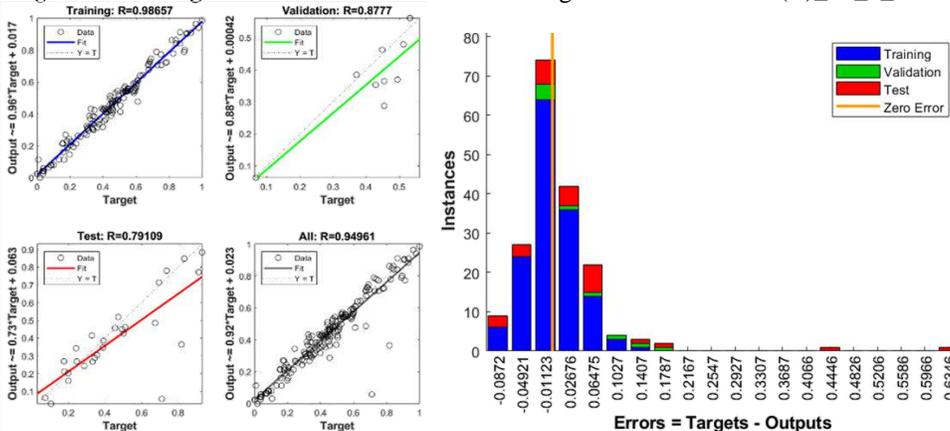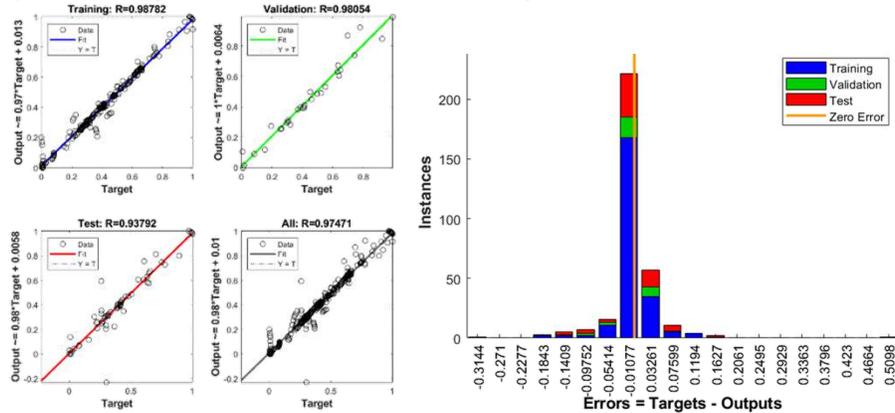

Figure B5.56 Regression coefficient and error histogram for model C+F(C)_80_5_15-23
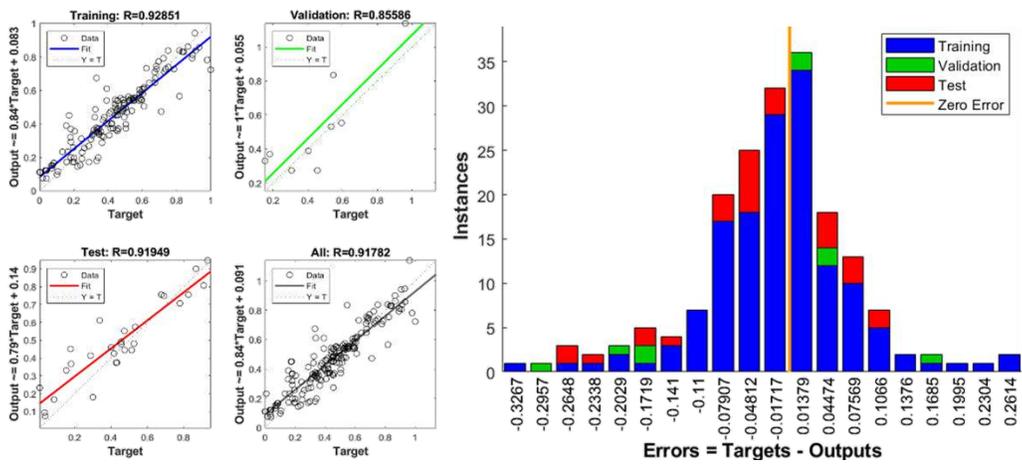
Figure B5.57 Regression coefficient and error histogram for model C+F(C)_80_5_15-33
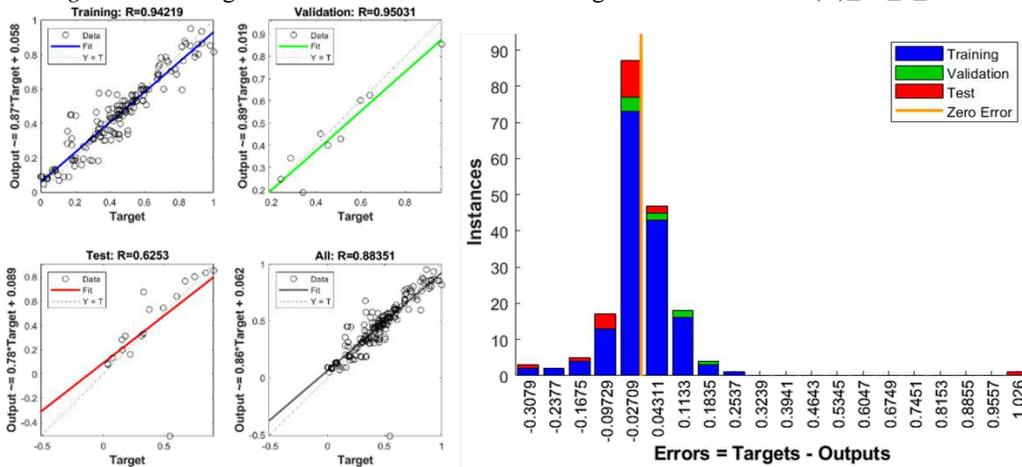
Figure B5.58 Regression coefficient and error histogram for model C+F(C)_85_5_10-11
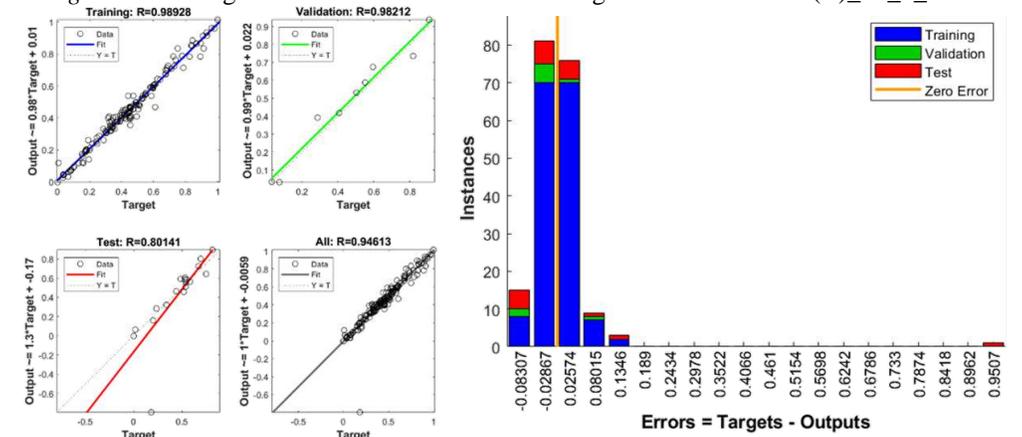
Figure B5.59 Regression coefficient and error histogram for model C+F(C)_85_5_10-23
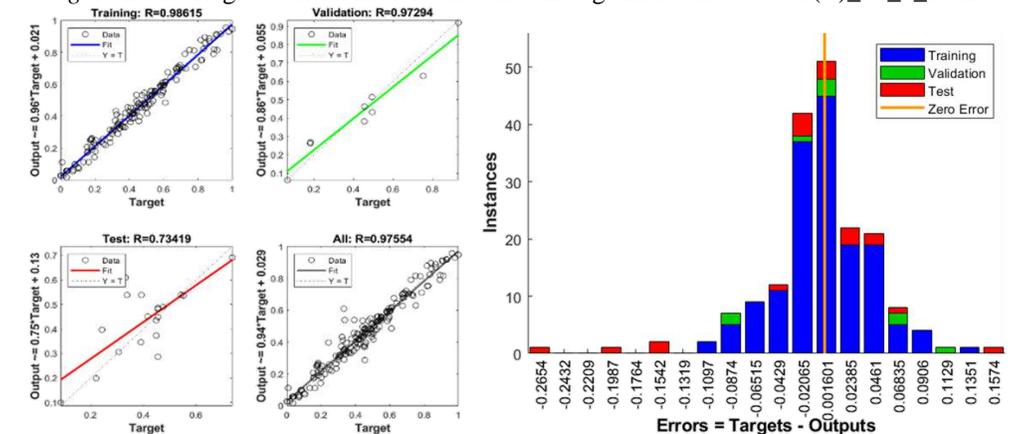
Figure B5.60 Regression coefficient and error histogram for model C+F(C)_85_5_10-33
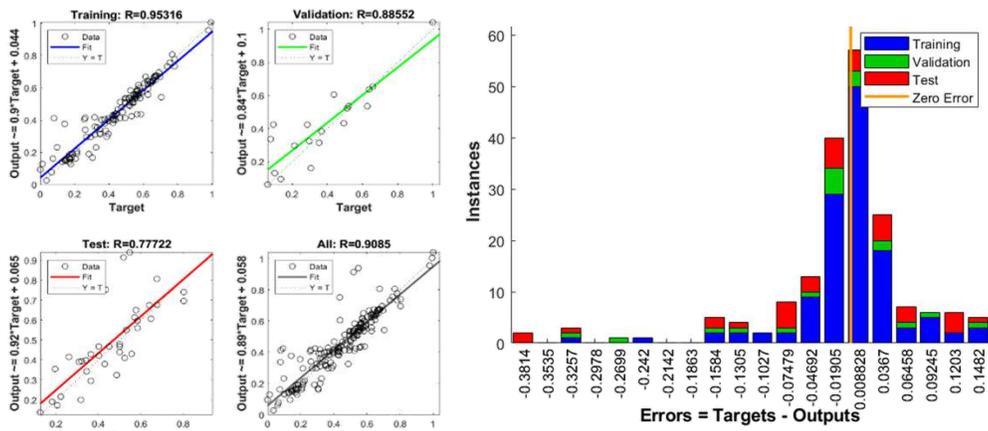
Figure B5.61 Regression coefficient and error histogram for model C+F(F)_70_10_20-11
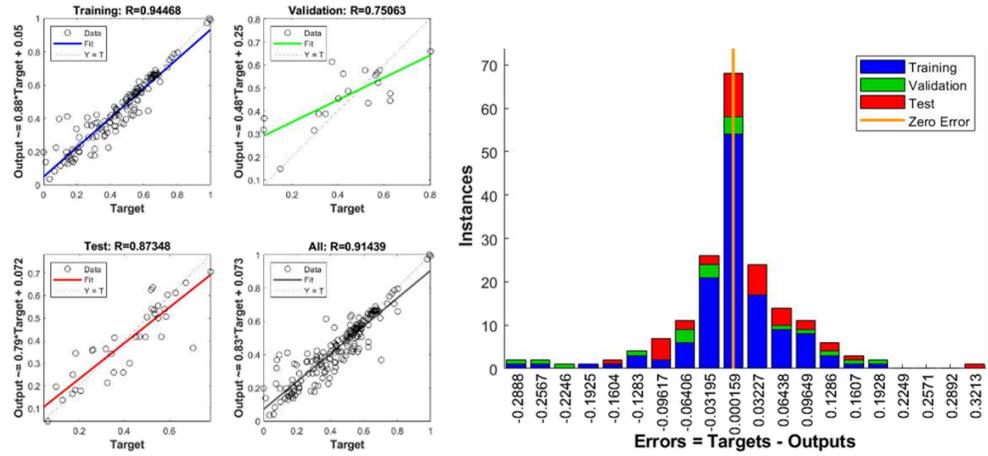
Figure B5.62 Regression coefficient and error histogram for model C+F(F)_70_10_20-23
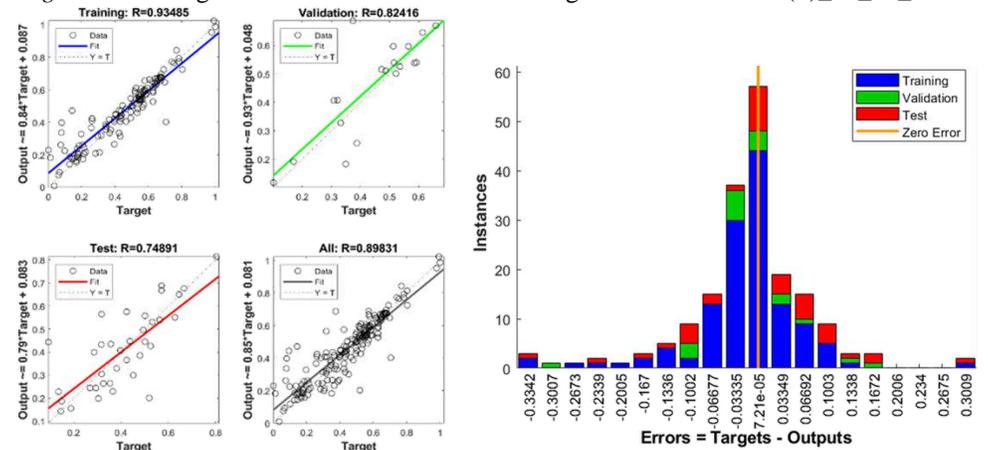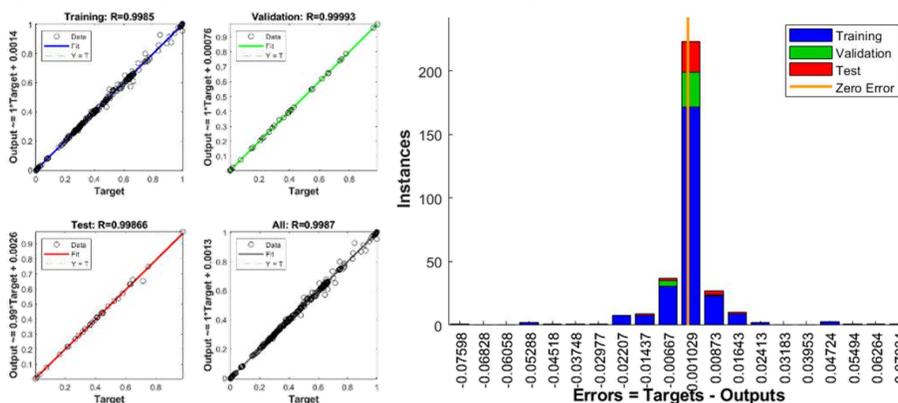

Figure B5.63 Regression coefficient and error histogram for model C+F(F)_70_10_20-33
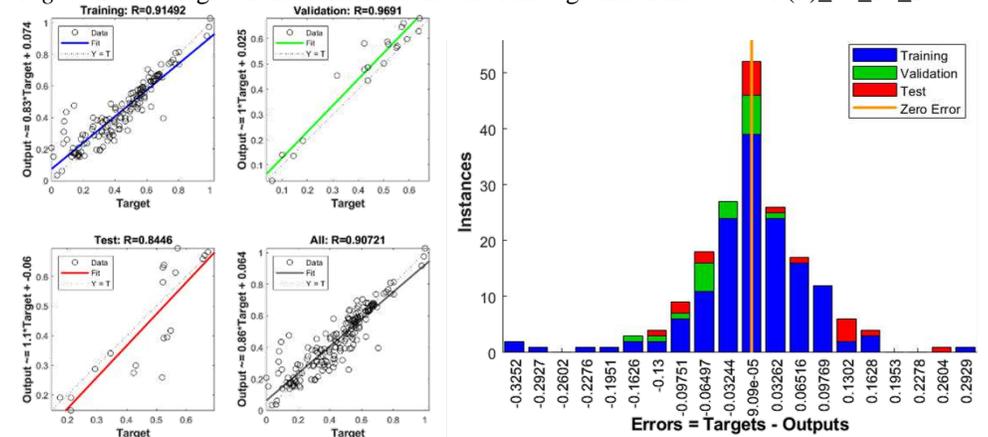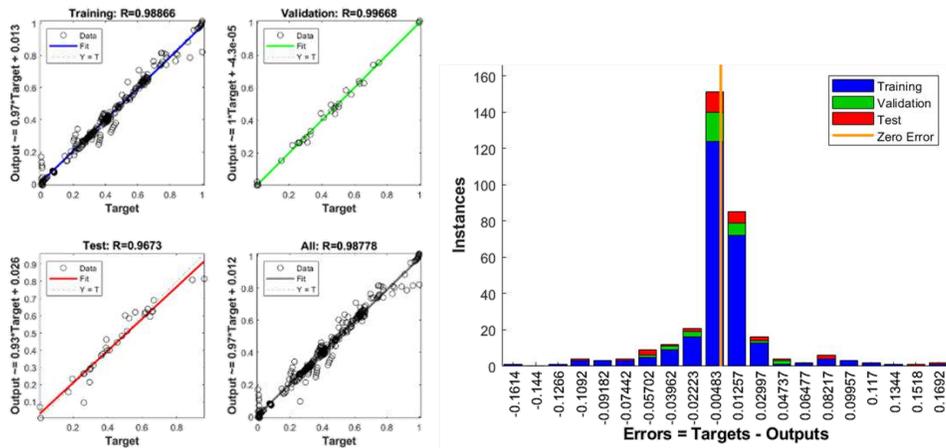

Figure B5.64 Regression coefficient and error histogram for model C+F(F)_80_10_10-11
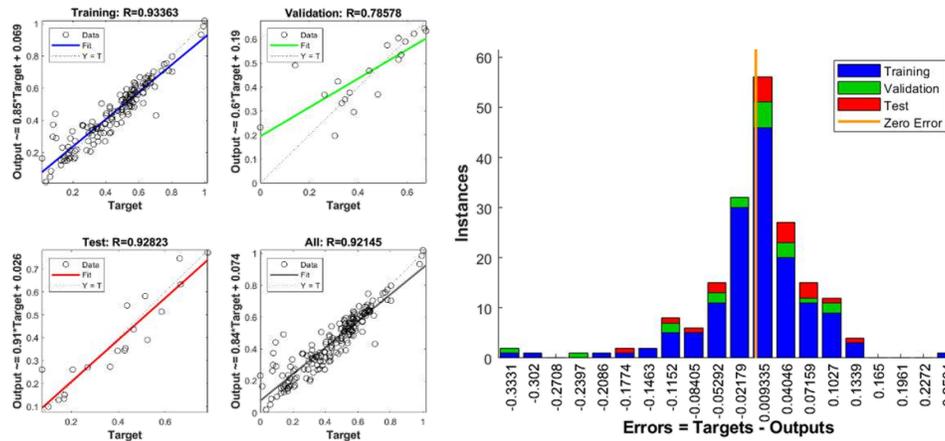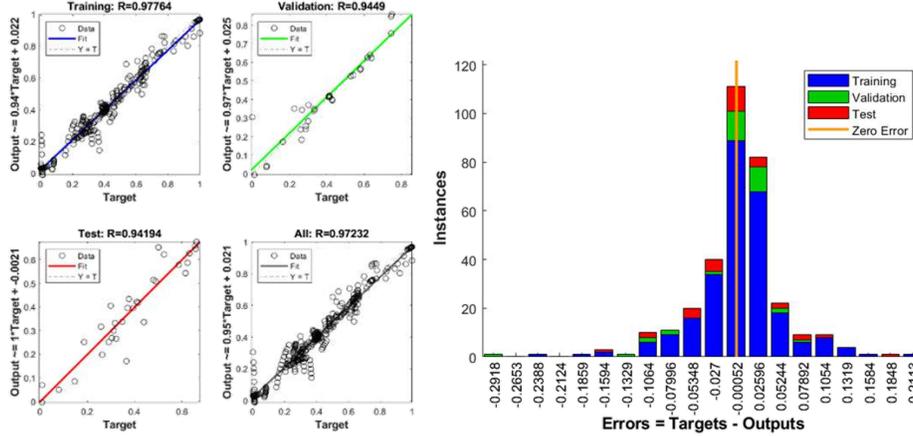
Figure B5.65 Regression coefficient and error histogram for model C+F(F)_80_10_10-23
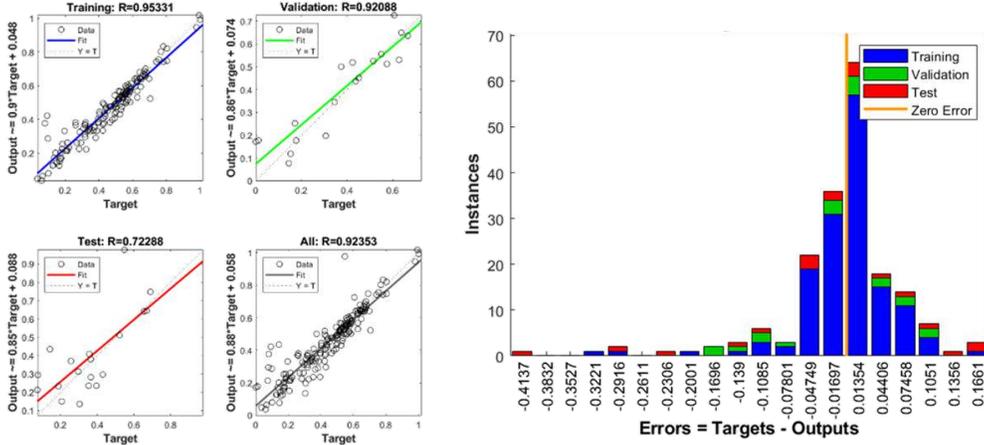
Figure B5.66 Regression coefficient and error histogram for model C+F(F)_80_10_10-33
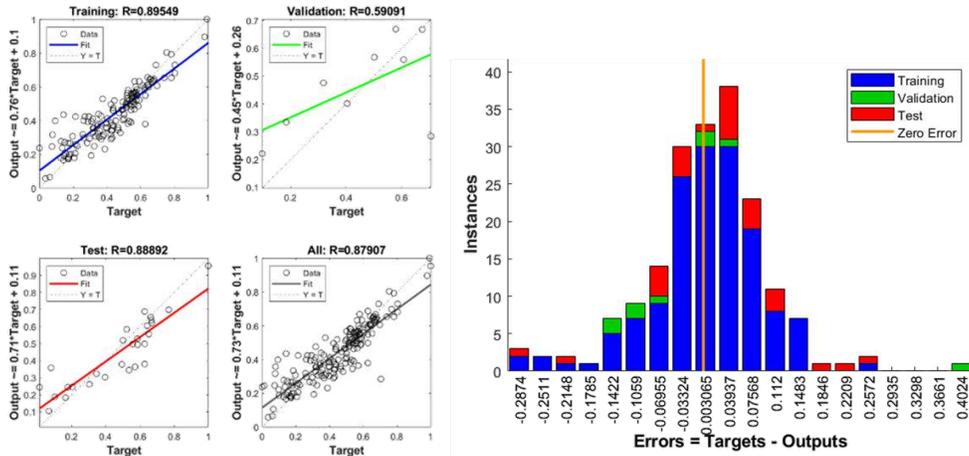
Figure B5.67 Regression coefficient and error histogram for model C+F(F)_80_5_15-11
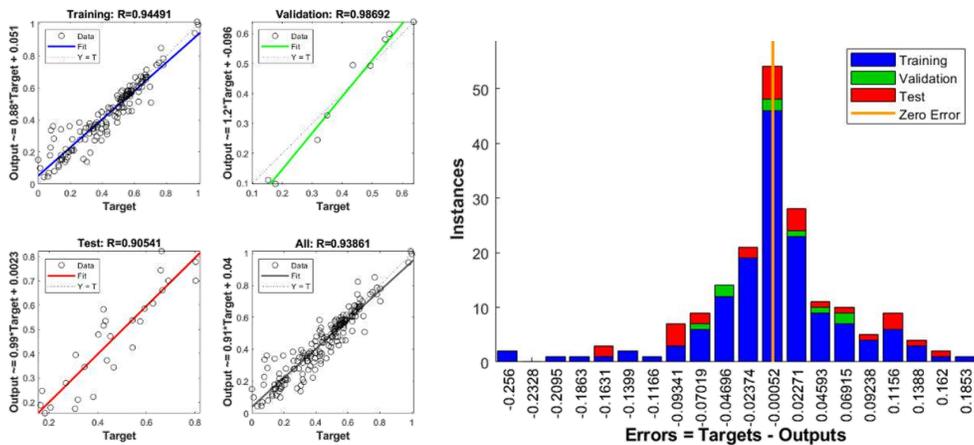
Figure B5.68 Regression coefficient and error histogram for model C+F(F)_80_5_15-23
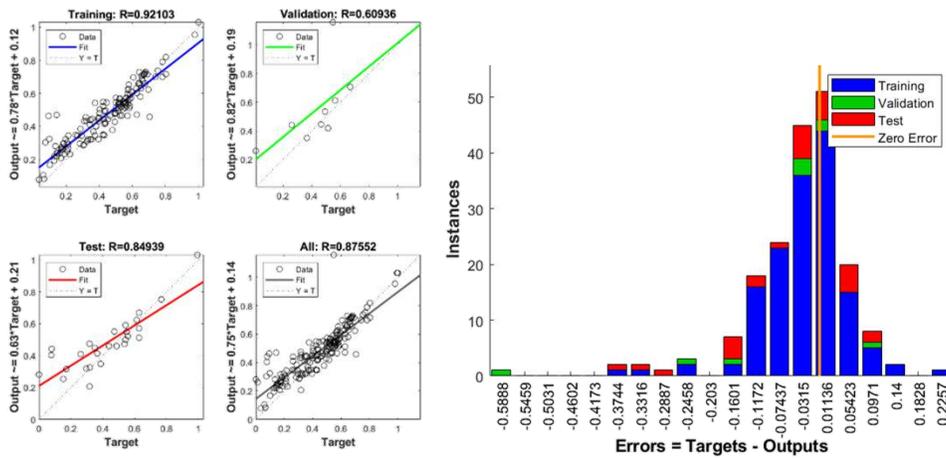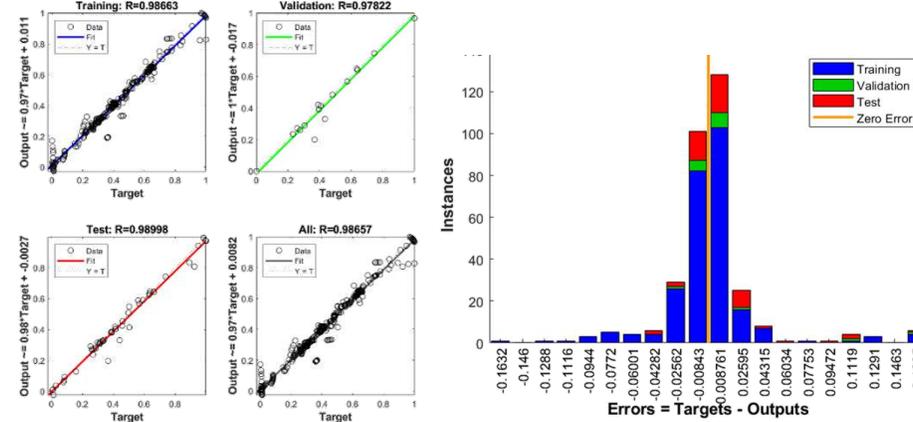
Figure B5.69 Regression coefficient and error histogram for model C+F(F)_80_5_15-33
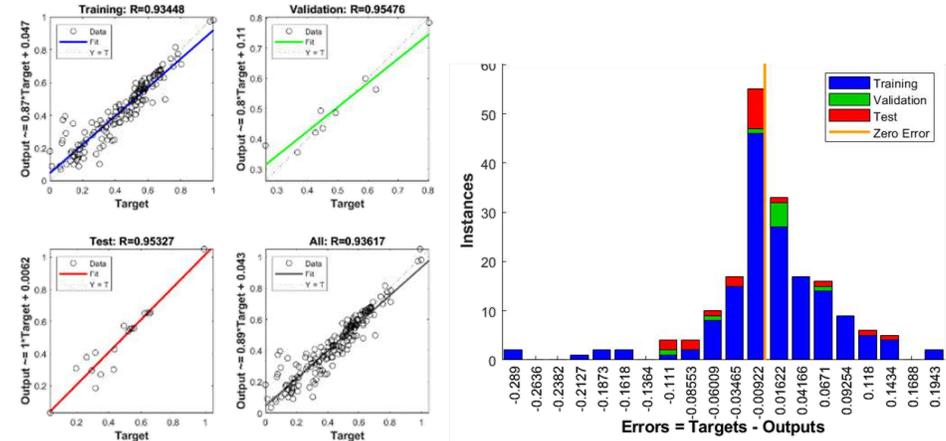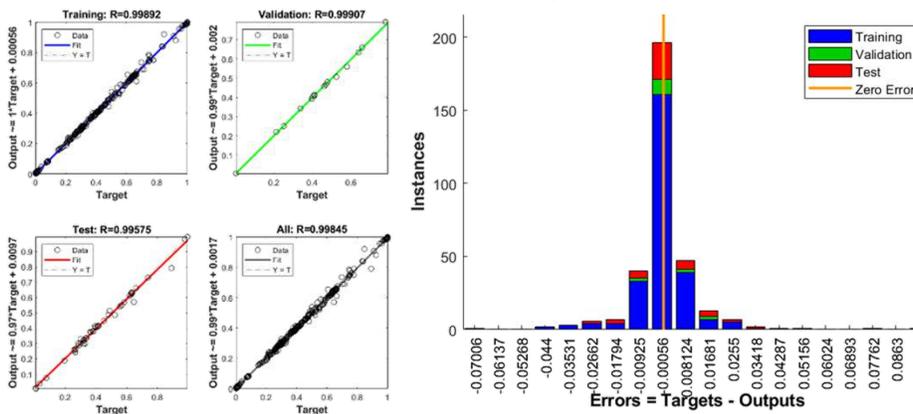

Figure B5.70 Regression coefficient and error histogram for model C+F(F)_85_5_10-11
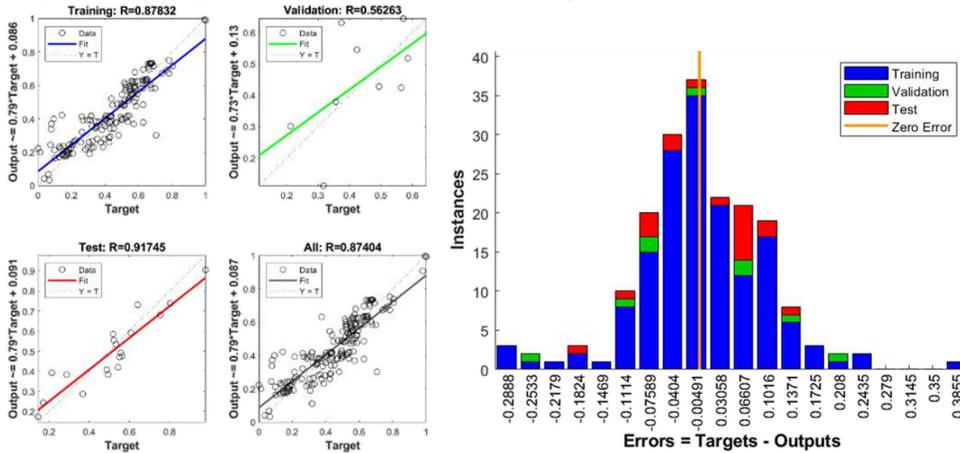
Figure B5.71 Regression coefficient and error histogram for model C+F(F)_85_5_10-23
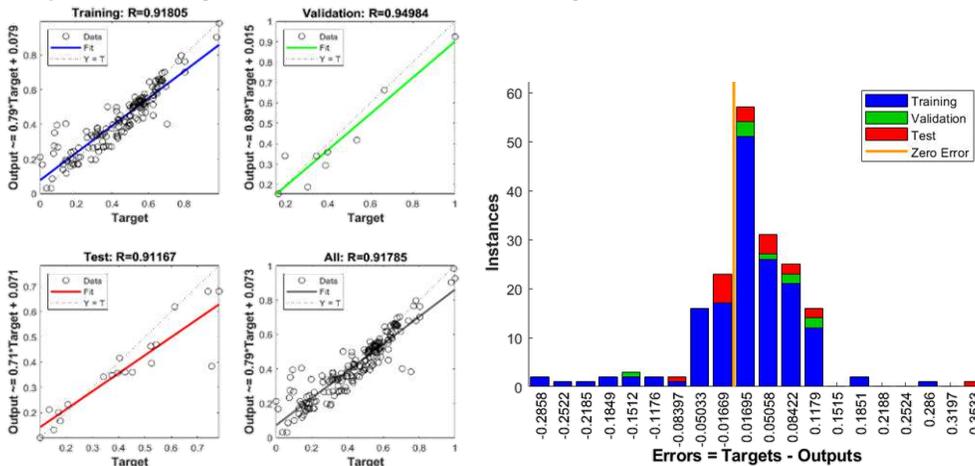
Figure B5.72 Regression coefficient and error histogram for model C+F(F)_85_5_10-33

90
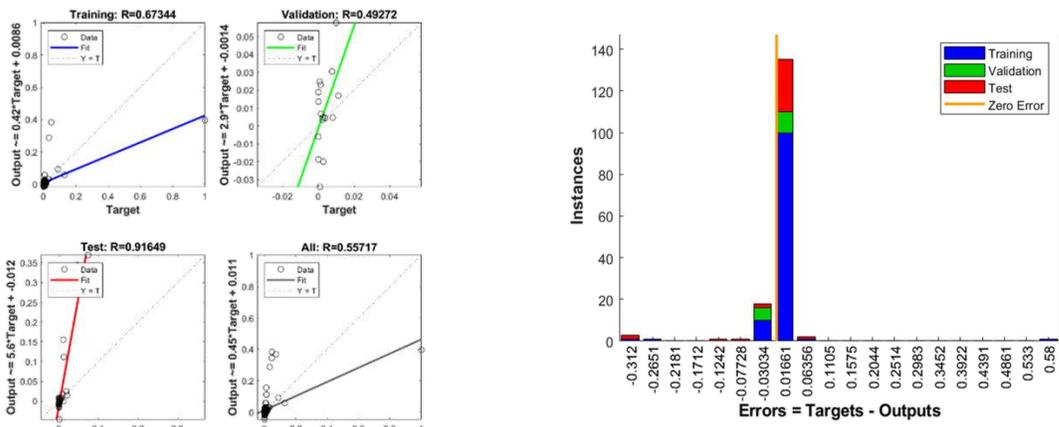
Figure B5.73 Regression coefficient and error histogram for model R-RES_70_10_20-18
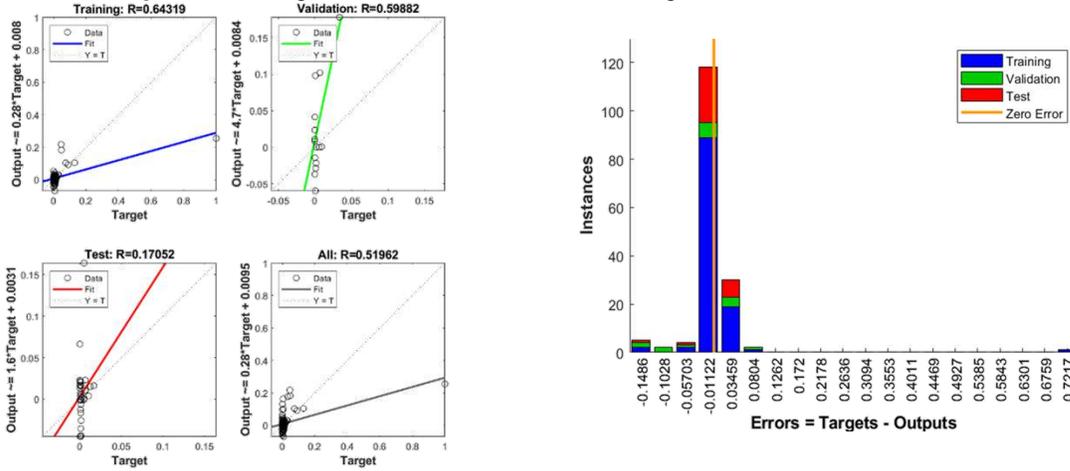
Figure B5.74 Regression coefficient and error histogram for model R-RES_70_10_20-37
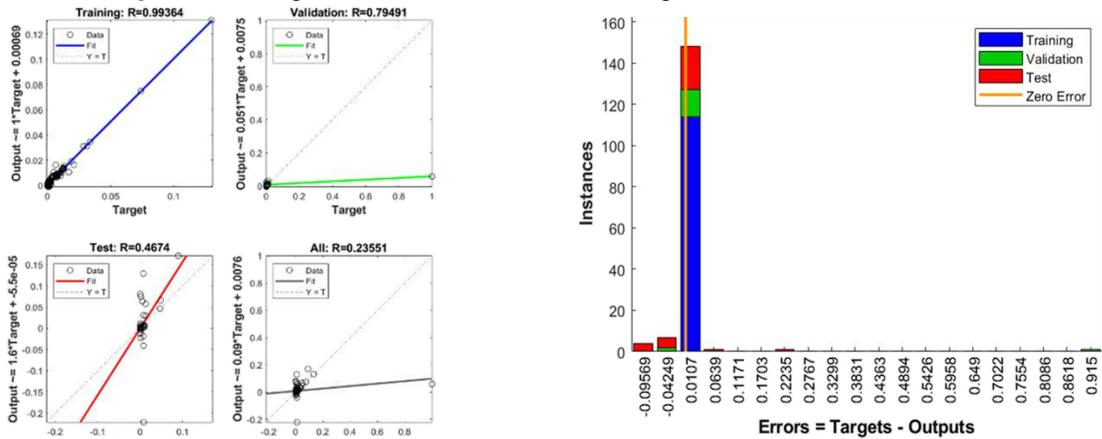
Figure B5.75 Regression coefficient and error histogram for model R-RES_70_10_20-54
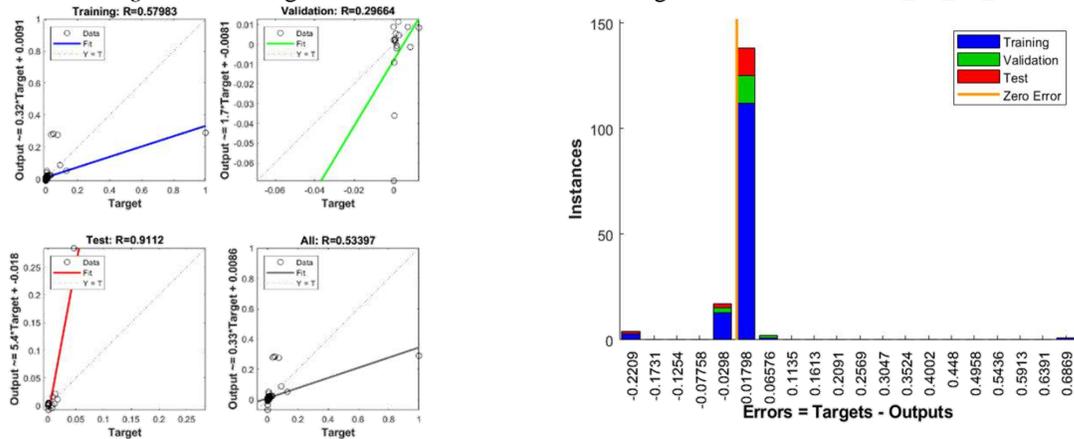
Figure B5.76 Regression coefficient and error histogram for model R-RES_80_10_10-18
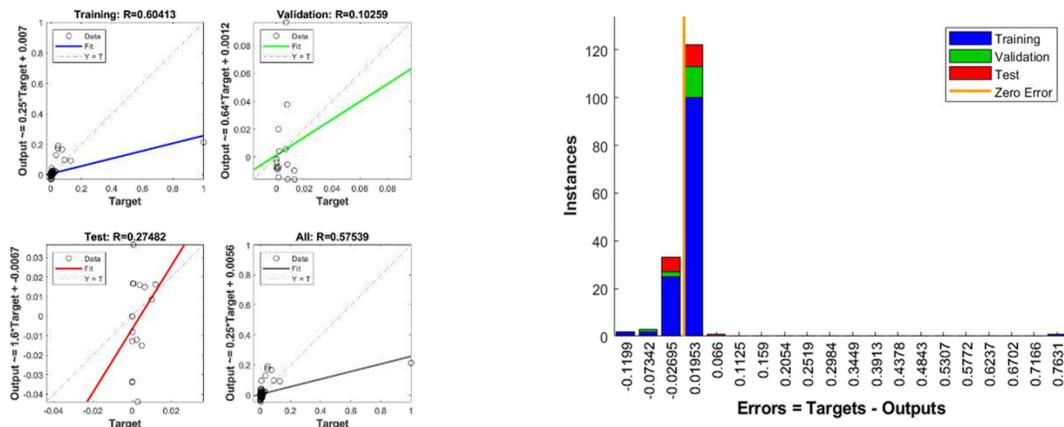
Figure B5.77 Regression coefficient and error histogram for model R-RES_80_10_10-37
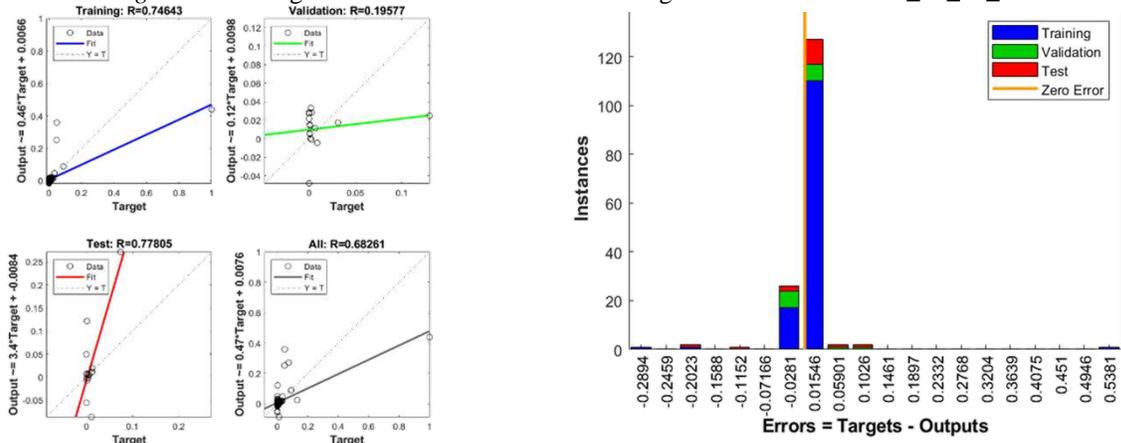
Figure B5.78 Regression coefficient and error histogram for model R-RES_80_10_10-54
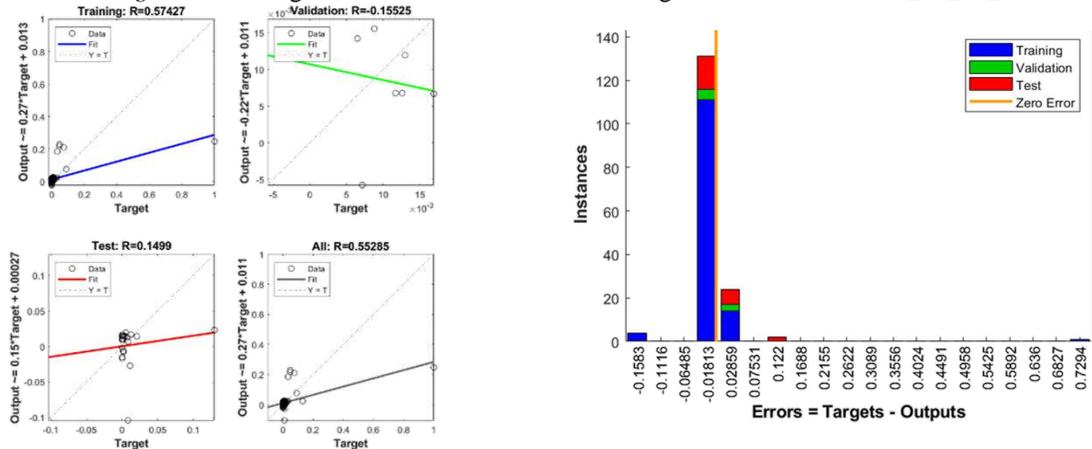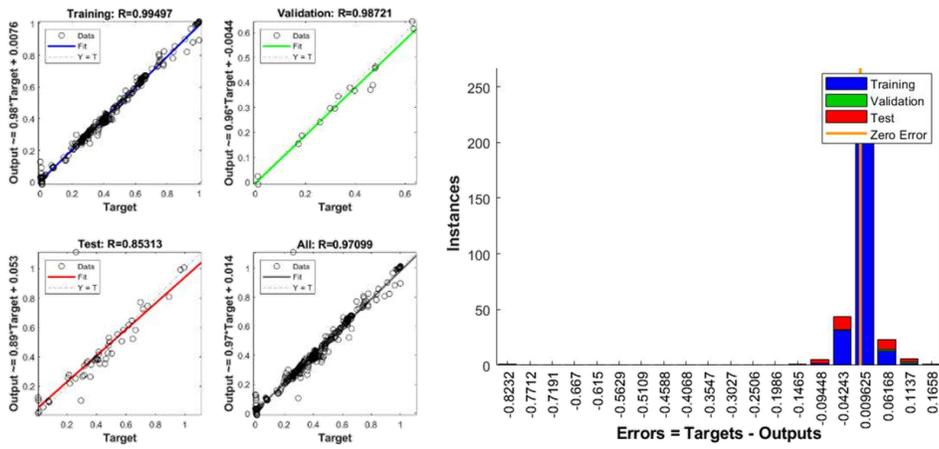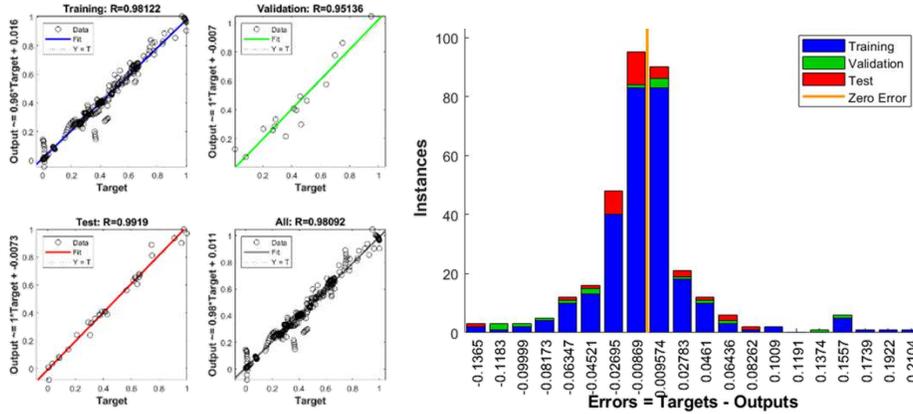

Figure B5.79 Regression coefficient and error histogram for model R-RES_80_5_15-18
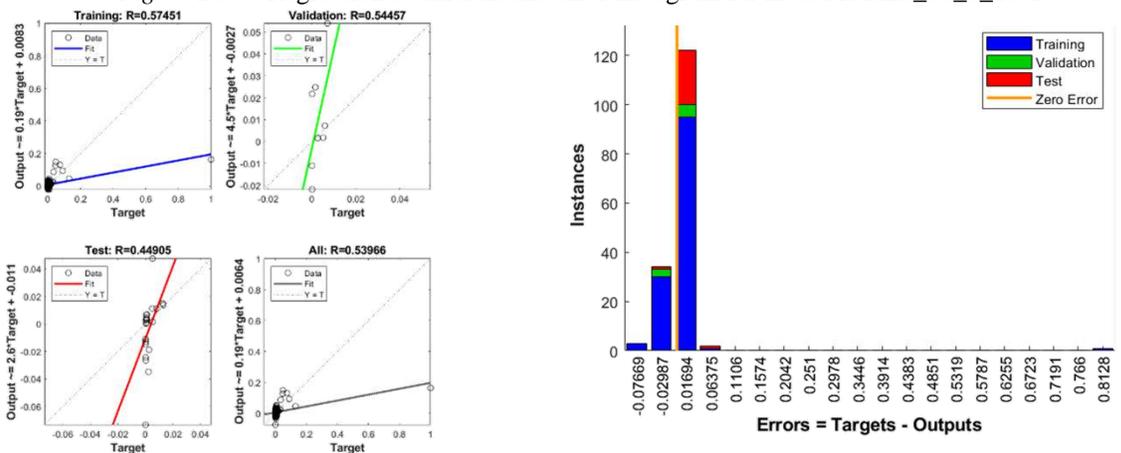
Figure B5.80 Regression coefficient and error histogram for model R-RES_80_5_15-37
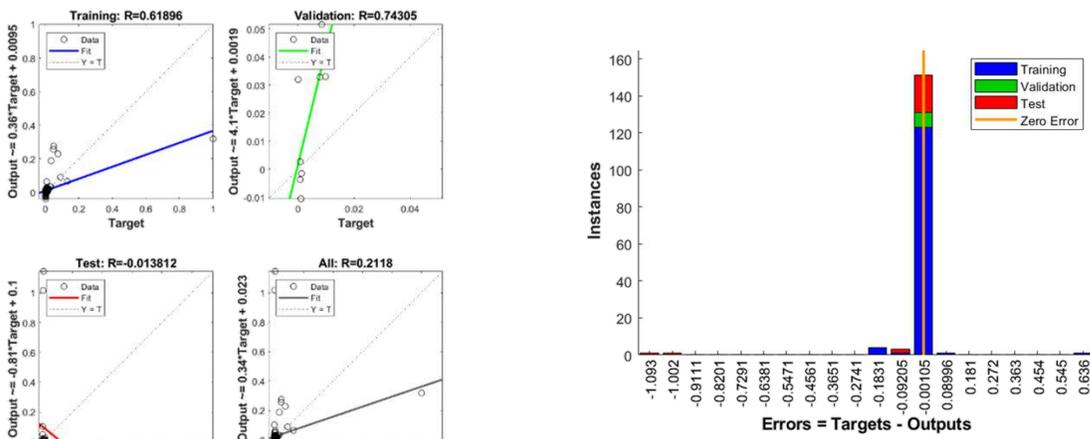
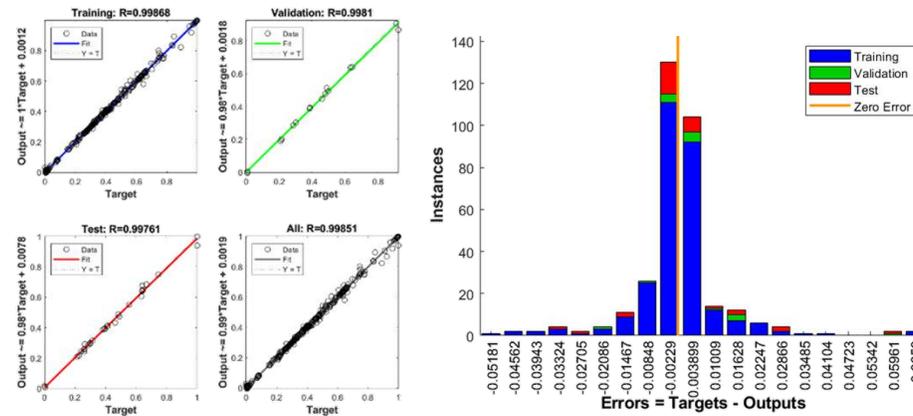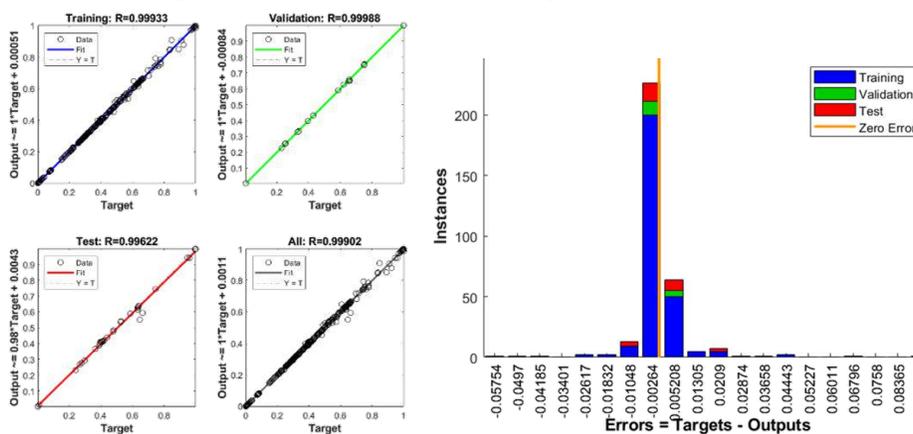*Figure B5.81* Regression coefficient and error histogram for model R-RES_80_5_15-54
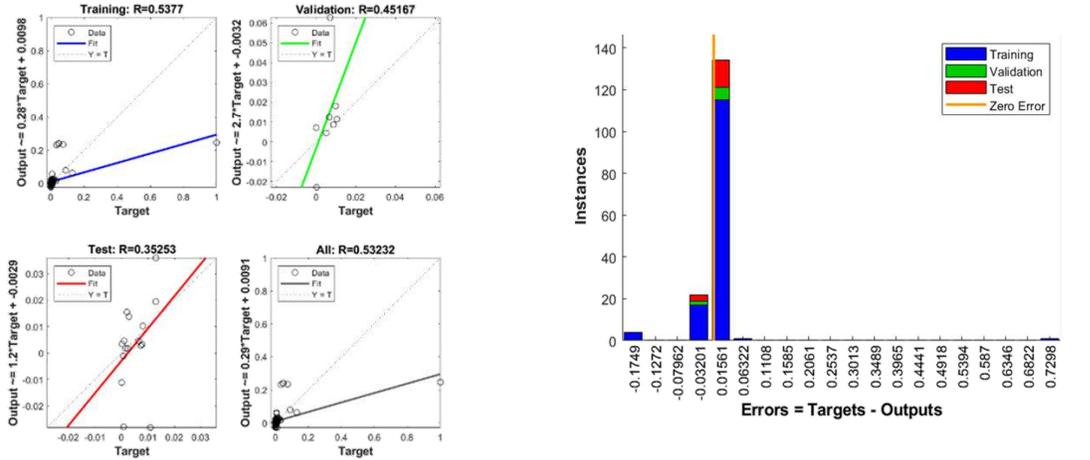
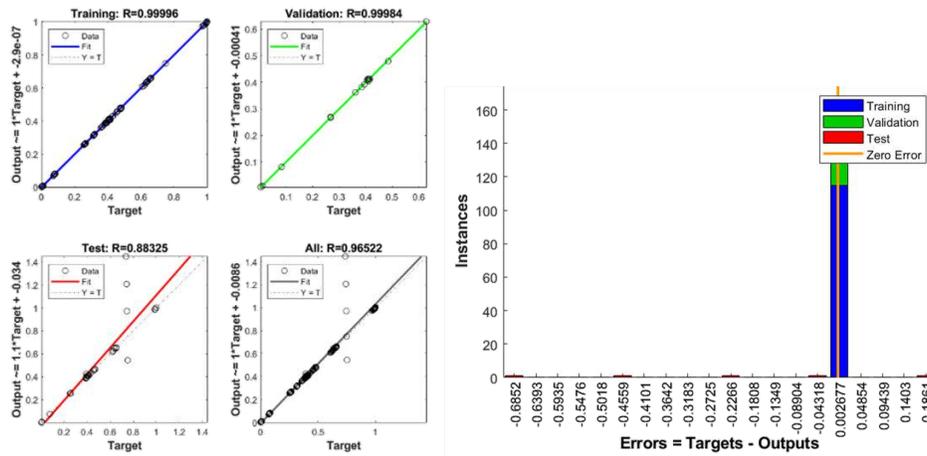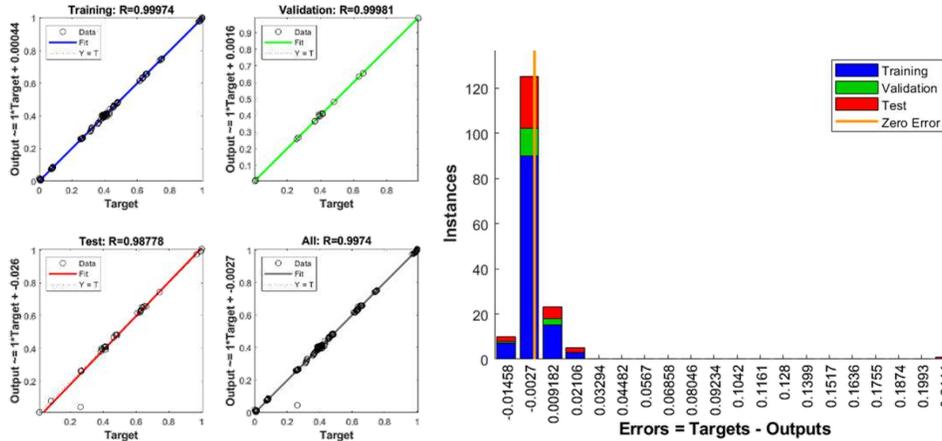*Figure B5.82* Regression coefficient and error histogram for model R-RES_85_5_10-18
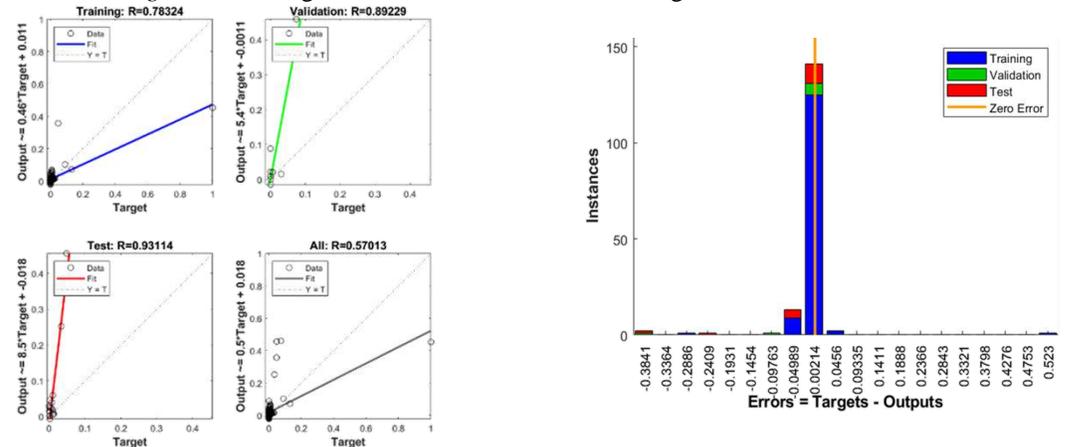
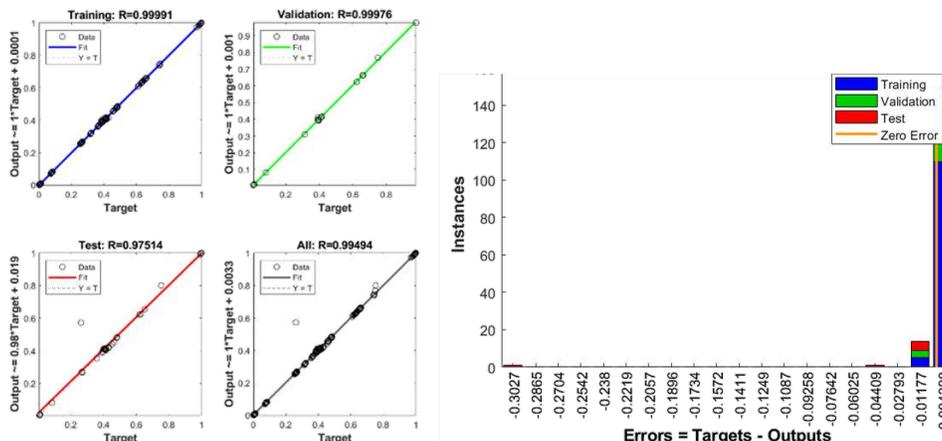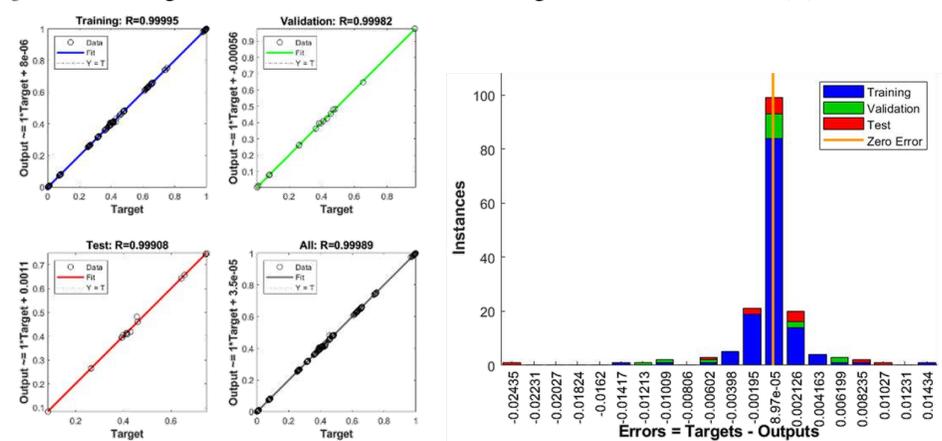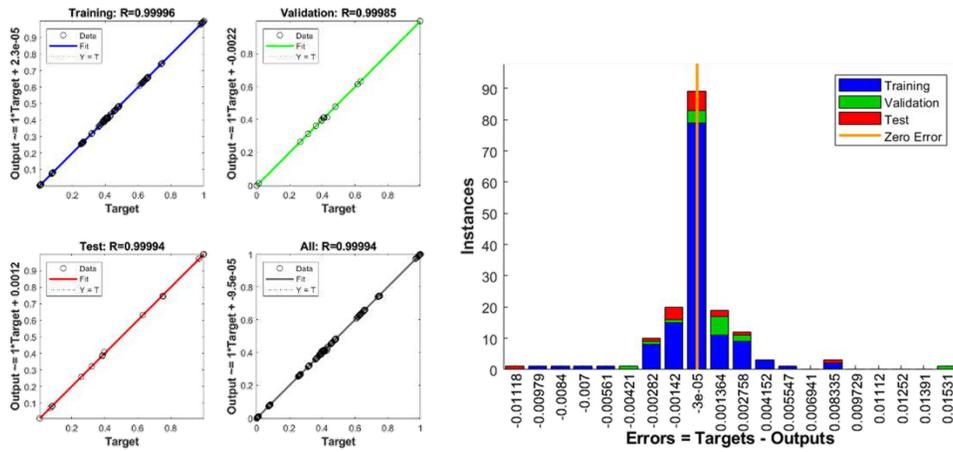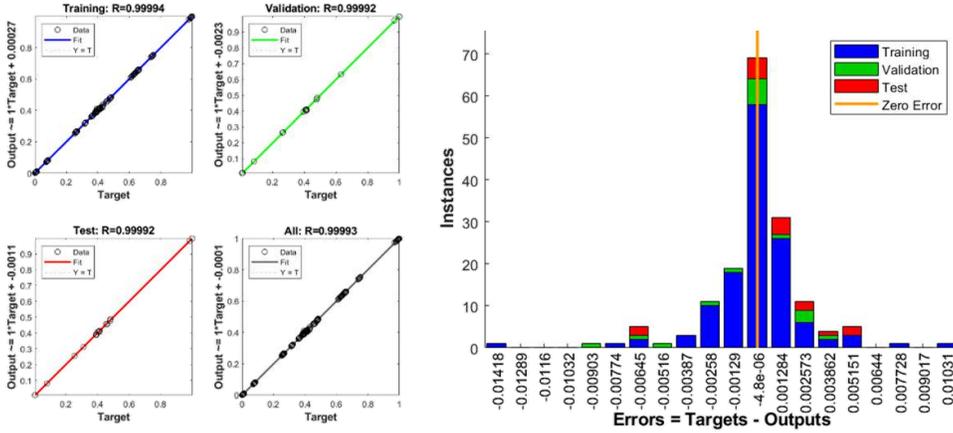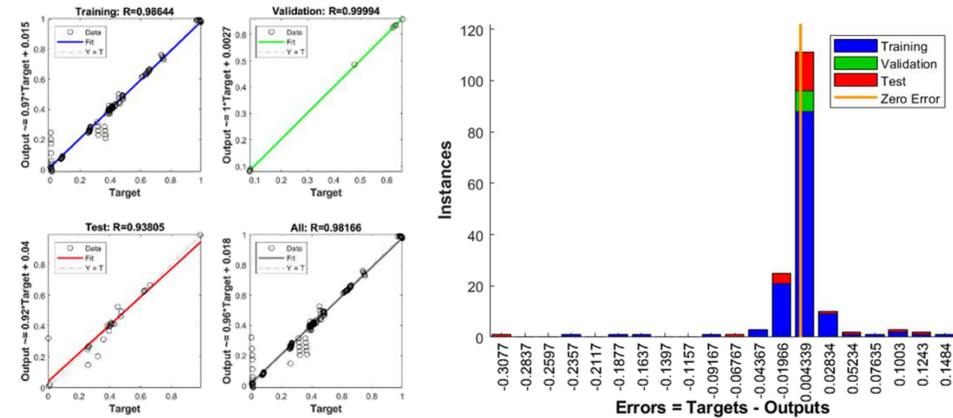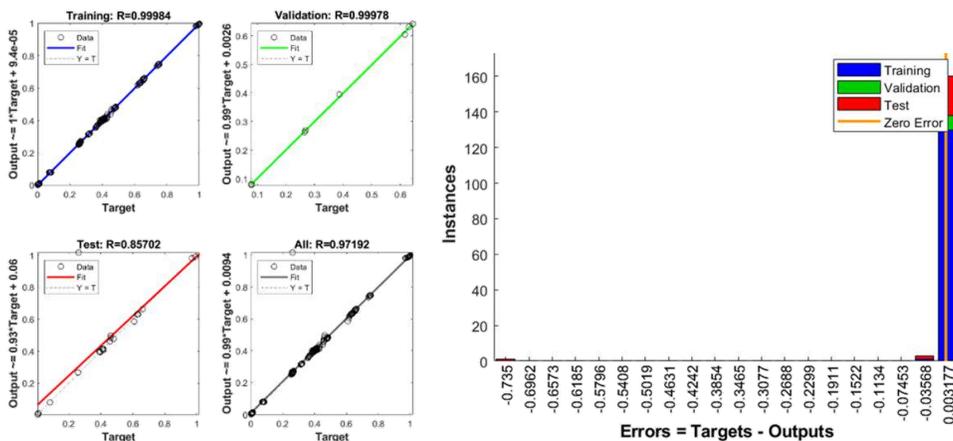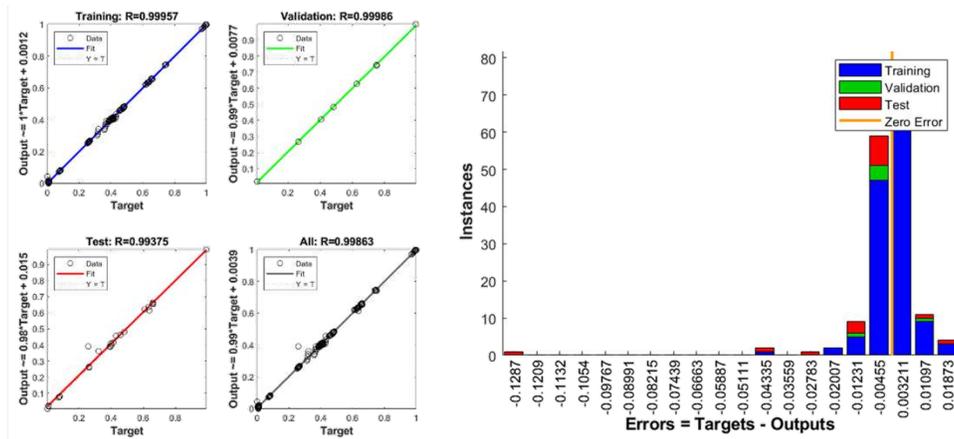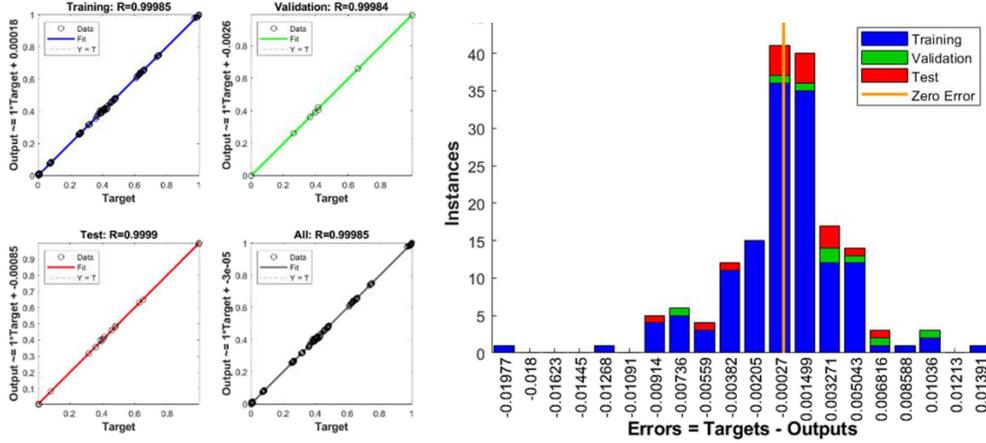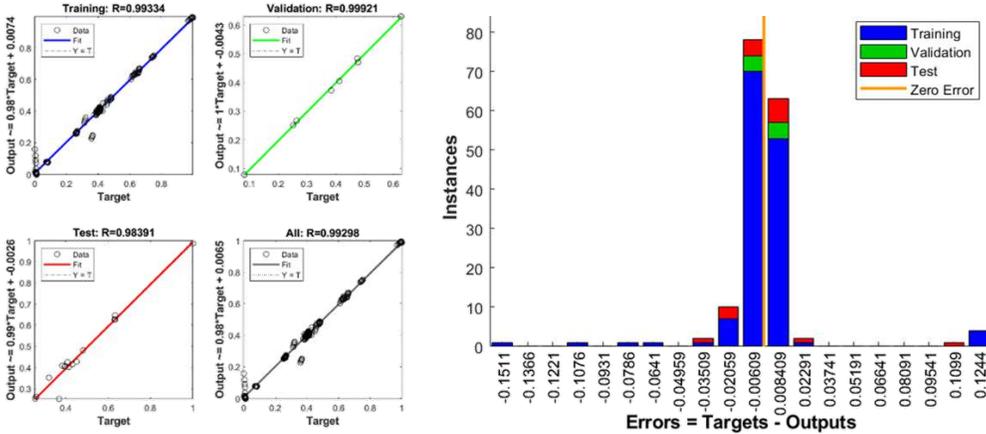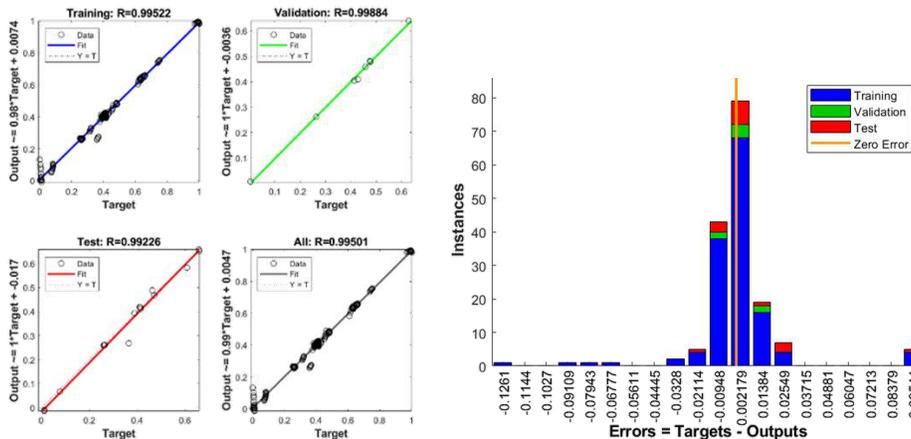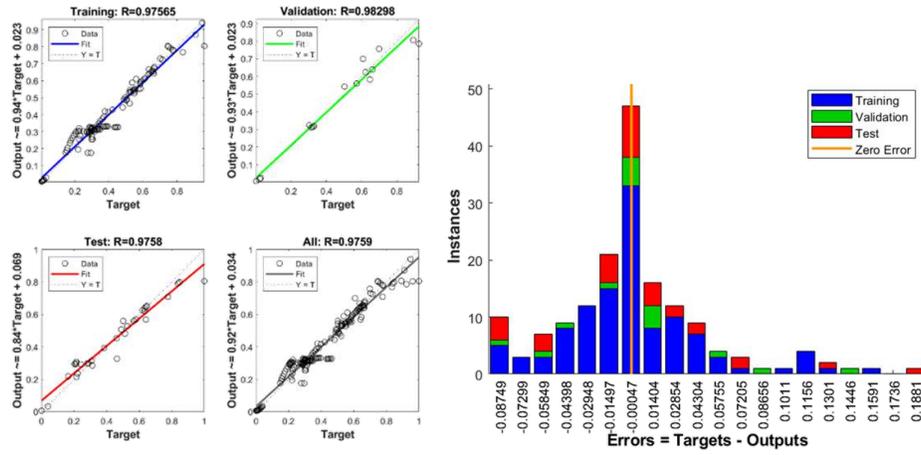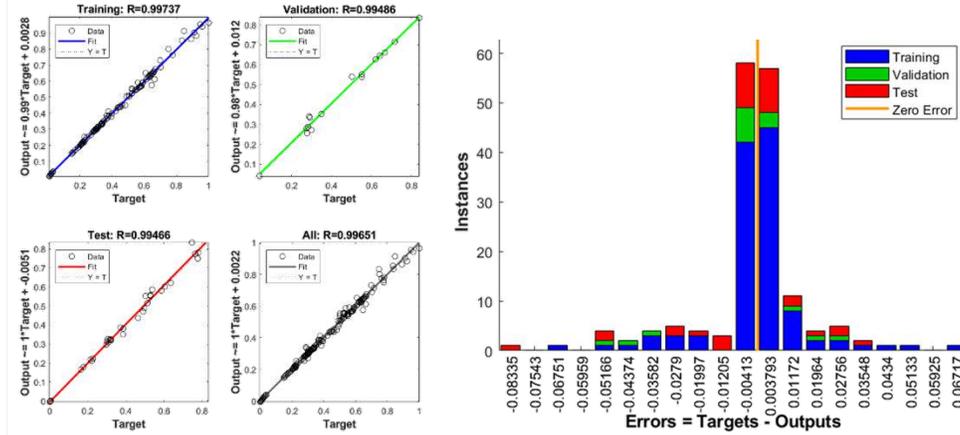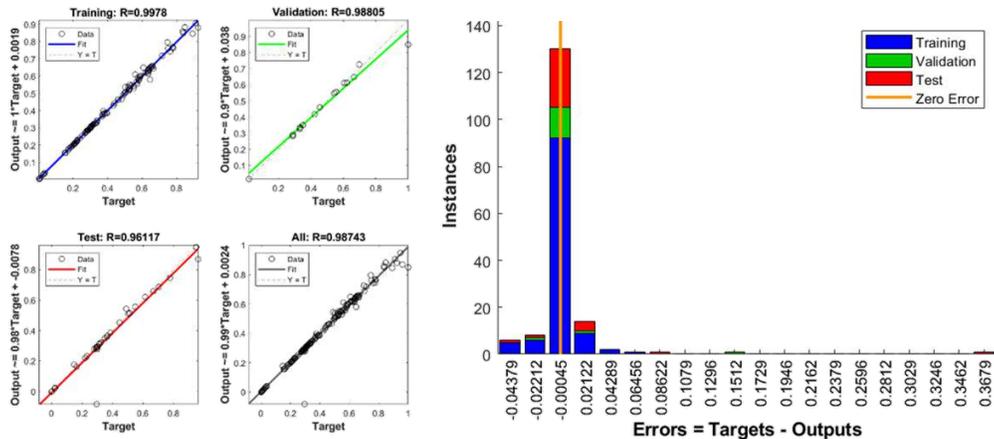*Figure B5.83* Regression coefficient and error histogram for model R-RES_85_5_10-37
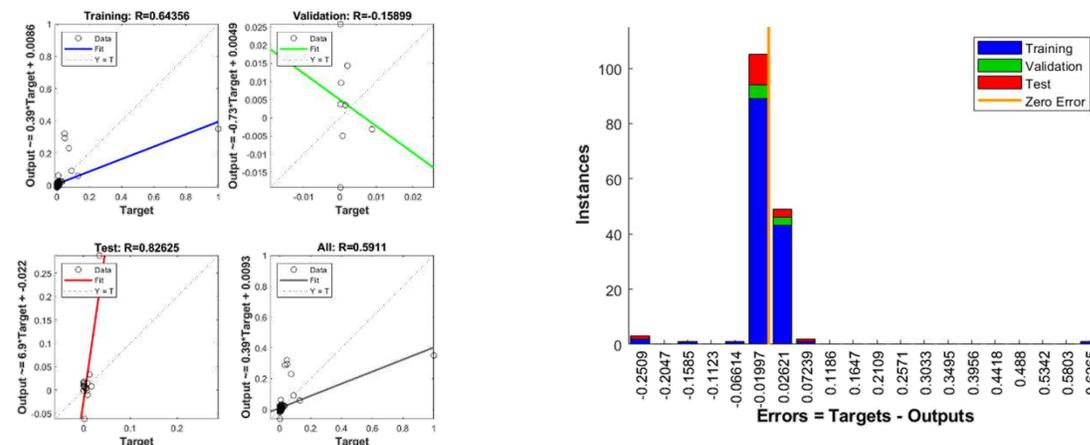
Figure B5.84 Regression coefficient and error histogram for model R-RES_85_5_10-54

Table B5.1 Results for prescribed models based on datasets from Group I

#	Model	Regression coefficient - training	Regression coefficient - validation	Regression coefficient - testing	Regression coefficient - total	Mean squared error	Epoch
1	COMP_70_10_20-20	0.96343	0.91117	0.93691	0.95267	0.0041683	11
2	COMP_70_10_20-41	0.9764	0.95823	0.95837	0.9688	0.0035684	10
3	COMP_70_10_20-60	0.96892	0.92014	0.97275	0.96502	0.0027543	11
4	COMP_80_10_10-20	0.98057	0.80865	0.96564	0.96367	0.0074847	12
5	COMP_80_10_10-41	0.98506	0.97668	0.95219	0.98091	0.00166	23
6	COMP_80_10_10-60	0.99134	0.92773	0.96242	0.9791	0.0058959	29
7	COMP_80_5_15-20	0.99243	0.96302	0.93571	0.96256	0.0026369	32
8	COMP_80_5_15-41	0.94902	0.84651	0.90042	0.93784	0.0065029	8
9	COMP_80_5_15-60	0.9734	0.96289	0.9181	0.96813	0.0020171	9
10	COMP_85_5_10-20	0.97739	0.96833	0.925	0.97202	0.0020394	27
11	COMP_85_5_10-41	0.98662	0.97242	0.91848	0.97858	0.0008891	24
12	COMP_85_5_10-60	0.97492	0.97925	0.96085	0.97274	0.0017733	11
13	FLEX_70_10_20-16	0.92275	0.93164	0.89117	0.91543	0.0052991	15
14	FLEX_70_10_20-33	0.90767	0.76191	0.88383	0.89097	0.011561	9
15	FLEX_70_10_20-48	0.97482	0.86785	0.76975	0.92254	0.011327	24
16	FLEX_80_10_10-16	0.87989	0.9049	0.89932	0.87775	0.015987	9
17	FLEX_80_10_10-33	0.90666	0.78076	0.91404	0.89732	0.012209	9
18	FLEX_80_10_10-48	0.95267	0.85083	0.66631	0.90198	0.0085164	23
19	FLEX_80_5_15-16	0.93545	0.87768	0.90633	0.92508	0.016499	20
20	FLEX_80_5_15-33	0.89835	0.5976	0.74502	0.86385	0.03847	8
21	FLEX_80_5_15-48	0.92223	0.95752	0.741	0.87383	0.0042048	10
22	FLEX_85_5_10-16	0.95091	0.98268	0.86206	0.94388	0.0020087	32
23	FLEX_85_5_10-33	0.94225	0.87925	0.92333	0.93602	0.014196	18
24	FLEX_85_5_10-48	0.93335	0.86572	0.71228	0.91121	0.0039731	10
25	RES_70_10_20-17	0.5818	0.49059	0.6872	0.56728	0.00032702	14
26	RES_70_10_20-35	0.6475	0.53495	0.38105	0.51622	0.0013192	11
27	RES_70_10_20-51	0.64343	0.44434	0.48697	0.45509	0.0016305	9
28	RES_80_10_10-17	0.70888	0.60544	0.55122	0.40192	0.040419	9
29	RES_80_10_10-35	0.91682	0.97327	0.2134	0.28895	0.000021093	12
30	RES_80_10_10-51	0.83741	0.52461	0.001682	0.68019	0.0060926	23
31	RES_80_5_15-17	0.96313	0.65467	0.78845	0.41224	0.00005	10
32	RES_80_5_15-35	0.64482	0.87646	0.42918	0.52067	0.00016986	11
33	RES_80_5_15-51	0.65712	0.70799	0.59939	0.50021	0.012333	8
34	RES_85_5_10-17	0.57762	0.92076	0.78307	0.54735	0.00013974	10
35	RES_85_5_10-35	0.5876	0.61604	0.10975	0.56962	0.00009043	11
36	RES_85_5_10-51	0.66185	0.95774	0.80715	0.60146	0.00002876	11
37	C+F_70_10_20-11	0.90648	0.69973	0.78576	0.86913	0.016046	10
38	C+F_70_10_20-23	0.92494	0.72127	0.90038	0.90129	0.021428	12
39	C+F_70_10_20-33	0.95484	0.91919	0.76254	0.88072	0.0065711	18
40	C+F_80_10_10-11	0.96269	0.89552	0.83256	0.93468	0.01262	27
41	C+F_80_10_10-23	0.96423	0.89838	0.8659	0.95102	0.0088218	21
42	C+F_80_10_10-33	0.94185	0.61875	0.48269	0.83489	0.042762	16
43	C+F_80_5_15-11	0.94032	0.97165	0.93642	0.94066	0.0043099	19
44	C+F_80_5_15-23	0.94552	0.93936	0.90559	0.93937	0.0070353	16
45	C+F_80_5_15-33	0.95811	0.97166	0.89735	0.95118	0.0030363	12
46	C+F_85_5_10-11	0.85493	0.7315	0.79043	0.83851	0.021476	10
47	C+F_85_5_10-23	0.91374	0.80006	0.51481	0.88078	0.020807	10
48	C+F_85_5_10-33	0.93165	0.89101	0.7667	0.90683	0.0068863	10

49	C+F(C)_70_10_20-11	0.94306	0.88933	0.79261	0.90407	0.006382	16
50	C+F(C)_70_10_20-23	0.99035	0.93642	0.91792	0.97062	0.001096	36
51	C+F(C)_70_10_20-33	0.99088	0.92069	0.53997	0.83021	0.001047	21
52	C+F(C)_80_10_10-11	0.8804	0.96462	0.92023	0.89466	0.01221	12
53	C+F(C)_80_10_10-23	0.98931	0.97563	0.85569	0.97368	0.0012175	41
54	C+F(C)_80_10_10-33	0.99117	0.94651	0.8712	0.97231	0.000967	40
55	C+F(C)_80_5_15-11	0.91441	0.86477	0.76372	0.8765	0.009125	14
56	C+F(C)_80_5_15-23	0.98657	0.8777	0.79109	0.94961	0.001538	25
57	C+F(C)_80_5_15-33	0.92851	0.85586	0.91949	0.91782	0.007535	9
58	C+F(C)_85_5_10-11	0.94219	0.95031	0.6253	0.88351	0.0061	20
59	C+F(C)_85_5_10-23	0.98928	0.98212	0.80141	0.94613	0.001173	28
60	C+F(C)_85_5_10-33	0.98615	0.97294	0.73419	0.97554	0.001657	19
61	C+F(F)_70_10_20-11	0.95316	0.88552	0.77722	0.9085	0.003713	21
62	C+F(F)_70_10_20-23	0.94468	0.75063	0.87348	0.91439	0.004592	14
63	C+F(F)_70_10_20-33	0.93485	0.82416	0.74891	0.89831	0.006237	10
64	C+F(F)_80_10_10-11	0.91492	0.9691	0.8446	0.90721	0.007103	17
65	C+F(F)_80_10_10-23	0.93363	0.78578	0.92823	0.92145	0.005278	11
66	C+F(F)_80_10_10-33	0.95331	0.92088	0.72288	0.92353	0.00356	13
67	C+F(F)_80_5_15-11	0.89549	0.59091	0.88892	0.87907	0.00736	10
68	C+F(F)_80_5_15-23	0.94491	0.98692	0.90541	0.93861	0.00455	27
69	C+F(F)_80_5_15-33	0.92103	0.60936	0.84939	0.87552	0.006775	8
70	C+F(F)_85_5_10-11	0.93448	0.95476	0.95327	0.93617	0.005235	21
71	C+F(F)_85_5_10-23	0.87832	0.56263	0.91745	0.87404	0.009377	8
72	C+F(F)_85_5_10-33	0.91805	0.94984	0.91167	0.91785	0.006489	9
73	R-RES_70_10_20-18	0.67344	0.49272	0.91649	0.55717	0.00041239	15
74	R-RES_70_10_20-37	0.64319	0.59882	0.17052	0.51962	0.0040962	9
75	R-RES_70_10_20-54	0.99364	0.79491	0.4674	0.23551	0.055495	11
76	R-RES_80_10_10-18	0.57983	0.29664	0.9112	0.53397	0.00040928	10
77	R-RES_80_10_10-37	0.60413	0.10259	0.27482	0.57539	0.00074849	10
78	R-RES_80_10_10-54	0.76463	0.19577	0.77805	0.68261	0.0011138	15
79	R-RES_80_5_15-18	0.57427	0.15525	0.1499	0.55285	0.00007205	9
80	R-RES_80_5_15-37	0.57451	0.54457	0.44905	0.53966	0.00047872	9
81	R-RES_80_5_15-54	0.61896	0.74305	-0.013812	0.2118	0.00052809	10
82	R-RES_85_5_10-18	0.5377	0.45167	0.35253	0.53232	0.00047318	11
83	R-RES_85_5_10-37	0.78324	0.89229	0.93224	0.57013	0.019719	11
84	R-RES_85_5_10-54	0.64356	-0.15899	0.82625	0.5911	0.00018284	10

B6. Results for scripted models – Group I
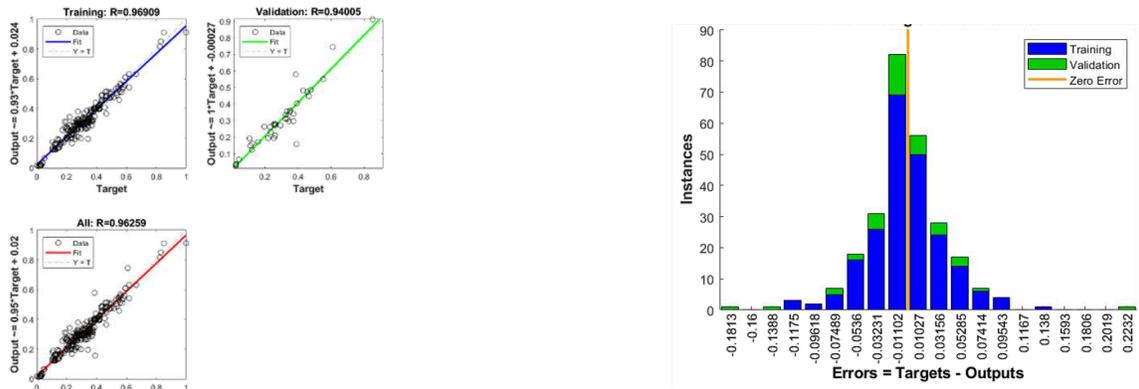
Figure B6.1 Regression coefficient and error histogram for model COMP Initial
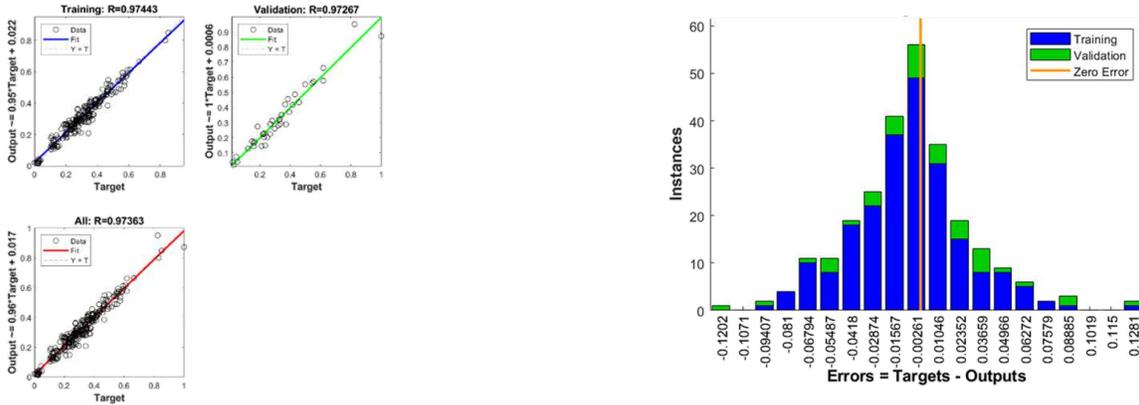
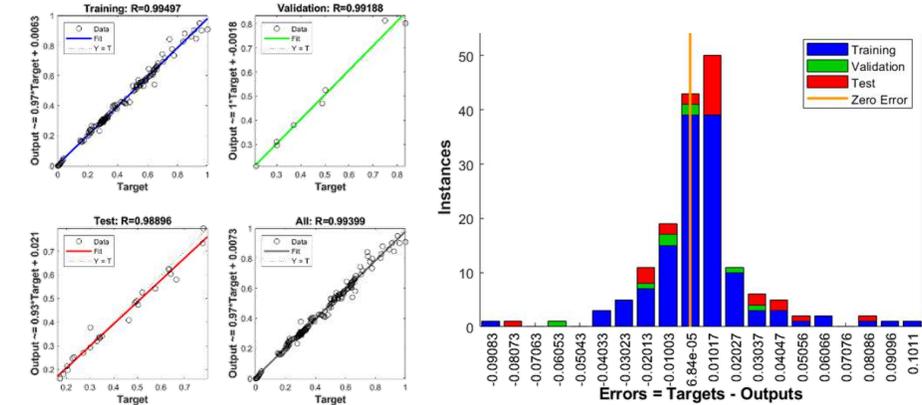*Figure B6.2* Regression coefficient and error histogram for model COMP Optimized n=25
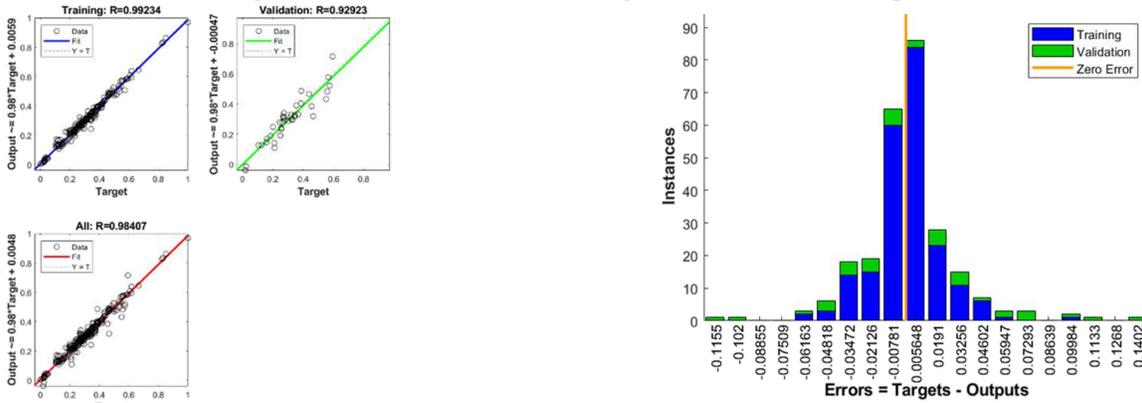
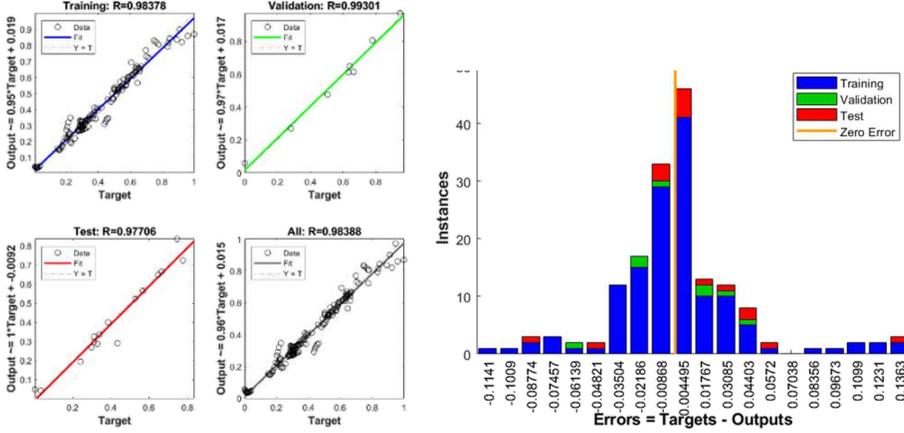*Figure B6.3* Regression coefficient and error histogram for model COMP Optimized n=31
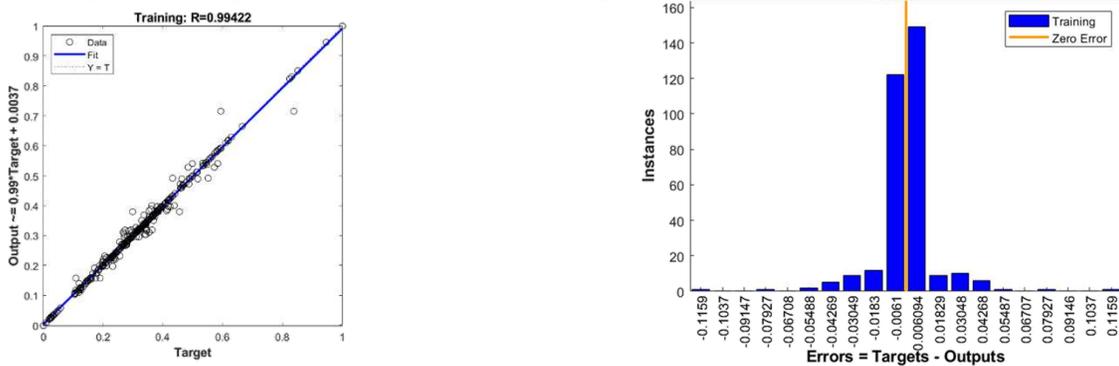
Figure B6.4 Regression coefficient and error histogram for model COMP Working
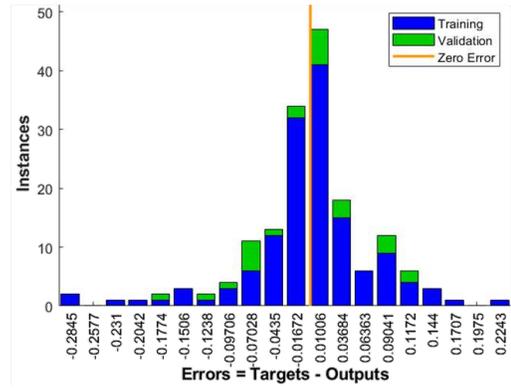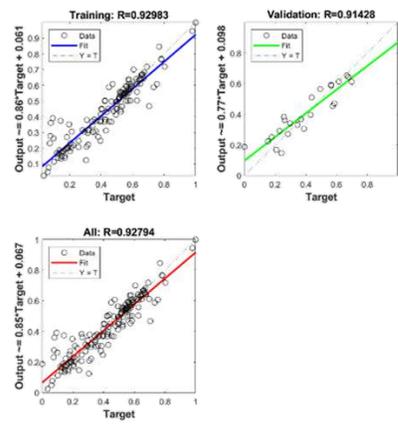
Figure B6.5 Regression coefficient and error histogram for model FLEX Initial
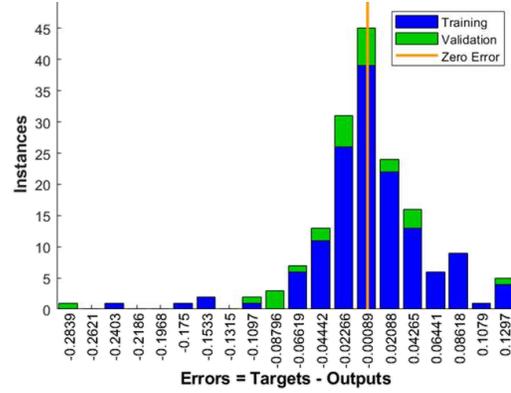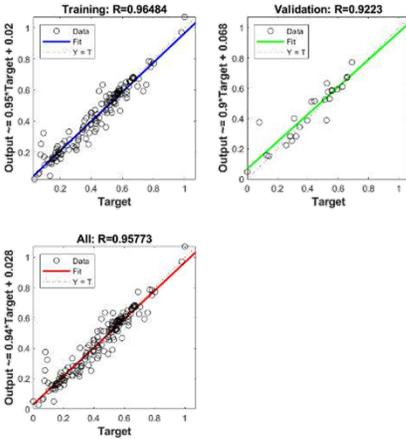
Figure B6.6 Regression coefficient and error histogram for model FLEX Optimized n-21
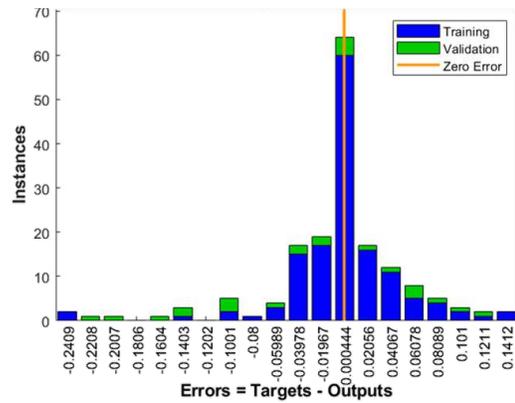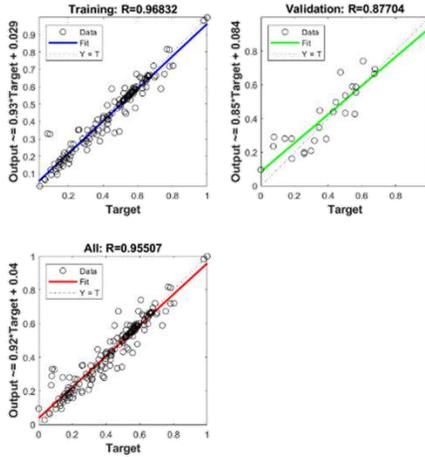
Figure B6.7 Regression coefficient and error histogram for model FLEX Optimized n=30
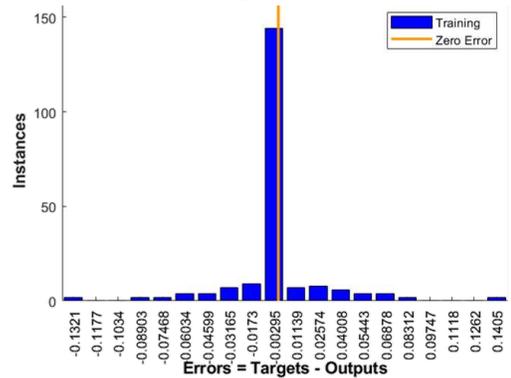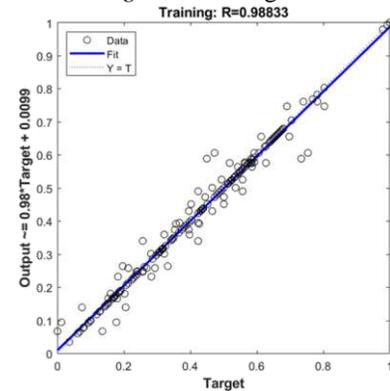
Figure B6.8 Regression coefficient and error histogram for model FLEX Working

Figure B6.9 Regression coefficient and error histogram for model COMP+FLEX Initial
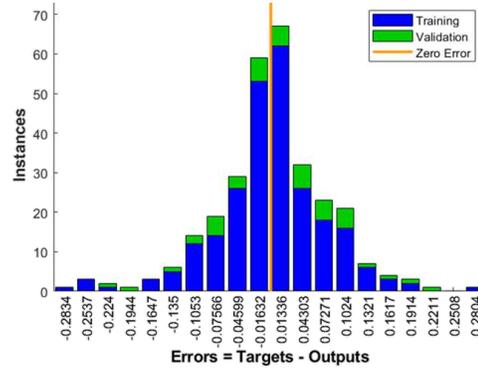
Figure B6.10 Regression coefficient and error histogram for model COMP+FLEX Optimized n=18
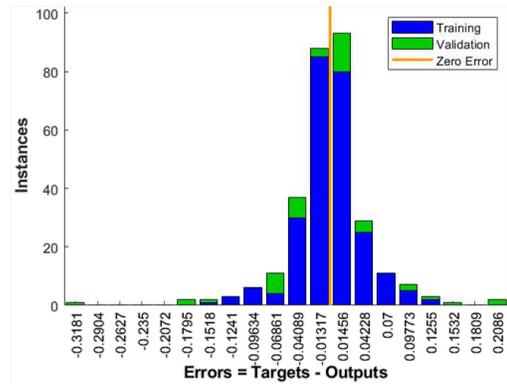
Figure B6.11 Regression coefficient and error histogram for model COMP+FLEX Optimized n=24

Figure B6.12 Regression coefficient and error histogram for model COMP+FLEX Working
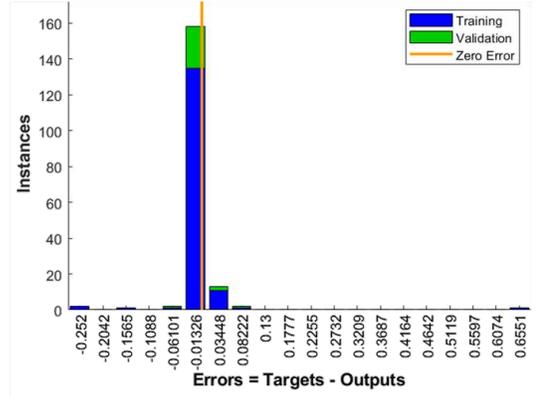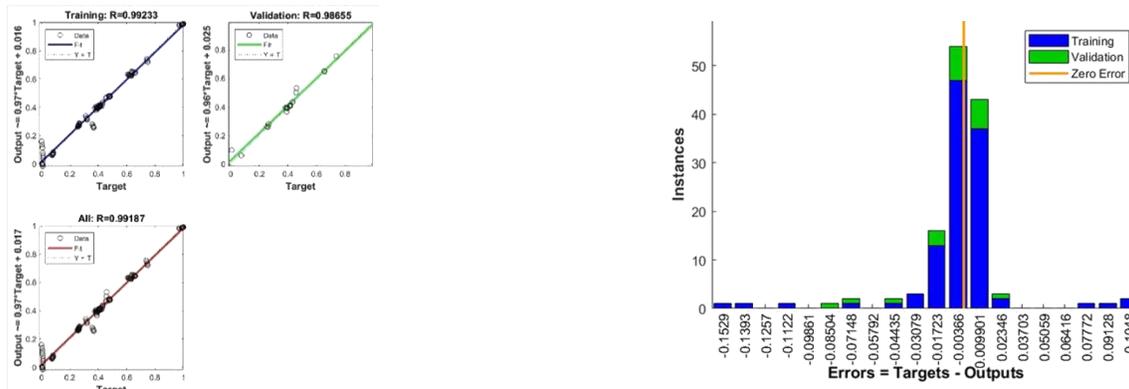
Figure B6.13 Regression coefficient and error histogram for model RESIST Initial
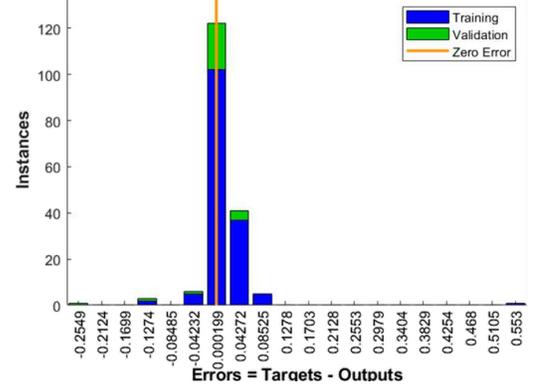
Figure B6.14 Regression coefficient and error histogram for model RESIST Optimized n=23
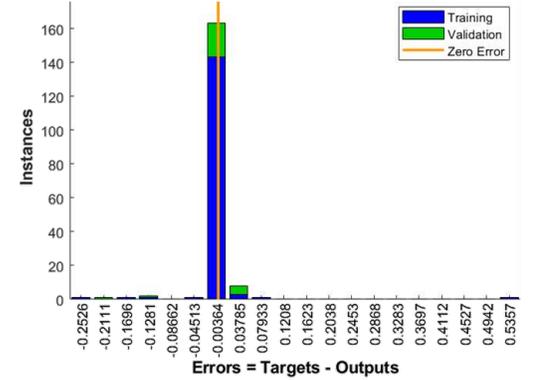
Figure B6.15 Regression coefficient and error histogram for model RESIST Optimized n=31
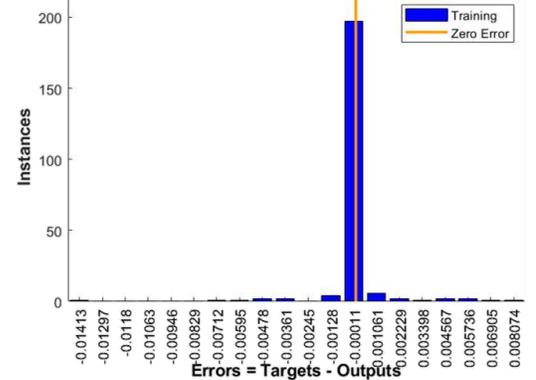
Figure B6.16 Regression coefficient and error histogram for model RESIST Working

#	Model	Regression coefficient - training	Regression coefficient - validation	Regression coefficient - total	Mean squared error - MSE	Root mean squared error - RMSE
1	COMP Initial	0.9609	0.94005	0.96259	0.0007135	0.0023
2	COMP Optimized n=25	0.97443	0.97267	0.97363	0.0012	0.0073
3	COMP Optimized n=31	0.99234	0.92923	0.98407	0.00039729	0.000019355
4	COMP Working	0.99422	/	0.99422	0.0004653	0.0001329
5	FLEX Initial	0.92983	0.91428	0.92794	0.0056	0.00043963
6	FLEX Optimized n=21	0.96484	0.9223	0.95773	0.0028	0.0029
7	FLEX Optimized n=30	0.96832	0.87704	0.95507	0.0025	0.000071645
8	FLEX Working	0.98833	/	0.98833	0.00093724	0.00065467
9	COMP+FLEX Initial	0.92493	0.83462	0.9103	0.018	0.134
10	COMP+FLEX Optimized n=18	0.93889	0.90908	0.93429	0.0986	0.2495
11	COMP+FLEX Optimized n=24	0.9831	0.91993	0.97254	0.0813	0.2851
12	COMP+FLEX Working	0.99363	/	0.99363	0.0892	0.3033
13	RESIST Initial	0.6207	0.67322	0.6173	0.0042	0.0003617
14	RESIST Optimized n=23	0.78144	0.8495	0.68137	0.0031	0.0149
15	RESIST Optimized n=31	0.76537	-0.030763	0.71474	0.003	0.0011
16	RESIST Working	0.99969	/	0.99969	0.0000028819	0.0011

B7. Results for prescribed models – Group II

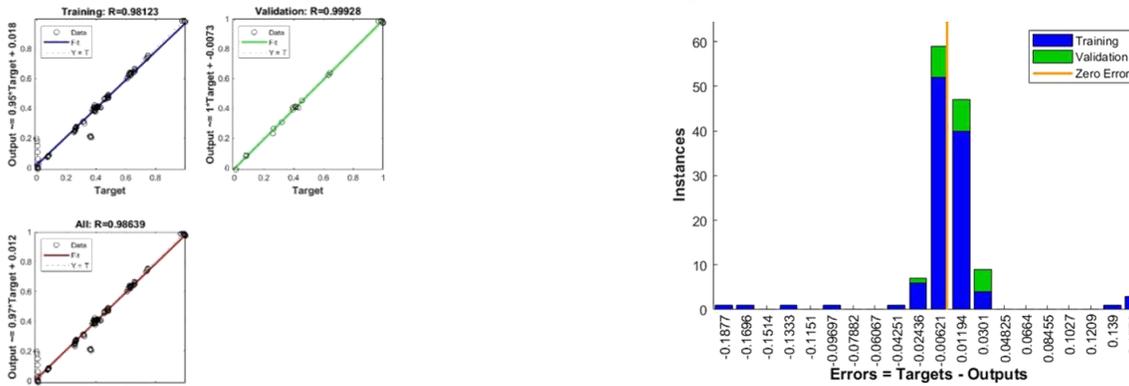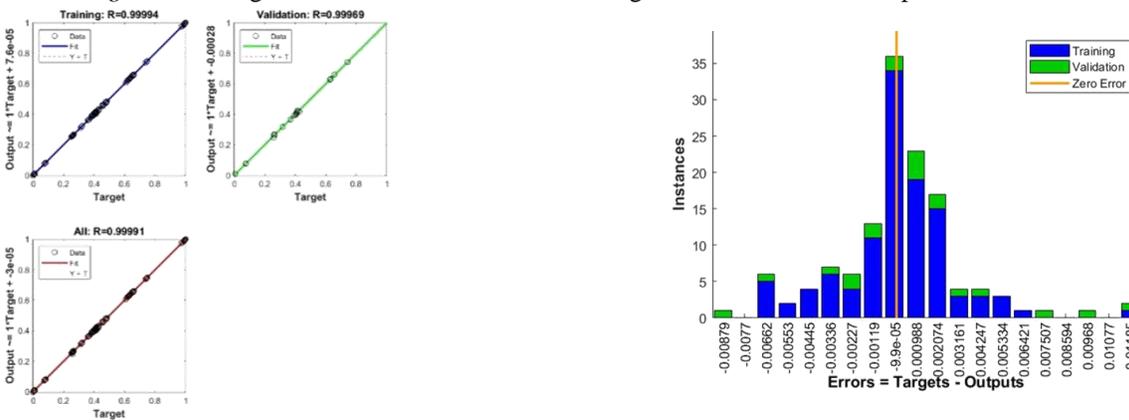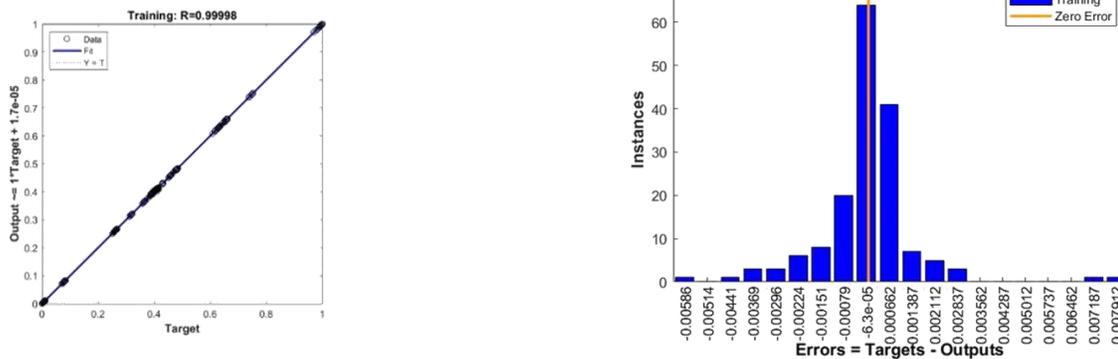*Figure B7.1* Regression coefficient and error histogram for model S_C+F_70_10_20-8

Figure B7.2 Regression coefficient and error histogram for model S_C+F_70_10_20-17

Figure B7.3 Regression coefficient and error histogram for model S_C+F_70_10_20-24

Figure B7.4 Regression coefficient and error histogram for model S_C+F_80_10_10-8
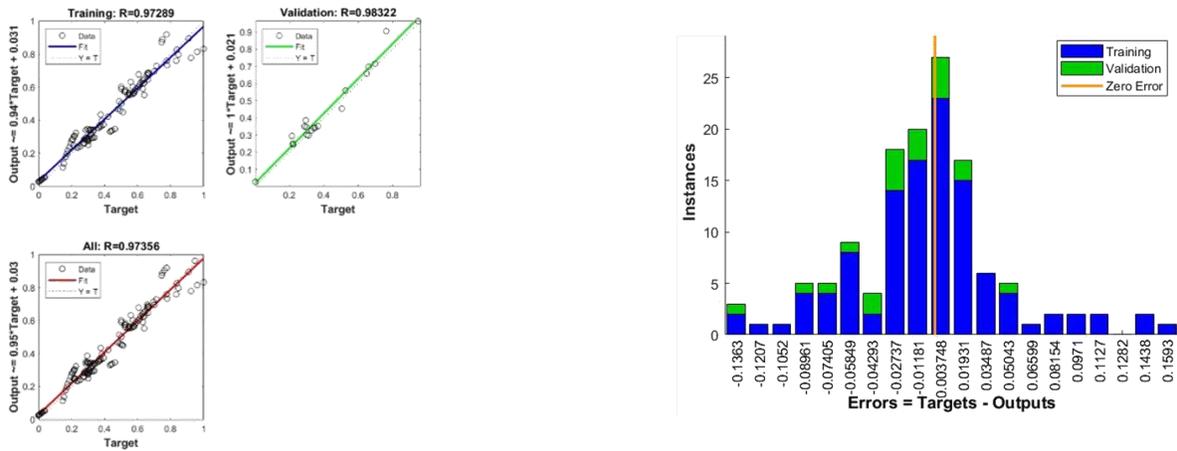
Figure B7.5 Regression coefficient and error histogram for model S_C+F_80_10_10-17

Figure B7.6 Regression coefficient and error histogram for model S_C+F_80_10_10-24

Figure B7.7 Regression coefficient and error histogram for model S_C+F_80_5_15-8

Figure B7.8 Regression coefficient and error histogram for model S_C+F_80_5_15-17

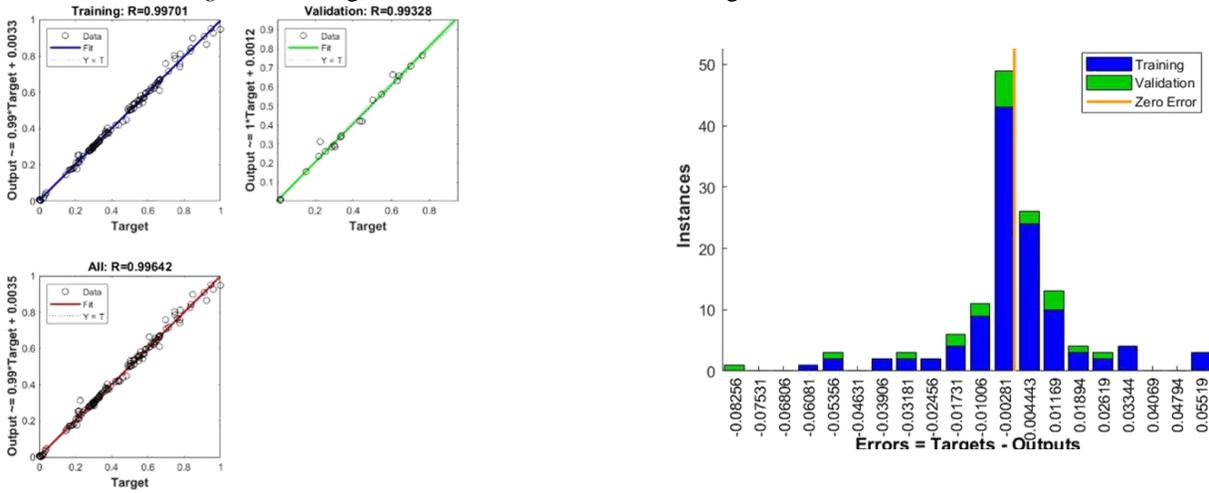*Figure B7.9* Regression coefficient and error histogram for model S_C+F_80_5_15-24

Figure B7.10 Regression coefficient and error histogram for model S_C+F_85_5_10-8

Figure B7.11 Regression coefficient and error histogram for model S_C+F_85_5_10-17

Figure B7.12 Regression coefficient and error histogram for model S_C+F_85_5_10-24

Figure B7.13 Regression coefficient and error histogram for model S_C+F(C)_70_10_20-8

Figure B7.14 Regression coefficient and error histogram for model S_C+F(C)_70_10_20-17

Figure B7.15 Regression coefficient and error histogram for model S_C+F(C)_70_10_20-24

Figure B7.16 Regression coefficient and error histogram for model S_C+F(C)_80_10_10-8

Figure B7.17 Regression coefficient and error histogram for model S_C+F(C)_80_10_10-17

Figure B7.18 Regression coefficient and error histogram for model S_C+F(C)_80_10_10-24
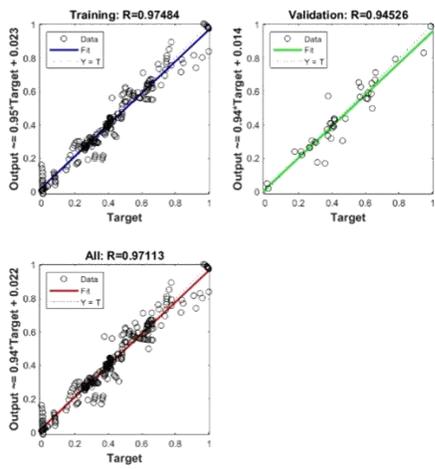

Figure B7.19 Regression coefficient and error histogram for model S_C+F(C)_80_5_15-8

Figure B7.20 Regression coefficient and error histogram for model S_C+F(C)_80_5_15-17

Figure B7.21 Regression coefficient and error histogram for model S_C+F(C)_80_5_15-24

Figure B7.22 Regression coefficient and error histogram for model S_C+F(C)_85_5_10-8

Figure B7.23 Regression coefficient and error histogram for model S_C+F(C)_85_5_10-17

Figure B7.24 Regression coefficient and error histogram for model S_C+F(C)_85_5_10-24

Figure B7.25 Regression coefficient and error histogram for model S_C+F(F)_70_10_20-8

Figure B7.26 Regression coefficient and error histogram for model S_C+F(F)_70_10_20-17

Figure B7.27 Regression coefficient and error histogram for model S_C+F(F)_70_10_20-24
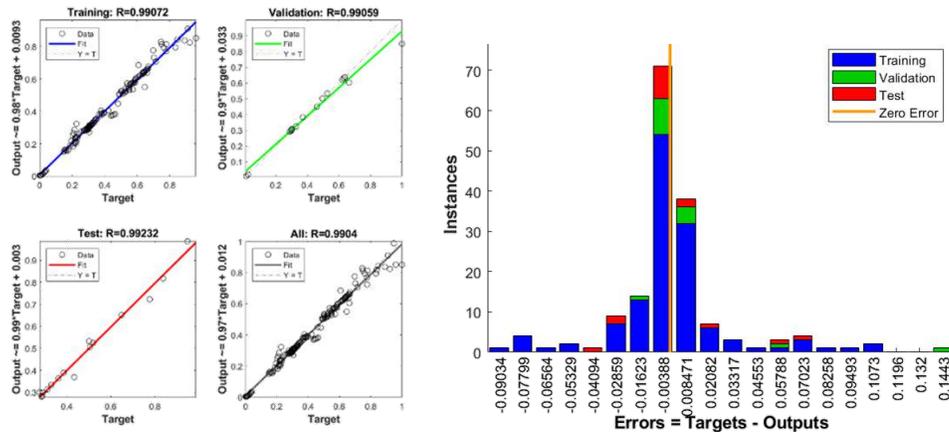
Figure B7.28 Regression coefficient and error histogram for model S_C+F(F)_80_10_10-8
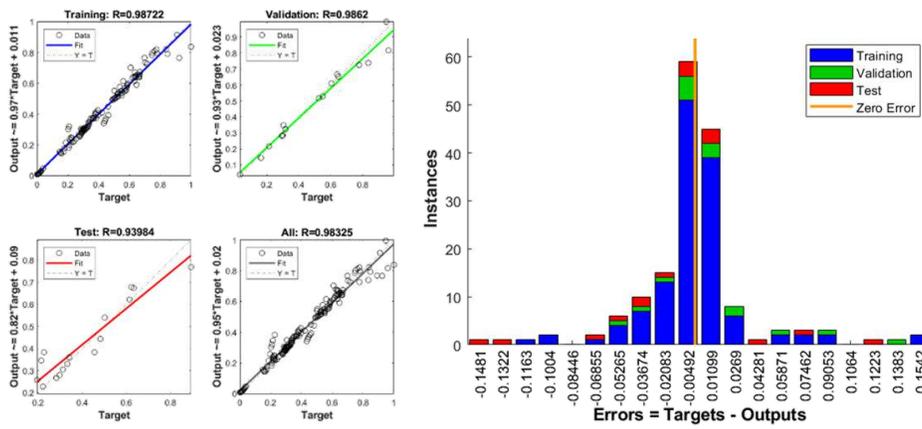
Figure B7.29 Regression coefficient and error histogram for model S_C+F(F)_80_10_10-17
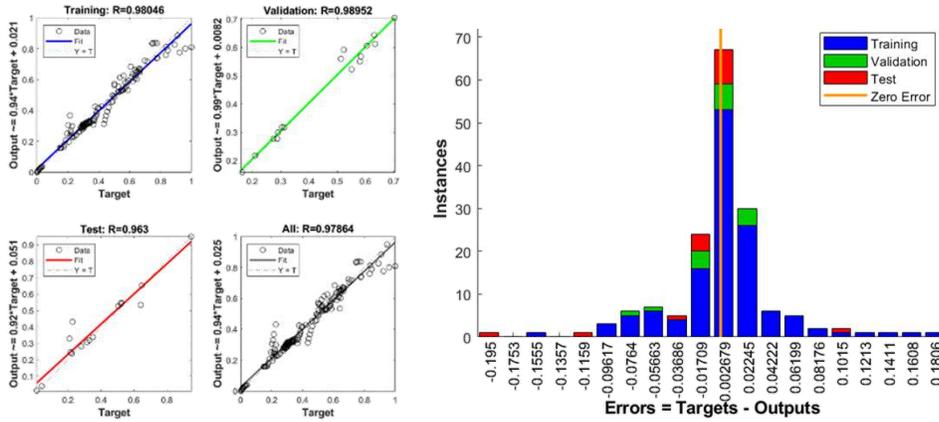
Figure B7.30 Regression coefficient and error histogram for model S_C+F(F)_80_10_10-24

Figure B7.31 Regression coefficient and error histogram for model S_C+F(F)_80_5_15-8
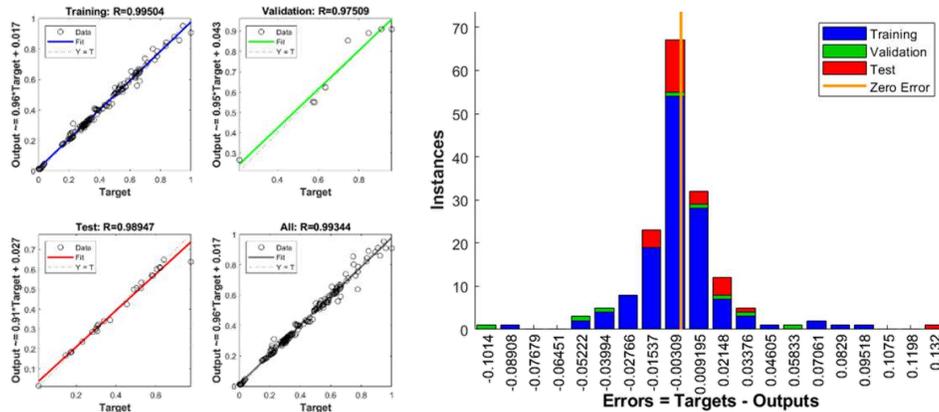
Figure B7.32 Regression coefficient and error histogram for model S_C+F(F)_80_5_15-17
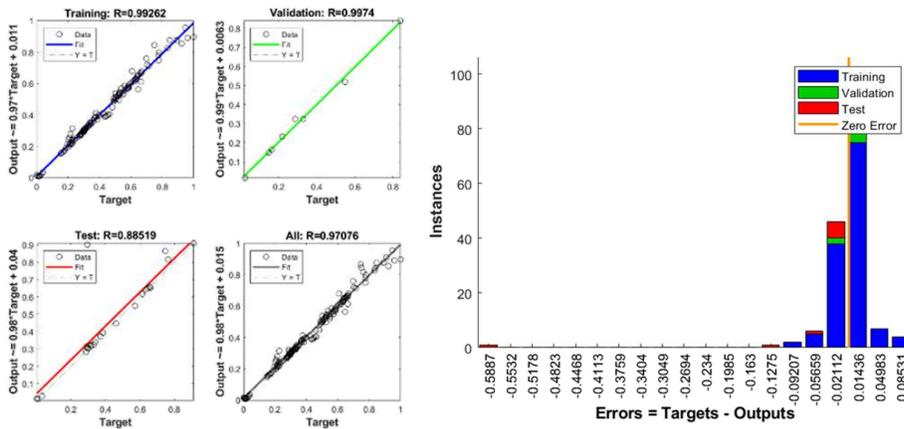
Figure B7.33 Regression coefficient and error histogram for model S_C+F(F)_80_5_15-24

Figure B7.34 Regression coefficient and error histogram for model S_C+F(F)_85_5_10-8
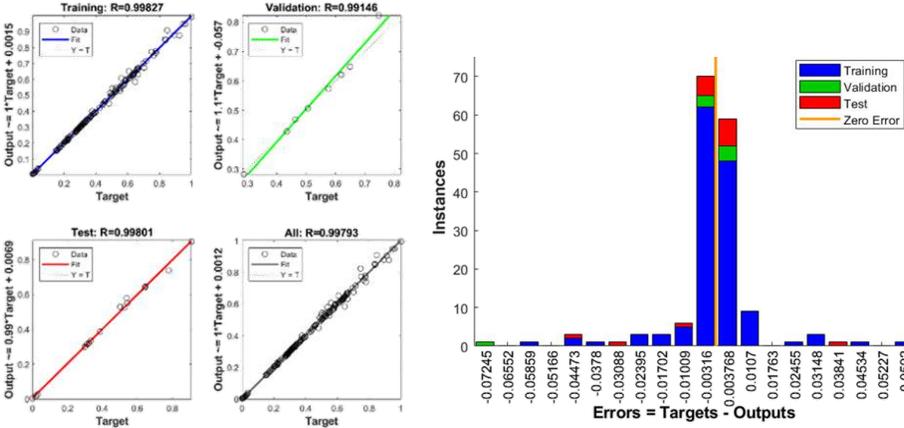
Figure B7.35 Regression coefficient and error histogram for model S_C+F(F)_85_5_10-17
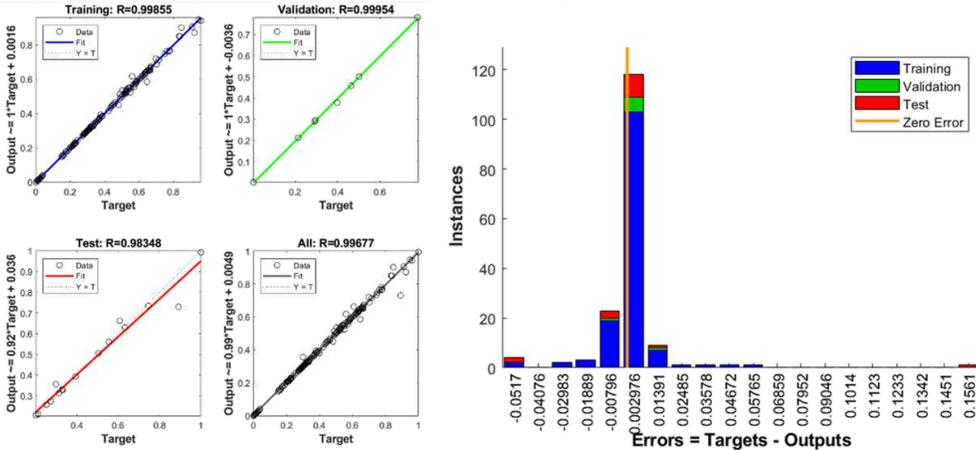
Figure B7.36 Regression coefficient and error histogram for model S_C+F(F)_85_5_10-24

Table B7.1 Results for prescribed models based on datasets from Group II

#	Model	Regression coefficient - training	Regression coefficient - validation	Regression coefficient - testing	Regression coefficient - total	Mean squared error - MSE	Epoch
1	S_C+F_70_10_20-8	0.99629	0.98852	0.98441	0.99333	0.00041914	70
2	S_C+F_70_10_20-17	0.99918	0.99693	0.9643	0.99401	0.00009324	81
3	S_C+F_70_10_20-24	0.98782	0.98054	0.93792	0.97471	0.0012624	24
4	S_C+F_80_10_10-8	0.9985	0.99993	0.99866	0.9987	0.0001597	183
5	S_C+F_80_10_10-17	0.98866	0.99668	0.9673	0.98778	0.001245	33
6	S_C+F_80_10_10-24	0.97764	0.9449	0.94194	0.97232	0.002636	12
7	S_C+F_80_5_15-8	0.98663	0.97822	0.98998	0.98657	0.0013906	38
8	S_C+F_80_5_15-17	0.99892	0.99907	0.99575	0.99845	0.0001255	47
9	S_C+F_80_5_15-24	0.99497	0.98721	0.85313	0.97099	0.00056264	27
10	S_C+F_85_5_10-8	0.98122	0.95136	0.9919	0.98092	0.00190345	38
11	S_C+F_85_5_10-17	0.99868	0.9981	0.99761	0.99851	0.0001442	78
12	S_C+F_85_5_10-24	0.99933	0.99988	0.99622	0.99902	0.0000703	113
13	S_C+F(C)_70_10_20-8	0.99996	0.99984	0.88325	0.96522	0.0000045	101
14	S_C+F(C)_70_10_20-17	0.99974	0.99981	0.98778	0.9974	0.00003163	46
15	S_C+F(C)_70_10_20-24	0.99991	0.99976	0.97514	0.99494	0.0000101	51
16	S_C+F(C)_80_10_10-8	0.99995	0.99982	0.99908	0.99989	0.00000696	176
17	S_C+F(C)_80_10_10-17	0.99996	0.99985	0.9994	0.99994	0.00000473	143
18	S_C+F(C)_80_10_10-24	0.9999	0.99992	0.99992	0.99993	0.0000067	54
19	S_C+F(C)_80_5_15-8	0.98644	0.99994	0.93805	0.98166	0.001706	21
20	S_C+F(C)_80_5_15-17	0.99984	0.99978	0.85702	0.97192	0.0000197	32
21	S_C+F(C)_80_5_15-24	0.99957	0.99986	0.99375	0.99863	0.0000495	32
22	S_C+F(C)_85_5_10-8	0.99985	0.99984	0.9999	0.99985	0.0000178	57
23	S_C+F(C)_85_5_10-17	0.99334	0.99921	0.98391	0.99298	0.0008709	28
24	S_C+F(C)_85_5_10-24	0.99522	0.99884	0.99226	0.99501	0.0006186	24
25	S_C+F(F)_70_10_20-8	0.97565	0.98298	0.9758	0.9759	0.0020427	12
26	S_C+F(F)_70_10_20-17	0.99737	0.99486	0.99466	0.99651	0.0002681	39
27	S_C+F(F)_70_10_20-24	0.9978	0.98805	0.96117	0.98743	0.0002038	61
28	S_C+F(F)_80_10_10-8	0.99072	0.99059	0.99232	0.9904	0.0008968	45
29	S_C+F(F)_80_10_10-17	0.98722	0.9862	0.93984	0.98325	0.0011868	17
30	S_C+F(F)_80_10_10-24	0.98046	0.98952	0.962	0.97864	0.001998	10
31	S_C+F(F)_80_5_15-8	0.99497	0.99188	0.98896	0.99399	0.0005593	45
32	S_C+F(F)_80_5_15-17	0.99504	0.97509	0.98947	0.99344	0.000515	34
33	S_C+F(F)_80_5_15-24	0.99262	0.9974	0.88519	0.97076	0.0006981	13
34	S_C+F(F)_85_5_10-8	0.98378	0.99301	0.97706	0.98388	0.0015214	15
35	S_C+F(F)_85_5_10-17	0.99827	0.99146	0.99801	0.99793	0.0001675	105
36	S_C+F(F)_85_5_10-24	0.99855	0.99954	0.98348	0.99677	0.0001397	102

B8. Results for scripted models – Group II

Figure B8.1 Regression coefficients and error histogram for model COMP Initial

Figure B8.2 Regression coefficients and error histogram for model COMP Optimized n=10

Figure B8.3 Regression coefficients and error histogram for model COP Optimized n=13

Figure B8.4 Regression coefficients and error histogram for model COMP Working

Figure B8.5 Regression coefficients and error histogram for model FLEX Initial

Figure B8.6 Regression coefficients and error histogram for model FLEX Optimized n=10
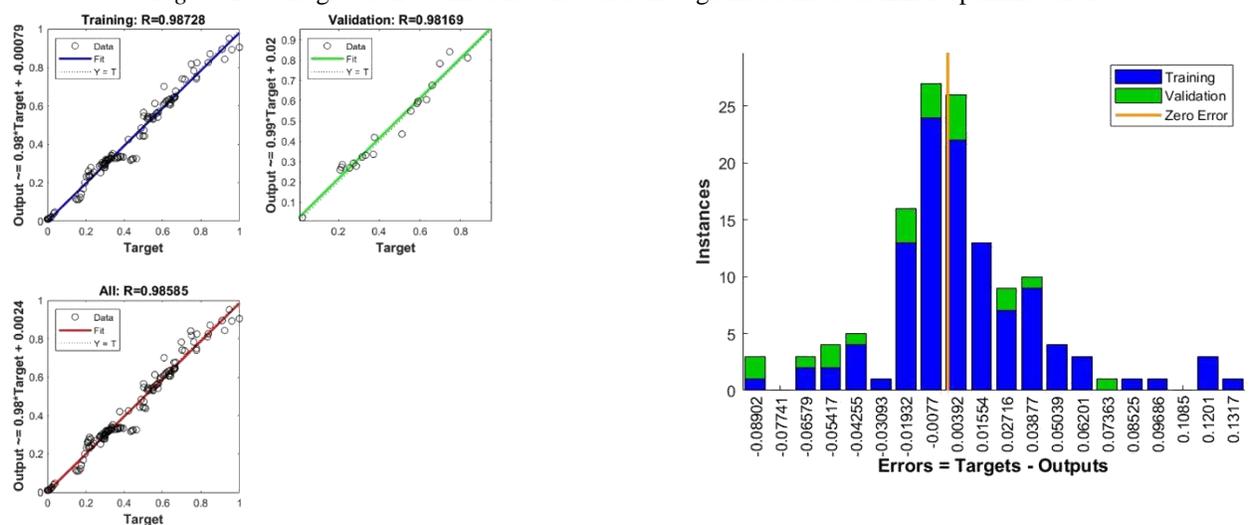
Figure B8.7 Regression coefficients and error histogram for model FLEX Optimized n=13
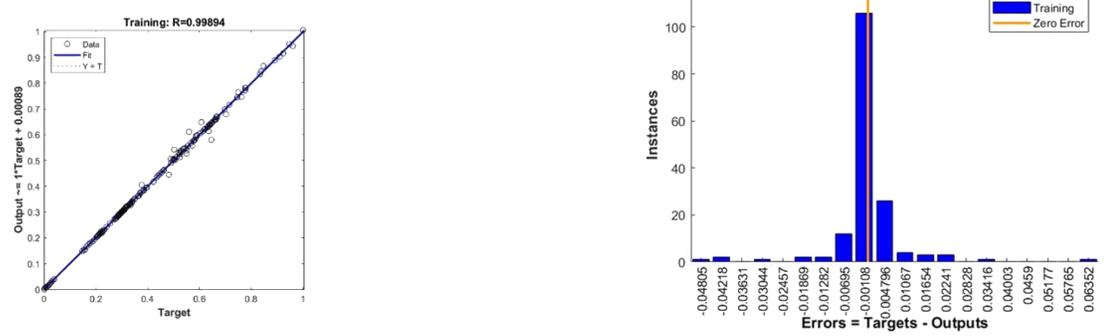
Figure B8.8 Regression coefficients and error histogram for model FLEX Working

112
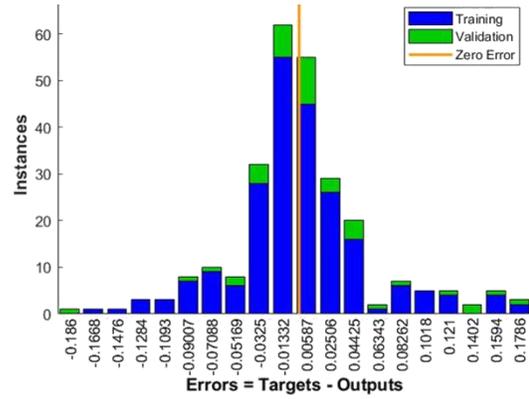
Figure B8.9 Regression coefficients and error histogram for model COMP+FLEX Initial
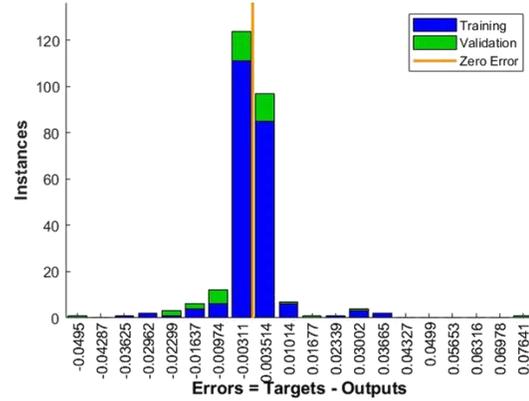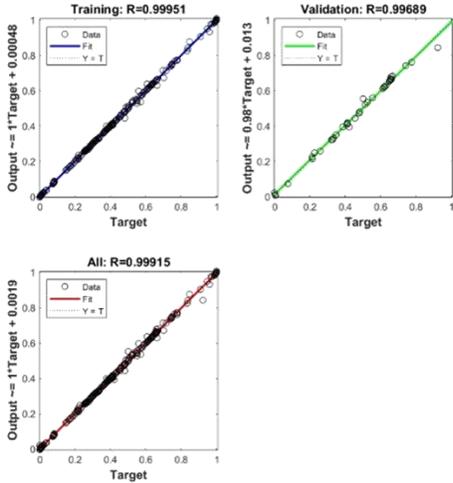
Figure B8.10 Regression coefficients and error histogram for model COMP+FLEX Optimized n=13
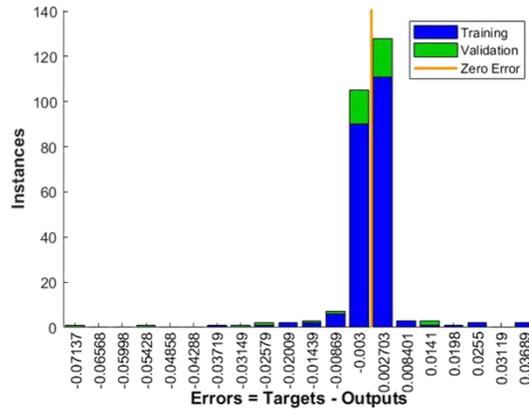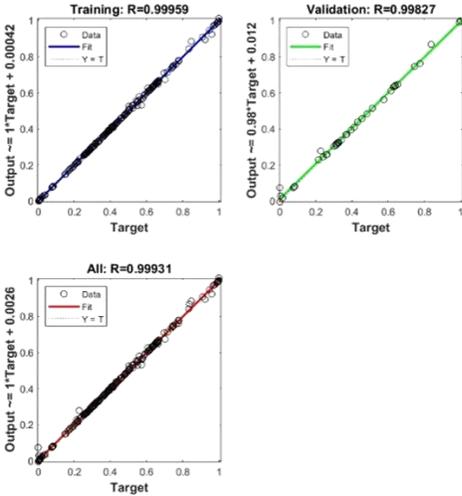
Figure B8.11 Regression coefficients and error histogram for model COMP+FLEX Optimized n=17
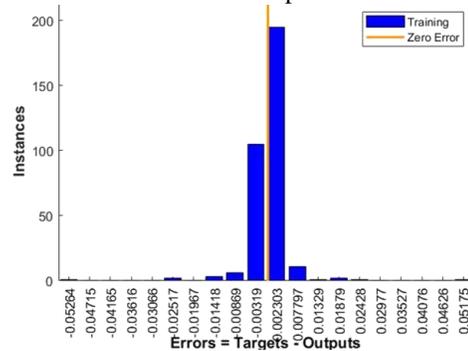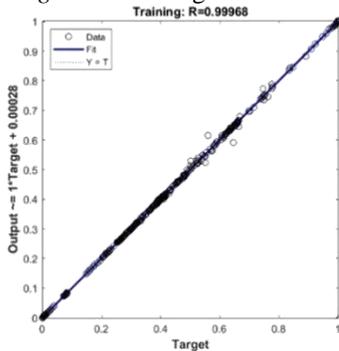
Figure B8.12 Regression coefficients and error histogram for model COMP+FLEX Working

#	Model	Regression coefficient - training	Regression coefficient - validation	Regression coefficient - total	Mean squared error - MSE	Root mean squared error - RMSE
1	COMP Initial	0.99233	0.98655	0.99187	0.001	0.0319
2	COMP Optimized n=10	0.98123	0.99928	0.98639	0.0019	0.00065577
3	COMP Optimized n=13	0.9994	0.99969	0.99991	0.000007986	0.0028
4	COMP Working	0.99998	/	0.99998	0.00000231	0.0028
5	FLEX Initial	0.97289	0.98322	0.97356	0.0028	0.0533
6	FLEX Optimized n=10	0.99701	0.99238	0.99642	0.0003194	0.00006157
7	FLEX Optimized n=13	0.98728	0.98169	0.98585	0.0014	0.0378
8	FLEX Working	0.99894	/	0.99894	0.0001047	0.0378
9	COMP+FLEX Initial	0.97484	0.94526	0.97113	0.1461	0.3823
10	COMP+FLEX Optimized n=13	0.99951	0.99689	0.99915	0.1438	0.2505
11	COMP+FLEX Optimized n=17	0.99959	0.99827	0.99931	0.135	0.3674
12	COMP+FLEX Working	0.99968	/	0.99968	0.138	0.3674

Table B8.1 Results for scripted models based on datasets from Group II

B9. Results – Evaluation

Evaluation of models in Group I
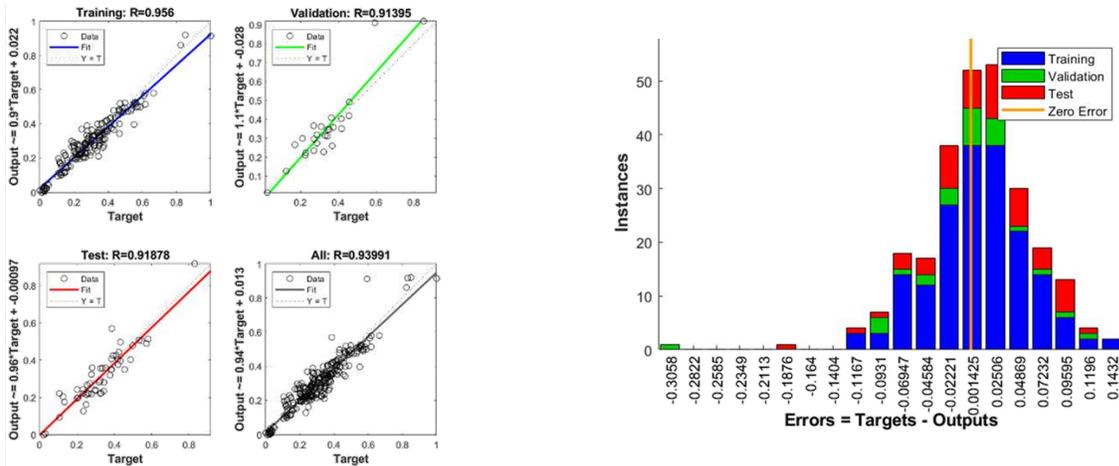
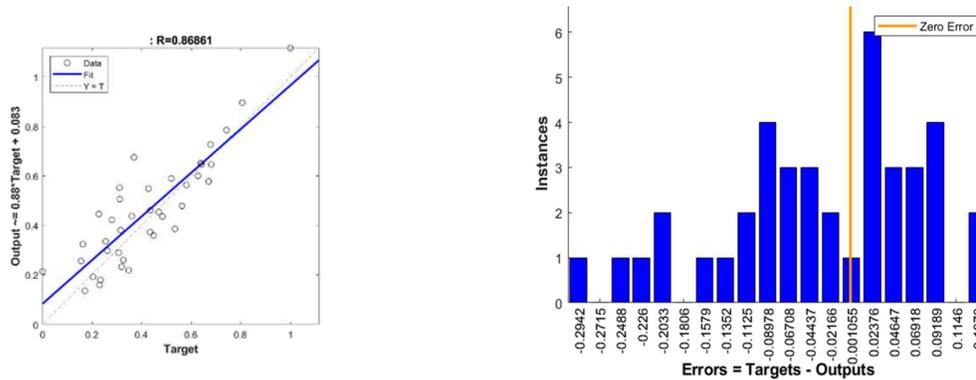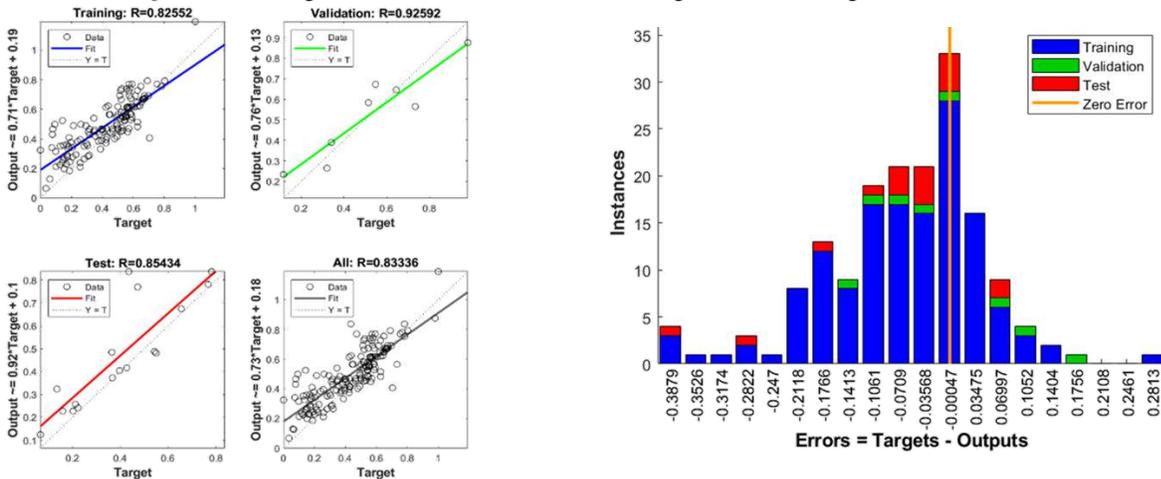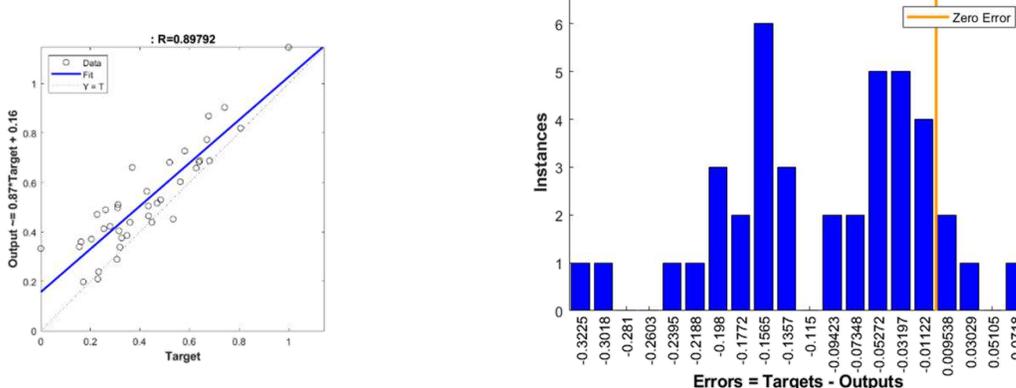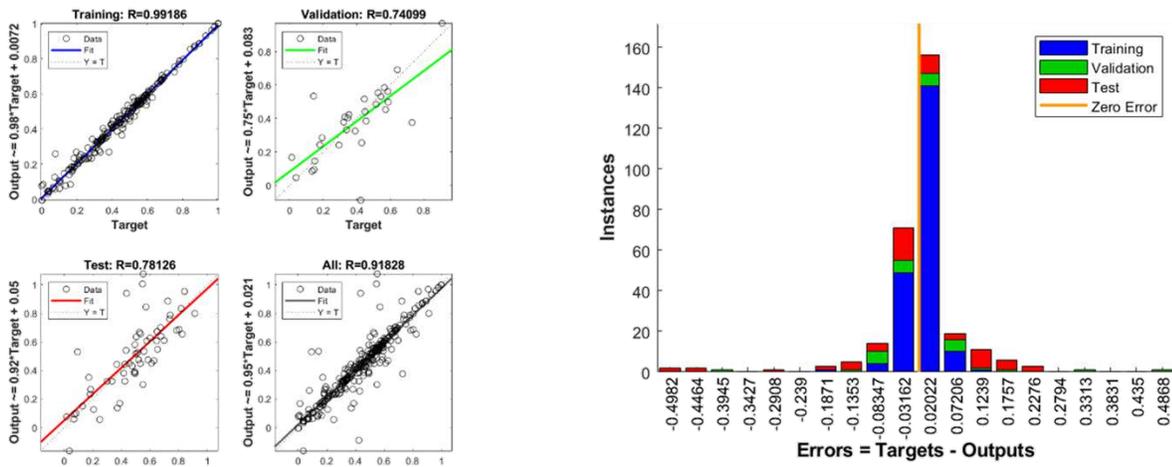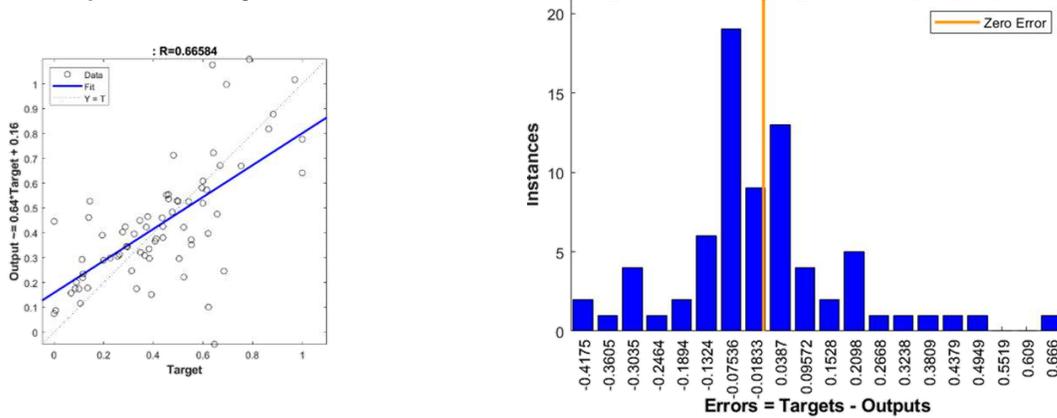*Figure B9.1* Regression coefficient and error histogram after training EV-COMP_70_10_20-41
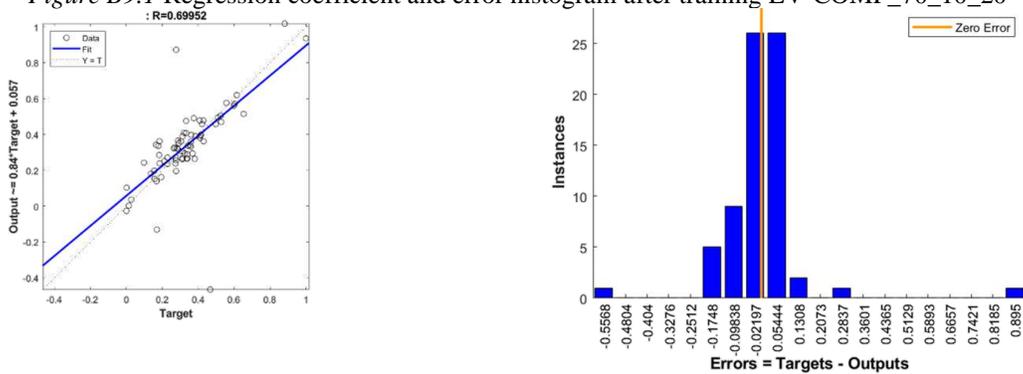
Figure B9.2 Regression coefficient and error histogram after testing EV-COMP_70_10_20-41
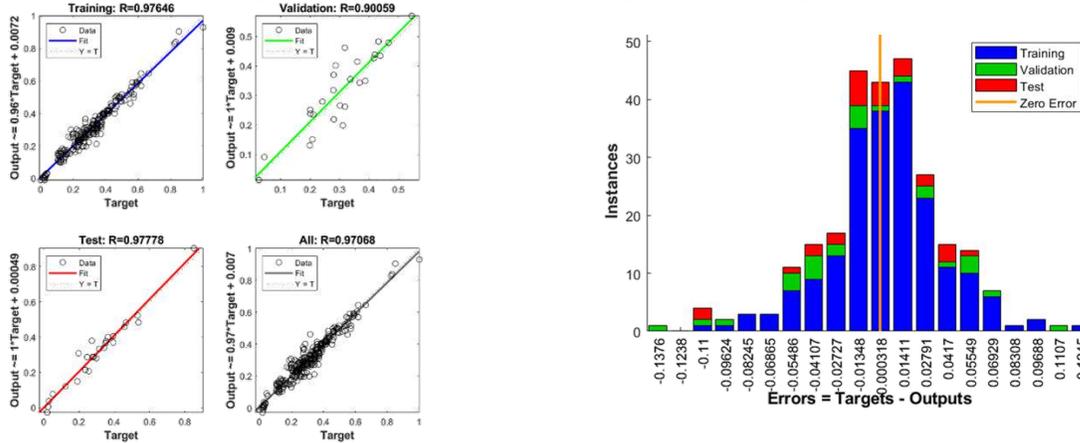
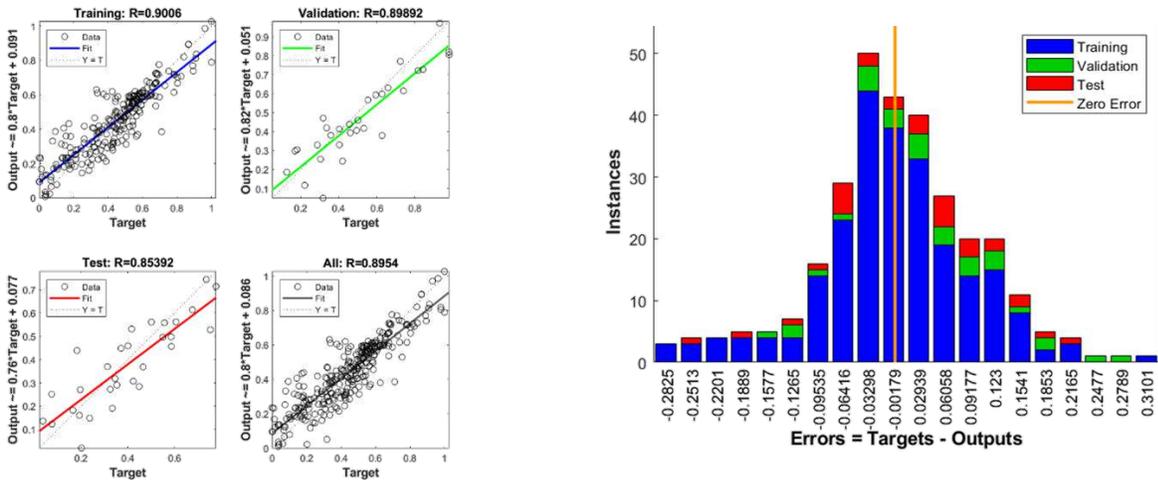*Figure B9.3* Regression coefficient and error histogram after training EV-COMP_80_10_10-60
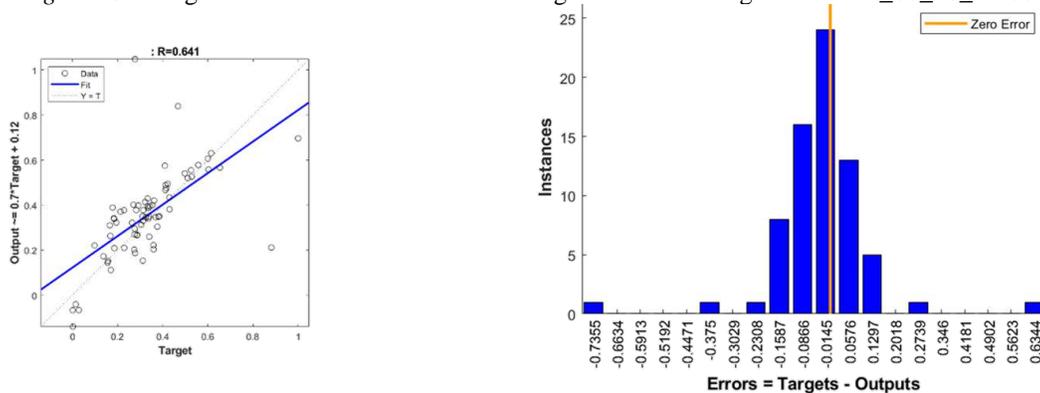
Figure B9.4 Regression coefficient and error histogram after testing EV-COMP_80_10_10-60
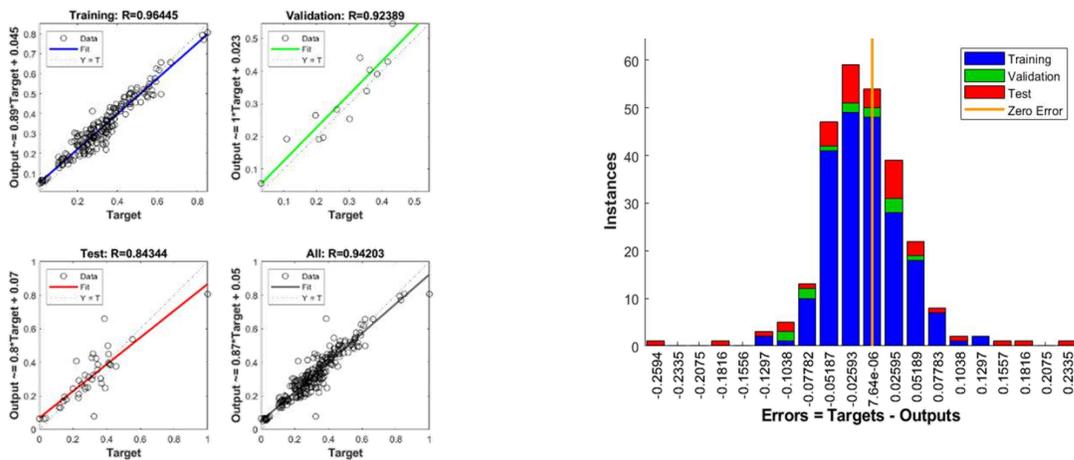
Figure B9.5 Regression coefficient and error histogram after training EV-COMP_80_5_15-20
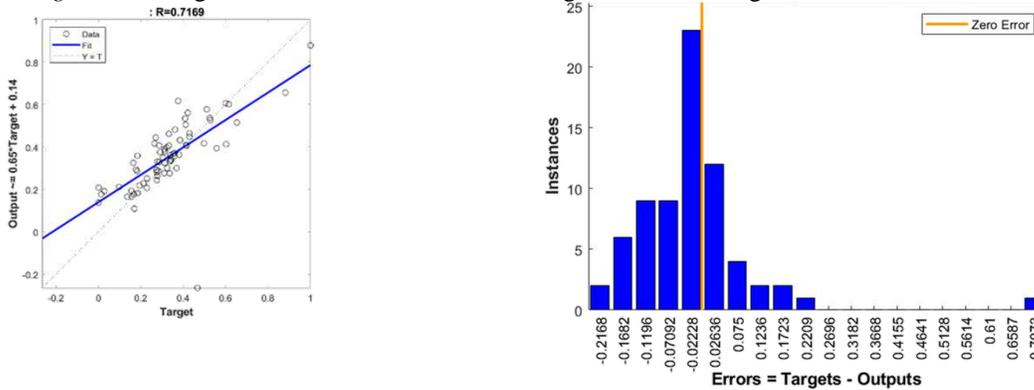
Figure B9.6 Regression coefficient and error histogram after testing EV-COMP_80_5_15-20
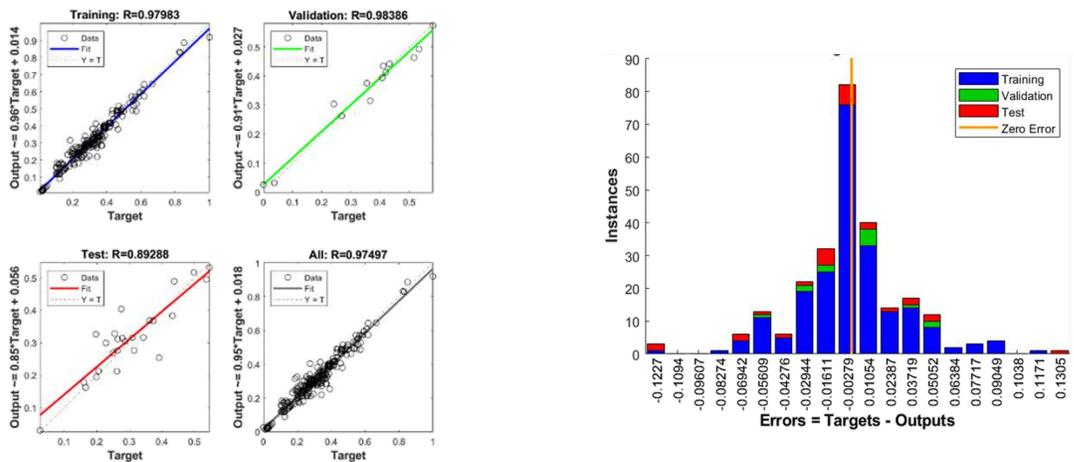
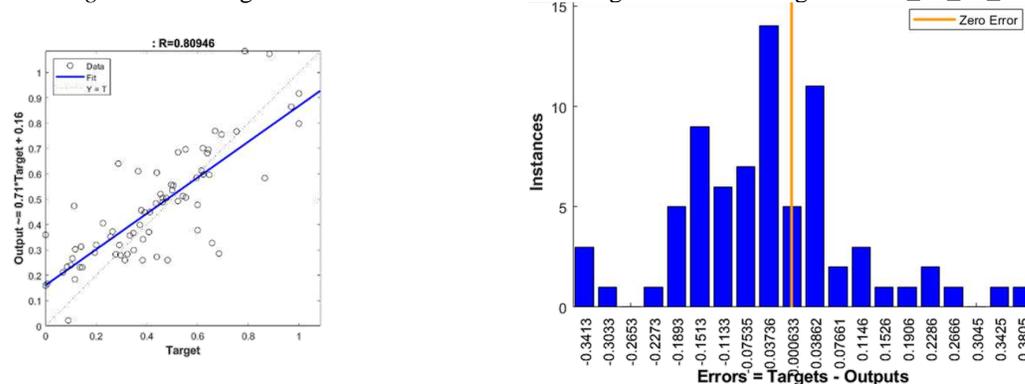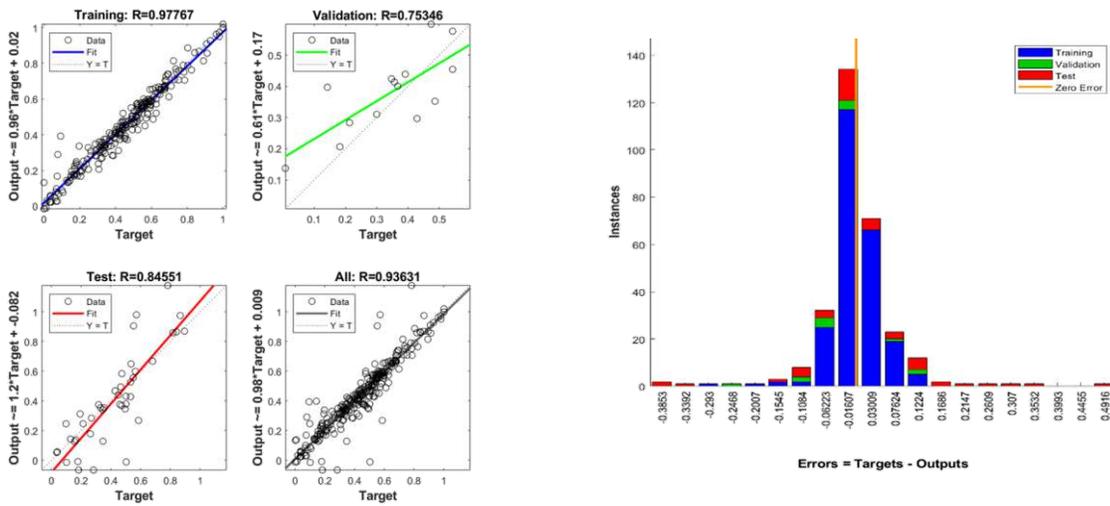*Figure B9.7* Regression coefficient and error histogram after training EV-COMP_85_5_10-41
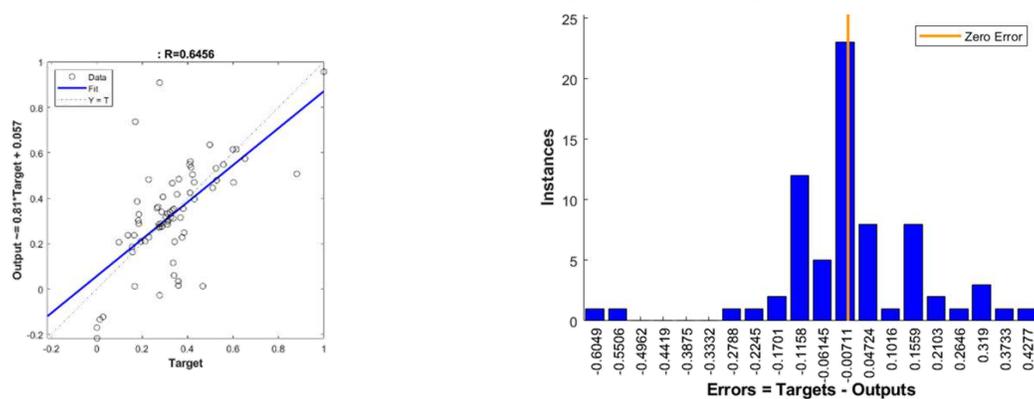
Figure B9.8 Regression coefficient and error histogram after testing EV- COMP_85_5_10-41
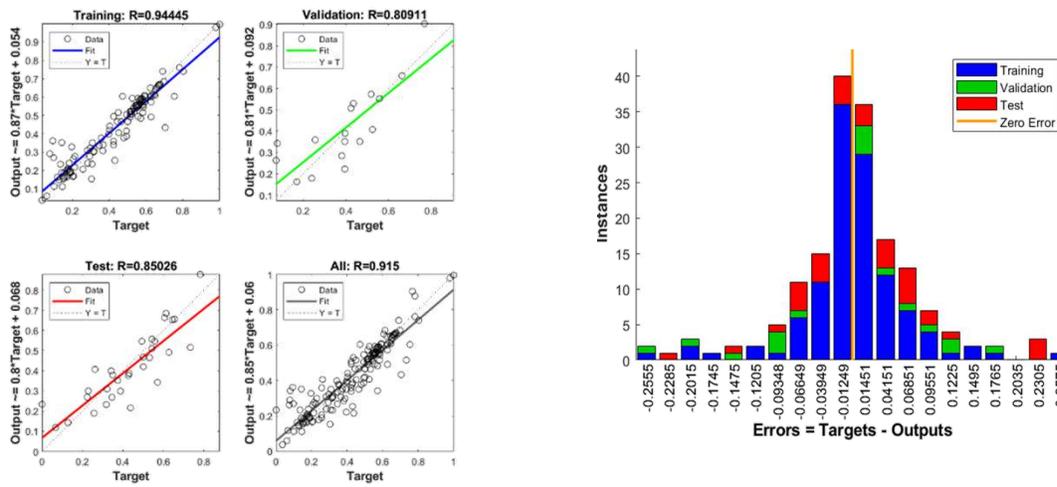
Figure B9.9 Regression coefficient and error histogram after training EV-FLEX_70_10_20-48
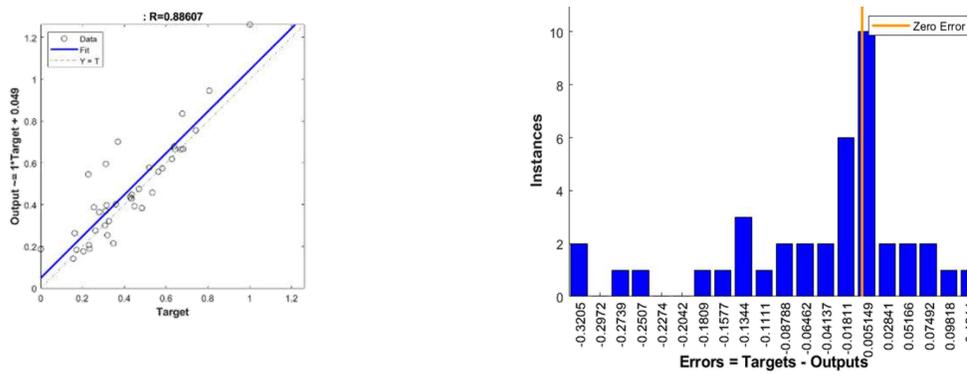
Figure B9.10 Regression coefficient and error histogram after testing EV- FLEX_70_10_20-48
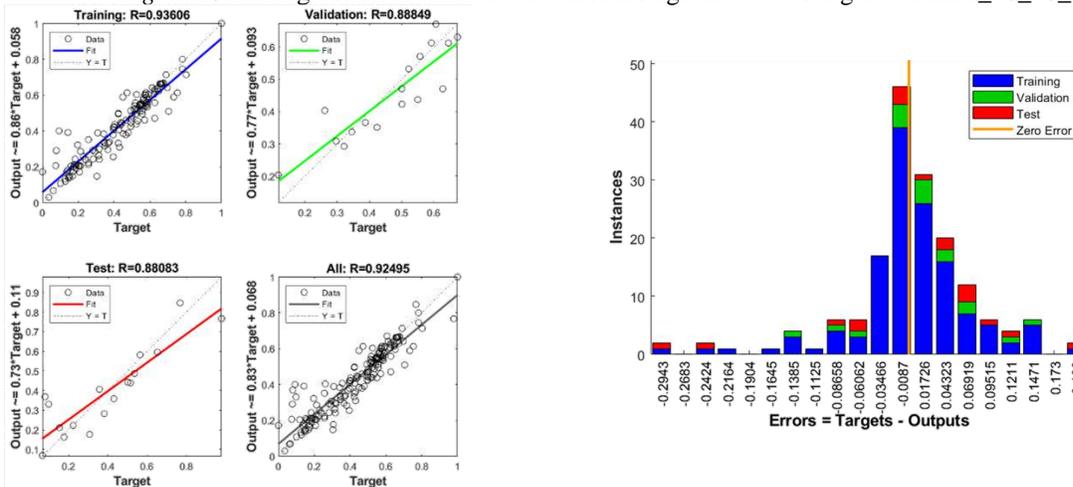
Figure B9.11 Regression coefficient and error histogram after training EV-FLEX_80_10_10-48
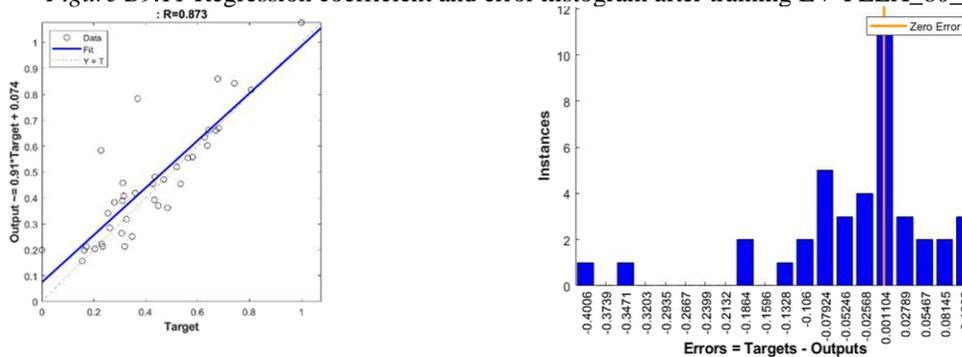
Figure B9.12 Regression coefficient and error histogram after testing EV- FLEX_80_10_10-48
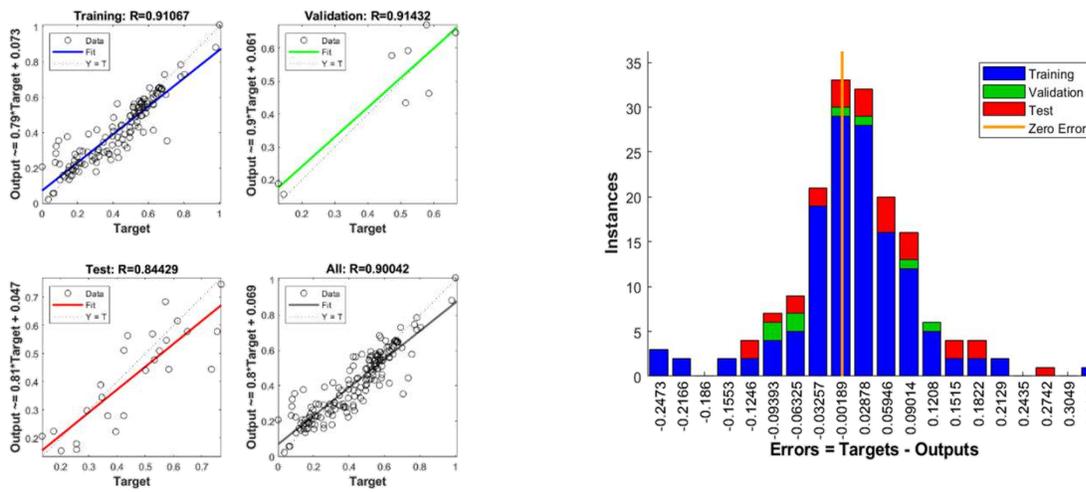
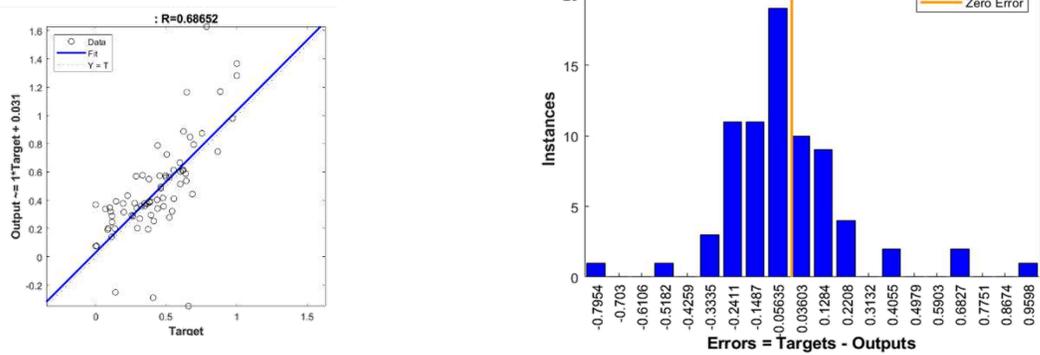*Figure B9.13* Regression coefficient and error histogram after training EV-FLEX_80_5_15-16

Figure B9.14 Regression coefficient and error histogram after testing EV- FLEX_80_5_15-16
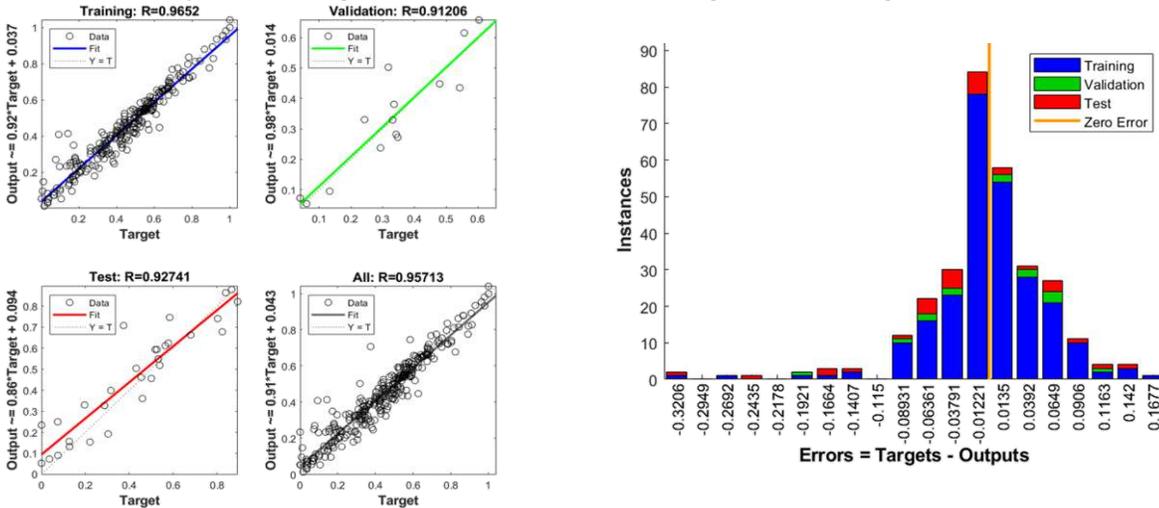

Figure B9.15 Regression coefficient and error histogram after training EV-FLEX_85_5_10-16

Figure B9.16 Regression coefficient and error histogram after testing EV- FLEX_85_5_10-16

Figure B9.17 Regression coefficient and error histogram after training EV-C+F_70_10_20-33

Figure B9.18 Regression coefficient and error histogram after testing EV-C+F_70_10_20-33

Figure B9.19 Regression coefficient and error histogram after training EV-C+F_80_10_10-11

Figure B9.20 Regression coefficient and error histogram after testing EV-C+F_80_10_10-11

Figure B9.21 Regression coefficient and error histogram after training EV-C+F_80_5_15-11

Figure B9.22 Regression coefficient and error histogram after testing EV-C+F_80_5_15-11

Figure B9.23 Regression coefficient and error histogram after training EV-C+F_85_5_10-33
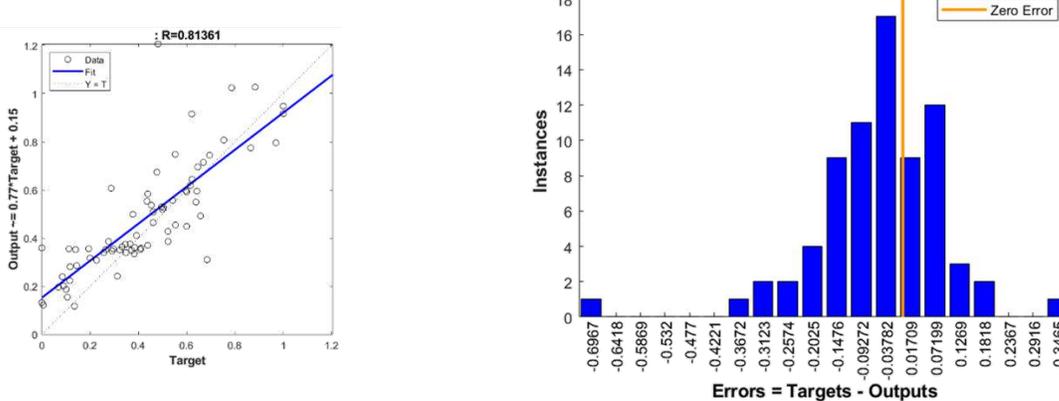

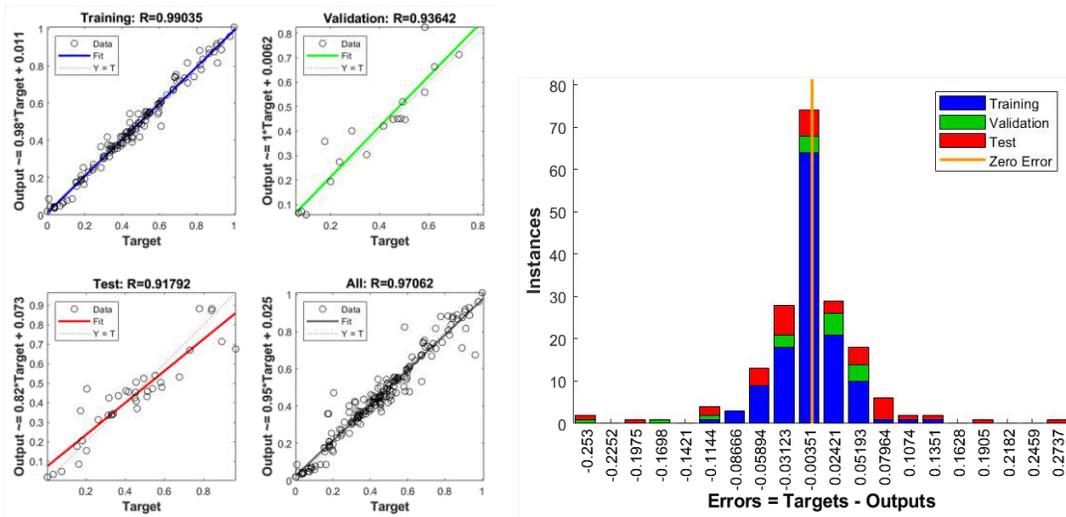*Figure B9.24* Regression coefficient and error histogram after testing EV-C+F_85_5_10-33

Figure B9.25 Regression coefficient and error histogram after training EV-C+F(C)_70_10_20-23
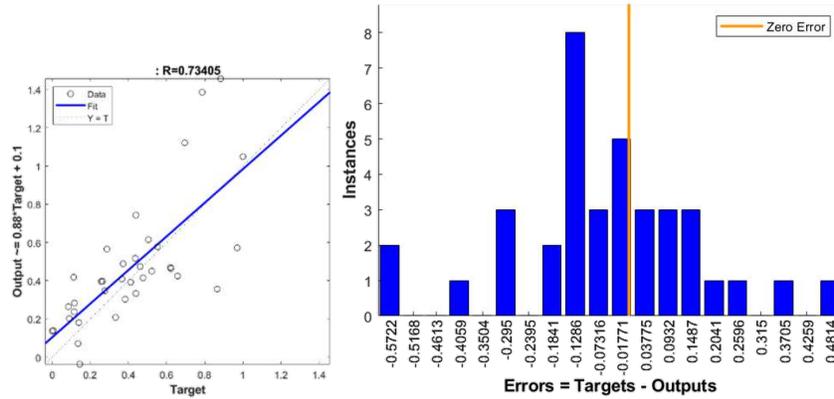

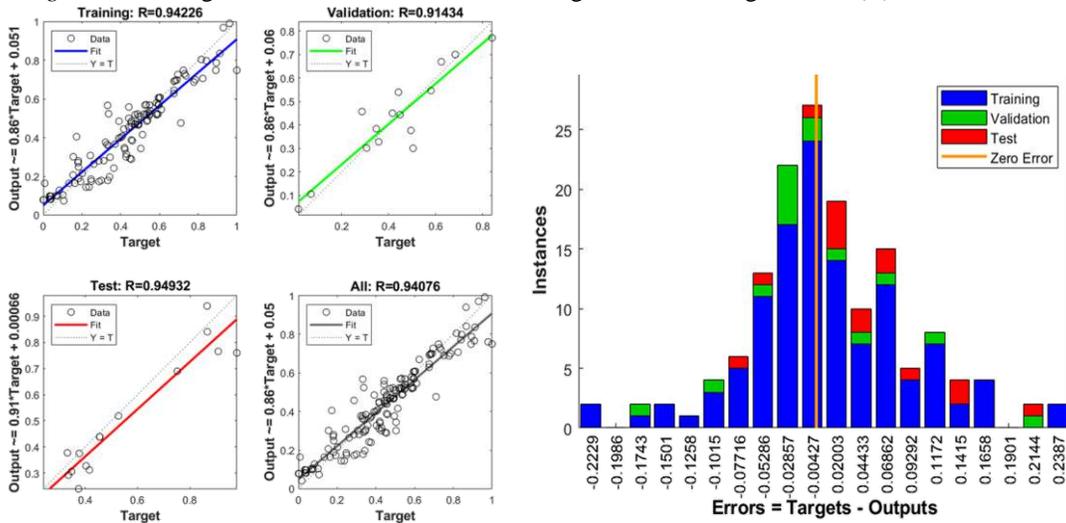*Figure B9.26* Regression coefficient and error histogram after testing EV-C+F(C)_70_10_20-23

Figure B9.27 Regression coefficient and error histogram after training EV-C+F(C)_80_10_10-33
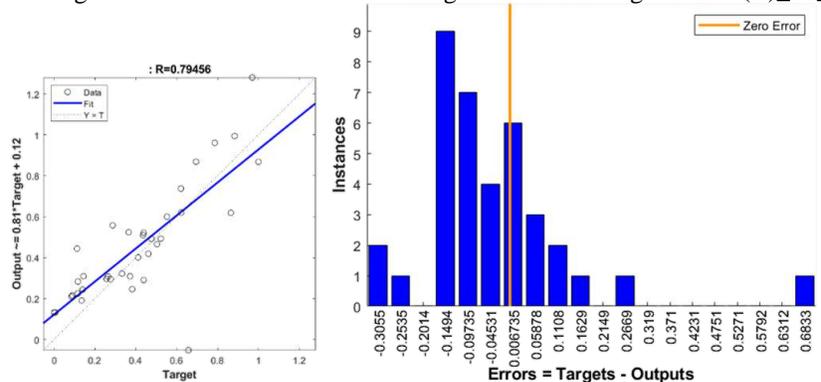

Figure B9.28 Regression coefficient and error histogram after testing EV-C+F(C)_80_10_10-33

Figure B9.29 Regression coefficient and error histogram after training EV-C+F(C)_80_5_15-23

Figure B9.30 Regression coefficient and error histogram after testing EV-C+F(C)_80_5_15-23
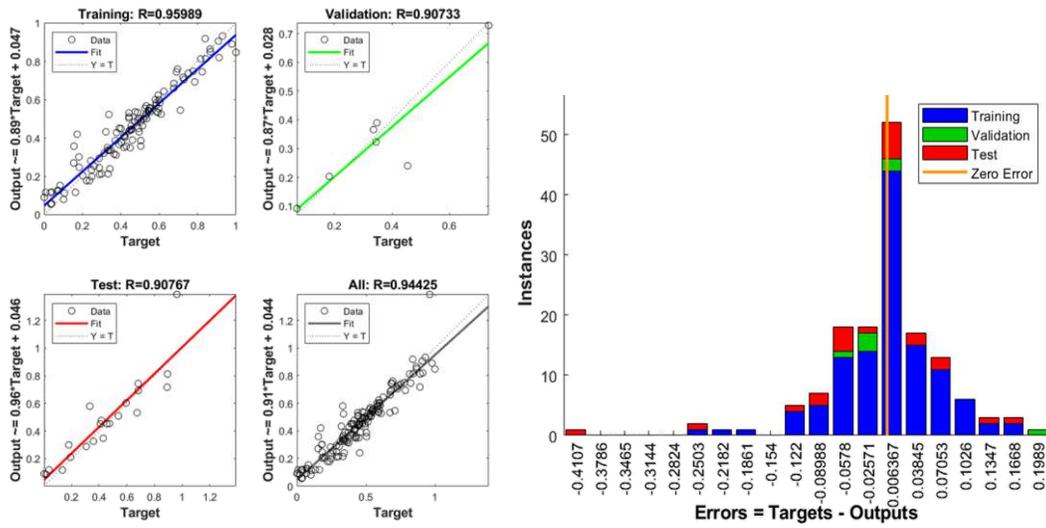

Figure B9.31 Regression coefficient and error histogram after training EV-C+F(C)_85_5_10-33

Figure B9.32 Regression coefficient and error histogram after testing EV-C+F(C)_85_5_10-33

Figure B9.33 Regression coefficient and error histogram after training EV-C+F(F)_70_10_20-23

Figure B9.34 Regression coefficient and error histogram after testing EV-C+F(F)_70_10_20-23

Figure B9.35 Regression coefficient and error histogram after training EV-C+F(F)_80_10_10-23

Figure B9.36 Regression coefficient and error histogram after testing EV-C+F(F)_80_10_10-23

Figure B9.37 Regression coefficient and error histogram after training EV-C+F(F)_80_5_15-23
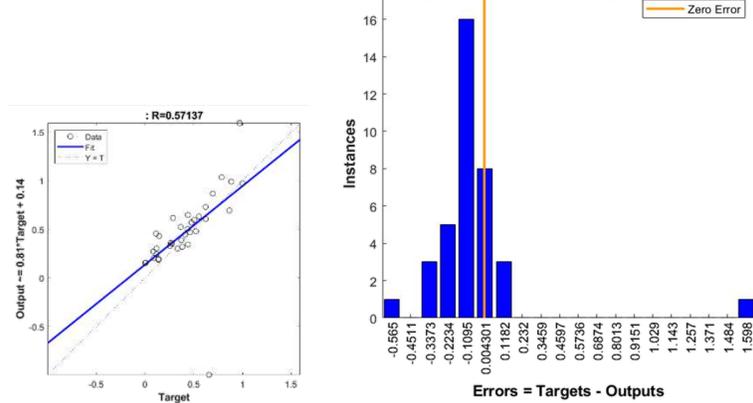

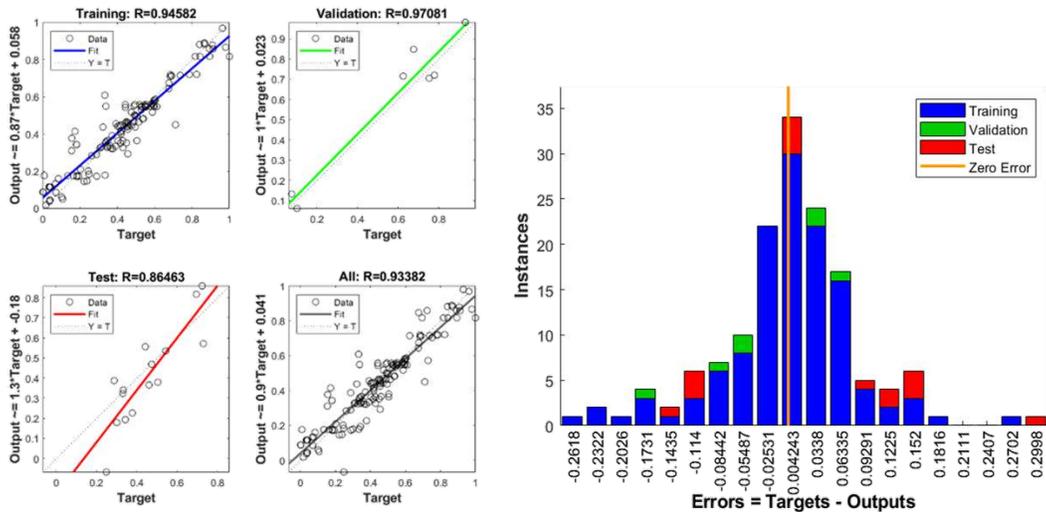*Figure B9.38* Regression coefficient and error histogram after testing EV-C+F(F)_80_5_15-23

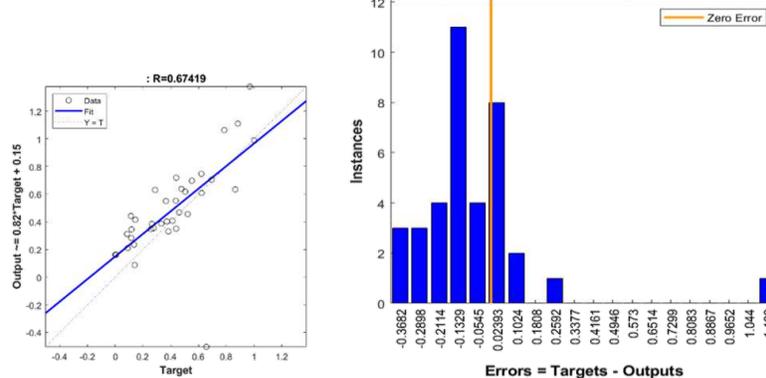*Figure B9.39* Regression coefficient and error histogram after training EV-C+F(F)_85_5_10-11

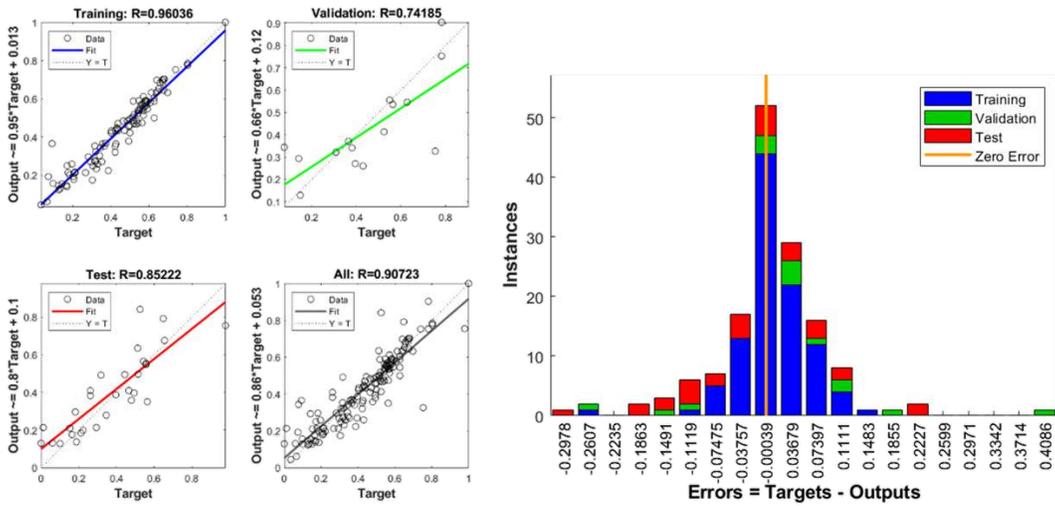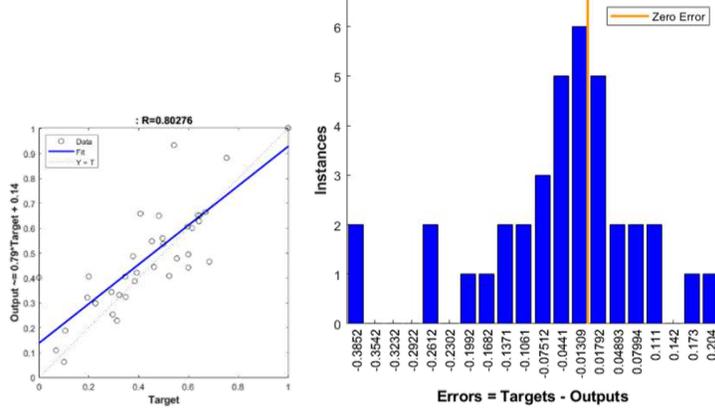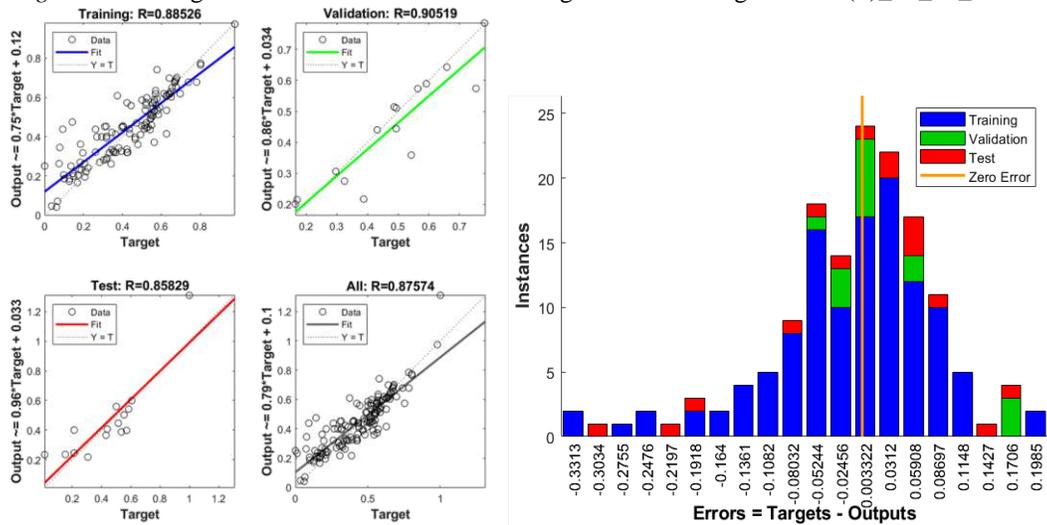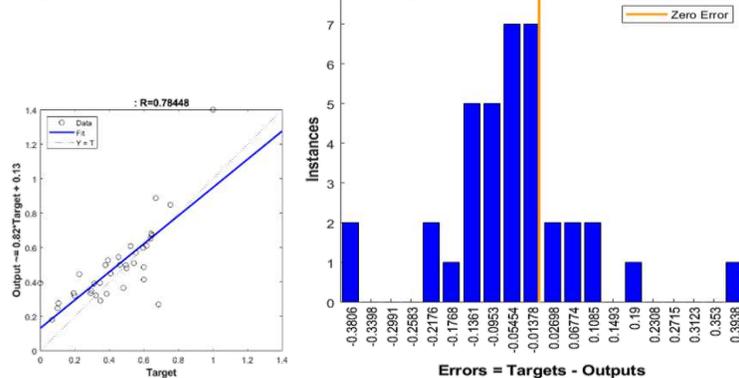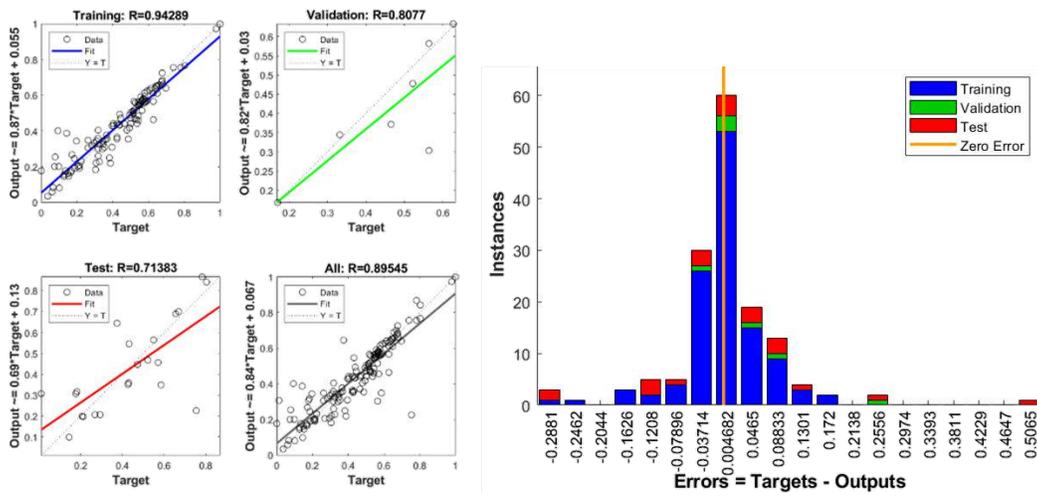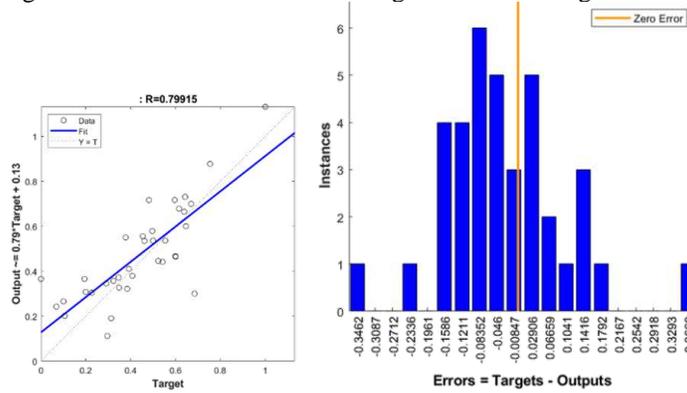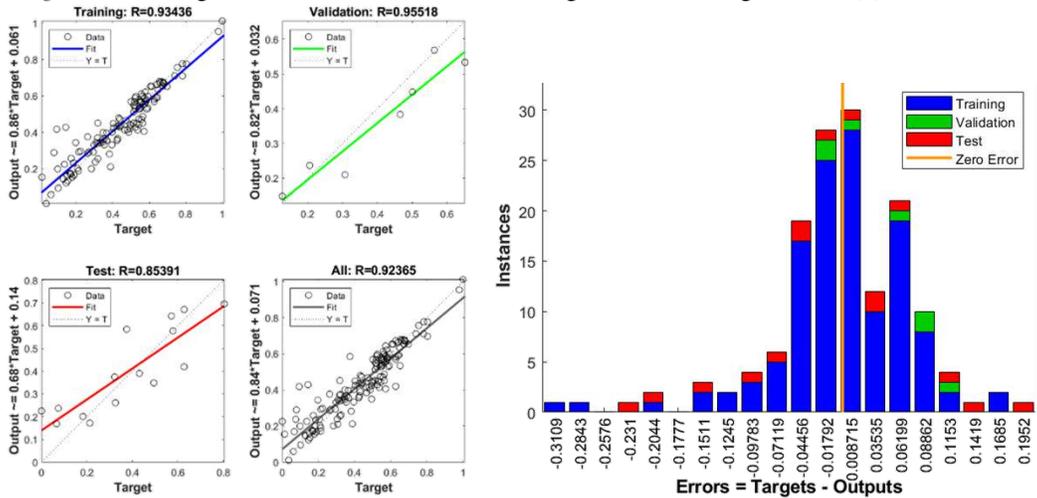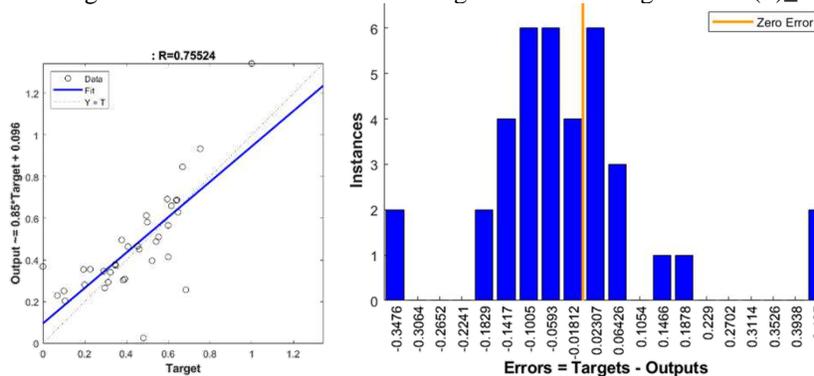*Figure B9.40* Regression coefficient and error histogram after testing EV-C+F(F)_85_5_10-11

Table B9.1 Results for evaluation ANN models based on dataset from Group I

#	Model	Training (80%)						Testing (20%)	
		Regression coefficient - training	Regression coefficient - validation	Regression coefficient - testing	Regression coefficient - total	Mean square error	Epoch	Regression coefficient	Mean square error
1	EV-COMP_70_10_20-41	0.956	0.91395	0.91878	0.93991	0.0035684	10	0.6995	0.02325
2	EV-COMP_80_10_10-60	0.97646	0.90059	0.97778	0.97068	0.0034543	10	0.641	0.02477
3	EV-COMP_80_5_15-20	0.96445	0.93289	0.84344	0.94203	0.0032266	11	0.717	0.0164
4	EV-COMP_85_5_10-41	0.97983	0.98386	0.89288	0.97497	0.00101	38	0.6455	0.0295
5	EV-FLEX_70_10_20-48	0.94445	0.80911	0.85026	0.915	0.01323	14	0.886	0.01385
6	EV-FLEX_80_10_10-48	0.93606	0.88849	0.88083	0.92495	0.005062	14	0.873	0.01281
7	EV-FLEX_80_5_15-16	0.91067	0.91432	0.84429	0.90042	0.0062921	10	0.869	0.01255
8	EV-FLEX_85_5_10-16	0.82552	0.92592	0.85434	0.83336	0.0097763	8	0.898	0.0189
9	EV-C+F_70_10_20-33	0.99186	0.74099	0.78126	0.91828	0.022628	25	0.6658	0.0379
10	EV-C+F_80_10_10-11	0.9006	0.89892	0.85392	0.8954	0.012551	11	0.8098	0.0218
11	EV-C+F_80_5_15-11	0.97767	0.75346	0.84551	0.93631	0.011428	56	0.68652	0.06705
12	EV-C+F_85_5_10-33	0.9652	0.91206	0.92741	0.95713	0.0055437	27	0.81361	0.02378
13	EV-C+F(C)_70_10_20-23	0.99035	0.93642	0.91792	0.97062	0.0071608	16	0.73405	0.05242
14	EV-C+F(C)_80_10_10-33	0.94226	0.91434	0.94932	0.94076	0.0071479	12	0.7946	0.03228
15	EV-C+F(C)_80_5_15-23	0.95989	0.90733	0.90767	0.94425	0.0071872	15	0.5714	0.10445
16	EV-C+F(C)_85_5_10-33	0.94582	0.97081	0.86463	0.93382	0.0072292	14	0.6742	0.06634
17	EV-C+F(F)_70_10_20-23	0.96036	0.74185	0.85222	0.90723	0.023928	22	0.8028	0.01907
18	EV-C+F(F)_80_10_10-23	0.88526	0.90519	0.85829	0.87574	0.0070207	8	0.7845	0.02238
19	EV-C+F(F)_80_5_15-23	0.94289	0.8077	0.71383	0.89545	0.011334	16	0.7992	0.01834
20	EV-C+F(F)_85_5_10-11	0.93436	0.95518	0.85391	0.92365	0.0049388	20	0.7552	0.0256

Evaluation of models in Group II

Figure B9.41 Regression coefficient and error histogram after training EV-S_C+F_70_10_20-8

Figure B9.42 Regression coefficient and error histogram after testing EV-S_C+F_70_10_20-8

Figure B9.43 Regression coefficient and error histogram after training EV-S_C+F_80_10_10-8

Figure B9.44 Regression coefficient and error histogram after testing EV-S_C+F_80_10_10-8

Figure B9.45 Regression coefficient and error histogram after training EV-S_C+F_80_5_15-17

Figure B9.46 Regression coefficient and error histogram after testing EV-S_C+F_80_5_15-17

Figure B9.47 Regression coefficient and error histogram after training EV-S_C+F_85_5_10-17

Figure B9.48 Regression coefficient and error histogram after testing EV-S_C+F_85_5_10-17
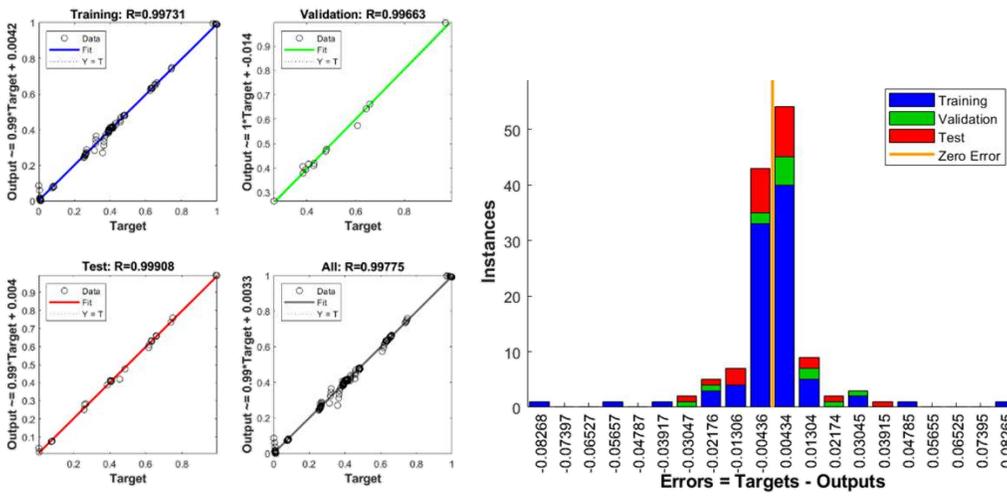
Figure B9.49 Regression coefficient and error histogram after training EV-S_C+F(C)_70_10_20-17
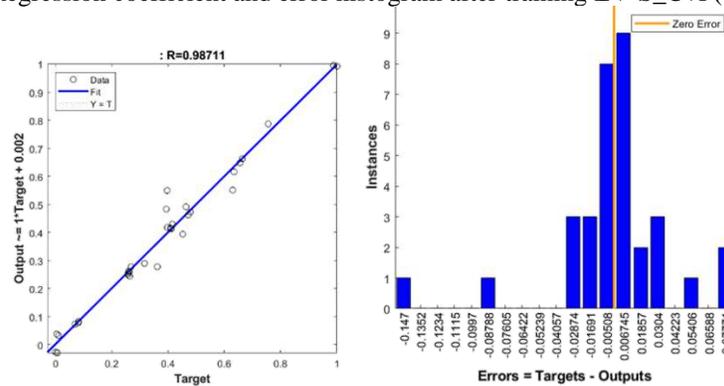
Figure B9.50 Regression coefficient and error histogram after testing EV-S_C+F(C)_70_10_20-17
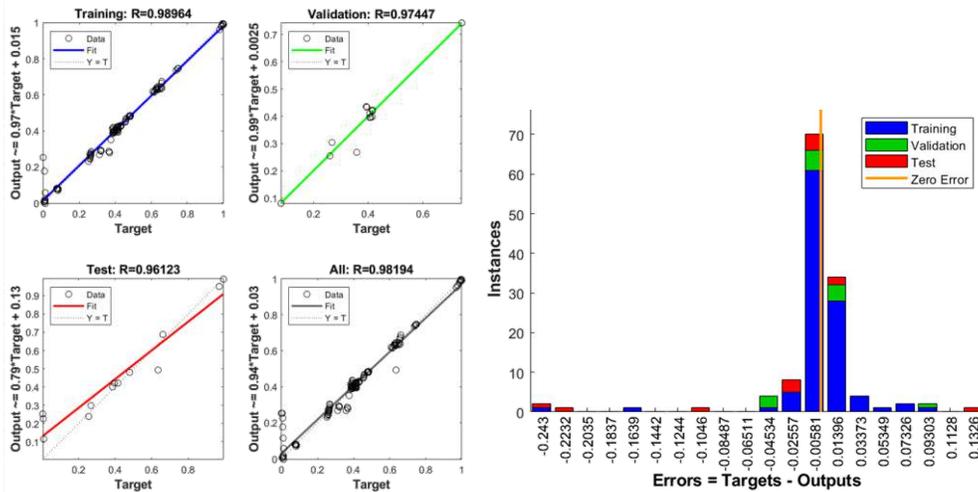
Figure B9.51 Regression coefficient and error histogram after training EV-S_C+F(C)_80_10_10-17
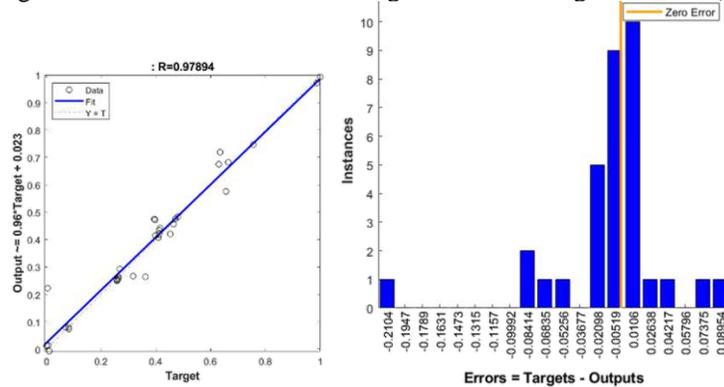
Figure B9.52 Regression coefficient and error histogram after testing EV-S_C+F(C)_80_10_10-17
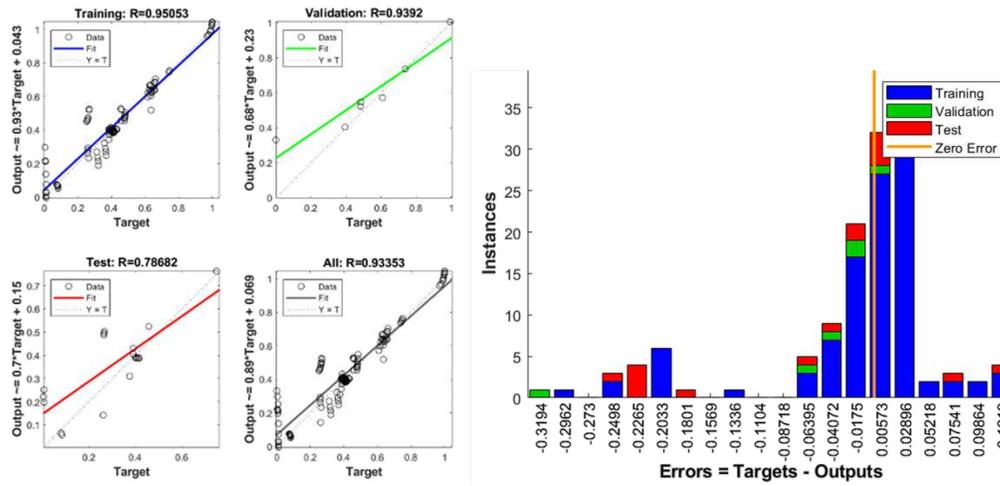
Figure B9.53 Regression coefficient and error histogram after testing EV-S_C+F(C)_80_5_15-8
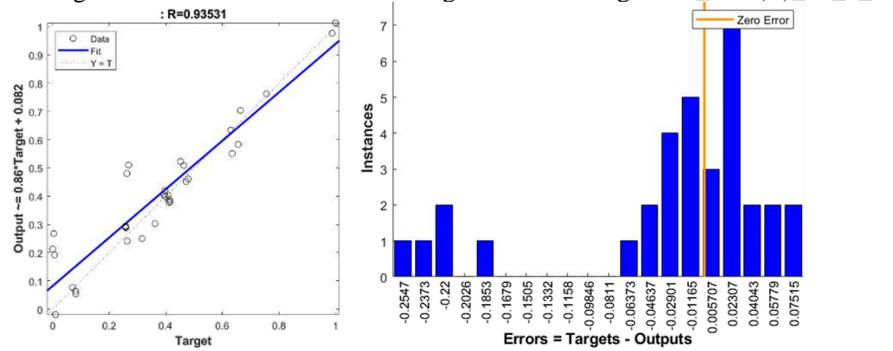
Figure B9.54 Regression coefficient and error histogram after training EV-S_C+F(C)_80_5_15-8
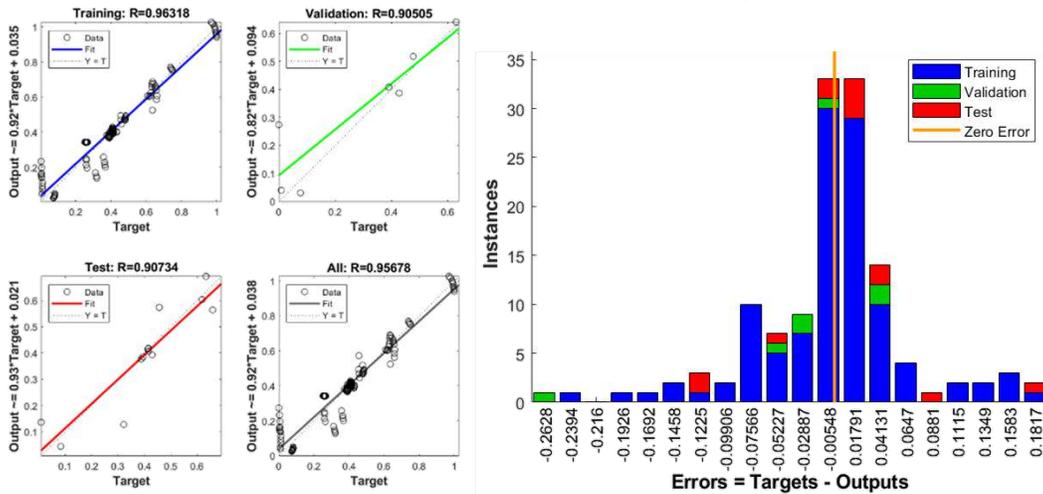
Figure B9.55 Regression coefficient and error histogram after testing EV-S_C+F(C)_85_5_10-8
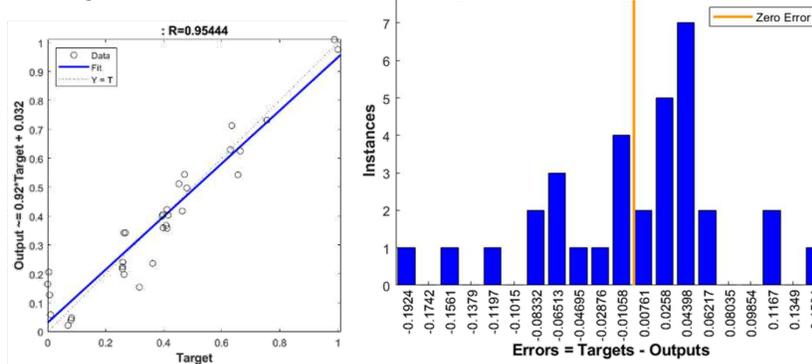
Figure B9.56 Regression coefficient and error histogram after testing EV-S_C+F(C)_85_5_10-8
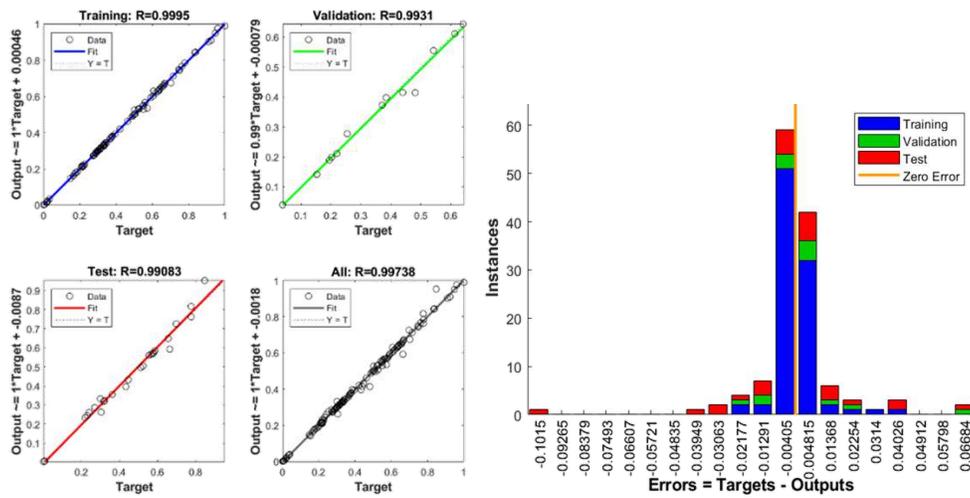
Figure B9.57 Regression coefficient and error histogram after training EV-S_C+F(F)_70_10_20-17
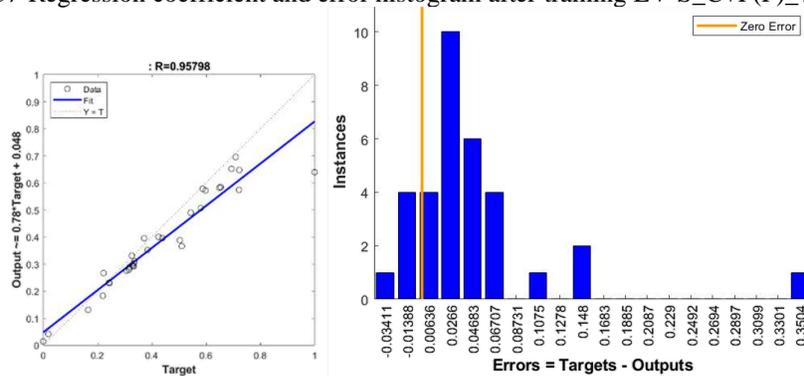
Figure B9.58 Regression coefficient and error histogram after testing EV-S_C+F(F)_70_10_20-17
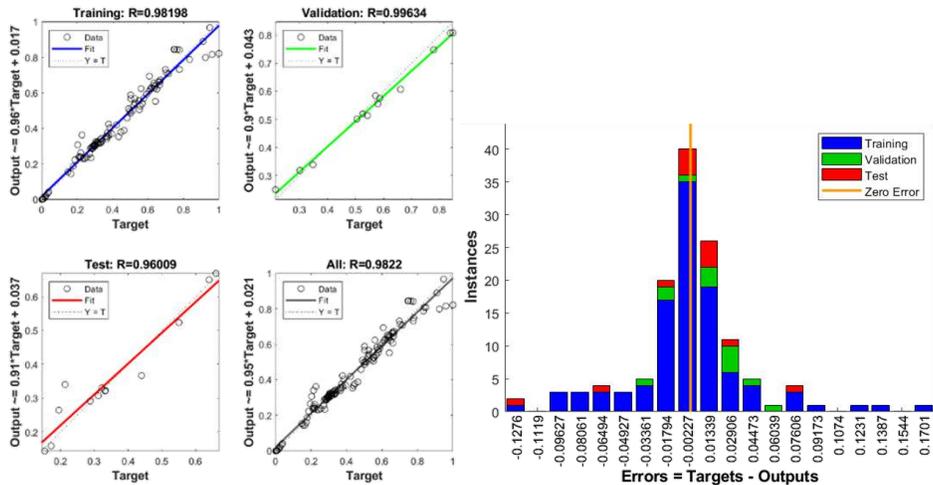
Figure B9.59 Regression coefficient and error histogram after training EV-S_C+F(F)_80_10_10-8
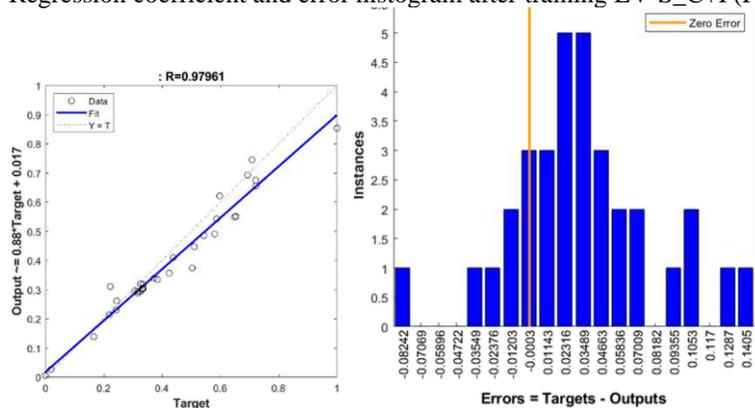
Figure B9.60 Regression coefficient and error histogram after testing EV-S_C+F(F)_80_10_10-8
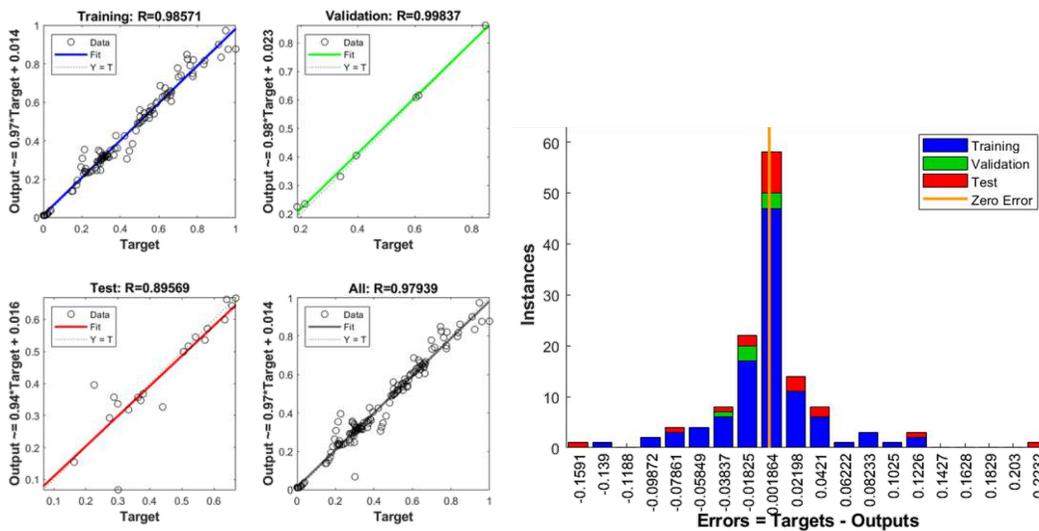
Figure B9.61 Regression coefficient and error histogram after training EV-S_C+F(F)_80_5_15-8
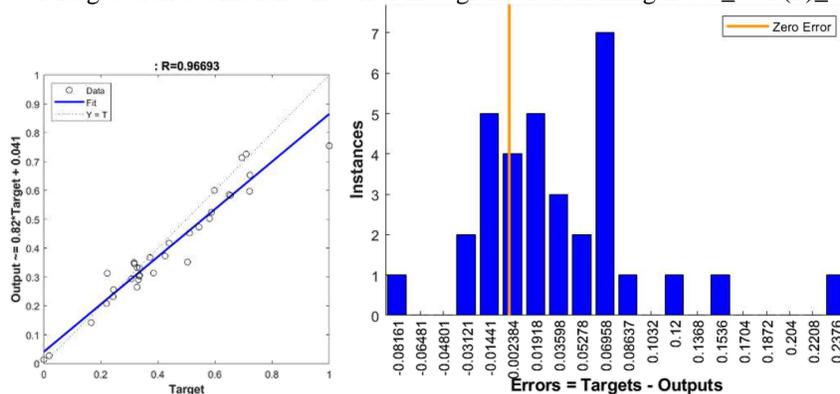
Figure B9.62 Regression coefficient and error histogram after testing EV-S_C+F(F)_80_5_15-8
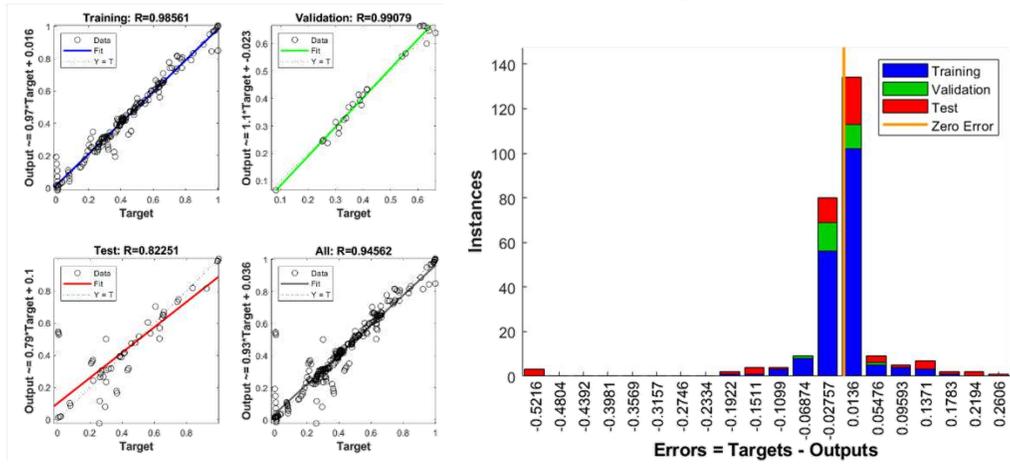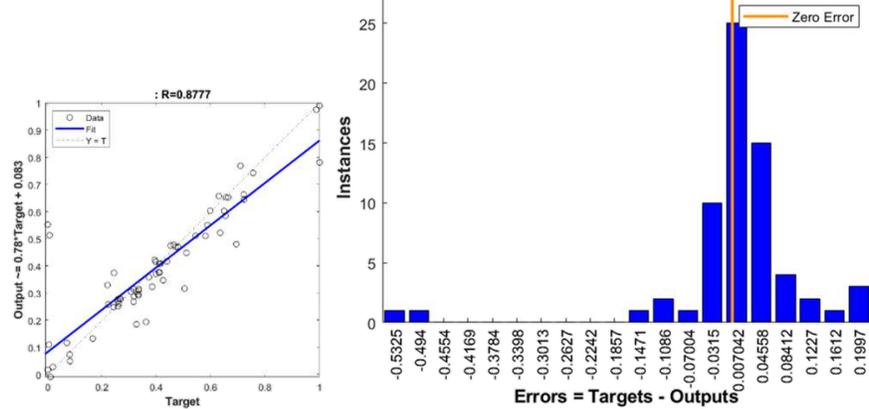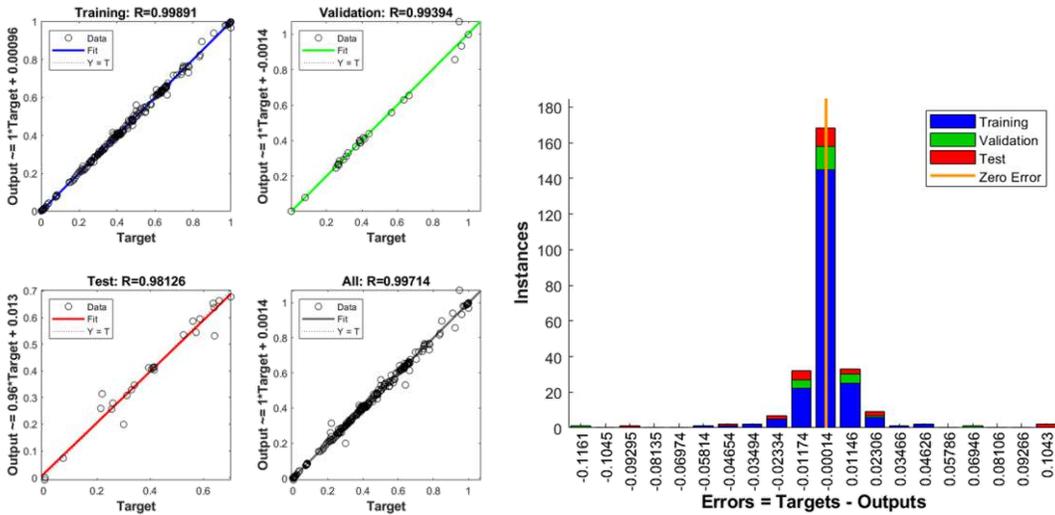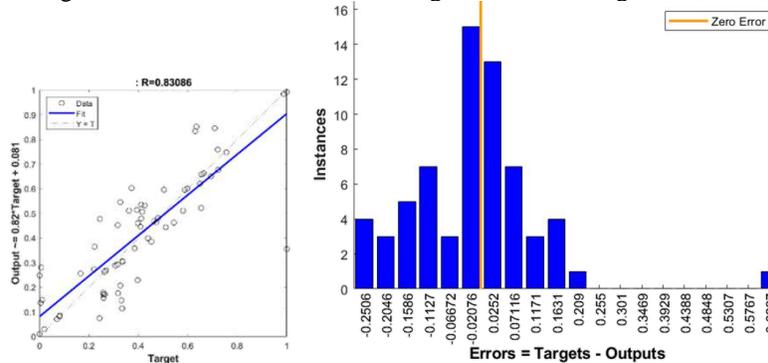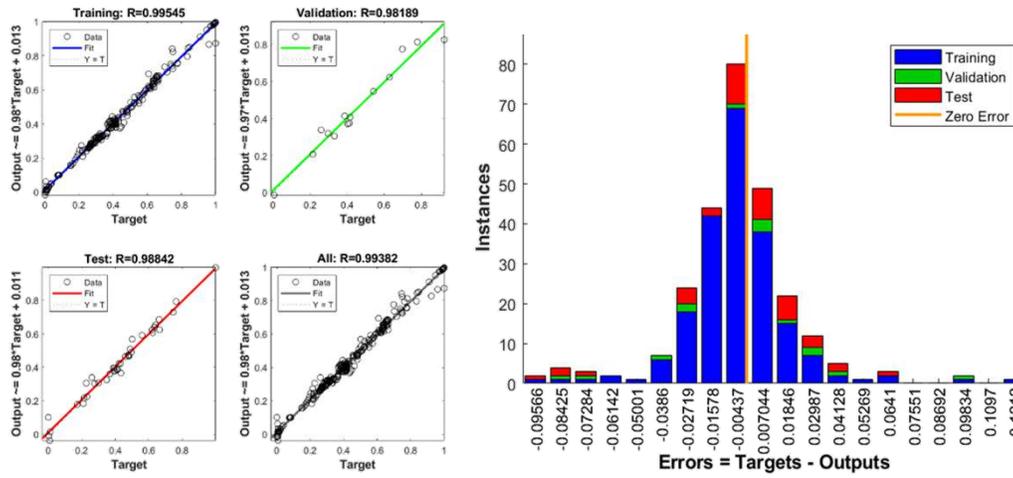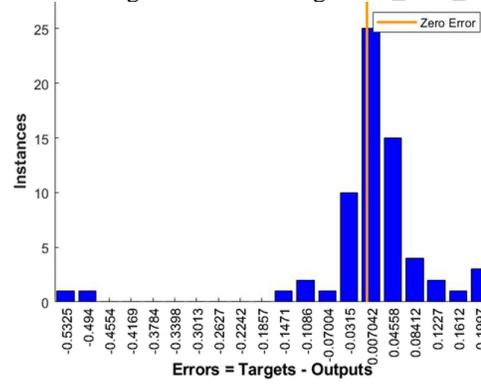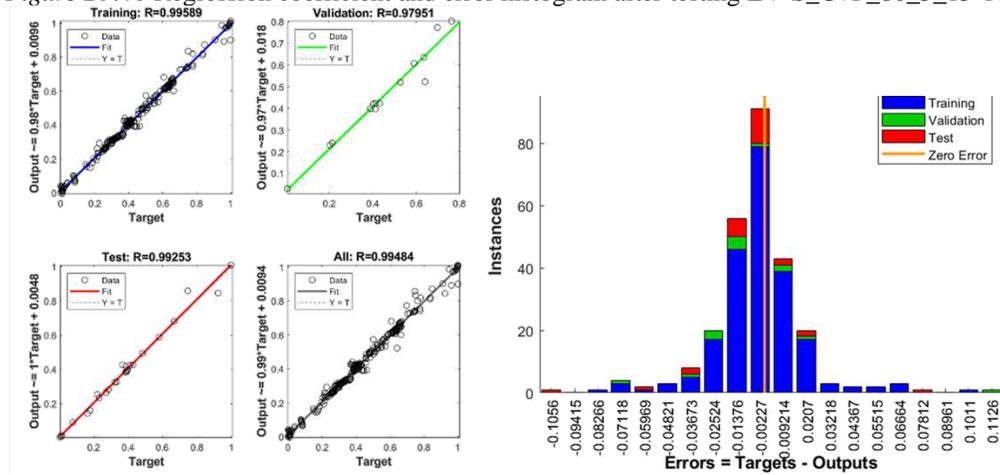

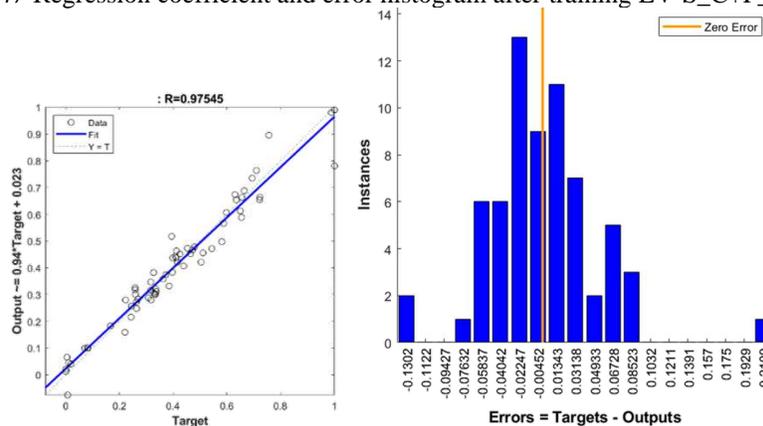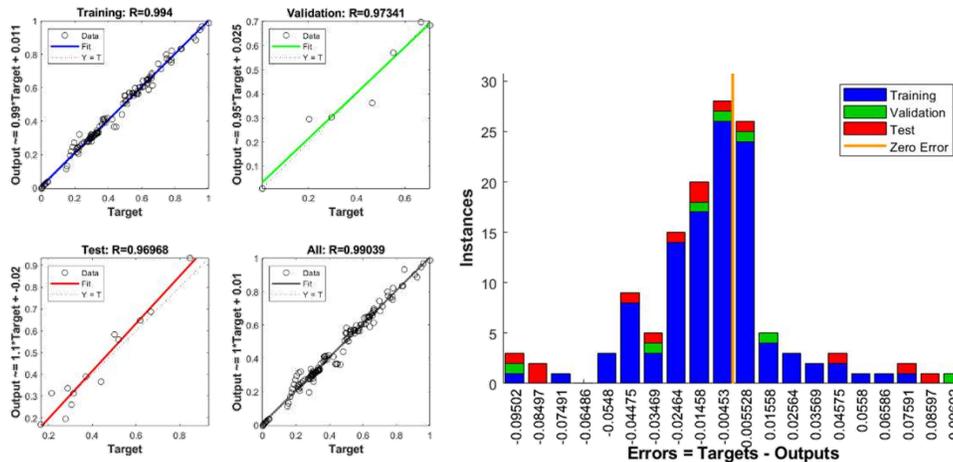*Figure B9.63* Regression coefficient and error histogram after training EV-S_C+F(F)_85_5_10-8
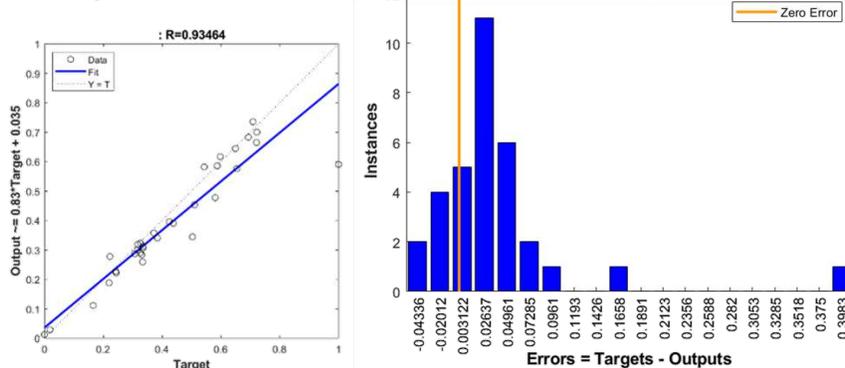
Figure B9.64 Regression coefficient and error histogram after testing EV-S_C+F(F)_85_5_10-8

Table B9.2 Results for evaluation ANN models based on dataset from Group II

#	Model	Training (80%)						Testing (20%)	
		Regression coefficient - training	Regression coefficient - validation	Regression coefficient - testing	Regression coefficient - total	Mean square error	Epoch	Regression coefficient	Mean square error
1	EV-S_C+F_70_10_20-8	0.98561	0.99079	0.82251	0.94562	0.0016205	30	0.8957	0.01294
2	EV-S_C+F_80_10_10-8	0.99891	0.99394	0.98126	0.99714	0.0001238	104	0.8222	0.01889
3	EV-S_C+F_80_5_15-17	0.99545	0.98189	0.98842	0.99382	0.0005492	47	0.9806	0.00273
4	EV-S_C+F_85_5_10-17	0.99589	0.97951	0.99253	0.99484	0.0004696	36	0.9765	0.00422
5	EV-S_C+F(C)_70_10_20-17	0.99731	0.99663	0.99908	0.99775	0.0003804	34	0.9871	0.0017
6	EV-SC+F(C)_80_10_10-17	0.98964	0.97447	0.96123	0.98194	0.001232	18	0.9789	0.0028
7	EV-S_C+F(C)_80_5_15-8	0.95053	0.9392	0.78682	0.93353	0.005928	14	0.93531	0.00892
8	EV-S_C+F(C)_85_5_10-8	0.96318	0.90505	0.90734	0.95678	0.004469	14	0.9544	0.00578
9	EV-S_C+F(F)_70_10_20-17	0.9995	0.9931	0.99083	0.99738	0.0000548	97	0.958	0.00697
10	EV-S_C+F(F)_80_10_10-8	0.98198	0.99634	0.96009	0.9822	0.001962	19	0.9796	0.00329
11	EV-S_C+F(F)_80_5_15-8	0.98571	0.99837	0.89569	0.97939	0.00165	18	0.9669	0.00483
12	EV-S_C+F(F)_85_5_10-8	0.994	0.97341	0.96968	0.99039	0.000704	53	0.9346	0.00741

B10. Results – Sensitivity analysis

Table B10.1 Weights and bias for model COMP from Group I

w1

1.45	2.10	4.05	0.89	2.20	-4.74	1.93	0.66	2.62	0.08	0.70	-0.22	-1.56	-0.16	0.19	-0.27	-0.83	-0.04	-0.08	-0.98
0.49	1.05	0.96	-0.08	-0.77	-2.61	0.79	0.57	1.32	-0.21	0.22	0.01	0.44	-0.18	-0.14	0.43	0.19	-0.45	-0.04	0.55
0.50	0.13	1.04	0.58	-3.22	8.56	0.47	0.75	0.65	-0.59	-1.71	0.02	-0.12	-1.36	-0.20	0.03	-0.11	0.46	0.20	-0.75
0.43	-0.05	0.05	-0.61	0.20	-0.21	2.02	-0.16	-0.84	-0.17	0.15	0.68	-0.89	-0.87	-0.06	-0.27	0.26	-0.41	0.26	0.93
2.24	0.61	1.25	-0.48	-0.28	1.80	0.22	0.03	1.05	-0.37	-0.16	0.43	-0.76	0.59	-0.08	0.14	0.19	-0.36	-0.17	0.54
-0.66	-0.78	0.31	0.11	0.07	-0.39	0.38	0.09	-0.22	-0.18	-0.94	-0.21	0.22	0.27	-0.26	-0.13	-0.59	0.60	-0.57	-0.61
2.03	1.96	-2.28	-0.42	2.49	-13.13	-1.92	3.35	5.55	0.77	2.05	1.33	4.65	1.55	-3.08	-1.34	-1.93	-0.82	0.08	-0.27
-2.17	1.77	1.52	0.17	-3.07	2.19	0.22	-1.29	-0.37	0.49	-0.03	1.14	-0.62	-1.07	0.71	0.36	-0.41	1.55	-0.30	0.30
-0.87	-0.74	-1.82	0.46	0.02	-4.10	1.14	0.00	-0.72	-0.68	-1.78	0.90	1.58	-0.11	-0.10	0.15	-0.12	0.54	0.75	-2.46
-0.95	-0.74	0.52	-0.17	-1.24	-1.64	-0.70	-0.18	0.35	0.02	0.71	0.15	0.51	1.83	0.11	0.14	0.14	-1.00	0.46	3.14
-0.10	0.46	-0.35	-0.44	-0.28	0.62	-0.43	-0.36	-0.50	-0.58	-0.13	-0.31	-0.41	-0.58	0.01	-0.40	0.15	-0.04	0.23	0.43
-1.21	1.84	-1.39	-1.06	-0.16	-1.99	0.02	-0.02	1.20	1.13	-0.74	0.01	0.28	0.82	0.06	0.79	0.73	0.49	0.50	-2.73
1.53	2.93	-1.35	0.56	0.34	5.50	-1.24	0.97	-0.78	-0.89	-1.26	-0.11	1.77	0.16	0.46	-0.18	-0.51	1.07	-0.08	-1.30
-1.98	-0.95	0.57	0.69	3.03	6.94	-1.73	-0.62	-0.05	-1.16	-1.53	0.96	0.48	-1.04	-0.80	-0.35	-2.16	-1.20	-1.28	0.14
-0.05	0.51	-0.68	-0.47	0.96	1.56	1.18	1.06	1.53	0.09	0.27	-0.11	-0.16	-1.19	0.75	-0.02	0.13	0.62	0.54	-4.99
0.93	2.11	0.84	-0.57	-0.48	-3.29	-0.09	0.50	0.11	-0.63	-0.92	-0.39	-0.13	0.39	-0.03	0.27	-0.26	-0.29	-0.50	1.01
-0.60	0.68	0.86	0.09	-0.89	0.76	-1.97	1.06	-0.27	0.70	0.05	0.10	0.42	-0.23	-0.84	0.12	-0.42	-0.19	-0.19	1.33
-2.65	-2.05	-2.38	0.10	2.18	3.06	-0.88	0.19	0.64	-0.84	-2.38	0.28	1.36	-0.51	-0.78	-0.67	-0.86	-0.23	-0.63	-0.58
-0.43	-0.38	-0.26	-0.02	2.69	4.98	-1.37	1.73	-1.65	-0.75	-0.56	-1.07	1.05	-0.33	-1.76	-0.21	-0.17	-0.67	-0.20	1.00
1.44	1.70	0.45	0.57	-3.11	6.56	0.28	-0.95	-0.22	-0.16	-0.08	-0.55	0.51	-2.37	-0.89	0.10	-0.36	-0.92	-0.54	-0.66
-1.93	-1.85	2.28	-0.74	-0.36	-0.15	0.58	-0.43	0.53	-0.37	0.96	-0.45	-0.49	-0.18	0.29	-0.83	-0.51	-0.62	0.22	1.01
0.45	0.30	-0.68	0.64	1.65	-2.33	-1.76	-0.68	0.01	0.49	0.16	-0.17	0.80	-0.20	0.89	-0.36	-0.61	-0.44	0.17	-0.56
-2.96	-1.01	-1.20	-1.19	0.24	1.39	0.15	1.05	0.88	-0.44	-0.34	0.23	0.71	-0.74	-1.16	-0.08	0.29	0.00	-0.29	2.79
3.31	1.34	1.07	1.59	-0.96	7.87	0.27	0.33	-1.07	-0.34	-1.14	-0.82	-0.65	0.40	-1.42	-0.13	-0.61	-0.37	-1.19	-6.71
0.22	-0.73	0.78	0.16	-1.68	0.89	-0.83	0.28	0.62	-0.52	0.22	0.35	0.92	0.65	-0.48	-0.02	0.64	-0.09	-0.51	-1.31
0.80	1.53	-1.45	-0.86	-1.64	0.97	0.43	-1.40	-1.16	-0.21	0.38	0.16	-1.07	0.58	0.72	-0.78	-0.28	-0.84	0.19	-1.23
-0.60	-0.36	-0.59	-0.48	0.76	2.55	-0.64	-0.53	1.14	-0.99	-0.27	0.04	-0.16	0.82	-1.38	-1.71	-0.09	-1.04	-0.18	3.77
-2.18	-1.56	2.33	0.15	-2.43	7.49	-1.19	0.15	-1.90	-0.44	0.87	1.39	-4.06	-0.05	2.65	0.47	-0.14	0.04	-0.76	3.47
0.57	2.59	2.06	0.96	3.44	7.78	-2.00	-0.12	0.66	-1.49	0.23	0.45	-0.66	-0.78	-0.75	-1.50	-1.62	-1.32	-0.98	0.59
0.33	-0.16	-2.11	-0.39	-0.80	5.37	-1.29	0.87	0.20	-0.52	0.16	0.94	0.01	-1.36	-1.58	0.02	-0.03	0.57	0.42	0.30
-1.63	0.46	0.80	-0.20	-3.95	0.76	-1.94	0.76	0.39	0.42	-1.97	0.13	-0.65	0.65	1.36	0.98	1.01	1.02	0.50	2.68

b1

-1.4892	-1.7065	2.1388	-1.0599	-1.1131	1.1059	-1.646	0.6807	0.4672	0.5155	0.5648	-0.0146	-0.1939	1.2575	-0.3828
0.1237	-0.22	0.2894	0.0433	1.1382	-0.401	-0.6888	-0.5702	1.4167	0.9006	1.2206	1.5342	2.6611	1.7775	-2.189

w2

2.9125	2.5174	-4.3277	-1.9946	2.916	-1.0941	-5.9358	4.9758	3.2575	3.9558	0.1834	-4.2854	3.3721	5.0374	3.6591
3.4051	-0.7486	-4.2521	5.4535	-5.2974	-3.9373	-3.1591	-4.1178	2.7175	2.705	-2.9014	4.7066	-2.9845	4.8757	-3.661

b2

-0.2259

Table B10.2 Weights and bias for model FLEX from Group I

w1

-0.11	0.10	0.35	-0.26	0.82	-0.53	0.36	0.74	0.87	-0.12	-0.37	-0.27	0.58	-0.81	-0.02	-0.45
0.06	-0.50	1.95	1.11	-0.47	-2.79	1.60	-0.09	0.58	0.39	0.80	-0.64	0.68	1.22	0.40	-1.59
-0.24	1.59	2.22	-0.54	-0.44	-4.59	0.73	-1.22	0.20	0.40	0.01	0.57	-0.49	0.77	-0.49	0.34
1.02	-0.56	0.17	0.75	-0.03	-2.28	0.21	-0.30	0.46	0.62	-0.57	0.19	0.03	0.72	-0.68	-1.11
-1.06	0.23	-1.34	1.03	-2.75	-4.05	-1.50	-0.52	1.41	0.43	1.25	-0.79	0.73	0.38	0.24	1.17
-0.27	-0.96	-0.38	0.19	0.50	-0.39	-0.29	-0.80	-0.25	0.47	0.38	-0.38	-0.73	-0.39	0.12	-0.22
-0.16	0.06	-1.88	1.02	0.01	0.92	-0.12	0.34	-0.57	-0.88	0.15	-1.34	0.15	-0.14	-0.54	-2.09
1.99	-1.37	0.36	-1.18	1.72	1.88	-0.94	0.89	0.39	-1.15	0.74	0.00	-0.17	0.25	-0.80	-1.16
-0.01	0.29	9.73	1.00	1.96	7.39	-0.70	-1.53	-0.65	-1.30	-1.47	-0.71	-1.26	0.03	-0.50	0.36
-0.38	1.46	-2.18	0.05	-1.94	1.36	-0.39	0.28	-0.28	-0.01	-0.30	0.24	0.80	-0.29	-0.55	1.51
0.63	3.21	-0.04	0.10	-0.99	0.47	-3.76	3.65	0.49	0.23	-0.26	0.55	-0.21	0.97	1.22	3.48
0.36	-1.21	-0.13	-0.79	-0.61	-1.91	1.04	-0.48	-0.68	0.32	-0.08	1.05	0.81	-1.27	-0.28	2.61
2.70	-0.11	-0.48	0.68	-0.91	0.64	1.52	0.76	0.42	0.10	-1.59	0.03	-0.12	1.41	1.11	-3.15
-0.33	-0.22	-1.19	-0.32	-1.64	-3.42	-0.47	-1.23	0.04	0.78	0.30	-0.05	-0.13	0.27	-0.15	-0.16
1.63	2.05	-2.12	0.99	0.73	-2.18	-1.43	0.33	-1.21	-0.33	0.69	0.27	0.07	-0.04	0.19	2.19
-2.41	-0.77	5.23	1.03	1.12	3.67	1.62	-0.35	0.95	-0.04	-0.30	0.34	-0.20	0.46	-0.18	-1.41
-1.24	1.91	1.09	0.03	-0.03	1.41	-0.72	-1.95	-0.46	-0.27	-0.44	0.06	-0.25	0.07	-0.04	2.96
1.16	-2.20	0.08	-0.21	-1.44	0.59	1.65	-0.18	0.10	0.76	-0.29	1.02	-0.06	-0.47	-0.40	2.14
0.36	-0.26	0.09	0.71	0.56	-0.29	-0.11	0.62	0.84	0.67	0.26	0.56	0.10	0.08	0.55	0.48
-0.65	0.86	0.44	-0.16	-0.78	-1.64	-1.63	1.70	-0.09	-0.09	0.59	0.76	0.10	0.01	-0.49	-1.77
-3.99	-5.56	-0.11	1.69	1.70	7.07	1.06	1.66	-1.11	-0.13	-0.86	0.91	-0.13	-1.19	0.69	-0.26
-0.51	0.11	-0.31	-0.77	-0.56	0.39	0.60	-0.05	-0.16	-0.51	0.37	-0.31	0.41	0.31	0.55	-0.13
2.98	0.19	0.71	0.22	1.21	1.28	0.46	2.35	0.93	0.56	-1.35	0.02	0.46	0.10	-0.29	0.12
0.92	-1.06	-1.19	-2.13	2.52	5.47	-0.86	-1.44	-1.32	-1.50	-2.20	-0.05	0.26	1.03	-0.74	-0.57
-0.56	2.17	4.32	0.35	-3.65	6.27	-0.42	-2.21	-2.10	-0.73	0.75	-1.20	-1.20	0.09	-1.28	-0.10
0.00	-0.59	0.48	-0.59	-0.37	0.47	0.47	-0.52	-0.33	-0.01	0.49	0.33	0.84	-0.43	0.62	0.43
-1.45	2.10	-0.56	1.75	-1.53	-2.55	0.27	0.28	-0.72	-0.66	0.38	0.41	1.30	0.75	-0.03	-0.73
-1.86	1.02	-0.31	1.39	-0.09	-3.00	-1.76	-0.56	-1.39	0.67	-0.28	0.82	0.47	0.99	0.66	-1.20
-0.25	0.54	0.22	-0.07	0.60	0.67	0.33	-0.34	-0.62	-0.11	-0.14	-0.17	0.37	0.78	0.19	0.58
4.73	4.17	2.67	-0.22	1.03	-8.62	-0.25	-2.86	1.85	1.04	-1.24	1.63	0.21	0.04	0.74	-1.11

b1

-1.572	1.028	1.288	1.300	0.57	-1.054	-0.84	-0.424	2.595	-1.073	-1.178	-0.81	-0.56	-0.345	-0.383
0.6332	0.142	0.397	0.365	-0.76	-0.23	-0.9	0.972	1.633	-0.584	1.075	-1.865	-2.42	-1.722	1.039

w2

1.8925	-2.689	3.564	2.015	-2.712	0.733	-2.55	-2.296	5.68	2.919	-4.175	-2.481	-3.135	-3.2163	-2.892
-3.627	-3.33	3.437	0.941	2.237	-5.84	0.80	2.580	3.966	-6.22	0.24	5.116	-2.954	1.2523	-3.292

b2

-1.5203

Table B10.3 Weights and bias for model COMP+FLEX from Group I

w1										
0.91	-1.44	-2.77	3.26	-6.06	-0.08	2.41	-0.63	-2.30	1.06	-2.45
-3.37	0.35	2.23	3.17	3.26	0.24	-1.06	3.34	0.96	-1.84	-3.31
-1.07	-5.35	-0.76	-0.75	2.45	0.57	-2.07	3.97	-0.26	-4.75	11.09
-0.57	-1.10	-1.63	-1.33	0.26	-0.26	-0.99	-3.61	1.34	-1.87	1.70
5.40	-3.39	2.47	0.00	-2.24	7.60	-1.23	-0.28	-3.04	-1.12	-0.39
-3.36	-5.70	0.15	4.88	-3.62	5.29	-1.86	-3.46	-0.01	-0.07	5.83
-0.34	-2.06	2.93	3.12	-3.12	4.88	0.11	1.22	-0.38	-2.69	-1.00
-3.13	-5.21	-5.16	0.19	-0.81	3.41	-1.38	-0.25	1.76	-0.66	0.03
1.68	3.95	-3.65	-2.03	1.91	-4.18	0.25	-5.55	6.12	-1.10	-0.26
-3.40	4.02	0.00	-1.67	-1.06	0.76	-1.50	-0.04	-0.09	0.22	-1.72
-2.21	-5.13	-3.03	2.30	2.21	-0.11	-2.28	2.49	1.58	-3.31	7.44
-11.39	-15.79	-7.81	-6.27	2.34	-10.89	6.42	9.17	-1.51	2.06	-0.25
1.19	-1.28	-0.23	1.28	5.79	1.16	-5.66	-4.43	-1.37	-0.85	-6.83
8.59	5.66	1.05	1.68	0.29	7.59	1.48	4.78	-11.60	-0.93	-0.35
-0.14	-1.90	-3.90	-1.26	1.09	-5.76	0.04	0.98	-3.11	4.56	0.06
0.97	1.98	5.46	0.75	-1.33	-8.44	0.96	-0.10	10.71	-3.61	0.30
-4.18	-4.71	10.15	2.28	-4.00	6.29	6.14	3.77	-3.95	4.69	-0.23
-3.02	-0.55	-4.55	-2.05	1.04	-0.14	-2.02	0.79	-0.92	1.31	-3.31
-4.45	2.87	-0.70	0.07	-3.23	-0.85	0.85	3.16	0.66	0.01	0.69
-1.91	2.07	3.09	-0.33	0.58	-3.48	-1.71	0.50	-0.90	0.29	-0.14
-3.17	-6.13	-4.69	3.17	-4.40	4.01	-1.27	4.54	2.23	1.23	0.08
3.63	-0.42	-2.22	-4.68	-2.26	-0.24	1.32	-6.44	-0.72	-2.89	3.25
10.32	-5.49	-0.98	3.80	10.87	30.76	-0.78	1.66	21.57	0.08	0.34
-0.63	2.74	2.40	1.40	-2.73	7.61	2.13	0.49	-9.15	0.73	-0.23
b1										
0.8635	2.5439	4.6607	1.4773	-1.0019	-1.7198	1.8923	1.2242	0.3735	-1.023	3.3363
-8.8828	-0.2786	0.9722	-5.1459	0.9158	-4.8249	-4.3672	-1.9168	0.3957	-2.7919	2.5415
2.729	-2.6959									
w2										
3.05	-6.56	-0.71	2.49	-1.54	-0.11	-3.27	6.92	6.81	-2.88	2.90
-1.76	0.03	1.53	0.09	0.06	1.59	-1.85	-1.07	-2.45	-7.10	-9.57
-0.86	-1.35	-6.09	10.18	-0.80	-8.00	7.84	-1.15	1.76	5.17	-4.20
-1.87	1.26	-9.23								
b2										
				2.2647	-6.2974					

Table B10.4 Weights and bias for model RESIST from Group I

w1

-0.75	0.44	0.59	-0.55	0.44	-0.27	-0.30	0.45	-0.25	0.26	0.26	-0.54	-0.68	-0.14	0.11	0.13	-0.09
1.08	-0.61	0.81	1.41	0.18	-2.08	-3.86	-0.67	-0.20	-0.38	0.76	0.89	-1.10	1.51	1.10	0.27	0.43
0.28	-1.14	0.99	-0.05	-0.52	1.42	-0.16	-0.42	-0.02	0.32	-0.13	-0.60	0.47	-0.18	0.51	1.41	-0.18
-0.42	0.40	-0.09	-0.62	0.11	0.71	0.11	0.28	-0.48	-0.20	0.50	0.22	0.53	-0.73	-0.62	0.38	0.52
0.70	0.56	-0.78	-0.33	0.32	-1.18	-0.50	0.18	0.69	-0.16	0.57	0.09	0.25	-0.36	-0.08	-0.54	0.49
-0.55	-0.89	-0.02	0.32	-0.36	-2.26	-1.45	-1.48	-0.58	0.46	-0.53	0.76	-0.82	1.07	-0.28	-0.45	0.01
-1.06	-0.75	1.52	-0.09	0.60	1.30	0.93	-0.39	0.11	-0.41	-0.30	-0.34	0.12	0.68	-0.01	-0.71	-0.27
1.49	1.89	1.10	3.18	1.42	-11.15	-13.22	-3.80	0.04	3.78	4.13	2.50	1.07	6.28	1.64	2.19	-0.89
1.10	-0.68	1.61	1.10	1.04	-1.50	-0.79	-0.37	-0.56	0.90	-0.71	0.56	-0.29	-0.30	-0.73	0.26	-0.96
0.17	-0.27	-0.21	0.06	0.06	0.46	0.87	-0.19	-0.45	-0.38	0.09	0.70	-0.47	0.49	0.80	0.56	-0.18
0.40	0.74	-0.44	1.02	-0.36	0.00	-0.67	-0.41	-0.29	0.11	-0.27	-0.50	0.04	-0.46	-0.34	0.14	0.15
-0.26	-0.74	0.44	0.11	-0.51	-0.95	-1.50	-0.56	-0.07	0.86	-0.64	0.45	1.92	0.53	0.54	0.24	-0.46
0.49	-0.40	-0.29	-0.66	0.04	0.48	0.96	0.47	-0.57	-0.52	0.14	0.75	-0.05	0.30	-0.17	-1.00	0.61
0.37	1.22	-0.71	-0.55	-0.40	2.33	2.83	0.20	0.36	0.57	0.25	1.37	-1.60	-0.60	0.28	-0.70	-0.20
-0.64	-0.22	-0.95	1.23	1.26	-1.22	-2.87	-1.08	-0.52	1.31	0.44	0.19	-0.54	0.04	0.77	0.63	-1.05
-0.56	-0.94	0.21	0.24	-0.83	-1.03	-0.80	-0.79	-0.87	0.42	-1.33	0.50	0.23	-0.15	0.25	0.30	-0.03
0.53	0.25	-0.87	0.07	0.96	-1.37	-1.01	-1.43	-0.68	0.04	-0.15	0.06	0.62	0.97	0.08	-0.67	-0.15
-0.62	-1.02	0.79	0.55	0.50	0.32	0.06	0.59	-0.95	-0.34	-0.29	0.42	0.79	0.27	-0.41	-0.83	-0.46
-0.56	0.54	0.23	-0.42	-0.26	-1.81	-0.96	-0.51	-0.60	0.52	0.32	1.34	-0.67	0.29	-0.05	-0.13	-0.65
-0.24	0.59	-1.56	-0.01	-0.58	0.11	-0.29	-0.08	1.00	-0.62	0.73	-0.29	-0.48	0.05	0.00	1.48	0.85
-0.80	-0.69	1.38	0.48	-0.16	-1.03	-1.53	-0.52	0.21	1.06	-0.42	-0.73	0.68	0.27	-0.75	0.74	0.41
-0.03	0.56	-0.05	-0.56	-0.18	-0.85	0.22	0.65	0.18	-0.02	0.09	-0.51	0.43	-0.54	-0.55	0.14	0.22
-0.27	-0.02	-0.97	-1.12	0.14	-1.26	-1.48	-0.10	0.12	1.13	-0.27	1.16	-0.18	0.72	-0.02	0.53	-0.11
0.13	0.95	-1.15	0.08	0.85	-0.18	0.08	-0.04	-1.02	-0.55	0.81	0.59	-0.07	-0.28	0.76	0.03	0.76
0.61	-0.50	-1.08	-0.23	-0.19	0.56	0.97	-0.51	-0.65	-0.12	-0.60	0.81	-0.16	0.14	-0.10	-0.13	-0.81
-0.55	-0.57	0.76	-0.41	-0.55	1.36	0.37	-0.08	0.41	-0.84	-0.89	-0.11	-0.13	0.54	0.12	-0.06	-0.98
-0.37	0.62	1.03	0.15	-0.24	-0.15	-1.43	-0.43	0.46	0.09	-0.09	-0.36	-0.79	-0.57	-0.55	-0.40	0.67
-0.39	-0.07	-0.84	-0.45	-0.22	0.75	-0.70	-0.13	-0.39	0.73	-0.32	0.28	-0.16	0.26	-0.94	-0.66	-0.64
-0.30	-0.54	0.36	0.63	0.15	0.38	1.04	-0.29	0.00	-0.66	0.32	-0.62	0.61	-0.16	-0.05	0.09	-0.24
-0.39	0.42	1.41	-0.64	-0.16	-1.30	-1.85	-0.82	-0.59	-0.14	-0.34	0.35	-0.90	1.45	1.11	0.77	-0.15
0.08	0.29	-0.56	0.00	0.15	-1.47	-1.03	-0.25	-0.92	-0.62	0.23	1.09	1.06	0.09	0.26	-0.72	-0.58

b1

1.728	-2.30	-1.57	1.393	-1.296	-1.652	0.978	-6.523	-1.108	-0.648	-0.677	-0.217	-0.185	0.097	-0.517	-0.241	-0.561
-0.11	-0.816	-0.345	-0.715	-0.69	-1.0	0.979	0.628	-0.925	-1.105	-1.412	-1.347	-2.128	-1.958			

w2

0.385	-4.165	-1.59	1.75	-0.953	2.294	2.558	11.08	-3.161	-1.599	-0.338	-2.85	1.032	3.873	2.751	1.569	2.43
1.037	-2.127	2.254	2.132	1.607	-2.255	2.133	-1.432	1.404	2.275	-2.12	0.245	2.396	-2.562			

b2

0.1194

Table B10.5 Weights and bias for model COMP from Group II

w1							
-1.1884	0.182	-0.9374	0.5679	-0.3351	-0.2558	-5.2589	-0.2763
-2.1869	2.8866	1.0088	-1.1248	-0.3941	0.0182	1.3825	-0.1151
-0.128	-1.2021	-0.104	2.8037	-1.3061	0.2297	0.6826	0.0102
-0.0207	1.4448	-0.465	-0.9313	-2.4762	0.0045	2.6815	1.2749
1.2701	1.0125	1.1661	-1.6151	-0.0083	0.5806	0.6177	1.1375
1.0311	0.5092	0.621	-1.1284	-0.2551	0.1715	-2.1946	-2.4888
1.8734	1.1565	2.357	-0.7279	-0.4765	-0.0271	1.1609	-0.3669
2.9708	0.431	-4.8571	-0.7982	-3.2505	-0.0773	-2.9495	-3.7917
-2.1509	-0.4917	-2.5108	-0.7216	-2.9942	0.0219	2.1745	0.2284
1.2086	1.2293	0.3426	-0.648	0.5133	0.4959	-1.6349	-1.6647
1.4481	2.3669	-1.301	-1.4687	4.8688	-0.0642	1.4993	0.1309
0.9894	-0.3978	-0.335	0.2886	0.8468	-2.0167	0.6984	-0.1969
0.8371	-0.4969	0.6019	-0.1619	2.041	-0.5576	-0.1745	1.8093
b1							
2.346	3.0436	-1.3634	0.5554	-0.498	-0.1821	0.0481	2.0566
-1.674	0.5284	-1.2239	-2.8439	1.8328			
w2							
1.5937	-3.8043	-3.2674	-1.637	0.336	-1.7192	4.5619	-2.4575
4.0304	0.4845	-1.565	-1.3314	0.4188			
b2							
-0.2534							

Table B10.6 Weights and bias for model FLEX from Group II

w1							
-1.4488	-0.8221	-0.502	2.7211	-0.0675	0.2174	0.1212	-0.7504
0.8543	0.2628	1.8752	1.2488	-1.1405	0.7772	-0.8542	-1.4933
-1.2083	-0.1092	-1.5005	-0.1481	0.6398	-0.5635	1.1665	1.6845
-1.769	-1.3208	-4.1244	-0.0042	-0.5436	-3.902	-5.9445	3.1523
-2.7013	-3.9625	-9.5696	3.8317	0.4865	4.6621	1.7553	3.9148
-2.3995	0.2943	9.169	-7.4938	-7.296	0.6183	-1.5866	0.0283
11.4797	-1.5484	9.4932	-2.3609	8.5039	-0.9344	-4.0579	-1.6971
-0.8368	-3.097	19.8282	-7.2423	-15.6804	2.0247	1.8409	-5.4337
-2.3159	-1.1394	-2.9464	1.0291	2.4679	-0.0572	-1.6116	-0.0797
1.3174	3.0794	1.2668	1.3446	0.7181	-1.0816	-3.2753	-1.2864
b1							
1.9638	1.4822	-0.7477	0.0545	-1.5794	-3.9594	2.3601	7.1784
0.5741	4.2847						
w2							
8.9119	2.7676	6.6768	-7.0178	0.1871	10.284	2.7118	-3.5751
-5.4928	4.0319						
b2							
0.1831							

w1							
0.4057	-3.4642	-6.0935	0.8761	3.5704	-1.5785	-1.6205	-1.192
-2.2973	-3.3549	4.0355	-0.5293	-2.3551	-16.0927	-2.2156	3.3834
2.4752	1.1469	-4.3217	2.1472	-1.054	4.3662	0.1911	2.3316
-1.0286	-2.1904	-1.445	-0.021	-2.8822	-0.0356	2.4545	0.9563
-0.486	-2.2571	3.0784	1.8721	-2.061	-0.0449	1.5076	0.5353
-0.0431	-0.2914	1.1077	0.3167	1.1889	0.3559	-0.6339	-3.0184
-1.2901	0.6595	0.8311	-0.7221	0.6385	0.0546	-1.3238	-0.543
0.4945	-4.306	0.0916	-2.063	-0.0161	0.0177	-0.2556	-0.8865
2.0755	-0.8918	-0.866	0.0306	7.4444	0.0675	-5.5135	-0.8417
3.3736	0.7742	-0.2385	1.7644	-0.6616	0.2131	-1.1627	1.5934
-0.4376	-3.2113	-2.917	-0.4292	-0.5983	0.4761	2.3449	0.0592
-5.6668	-1.3495	-6.2314	3.7799	0.7846	-1.4832	-6.7488	-0.9901
0.1437	3.5828	2.9856	2.8431	0.6768	-0.8325	-0.0725	-0.4212
0.5898	-1.9165	-9.4482	0.5304	5.59	0.0564	2.9246	1.6678
-0.3042	-2.4195	-8.2131	-2.22	-5.4227	-2.2726	-6.0587	1.9952
0.7098	-0.3472	-1.9458	0.1555	-18.8732	-1.4917	-3.4175	-6.8389
4.0293	0.1033	-3.3914	-1.3056	0.9756	-0.1814	-0.4908	0.7369
b1							
-4.3981	4.1709	-2.7377	0.341	0.1609	1.305	-1.428	-0.5244
-0.5944	1.1347	1.2699	-4.0717	3.777	-3.2041	0.1645	2.0072
3.047							
w2							
0.0519	0.0072	0.0254	-1.8906	-2.11	-1.0874	-0.1308	1.1345
-1.1354	-1.2396	0.5623	-0.1067	0.3931	1.6966	2.2881	-0.5978
-1.6474							
-1.5204	-0.1465	-0.2333	3.8884	0.8843	0.9265	-5.5619	1.473
6.7699	0.4607	-7.9291	0.7627	-4.7897	-11.6289	-15.3434	3.9745
-2.956							
b2							
-0.0072				3.8507			